THE PHYSICAL REVIEW

VOLUME 90 Second Series NUMBER 4

MAY 15, 1953

Published for the

AMERICAN PHYSICAL SOCIETY

by the

AMERICAN INSTITUTE OF PHYSICS

LANCASTER, PA., AND NEW YORK, N. Y.

REVIEW

A journal of [illegible]

Published by the American Institute of Physics
for the
AMERICAN PHYSICAL SOCIETY

Officers

President

Enrico Fermi
Institute for Nuclear Studies
University of Chicago
Chicago 37, Illinois

Vice-President

H. A. Bethe
Cornell University
Ithaca, New York

Secretary

S. K. Allison
Ryerson Physical Laboratory
Office
Columbia University
New York 27, New York

Treasurer

G. B. Pegram
Columbia University
New York 27, New York

Local Secretary
for the Pacific Coast

[illegible]
University of California at
Los Angeles
Los Angeles, California

Managing Editor

E. A. Gurnett
Brookhaven National Laboratory
Upton, Long Island
New York

[illegible] OF PHYSICS

[illegible]

[illegible]

[illegible]

THE
PHYSICAL REVIEW

A journal of experimental and theoretical physics established by E. L. Nichols in 1893

SECOND SERIES, VOL. 90, NO. 4 MAY 15, 1953

The Energy Loss of Protons in Metallic Foils and Mica*

DAVID KAHN†
Department of Physics and Institute for Nuclear Studies, University of Chicago, Chicago, Illinois
(Received January 19, 1953)

The rate of loss of energy of 500- to 1300-kev protons in various metals and mica has been determined. Foils of Be, Al, Cu, and Au were prepared by evaporation techniques, and the density of the foil was determined by weighing the amount of metal deposited on a known area. The energy loss rate $\Delta E/\Delta x$ was measured with a standard deviation of <3 percent. The energy loss curve was found to join smoothly to the previously measured curve for lower energy protons (50 kev$<E<350$ kev), and to approach the theoretical curves of Bethe and Bloch at the high energy end.

I. INTRODUCTION

THE energy loss of charged particles in matter has been of interest since the early days of nuclear physics. The range of an energetic charged particle has long been used to measure its energy; but the importance of the energy loss phenomenon is due not only to its close connection with the problem of range-energy relations, but also in that it allows an evaluation of our ideas concerning the interactions of charged particles with atoms and electrons.[1]

The problem of particle interaction with matter was first experimentally investigated by observing the range and ionization of naturally occurring α-particles in various gases.[2] To understand better the resultant data, the problem was investigated theoretically on a classical basis by Bohr[3] and from a quantum-mechanical standpoint by Bethe[4] and Bloch.[5] These equations could be tested by determining the energy loss of α-particles in foils of known thickness.

The first observations on protons were made by utilizing the recoil protons resulting from collisions of α-particles in gases containing an admixture of hydrogen.[6] The range-energy curve for protons over a wider energy range was constructed by relating the proton curve to that for α-particles (which was based on more plentiful and accurate data) by means of formulas, both theoretical[2] and empirical.[7]

The development of particle accelerators provided a source of protons of variable and accurately known energies, and observations on the range of artificially accelerated protons were made in 1937.[8] While the experimental results of energy loss and range agree suitably with the theory for high particle energies,[1] the agreement is unsatisfactory at lower energies where the assumptions made in deriving the formulas are increasingly invalid. For the regions in which the theory is not applicable resort must be made to empirically determined data if the energy loss of particles is to be known for these energies. The energy loss in metallic foils for protons with energies in the region 50 to 400 kev has been measured in this laboratory using the Cockcroft-Walton proton accelerator.[9] Some measurements have been made at higher energies in gold[10] and beryllium.[11]

In order to extend the range of measurement, the Van de Graaff accelerator of the Institute of Radiobiology and Biophysics was used to measure the energy loss of

* Supported in part by the U. S. Atomic Energy Commission.
† U. S. Atomic Energy Commission Predoctoral Fellow.
[1] A. E. Taylor, Repts. Progr. Phys. **15**, 49 (1952).
[2] M. S. Livingston and H. A. Bethe, Revs. Modern Phys. **9**, 245 (1937). This article contains an extensive bibliography and review of experimental and theoretical work done prior to 1937.
[3] N. Bohr, Phil. Mag. **25**, 10 (1913).
[4] H. A. Bethe, Ann. Physik **5**, 325 (1930).
[5] F. Bloch, Ann. Physik **16**, 285 (1935).
[6] P. M. S. Blackett and D. S. Lees, Proc. Roy. Soc. (London) **134**, 658 (1932).
[7] W. P. Jesse and J. Sadauskis, Phys. Rev. **75**, 1110 (1949); **78**, 1 (1950).
[8] Parkinson, Herb, Bellamy, and Hudson, Phys. Rev. **52**, 75 (1937).
[9] S. D. Warshaw, Phys. Rev. **76**, 1759 (1949).
[10] T. Huus and C. B. Madsen, Phys. Rev. **76**, 323 (1949).
[11] C. B. Madsen and P. Venkateswarlu, Phys. Rev. **74**, 648 (1948); **74**, 1782 (1948).

protons with energies between 500 and 1400 kev in several metals and mica.[12]

II. APPARATUS

In order to obtain as uniform foils as possible, evaporation techniques were used in preparing them.[13] Glass microscope slides were successively washed with detergent, distilled water, hydrogen peroxide, ether, and ethyl alcohol, and then dried. These slides were then dipped into a 5 percent solution of Parlodion (celluloid) in equal parts of ether and alcohol, and dried. The Al, Cu, and Au foils were deposited onto the coated slides by evaporation from a heated tungsten filament in a vacuum of less than 10^{-4} mm Hg. An equal amount of metal was deposited simultaneously onto two previously weighed platinum foils exposed behind a mesh with circular apertures of known area.

The Parlodion coating containing the metal foil was then stripped from the glass and mounted on rectangular frames with an opening of approximately one by one-half centimeter. The remaining Parlodion backing was removed by immersing the frame and foil into the ether-alcohol solvent. The last traces of the backing were removed by placing the frames cooled by dry ice above the gently warmed solvent mixture.

The proton beam was produced by a Van de Graaff electrostatic accelerator.[14] The construction of the machine is similar to that of the previous models.[15] After acceleration and magnetic analysis, the emerging proton beam defined by the Van de Graaff slit system struck a beryllium target button supporting an evaporated layer of gold approximately 0.0076 mg/cm² thick. The thickness of the gold layer was determined from the evaporation geometry. The beryllium button was insulated from the rest of the apparatus, and the current from the button to ground was used to monitor the proton current. Those protons scattered through a ninety degree angle either (a) passed through an electrostatic analyzer, giving the initial energy E_0,[16] or (b) first passed through the metal foil between the button and the entrance slit of the analyzer, giving the final energy E_f. The scattered protons, rather than the direct beam from the Van de Graaff, were used for the dE/dx measurements, since there was sufficient intensity and thin foils were more liable to rupture in the direct beam.

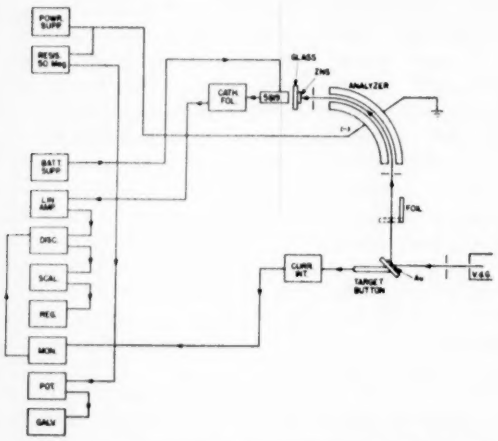

FIG. 1. Schematic diagram of the apparatus and a plan of the electrical circuits. The arrows indicate the flow of information.

The analyzer thus measured either the energy distribution with its peak at E_0 of the protons scattered from the gold layer of the target button, or if the metal foil was placed in the beam, the energy spread with its peak at E_f of the proton beam after penetrating the foil. The most probable energy loss is then E_0-E_f.[17]

The apparatus for supporting the foils was arranged so that two foils could be placed in the vacuum system at once. A stop was provided so that positioning the foils perpendicular to the proton beam could be easily done once the equipment was aligned with respect to the proton beam.

A schematic diagram of the apparatus and electronic control circuits is shown in Fig. 1.

For proton energies between 400 and 800 kev, a 90° electrostatic analyzer with a mean radius of 25.400 cm was used. With the slit positions and charging arrangement used in the present work the value of the constant k[18] of the analyzer was determined to be 19.77 with a standard deviation of 0.11.[19] For energies between 800 and 1400 kev, a 90° cylindrical electrostatic analyzer with a mean radius of 15.167 cm and a constant of 45.23 was used.[18]

The exit port of the analyzer housing was closed by a glass disk, covered on the inside by an evaporated layer of aluminum. The metal was removed from an area one-quarter inch wide and one inch high directly in back of the exit slit. This transparent area was first covered with a very thin layer of silicone grease and then covered with a single layer of phosphorescent ZnS crystals (RCA type 33-Z-20A) having an average diameter of 15μ.

The aluminum coating was used to diminish the pulses produced in the phototube by discharges in the analyzer at high voltages.

---

[12] I wish to thank Dr. Raymond Zirkle and Dr. William Bloom for their kind permission to use the accelerator, and Mrs. L. Wang for preparing the mica foils.

[13] S. D. Warshaw, Rev. Sci. Instr. **20**, 623 (1949).

[14] The accelerator, model AH, was built by the High Voltage Engineering Company, Cambridge, Massachusetts.

[15] Buechner, Van de Graaff, Sperduto, McIntosh, and Burrill *et al.*, Rev. Sci. Instr. **18**, 754 (1947).

[16] Equal to (196/198) E_A, where E_A is the energy of the protons leaving the accelerator.

[17] It can be shown that the average energy loss is also equal to E_0-E_f.

[18] The analyzer constant k is given by $k=W_0/(V_1-V_2)$, where W_0 is the kinetic energy, in electron kilovolts, of a proton as it leaves the foil, in a region of zero (ground) potential; and V_1 and V_2 are the potentials which, when applied to the inner and outer plates of the analyzer, will cause a proton to pass through the instrument and through the defining exit slit.

[19] Allison, Skaggs, and Smith, Phys. Rev. **54**, 171 (1938).

A type 5819 photoelectron multiplier tube was placed directly against the outer surfaces of the glass disk to detect the scintillations caused by the protons hitting the ZnS crystals. The phototube was powered by batteries. The pulses emitted from the phototube after passing through a cathode follower stage entered a linear amplifier of conventional design,[20] where the average signal pulse height was increased to about twenty volts. The pulses then passed to a Schmitt discriminator circuit[21] and thence to a scaler and register.

The current from the proton beam which struck the Be target button was measured by a current integrator and used to monitor the proton counts. To eliminate errors due to unsteadiness in the output current of the Van de Graaff accelerator, the discriminator circuit was turned off after a predetermined amount of current had struck the button. The time for each run was measured as a check on the constancy of output from the accelerator.

The deflecting voltage for the electrostatic analyzer was supplied by a 50-kv voltage doubler circuit of conventional design.[22] The analyzer plate voltage was measured by determining the current drain through a 50 megohm ±0.1 percent resistor stack in parallel with the analyzer plate by means of a 50 ohm ±0.01 percent shunt and potentiometer (Rubicon type 2703). The potentiometer was also used to measure the analyzing magnet current by means of a shunt in the circuit as a check on the constancy of the energy of the beam from the Van de Graaff accelerator.

III. PROCEDURE OF MEASUREMENT

The Van de Graaff accelerator was prepared for a run by adjusting the analyzing magnet of the accelerator to its proper value and then varying the other parameters of the machine (charging current, corona point spacing, focus, etc.) until a steady beam of the desired energy was produced. The vertical position of the emergent beam was then adjusted for the varying type of foil holder used.

When the equipment had been adjusted for maximum geometrical transmission for each run, the analyzer voltage was first roughly adjusted for maximum counting rate with the foil either in or out of the beam. This value of the voltage was determined by means of the potentiometer. The potentiometer was then set at a value approximately 0.3 kev higher than the maximum, and successive runs were made for equal current hitting the target button while lowering the analyzer voltage 0.05 kev each time (Fig. 2). The total number of protons and the duration of each run was recorded. Usually a duration of ~0.5 min produced enough counts so that the statistical error was sufficiently low. The error signal of

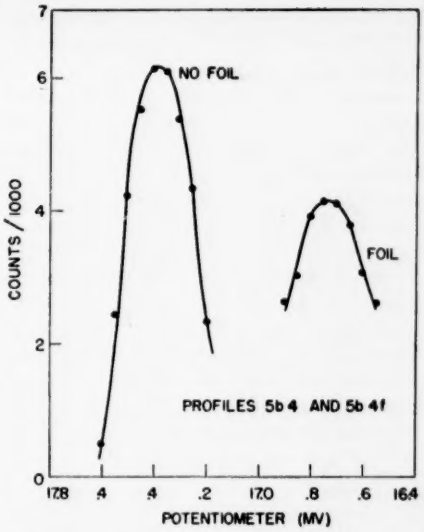

FIG. 2. Representative E_0 and E_f profiles. The abscissas can be converted into kev by multiplying by 45.23.

the potentiometer was measured on a galvanometer equipped with an optical lever. The potentiometer was compared frequently with the standard cell to prevent a significant drift. The successive counts as a function of the analyzer voltage gave an energy profile of the beam entering the analyzer. The position of the foil was then changed and the process repeated. It was found that the shape of the profile was independent of the order in which the successive points were taken.

A check was made of the duration for each run. It was considered that the machine was operating with sufficient steadiness if the time for each run was constant to within approximately 10 percent. Points for which the variation was appreciably greater were re-run.

IV. ERROR ANALYSIS

Part of the spread in the energy profile of E_0 and E_f is caused by the fact that the analyzer has a finite resolution, which is necessary in order to have a reasonable transmission through the instrument. The "25-cm" analyzer had fixed entrance and exit slits resulting in a theoretical limit of resolution of $0.008E$, where E is the energy of the ions traversing the instrument. Measurements of energy profiles with no foil in the beam showed an energy spread which agreed with that predicted.

In this experiment the "15-cm" analyzer slit width was usually 1 mm or less, corresponding to a resolution of 0.32 percent.

The resistor stack in parallel with the analyzer plate was composed of ten 5±0.005 megohm resistors (Shallcross Type XR5). The shunt in series with the stack to measure the current drain through the resistance was 50±0.05 ohms (Rubicon, Type B, No. 1015 resistance box).

[20] T. E. Cranshaw and J. A. Harvey, Can. J. Research **26**, 243 (1948).

[21] W. C. Elmore and M. Sands, *Electronics* (McGraw-Hill Book Company, Inc., New York, 1949), pp. 99–103.

[22] The 0–50 kv DC Power Supply Model No. 2008 was manufactured by the Beta Electric Corporation, New York, New York.

TABLE I. The proton energy loss as a function of energy. The values for proton energies above 200 kev are taken from the solid curves of Fig. 3(a) and (b). The values below 200 kev are taken from Warshaw's curves (reference 9).

Proton energy (kev)	dE/dx kev/(mg/cm²) Be	Mica	Al	Cu	Au
25	546.0				
50	617.0		422.0	185.0	61.0
75	640.0		439.0	212.0	77.0
100	615.0		416.0	223.5	87.0
150	521.0		366.0	228.0	90.0
200	467.5		333.5	222.0	88.5
250	433.0		314.5	212.0	84.5
300	405.0		297.0	200.0	80.5
350	380.8	312.0	283.0	189.5	77.2
400	360.0	286.5	271.0	180.5	74.5
450	342.0	266.5	260.0	172.5	72.0
500	325.0	250.0	250.0	166.0	69.5
550	310.8	236.0	241.0	160.0	67.5
600	297.5	224.0	233.0	154.0	66.0
650	284.2	213.5	223.5	148.5	64.5
700	272.5	204.0	217.0	144.0	63.5
750	266.3	196.0	210.0	140.0	62.0
800	250.9	189.0	202.5	136.0	60.2
850	241.0	182.0	196.0	132.0	59.0
900	231.7	176.5	189.5	128.7	58.5
950	223.0	171.0	183.0	126.0	58.0
1000	215.0	165.0	177.0	122.0	57.0
1050	206.3	160.0	171.0	119.5	56.5
1100	198.0	154.5	166.5	117.0	55.2
1150	190.8	150.0	162.0	114.7	54.7
1200	184.5	146.0	157.5	112.5	54.0
1250	178.8	143.0	154.0	110.0	53.5
1300	173.3	140.0	150.5	109.0	
1350	168.5	137.0	146.5	107.0	

Since it was necessary to measure only the ratio and not the magnitude of each of these resistors to check the accuracy of the analyzer voltage measurements, the two resistors were placed in a bridge circuit with other known resistors. The ratio of the two was found to be $1.0019\pm0.0012\times10^6$.

The individual settings of the potentiometer could be easily estimated to within 0.01 percent of the range. The guaranteed accuracy of the potentiometer is 0.1 percent, but the actual adjustment is much closer. As a further check, the potentiometer was compared with two other similar instruments using a current meter with an accuracy of 0.5 percent (Weston Model 622 milliameter). All potentiometers were in agreement within the accuracy of the meter.

The error signal of the potentiometer was registered continually on a "spot light" galvanometer (Rubicon No. 3404HB). The 0.05-kev analyzer voltage steps used in obtaining a profile corresponded to a galvanometer displacement of one cm. By means of a fine control on the autotransformer in the primary circuit of the high voltage power supply, the galvanometer movement during a run was kept constant to within one mm. This corresponded to a fluctuation at the analyzer plate of ±0.114 kev.

The ac ripple of the analyzer voltage supply was measured and found to have a peak to peak value of 0.08 percent.

The energy spread of the accelerator beam was kept as small as possible to reduce the width of the energy profiles. This spread was largely determined by the width of the accelerator exit slit. The effect of this slit can be easily estimated by considering the change in the radius dr of a beam of protons with slightly different energies traversing the analyzing magnet through which it moves in an arc with a 17-inch radius. If we consider dr as the displacement at the slit due to an energy difference dE, we shall have a good first-order approximation. From elementary principles we have

$$dr=d[(2mE)^{\frac{1}{2}}C/eH]=(r/2E)dE.$$

The Van de Graaff exit slit width was approximately 0.5 mm. For such a slit opening, the energy spread will be a constant percentage of the energy equal to

$$dE/E=2dr/r=2.05/17(2.54)=0.23 \text{ percent}.$$

The effect of this energy spread will be merely to increase the width of the energy profile, unless, during the course of a run, the energy distribution of the protons within this spread should change. To estimate the magnitude of this effect a series of measurements of $\Delta E/\Delta x$ at the same proton energy was made with resulting values unchanged to within the limit of error arising from other causes.

It would seem reasonable to assign an uncertainty in the determination of E_0 due to this cause of 10 percent of the energy spread, or

$$\Delta E_0/E_0=0.1(dE_0/E_0)=0.00023E_0.$$

The proton pulse-height distribution was of such a shape that it was possible to set the discriminator to such a value that the noise pulses could be eliminated and yet have no effect on the proton pulses.

The position of the maximum was determined by finding the axis of symmetry of the energy profile. The agreement between several such estimations and the calculated value of the mean agreed to within 0.113 kev. Accordingly the value for the uncertainty in determining the maximum of the profile is taken to be ±0.113 kev. The error in determining the maximum of the profile due to the finite number of counts for each point can be shown to be negligible providing each point of the curve includes at least a thousand counts. This is almost always the case in this experiment.

Since the solid angle at the foils defined by the analyzer exit slit was approximately 0.00077 steradian, any errors due to multiple scattering in the foil should be negligible.

There seemed to be no regular folding of the foils, which would reveal itself in the form of a double peak in the E_f energy profile. Although some wrinkles were observed, the foils appear as though the greater portion of the foil is flat and deviates, perhaps, within $\pm3°$ from the plane of the foil holder, which is perpendicular to the proton beam. This wrinkling would result in a slight shift of the final energy profile toward the low energy

end, giving a too high value for E_0-E_f. This effect results in a measured value for E_f which is too low by 0.068 ± 0.068 percent. Since the foils are kept in a vacuum and moved in and out of the beam slowly, the effect due to wrinkling should be the same for all measurements with the same foil.

The energy loss in the foils varied from 13 kev to 78 kev for the metallic foils and up to 138 kev in the case of the mica foil. By the use of two foils of differing thicknesses (except for Be and mica) the energy loss was kept to a value of approximately 10 percent of the initial proton energy. Although, for very thin foils and low specific ionization, the energy loss profile is asymmetric, the proton energies and foil thicknesses used in this experiment result in profiles which from theoretical considerations should be symmetrical.[23] That this is so may be seen from the profile shown in Fig. 2. An analytical analysis of the experimentally obtained E_0 and E_f profiles shows them to be very nearly symmetrical.

The foils were placed in the vacuum system immediately before use so as to avoid the formation of oil layers on the foils. The arrangement used for evaporation[24] produced a very nearly uniform deposition of metal both on the Parlodion coated slides and the platinum foils. The variation of the foil thickness at various points on the glass slide and the variation of thickness between the platinum foil and the glass slides was calculated to be less than ±0.25 percent.

The area of deposition on the platinum foil was measured to within an error of ±0.21 percent.

The platinum foils were weighed before and after the evaporation with a microbalance.[25] The sensitivity of the balance was measured periodically and found to be approximately 2 μg/division. By averaging the results of several weighings, it was possible to make a weight determination to within ±1 μg.

Several "control" evaporations (no metal evaporated) were made and the difference in foil weights before and after the operation differed within a few micrograms. The error in determining the amount of evaporated metal ranged from ±1 percent for 200 μg of deposited metal to ±0.5 percent for amounts up to 1 milligram.

The surface density of the beryllium and mica foils was determined by weighing a portion of the foil and then determining its area. A photographic enlargement was made of the foil specimen resulting in an area of approximately 100 cm^2 which was determined accurately by means of a planimeter. The magnification of the image was found by enlarging known lengths at various positions covered by the foil to minimize local distortion of the photograph. The planimeter readings were found to be reproducible to within one percent. The weight determination in the case of the beryllium foil was subject to a considerable error ($\sim$15 percent) since the piece of foil weighed was, unfortunately, quite small. The absolute value of dE/dx for the beryllium curve may contain this much error, and the good agreement between the results of this experiment and other determinations may be fortuituous. The relative values between points at different proton energies are not, of course, affected by the weight determination. The error in weighing the mica foils because of its large weight (1.715 mg) is less than one percent. The mica used is muscovite.

The metal foils used in this experiment seem to be fairly smooth. An estimate of the roughness can be made from the shape of the energy loss profile. Assuming that all of the spread in traversing the foil is due to roughness, the relative variation in thickness appears to be 7 percent. It is unlikely that the variation is other than random—as can be seen from shadow photographs of similarly prepared foils[26]—and a symmetrical broadening of the E_f profile is to be expected.

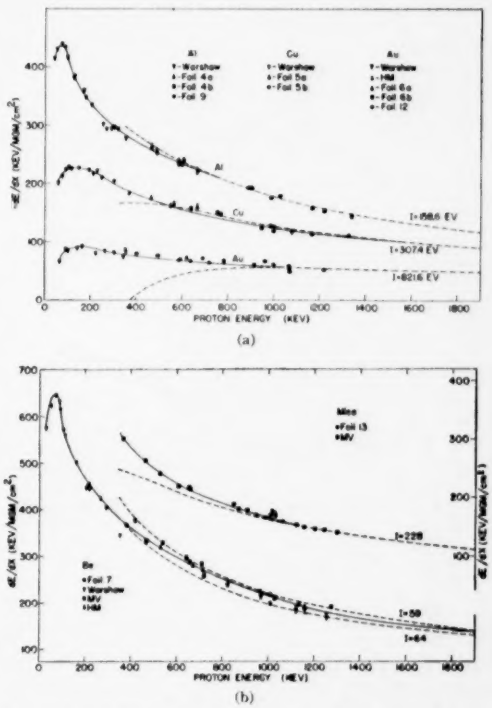

FIG. 3(a) and (b). Proton energy loss as a function of energy. The experimental curves are solid. The dashed lines are calculated from Eq. (1). The references to other determinations of dE/dx are S. D. Warshaw, Phys. Rev. **76**, 1759 (1949); HM, T. Huus and C. P. Madsen, Phys. Rev. **76**, 323 (1949); MV, C. P. Madsen and P. Venkateswarlu, Phys. Rev. **74**, 1782 (1948). The error in the Be measurements due to the uncertainty in weighing is not shown. Numerical values of dE/dx can conveniently be read from Table I.

[23] L. Landau, J. Phys. U.S.S.R. **8**, 201 (1944).

[24] J. Strong, *Procedures in Experimental Physics* (Prentice-Hall, Inc., New York, 1945), p. 198.

[25] Type FDJ, manufactured by Wm. Ainsworth and Sons, Inc., Denver, Colorado.

[26] R. C. Williams and P. C. Backus, J. Appl. Phys. **20**, 98 (1949).

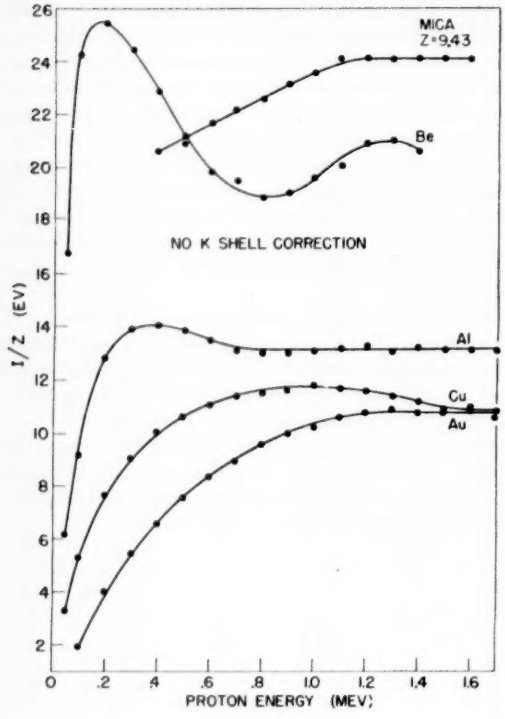

(a)

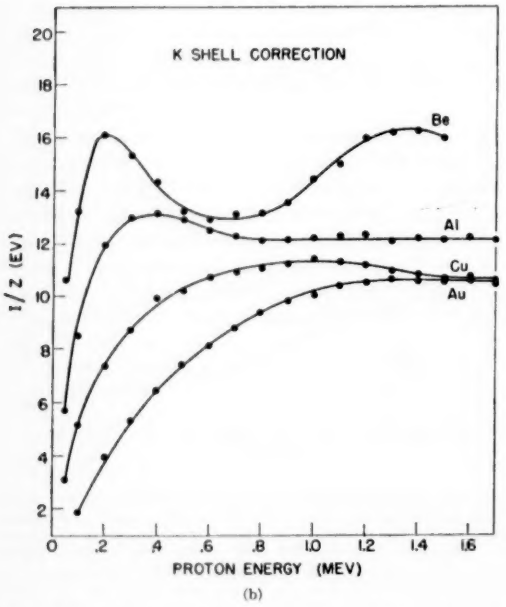

(b)

FIG. 4. The average excitation potential. (a) The values of I were obtained from the data of Table I using Eq. (1) of the text with C set equal to zero; (b) The values of I were obtained from the data of Table I using Eq. (1) of the text.

V. RESULTS

The results of the experimental determinations of $\Delta E/\Delta x$ are given in Table I and Fig. 3(a) and (b). The curves are seen to join smoothly at the lower energy end with the results of Warshaw. At the high energy end the curves fit smoothly with the formulas of Bethe[4] and Bloch.[5] The experimental curves are shown solid. The dashed curves were calculated using the formula

$$-\frac{dE}{dx}=\frac{4\pi e^4 z^2 N}{mv^2}\left[Z\ln\frac{2mv^2}{I}-C_k(\eta)\right];\quad \eta=\frac{mv^2}{2(Z-0.3)^2\mathrm{Ry}}. \tag{1}$$

Although this formula is valid only for large values of η,[27] nevertheless this formula was used as a means of smoothly extrapolating from the energies used here to much higher energies where C_k approaches zero. The value of I for aluminum was obtained by Bloembergen and van Heerden using 70-Mev protons.[28] The dashed curve then represents a very reasonable extrapolation to higher energies. The value of I for copper was determined by Mather and Segrè using 340-Mev protons.[29] The value of I for gold was chosen to fit the experimental curve. Reference 1 contains a collation of the determinations of I for various elements.

The value of the average excitation potential I calculated from the smoothed curves as a function of the proton energy is given in Figs. 4(a) and (b). The calculated value of I with and without the K shell corrections is given. The rise in the value of I for Be and Al at the lower proton energies has no physical significance. It arises from the fact that the logarithmic term in the theoretical formula causes it to approach $-\infty$ and hence to cross the experimental curve. At this point the value of I calculated from the experimental curve using the theoretical formula must again equal the value of I for high proton energies.

The expression for $\Delta E/\Delta x$ may be written

$$\Delta E/\Delta x=\alpha(V_f-V_0)/\Delta x,$$

where α is a constant, Δx is the thickness and V_0 and V_f are the potentiometer readings corresponding to the maxima of the E_0 and E_f profiles, respectively.

The presence of a subtraction in the formula for the stopping power tends to divide the errors in measurement into two groups. The errors in the quantities being subtracted are emphasized if the difference between the quantities is small compared to the quantities themselves; as is the case in this experiment. The other errors do not exert as much influence on the final error and need not be so diligently reduced.

The largest errors in α are the result of the uncertainty in the values of the analyzer constants and

[27] L. M. Brown, Phys. Rev. **79**, 297 (1950).
[28] N. Bloembergen and P. J. van Heerden, Phys. Rev. **83**, 561 (1951).
[29] R. Mather and E. Segrè, Phys. Rev. **84**, 191 (1951).

resolutions; the uncertainties in the parameters of the 25-cm instrument being about two times those for the 15-cm analyzer. The largest error in Δx arises from the error in foil weighing and the uncertainty in the backing removal. The only estimation of the backing error that can be made is an upper bound obtained from considering the errors involved in weighing. There is reason to believe that the actual error is quite small, but the upper bound will be used in computing the over-all error. The uncertainty in α and Δx, however, affects the experimental results only by changing the scale of the curve and alters the shape only as a second-order effect.

The most important errors in determining V_0 and V_f are the analyzer voltage ripple and the uncertainty in determining the mode. The voltage ripple results in the observed curve being a "moving average" of the actual curve.[30] Since the actual curves should be nearly symmetrical, the averaging effect of the voltage ripple should cause a small variation in the position of the maximum.

Since the accuracy of $\Delta E/\Delta x$ depends so much on the difference between V_0 and V_f, it is not possible to give one value for the accuracy which is true for each point on a curve. The accuracy of the individual points in Fig. 3 is given by the vertical lines at each point.

The author wishes to thank Professor Samuel K. Allison for suggesting this problem, for extending the facilities of his laboratory, and for his constant advice and encouragement without which this work would not have been completed. Grateful acknowledgment is also made of the assistance of Gordon DuFloth, Peter Weyl, and others of the Kevatron Group; and to George Moulton, Charles E. Soderquist, and other members of the Institute of Radiobiology and Biophysics.

Note added in proof:—Since this paper was submitted for publication, private communications have been received from C. B. Madsen, reporting further dE/dx measurements at Copenhagen, and from A. B. Chilton and J. N. Cooper at Ohio State University giving stopping powers of copper and nickel for protons. Madsen's data include stopping powers for 2000-kev protons, and using them (directly, for beryllium, mica, and gold, and with some adjustment to our curve for copper and aluminum) it is concluded that the following are the best values at present for 2000 kev. Be, 140; mica, 102; Al, 116; Cu, 75; Au, 43. These should be more reliable than the theoretically extrapolated points above 1350 kev of Fig. 3. The data of Chilton and Cooper on copper lie in the proton energy range 406–1050 kev; their values of dE/dx are about 4 percent lower, on the average, than those reported here.

[30] B. Van der Pol and H. Bremmer, *Operational Calculus* (Cambridge University Press, Cambridge, 1950), pp. 293–300.

Penetration and Diffusion of Hard X-Rays: Polarization Effects*

L. V. SPENCER AND CHARLES WOLFF†
National Bureau of Standards, Washington, D. C.
(Received December 15, 1952)

Most calculations of x-ray penetration and diffusion neglect the polarization of the scattered photons. In this paper an investigation is made of the effect of polarization in a typical x-ray penetration problem. The Boltzmann equation for polarizable photons is expanded into suitable angular and spatial polynomial systems; and a calculation based on this Boltzmann equation is compared with a similar calculation which neglects polarization. The polarization effect increases the intensity of the 100–200 kev secondaries by a few percent.

I. INTRODUCTION

IN recent years a number of methods have been developed for calculating spectral intensities of scattered x-rays at various penetrations.[1, 1a, 2] Nearly all calculations have neglected the effect of polarization in successive Compton scatterings. It is of interest to know just how far one is justified in this. An attempt to evaluate the effect of polarization was made four years ago by Monte Carlo sampling techniques.[3] The results indicated that the effect is quite small.

It can be argued qualitatively that polarization should increase the x-ray flux slightly at large penetrations since the effect of polarization is to increase the likelihood that the successive directions of scattering of a photon will be coplanar. The effect should be more important at low than at high photon energies.

In this paper we have extended the method of reference 1 to calculate spectral intensities generated by a point isotropic source in an infinite medium, taking into account polarization. The results confirm our expectations of slightly greater flux at great depths than is predicted by the simpler theory. Since the method for performing such a calculation may be of fairly general interest, we present it in some detail in the following sections.

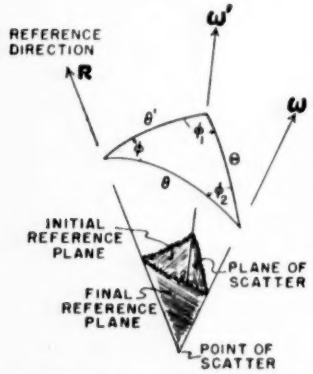

FIG. 1. The geometry of a Compton scattering. A photon traveling initially in the direction ω' is scattered into a new direction ω. The plane of scatter includes the two photon directions, and the initial and final reference planes relate ω', ω to a reference direction **R**.

II. THE DIFFUSION EQUATION

A beam of partially polarized radiation can be completely described by the four parameters of Stokes:[4, 5] I^0, I^1, I^2, and I^3, where I^0 refers to the intensity of the beam, I^1 and I^2 together describe the degree and direction of plane polarization, and I^3 represents the degree of circular polarization. We need not consider circular polarization because it does not affect the penetration of x-rays unless the electrons in the medium are spin polarized.

In order to write down the Boltzmann equation in terms of Stokes parameters we need to know how the Stokes parameters transform if their reference plane is rotated.[6] To determine this we consider a partially polarized beam of photons which passes through a "polarization analyzer." Since the measurement of the analyzer is independent of our description of the beam, the Stokes parameters relating to reference planes inclined to the plane of the analyzer by angles α_1 and α_2 must satisfy the relation[4]

$$I_1^0+I_1^1\cos2\alpha_1+I_1^2\sin2\alpha_1 = I_2^0+I_2^1\cos2\alpha_2+I_2^2\sin2\alpha_2, \quad (1)$$

where the subscripts on the I's refer to the reference plane. If the angle between the reference planes is Φ, i.e., $\alpha_1+\Phi=\alpha_2$, the I_2's can be obtained from the I_1's by the operation

$$\begin{pmatrix} I_2^0 \\ I_2^1 \\ I_2^2 \end{pmatrix} = \begin{pmatrix} 1 & 0 & 0 \\ 0 & \cos2\Phi & -\sin2\Phi \\ 0 & \sin2\Phi & \cos2\Phi \end{pmatrix} \cdot \begin{pmatrix} I_1^0 \\ I_1^1 \\ I_1^2 \end{pmatrix}. \quad (2)$$

* Work supported by the U. S. Office of Naval Research and the U. S. Atomic Energy Commission.
† Now at the University of Chicago, Chicago, Illinois.
[1] L. V. Spencer and U. Fano, J. Research Natl. Bur. Standards **46**, 446 (1951).
[1a] L. V. Spencer, Phys. Rev. **88**, 793 (1952).
[2] G. H. Peebles, Rand Corporation Report RM-653, Part 1, 1951; Part 2, 1952 (unpublished).
[3] L. V. Spencer, National Bureau of Standards Interim Report on Contract with the U. S. Office of Naval Research, 1948 (unpublished).
[4] U. Fano, J. Opt. Soc. Am. **39**, 859 (1949).
[5] S. Chandrasekhar, *Radiative Transfer* (University Press, Oxford, 1950), Chap. I.
[6] The Stokes parameters are defined operationally by means of measurements made with a "polarization analyzer." These measurements are made with the plane of the analyzer inclined several different angles to a so-called arbitrary "reference plane."

If the Stokes parameters of incident and scattered radiation are referred to the plane of scatter,[7] the Klein-Nishina cross section can be expressed as a matrix which relates the parameters of the scattered radiation to the parameters of the incident radiation:[4]

$$\frac{3\lambda'}{8\lambda}\mu_{Th}\begin{pmatrix} 1+\cos^2\Xi+\left(\frac{1}{\lambda'}-\frac{1}{\lambda}\right)(1-\cos\Xi) & -\sin^2\Xi & 0 \\ -\sin^2\Xi & 1+\cos^2\Xi & 0 \\ 0 & 0 & 2\cos\Xi \end{pmatrix} = \frac{3\lambda'}{8\lambda}\mu_{Th}\begin{pmatrix} k_{00}(\lambda',\lambda) & k_{01}(\lambda',\lambda) & 0 \\ k_{10}(\lambda',\lambda) & k_{11}(\lambda',\lambda) & 0 \\ 0 & 0 & k_{22}(\lambda',\lambda) \end{pmatrix}, \quad (3)$$

where λ', λ are the wavelengths in Compton units of the incident and scattered radiation respectively, $\cos\Xi$ is $(1-\lambda+\lambda')$ and must, according to the Compton condition, equal $\cos\Theta$ where Θ is the angle between incident and scattered directions, and μ_{Th} is the Thomson scattering cross section.

We now want to consider a beam of photons which is traveling in a direction $\boldsymbol{\omega}'$ and which is described by Stokes parameters relating to a plane defined by the direction $\boldsymbol{\omega}'$ and a reference direction $\mathbf{R}$. If these photons are scattered into a direction $\boldsymbol{\omega}$, we shall want the Stokes parameters of the scattered radiation related to the plane $(\boldsymbol{\omega}, \mathbf{R})$. To this end we rotate the reference plane of the original parameters through an angle ϕ_1 into coincidence with the plane of scatter (see Fig. 1), apply the Klein-Nishina scattering matrix (3), and finally rotate the plane of the scattered photons back to the new reference plane through an angle $(\phi_2+\pi)$. This sequence of operations is expressed in the following manner:

$$\begin{pmatrix} I_2^0 \\ I_2' \\ I_2^2 \end{pmatrix} = \frac{3\lambda'}{8\lambda}\mu_{Th}\begin{pmatrix} 1 & 0 & 0 \\ 0 & \cos2(\phi_2+\pi) & -\sin2(\phi_2+\pi) \\ 0 & \sin2(\phi_2+\pi) & \cos2(\phi_2+\pi) \end{pmatrix} \cdot \begin{pmatrix} k_{00}(\lambda',\lambda) & k_{01}(\lambda',\lambda) & 0 \\ k_{10}(\lambda',\lambda) & k_{11}(\lambda',\lambda) & 0 \\ 0 & 0 & k_{22}(\lambda',\lambda) \end{pmatrix}$$

$$\cdot \begin{pmatrix} 1 & 0 & 0 \\ 0 & \cos2\phi_1 & -\sin2\phi_1 \\ 0 & \sin2\phi_1 & \cos2\phi_1 \end{pmatrix} \cdot \begin{pmatrix} I_1^0 \\ I_1^1 \\ I_1^2 \end{pmatrix}. \quad (4)$$

If we define

$$\mathbf{I} \equiv \begin{pmatrix} I^0 \\ I^1 \\ I^2 \end{pmatrix},$$

and if we perform the multiplications, we may write this relation in the form $\mathbf{I}_2 = \mathbf{S}\cdot\mathbf{I}_1$, where

$$\mathbf{S} = \frac{3\lambda'}{8\lambda}\mu_{Th}\begin{pmatrix} k_{00} & k_{01}\cos2\phi_1 & -k_{01}\sin2\phi_1 \\ k_{10}\cos2\phi_2 & k_{11}\cos2\phi_2\cos2\phi_1 - k_{22}\sin2\phi_2\sin2\phi_1 & -k_{11}\cos2\phi_2\sin2\phi_1 - k_{22}\sin2\phi_2\cos2\phi_1 \\ k_{10}\sin2\phi_2 & k_{11}\sin2\phi_2\cos2\phi_1 + k_{22}\cos2\phi_2\sin2\phi_1 & -k_{11}\sin2\phi_2\sin2\phi_1 + k_{22}\cos2\phi_2\cos2\phi_1 \end{pmatrix}. \quad (5)$$

With these definitions, the equation governing the propagation of radiation is the following:

$$\boldsymbol{\omega}\cdot\mathrm{grad}\mathbf{I}(\mathbf{r},\boldsymbol{\omega},\lambda) = -\mu(\lambda)\mathbf{I}(\mathbf{r},\boldsymbol{\omega},\lambda) + \int_0^{\lambda} d\lambda' \int_{4\pi} d\boldsymbol{\omega}'(1/2\pi)\delta(\boldsymbol{\omega}\cdot\boldsymbol{\omega}'-\cos\Xi)\mathbf{S}\cdot\mathbf{I}(\mathbf{r},\boldsymbol{\omega}',\lambda') + \text{source}, \quad (6)$$

where

$$\mathbf{I}(\mathbf{r},\boldsymbol{\omega},\lambda) = \begin{pmatrix} I^0(\mathbf{r},\boldsymbol{\omega},\lambda) \\ I^1(\mathbf{r},\boldsymbol{\omega},\lambda) \\ I^2(\mathbf{r},\boldsymbol{\omega},\lambda) \end{pmatrix}. \quad (7)$$

In these relations, $I^0(\mathbf{r},\boldsymbol{\omega},\lambda)$ is the spectral energy density of the x-rays,[1a] $\mathbf{r}$ is the position vector, $\mu(\lambda)$ is the total narrow beam attenuation coefficient, $\boldsymbol{\omega}, \boldsymbol{\omega}'$ are unit direction vectors, δ is the Dirac delta-function, and $\cos\Xi = (1-\lambda+\lambda')$.

[7] The plane of scatter is the plane which includes the photon directions before and after the scattering.

If we restrict ourselves to a point isotropic source, the only position parameter necessary is the distance of the photon from the source. If, further, we specify a monoenergetic source and choose as a reference direction **R** the line from the source to the position of the photon, Eq. (7) becomes[1]

$$\omega_r\frac{\partial \mathbf{I}(r,\omega_r,\lambda)}{\partial r}+\frac{(1-\omega_r^2)}{r}\frac{\partial \mathbf{I}(r,\omega_r,\lambda)}{\partial \omega_r}=-\mu(\lambda)\mathbf{I}(r,\omega_r,\lambda)$$
$$+\int_{\lambda_0}^{\lambda}d\lambda'\int_{4\pi}d\omega'(1/2\pi)\delta(\cos\Theta-\cos\Xi)\mathbf{S}\cdot\mathbf{I}(r,\omega_r',\lambda')+\lambda_0\delta(\lambda-\lambda_0)\frac{\delta(r)}{4\pi r^2}\mathbf{1} \quad (8)$$

where

$$\mathbf{1}=\begin{pmatrix}1\\0\\0\end{pmatrix},$$

$r=|\mathbf{r}|$, $\omega_r=\boldsymbol{\omega}\cdot\mathbf{R}=\cos\vartheta$, $\omega_r'=\boldsymbol{\omega}'\cdot\mathbf{R}=\cos\vartheta'$, $\cos\Theta=\boldsymbol{\omega}\cdot\boldsymbol{\omega}'$, and λ_0 is the wavelength of the source radiation.

III. REDUCTION OF THE DIFFUSION EQUATION

We want to expand Eqs. (8) into spherical harmonics. In making this expansion, we find that each of the elements of **S** leads to integrals which are special cases of the quantity

$$D(m_1,m_2)=(1/2\pi)\int_0^{2\pi}d\phi e^{i(m_1\phi_1+m_2\phi_2)}\delta(\cos\Theta-\cos\Xi). \quad (9)$$

The evaluation of $D(m_1,m_2)$ can be accomplished by means of the symmetrical top wave functions $\psi(l,m_1,m_2)$.[8] These functions are especially adapted to this problem because they relate to the most general possible rotation of axes, involving all three Euler angles.

If we make use of the orthogonality property of these wave functions we may write

$$D(m_1,m_2)=(1/2\pi)\int_0^{2\pi}d\phi e^{i(m_1\phi_1+m_2\phi_2)}4\pi^2\sum_l\psi(l,m_1,m_2;0,\Xi,0)\psi(l,m_1,m_2;0,\Theta,0)$$
$$=e^{-im_2\pi}(1/2\pi)\int_0^{2\pi}d\phi 4\pi^2\sum_l\psi(l,m_1,m_2;0,\Xi,0)\psi(l,m_1,m_2;\phi_1,\Theta,\pi+\phi_2). \quad (10)$$

We now want to make use of an addition formula for the ψ's which relates to the fact (see Fig. 1) that a general rotation of axes involving:

(a) A rotation around one axis by an angle ϕ_1,
(b) A tipping of this axis by an angle Θ,
(c) Another rotation around the tipped axis by an angle $\pi+\phi_2$, which is the transformation to which $\psi(l,m_1,m_2;\phi_1,\Theta,\pi+\phi_2)$ corresponds, is identical to the following transformation:

(a) A tipping of the axis by an angle ϑ',
(b) A rotation around the tipped axis by an angle $(\pi-\phi)$,
(c) A further tipping of the axis by an angle ϑ.
(d) A rotation about this final axis by the angle π.

The addition formula relating to this identity is the following:

$$\psi(l,m_1,m_2;\phi_1,\Theta,\pi+\phi_2)=\sum_i\left(\frac{8\pi^2}{2l+1}\right)^{\frac{1}{2}}\psi(l,m_1,i;0,\vartheta',\pi-\phi)\psi(l,i,m_2;0,\vartheta,\pi). \quad (11)$$

[8] These (normalized) functions are given by the following formula (l, m_1, m_2 integers):

$$\psi(l,m_1,m_2;\phi_1,\Theta,\phi_2)=Ae^{i(m_1\phi_1+m_2\phi_2)}[\tfrac{1}{2}(1-\cos\Theta)]^{d/2}[\tfrac{1}{2}(1+\cos\Theta)]^{s/2}F[-p,(1+d+s+p);(1+d);\tfrac{1}{2}(1-\cos\Theta)],$$

where

$$A=\left\{\frac{2l+1}{8\pi^2}\frac{(d+s+p)!(d+p)!}{p!(d!)^2(s+p)!}\right\}^{\frac{1}{2}},$$
$$d=|m_1-m_2|,\quad s=|m_1+m_2|,\quad p=l-\tfrac{1}{2}(s+d).$$

We obtained this formula for the normalized functions from Ruark and Urey, *Atoms, Molecules, and Quanta*, p. 671 (McGraw-Hill Book Company, Inc., New York, 1930). The ψ's are also called the representations $\mathfrak{D}^{(l)}$ of the group of space rotations. We are very grateful to U. Fano for this method of evaluating $D(m_1,m_2)$.

If we substitute this into (10) and carry out the integration, we have the result:

$$D(m_1, m_2) = 4\pi^2 \sum_l \left(\frac{8\pi^2}{2l+1}\right)^{\frac{1}{2}} \psi(l, m_1, m_2; 0, \Xi, 0)\psi(l, m_1, 0; 0, \vartheta', 0)\psi(l, 0, m_2; 0, \vartheta, 0)$$

$$= 4\pi^2 \sum_l \left\{\frac{2l+1}{8\pi^2} \frac{(l-m_1)!(l-m_2)!}{(l+m_1)!(l+m_2)!}\right\}^{\frac{1}{2}} \psi(l, m_1, m_2; 0, \Xi, 0) P_l^{m_1}(\omega_r') P_l^{m_2}(\omega_r). \tag{12}$$

Notice that according to (12), $D(m_1, m_2)$ is real. The part of $D(m_1, m_2)$ which changes sign if the signs of both ϕ_1 and ϕ_2 are reversed vanishes with the integration over ϕ. Now, the elements of **S** are either even or odd with respect to a reversal of the sign of both ϕ_1 and ϕ_2. Since all elements lead to the integrals $D(m_1, m_2)$ (plus or minus the complex conjugate), those elements which are odd vanish when the integral over ϕ is performed. We may as well omit these odd elements and write

$$\mathbf{S} = \frac{3\lambda'}{8\lambda}\mu_{\mathrm{Th}} \begin{pmatrix} k_{00} & k_{01}\cos 2\phi_1 & 0 \\ k_{10}\cos 2\phi_2 & k_{11}\cos 2\phi_2 \cos 2\phi_1 - k_{22}\sin 2\phi_2 \sin 2\phi_1 & 0 \\ 0 & 0 & -k_{11}\sin 2\phi_2 \sin 2\phi_1 + k_{22}\cos 2\phi_2 \cos 2\phi_1 \end{pmatrix}. \tag{13}$$

It is apparent from (13) that the lower right corner element of **S** is isolated. This has the consequence that, if the source radiation is unpolarized, $I^2(r, \omega_r, \lambda)$ remains identically zero, since there is no means by which it can be generated. (This result can be readily obtained directly from symmetry considerations.)

If we define quantities I_{ln}^0, I_{ln}^1 by the relations

$$I_{ln}^0(\lambda) = (n!)^{-1} \int_0^\infty dr(4\pi r^2) r^n \int_{4\pi} d\omega (2\pi)^{-1} P_l(\omega_r) I^0(r, \omega_r, \lambda),$$

$$I_{ln}^1(\lambda) = (n!)^{-1} \int_0^\infty dr(4\pi r^2) r^n \int_{4\pi} d\omega (2\pi)^{-1} P_l^2(\omega_r) I^1(r, \omega_r, \lambda), \tag{14}$$

and if we expand (8) after the manner of reference 1, Eq. (23), we obtain the following interlinked system of equations:

$$-\frac{1}{n(2l+1)}[(l+1)(n-l)I_{l+1,\,n-1}^0(\lambda) + l(l+n+1)I_{l-1,\,n-1}^0(\lambda)] = -\mu(\lambda)I_{ln}^0(\lambda)$$

$$+ \int_{\lambda_0}^{\lambda} d\lambda' \left\{k_{00}P_l(\cos\Xi)I_{ln}^0(\lambda') + k_{01}\frac{(l-2)!}{(l+2)!}P_l^2(\cos\Xi)I_{ln}^1(\lambda')\right\} + \delta(\lambda-\lambda_0)\delta_{n0}\delta_{l0},$$

$$-\frac{1}{n(2l+1)}[(l-1)(n-l)I_{l+1,\,n-1}^1(\lambda) + (l+2)(l+n+1)I_{l-1,\,n-1}^1(\lambda)] = -\mu(\lambda)I_{ln}^1(\lambda) \tag{15}$$

$$+ \int_{\lambda_0}^{\lambda} d\lambda' \{k_{10}P_l^2(\cos\Xi)I_{ln}^0(\lambda') + \tfrac{1}{2}[k_{11}\{\psi(l, 2, 2) - \psi(l, 2, -2)\} + k_{22}\{\psi(l, 2, 2) + \psi(l, 2, -2)\}]I_{ln}^1(\lambda')\},$$

where $k_{ij} = k_{ij}(\lambda', \lambda)$ and $\psi(l, 2, \pm 2) = \psi(l, 2, \pm 2; 0, \Xi, 0)$.

This double system of equations can best be interpreted with the aid of Fig. 2. If l is zero or one, I_{ln}^1 is identically zero. This is a consequence of (14) rather than (15). If l is equal to n, the interlinkage terms $I_{l+1,\,n-1}^0$, $I_{l+1,\,n-1}^1$ in (15) are destroyed by the factor $(n-l)$. This means that the elements in Fig. 2 which are left of the diagonal are not linked to the elements which are to the right of the diagonal. The integral equations for I_{ln}^0, I_{ln}^1 must in general be solved simultaneously, since both quantities appear in both integral terms of (15). As in reference 1, by proceeding from small to large n it is possible to unravel the system (15) and solve for as many I_{ln}^0, I_{ln}^1 as desired, since the inhomogeneous terms in the equations for $I_{l,\,n+1}^0$, $I_{l,\,n+1}^1$ involve only quantities which have already been determined at an earlier stage of calculation.

IV. CALCULATIONS

For purposes of comparison, two calculations were performed by identical methods. In the first (polariza-

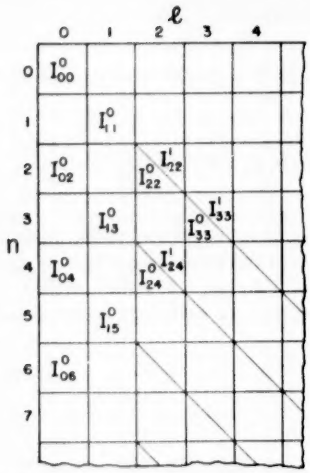

FIG. 2. A diagram showing the quantities determined in the polarization calculation. Two quantities within the same square must be solved for simultaneously. The solution starts in the upper left corner and proceeds down and to the right.

tion included) calculation, a number of Eqs. (15) were solved numerically. In the second (polarization neglected), the corresponding equations of reference 1 were used. (These are the equations obtained by arbitrarily setting all $I_{ln}{}^1$ equal to zero.)

The position variable was taken to be the dimensionless quantity $(\mu_0 r)$, μ_0 being the total attenuation coefficient of the source radiation. The source energy was chosen to be 1.277 Mev and the scattering medium was water. The solution was not carried out directly for the space moments $I_{ln}{}^{0,1}$, but rather for the coefficients of the $U_n{}^l(\mu_0 r)$ polynomials,[1,9] which are small differences between the $I_{ln}{}^{0,1}$ moments.

The integration was performed in accordance with Stirling's formula, with an adjustment for situations involving an odd number of integration steps. No integrations were performed for photon energies below 116 kev. The quantities determined correspond with those listed explicitly in Fig. 2, i.e., the coefficients of the first four $U_n{}^0(\mu_0 r)$ polynomials in the polynomial expansion of the spectral energy density. A considerable simplification in the integration results from the fact that $k_{01}(\lambda,\lambda)=k_{10}(\lambda,\lambda)=0$. Because of this the simultaneous solution of the equations for $I_{ln}{}^0, I_{ln}{}^1$ does not involve awkward algebraic difficulties.

V. RESULTS

The results of these calculations are summarized in Fig. 3, in which is plotted the percentage increase in the spectral energy density at a given depth resulting from polarization. The effect is small ($\sim$1 percent) and positive, as expected. It disappears at high energies. At low energies it is constant because the angular distributions are isotropic. One characteristic which does not appear in Fig. 3 is an approach to an equilibrium (maximum) effect as r increases. It is difficult to predict the penetration at which this maximum effect will be reached, and it is perhaps not surprising that Fig. 3 does not show it.

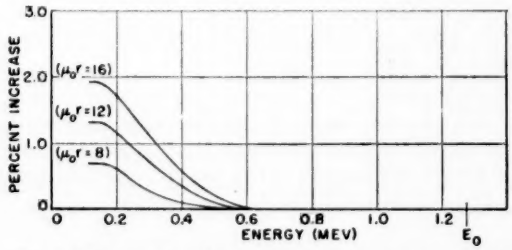

FIG. 3. The percentage increase in the spectral energy density due to polarization. The source energy is $E_0=1.277$ Mev. The leveling off at low energies relates to the fact that photon directional distributions become isotropic at low energies.

[9] L. V. Spencer and F. Stinson, Phys. Rev. **85**, 662 (1952).

Corrected Values of Fowler-Nordheim Field Emission Functions $v(y)$ and $s(y)$

R. E. BURGESS, *Radio Research Station, Dilton Park, Slough, Bucks, England*
H. KROEMER, *Fernmeldetechnisches Zentralamt, Darmstadt, Germany*

AND

J. M. HOUSTON,* *Research Laboratory of Electronics, Massachusetts Institute of Technology, Cambridge, Massachusetts*
(Received February 10, 1953)

Corrected values are given for the function $v(y)$ which appears in the exponent of the Fowler-Nordheim equation for field emission from a metal. Values are also given for the function $s(y)$ which relates to the slope of logarithmic plots of the Fowler-Nordheim equation.

NORDHEIM[1] has given an expression for a function $v(y)$, which appeared when he calculated the probability that an electron might pass through a potential barrier composed of a mirror-image potential plus a linear potential that resulted from an applied electric field. This function appears in the exponent of the Fowler-Nordheim equation for electron field emission from a metal. The variable y is a nondimensional function of the applied electric field and the surface work-function.

Burgess and Kroemer have recently independently discovered a mathematical error in Nordheim's analysis. The correct expression for $v(y)$ is:

$$v(y)=2^{-\frac{1}{2}}[1+(1-y^2)^{\frac{1}{2}}]^{\frac{1}{2}} \times\{E(k^2)-y^2K(k^2)/[1+(1-y^2)^{\frac{1}{2}}]\},$$

where

$$E(k^2)=\int_0^{\pi/2}(1-k^2\sin^2\phi)^{\frac{1}{2}}d\phi,$$

$$K(k^2)=\int_0^{\pi/2}(1-k^2\sin^2\phi)^{-\frac{1}{2}}d\phi,$$

$$k^2=2(1-y^2)^{\frac{1}{2}}/[1+(1-y^2)^{\frac{1}{2}}].$$

$K(k^2)$ and $E(k^2)$ are the complete elliptic integrals of the first and second kind. In his paper Nordheim defined k incorrectly.

This error renders incorrect Houston's[2] tables of $v(y)$ and $s(y)$, the latter being defined as: $s(y)=v(y)-\frac{1}{2}ydv/dy$. The function $s(y)$ appears in expressions[2] for the slope of logarithmic plots of the Fowler-Nordheim equation. In Table I are listed recalculated values of $v(y)$ and $s(y)$ correct to four figures.

TABLE I. Values of $v(y)$ and $s(y)$.

y	$v(y)$	$s(y)$
0	1.0000	1.0000
0.05	0.9948	0.9995
0.1	0.9817	0.9981
0.15	0.9622	0.9958
0.2	0.9370	0.9926
0.25	0.9068	0.9885
0.3	0.8718	0.9835
0.35	0.8323	0.9777
0.4	0.7888	0.9711
0.45	0.7413	0.9637
0.5	0.6900	0.9554
0.55	0.6351	0.9464
0.6	0.5768	0.9366
0.65	0.5152	0.9261
0.7	0.4504	0.9149
0.75	0.3825	0.9030
0.8	0.3117	0.8903
0.85	0.2379	0.8770
0.9	0.1613	0.8630
0.95	0.0820	0.8483
1.	0	0.8330

* This work was supported in part by the Signal Corps, the Air Materiel Command, and the U. S. Office of Naval Research.
[1] L. Nordheim, Proc. Roy. Soc. (London) **121**, 626 (1928).
[2] J. M. Houston, Phys. Rev. **88**, 349 (1952).

Active Nitrogen

S. K. MITRA
Institute of Radio Physics and Electronics, University of Calcutta, Calcutta, India
(Received December 29, 1952)

Criticisms have been made of the ionic theory of active nitrogen, proposed by the author some years ago, on the ground that experiments carried out since then with the specific purpose of detecting N_2^+ ions in the glowing gas have yielded negative results. Need is felt therefore for re-examining the older theories in particular the atomic theory and its variations. It is shown in the paper that by collating the suggestions made in respect of this theory in recent years one may make the following hypothesis: Active nitrogen is a mixture of nitrogen atoms in the ground state ^4S and the metastable states ^2D and ^2P (the last named in small proportion) produced by dissociative recombination of N_2^+ ions and electrons always present in a strong electric discharge in nitrogen. The N_2^+ ions and electrons are thus the parent bodies of the active substance instead of being themselves the active substance, as had been proposed in the ionic theory. The reason the production of the atoms is supposed to be due to dissociative recombination and not to electronic bombardment of N_2 molecules, is that it has been known for a long time that the production of active nitrogen is closely associated with the presence and production of N_2^+ ions. The two outstanding properties of active nitrogen (besides its chemical activity) e.g., long-duration afterglow emitting its characteristic band spectrum, and the invariable presence of ionization in the glowing gas, are thus explained as follows: The nitrogen atoms recombine by a preassociation process (as first suggested by Gaydon) to produce N_2 molecules in the high vibrational levels of the B state from which the first positive bands, with the characteristic intensity distribution, are emitted. The long life of the afterglow is explained as resulting from the fact that the wall recombination of the N atoms is prevented by the formation of an adsorbed layer of N_2 molecules on the wall surface. (Formation of such an adsorbed layer was also assumed in the ionic theory.) The invariable presence of ionization in the glowing gas is explained as resulting from ionizing recombination of metastable atoms, $N(^2D)+N(^2P)\rightarrow N_2^+ + e$. Possible explanations of the negative temperature coefficient of the glow intensity, of the so-called dark modification, and also of some of the other properties of active nitrogen, are suggested.

1. INTRODUCTION. THE IONIC THEORY

THE author of this note put forward some time ago the theory that the active substance in the well-known nitrogen afterglow (Lewis-Rayleigh type) consists of a mixture of N_2^+ ions and electrons.[1,2] The theory further postulated that the walls of the afterglow vessel are so conditioned by the formation of an adsorbed "layer" (probably of N_2) that only a small fraction of the impinging electrons attach themselves to the walls to form electronic surface charge. The neutralization of ions and electrons on the surface (which is a very fast process) being thus prevented, the recombination takes place mainly in the volume by a three-body process,

$$N_2^+ + e + M \rightarrow N_2(\text{excited}) + M(\text{excited}),$$

in course of which the characteristic afterglow spectrum is emitted. Here M is the third body (a nitrogen molecule) which takes up the excess of energy and momentum. The three-body collision process being necessarily a slow one, the long life of the afterglow is explained.

Critisicms of this "ionic theory" of active nitrogen have been made from time to time mainly on grounds of newer experimental results. These are as follows:

In 1948 Worley[3] carried out experiments to detect absorption, in the visible range, in a long column of the glowing gas (13 meters). It was expected that the transition $N_2^+(X')+h\nu \rightarrow N_2^+(A')$ would cause strong absorption because the reverse transition, $N_2^+(A')\rightarrow N_2^+(X')+h\nu$, is an allowed one leading to the emission of the familiar first negative bands in strong nitrogen discharge. The obvious inference from the experimental result is that N_2^+ ions are not present in sufficient number in the glowing gas.

Very recently Benson[4] has carried out interesting measurements of some of the physical properties of active nitrogen employing modern microwave techniques. He concludes from his results that the observed ionization in a stream of active nitrogen is incidental rather than essential to the production of the Lewis-Rayleigh afterglow (an opinion expressed also by other workers) and that the ionization appears to be due mainly to electrons. Further, the concentration of the electrons in the glowing gas is many orders less than that of the active particles.

In view of these criticisms is becomes necessary to re-examine some of the older theories of active nitrogen.

2. THE OLDER THEORIES

The oldest theory of active nitrogen is that the active substance in the afterglow is nitrogen atoms. The suggestion was first made by Rayleigh[5] in 1911 and is a very natural one since hydrogen afterglow—albeit of much shorter duration—is known to be due to recombination of hydrogen atoms. Sponer[6] in 1925 gave the theory a more definite form by suggesting that the

[1] S. K. Mitra, Science and Culture (Calcutta) **9**, 46 (1943-44); Nature **154**, 212 (1944).
[2] S. K. Mitra, *Active Nitrogen—A New Theory* (Indian Association for the Cultivation of Science, Jadavpur, Calcutta, 1945). Part I gives a summary of the properties and phenomena of active nitrogen.
[3] R. Edwin Worley, Phys. Rev. **73**, 531 (1948).
[4] James M. Benson, J. Appl. Phys. **23**, 757 (1952).
[5] Lord Rayleigh (Strutt), Proc. Roy. Soc. (London), **A85**, 219 (1911).
[6] H. Sponer, Z. Physik **34**, 622 (1925); **41**, 611 (1927).

nitrogen atoms recombine by a three-body process,

$$N+N+M \rightarrow N_2(\text{excited})+M(\text{excited}),$$

in course of which the afterglow is emitted. If the excited nitrogen molecule be assumed to be formed in the higher vibrational levels of the $B\ ^3\Pi_g$ state, then the emission of the afterglow spectrum (first positive bands) is explained (see Fig. 1). The reaction is energetically possible if Gaydon's value[7] of dissociation energy of the N_2 molecule (9.76 ev) is accepted. Further, since three-body collision is a slow process, the long life of the afterglow is explained. The reaction, however, does not explain why only selected bands of first positive group (see below) are emitted.

To obviate this difficulty Cario and Kaplan[8] proposed that the active substance in the afterglow is a mixture of metastable molecules in the A state, and metastable atoms in ^2P and ^1D states. [The energies of these states are 3.56 ev and 2.37 ev, respectively, (see Fig. 2).] It is supposed that the molecule in the A state is excited to the B state (from which the characteristic first positive bands are emitted) by collision with a metastable atom. Since the energy of the A state is 6.1 ev, the enhancement of selected bands of the first positive group is explained (see below).

There have also been rather speculative theories[9–11] suggesting that the active substance is a molecule in some highly metastable state or is a "collision complex (NN)" formed of two metastable nitrogen atoms.

The main concern of the above theories had been to explain the excitation of the characteristic afterglow spectrum and, to some extent, its long life. They do not make any attempt to explain the many other properties and phenomena of active nitrogen. This was first done in the ionic theory proposed by the author. But unfortunately, as already mentioned in the introduction, experimental evidence seems to go against the existence of N_2^+ ions and electrons, in sufficient numbers at least, in the glowing gas. It will however be shown in the next section that it is possible to develop a theory (an atomic theory) in which the N_2^+ ions and electrons, though they are not themselves the active substance, are the parent bodies of the same, namely metastable nitrogen atoms. This metastable atomic theory, unlike the theory of Cario and Kaplan, does not require the essential presence of the metastable molecules to explain the afterglow spectrum. It will further be shown that it is possible to explain by this theory not only the two outstanding properties of active nitrogen (besides its chemical activity), namely the long-duration afterglow emitting its characteristic spectrum and the invariable presence of ionization in the glowing gas, but also the other characteristics like negative temperature coefficient and the so-called dark modification.

[7] A. G. Gaydon, Nature **153**, 407 (1944).
[8] G. Cario and J. Kaplan, Z. Physik **58**, 769 (1929).
[9] R. T. Birge, Phys. Rev. **23**, 294 (1924).
[10] D. E. Debeau, Phys. Rev. **61**, 668 (1942).
[11] A. van der Ziel, Physica **1**, 353 (1934); **4**, 373 (1937).

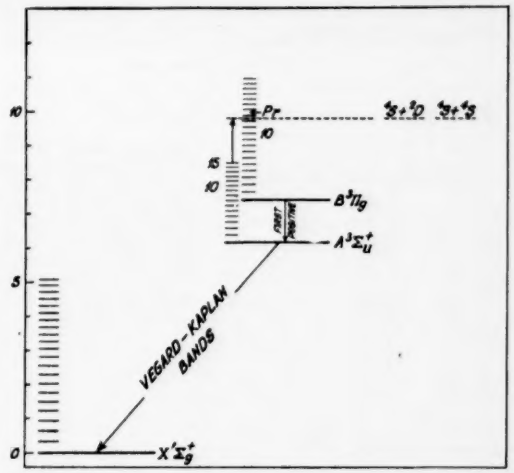

FIG. 1. Energy levels of N_2 molecule which are of interest in the emission of the Lewis-Rayleigh afterglow. The molecule in the excited A state dissociates when the energy of the vibration level is 9.76 ev. The two dissociated nitrogen atoms are in the ground state (^4S) if the dissociation energy is 9.76 ev, or one atom in the ground state and the other in the metastable ^2D state if the dissociation energy is 7.38 ev. There is predissociation of the excited molecule in the B state at the vibration levels $v=13$ to 16.

3. METASTABLE ATOM THEORY

It will be helpful and instructive if the statement of the theory is preceded by a little inductive reasoning.

One of the most firmly established facts in the whole group of phenomena of active nitrogen is that the spectrum of the Lewis-Rayleigh afterglow consists only of selected bands of the first positive group ($B^3\Pi_g \rightarrow A^3\Sigma_u$) as originate from the higher vibrational levels $v''=12$, 11, 10, etc. The energy of the highest vibrational level is about 9.7 ev. The intensity distribution in the bands differs, in fact, markedly from that in the spectrum of the ordinary glow discharge when active nitrogen is *not* being produced.

From the above fact one may at once infer that the active substance, whatever may be its nature, must be producing N_2 molecules in the higher vibrational levels of the B state even after the discharge is cut off.

Let us therefore consider the probable mode of production of such excited N_2 molecules in the glowing gas.

Detailed study of the N_2 band spectra shows that there is predissociation of the $N_2(B)$ molecule at the vibrational levels $v=13$ to 16 (Fig. 1). The predissociated products may be two nitrogen atoms in the ground state $N(^4S)$ if Gaydon's value of dissociation energy (9.76 ev) is accepted, or one atom in the ground state $N(^4S)$ and the other in the metastable $N(^2D)$ state if the older value of dissociation energy (7.38 ev) is assumed. Now corresponding to predissociation there is also the opposite process of preassociation in which the dissociated atoms, when they collide, have a probability of combining to produce the molecule in the

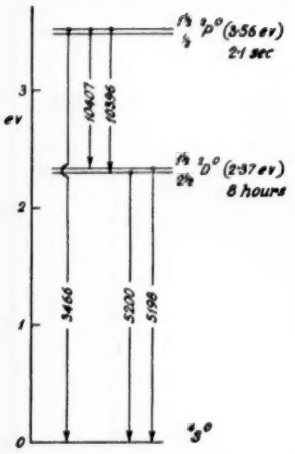

FIG. 2. Energy levels of the metastable states of the nitrogen atom. Nitrogen atoms in the ground and metastable states (which constitute active nitrogen) are produced by dissociative recombination of N_2^+ ions and electrons.

vibrating electronic state in which the predissociation occurred. The dissociated N atoms will, therefore, have a probability of recombining by radiationless transition in one of the high vibrational levels near $v=13$. The possibility of the production of excited N_2 molecules from which the characteristic emission of the afterglow spectrum takes place by such preassociation of N atoms has been discussed by Gaydon.[12] (The $N_2(B)$ molecules may also be produced by radiative recombination of two metastable N atoms. But the probability of such recombination is extremely small.)

Next let us consider how the N atoms—assuming that they constitute the active substance in the afterglow—may be produced in the discharge tube. No definite suggestion regarding this is made in the older theories. Perhaps there was the tacit assumption that the N_2 molecules are dissociated by impacts of high energy electrons. This however does not explain the fact—as observed by many workers—that the production of N_2^+ ions is closely associated with the production and the presence of the active substance. We may cite here two instances of such observation.

It has been observed by Rayleigh[13] that the yield of active nitrogen is the highest in the neighborhood of the cathode of the discharge tube. Also it is well known that the concentration of the positive ions is also the highest in the neighborhood of the cathode.

Kenty and Turner[14] found that in order to produce active nitrogen, one has to bombard nitrogen gas by electrons of energy 16.3 ev which is just above the first ionization potential of N_2. They further found that the maximum effect begins when the energy is nearing 20 ev, which is a little above the second ionization potential of N_2, 18.75 ev. This indicates that the bombarding electrons are producing N_2^+ ions in the excited A' state from which the first negative bands are emitted.

The essential presence of N_2^+ ions in the production of the active substance, the N atoms, can be understood if we assume that they are produced by dissociative recombination of N_2^+ ion and electron as follows:

$$N_2^+ + e \rightarrow N(\text{excited}) + N(\text{excited}).$$

Such dissociative recombination process has, according to Bates,[15] a very high probability. The dissociated N atoms may both be in the ^2D state or one in the ^2D and other in the ^2P state. The energy relations in the reaction are as follows: The energy released by recombination is the equivalent of 15.58 ev, the first ionization potential of N_2. The energy taken up on the right-hand side is the dissociation energy of N_2, 9.76 ev (Gaydon's value) plus the energies of excitation of the two atoms. The latter, if both the atoms are in ^2D state, is 4.74 ev, or if one of the atoms be in the ^2D and the other in the ^2P state, is 5.93 ev. In the first case there is an excess of 1.08 ev of energy, and in the latter there is a defect of 0.11 ev. The defect in the latter case can be made up if, as suggested by the author of this note,[16] the recombining N_2^+ ion be in a low vibrationality excited state or simply, as suggested by Bates,[17] if the colliding electron is sufficiently energetic. Of the two metastable states, ^2D has a very long life (about 8 hours), and hence it does not easily drop to the ground state. The ^2P state on the other hand has a life of about 2.1 seconds only and can drop to the ground state by radiation or by collision with the wall. It may be noted in this connection the line $\lambda 3466$ due to the transitions $^2P \rightarrow {}^4S$ has been observed by Kaplan[18] in the spectrum of the strong discharge which produces active nitrogen. (With the older value of the dissociation energy, both the dissociated N atoms may be in the ^2P state.)

It is to be mentioned, that Kaplan, in discussing the behavior of the spectrum of the special types of intense short-lived nitrogen afterglows (which may properly be called Kaplan afterglow) discovered by him, has suggested that excited N atoms, as may be produced by dissocivative recombination of N_2^+ ions, play a part not only in these special types of afterglow, but also probably in the Lewis-Rayleigh afterglow.[18]

In view of the above discussion we may state our metastable atom theory as follows.

The active substance in the glowing nitrogen gas (Lewis-Rayleigh afterglow) is a mixture of nitrogen atoms in the ground state ^4S and in the metastable states ^2D and ^2P (the last named in only small proportion) produced by dissociative recombination of N_2^+ ion and electron produced under strong electric discharge.

It is to be noted that this mode of production of N

[12] A. G. Gaydon, *Dissociation Energies* (Chapman and Hall, Ltd., London, 1947), p. 160.
[13] Lord Rayleigh (Strutt), Proc. Roy. Soc. (London), **A92**, 438 (1916).
[14] C. Kenty and L. A. Turner, Phys. Rev. **32**, 799 (1928).
[15] D. R. Bates, Phys. Rev. **78**, 492 (1950).
[16] S. K. Mitra, Nature **167**, 897 (1951).
[17] D. R. Bates (private communication).
[18] J. Kaplan, Phys. Rev. **73**, 484 (1948).

atoms provides a link between the metastable atom theory as now formulated and the ionic theory as had been previously suggested the author of this note. The N_2^+ ion and electron are, as it were, the parent bodies of the active substance though they are not themselves so directly.

Let us now discuss how far this metastable atom theory explains the various properties and phenomena of active nitrogen.

4. DISCUSSION[19]

Wall Effect and Long Life

The life of the afterglow is known to depend markedly on the condition of the wall surface of the containing vessel. All workers agree that the formation of a "layer" on the wall promotes the production and prevents the destruction of the active substance. In the proposed theory the parent bodies of the active substance being N_2^+ ions and electrons, their recombination on the wall may be prevented if on the wall surface there is an adsorbed layer of molecules with little electron affinity. Only a small fraction of the electrons striking the wall will then be able to attach themselves to the wall to form an electronic surface charge. An adsorbed layer of N_2 molecules may have such a property. Further, such a layer would also prevent the destruction of the active substance, that is, prevent the recombination of the N atoms on the surface. One may imagine that the production itself of the adsorbed layer of N_2 molecules is a result of wall recombination of the N atoms.

The inhibition of the recombination of the N atoms on the wall at once explains the long life of the glow because recombination by the preassociation process, $N(^4S)+N(^4S)\rightarrow N_2\ ^3\Pi_g$, cannot be a fast one.

Chemical Activity

The chemical activity of active nitrogen consists generally in the formation of nitrides of the substance introduced (in the form of vapor) into the glowing gas. Since nitrogen in the atomic state is highly active, the chemical activity is at once explained.

Spectroscopic Excitation

This consists of excitations of the spectra of the substances introduced and also of the compounds formed of the same. The latter is easily explained as the molecule of nitride may be formed in an optically excited state. For the former however one has to assume a three-body collision process as follows:

$$N+N+M\rightarrow N_2+M(\text{excited}),$$

where M is the atom of the substance introduced. The maximum energy imparted by the active substance in spectroscopic excitation is known to be 9.52 ev. With Gaydon's value of the dissociation energy, this amount will be available on the recombination of the two atoms in the ground state. With the older value, however, one of the atoms at least has to be in the metastable ^2D (or ^2P) state.

Ionization

Ionization is always associated with the glow: The decrease of the one is accompanied by the decrease of the other, though the rates are not the same. Further, the ionization persists—being diminished only by a few percent—even after the glowing gas from the discharge has been drawn through the space between a pair of electrodes ("ion trap") across which a saturation current is flowing. This observation shows that either the ion trap is ineffective in stopping the flow of ions from the discharge or that the ions are being generated in the glowing gas. The author of this note held the former view in connection with his ionic theory. One may however explain the production of ions and electrons according to the metastable atom theory as follows.

It has been postulated that the metastable atoms are produced by dissociative recombination of N_2^+ ions and electrons. Corresponding to this process we can also imagine the reverse one, namely ionizing recombination of two metastable atoms

$$N(^2D)+N(^2P)\rightarrow N_2^++e.$$

As already indicated, there is enough energy available for this reaction to occur with Gaydon's value of the dissociation energy. With the older values of the same, there is a deficit of 1.08 ev even if both the atoms are in the ^2P state. But this may be supplied by the relative kinetic energy of the colliding atoms.

Negative Temperature Coefficient

If the temperature of the glowing gas is lowered keeping the pressure constant, then making allowance for the increase in intensity due to increase in concentration of the active substance, the reaction rate is found to increase. Heating decreases the intensity of the glow.

These effects may be explained if it is recalled that the predissociation of the two nitrogen atoms occurs in the vibration levels between $v=13$ and 16 of the B state. At higher vibrational levels the predissociation disappears. This means that for the converse process of preassociation, the colliding atoms must not possess relative kinetic energy much larger than that with which they were separated at predissociation. It is possible that the lowering of the temperature brings the kinetic energy of more atoms within this limit and thus increases the chance of preassociation. This increased chance more than compensates for the decrease of the rate of preassociation through the decrease in

[19] Accounts of the various afterglow and active nitrogen phenomena, as discussed in this section, are to be found in reference 2.

the number of collisions caused by the lowering of the temperature. The opposite phenomenon occurs on heating and thus explains the decrease of the glow intensity with increase of temperature.

Dark Modification

It has been found that though heating destroys the glow it does not destroy the chemical activity of the glowless gas, or its ability to excite the spectrum of substances introduced in it. The considerations in the preceding sub-section regarding the effect of heating provide a simple explanation of this so-called dark modification of active nitrogen. The heating affects only the rate of preassociation of the atoms (which produces the afterglow); it cannot affect in any way their chemical activity or their ability to excite the spectra by three-body collision.

Besides the above, there are many other characteristic phenomena of active nitrogen, detailed explanations of which are not attempted here.

For example, in regard to the formation of the adsorbed layer on the surface, it is well established that contamination of the nitrogen used with some foreign gas in very small proportion, promotes the afterglow. It is possible that the contaminating gas acts as a catalytic agent to the formation of the layer. (The contamination which is most commonly used for promoting the afterglow in oxygen.)

Again according to Rayleigh's measurements, when the decay of the glow occurs mainly in the volume (the destruction of the active substance on the wall being kept at a minimum by special treatment of the wall and by use of large vessels), the law of decay is that for bimolecular reaction. This is as it should be according to the present theory. However, other experiments of Rayleigh show that, if the glowing gas is compressed or rarefied, the glow intensity varies as the cube of the concentration. This is a characteristic of termolecular reaction and cannot be reconciled with the theory. The same remark applies to the observation that increasing the concentration of the inert gas, keeping that of the active substance constant, increases considerably the intensity of the glow. Perhaps spectroscopic considerations of the preassociation process will provide explanations of these phenomena.

The question of the energy content of the active substance, in reference to Rayleigh's experiments of the heating of metal foils in the glowing gas, has also to be considered. According to Rayleigh, the energy imparted is at least 12.9 ev per act of destruction of the active substance on the metal foil. To explain this one has to assume that nearly all the molecules in the glowing gas have been dissociated and that metastable atoms are taking part in the surface recombination. (In later experiments Rayleigh obtained values even higher than 12.9 ev.) It is not possible to reconcile these observations with the metastable atom theory. Perhaps, as many of the investigators in this field maintain, the heating effect observed by Rayleigh was due to cathode rays in addition to the action of the active substance.

There is one point regarding the afterglow spectrum which appears to be puzzling. The spectrum does not show the Vegard-Kaplan bands, though the emission of the first positive bands leaves the molecules in the A state. It is of course agreed that since the $A \rightarrow X$ transition, yielding the Vegard-Kaplan bands, is a forbidden one, these bands will not ordinarily be observed. However, it is to be remembered that they have been identified by Kaplan in the special short-lived nitrogen afterglow studied by him. One would therefore have expected that the Vegard-Kaplan bands, though not ordinarily observable in the Lewis-Rayleigh type of afterglow, could be obtained by suitable adjustments of pressure and wall condition. However, though the Lewis-Rayleigh glow has been studied over wide ranges of pressures and wall condition, no trace of the Vegard-Kaplan bands has been found. (It may be argued that neither have emissions due to transitions of the N atoms from the metastable states been observed. But it is to be remembered that the ^2D state has the extraordinarily long life of 8 hours and that the ^2P atoms are present only in small number.) One explanation of the absence of the Vegard-Kaplan bands may be (as suggested by Cario and Kaplan[8]) that the N_2 molecules in the A state, before they have a chance of dropping to the X state by radiation, are raised to the B state by collision with the ^2D atoms,

$$N_2(A)+N(^2D)\rightarrow N_2(B)+N(^4S).$$

The energy relation shows that the $N_2(B)$ molecule will be formed in the high vibrational levels as required. The Cario-Kaplan process may therefore also contribute to the maintenance of the afterglow.

5. CONCLUDING REMARKS

The metastable atom theory of active nitrogen as developed in the preceding sections appears to give satisfactory explanations not only of the long life and the emission characteristic of the afterglow spectrum, but also of the other important associated properties, such as the invariable presence of ionization in the glow, the negative temperature coefficient, and the dark modification. The metastable atom theory may thus be an acceptable theory of active nitrogen. The author, however, feels diffident in making a more categorical statement regarding the merit of the theory, as his experience with the fate of the ionic theory (which he had developed in elaborate detail) warns him of the many pitfalls awaiting the unwary investigator of this elusive substance. What is now needed is a more thorough spectroscopic examination of the predissociation of $N_2(B)$ molecule, because there still appears to be some difference of opinion about its exact nature.

A straightforward proof of the theory would be to prove experimentally the presence of nitrogen atoms in the glowing gas (after the discharge has been cut off). Since the nitrogen atom possesses resonance lines near 1200A, absorption experiments in this region with a long column of the glowing gas would furnish this proof. Experiments to study this absorption are in progress under the direction of Professor G. Herzberg.[20] If the experiments prove the presence of nitrogen atoms in sufficient concentration in the glowing gas, the long series of speculations regarding the nature of active nitrogen will be ended.

[20] G. Herzberg (private communication).

PHYSICAL REVIEW VOLUME 90, NUMBER 4 MAY 15, 1953

The Solubility of Silicon and Germanium in Gallium and Indium*

PAUL H. KECK AND JACOB BRODER
Signal Corps Engineering Laboratories, Fort Monmouth, New Jersey
(Received January 8, 1953)

The solubilities of silicon and germanium in liquid gallium and in indium were determined over a wide temperature range. If the logarithms of the solubilities are plotted against the inversed absolute temperatures, straight lines are obtained the slopes of which yield the heats of solution. For the investigated systems it was found that the heats of solution are approximately proportional to the third power of the radii of the solvent atoms. Upon slow cooling of the saturated solutions silicon and germanium crystals of fair purity were obtained. The solubility data are of interest for the preparation of junction transistors.

KLEMM and co-workers[1] studied the phase diagrams of the systems Si-Ga and Si-In among others. The diagrams are of eutectic type and indicate for high temperatures an appreciable solubility of silicon in liquid gallium and indium which drops sharply with decreasing temperature. Apparently no published data are available in the temperature range where only small solubilities occur. Since we were interested in the crystallization of silicon from solutions in gallium and in indium, the solubility over a wide range of temperatures covering essentially the range of small solubilities was determined.

Gallium or indium was heated to a predetermined temperature in a quartz tube, using argon as an inert atmosphere. A piece of pure silicon was attached to a quartz hook and was kept immersed in the melt until saturation had been reached. The undissolved silicon was then pulled out of the melt and the apparatus cooled to room temperature. The amount of silicon which had dissolved at the test temperature was obtained from the difference in weight. Since the determination by weight was not accurate enough for values smaller than 0.1 atomic percent the lowest solubilities were measured spectrochemically.[2]

The solubilities of silicon in gallium and indium are plotted in Fig. 1 together with the data given in Klemm's paper. The logarithms of the solubilities in the concentration range below 10 atomic percent silicon when plotted against the inversed absolute temperature are fairly well represented by straight lines, the slopes of which yield the heats of solution at saturation, given in Table I.

For high concentration a marked deviation from a straight line takes place which is larger for silicon dissolved in indium than for silicon in gallium. Near 100 atomic percent silicon the slope of the solubility curve seems to approach the heat of fusion of silicon which is represented in Fig. 1 by the slope of line "Si."

Corresponding solubility measurements were made with the systems Ge-Ga and Ge-In. The experimental method used was the same as described above. However, a Pyrex tube was substituted for quartz glass since the temperature range under study was from 200 to 500°C only. Figure 2 is a plot of the results. It includes also the data of Klemm and co-workers.[1] As with silicon the solutions behave ideally in the range of low concentrations and the slopes of the straight lines yield the heats of solution at saturation. For high concentration

TABLE I. The heats of solution at saturation and the radii of the solvent atoms for the systems Si-Ga, Si-In, Ge-Ga, and Ge-In.

Heat of solution in kcal/mole	Atomic radii[a]	$\Delta H/r^3$
$\Delta H_{Si\ in\ Ga} = 16.2$	$r_{Ga} = 1.35$	6.6
$\Delta H_{Si\ in\ In} = 25.8$	$r_{In} = 1.57$	6.7
$\Delta H_{Si\ fusion} = 9.46^{a} - 11.1^{b}$	$r_{Si} = 1.17$	5.9–6.9
$\Delta H_{Ge\ in\ Ga} = 8.3$	$r_{Ga} = 1.35$	3.4
$\Delta H_{Ge\ in\ In} = 11.9$	$r_{In} = 1.57$	3.1
$\Delta H_{Ge\ fusion} = 8.3^{b}$	$r_{Ge} = 1.39$	3.1

[a] H. D. Hubbard and W. F. Meggers, *Periodic Chart of the Atoms* (W. W. Welch Scientific Company, Chicago, 1950).
[b] L. L. Quill, *The Chemistry and Metallurgy of Miscellaneous Materials* (McGraw-Hill Book Company, Inc., New York, 1950), Table 3.7, p. 28.

* Presented at the American Physical Society Meeting at Cambridge, Massachusetts, January 22, 1953.
[1] Klemm, Klemm, Hohmann, Volk, Orlamuender, and Klein, Z. anorg. Chem. **256**, 239 (1948).
[2] The authors are indebted to Mr. J. Mellichamp for carrying out the spectrochemical analysis.

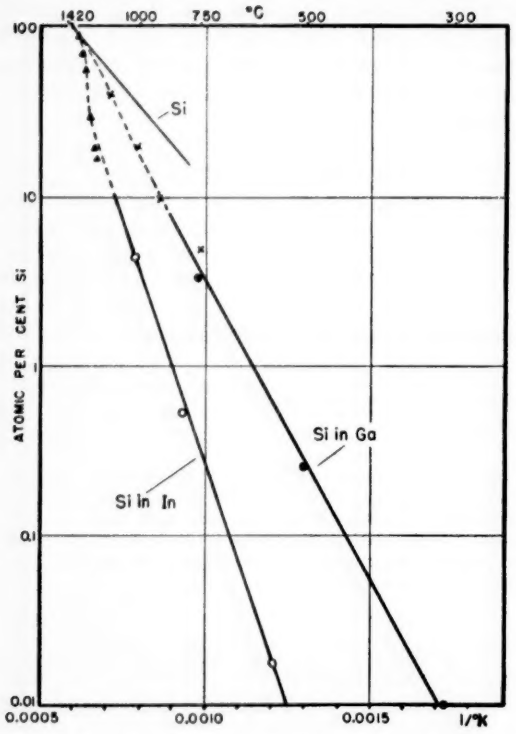

FIG. 1. Solubility of silicon in gallium and in indium *versus* inverse absolute temperature. × and ▲: values taken from Klemm and co-workers. (See reference 1.) ● and ○: authors' measurements.

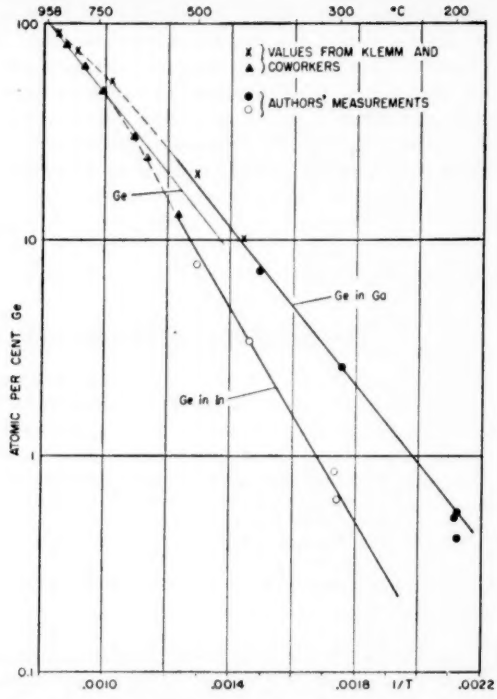

FIG. 2. Solubility of germanium in gallium and in indium *versus* inverse absolute temperature.

marked deviations take place and the curves approach the heat of fusion of germanium at 100 atomic percent.

In the systems discussed the partners do not form compounds with each other, and moreover, they have comparable electron configurations. It is obvious that here the heats of solution are closely related to the size of the atoms of the solute and the solvent. It was found that the heats of solution as derived from the slopes of the solubility curves are approximately proportional to the third power of the radii of the solvent atoms. This also holds with fair approximation for the heats of fusion of pure silicon and of pure germanium if the melting process is considered as a solution of the solid phase into the liquid phase at the melting point. The validity of this correlation is indicated in Table I since the values $\Delta H/r^3$ are approximately constant.

The solubility values are of practical interest for the preparation of junction transistors wherein gallium or indium is allowed to dissolve parts of a germanium or silicon wafer at an elevated temperature.

Another practical aspect of the solubility of silicon and germanium in gallium and in indium is the possibility of growing silicon or germanium crystals from solutions. Upon slow cooling of a saturated solution of silicon in gallium, silicon crystals up to a length of 15 mm were obtained. Measurements of the electrical conductivity indicated that these crystals contain approximately 10 gallium atoms per million silicon atoms.

It is a pleasure to thank Dr. G. Hass for stimulating discussions.

The Adiabatic Hall Effect in Semiconductors*

V. A. JOHNSON AND F. M. SHIPLEY†
Department of Physics, Purdue University, Lafayette, Indiana
(Received February 9, 1953)

Calculations are carried out to determine the relative difference between the isothermal and adiabatic Hall coefficients of typical semiconductors. The isothermal Hall effect requires a constant temperature in the plane of the electric current flow and Hall field, whereas the adiabatic Hall effect is defined by the alternative requirements that the temperature gradient be zero in the direction of the electric current flow and the heat current be zero in the direction of the Hall field. The relative difference $(R_a-R_i)/R_i$ is studied for the (1) classical impurity semiconductor, (2) degenerate semiconductor, and (3) classical semiconductor at high temperatures. For the thermal and electrical conductivities characteristic of silicon and germanium, the relative differences are found to be of the order one percent or less, thus indicating that it usually is not necessary to distinguish between the isothermal and adiabatic conditions in interpreting measured Hall values. Tabulated values are presented in such form that the relative difference may be readily calculated for any semiconducting sample of known electrical conductivity, thermal conductivity, and variation of carrier density with temperature.

I. INTRODUCTION

THE Hall effect[1] is the production of a transverse electric potential difference across a conducting sample as a result of the deflection of current carriers when a magnetic field is applied in a direction perpendicular to the current flow. At equilibrium the electrostatic force due to the Hall field balances the magnetic force on the moving charges composing the current. The Hall coefficient, R, is defined by the relation[2]

$$R=E_y/j_xH_z, \tag{1}$$

where j_x is the longitudinal electric current density, E_y the transverse electric field intensity, and H_z the magnetic field intensity. The transverse electric current density j_y is assumed to be zero. Kinetic theory of conduction indicates that, if the current carriers all have the same sign, R depends upon n, the number of carriers per unit volume, and e, the magnitude of charge on each carrier:

$$R=\pm r/ne, \tag{2}$$

where r is a numerical factor and the sign of R is the sign of the charge on the carriers.

Accurate determination of electron density from measured values of the Hall coefficient requires knowledge of the proportionality factor r, which depends upon (1) the statistical distribution of the electron velocities in the presence of electric and magnetic fields, (2) the dependence of the mean free path upon electron velocity, and (3) the temperature variation and heat flow in the sample.

The "isothermal" Hall effect[3] requires a constant temperature in the plane of the current and Hall field; i.e., the temperature gradients dT/dx and dT/dy must be zero. The absence of a temperature gradient does not insure the absence of the heat current resulting from the electrons if electric or magnetic fields are applied. Thus, the "adiabatic" Hall effect is defined by the alternative requirements that dT/dx and the heat current in the Y direction must be zero. In actual Hall effect measurements, it is usually impracticable to take the precautions necessary to eliminate the transverse temperature gradient; and so there is doubt as to whether the isothermal or the adiabatic conditions apply the more closely to an experimental situation. The object of this paper is to calculate the difference between the isothermal and adiabatic Hall coefficients under varying assumptions as to the nature of the sample; these assumptions correspond particularly to the observed characteristics of silicon, germanium, and tellurium samples.

II. GENERAL EXPRESSION FOR THE ADIABATIC HALL COEFFICIENT

The kinetic theory of conduction,[3-5] based upon the Lorentz solution of the Boltzmann equation, leads to the following set of equations for the electrical and thermal current densities:

$$\begin{aligned}
j_x&=L_{11}E_x+L_{12}H_zE_y+L_{13}dT/dx+L_{14}H_zdT/dy,\\
j_y&=-L_{12}H_zE_x+L_{11}E_y-L_{14}H_zdT/dx+L_{13}dT/dy,\\
w_x&=L_{31}E_x+L_{32}H_zE_y-(L_{33}+\kappa_L)dT/dx\\
&\qquad+L_{34}H_zdT/dy,\\
w_y&=-L_{32}H_zE_x+L_{31}E_y-L_{34}H_zdT/dx\\
&\qquad-(L_{33}+\kappa_L)dT/dy.
\end{aligned} \tag{3}$$

Here w_x and w_y represent thermal current per unit area in the X and Y directions, respectively, and κ_L is the

* Work assisted by contract between U. S. Signal Corps and Purdue Research Foundation.
† Now at Naval Ordnance Plant, Indianapolis, Indiana.
[1] E. H. Hall, Am. J. Math. **2**, 287 (1879); Phil. Mag. **10**, 301 (1880).
[2] Derivations in this paper are carried out in the electromagnetic system of units.
[3] The terms "isothermal Hall effect" and "adiabatic Hall effect" were introduced by R. Gans, Ann. Physik **20**, 293 (1906).
[4] H. A. Lorentz, *The Theory of Electrons* (G. E. Stechert and Company, New York, 1923), p. 63 and note 29.
[5] A. Sommerfeld and N. H. Frank, Revs. Modern Phys. **3**, 1 (1931).

TABLE I. Coefficients appearing in the electrical and thermal current density equations[a] (current carried by electrons only[b]).

$$L_{11}=-\frac{4\pi e^2}{3}\int_0^\infty v^2 l\frac{\partial f_0}{\partial\epsilon}vdv$$

$$L_{12}=\frac{4\pi e^2}{3m}\int_0^\infty vl^2\frac{\partial f_0}{\partial\epsilon}vdv$$

$$L_{13}=-\frac{4\pi e}{3}\int_0^\infty v^2 l\frac{\partial f_0}{\partial\epsilon}\left\{\frac{\epsilon}{T}+T\frac{d}{dT}\left(\frac{\zeta}{T}\right)\right\}vdv$$

$$L_{14}=\frac{4\pi e^2}{3m}\int_0^\infty vl^2\frac{\partial f_0}{\partial\epsilon}\left\{\frac{\epsilon}{T}+T\frac{d}{dT}\left(\frac{\zeta}{T}\right)\right\}vdv$$

$$L_{31}=\frac{4\pi me}{6}\int_0^\infty v^4 l\frac{\partial f_0}{\partial\epsilon}vdv$$

$$L_{32}=-\frac{4\pi e^2}{6}\int_0^\infty v^3 l^2\frac{\partial f_0}{\partial\epsilon}vdv$$

$$L_{33}=-\frac{4\pi m}{6}\int_0^\infty v^4 l\frac{\partial f_0}{\partial\epsilon}\left\{\frac{\epsilon}{T}+T\frac{d}{dT}\left(\frac{\zeta}{T}\right)\right\}vdv$$

$$L_{34}=-\frac{4\pi e}{6}\int_0^\infty v^3 l^2\frac{\partial f_0}{\partial\epsilon}\left\{\frac{\epsilon}{T}+T\frac{d}{dT}\left(\frac{\zeta}{T}\right)\right\}vdv$$

[a] The symbol f_0 represents the unperturbed electron distribution function, l the mean-free-path, and ϵ the kinetic energy $mv^2/2$, where m is the effective mass. The symbol ζ represents the chemical potential (or Fermi level).

[b] Those coefficients which include an odd power of the electron charge are reversed in sign, and those with an even power of ϵ retain the same sign if holes, rather than electrons, carry the current.

thermal conductivity associated with the lattice vibrations, as distinct from the thermal conductivity associated with kinetic energy transfer by conduction electrons. The coefficients L_{jk} are integrals dependent upon the mean free path, the distribution function, and the chemical potential (Fermi level); these coefficients are given explicitly in Table I.

The total thermal conductivity κ is defined as $-w_x/(dT/dx)$ under the conditions $j_x=dT/dy=H_z=0$. Equations (3) yield the expression

$$\kappa=(L_{13}L_{31}/L_{11})+L_{33}+\kappa_L\equiv\kappa_e+\kappa_L, \tag{4}$$

where κ_e represents the conduction electron contribution to the thermal conductivity.

The isothermal Hall coefficient R_i is found from Eqs. (3) by setting $j_y=dT/dx=dT/dy=0$ and solving for

$$R_i=E_y/j_xH_z=L_{12}(L_{11}^2+L_{12}^2H_z^2)^{-1}. \tag{5}$$

The weak field approximation that terms containing the second or higher power of the magnetic field strength are negligible is used in this paper; hence Eq. (5) reduces to

$$R_i=L_{12}/L_{11}^2. \tag{6}$$

The adiabatic Hall coefficient R_a is also obtained from Eqs. (3), but the auxiliary conditions are $j_y=dT/dx=w_y=0$. Thus one obtains

$$R_a=\frac{L_{12}\{L_{33}+\kappa_L+(L_{13}L_{32}/L_{12})\}}{L_{11}^2\{L_{33}+\kappa_L+(L_{13}L_{31}/L_{11})\}}. \tag{7}$$

Equations (4) and (6) are used to reduce the above to

$$R_a=R_i\left\{1+\frac{L_{13}}{\kappa}\left(\frac{L_{32}}{L_{12}}-\frac{L_{31}}{L_{11}}\right)\right\}. \tag{8}$$

This relation serves as the basis for comparing the adiabatic and isothermal Hall coefficients through evaluation of the ratio R_a/R_i or the relative difference $(R_a-R_i)/R_i$.

The following discussion explicitly applies to n-type or electron conductors, but an exactly parallel treatment applies to p-type or hole conductors; thus the results obtained in the following sections are equally valid for n- and p-type conductors.

III. THE ADIABATIC HALL COEFFICIENT FOR A CLASSICAL IMPURITY SEMICONDUCTOR

At low temperatures conduction in a semiconductor is due to electrons which have been excited from the impurity levels to the conduction band. At a temperature depending upon the sample, nearly all of the impurity atoms are ionized and "exhaustion" occurs. At higher temperatures electrons may be excited from the filled band to the conduction band (intrinsic conduction). The classical impurity region is defined as lying above the temperature at which it is necessary to use quantum statistics but below the temperature at which intrinsic conduction becomes significant. In this range one uses the distribution function

$$f_0=\frac{2m^3}{h^3}\exp\left(\frac{\zeta-\epsilon}{kT}\right), \tag{9}$$

where m denotes effective mass, ζ the chemical potential or Fermi level, and ϵ the electron kinetic energy; the zero of energy is taken as the bottom of the conduction band.

The coefficients L_{jk} of Eqs. (3) all involve integrals of the form

$$\int_0^\infty v^{2\alpha}l^\beta\partial f_0/\partial\epsilon v dv, \tag{10}$$

where 2α and β are integers. Define

$$u=\epsilon/kT; \tag{11}$$

then the integral (10) may be written as

$$-(2kT)^\alpha m^{-(\alpha+1)}\int_0^\infty u^\alpha l^\beta f_0 du\equiv(2kT)^\alpha m^{-(\alpha+1)}K_{\alpha,\beta}. \tag{12}$$

Equation (8) combined with Table I and Eq. (12), gives the result

$$R_a=R_i\left\{1+\frac{\sigma T}{\kappa}\frac{k^2}{e^2}F(l,\zeta,T)\right\}, \tag{13}$$

where σ is the electrical conductivity (L_{11}) and where

$$F(l,\zeta,T)=\left\{\frac{K_{2,1}}{K_{1,1}}-\frac{K_{\frac{1}{2},2}}{K_{\frac{1}{2},2}}\right\}\left\{\frac{K_{2,1}}{K_{1,1}}+\frac{T}{k}\frac{d}{dT}\left(\frac{\zeta}{T}\right)\right\}. \tag{14}$$

The Fermi level for a classical semiconductor is given by

$$\zeta = kT \ln\left\{\frac{nh^3}{2(2\pi mkT)^{\frac{3}{2}}}\right\}, \tag{15}$$

and thus

$$\frac{d}{dT}\left(\frac{\zeta}{T}\right) = \frac{k}{n}\frac{dn}{dT} - \frac{3}{2}\frac{k}{T}. \tag{16}$$

In the classical impurity region, scattering of the conduction electrons both by the lattice and by impurity ions may be important. Hence it is of interest to consider the mean free path as given by

$$l = \gamma \epsilon^p. \tag{17}$$

When $p=0$, the mean free path is constant with respect to energy, corresponding to the case when lattice scattering[6] alone is present; if $p=2$, the mean free path is approximately that associated with impurity scattering.[7] One can write

$$K_{\alpha,\beta} = -2m^3h^{-3}e^{\zeta/kT}\{\gamma(kT)^p\}^\beta \Gamma(\alpha+p\beta+1), \tag{18}$$

and thus Eq. (14) reduces to

$$F(l,\zeta,T) = (\tfrac{1}{2}-p)\left(p+\frac{1}{2}+\frac{T}{n}\frac{dn}{dT}\right). \tag{19}$$

For lattice scattering only ($p=0$), Eq. (13) becomes

$$R_a = R_i\left\{1+\frac{\sigma T}{k}\frac{k^2}{e^2}\left(\frac{1}{4}+\frac{1}{2}\frac{T}{n}\frac{dn}{dT}\right)\right\}, \tag{20}$$

and for impurity scattering only ($p=2$), it becomes

$$R_a = R_i\left\{1+\frac{\sigma T}{\kappa}\frac{k^2}{e^2}\left(-\frac{15}{4}-\frac{3}{2}\frac{T}{n}\frac{dn}{dT}\right)\right\}. \tag{21}$$

It is seldom that either of the two limiting cases, completely dominant lattice scattering or completely dominant impurity scattering, exists throughout the impurity temperature range. The effective mean free path l for combined scattering may be taken as

$$1/l = 1/l_L + 1/l_I, \tag{22}$$

where $l_I = \gamma\epsilon^2 = \gamma(kT)^2u^2$ and l_L is independent of ϵ. Then

$$K_{\alpha,\beta} = -\frac{2m^3}{h^3}e^{\zeta/kT}l_L{}^\beta \int_0^\infty \frac{e^{-u}u^{\alpha+2\beta}du}{(u^2+b^2)^\beta}, \tag{23}$$

where

$$b^2 \equiv l_L/\{\gamma(kT)^2\} = 6\rho_I/\rho_L, \tag{24}$$

in which ρ_I and ρ_L are the resistivities due to impurity and lattice scattering, respectively.[8] Define the functions

$$G_k(b) = \int_0^\infty e^{-u}u^k(u^2+b^2)^{-1}du \tag{25}$$

and

$$H_k(b) = \int_0^\infty e^{-u}u^k(u^2+b^2)^{-2}du; \tag{26}$$

then Eq. (14) becomes

$$R_a = R_i\left[1+\frac{\sigma T}{\kappa}\frac{k^2}{e^2}\left\{\frac{G_4(b)}{G_3(b)}-\frac{H_{11/2}(b)}{H_{9/2}(b)}\right\} \times\left\{\frac{G_4(b)}{G_3(b)}-\frac{3}{2}+\frac{T}{n}\frac{dn}{dT}\right\}\right]. \tag{27}$$

The required functions $G_k(b)$ and $H_k(b)$ have been evaluated by numerical methods.

Examination of Eqs. (20), (21), and (27) shows that the ratio R_a/R_i is dependent upon temperature, electrical conductivity, thermal conductivity, the temperature rate of change of carrier density, and the nature of the scattering encountered by the carriers. In the following paragraphs R_a/R_i is evaluated under several sets of conditions chosen to correspond to the observed characteristics of semiconducting samples.

A. The Gans Expression

Gans[3] considered only the electronic contribution to the thermal conductivity and took the mean free path as independent of energy. He used $\kappa/\sigma T = \kappa_e/\sigma T = 2k^2/e^2$ and hence found

$$\frac{R_a-R_i}{R_i} = \frac{1}{8}+\frac{1}{4}\frac{T}{n}\frac{dn}{dT}. \tag{28}$$

This indicates an appreciable difference between the isothermal and adiabatic Hall coefficients; the difference is even more pronounced for impurity scattering in which case one obtains

$$\frac{R_a-R_i}{R_i} = -\frac{3}{2}-\frac{3}{5}\frac{T}{n}\frac{dn}{dT}. \tag{29}$$

However, the measured heat conductivity of a semiconductor at ordinary temperature is far greater than that obtained by the assumption of electronic thermal current alone. This fact indicates a large contribution to heat conductivity from the lattice, so that Eqs. (28) and (29) are not valid.

B. Exhaustion Temperature Range: $dn/dT = 0$

In many samples the conduction electron density does not change measurably over a portion of the tem-

[6] A. Sommerfeld and H. Bethe, *Handbuch der Physik* (Julius Springer, Berlin, 1934), Vol. **24**, No. 2, p. 558.
[7] E. Conwell and V. F. Weisskopf, Phys. Rev. **77**, 388 (1950).
[8] V. A. Johnson and K. Lark-Horovitz, Phys. Rev. **82**, 977 (1951).

TABLE II. $F(l, \zeta, T)$ as a function of the ratio of impurity to lattice scattering in a classical impurity semiconductor.

$\rho_I/(\rho_I+\rho_L)$	$b^2=6\rho_I/\rho_L$	$F(l, \zeta, T)$
0.0	0	0.2500
0.1	2/3	0.0816
0.2	3/2	−0.0160
0.3	18/7	−0.113
0.4	4	−0.250
0.5	6	−0.375
0.6	9	−0.581
0.7	14	−0.816
0.8	24	−1.15
0.9	54	−1.72
1.0	∞	−3.75

perature range. In this "exhaustion" region the assumption $dn/dT=0$ may be made and the function F simplified accordingly. Equation (20) leads to

$$\frac{R_a-R_i}{R_i}=-\frac{1}{4}\frac{\sigma T}{\kappa}\frac{k^2}{e^2}, \tag{30}$$

which is applicable in the exhaustion range if only lattice scattering exists.

Measurements of the heat conductivity of germanium[9,10] give 0.59 watt/cm-°K at room temperature and little deviation from this value over a wide temperature range in the neighborhood of 300°K. Since the thermal conductivity of silicon[11] is about the same as for germanium, the $(R_a-R_i)/R_i$ values are also about the same for equivalent σT values; the thermal conductivity of tellurium[12] at 300°K is about one-tenth that of germanium and hence the fraction $(R_a-R_i)/R_i$ is ten times higher for tellurium than for germanium for a given σT value.

The relative difference between the adiabatic and isothermal Hall coefficients, as calculated from Eq. (30) with $\kappa=0.59$ watt/cm-°K, varies from 2×10^{-8} for $\sigma T=6$°K mho/cm to 3×10^{-3} for $\sigma T=9\times10^5$°K mho/cm. Hence one can conclude that the adiabatic and isothermal Hall coefficients are practically indistinguishable for the type of sample to which Eq. (30) applies.

If impurity scattering dominates, as may occur at the low temperature end of the exhaustion range for a low resistivity sample, Eq. (21) predicts that

$$\frac{R_a-R_i}{R_i}=-\frac{15}{4}\frac{\sigma T}{\kappa}\frac{k^2}{e^2}. \tag{31}$$

This relation is applicable under conditions such that σT is in the range 10^4-10^5 °K mho/cm, and thus Eq. (31) leads to $(R_a-R_i)/R_i$ values in the range -5×10^{-4} to -5×10^{-3}. Again the adiabatic and isothermal values are practically indistinguishable.

If both lattice and impurity scattering are considered, the function F is evaluated numerically in accordance with Eq. (27); the results are given in Table II. If one takes $\kappa=0.59$ watt/°K-cm and $\sigma T=3\times10^5$ °K-mho/cm, the fractional difference $(R_a-R_i)/R_i$ varies from +0.1 percent to −1.4 percent as the proportion of impurity scattering increases from zero to unity.

C. Low Temperature Range: $dn/dT\neq0$

The assumption $dn/dT=0$ is not a good approximation throughout the classical impurity region. An expression for dn/dT may be obtained from the classical equilibrium equation:[13]

$$\frac{n^2}{N-n}=\frac{2(2\pi mkT)^{\frac{3}{2}}}{h^3}\exp\left(-\frac{E_D}{kT}\right), \tag{32}$$

TABLE III. Relative difference between adiabatic and isothermal Hall coefficients at 100°K calculated with dn/dT found from dissociation equation.

N cm^{-3}	E_D ev	n cm^{-3}	$\rho_I/(\rho_I+\rho_L)$	$F(l, \zeta, T)$	σ mho/cm	$(R_a-R_i)/R_i$
10^{15}	0.07	6.784×10^{14}	0.1	0.299	1.3	0.49×10^{-6}
			0.2	−0.0514	1.1	-0.072×10^{-6}
			0.3	−0.334	0.93	-0.39×10^{-6}
			0.4	−0.697	0.79	-0.70×10^{-6}
10^{17}	0.03	6.846×10^{16}	0.5	−0.685	66	-57×10^{-6}
			0.6	−1.02	53	-69×10^{-6}
			0.7	−1.39	42	-74×10^{-6}
10^{18}	0.01	6.875×10^{18}	0.8	−1.54	285	-560×10^{-6}
			0.9	−2.23	163	-460×10^{-6}

where N is the number of ionizable impurities (donors) per unit volume and E_D the activation energy required to excite an electron from the donor level to the conduction band. From Eq. (32) one obtains

$$\frac{dn}{dT}=\frac{n}{T}\left(\frac{3}{2}+\frac{E_D}{kT}\right)\left(\frac{N-n}{2N-n}\right). \tag{33}$$

Table III gives values of $(R_a-R_i)/R_i$ calculated from Eq. (27) by using the dn/dT expression of Eq. (33). Numerical values of N, E_D, ρ_I/ρ_L, and σ have been chosen so as to be representative of germanium sample of varying degrees of purity; the value 0.59 watt/cm-°K has been used for the thermal conductivity. The largest difference, about 0.5 percent, is found in the impure material having $N=10^{18}$ per cm^3. Recent measurements[14,15] of the thermal conductivity of germanium at at low temperatures indicate that at 100°K the value

[9] K. Lark-Horovitz, National Defense Council Report 14-585, p. 61, Nov., 1945, unpublished.
[10] A. Grieco and H. C. Montgomery, Phys. Rev. **86**, 570 (1952).
[11] Given as 0.84 watt/cm-°K by J. W. Mellor, *Comprehensive Treatise of Inorganic Chemistry* (Longmans, Green and Company, New York, 1925), Vol. VI, p. 152.
[12] W. W. Scanlon, Purdue Progress Report on Semiconductor Research (January, 1948).
[13] R. H. Fowler, Proc. Roy. Soc. (London) **A140**, 505 (1933).
[14] I. Estermann and J. E. Zimmerman, U. S. Office of Naval Research report from Carnegie Institute of Technology, 1950, unpublished.
[15] J. F. Goff, Purdue University, private communication.

of κ may be as high as 3 watt/cm-°K, and thus the $(R_a-R_i)/R_i$ values of Table III may be too high by a factor as large as 5.

IV. THE ADIABATIC HALL COEFFICIENT OF A DEGENERATE SEMICONDUCTOR

Hall effect measurements of germanium and silicon samples show that samples with large impurity content become degenerate at low temperatures.[16–18] In this case the classical distribution function of Eq. (9) is replaced by the Fermi-Dirac distribution function

$$f_0=\frac{2m^3}{h^3}\left\{1+\exp\left(\frac{\epsilon-\zeta}{kT}\right)\right\}^{-1} =\frac{2m^3}{h^3}(1+e^{u-\zeta^*})^{-1}, \tag{34}$$

where $\zeta^*=\zeta/kT$. In a degenerate sample the impurity content is high and the temperature relatively low; thus impurity scattering dominates and one can take $l=l_I=\gamma\epsilon^2=\gamma(kT)^2u^2$. Equation (18) is replaced by

$$K_{\alpha,\beta}=-\frac{2m^3}{h^3}\gamma^\beta(kT)^{2\beta}\int_0^\infty\frac{u^{\alpha+2\beta}e^{u-\zeta^*}du}{(1+e^{u-\zeta^*})^2} =-\frac{2m^3}{h^3}\gamma^\beta(kT)^{2\beta}(\alpha+2\beta)\int_0^\infty\frac{u^{\alpha+2\beta-1}du}{1+e^{u-\zeta^*}} =-\frac{2m^3}{h^3}\gamma^\beta(kT)^{2\beta}(\alpha+2\beta)J_{\alpha+2\beta-1}(\zeta^*), \tag{35}$$

where $J_k(\zeta^*)$ is the Fermi-Dirac integral of kth order. With the change of statistics, $d/dT(\zeta/T)$ is no longer given by Eq. (16); instead

$$\frac{d}{dT}\left(\frac{\zeta}{T}\right)=\left(\frac{2k}{n}\frac{dn}{dT}-\frac{3k}{T}\right)\frac{J_{\frac{1}{2}}(\zeta^*)}{J_{-\frac{1}{2}}(\zeta^*)}. \tag{36}$$

Now the adiabatic Hall coefficient can be written in the form of Eq. (13) with

$$F(l,\zeta,T)=\left\{\frac{4}{3}\frac{J_3(\zeta^*)}{J_2(\zeta^*)}-\frac{11}{9}\frac{J_{9/2}(\zeta^*)}{J_{7/2}(\zeta^*)}\right\} \times\left\{\frac{4}{3}\frac{J_3(\zeta^*)}{J_2(\zeta^*)}-\left(3+\frac{2T}{n}\frac{dn}{dT}\right)\frac{J_{\frac{1}{2}}(\zeta^*)}{J_{-\frac{1}{2}}(\zeta^*)}\right\}. \tag{37}$$

The integral $J_k(\zeta^*)$ has been discussed by McDougall and Stoner,[19] who treat the evaluation of the integral in three different ways, depending upon the value of ζ^*:

(1) $\zeta^*\leq 0$:

$$J_k(\zeta^*)=\sum_{r=1}^{\infty}(-1)^{r-1}e^{r\zeta^*}r^{-(k+1)}\Gamma(k+1). \tag{38}$$

(2) $\zeta^*\gg 0$: An asymptotic expansion due to Sommerfeld[20] can be used:

$$J_k(\zeta^*)=(\zeta^*)^{k+1}\{1+\sum_{r=1}^{n}a_{2r}(\zeta^*)^{-2r}\}+\Re_{2n}, \tag{39}$$

where

$$a_{2r}=2C_{2r}(k+1)(k)\cdots(k-2r+2),$$

$$C_{2r}=(1-2^{1-2r})\sum_{m=1}^{\infty}m^{-2r},$$

and the remainder $\Re_{2n}$ is given an upper limit by the relation

$$\Re_{2n}<(2n+2)a_{2n}+2(\zeta^*)^{k-2n-1}.$$

(3) ζ^* a small positive quantity: For ζ^* between 0 and about 4, the error incurred by using the asymptotic expression (39) is prohibitive. In this range $J_k(\zeta^*)$ must be found by numerical methods. The integrals $J_{\frac{1}{2}}(\zeta^*)$, and $J_{-\frac{1}{2}}(\zeta^*)$ have been tabulated by McDougall and Stoner[11] at close intervals in the range $-4\leq\zeta^*\leq 20$. Table IV gives values of $J_k(\zeta^*)$, for $k=2$, 3, 7/2, and 9/2, evaluated by the authors for use in this paper.

Table IV also gives value of $F(l,\zeta,T)$ calculated from Eq. (37) for $-4\leq\zeta^*\leq 20$; dn/dT is taken as zero in this evaluation. As ζ^* assumes large positive values, F approaches zero; this is consistent with the conclusion of Sommerfeld that $R_a=R_i$ for a metal.

Estermann and Zimmerman[14] have measured the thermal conductivity, at low temperatures, of an

TABLE IV. Values of the Fermi-Dirac integral $J_k(\zeta^*)$ and $F(l,\zeta,T)$ for a degenerate semiconductor (impurity scattering only).

ζ^*	$J_2(\zeta^*)$	$J_3(\zeta^*)$	$J_{7/2}(\zeta^*)$	$J_{9/2}(\zeta^*)$	$-F(l,\zeta,T)$
−4.0	0.03656	0.10977	0.21287	0.95830	3.736
−3.5	0.06018	0.18084	0.35078	1.57956	3.729
−3.0	0.09896	0.29780	0.57782	2.60314	3.714
−2.5	0.16252	0.49002	0.95137	4.28883	3.691
−2.0	0.26626	0.80532	1.56496	7.06295	3.656
−1.5	0.43456	1.32088	2.57067	11.6329	3.612
−1.0	0.70510	2.15984	4.21327	19.105	3.560
−0.5	1.1343	3.51520	6.88232	31.347	3.396
0.0	1.803	5.68220	11.184	51.290	3.324
1.0	4.312	14.39	28.83	135.4	2.773
2.0	9.445	34.30	70.76	346.6	2.232
3.0	18.87	75.73	162.6	846.2	1.736
4.0	34.49	154.3	346.7	1947	1.34
5.0	58.12	291.0	687.3	4200	1.04
6.0	91.74	513.0	1273	8500	0.814
7.0	137.36	853.4	2223	16 206	0.647
8.0	196.99	1351	3687	29 279	0.522
9.0	272.61	2051	5847	50 430	0.429
10	366.23	3005	8926	83 281	0.357
11	479.86	4269	13 184	132 532	0.301
12	615.48	5806	18 920	204 150	0.257
13	775.10	7986	26 482	305 550	0.223
14	960.72	10 583	36 257	445 804	0.194
15	1174.3	13 778	48 684	635 840	0.170
16	1418.0	17 659	64 248	888 663	0.151
17	1693.6	22 318	83 488	1 219 590	0.134
18	2003.2	29 854	106 992	1 646 455	0.120
19	2348.8	34 373	135 402	2 189 874	0.108
20	2732.5	41 985	169 419	2 873 483	0.0981

[16] W. W. Scanlon, Ph.D. thesis, Purdue University, 1948, unpublished.
[17] G. L. Pearson and J. Bardeen, Phys. Rev. **75**, 865 (1949).
[18] C. S. Hung and J. R. Gliessman, Phys. Rev. **79**, 726 (1950).
[19] J. McDougall and E. C. Stoner, Trans. Roy. Soc. (London) **A237**, 67 (1936).
[20] A. Sommerfeld, Z. Physik **47**, 1 (1928).

impure germanium sample having a 25°C resistivity of 0.0021 ohm-cm. They found κ (in watt/cm-°K) equal to 1.9 at 65°K, 1.1 at 15°K, and 0.05 at 3.6°K. If these κ values are used, Eqs. (37) and (13) yield values of $(R_i-R_a)/(\sigma R_i)$, at 65°K, dropping from 9.3×10^{-6} to 0.89×10^{-6} ohm-cm as ζ^* increases from -4 to 10; the corresponding variation at 15°K is from 3.8×10^{-6} to 0.36×10^{-6}, and at 3.6°K the range is from 2.0×10^{-6} to 0.19×10^{-6}. Since σ for degenerate germanium samples is between 100 and 1000 mho/cm in this temperature range, one finds that $(R_i-R_a)/R_i$ is of the order 10^{-4} to 10^{-3} and thus that there is no appreciable difference between the adiabatic and isothermal Hall coefficients of a degenerate germanium sample.

V. THE ADIABATIC HALL COEFFICIENT OF A CLASSICAL SEMICONDUCTOR AT HIGH TEMPERATURES

The high temperature behavior of a semiconductor is characterized by thermal excitation of electrons from the full band to the conduction band. When both electrons and holes take part in conduction, the two currents are additive. It is convenient to retain the formal notation for the electrical and thermal current density equations (3) in applying them to semiconductors displaying both electron and hole conduction. This may be done by defining "total" coefficients $L_{jk}(t)$ which are appropriate algebraic sums of coefficients $L_{jk}(1)$, ascribed to electrons, and $L_{jk}(2)$, due to holes. The $L_{jk}(1)$ and $L_{jk}(2)$ coefficients are the expressions of Table I except that the mass, mean free path, and carrier density carry the subscript 1 (electrons) or 2 (holes). The difference in the sign of charge is correctly taken into account if those coefficients $L_{jk}(2)$, such as $L_{12}(2)$, which include e to an odd power are prefixed by a negative sign. By following this convention one obtains

$$\begin{aligned}
&L_{11}(t)=L_{11}(1)+L_{11}(2), \quad L_{12}(t)=L_{12}(1)-L_{12}(2),\\
&L_{13}(t)=L_{13}(1)-L_{13}(2), \quad L_{14}(t)=L_{14}(1)+L_{14}(2),\\
&L_{31}(t)=L_{31}(1)-L_{31}(2), \quad L_{32}(t)=L_{32}(1)+L_{32}(2),\\
&L_{33}(t)=L_{33}(1)+L_{33}(2), \quad L_{34}(t)=L_{34}(1)-L_{34}(2).
\end{aligned} \tag{40}$$

Since the sign of charge has now been provided for, e denotes only the magnitude of the electron charge, a positive quantity, in all of the $L_{jk}(1, 2)$ integrals.

Classical statistics and a mean free path independent of energy are used in evaluating $L_{jk}(t)$. Table V gives these coefficients in terms of the electron and hole mobilities, μ_1 and μ_2, respectively. Equation (8) is valid if each L_{jk} appearing therein is taken as a "total" $L_{jk}(t)$. Thus one gets

$$R_a=R_i\left(1+\frac{T}{\kappa}\frac{k^2}{e^2}AB\right), \tag{41}$$

where

$$A=\mu_2(n_1c-n_2)+2\mu_2T(cdn_1/dT-dn_2/dT),$$

$$B=\frac{n_1c-n_2}{n_1c+n_2}-\frac{3}{4}\frac{n_1c^2+n_2}{n_1c^2-n_2},$$

and $c=\mu_1/\mu_2$. The quantities dn_1/dT and dn_2/dT are estimated from the equilibrium condition:[21]

$$n_1n_2=32h^{-6}(m_1m_2)^{\frac{3}{2}}(\pi kT)^3\exp(-E_G/kT), \tag{42}$$

where E_G is the width of the forbidden energy gap. If $n_1=n_2+N$ and $dN/dT=0$, then

$$\frac{dn_1}{dT}=\frac{dn_2}{dT}=\frac{n_1n_2}{T}\left(3+\frac{E_G}{kT}\right)(N^2+4n_1n_2)^{-\frac{1}{2}}. \tag{43}$$

The relative difference between R_a and R_i is calculated for germanium samples from Eq. (41) and presented in Table VI. The following numerical values were used in these computations:

$$E_G=0.74 \text{ ev.},[22] \quad c=1.5,[23]$$
$$\mu_1=1.7\times10^7T^{-\frac{3}{2}} \text{ cm}^2/\text{volt-sec},[24]$$
$$\kappa=0.586 \text{ watt/cm-°K}.[9,10]$$

The values of Table VI show again that there is no appreciable difference between R_a and R_i since $(R_a-R_i)/R_i$ is of the order of one percent or less for temperatures as high as 900°K and conduction electron concentrations as low as 10^{15} cm^{-3}.

TABLE V. Coefficients $L_{jk}(t)$ for a high temperature semiconductor.

$$L_{11}(t)=n_1e\mu_1+n_2e\mu_2$$
$$L_{12}(t)=-\frac{3\pi e}{8}(n_1\mu_1^2-n_2\mu_2^2)$$
$$L_{13}(t)=\frac{k}{2}(n_1\mu_1-n_2\mu_2)+kT\left(\mu_1\frac{dn_1}{dT}-\mu_2\frac{dn_2}{dT}\right)$$
$$L_{14}(t)=\frac{3\pi}{8}kT\left(\mu_1^2\frac{dn_1}{dT}-\mu_2^2\frac{dn_2}{dT}\right)$$
$$L_{31}(t)=-2kT(n_1\mu_1-n_2\mu_2)$$
$$L_{32}(t)=\frac{9\pi}{16}kT(n_1\mu_1^2+n_2\mu_2^2)$$
$$L_{33}(t)=\frac{3k^2T}{e}(n_1\mu_1+n_2\mu_2)+2\frac{k^2T^2}{e}\left(\mu_1\frac{dn_1}{dT}+\mu_2\frac{dn_2}{dT}\right)$$
$$L_{34}(t)=\frac{9\pi}{16}\frac{k^2T}{e}\left(n_1\mu_1^2-n_2\mu_2^2+T\mu_1^2\frac{dn_1}{dT}-T\mu_2^2\frac{dn_2}{dT}\right)$$

$$\mu_{1,2}=\frac{2}{3}\frac{(2)^{\frac{1}{2}}}{\pi}el_{1,2}(m_{1,2}kT)^{-\frac{1}{2}}$$

[21] A. H. Wilson, *The Theory of Metals* (Cambridge University Press, Cambridge, 1936), p. 67.
[22] Lark-Horovitz, Middleton, Miller, and Walerstein, Phys. Rev. **69**, 258 (1946).
[23] G. L. Pearson, Phys. Rev. **76**, 179 (1949).
[24] Pearson, Haynes, and Shockley, Phys. Rev. **78**, 295 (1950).

VI. SUMMARY

The relative difference between the adiabatic and isothermal Hall coefficients has been calculated for various sets of assumptions chosen to correspond to the observed behavior of semiconducting samples in the different temperature ranges.

A. Classical Impurity Semiconductor in the Exhaustion Range

In this case classical statistics are employed, both impurity and lattice scattering are considered, and the carrier density is taken as independent of the temperature. The quantity F of Eq. (13) takes values between 0.25 and -3.75. When this is combined with a thermal conductivity of 0.6 watt/°K-cm and an electrical conductivity of 1000 mho/cm, $(R_a-R_i)/R_i$ varies between 10^{-3} and 10^{-2} at 300°K.

B. Classical Impurity Semiconductor at Temperatures below the Exhaustion Range

The variation of the carrier density with temperature is calculated from the dissociation equation, and the conductivities used are varied to correspond to different impurity contents in germanium. The resulting $(R_a-R_i)/R_i$ values at 100°K range between 10^{-6} and 10^{-3}, depending upon impurity content and impurity activation energy.

C. Degenerate Impurity Semiconductor

This treatment applies at low temperatures to samples having high impurity content. Fermi-Dirac statistics are employed, impurity scattering is assumed to be dominant, and the carrier density is approximately temperature independent. As ζ^* goes from negative values, through zero, to increasing positive values, F values go from -3.75 toward 0, and hence $(R_a-R_i)/R_i$ approaches zero under these conditions.

TABLE VI. $(R_a-R_i)/R_i$ for a semiconductor at high temperatures.

T(°K)	N(cm^{-3})	n_1(cm^{-3})	n_2(cm^{-3})	$(R_a-R_i)/R_i$
300	1.0×10^{18}	1.0×10^{18}		50×10^{-6}
300	0.1×10^{18}	0.1×10^{18}		5×10^{-6}
300	0.001×10^{18}	0.001×10^{18}		0.05×10^{-6}
600	1.0×10^{18}	1.01×10^{18}	0.014×10^{18}	-4×10^{-6}
600	0.1×10^{18}	0.18×10^{18}	0.077×10^{18}	-60×10^{-6}
600	0.001×10^{18}	0.12×10^{18}	0.12×10^{18}	-180×10^{-6}
900	1.0×10^{18}	3.0×10^{18}	3.0×10^{18}	-5.5×10^{-3}
900	0.1×10^{18}	1.6×10^{18}	1.6×10^{18}	-12×10^{-3}
900	0.001×10^{18}	1.4×10^{18}	1.4×10^{18}	-13×10^{-3}

D. Classical Semiconductor at High Temperatures

The expression for $(R_a-R_i)/R_i$ reflects the fact that both electrons and holes take part in conduction. The magnitude of the relative difference increases strongly with temperature, especially for relatively pure material. However, even at 900°K, $(R_a-R_i)/R_i$ is not over about 10^{-2} for germanium and silicon samples.

Thus one can conclude that the adiabatic and isothermal Hall coefficients are practically indistinguishable as long as the ratio of electrical conductivity to thermal conductivity, σ/κ, does not appreciably differ from the values, characteristic of germanium and silicon, used in the foregoing calculations. For a material such that σ/κ is appreciably larger, the relative difference between R_a and R_i may be readily estimated from the tabulated values of the $F(l, \zeta, T)$ function.

The authors wish to thank Dr. K. Lark-Horovitz for his valuable suggestions during the course of this work.

Magnetic Susceptibility of Colored Potassium Chloride from 1°K to 300°K*

C. V. Heer and C. Rauch
Department of Physics and Astronomy, Ohio State University, Columbus, Ohio
(Received February 2, 1953)

The magnetic susceptibility of potassium chloride crystals additively colored with an excess of potassium was measured from 1°K to 300°K. The excess magnetic susceptibility or the susceptibility of the color centers can be described by a temperature independent term which is predominant at room temperatures plus a temperature dependent term which obeys Curie's law and predominates in the liquid helium temperature range. It is suggested that the portion of the susceptibility following Curie's law is due to F-centers, and the temperature-independent contribution is due to color center complexes.

THE magnetic susceptibility of colored alkali-halides at room temperatures has been measured by Jensen[1] and more recently by Scott, Hrostowski, and Bupp.[2] The work of Jensen indicated a paramagnetic susceptibility which increased linearly with the concentration of the F-centers; the work of Scott and coworkers indicated that the susceptibility at room temperature depended both on the concentration of F-centers and R-centers.

In order to investigate the nature of F-centers and other color-centers formed in KCl additively colored with an excess of potassium, the temperature-dependent magnetic susceptibility of an additively colored crystal was measured between 1°K and 300°K. If an F-center is regarded as an electron trapped in a chloride ion vacancy as suggested by de Boer,[3] the magnetic properties of the center should be similar to those of an atomic S-state. Since by Kramers' theorem[4] the twofold degeneracy of the trapped electron cannot be lifted by the surrounding crystalline field alone, the susceptibility due to an F-center should follow Curie's law until either an exchange or magnetic interaction between spins becomes sufficiently large to remove the degeneracy. The paramagnetic resonance absorption[5] of F-centers suggests that the spin system is essentially free down to liquid air temperatures, since a g-value of approximately 2 and a line width of less than 100 gauss are observed.

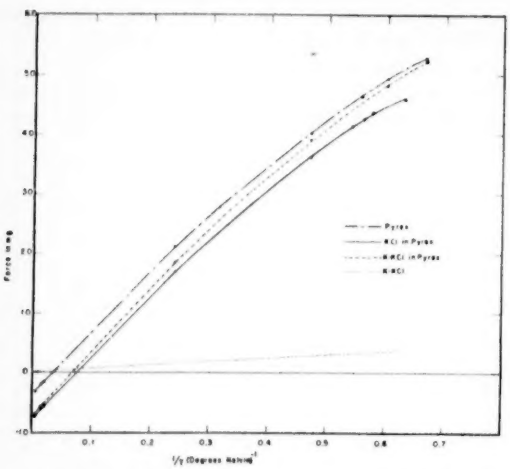

FIG. 1. Change in weight upon application of a field of 5120 gauss for the empty Pyrex container, the container plus pure KCl, the container plus colored KCl, and the excess weight due to the color centers.

The Gouy method for measuring magnetic susceptibility was selected since it allows a direct measurement of the susceptibility and is easily adapted to experiments in the temperature range from 1°K to 300°K. A cryostat operating in this temperature range was combined with an Ainsworth type BB analytical balance. The balance was mounted inside a vacuum case, and controls operating the chainweight were brought out of the vacuum case through Teflon seals. This arrangement allows changes in weight from 0.1 to 100 milligrams to be observed for samples weighing as much as 200 grams with a sensitivity of 0.05 milligram. Two permanent magnets with fields of 5120 and 2220 gauss were used to supply the magnet fields.

Potassium chloride crystals of the optical type which were obtained from the Harshaw Chemical Company were prepared by sealing the crystals in a copper cylinder with a small piece of potassium; the unit was baked at a temperature of 750°C for a period of two hours and then rapidly quenched. Using the work of Rögener,[6] a concentration of the order of 1×10^{19} F-centers per cm^3 is predicted. A subsequent chemical determination of the excess potassium in the colored crystal by measurement of the change in pH yielded a value of $1.0\pm0.2\times10^{19}$ excess potassium atoms per cm^3. The colored KCl crystals were finely ground and placed in a Pyrex glass container with a sample cross-sectional area of 0.50 cm^2 and with a powder density of 1.28 grams/cm^3 as compared with 1.98 grams/cm^3 for the bulk crystals.

In Fig. 1 the change in weight upon application of a magnetic field of 5120 gauss as a function of the re-

* Assisted by a contract between the U. S. Atomic Energy Commission and the Ohio State University Research Foundation.
[1] P. Jensen, Ann. Physik **34**, 161 (1939).
[2] Scott, Hrostowski, and Bupp, Phys. Rev. **79**, 346 (1950).
[3] J. H. de Boer, Rec. trav. chim. **56**, 301 (1937).
[4] H. A. Kramers, Proc. Amsterdam Acad. Sci. **33**, 962 (1930).
[5] C. A. Hutchison and G. A. Noble, Phys. Rev. **87**, 1125 (1952).
[6] H. Rögener, Ann. Physik **29**, 386 (1937).

ciprocal temperature is shown for the empty Pyrex container, the container plus pure KCl, the container plus colored KCl, and the excess weight due to the color centers. The excess susceptibility per gram of the colored crystal as a function of the reciprocal temperature is shown in Fig. 2.

The magnetic susceptibility of the pure KCl between 1.5°K and 300°K is temperature independent within the experimental accuracy and yielded a value of $\chi=-0.49\pm0.01\times10^{-6}$ emu/gram, as compared with previously quoted values[7] of -0.516×10^{-6} emu/gram.

The sample of Pyrex glass selected for this experiment was a particularly poor choice of container because of its large susceptibility, but it yields the rather interesting result that in a magnetic field of 2220 gauss, Pyrex glass follows Curie's law down to 1.4°K with a volume susceptibility given by $\kappa=49/T\times10^{-6}$ emu/cm³. The curvature of the susceptibility curve for Pyrex at low temperatures (see Fig. 1) and in a field of 5120 gauss is the result of saturation effects.

The excess magnetic susceptibility of the colored KCl varies linearly with the reciprocal temperature (see Fig. 2) at the lower temperatures, and the curve can be fitted by the equation,

$$\kappa=3\times10^{-8}+1.36\times10^{-6}/T \text{ emu/cm}^3. \quad (1)$$

For a system composed of n magnetic spins per cm³ with spin magnetic quantum number $\frac{1}{2}$, $g=2$, and obeying Boltzmann statistics, the paramagnetic susceptibility is given by

$$\kappa=n\mu_B^2/kT=6.18\times10^{-25}n/T \text{ emu/cm}^3. \quad (2)$$

A comparison of the slopes of Eqs. (1) and (2) suggests that there are 2.3×10^{18} spins/cm³ contributing to the temperature-dependent paramagnetic susceptibility, a factor of 4 smaller than the number of excess potassium atoms. Although the measurements at room and liquid nitrogen temperatures are subject to large errors, the error being of the order of 1.2×10^{-8} emu/cm³ over the entire temperature range, the susceptibility at room temperature is much larger than expected from an extrapolation of Curie's law to the higher temperature range. A direct application of Eq. (2) to the room temperature value would suggest 1.4×10^{19} centers/cm³,

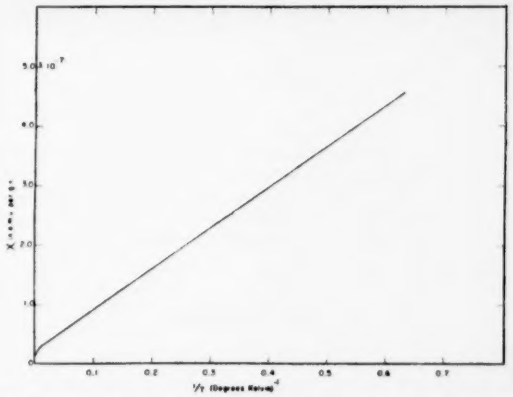

FIG. 2. Excess magnetic susceptibility of the colored KCl crystals.

a result which is in much better agreement with the vapor pressure and chemical determinations. A similar result was observed by Hutchinson and Noble[5] in the measurement of the paramagnetic resonance absorption of colored KCl, their measurement indicating that the number of active spins causing the absorption was considerably smaller than the number of excess potassium ions.

If we use a model for the F-center as suggested by de Boer, it seems reasonable to interpret the temperature-dependent magnetic susceptibility resulting from the F-centers, and the temperature-independent susceptibility as resulting from the interacting spin systems, i.e., F-centers in close proximity or other color-center complexes.[8] In order to determine the complete relationship between the magnetic susceptibility and the number and type of these other centers present in colored crystals, experiments are being planned to correlate optical absorption data with the magnetic susceptibility.

We wish to thank Dr. J. G. Daunt for his aid and discussions, particularly with regard to the possible future use of colored alkali halides for magnetic cooling processes. We thank also the Research Corporation and the Ohio State University Research Foundation for their valued grants-in-aid, which have materially assisted the work.

[7] *International Critical Tables* (McGraw-Hill Book Company, Inc., New York, 1926).

[8] F. Seitz, Revs. Modern Phys. **18**, 384 (1946).

The Energy Loss of Low Energy Protons in Some Gases*

JAMES A. PHILLIPS
University of California, Los Alamos Scientific Laboratory, Los Alamos, New Mexico
(Received January 29, 1953)

Experimental values for the energy loss of protons in H_2, He, N_2, O_2, A, Kr, H_2O, CO_2, and CCl_4 have been obtained in the region from 10 to 80 kev. The energy loss ($\Delta E/\Delta x$) can be expressed for the elementary gases measured in terms of a single curve, with two constants $\Delta E/\Delta x = Lf(ME)$. The energy loss per atom is independent of the target density over the range 0 to 1.5-mm Hg, and the energy loss for compound gases is equal to the sum of their components.

I. INTRODUCTION

IN traversing a target, a charged particle has a maximum rate of energy loss in the region where the velocity is comparable with the orbital electron velocities in the target atoms. Although abundant measurements of the energy loss have been made on the high energy side of the maximum, the data are scanty on the low side, and the present work was undertaken to provide data in this region.

In 1942, Crenshaw[1] measured the energy lost by protons and deuterons in some gases above an energy of about 100 kev. More recently, Wilcox[2] and Warshaw[3] have reported measurements on the stopping power for protons in several metals in the energy range from 50 to 400 kev. Also Wenzel and Whaling[4] have measured the energy loss of protons in heavy ice in the energy interval from 18 to 540 kev.

The present experiment was designed to measure the energy loss due to ionization, excitation, and charge exchange but not that due to nuclear scattering. Thus only those particles which entered and left the apparatus in a narrow pencil of angle 2.5° were measured. The apparatus and techniques used for the reaction cross-section experiments completed previously lent themselves rather readily for use in making the energy loss measurements in the same energy range. Since these techniques have been reported elsewhere[5] in detail they will not be fully described here. Measurements were made on H_2, He, N_2, O_2, A, Kr, H_2O, CO_2, and CCl_4.

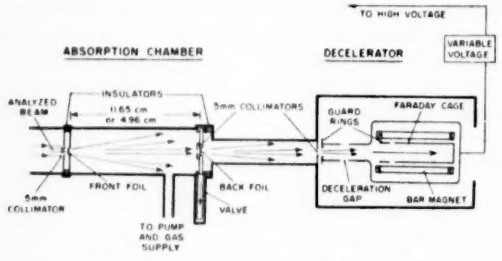

FIG. 1. A schematic diagram of the absorption chamber and decelerator.

II. APPARATUS AND PROCEDURE

Analyzed protons of energy 10 to 80 kev from a Cockcroft-Walton accelerator passed through a gas absorption chamber via thin (5 to 10 kev) windows into a decelerator. The decelerator measured the current received, as a function of retarding voltage, and hence the energy and energy distribution in the beam. Changing the gas density in the absorption chamber then gave the energy loss in the gas by difference.

The absorption chamber is shown in Fig. 1. The beam was collimated by an aperture 5 mm in diameter. The front foil was mounted on foil holders of different length so that the path length of the beam in the gas could readily be changed. The back foil was mounted on the sliding vane of a valve.[6] When the valve was opened, the back foil was removed from the beam and the energy loss of the front foil could be measured. The valve then could be closed and a gas-tight chamber obtained. A 5-mm diameter collimator was located immediately in front of the back foil. The absorption chamber was insulated from ground so that the beam current to the chamber could be monitored.

Two lengths of the absorption chamber were used, 11.65 and 4.96 cm. The longer chamber was used at high proton energies and with gases having small stopping powers. At lower energies the scattering of the beam by the foils became serious, and in order to have sufficient intensities at the decelerator, the shorter chamber was used.

The preparation and properties of the SiO foils used as windows have been described elsewhere.[7] In these experiments, the foils were 8 mm in diameter and the beam had a diameter of 5 mm. The foils were strong enough to hold a pressure of 2- to 3-mm Hg and the gas leakage was usually negligible. Because these foils are insulators, it was necessary to expose them to an excess of electrons when a beam passed through them in a vacuum. Thus, the foils were prevented from charging up and destroying themselves.

Each of the two foils of the absorption chamber scat-

* Work performed under the auspices of the U. S. Atomic Energy Commission.
[1] C. M. Crenshaw, Phys. Rev. **62**, 54 (1942).
[2] H. Wilcox, Phys. Rev. **74**, 1747 (1948).
[3] S. D. Warshaw, Phys. Rev. **76**, 1759 (1949).
[4] W. Wenzel and W. Whaling, Phys. Rev. **87**, 499 (1952).
[5] Los Alamos Report, La-1479 (unpublished).
[6] Wahl, Forbes, Nyer, and Little, Rev. Sci. Instr. **23**, 379 (1952).
[7] G. A. Sawyer, Rev. Sci. Instr. **23**, 604 (1952).

tered the beam, and only a small part of the beam incident on the front foil passed through to the decelerator. Since the scattering becomes greater, the lower the energy of the beam, it became a serious problem to obtain sufficient beam current at the decelerator without destroying the foils. This set the lower limit of energy in this experiment at which effective measurements could be made. Replacing protons in the beam by deuterons and tritons allowed the lower limit of the energy to be extended downward in the following way: it has been shown by Crenshaw and Warshaw (and this experiment) that isotopes having the same velocity have the same energy loss. Thus, a hydrogen isotope of mass M and energy E will have the same energy loss as a proton of energy $(M_p/M)E$, where M_p is the mass of the proton. The scattering in a foil of the different isotopes at the same energy, however, is the same. Thus, at an incident energy E, the scattering, and consequently, the attenuation, of protons, deuterons, and tritons will be the same, but the differential energy losses observed correspond to protons of energy E, $E/2$, and $E/3$.

The energy of the beam was measured by a decelerator which had been previously developed and is shown in Fig. 1. This device measured the deceleration voltage which was required just to bring the charged ions of the beam to rest. The beam from the absorption chamber was collimated by an aperture 5 mm in diameter before entering the deceleration gap. A guard ring, which was at -300 volts with respect to ground, prevented secondary electrons from entering the deceleration gap (acceleration for electrons). A Faraday cage inside the high voltage terminal collected the beam current. A guard ring and a crossed magnetic field supplied by bar magnets controlled the motion of secondary electrons. The guard ring was -300 volts and the outer shell -2000 volts with respect to the Faraday cage. The current to the Faraday cage was as small as 10^{-10} amp and was measured by an electrometer circuit. A power supply was used to vary the potential of the Faraday cage with respect to the high voltage of the accelerator.

Typical results are shown in Fig. 2. When the beam unobstructed by a foil was passed into the decelerator, it was stopped by a potential about 100 volts lower than the potential on the anode of the ion source. This showed that the plasma in the ion source from which the ions originate was below the ion source anode potential by this amount. It was found that the gas pressure of the ion source was the most important factor in changing the energy of the ions with respect to the anode. However, if the pressure of the ion source was kept relatively constant during an experiment, no appreciable error was introduced. Figure 2 shows that the energy spread of the unobstructed beam was about 150 volts.

When a SiO foil was placed in the beam a deceleration curve was obtained as shown in Fig. 2. For this foil the

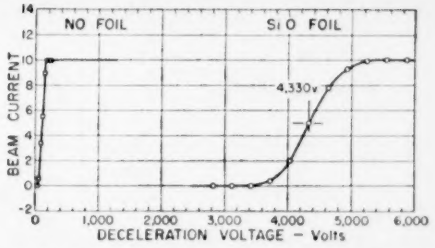

FIG. 2. Deceleration curves showing the energy distribution of the analyzed beam from the accelerator and the energy distribution of the beam after it had passed through a SiO foil.

average energy loss was 4.330 kev. The large straggling was surprising at first. However, since the foils were only about 100 atoms thick and the number of collisions in the foil was only about 50 (there being about 100 ev lost per collision), the statistics of the number of collisions explain the straggling.

Figure 2 shows that the straggle is approximately symmetrical about a mean energy. More sensitively, it was tested to be Gaussian in nature by plotting on probability paper. In such a plot a Gaussian distribution appears as a straight line. This method has the advantage of using the data in an optimum way, and the data gave good straight lines.

By changing the energy of the incident beam, the energy loss of a foil as a function of proton energy was obtained.[5] The relative $\Delta E/\Delta x$ curve for the window material proved to be quite reproducible so that it could be used to predict the energy loss in foils at other energies from a measured loss at one energy. (No very satisfactory method of measuring the mass density of the films is known to us, so that absolute $\Delta E/\Delta x$ values for the foil material remains unknown.)

The gas pressure in the absorption chamber was measured by a Consolidated Engineering Company micromanometer pressure gauge. This all-metal instrument contains a diaphragm which is bowed (to a greater or lesser amount) by pressure. The capacity between the diaphragm and a fixed plate has a value which is a reproducible function of the pressure. The gauge was calibrated by an oil manometer and was found to be stable to within 1 percent during the experiment.

The temperature of the gas was assumed to be the same as the room temperature as measured close to the absorption chamber. With the beam currents used in these experiments a thermocouple placed in the gas of the target chamber showed that the gas temperature was the same as the target chamber walls temperature to within $\pm 0.5°C$.

The gases were handled in the following ways:

1. Hydrogen. Uranium metal absorbers were used to store the hydrogen. A mass spectrographic analysis was made and the gas found to be 99.8 percent hydrogen.

2. Water vapor and CCl_4. Distilled water and chemically pure CCl_4 were frozen to dry ice tem-

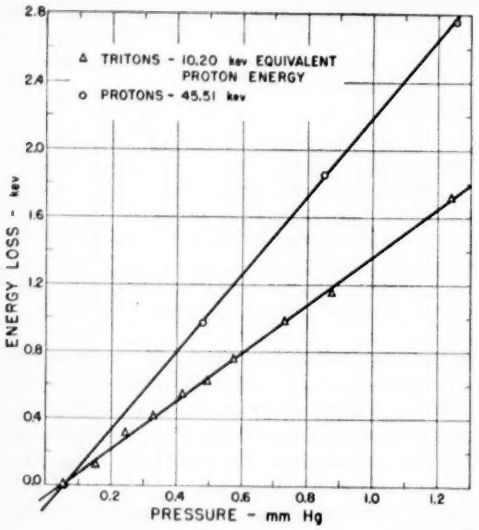

FIG. 3. The energy lost by a proton and a triton beam in passing through hydrogen gas in the absorption chamber as a function of the pressure.

perature and pumped to remove the air originally absorbed in the samples. This was repeated several times. For the last few times liquid air was used to freeze the liquid to reduce the vapor pressure of the sample to a minimum.

3. Samples of the other gases were as pure as could be obtained, being spectroscopically pure in most instances. A mass spectrographic analysis was performed when there was question of a sample's purity.

III. PROCEDURE

The experiment consisted essentially of measuring the increased energy lost by the beam passing through the absorption chamber as gas was admitted to the chamber. In order to obtain the average energy of the beam at the center of the absorption chamber and to calculate changes in the energy lost in the back foil because of the addition of the gas, the following procedure was adopted:

1. At some incident beam energy E, the energy loss in the front foil was measured. The back foil could be drawn out of the way during this measurement by opening the valve on which it was mounted. Subtracting the energy lost in the front foil from the incident energy of the beam gave the average energy of the beam as it entered the gas.

2. The second foil was placed in position and the energy lost by both foils was measured. The difference between the two measurements gave the energy loss in the back foil. The average energy of the beam passing through the back foil was equal to the energy of the beam after it left the first foil minus one-half the energy loss in the second foil. With a knowledge of the relative energy lost by a proton beam in the foils as a function of energy, it was possible to calculate the energy lost in the back foil at any energy of the beam emergent from the second foil.

3. Measurements of the foil stopping power were unreliable in a high vacuum, because the window was then cooled by radiation only and became hot enough to change in stopping power by as much as 100 ev. Gas was thus added to the absorption chamber to a pressure of 0.050-mm Hg and used as the reference pressure. Any change in the energy loss of the two foils, when measured in a vacuum and at the reference pressure, was assumed to be the same in both foils.

4. Gas was added to the desired pressures, and at each pressure the energy lost by the beam in passing through the absorption chamber was measured.

5. Finally, the energy lost by the beam at the reference pressure of 0.050-mm Hg was again measured to determine whether the foils had changed during the run. It was usually found that the energy loss of the two foils had increased by as much as 400 ev. It was thought that the loss was due to condensation of oil vapors on the foils. Examination of the data showed that the rate of foil growth was to a good approximation constant, while the beam was passing through the foil.

Since the energy of the emergent beam was known at each pressure, the energy loss in the back foil was calculable from the known stopping power energy curve of SiO. As the pressure of the gas was increased, the average energy of the beam passing through the second foil was decreased, and thus the energy lost by the beam in the back foil was decreased.

The energy lost by the gas at each pressure was then calculated by subtracting the energy lost in the two

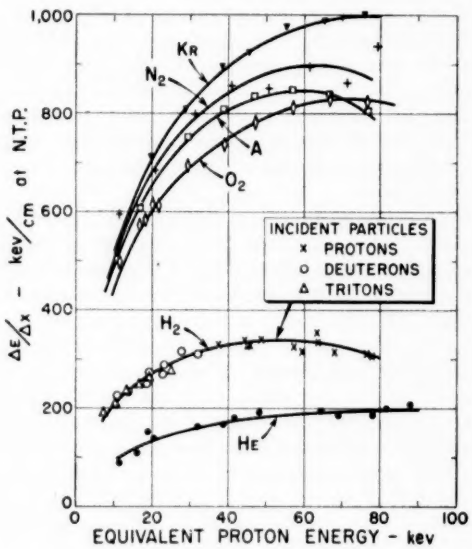

FIG. 4. The experimental values of the energy loss for protons in passing through the gases examined. The smooth curves are calculated from the equation $\Delta E/\Delta x = Lf(ME)$.

foils from the total energy lost by the beam in passing through the absorption chamber.

IV. RESULTS

A. Pressure Dependence

At each energy at least three different pressures were used in the measurement of the energy lost by the beam in the gas. In all cases when the energy loss was plotted as a function of pressure, a straight line was obtained within the experimental error. Typical results are shown in Fig. 3. The straight line passes through zero energy loss at a pressure of 0.050-mm Hg, the reference pressure. These results lead to the conclusion that, in the pressure range 0.050- to 1.50-mm Hg and the energy range examined, the energy loss by a hydrogen beam is proportional to the target density.

B. Effect of Gas on Foil Energy Loss

So far, it has been assumed that a foil stopping power measured in vacuum would continue to apply when gas was present. There is considerable difference in the physical state of the foil in these two cases: in vacuum, the foil is slack and hot enough to radiate the energy lost in it by the beam, but when gas is present, the foil is stretched and cool.

To test this assumption, an experiment was made in which two foils were mounted with a spacing of only 0.3 mm, and the stopping power of the combination was measured with several gases as described above. Within experimental error an energy loss *versus* pressure curve gave a straight line for each gas. Given an approximate value of the energy loss for each gas, calculation showed that as a gas was added to the absorption chamber the foils behaved as if there was a constant separation between the two foils of 2.9 ± 0.3 mm. Since the foil holders were 0.3 mm apart, the bowing of the foils and any diffusion of the gas through them added up to an effective gas length of 2.6 ± 0.3 mm. This correction was added to the measured length of the absorption chamber and the final $\Delta E/\Delta x$ values calculated.

C. Effect of Scattering

In the present experiment, the energy loss of the beam caused by scattering was not to be included. That scattering did occur in the gas was readily apparent, since as the gas pressure in the absorption chamber was increased, the fraction of the incident beam detected by the decelerator was decreased by as much as 50 percent with some gases. The part of the beam which was scattered by the gas did not pass through the collimator in front of the back foil and into the decelerator and was not included in the measurement.

However, the possibility of inscattering by the gas of the beam scattered by the front foil had to be considered. A calculation of this correction, using the simplifying but comparable assumption that all the gas is condensed on a plane midway between the two foils, gave a value of 0.2 percent, and it was therefore neglected.

TABLE I. Probable errors in determination of $\Delta E/\Delta x$.

1. Energy determination	
The probable error in a deceleration	±25 ev
The probable error of the energy loss in the gas, the result of three decelerations, assuming $\Delta E=1.5$ kev	±3 percent
2. Gas pressure	±3 percent
3. Gas purity	±1 percent
4. Length of the absorption chamber	±1 percent
5. Temperature	±0.3 percent
Total probable error in $\Delta E/\Delta x$ (rms)	±5 percent

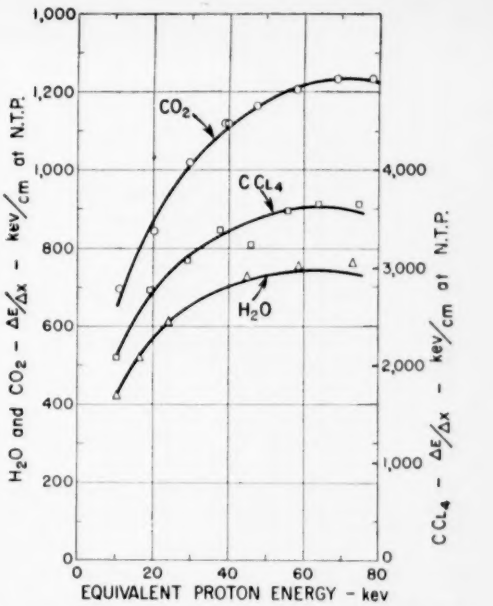

FIG. 5. The experimental values of the energy loss for three compounds. The smooth curves are the sums of the energy loss of the constituents of the compounds calculated from the equation $\Delta E/\Delta x = Lf(ME)$.

D. $\Delta E/\Delta x$ Results

In Figs. 4 and 5 the experimental values of $\Delta E/\Delta x$ are shown for the different gases. The energy loss $\Delta E/\Delta x$ is in units of kev per cm at 0°C and 76-cm Hg. Each of the experimental points is the result of the calculation of the slope of an energy loss *versus* pressure curve as in Fig. 3.

V. ERRORS

The probable errors assigned to the factors which enter into the determination of $\Delta E/\Delta x$ are given in Table I. The total probable error in $\Delta E/\Delta x$ is ±5 percent.

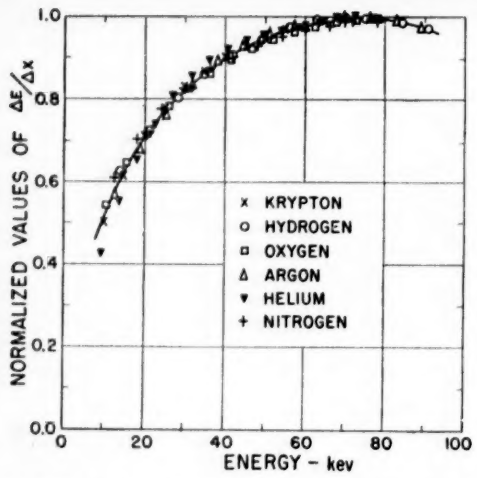

FIG. 6. The energy loss curves of the elementary gases examined normalized to that of krypton. The smooth curve is the average which determines the function f.

With water vapor, it was found difficult to control the pressure in the absorption chamber. When water vapor was added, much of the gas was absorbed in the walls of the chamber requiring a rather long time for the pressure to become stable. When the pressure was then reduced, the water vapor would come out of the walls making it difficult to arrive at a lower pressure. Over the relatively long periods of time which elapsed between decelerations at different pressures there was the possibility that the energy loss of the foils did change. It is expected that the data with water vapor should show a greater scatter than with other gases.

VI. DISCUSSION OF THE RESULTS

1. An examination of the curves of energy loss *versus* energy for the elementary gases reveals a certain similarity in shape. The simplest method of checking this was to match the curves to a standard curve, by linear transformations of the coordinates, i.e.,

$$\left(\frac{1}{L_i}\frac{\Delta E}{\Delta x}\right)=f(M_iE), \tag{1}$$

where L_i and M_i are constants for gas i.

The function f was determined empirically by drawing smooth curves through the experimental points for each gas and normalizing to that for krypton. Plotting the results for the gases on the same graph gave the result shown in Fig. 6. An average was then drawn through these points to obtain f. The function f and the normalizing constants L_i and M_i are shown in Tables II and III. In Figs. 4 and 5, the experimental points may be compared with the smooth curves for the calculated values. The two agree within the experimental error. The same standard f curve fits equally well with Warshaw's[3] data for the energy loss in solid targets 50 to 100 kev.

An analytical expression has not been found for the function f which will connect the $E^{\frac{1}{2}}$ dependence[8] at very low energies with the $E^{-1}\log E$ dependence[9] at high energies. Assuming, however, an expression of the form $f(E)=A(E)E^{n(E)}$, $n(E)$ approaches the value 0.5 as E decreases.

No significant regularity in L and M has been found in terms of the atomic constants among the limited number of elementary gases measured. There is, of course, a common reason for a rising $\Delta E/\Delta x$ at low energies, and a falling one at high, but the constants L and M doubtless depend on the properties of the outer electrons of these target gases and on the nuclear charge.

2. The results reported here for H_2 and air are in good agreement ($\sim$3 percent) with those reported by Crenshaw.[1] With He and H_2O there is some disagreement with the present values being $\sim$18 percent higher. Crenshaw's data have been corrected for a temperature of the target gas in his experiment of 30°C.[10]

TABLE II. Values of the function f in the equation $\Delta E/\Delta x=L_if(M_iE)$.

E	f	E	f
0.133	0.515	0.600	0.926
0.200	0.627	0.700	0.958
0.300	0.743	0.800	0.980
0.400	0.822	0.900	0.993
0.500	0.881	1.000	1.000

TABLE III. The normalizing constants L and M for the gases measured.

Element	L	M
Hydrogen, $\frac{1}{2}H_2$	169	53.2 kev
Helium	196	82.5
Carbon	404	70.5
Nitrogen, $\frac{1}{2}N_2$	449	62.2
Oxygen, $\frac{1}{2}O_2$	416	72.0
Chlorine, $\frac{1}{2}Cl_2$	807	61.5
Argon	848	59.2
Krypton	999	75.0

3. For water vapor, the vapor has the same stopping power as that calculated from hydrogen and oxygen, indicating that the sum of $\Delta E/\Delta x$ of the constituents equals that of the compound. The results are shown in Fig. 5. Comparison with the results for D_2O ice obtained by Wenzel and Whaling[4] shows that the vapor gives a value for the stopping power 17 percent higher than that for the solid. A density effect in this energy range might thus be indicated.

4. The $\Delta E/\Delta x$ of carbon was obtained from CO_2

[8] E. Fermi and E. Teller, Phys. Rev. **72**, 399 (1947).
[9] M. S. Livingston and H. A. Bethe, Revs. Modern Phys. **9**, 245 (1937).
[10] C. M. Crenshaw (private communication).

and O_2, assuming the sum of the energy losses of the constituents equals that of the compound. Using this value for carbon one may then obtain chlorine from CCl_4. Calculating the L and M values for carbon and chlorine, it is then possible to calculate, using Eq. (1), the energy loss for the compounds. The calculated results are drawn as the smooth curves in Fig. 5.

5. From data taken with hydrogen for equal velocities, the energy loss of protons, deuterons, and tritons is the same within the experimental error.

The collaboration of my colleagues in the group, W. R. Arnold, G. A. Sawyer, and E. J. Stovall, Jr., is gratefully acknowledged. Further, it is a pleasure to record the guidance and support of J. L. Tuck.

PHYSICAL REVIEW VOLUME 90, NUMBER 4 MAY 15, 1953

The Microwave Absorption Spectum of $(O^{16})_2$ and $O^{16}O^{17}$*

S. L. MILLER† AND C. H. TOWNES
Radiation Laboratory, Columbia University, New York, New York

(Received January 12, 1953)

The theory of the fine structure of O_2 is made somewhat more complete and fitted to the observed microwave spectrum. This gives $B_0=43\,102\pm5$ Mc/sec for $O^{16}O^{16}$. In addition there is evidence for the effect of higher order terms such as centrifugal distortion on the magnetic interaction constants. Magnetic hyperfine structure has been observed in the spectrum of $O^{16}O^{17}$. The spectrum agrees with that predicted on the basis of a perturbation Hamiltonian $b\mathbf{I}\cdot\mathbf{S}+cI_zS_z$, where $b=-102$ Mc/sec and $c=140$ Mc/sec. The value of 5/2 for the spin of O^{17} is confirmed.

INTRODUCTION

THE oxygen molecule is unusual in having a $^3\Sigma$ ground state; that is, it has an electron spin momentum of unity rather than the value zero which occurs in the ground state of most molecules. This spin angular momentum adds vectorially to the angular momentum K of the "end-over-end" rotational motion of the molecule to give a total angular momentum J which may have the values $K-1$, K, or $K+1$. Transitions between these three different fine structure or ρ-type triplet levels are allowed, because of the magnetic dipole moment associated with the electron spins, with the selection rule $\Delta J=0,\pm1$. The transitions with $\Delta J=\pm1$ give a microwave absorption spectrum in the region of 60 000 Mc/sec.

Since the total orbital angular momentum of the electrons has zero component along the internuclear axis, there should be no multiplet structure of the ordinary type arising from the interaction of the electronic spin with the orbital motion of the electrons. Kramers[1] has shown that the interaction of the two unpaired electron spins, when averaged over the rotation of the molecule, is equivalent to a coupling between the total spin and the figure axis proportional to $3\cos^2\theta-1$, where θ is the angle between the two. Using this interaction and the $\mathbf{S}\cdot\mathbf{K}$ interaction between the total spin and the magnetic moment caused by the end-over-end rotation of the molecule, Kramers derived an expression for the three energy levels corresponding to $J=K+1$, K, and $K-1$.

Although the Σ-state has a zero average electronic orbital angular momentum, there is an angular momentum component perpendicular to the axis of the molecule and precessing about it. Hebb[2] considered only the interaction between this component and the total spin $S=1$ and arrived at a formula of exactly the same form as Kramers.[1] This interaction is equivalent to a perturbation of the ground state by neighboring Π-states.

In order to get satisfactory agreement between the fine structure theory and optically obtained data, Schlapp[3] recalculated the energy levels allowing for the fact that the coupling between the electron spin and the molecular rotation is appreciable compared with the rotational energy of the molecule. Schlapp's expressions for the energy differences between the members of a ρ-type triplet are:

$$\nu_+(K)=(W_{J=K}-W_{J=K+1})/h=\lambda-\mu(K+1)-(2K+3)B+[\lambda^2-2\lambda B+(2K+3)^2B^2]^{\frac{1}{2}},$$
$$\nu_-(K)=(W_{J=K}-W_{J=K-1})/h=\lambda+\mu K+(2K-1)B-[\lambda^2-2\lambda B+(2K-1)^2B^2]^{\frac{1}{2}}, \quad (1)$$

where λ is a parameter which gives the magnitude of the interaction proportional to $\cos^2\theta$, and μ is a parameter giving the magnitude of the interaction proportional to $\cos\theta$. From this it is readily seen that

$$\nu_+(K-2)+\nu_-(K)=2\lambda+\mu,$$

where $2\lambda+\mu$ is presumably a constant.

* Research supported jointly by the Signal Corps and the U. S. Office of Naval Research.

† U. S. Atomic Energy Commission Predoctoral Fellow. Present address: Bell Telephone Laboratories, Murray Hill, New Jersey.

[1] H. A. Kramers, Z. Physik **53**, 422 (1929).

[2] M. H. Hebb, Phys. Rev. **49**, 610 (1936).

[3] R. Schlapp, Phys. Rev. **51**, 342 (1937).

TABLE I. Tabulation of experimental and calculated frequencies, in Mc/sec, for $O^{16}O^{16}$ fine structure lines. The calculated frequencies were obtained with values $\lambda_K = 59\,501.6 + 0.0575K(K+1)$ Mc/sec, $B_K = 43\,101.6 - 0.14K(K+1)$ Mc/sec, and $\mu = -252.72$ Mc/sec for all values of K.

		Experimental $\nu_+(K)$			Experimental $\nu_-(K)$	
K	Calc. $\nu_+(K)$	Burkhalter	Gokhale	Calc. $\nu_-(K)$	Burkhalter	Gokhale
1	56 264.5	56 265.1	56 265.2±0.5	118 750.7	118 745.5	
3	58 446.7	58 446.2	58 446.3±0.4	62 486.4	62 486.1	62 486.2±0.4
5	59 591.2	59 610[a]		60 307.0	60 306.4	
7	60 435.1	60 436[a]		59 163.9	59 163.4	59 164.2±0.2
9	61 150.9	61 120[a]		58 323.5	58 324.0	58 324.9±0.3
11	61 800.4	61 890.2		57 612.2	57 612.0	57 612.3±0.4
13	62 411.7	62 411.7	62 412.9±0.8	56 968.3	56 968.7	
15	62 997.9	62 970[a]		56 363.0	56 362.8	56 364.2±0.5
17	63 568.1	63 568.3		55 783.7	55 784.1	
19	64 126.8	64 127.6		55 221.5	55 220.8	
21	64 677.5	64 678.9		54 671.8	54 672.5	
23	65 221.7	65 220[a]		54 131.2	54 130.0	
25	65 761.6	65 770[a]		53 597.5	53 592.2	

[a] Wave meter reading.

These transitions were observed by Beringer[4] and by Strandberg, Meng, and Ingersoll[5] at pressures near one atmosphere and therefore in an unresolved form. Burkhalter *et al.*[6] resolved the $O^{16}O^{16}$ spectrum at low pressure. They found experimentally that $\nu_+(K-2) + \nu_-(K)$ is not a constant, but varies by about one part in two thousand over twenty rotational states ($K=3$ to $K=23$). Thus no constant values of λ and μ can be found which will fit the experimental data to Schlapp's formula as it stands. Burkhalter[6] empirically fitted the data by adding $\delta K + \alpha/[K(K+1)]^{\frac{1}{2}}$ to the expression for $\nu_-(K)$, where α and δ are suitable constants. Gokhale and Strandberg[7] have remeasured some of the $O^{16}O^{16}$ fine structure lines, and recently the $\nu_-(1)$ line, theoretically given by $2\lambda+\mu$ has been reported at 118 745.5 Mc/sec.[8] All measured frequencies for these lines are given in Table I. It may be noted that only odd K values are listed, because the zero spin of O^{16} and the fact that it obeys Bose-Einstein statistics forbid the existence of even K values.

RE-EXAMINATION OF THE FINE-STRUCTURE THEORY

It seems obvious that great care must be exercised in neglecting "small" terms in the derivation of the formula for the ρ-type triplet intervals when that formula is to be used to predict microwave absorption lines to an accuracy better than 1 Mc/sec. Inspection of Schlapp's expressions (1) indicates that second powers of μ have been omitted. Hence, as a first step in an attempt to obtain better agreement between theory and experiment, the Schlapp (Kramers) and Hebb formulas were rederived without discarding any terms.

Hill and Van Vleck[9] give the matrix elements for the $\cos^2\theta$ interaction between the spin and the figure axis. The matrix elements of the $\mathbf{S}\cdot\mathbf{K}$ interaction are easily obtained from the vector model. Therefore the energy levels arising from Kramers' interaction are the solutions of the secular determinant:

$$\begin{vmatrix} & K=J+1 & K=J & K=J-1 \\ K=J+1 & 2\lambda[J/(2J+1)]+B(J+1)(J+2) & 0 & 2\lambda[J(J+1)/(2J+1)^2]^{\frac{1}{2}} \\ & -(J+2)\mu-W & & \\ K=J & 0 & 2\lambda-\mu+BJ(J+1)-W & 0 \\ K=J-1 & 2\lambda[J(J+1)/(2J+1)^2]^{\frac{1}{2}} & 0 & 2\lambda[(J+1)/(2J+1)]+BJ(J-1) \\ & & & +(J-1)\mu-W \end{vmatrix} = 0.$$

This gives for the fine structure separations:

$$\begin{aligned}\nu_+(K) &= (W_{J=K} - W_{J=K+1})/h \\ &= \lambda - \mu(K+1) - (2K+3)(B-\tfrac{1}{2}\mu) \\ &\quad + [\lambda^2 - 2\lambda(B-\tfrac{1}{2}\mu) + (2K+3)^2(B-\tfrac{1}{2}\mu)^2]^{\frac{1}{2}},\end{aligned}$$

$$\begin{aligned}\nu_-(K) &= (W_{J=K} - W_{J=K-1})/h \\ &= \lambda + \mu K + (2K-1)(B-\tfrac{1}{2}\mu) \\ &\quad - [\lambda^2 - 2\lambda(B-\tfrac{1}{2}\mu) + (2K-1)^2(B-\tfrac{1}{2}\mu)^2]^{\frac{1}{2}}. \quad (2)\end{aligned}$$

These expressions are the same as Schlapp's formulas except for the fact that B has been replaced throughout by $B-\frac{1}{2}\mu$.

Hebb[2] gives the matrix elements connecting $^3\Pi$ and $^3\Sigma$ states in Hund's case (a). The Hebb matrix may be transformed so that the "Σ" portion is in Hund's case

[4] R. Beringer, Phys. Rev. **70**, 53 (1946).
[5] Strandberg, Meng, and Ingersoll, Phys. Rev. **75**, 1524 (1949).
[6] Burkhalter, Anderson, Smith, and Gordy, Phys. Rev. **79**, 651 (1950).
[7] B. V. Gokhale and M. W. P. Strandberg, Phys. Rev. **84**, 844 (1951).
[8] Anderson, Johnson, and Gordy (to be published).
[9] E. L. Hill and J. H. Van Vleck, Phys. Rev. **32**, 269 (1928).

(b) representation. If the Van Vleck transformation[10] is then applied, the order of magnitude of the matrix elements connecting the Π and Σ states can be reduced. This leaves a "Σ" matrix of precisely the same form as that arising from the Kramers' interactions but with an additive constant in the diagonal terms. The small terms still connecting the "Π" and "Σ" matrices give contributions to the energy of higher order than λ^2. If these are neglected, the expressions for the fine structure separations derived from Hebb's interactions are thus of exactly the same form as Eq. (2), since the matrix to be solved has the same form as that for the Kramers' interaction. However, the constant λ has quite a different meaning than it does in the Kramers' expression, and the dependence of μ on other molecular parameters is evident from Hebb's treatment. If both Hebb's and Kramers' types of interaction are present, Eqs. (2) still hold, with the new constants λ and μ dependent on the sum of the two individual interactions.

COMPARISON WITH MEASURED FINE STRUCTURE

An examination of these fine structure expressions shows that $\nu_+(K-2)+\nu_-(K)$ still equals $2\lambda+\mu$. Therefore, if the theory is correct and complete, the experimental results show that $2\lambda+\mu$ must vary with K by about one part in two thousand. A small variation is not surprising, since some of the molecular parameters should change by about this amount as the molecule undergoes centrifugal distortion with increasing K. In addition, small higher order terms which have been neglected in the theory can be large enough to produce the apparent variation in $2\lambda+\mu$. These include the neglected terms in Hebb's interaction, and terms involving mixtures of singlet states resulting from the molecular rotation.

The theoretical expression for the variation in B with rotational quantum number is given by:

$$B_K = B_{K=0} - (4B^2/\omega^3)K(K+1) = B_{K=0} - 0.14K(K+1) \text{ Mc/sec},$$

where ω is the vibrational frequency. A careful study of the experimental data for $O^{16}O^{16}$ with allowance for the change in B shows that the most reasonable fit is obtained by allowing λ to vary while μ remains constant. Excellent agreement between theory and experiment for all K values up to 25 may be obtained by assuming λ to be given by $\lambda = 59\,501.6 + 0.0575K \times (K+1)$ Mc/sec. The variation in λ is thus of the form to be expected from centrifugal distortion, or possibly from some higher order terms. Some deviations remain for the lines corresponding to $K=1$ and 25. There is a 5 Mc/sec discrepancy in the frequency of the $\nu_-(1)$ and $\nu_-(25)$ line which is surprising, and which may warrant their remeasurement.

Comparisons between experimental and theoretical frequencies are given in Table I. The theoretical frequencies are calculated with $B_K = 43\,101.6 - 0.14K \times (K+1)$ Mc/sec, $\mu = -252.72$ Mc/sec, and with λ as given above. Certain lines which are marked by an asterisk in Table I were measured experimentally only with a wavemeter and not with a frequency standard as were the other lines. Hence the errors in their measured values are as large as about 30 Mc/sec, and the theoretical values are undoubtedly considerably more accurate than the experimental ones.

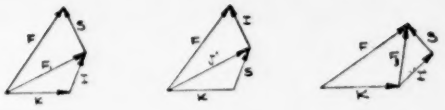

FIG. 1.

ISOTOPIC SPECIES OF O_2

Formula (2) was found equally applicable to the spectrum of $O^{16}O^{18}$ and $O^{18}O^{18}$ when B and μ were varied inversely with the reduced mass of the isotopic combination as would be expected from theory. Although a number of lines of these isotopic species were observed[11] they were not measured with accuracies better than about two megacycles. Their frequencies are not given, since theoretical values are probably more accurate than these experimental measurements.

In the case of $O^{16}O^{17}$ a more complex spectrum has been observed due to a hyperfine splitting of the $O^{16}O^{17}$ fine structure lines. The hyperfine structure results from the interaction of the magnetic moment of the O^{17} nucleus with the unpaired electrons in the molecule.

MAGNETIC HYPERFINE STRUCTURE THEORY

Frosch and Foley[12] have developed a theory for magnetic hyperfine structure in diatomic molecules which is applicable to the case of $O^{16}O^{17}$. From a treatment of the problem using the two-component Pauli equation as an approximation to the Dirac equation, they have derived a perturbation Hamiltonian,

$$H = aI_zL_z + b\mathbf{I}\cdot\mathbf{S} + cI_zS_z, \tag{3}$$

where

$$a = 2g_I\mu_0\mu_N(1/r^3)_{Av},$$

$$b = g_I\mu_0\mu_N\left[\frac{16\pi}{3}|\psi(0)|^2 - \left(\frac{3\cos^2\chi - 1}{r^3}\right)_{Av}\right],$$

$$c = 3g_I\mu_0\mu_N\left(\frac{3\cos^2\chi - 1}{r^3}\right)_{Av}$$

g_I = the gyromagnetic ratio for the nucleus, μ_0 and μ_N are the Bohr and nuclear magnetons, respectively, r is the distance between nucleus and electron, and χ is

[10] S. Golden and E. B. Wilson, J. Chem. Phys. **16**, 669 (1948); E. C. Kemble, *Fundamental Principles of Quantum Mechanics* (McGraw-Hill Book Company New York, 1937).

[11] Miller, Javan, and Townes, Phys. Rev. **82**, 454 (1951).

[12] R. A. Frosch and H. M. Foley, Phys. Rev. **88**, 1337 (1952).

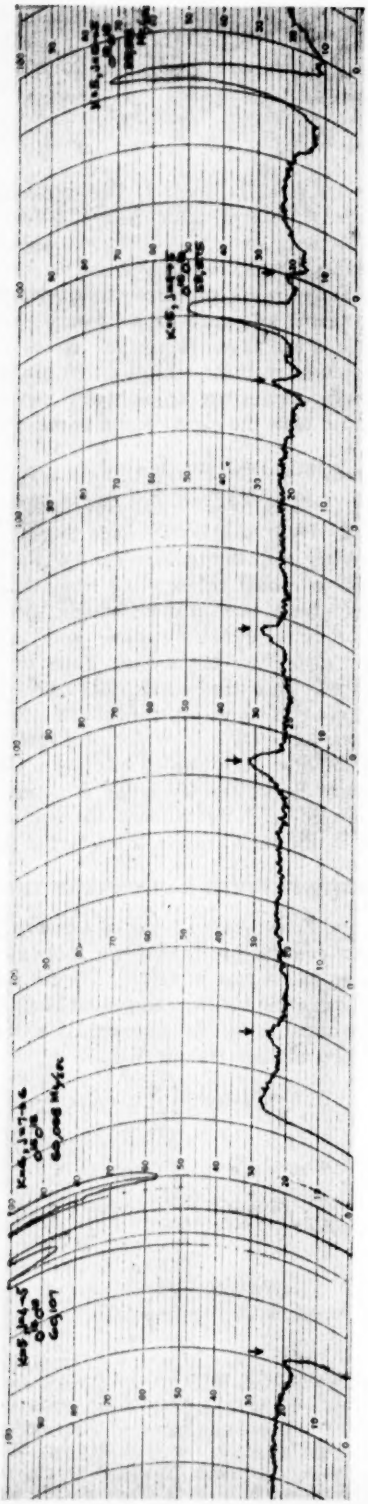

FIG. 2.

the angle between the internuclear axis and the radius vector from nucleus to electron. In a, b, and c the averages are taken over the wavefunctions of the unpaired electrons.

For a molecule in a Σ state such as O_2, $L_z=0$, so that only the terms involving b and c in (3) are of importance. It may be noted that, if the electron is spherically distributed with respect to the nucleus, the interaction (3) reduces to $b\mathbf{I}\cdot\mathbf{S}$, with $b=(16/3)\pi g_I\mu_0\mu_N|\psi(0)|^2$ as found by Fermi[13] for s electrons in an atom.

REPRESENTATION FOR $O^{16}O^{17}$

In order to find the eigenvalues of the perturbation Hamiltonian, it is important to choose a representation in which the energy is nearly diagonal. This will be achieved if a representation is chosen which is diagonal in the sum of the two vector quantities which are most tightly coupled.

There are three possible coupling schemes for I, S and K in the case of a molecule like $O^{16}O^{17}$. Vector diagrams for the three representations are shown in Fig. 1.

In $O^{16}O^{17}$ the choice of one of these simple representations is quite clear. The coupling of S to K which gives rise to the fine structure of the O_2 molecule is about 60 000 Mc/sec while the coupling between I and S which gives rise to the magnetic hyperfine structure is of the order of 100 Mc/sec. The coupling of I to K which depends on the electric quadrupole interaction is only about 3 Mc/sec, so that the second or J representation is best.

Since the choice is so clear, the contribution to the energies from off-diagonal matrix elements is very small. In this representation the perturbation Hamiltonian gives the following hyperfine structure shifts for a $^3\Sigma$ state to the first order in b and c.

$$J=K+1\quad\frac{F(F+1)-J(J+1)-I(I+1)}{2J(J+1)}\times(K+2)\left[b+\frac{c}{2K+3}\right],$$

$$J=K\quad\frac{F(F+1)-J(J+1)-I(I+1)}{2J(J+1)}(b+c),$$

$$J=K-1\quad\frac{F(F+1)-J(J+1)-I(I+1)}{2J(J+1)}\times(K-1)\left[-b+\frac{c}{2K-1}\right].$$

The terms containing the second order of b and c and the effect of nuclear quadrupole coupling were found to be negligible in this molecule.

[13] E. Fermi, Z. Physik **60**, 320 (1930).

APPARATUS AND MEASUREMENTS

The spectrum of $O^{16}O^{17}$ was observed in a sample of O_2 enriched to 1 percent abundance in O^{17}. The spectrum was measured with a recording Zeeman modulation spectrometer with a 100-kc/sec sine wave Zeeman field produced by a solenoid wound around the wave guide absorption cell. The 5-mm radiation was obtained from a Raytheon QK 295 klystron. It was necessary to cool the gas sample to liquid nitrogen temperature in order to intensify the lines enough to be detectable. Because of limitations of the frequency range of the available klystrons, the $O^{16}O^{17}$ spectrum was observed only between 59 250 Mc/sec and 60 300 Mc/sec. Figure 2 shows a portion of the recorded spectrum.

The frequencies of the observed hyperfine structure lines were determined by interpolation between $O^{16}O^{16}$, $O^{16}O^{18}$, and $O^{18}O^{18}$ fine structure lines appearing on the recorder trace. The traces taken were consistent with the assumption that expression (2) gave the frequencies of the latter lines correctly. The undisplaced positions of the $O^{16}O^{17}$ lines were assumed to be given by the same formula.

Table II lists the observed spectrum and that theoretically predicted for values of $b=-102$ Mc/sec and $c=+140$ Mc/sec. The observed and predicted relative intensities are also given. The relative intensities could be measured only very roughly because of variation in klystron power output and sample temperature. The predicted relative intensities were computed under the simplifying assumptions that all of the lines have the same width and Zeeman sensitivity. In view of this, it is felt that the relative intensities check well.

TABLE II. Tabulation of experimental and theoretical frequencies and relative intensities for $O^{16}O^{17}$ magnetic hyperfine structure lines between 59 250 Mc/sec and 60 300 Mc/sec. It is assumed that $b=-102$ Mc/sec and $c=+140$ Mc/sec for calculation of theoretical frequencies.

Transition	Frequency (Mc/sec) Experimental	Theoretical	Relative intensity Experimental	Theoretical
$K=4,\ J=5\rightarrow4,\ F=13/2\rightarrow11/2$	59 250	59 249	4	4.25
$K=7,\ J=6\rightarrow7,\ F=9/2\rightarrow11/2$	59 322	59 320	2.5	3.48
$K=5,\ J=6\rightarrow5,\ F=7/2\rightarrow5/2$	59 359	59 358	3	2.40
$K=6,\ J=5\rightarrow6,\ F=15/2\rightarrow17/2$	59 385	59 383	4.5	6.66
$K=7,\ J=6\rightarrow7,\ F=7/2\rightarrow9/2$	59 390	59 389	2.5	2.98
$K=4,\ J=5\rightarrow4,\ F=15/2\rightarrow13/2$	59 398	59 396	7	5.24
$K=5,\ J=6\rightarrow5,\ F=9/2\rightarrow7/2$	59 431	59 431	2	2.90
$K=6,\ J=5\rightarrow6,\ F=13/2\rightarrow15/2$	59 519	59 518	4	5.60
$K=5,\ J=6\rightarrow5,\ F=11/2\rightarrow9/2$		59 519		3.54
$K=5,\ J=6\rightarrow5,\ F=13/2\rightarrow11/2$	59 627	59 626	2.5	4.25
$K=6,\ J=5\rightarrow6,\ F=11/2\rightarrow13/2$	59 638	59 636	3	4.65
$K=6,\ J=5\rightarrow6,\ F=9/2\rightarrow11/2$	59 737	59 735	3	3.87
$K=5,\ J=6\rightarrow5,\ F=15/2\rightarrow13/2$	59 748	59 748	5	5.11
$K=6,\ J=7\rightarrow6,\ F=9/2\rightarrow7/2$	59 790	59 787	2.5	2.98
$K=6,\ J=7\rightarrow6,\ F=11/2\rightarrow9/2$	59 864	59 864	2.5	3.47
$K=5,\ J=6\rightarrow5,\ F=17/2\rightarrow15/2$	59 889	59 887	6	6.09
$K=6,\ J=7\rightarrow6,\ F=13/2\rightarrow11/2$	59 956	59 955	4	4.08
$K=5,\ J=4\rightarrow5,\ F=13/2\rightarrow15/2$	59 989	59 986	5.5	6.38
$K=6,\ J=7\rightarrow6,\ F=15/2\rightarrow13/2$	60 060	60 059	2	4.77
$K=5,\ J=4\rightarrow5,\ F=11/2\rightarrow13/2$	60 130	60 129		
$K=7,\ J=8\rightarrow7,\ F=11/2\rightarrow9/2$	60 170–180 (two lines)	60 172	2	3.20
$K=6,\ J=7\rightarrow6,\ F=17/2\rightarrow15/2$		60 179	3	5.55
$K=5,\ J=4\rightarrow5,\ F=9/2\rightarrow11/2$	60 240–250 (strong)	60 250	6	4.11
$K=7,\ J=8\rightarrow7,\ F=13/2\rightarrow11/2$		60 251		3.78

INTERPRETATION OF DATA

The B value for the $(O^{16})_2$ molecule extrapolated to the $K=0$ rotational state is 43 101.6±5 Mc/sec from the analysis of the fine structure spectrum. The internuclear distance is 1.2107A from this value of B_0. The value B_0 has also been very accurately measured by optical spectroscopy[14] to be 1.43777 ± 0.00001 cm^{-1}. Since the microwave measurement is a frequency measurement, and the optical measurement a determination of wavelength, the ratio of the microwave value of B_0 in cycles/sec to the optical value in wavenumbers affords a determination of the velocity of light. The result is $c=299\,781\pm33$ km/sec. This is not sufficiently accurate to be very useful, but in view of the discrepancy noted in a similar measurement involving HCN,[15] a refinement of the experimental measurements and the theory of the O_2 microwave spectrum to obtain more accuracy in the microwave value of B_0, and hence in this determination of c, may be worthwhile.

The theoretical hyperfine structure spectrum was computed on the basis of a nuclear spin $I=5/2$ for O^{17}. This spin value has been reported recently by Alder and Yu[16] and by Geschwind *et al.*[17] Alder and Yu found the spin from the intensity of a nuclear induction signal and Geschwind by the examination of the partially resolved quadrupole hyperfine structure of the $J=1\rightarrow2$ transition in $O^{17}CS$. The close agreement between the observed magnetic hyperfine structure and that predicted theoretically on the basis of $I=5/2$ affords an independent spin determination for O^{17} and confirms the earlier experimental results.

Experimental evaluation of the hyperfine constants b and c allows fairly direct determination of some properties of the O_2 electronic wave functions. These are discussed in the following paper.[18]

The authors wish to thank Professor A. O. Nier for supplying a sample of oxygen enriched in both O^{18} and O^{17}. They are also grateful to Messrs. A. L. Schawlow, T. M. Sanders, and W. A. Hardy who constructed the spectrometer on which the above measurements were made, and to Professor H. M. Foley and Dr. R. A. Frosch for many helpful discussions.

[14] H. D. Babcock and L. Herzberg, Astrophys. J. **108**, 167 (1948).
[15] Rank, Ruth, and Vander Sluis, Phys. Rev. **86**, 798 (1952).
[16] F. Alder and F. C. Yu, Phys. Rev. **81**, 1067 (1951).
[17] Geschwind, Gunther-Mohr, and Silvey, Phys. Rev. **85**, 474 (1952).
[18] Miller, Townes, and Kotani, Phys. Rev. **90**, 542 (1953).

The Electronic Structure of O_2*

S. L. MILLER† AND C. H. TOWNES, *Radiation Laboratory, Columbia University, New York, New York*

AND

M. KOTANI, *Tokyo University, Tokyo, Japan*

(Received January 12, 1953)

The magnetic hyperfine structure parameters which have been evaluated from an analysis of the spectrum of $O^{16}O^{17}$ are used to obtain information on the electronic structure of O_2. These values show that the unpaired electrons are primarily in $p\pi$ orbits but have approximately 2.5 percent s character.

THE observed magnetic hyperfine structure in the microwave spectrum of $O^{16}O^{17}$ can be fitted to the theoretical interaction energy of the form

$$H=b\mathbf{I}\cdot\mathbf{S}+cI_zS_z,$$

and hence experimental values of the constants b and c are obtained.[1] Here $\mathbf{I}$ is the nuclear spin of O^{17}, and $\mathbf{S}$ is the total electronic spin. The z direction is along the internuclear axis. Since the constants b and c depend on the distribution of electronic magnetic moment in the molecule, their observed values may be used to determine this distribution.

The constants b and c are given to a good approximation by[1]

$$b=2g_I\mu_0\mu_n\left[\frac{8\pi}{3}\psi^2(0)-\left(\frac{3\cos^2\chi-1}{2r^3}\right)_{Av}\right],$$
$$c=6g_I\mu_0\mu_n\left(\frac{3\cos^2\chi-1}{2r^3}\right)_{Av}, \tag{1}$$

where g_I is the g factor for O^{17}, or -0.7571;[2] μ_n is the nuclear magneton, assumed to be positive in sign; μ_0 is the Bohr magneton (taken as positive in sign); $\psi^2(0)$ is the electron density at the O^{17} nucleus for the electrons with unpaired spins and magnetic moments. χ is the angle between the molecular axis and the vector joining the nucleus and the electron; r is the length of this vector. The measured values of these constants are:[1] $b=-102$ Mc/sec and $c=140$ Mc/sec. This allows a direct determination of the two quantities $\psi^2(0)$ and $[(3\cos^2\chi-1)/2r^3]_{Av}$, each of which has a fairly simple interpretation in terms of the electronic structure of the molecule.

The oxygen atom has the configuration $(1s)^2(2s)^2(2p)^4$. The bond between the two oxygen atoms to form O_2 has been considered to consist of two 3-electron bonds and one single bond.[3] The single bond consists of overlapping $2p\sigma$ electron orbits with paired spins. The 3-electron bonds consist of two overlapping $2p\pi$ orbits, one of which contains a pair of electrons while the other is occupied by one electron. Any bond of the normal type which contains two electrons with paired spins contributes nothing to the hyperfine structure since the magnetic fields produced by the two electrons exactly cancel. Because b and c depend on $(1/r^3)_{Av}$, the part of the electronic wave function very near the O^{17} is by far the most important, and the contribution to this average of the wave function near the O^{16} nucleus is negligible.[4] According to the proposed model of the O_2 molecule, there is on the average one electron with unpaired spin in a $2p\pi$ orbit about the O^{17} nucleus, and from this the expected values of b and c may be determined if the atomic $2p$ wave functions are sufficiently well known. If overlap effects are neglected, the molecular orbital description of the oxygen molecule is the same for our purposes as the atomic orbital model.

From the experimental values of b and c and Eqs. (1), it follows that

$$\left(\frac{3\cos^2\chi-1}{2r^3}\right)_{Av}=-8.9\times10^{24}\text{ cm}^{-3},$$
$$\psi^2(0)=1.26\times10^{24}\text{ cm}^{-3}. \tag{2}$$

The negative value of $[(3\cos^2\chi-1)/2r^3]_{Av}$ immediately shows that the unpaired electrons are primarily in $p\pi$ rather than $p\sigma$ orbits, since $[(3\cos^2\chi-1)/2r^3]_{Av}$ is negative for a $p\pi$ and positive for a $p\sigma$ orbit. This is in satisfying agreement with what is expected from the electronic structure of O_2 described above. The value of $[(3\cos^2\chi-1)/2]_{Av}$ can easily be obtained for a $p\pi$ wave function as $-1/5$, so that from (2)

$$(1/r^3)_{Av}=4.45\times10^{25}\text{ cm}^{-3}. \tag{3}$$

One might expect to obtain a theoretical value of $(1/r^3)_{Av}$ from the radial wave functions for the O atom derived by the Hartree-Fock method.[5] This gives a value $(1/r^3)_{Av}=3.2\times10^{25}$ cm^{-3}, or 29 percent less than

* Research assisted by the U. S. Atomic Energy Commission.

† U. S. Atomic Energy Commission Predoctoral Fellow. Present address: Bell Telephone Laboratories, Murray Hill, New Jersey.

[1] S. L. Miller and C. H. Townes (preceding paper), Phys. Rev. **90**, 537 (1953).

[2] Obtained from data given by F. Alder and F. C. Yu, Phys. Rev. **81**, 1067 (1951).

[3] L. Pauling, *The Nature of the Chemical Bond* (Cornell University Press, Ithaca, 1945).

[4] See the similar quantity involved in nuclear quadrupole hyperfine structure, C. H. Townes, and B. P. Dailey, J. Chem. Phys. **17**, 982 (1949).

[5] Hartree, Hartree, and Swirles, Phil. Trans. Roy. Soc. (London) **A238**, 229 (1939).

the "experimental" value given by (3). This type of wave function should not, however, be expected to yield very accurate values of $(1/r^3)_{Av}$, since it is not particularly accurate near the nucleus.[6]

Probably the best value for $(1/r^3)_{Av}$ can be obtained from measurement of fine structure in the ground state $[(2p)^4\,{}^3P]$ of the O atom. Yamanouchi and Horie[6] have shown from this fine structure that

$$(Z-\sigma)\mu^2/hc(1/r^3)_{Av}=73.5\ \text{cm}^{-1}, \tag{4}$$

where σ is the screening constant and equals 3.074, and μ is the Bohr magneton. Expression (4) gives

$$(1/r^3)_{Av}=3.45\times10^{25}\ \text{cm}^{-3}. \tag{5}$$

This value agrees fairly well with the experimental value (3), but is smaller by as much as 23 percent.

The discrepancy between (3) and (5) will only be increased if the unpaired electrons in O_2 are assumed to be partially in $p\sigma$ orbits, since this would decrease the value of $[(3\cos^2\chi-1)/2]_{Av}$. Hence we can conclude that electronic configurations which put unpaired electrons in the $p\sigma$ orbit are unimportant in the O_2 molecule. Some of the discrepancy results from omission of the effects of overlapping of wave functions in the above discussion. Calculations of these effects using either molecular-orbital or atomic-orbital approximations do improve the agreement by a few percent, but still leave a discrepancy of about 15 percent. This remaining discrepancy is not large. However, it is probably significant and may indicate a distinct deviation of the molecule $p\pi$ wave function from an atomic wave function.

The value found for $\psi^2(0)$ may seem rather large. However, it corresponds to only 2.5 percent of the value of $\psi^2(0)$ for a $2s$ wave function as given by the Hartree-Fock method, hence it represents a rather small detail of the molecular wave function. A pure atomic p orbit of course gives a completely negligible value of $\psi^2(0)$, so that there must be a partial s character of the wave function. This s character for the molecular wave function of the unpaired electron might be attributed to a small probability of the unpaired electron being in a $p\sigma$ orbit which has some s character. The large value of $[(3\cos^2\chi-1)/2]_{Av}$ seems to rule this out as noted above.

In the case of O^+, Hartree, Hartree, and Swirles[5] have calculated the amount of configuration mixing by a variational method. They found that the wave function includes 96 percent $(1s)^2(2s)^2(2p)^3$ configuration and 4 percent $(1s)^2(2p)^5$. This perhaps indicates the ease with which some neglected electrostatic interactions can introduce the 2.5 percent s character found here in the O_2 molecular wavefunction.

CONCLUSION

Agreement between the measured coefficients b and c of the magnetic hyperfine structure of $O^{16}O^{17}$ and those expected from present ideas of the electronic structure of O_2 is strikingly good in view of the crudeness of our knowledge about molecules. Several qualitative features of the O_2 electronic structure are shown to be correct by the hyperfine structure. However there are significant discrepancies between the experimentally measured hyperfine constants and those obtained from the crude electronic wave functions used. More extensive calculations of the electronic distribution in the O_2 molecule are being investigated by one of the authors (M.K.). It is hoped that this will allow a still more detailed comparison between the observed and theoretically expected hyperfine structure.

[6] T. Yamanouchi and H. Horie, J. Phys. Soc. Japan **7**, 52 (1952).

The Transmission of Electrons through Thin Metallic Foils*

C. H. CHANG, C. S. COOK, AND H. PRIMAKOFF
Physics Department, Washington University, St. Louis, Missouri
(Received December 12, 1952)

Experimental studies have been made on the relative transmission of positrons and negatrons in the energy range 50–750 kev through aluminum and platinum windows of an end-window-type G-M counter. In qualitative agreement with the theoretical predictions that more scattering takes place in material having higher atomic number, a platinum foil having the same surface density as a corresponding aluminum foil shows lower relative transmission at any given energy even though the low energy cutoffs of the two windows are just about the same. Also in qualitative agreement with theory, a larger percentage of positrons than negatrons are transmitted at any given energy for the same platinum foil. Theoretical transmission curves, with an empirically determined constant, have been developed. These curves are in relatively good agreement with the experimental curves.

I. INTRODUCTION

FROM the point of view of the beta-ray spectroscopist studying nuclear beta- and gamma-ray spectra, a Geiger-Müller counter window introduces experimental distortions in the magnitudes and shapes of low energy spectra. In practice, methods have been devised either for the measurement of the transmission coefficient of the counter window[1–3] in order to correct for this effect, or, attempts have been made to eliminate the counter window entirely.[4] From a more fundamental aspect, however, the problem is actually a form of the general problem of the passage of electrons through matter which has been a subject of much study since the first discovery of cathode rays and which has recently been investigated intensively[5–10] in the range of energies considered in this paper. If attacked from this point of view, the transmission coefficient η of a G-M counter window foil may be considered as consisting of two parts which we shall call η_E and η_I. The quantity η_E is a measure of the amount of elastic scattering of the electrons within the foil. The elastic scattering is important, since some of the electrons do not pass completely through the foil and get into the sensitive region of the G-M counter because they are scattered through too large an angle to enter this region. The second quantity η_I is a measure of the inelastic scattering between the passing electron and the atoms of the foil; such inelastic scattering may lead to the actual stopping of the electron within the foil. The total coefficient is the product of these two parts ($\eta=\eta_E\eta_I$). Actually, of course, these two quantities are not entirely statistically independent one from the other, but handling them as separate entities appears valid in first approximation and leads to reasonably good results.

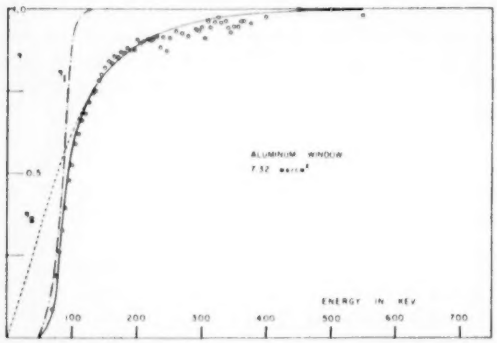

FIG. 1. Relative electron transmission η through a 7.32 mg/cm² aluminum G-M counter window as a function of the electron's incident kinetic energy. In this and subsequent figures the circles represent experimentally determined negatron transmissions, and the plus signs experimentally determined positron transmissions. The continuous line is the theoretical transmission coefficient, $\eta=\eta_E\eta_I$, as determined by the method discussed in the text. To show the relative importance of η_E and η_I at various energies the theoretically determined curves for these two quantities are also shown in this diagram.

II. EXPERIMENTAL RESULTS

The measurements made in the current experiments on the relative transmission of negatrons and positrons through various aluminum and platinum G-M counter windows are indicated in Figs. 1 through 5. These represent seven sets of data, since two of the figures give results for both positrons and negatrons for the same window. The solid lines represent a type of theoretical curve which will be discussed in the next section.

The experimental measurements were performed on the lens spectrometer previously used[3] for this purpose. However, the experimental data presented here were not obtained by means of the acceleration technique[3] but were obtained through a comparison method. Since all aluminum and platinum windows used for the cur-

* Assisted by the joint program of the U. S. Office of Naval Research and the U. S. Atomic Energy Commission.
[1] D. Saxon, Phys. Rev. **81**, 639 (1951).
[2] Heller, Sturcken, and Weber, Rev. Sci. Instr. **21**, 898 (1950).
[3] C. H. Chang and C. S. Cook, Nucleonics **10**, No. 4, 24 (1952).
[4] Langer, Motz, and Price, Phys. Rev. **77**, 798 (1950).
[5] Groetzinger, Humphrey, and Ribe, Phys. Rev. **85**, 78 (1952).
[6] H. J. Lipkin, Phys. Rev. **85**, 517 (1952).
[7] H. H. Seliger, Phys. Rev. **88**, 408 (1952).
[8] Christian, Dunning, and Martin, Nucleonics **10**, No. 5, 41 (1952).
[9] W. Paul and H. Reich, Z. Physik **131**, 326 (1952).
[10] E. Hisdal, Phil. Mag. **43**, 790 (1952).

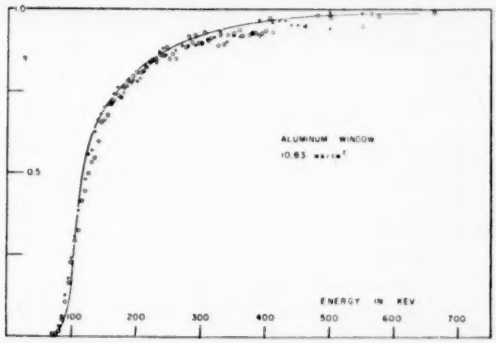

FIG. 2. Relative electron transmission η through a 10.83-mg/cm² aluminum window. See caption for Fig. 1 for explanation.

rent experiment are relatively thick, as G-M counter windows go, a thin Zapon window will transmit, within experimental error, 100 percent of the beta-particles at the energies under consideration. For this reason one can obtain spectra for the negatrons (Ag^{110}) and for the positrons (Cu^{61}) using a thin Zapon window and, by comparison with the spectra obtained using the thicker metallic windows, calculate a relative transmission curve for these thicker windows. This method could be applied quite simply to the Ag^{110} negatron source since its long half-life allowed the same source to be used for all measurements (with appropriate decay corrections). However, the short half-life of the Cu^{61} positron source forced the preparation of a new source for each set of data. The preparation of a Cu^{61} source has been, however, so standardized that it was possible to prepare two or more such sources almost identical one with the other. Corrections were made for small variations in the intensity of the different sources through comparison of the sources with a standard long-lived source under conditions of a standardized geometry.

When it can be applied and when measurements must be made on a number of different sources, the comparison method requires less expenditure of time than does the acceleration technique. However, slight discrepancies between the two techniques still appear in the energy region just above the window cutoff.

III. THE ELASTIC TRANSMISSION COEFFICIENT η_E

Monoenergetic electrons entering a foil may be elastically scattered through any (total) angle, depending upon the number of individual collisions between them and the atoms of foil and upon the angles of scattering in these collisions. The distribution of the electrons upon leaving the foil will be some function $P(\theta)$ of the (total) spatial angle of multiple scattering θ. The form of this function will depend upon the geometrical thickness L_0, the number density of the atoms in the foil N/V, the type of foil material (atomic number Z), the kinetic energy of the incident electrons E, and the polarity of the electron charge (negatrons, $Z'e=-e$, or positrons $Z'e=+e$). The elastic transmission coefficient η_E can then be expressed as

$$\eta_E=\int_0^{\theta_{\max}} P(\theta)d\theta, \tag{1}$$

where $\theta_{\max}$ is the maximum (total) angle through which an electron may be scattered by the G-M counter window foil and still enter the sensitive region of the G-M counter. For ease in calculation we shall normalize $P(\theta)$ in the interval $0\leq\theta<\infty$, even though physically $0\leq\theta<\pi$, since the form of $P(\theta)$ which we shall use is small for $\pi\leq\theta<\infty$.

In the present paper we will not attempt to derive the actual form of $P(\theta)$ from basic theoretical considerations. However, we will show that the crude assumption of a decreasing exponential function of θ for the scattering probability per unit solid angle will lead to results for η_E which can be brought into approximate agreement with the experimental observations. Such a normalized function is

$$P(\theta)d\theta=\alpha^2\exp(-\alpha\theta)\sin\theta d\theta\approx\alpha^2\exp(-\alpha\theta)\theta d\theta, \tag{2}$$

the choice of this function being initially justified on the basis that it is a simple function which at least roughly resembles the spatial distribution associated with the projected "Gaussian" plus "tail" distribution which has been used in most "small angle" multiple scattering theories. From Eqs. (1) and (2) one then obtains

$$\eta_E=1-\{\exp(-\alpha\theta_{\max})\}\{1+\alpha\theta_{\max}\},$$

with α determined via the mean square angle of multiple scattering by

$$\langle\theta^2\rangle=\int_0^{\pi}\theta^2P(\theta)d\theta=6/\alpha^2,$$

$$\alpha=2.45/\langle\theta^2\rangle^{\frac{1}{2}}. \tag{3}$$

There then remains only one arbitrary constant within the equation for η_E, namely, $\theta_{\max}$; for our counter ge-

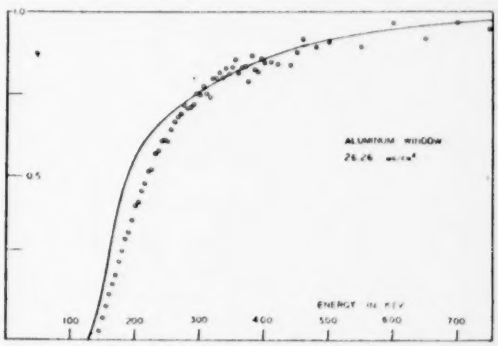

FIG. 3. Relative electron transmission η through a 26.26-mg/cm² aluminum window. See caption for Fig. 1 for explanation.

ometry, the assumption of $\theta_{max}=1$ radian appears reasonable. Thus, the equation from which η_E has to be determined for each window becomes

$$\eta_E=1-\{\exp[-2.45/\langle\theta^2\rangle^{\frac{1}{2}}]\}\{1+2.45/\langle\theta^2\rangle^{\frac{1}{2}}\}. \quad (4)$$

The mean square angle of multiple scattering can now be found (in the "small angle" approximation) from an expression involving the single scattering probability distribution through an angle ϕ.[11] Using, in addition, in this expression a "spin orbit correction" factor $\gamma(\phi)$,[12] we obtain a formula for the mean square angle of multiple scattering,

$$\langle\theta^2\rangle=\frac{8\pi NL_0}{V}\left(\frac{ZZ'e^2}{pv}\right)^2\int_0^{\pi/2}\frac{\phi^2\gamma(\phi)d\phi}{\{\phi^2+\phi_{min}^2\}^{\frac{1}{2}}}. \quad (5)$$

Here the foil contains NL_0/V atoms per unit area; p and $v=\beta c$ are, respectively, the momentum and velocity of the incident electron;

$$\phi_{min}=\{1.14mcZ^{\frac{1}{3}}/137p\}\{1.13+3.76(ZZ'/137\beta)^2\}^{\frac{1}{2}},$$

and for small angles,

$$\gamma(\phi)=1-\beta^2\left(\frac{\phi}{2}\right)^2-[\pi ZZ'\beta/137](\phi/2)[1-\phi/2].$$

Actually, for large Z, higher powers of $ZZ'/137$ than the first contribute to $\gamma(\phi)$, but these contributions are relatively unimportant at the rather small ϕ which make the major contribution[13] to $\langle\theta^2\rangle$.

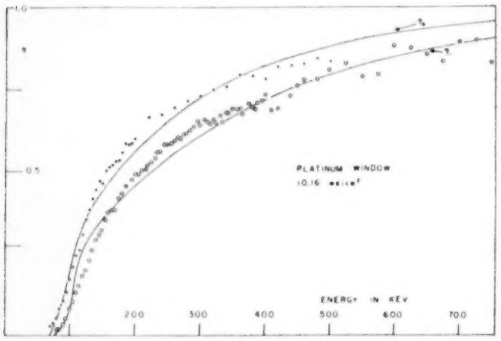

FIG. 4. Relative electron transmission η through a 10.16-mg/cm² platinum window. See caption to Fig. 1 for explanation. The theoretical transmission coefficient designated by the symbol η_+ is the one determined for positrons and that designated by the symbol η_- is the one determined for negatrons.

[11] G. Molière, Z. Naturforsch. **2a**, 133 (1947); **3a**, 78 (1948); S. Olbert, Phys. Rev. **87**, 319 (1952).

[12] W. A. McKinley and H. Feshbach, Phys. Rev. **74**, 1759 (1948); H. Feshbach, Phys. Rev. **88**, 295 (1952).

[13] We neglect the contribution to $\langle\theta^2\rangle$ for values of ϕ between $\pi/2$ and π. In this region both the Rutherford factor in Eq. (5) and the spin orbit correction factor are not accurately given by our very approximate expressions, but we may nevertheless estimate that the net contribution from this region in the integration over the correct single scattering distribution is small compared to the net contribution of the region between $\theta=0$ and $\theta=\pi/2$.

IV. THE INELASTIC TRANSMISSION COEFFICIENT η_I

The inelastic transmission coefficient is determined by the number of electrons which are stopped in the foil. Physically known quantities make it easier to calculate the number of electrons which are stopped rather than the number which penetrate the foil. Therefore it seems appropriate to define a quantity $\eta_S=1-\eta_I$ which represents the probability that an electron is stopped in the foil.

If an electron possessing a fairly high kinetic energy enters a piece of material having semi-infinite extent, it will continue to move until it has been robbed of essentially all its kinetic energy as a consequence of inelastic collisions involving the ionization and excitation of the atoms of the material. The total distance X (effective path length) which the electron travels before stopping will not be the same in all individual cases but will instead be distributed according to a probability function $P_S(X)$ which is in first approximation Gaussian:

$$P_S(X)dX=\exp(-y^2/2\langle y^2\rangle)dy/(2\pi\langle y^2\rangle)^{\frac{1}{2}}.$$

Here $y=X-R$, $\langle X\rangle=R$ is the range of the electron within the material, and $\langle y^2\rangle$, the mean square range straggling, is in first approximation,[14]

$$\langle y^2\rangle=(\langle X-R)^2\rangle=R^2/2\ln(E/I)$$
$$=E^4/32\pi^2(N/V)^2Z^2e^8[\ln(E/I)]^3,$$

where E is the kinetic energy of the incident electron and I is the average ionization energy (we use $13.6Z$ ev for this energy). The actual small difference between the R and the $\langle y^2\rangle$ values for (nonrelativistic) negatrons and for (nonrelativistic) positrons of a given energy is neglected. We then have

$$\eta_I=1-\eta_S=1-\int_0^L P_S(X)dX$$
$$=1-\{1/(2\pi\langle y^2\rangle)^{\frac{1}{2}}\}\int_{-R}^{L-R}\exp(-y^2/2\langle y^2\rangle)dy$$
$$=\tfrac{1}{2}-\{1/(2\pi\langle y^2\rangle)^{\frac{1}{2}}\}\left\{\int_0^{L-R}\exp(-y^2/2\langle y^2\rangle)dy\right.$$
$$\left.-\int_R^{\infty}\exp(-y^2/2\langle y^2\rangle)dy\right\}, \quad (7)$$

where L is the effective path length of an electron

[14] See, for example, H. W. Lewis, Phys. Rev. **85**, 20 (1952). Justification for the use of Lewis' theory of range and of range straggling for a *nonrelativistic* charged particle (negatron or positron) is based upon the fact that η_I affects only the lower energy portion of the transmission curve (see Fig. 1). For higher relativistic electron energies η_I is approximately unity and the transmission curve is determined solely from η_E.

traversing the foil. Using the results of Yang,[15] one has roughly, $L=(1+\langle\theta^2\rangle/4)L_0$; also, the second integral [in the last form of Eq. (7)] can be dropped since $R/(2\langle y^2\rangle)^{\frac{1}{2}}=[\ln(E/I)]^{\frac{1}{2}}\gg 1$, while the first integral can be found from available tables[16] and graphs.[17]

The results of these calculations for η_I, as well as those for η_E and the combined result $\eta=\eta_E\eta_I$, are shown for the 7.32-mg/cm² aluminum window in Fig. 1. Other graphs for the remaining windows show only the final theoretical result $\eta=\eta_E\eta_I$.

V. DISCUSSION

It will be noted that $\langle\theta^2\rangle$ plays a very important role in the present work, since it is instrumental in the determination of both η_E and η_I. Because of this use of the "scattering" approach to the problem of window transmission, it is valid to compare our results with those made through the study of the scattering by various materials of electrons in the energy range considered here (from about 30 kev to a few Mev). Qualitatively the results agree.

Our results show that, in a high Z material—platinum, at a given energy, the transmission coefficient for positrons is greater than for negatrons; in agreement with the observations[5–7] that there is a greater single scattering of negatrons than positrons at high Z. In addition, for a given foil surface density, the transmission coefficient for aluminum is greater than for platinum, in agreement with the observations[7,8] that the amount of single scattering increases with larger atomic number of the scattering material.

For comparison of our distribution function [Eq. (2)] with the measurements of Hisdal[10] on the scattering of 0.5-Mev electrons in an Ilford G5 emulsion, we must transform our distribution for spatial angles into an equivalent form for projected angles. Such a transformation shows that the projected distribution is approximately proportional to $\exp(-\alpha|\Theta|)[|\Theta|+1/\alpha]$ where Θ is the projected scattering angle. Using the data for Ilford G5 emulsions, as given by Voyvodic and Pickup,[18] and the cell length given by Hisdal, to determine α, our distribution is in rough agreement with Hisdal's experimental results.

[15] C. N. Yang, Phys. Rev. **84**, 599 (1951). This formula is, however, applicable only to small angles.

[16] *Table of Probability Functions*, prepared by Federal Works Agency, Works Project Administration, sponsored by National Bureau of Standards, 1941.

[17] E. Jahnke and F. Emde, *Tables of Functions* (Dover Publications, New York, 1945), fourth edition, pp. 23–25.

[18] L. Voyvodic and E. Pickup, Phys. Rev. **85**, 91 (1952).

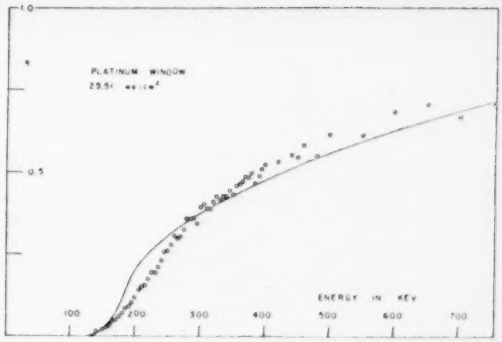

FIG. 5. Relative electron transmission η through a 25.51-mg/cm² platinum window. See caption to Fig. 1 for explanation.

As has already been mentioned, the distribution function for multiple elastic scattering used in the present calculations is of the same general shape in its "small angle" plane projected form as the more commonly used sum of a "Gaussian" plus "tail." Apart from this, possibly the only virtue of our distribution is its simplicity for numerical calculations. Considering this and the number of additional approximations which have been made in the determination of η_E and η_I, the theoretically determined curves for η are in not unsatisfactory agreement with the experimental observations.

These approximations, it will be recalled, are as follows: (a) the omission of any systematic treatment of the inelastic collision energy losses in the treatment of the multiple elastic scattering and the parallel omission of the effect of multiple elastic scattering in the treatment of the stopping probability due to inelastic collision;[19] (b) the use of a crude "small angle" exponential approximation to the "Gaussian" plus "tail" "small angle" multiple scattering distribution in a physical situation where some of the angles of multiple scattering become quite appreciable; and (c) the use of very approximate expressions for the electron range and range straggling. In spite of these perhaps mutually compensating approximations, the agreement between theory and experiment seems to indicate that a future rigorous calculation of the transmission coefficient η should yield results not too different from those developed here.

[19] Except in so far as our use of the approximate relation between L and L_0.

The Capture and Loss of Electrons by Fission Fragments*

GEORGE I. BELL†
Cornell University, Ithaca, New York
(Received January 2, 1953)

We calculate the effective charge of fission fragments passing through a low pressure gas. We first compute, on a classical basis, the cross section for capture of an electron by a fission fragment of relatively arbitrary charge and velocity. We then develop a rough theory which gives the cross section for loss of an electron through interaction with a gas atom. From these two cross sections we readily obtain the effective charge. The effective charge of a fragment will increase with the pressure of the substance through which it passes. We note the probable importance of anomalous effects in hydrogen and helium. We find general agreement between theoretical predictions and experimental results.

I. INTRODUCTION

IN this paper we will consider the problem of calculating the average number of electrons which a fission fragment possesses as a function of its nuclear charge, velocity, and the density and atomic weight of the material through which it passes. We take the term "effective charge of a fragment" to mean the fragment's nuclear charge minus the average number of electrons which it has under given conditions.

The problem of determining the effective charge of a fission fragment has been discussed by Bohr;[1-3] Lamb;[4] Knipp and Teller;[5] and Brunings, Knipp, and Teller.[6] All of these authors have agreed in treating the electrons of the fragments as a Fermi-Thomas gas. They then made physically reasonable but relatively arbitrary assumptions to obtain the effective charge as a function of fragment nuclear charge and velocity. It is the aim of the present paper to develop a theory which is somewhat less arbitrary or ambiguous than the previous formulations. It is believed that the calculations here made have some claim to quantitative accuracy.

Let us consider the passage through a gas of a fragment of nuclear charge $40e$ or $50e$, effective charge of the order of $10e$, and velocity of the order of $4\alpha c$, where $\alpha=(137)^{-1}$ and c is the velocity of light. Inasmuch as the effective charge of a fragment will at any instant be determined by a statistical balance between the fragment's capture and loss of electrons, we wish to calculate the cross section for the fragment to capture an electron from the gas atom, and the cross section for the fragment to lose an electron in an interaction with a gas atom. Since we are most interested in the ratio of these cross sections, it may be important to treat them by similar methods; we may thus hope that some inaccuracies inherent in the necessarily approximate methods employed will not affect the ratio.

Let us for the present consider that we have the fragment passing through a gas of moderate atomic number (of order 10: The special cases of hydrogen and helium will receive some attention in Sec. IV). Let us further assume that the successive collisions of a fragment with gas atoms are independent. This means that there is sufficient time between collisions in order that fragment electrons which were either raised to highly excited states or newly captured in such states in the last previous collision, will be able to decay to some of the lowest available fragment states before the next collision. We thus ignore ionization in two or more steps and take any captured electron to be no different from other fragment electrons in subsequent collisions. It appears that we hereby limit ourselves to passage through rather rarified gases as will be seen in Sec. V.

Theories of the capture of electrons by α-particles and protons have been developed classically by Thomas,[7] and quantum mechanically by Oppenheimer[8] and Brinkman and Kramers.[9] For our case the fission fragment will have an effective charge of the same order as the nuclear charge of the gas atom, and it is clear that a perturbation or Born approximation method is not valid for a treatment of the capture problem. On the other hand, the electrons will necessarily be captured in fairly high quantum states for which the picture of classical orbits has some validity, and thus a classical approach suggests itself. It is then important to make sure that we can define the positions of our electrons with sufficient accuracy to be able to introduce meaningful impact parameters. It must not be necessary to define electron momenta to an accuracy which would imply position uncertainties as large as the impact parameters. We shall see that, although this limitation is serious, it is generally possible to define the momentum and position of a gas atom electron well enough to justify qualitatively a classical approach.

* Part of this work was done in partial fulfillment of the requirements for a Ph.D. at Cornell University. Part was done while the author was a U. S. Atomic Energy Commission predoctoral fellow.

† Now at Los Alamos Scientific Laboratory, Los Alamos, New Mexico.

[1] N. Bohr, Phys. Rev. **58**, 654 (1940).
[2] N. Bohr, Phys. Rev. **59**, 270 (1941).
[3] N. Bohr, Kgl. Danske Videnskab Selskab, Mat.-fys. Medd. **18**, 8 (1948).
[4] W. E. Lamb, Jr., Phys. Rev. **58**, 696 (1940).
[5] J. Knipp and E. Teller, Phys. Rev. **59**, 659 (1941).
[6] Brunings, Knipp, and Teller, Phys. Rev. **60**, 657 (1941).
[7] L. H. Thomas, Proc. Roy. Soc. (London) **114**, 661 (1927).
[8] J. R. Oppenheimer, Phys. Rev. **31**, 349 (1928).
[9] H. C. Brinkman and H. A. Kramers, Proc. Acad. Sci. Amsterdam **33**, 973 (1930). See also J. D. Jackson and H. Schiff, Phys. Rev. **89**, 359 (1953).

A quantum-mechanical perturbation theory would seem to have more validity for the calculation of the loss cross section, since the influence of the gas atom on the tightly bound fragment electrons is generally small. But in view of the large amount of momentum that must be given to a fragment electron to remove it from the fragment, we may hope that the large allowable uncertainty in electron momentum may permit one to localize the electron position sufficiently to somewhat justify also a classical approach. To this we shall turn our attention in Sec. III, where it will be further argued that the gas atom may be approximately treated as a Coulomb potential, in which happy case classical and perturbation calculations coincide.

II. THEORY OF CAPTURE

It is difficult for a fragment to capture a free electron. This it can do only if the electron collides inelastically with a fragment electron or suffers a radiative collision; otherwise the total energy of the electron in the rest system of the fragment is non-negative, and the electron moves in a hyperbolic orbit. However, it is different for an electron bound in a gas atom: When fragment and gas atom are separated by a distance large compared to atomic dimensions, the fragment exerts virtually no influence on an electron bound in the gas atom. Since the atom is electrically neutral, it will experience only a small net polarization force and may approach quite close to the fragment without having its electrons particularly accelerated toward the fragment. Hence, when the electron is finally liberated from the gas atom, it may have a sufficiently small velocity so that its total energy in the fragment rest system is negative, allowing it to be captured.

During the early stages of a fragment-atom collision, the external force on a gas-atom electron is small compared to the force binding the electron in the atom. For any electron that is to be captured, there will come a time during the collision when the force on the electron caused by the fragment becomes larger than the binding force, and thereafter the force between gas atom and electron is of secondary importance. Thus the following treatment suggests itself as a simplification of the difficult two-center problem posed by capture: In considering the possible capture of any electron we ignore the effect of the fragment on the gas atom, i.e., polarization, until the force on the electron in question caused by the fragment is equal to the force binding the electron in the atom. Thereafter we ignore the effect of the gas atom and consider the newly liberated electron to be captured, if and only if its total energy in the rest system of the fragment is negative.

In this approach we use the Fermi-Thomas model of the atom in order to obtain the space and velocity distributions of electrons in the gas atom. We are favored in this choice because the outermost electrons, which are poorly described by the Fermi-Thomas model, are seldom captured and because several electrons contribute almost equally to the capture cross section, thus implying no inconsistency in a statistical model.

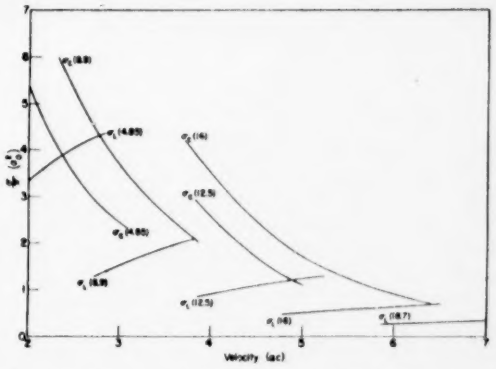

FIG. 1(a). Cross sections for capture σ_c and loss σ_L of an electron by fission fragments of nuclear charge $40e$ passing through low density oxygen; as functions of fragment velocity. The number of electrons z which the fragment lacks for electrical neutrality is indicated as $\sigma(z)$.

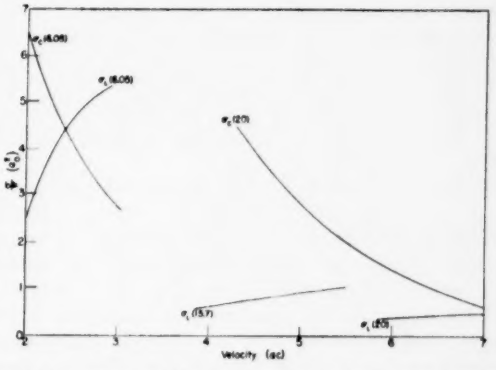

FIG. 1(b). Capture and loss cross sections for fragments of nuclear charge $50e$ in oxygen.

Consider the interaction of a fragment of effective charge z and velocity $\mathbf{v}$ with an electron which has a velocity $\mathbf{v}_e$ in its own Fermi-Thomas atom and is subject to a binding force $\mathbf{F}_e$. Assuming that the electron is liberated at fragment-atom separations large compared to the dimensions of the fragment or gas atom, the force on the electron due to the fragment will be equal to the binding force when gas atom and fragment are separated by r_0 such that $F_e = zr_0^{-2}$. At this separation we assume that the electron is liberated, and thereafter we ignore the gas atom. The electron's potential energy is now $-z_0 r_0^{-1}$, and its kinetic energy in the fragment rest system is $\frac{1}{2}m(\mathbf{v}+\mathbf{v}_e)^2$. It is convenient to introduce v_0, the minimum speed relative to the fragment which an electron at distance r_0 from the fragment nucleus must have in order to escape. Then the condition for capture is $|\mathbf{v}_e+\mathbf{v}| \leqslant v_0$. From simple geometry it follows that the probability of capture, $P(v, v_0, v_e)$, may

be written

$$\begin{aligned} P(v, v_0, v_e) &= 0, && |v-v_e| \geqslant v_0 \\ &= 1, && v+v_e \leqslant v_0 \\ &= \tfrac{1}{2}[v_0^2-(v-v_e)^2]/2vv_e. && v-v_e \leqslant v_0 \leqslant v+v_e \end{aligned} \quad (1)$$

For an electron which is initially located at a definite position r_e in the gas atom, the value of r_0 is determined (for given fragment charge). Our approximation consists in the assumption that *all* electrons of this type are liberated at r_0 so that the cross section for liberation of such electrons is πr_0^2. The cross section for their capture is $\sigma_c = \pi r_0^2 P(v, v_0, v_e)$. This expression must then be integrated over a distribution of electrons (r_0, v_e, v_0) consistent with the Fermi-Thomas model of the gas atom.

This calculation has been carried through for a number of fragments in oxygen, and some of the resulting total capture cross sections are plotted in Fig. 1. The calculation has also been carried far enough for fragments in argon to show that the total capture cross sections are very nearly twice the values for oxygen. It appears that over most of the periodic table, excluding very light elements, the capture cross section for any given fragment will increase with z of the gas somewhat more slowly than linearly, with the increase becoming slower with larger z.

Some general features of the capture process emerge in our calculation. First of all, as is physically evident, it is difficult for fast fragments to capture slow (outer) electrons or for slow fragments to capture fast (inner) electrons. More quantitatively, it is relatively improbable for a fragment of velocity $\simeq 4\alpha c$ to capture outer electrons which have velocities $\simeq \alpha c$, or inner electrons which have velocities $\simeq Z\alpha c$ if Z, here the atom nuclear charge, is $\geqslant 7$.

Second, we note that the capture cross section for a fragment of given effective charge decreases rapidly with the fragment velocity.[10] This is because, other things being equal, a fast fragment will be less likely than a slow fragment to capture the slower electrons of a gas atom which will be liberated with large cross sections. It will capture faster gas atom electrons better than the slow fragment, but these electrons are liberated with small cross sections. Hence, the total capture cross section will decrease with velocity.

It is of interest to compare this decrease with that recently observed in the case of protons[11,12] and with the theories of Bohr,[3] and Brinkman and Kramers.[9] The observed capture cross sections for protons in hydrogen and air decrease somewhat more steeply than our capture cross sections for fragments. Bohr estimated $\sigma_c \sim v^{-6}$, which is a stronger velocity dependence than found even in the proton experiments. The calculations of Brinkman and Kramers (giving $\sigma_c \sim v^{-12}$) are not strictly applicable to any of the above cases.

For consideration of the loss calculation it is important to note how the electronic structure of a gas atom disintegrates as a fragment passes by. To get an idea of this effect, suppose we divide the Fermi-Thomas oxygen atom into eight spherical shells, each containing one unit of charge, compute the binding force on each shell and thus the liberation radii r_{0i} for the shells. The liberation radii, so computed, for the outer six oxygen electrons in interaction with a fragment of effective charge 8.9 are successively 9.2, 5.9, 2.1, 1.2, 0.90, and $0.65a_0$, (a_0 = Bohr radius). Thus the oxygen atom begins to lose electrons already a long way, $\sim 10a_0$, from the fragment, and it loses of the order of half of its electrons in a collision with impact parameter a_0. Very few of these electrons can be captured by the fragment; most of them will simply escape.

We note that any attempt to refine these calculations in the framework of classical mechanics must be viewed with suspicion. If one attempted to localize the electron's position and follow its motion under the influence of the various forces more closely, one would imply uncertainties in the electron energy large compared to to the energy itself, and the whole correction would be spurious.

III. THEORY OF LOSS

We seek the probability for a fragment to lose an electron in a collision with a gas atom. For this problem a quantum-mechanical perturbation approach has some validity, at least if the nuclear charge of the gas atom is smaller than the effective charge of the fragment. One could consider the effect of the passing gas atom as a small perturbation of the electron wave function and calculate the probability for the electron to be knocked out of the fragment.

A difficulty in this calculation is the appropriate choice of the perturbing potential. As we have seen at the end of the last section, the gas atom becomes increasingly ionized as it approaches the fission fragment. In the approximation used in the last section, the successive ionizations occur at definite "liberation distances" from the fragment. Thus an oxgyen atom approaching a fragment of effective charge 8.9 will act like a singly charged ion between distances 9.2 and $5.9a_0$ from the fragment, like a quadruple charged ion between 1.2 and $0.9a_0$, etc. Given the impact parameter b and the velocity v, the perturbing potential due to the oxygen atom can therefore be written down as a function of time and its effect on the fragment electrons calculated by time-dependent perturbation theory.

While this calculation would be perfectly feasible, it was considered too cumbersome for the present work. A simpler method offers itself immediately. Consider first a fragment passing through hydrogen or helium. These light atoms will lose their electrons at relatively large distances from the fragment, and hence, during a

[10] The effect is somewhat mitigated in the physical case of capture, because the effective charge of a fragment will increase with velocity.

[11] H. Kanner and F. L. Ribe, Phys. Rev. **83**, 1217 (1951).

[12] H. Kanner, Phys. Rev. **84**, 1211 (1951).

close collision the fragment will see a proton or α-particle, vaguely accompanied by one or two electrons. We shall say more concerning the motion of these electrons in Sec. V. Anyway, it appears that appropriate perturbing potentials are those for a proton or α-particle.

With more complicated gas atoms the situation is not so clear. However, the consideration is simplified if we again treat the collision between gas atom and fragment electron by classical mechanics. This approach may be suggested by fairly large quantum numbers of the electron, and its justification will be discussed shortly. Because of the large binding energies of the fragment electrons, large amounts of momentum must be transferred from the gas atom to the electron to enable the electron to escape from the fragment. This is only possible classically for close collisions. Now the fragment electron is rather close to the fragment nucleus, and therefore close approach between gas atom and fragment electron automatically means close approach between atom and fragment itself. For such close approach, however, we know that the gas atom will be highly ionized. The perturbing potential at large distances and low degrees of ionization of the gas atom atom is therefore irrelevant, and we may consider the gas atom to have some high effective charge z *all* the time.

Quantitatively, we determine the effective charge z of the gas atom and the loss cross section σ simultaneously by the following consideration. For any *given* z, we can calculate the cross section for removal of a given fragment electron (i.e., one of given binding energy). Because we are now dealing with a perturbing Coulomb potential, this cross section is easily calculated and is essentially the same in classical and quantum mechanics; let us call it πl^2. Then, using a classical picture, essentially all passages with gas atom-electron impact parameters less than l will lead to ionization, those greater than l will not. We shall now choose z in such a way that the electric field at a distance l from the nucleus of the gas atom is just ze/l^2. In other words, z shall be an effective charge at the distance l from the gas atom nucleus, while at the same time πl^2 is the cross section for removal of the fragment electron by a Coulomb field of charge z.

If l and z are simultaneously determined in the manner described, it is found that z corresponds to about the highest degree of ionization which the gas atom can reach, barring direct hits on the fragment. An electron which passes at distance l from the gas atom will not appreciably penetrate the remaining electronic structure of the atom, hence will be perturbed by what is very nearly a pure Coulomb field. Electrons that pass even closer will enter regions of the "gas atom" where the field is stronger than assumed, but they will be lost in either picture.

The question arises as to the validity of these classical arguments. For its escape to be possible, a fragment electron must be given a large amount of energy. This means that a correspondingly large uncertainty in the initial electron momentum may be tolerated and that we can therefore localize the electron to a region small compared with, or of the order of, that given by relevant impact parameters without implying a prohibitively large momentum uncertainty. Interactions which produce loss will correspond to impact parameters of the order of $2Z_e^2/mv^2$, where $Z \leqslant$ the nuclear charge of the gas atom. For oxygen or heavier gases this will be of the order a_0, and the classical approach will have about as much validity as in the case of capture.

We now turn to the quantitative calculation of the loss cross section. Let $\hbar\mathbf{k}_e$ denote the initial momentum of the fragment electron relative to the fragment nucleus and $\hbar\mathbf{k}_m$ the momentum of an electron stationary in the fragment relative to the gas atom. Then $\hbar\mathbf{k}=\hbar(\mathbf{k}_m+\mathbf{k}_e)$ is the initial momentum of the fragment electron relative to the gas atom. If $\hbar\mathbf{k}_f$ is the final momentum of the electron relative to the gas atom, then $k_f=k$, and the momentum change $\hbar q$ will be given by $2\hbar k\sin(\theta/2)$, where θ is the angle of scattering. The final momentum relative to the fragment is $\hbar\mathbf{k}^1=\hbar\mathbf{k}_f-\hbar\mathbf{k}_m$. Now let $\hbar k_0$ be that minimum value of the momentum which the electron in question must have relative to the fragment in order to be free. Then the condition for ionization or loss of this electron which must be imposed on its final momentum is $k^1 \geqslant k_0$. All these momenta are shown in a k space diagram in Fig. 6.

For a Coulomb potential of strength z, the differential scattering cross section is

$$d\sigma/d\Omega=(2mz_e^2/\hbar^2)1/q^4. \tag{2}$$

To find the loss cross section for an electron characterized by $(\mathbf{k}_e, k_0)$ we must integrate $d\sigma$ for all $k^1 \geqslant k_0$. This integration is outlined in the Appendix. We may then calculate the average loss cross section as a function of the distance r of the fragment electron from the fragment nucleus. From the Fermi-Thomas model of the fragment we compute three parameters as a function of r, namely, (1) $k_0(r)$, (2) $k_a(r)$, where $\hbar k_a(r)$ is the maximum value of the initial momentum which an electron at r can have, i.e., the momentum of an electron at the Fermi level, and (3) $D(r)$, where $D(r)dr$ is the number of fragment electrons between r and $r+dr$.

The loss cross section per electron as a function of r is shown in the Appendix to be

Case I.—$(2k_m-k_0 \leqslant k_a)$

$$\sigma_L(k_m, k_0(r), k_a(r)) = \frac{3\pi z^2}{4a_0^2k_a^3k_m}\left[\left(\frac{2(k_0^2+k_m^2)}{k_0^2-k_a^2}-1\right)\ln\left(\frac{k_m+k_a}{k_0-k_m}\right) + \frac{k_m}{k_m+k_a}-\frac{2k_m}{k_0-k_a}-\frac{2k_m-k_0}{k_0-k_m}\right]. \tag{3a}$$

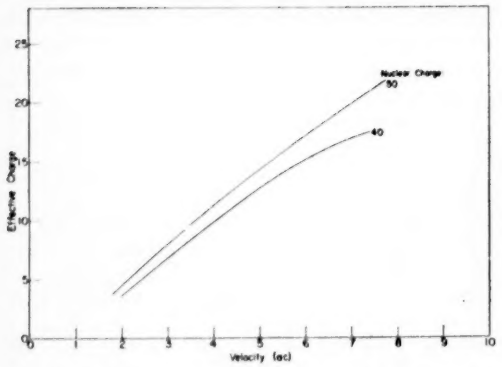

FIG. 2. Effective charges of fragments of nuclear charge 40e and 50e passing through low density oxygen, as functions of fragment velocity.

Case II.—$(2k_m - k_0 \gtrsim k_a)$

$$\sigma_L(k_m, k_0(r), k_a(r)) = \frac{3\pi z^2}{4a_0^2 k_a^3 k_m}\left[\left(\frac{2(k_m^2+k_0^2)}{k_0^2-k_a^2}-1\right)\ln\left(\frac{k_m+k_a}{k_m-k_a}\right) - k_a k_m\left[\frac{4}{k_0^2-k_a^2}+\frac{2}{k_m^2-k_a^2}\right]\right]. \quad (3b)$$

In addition, $\sigma_L = 0$ if $2k_m - k_0 < -k$.

Finally, the total cross section for loss by the fragment is obtained by integrating the cross section per electron multiplied by the electron density over the fragment volume,

$$\sigma(k_m, z) = \int_0^{r_{\max}} \sigma_L(k_m, k_0(r), k_a(r)) D(r) dr. \quad (4)$$

The integrand of Eq. (4) has a fairly pronounced maximum. This is because $D(r)$ is very small for r near $r_{\max}$ and σ_L decreases rapidly as r becomes smaller. The charge of the gas atom, z of Eqs. (3), is determined by demanding that the loss cross section per electron at the maximum of the integrand in (4) is equal to the geometrical cross-sectional area of that region of the gas atom within which there are one nucleus of charge Z and $Z-z$ electrons. As remarked earlier, the value of z thus obtained is in each case about equal to the number of gas atom electrons which have been liberated under the influence of the fragment, at the time when the gas atom and fragment are separated by a distance about equal to the fragment radius. We may essentially conclude that a fragment electron is with high probability removed from the fragment, if and only if it is "hit" by the gas atom, i.e., if the gas atom passes close enough to the fragment so that the fragment electron penetrates the remaining atom electronic structure.

Using Eqs. (3), (4) and the above criterion for determining z, we have computed loss cross sections for various fragments in oxygen. Some results are shown in Fig. 1. The values of effective z for oxygen which are obtained vary from about 2 with fragments of effective charge about 5 to about 6 for fragments of effective charge approximately 20. Loss cross sections have also been computed for fragments in argon, and these are found to be larger than those for oxygen by a factor which for effective fragment charge $\gtrsim 8$ is about 2.2 and is smaller for smaller fragment effective charge.

It is worth noting that the loss cross section for a *fixed* effective charge increases with fragment velocity in the region considered. This is apparently contrary to observations with protons[12,13] and the Born approximation, where σ_L decreases with velocity. However, since in reality the fragment effective charge increases with velocity, the loss cross section for a fragment will actually decrease with increasing fragment velocity.

IV. THE EFFECTIVE CHARGE

If we know the capture and loss cross sections as functions of fragment charge and velocity, it is a simple matter to find the most probable number of electrons in a fragment as a function of its velocity. We shall see that the most probable number is essentially the average number, and hence from the intersections of the capture and loss curves in Fig. 1 we may obtain effective charge as a function of velocity and nuclear charge. The effective charges of fragments of nuclear charges 40 and 50 in oxygen are plotted as functions of the velocity in Fig. 2.

Our results may be compared with previous calculations, which are summarized in reference 6. Bohr estimated the effective charge z of a fragment of nuclear charge Z to be $z = Z^{\frac{1}{3}}v$, where v is measured in units of αc. We see that Bohr's values of effective charge are greater than ours by factors of 1.30 or more. The effective charges calculated in (5) and (6), by Knipp, Teller, and Brunings, are greater than ours by the order of at least 30 percent for fragment velocities greater than $3\alpha c$, but are in better agreement with ours for smaller velocities. It appears that their second choice of "critical electron velocity" gives much better (i.e., lower) values of the effective charge for high fragment velocities. Our results are in rather close agreement (of the order of 10 percent) with those of Lamb.[4]

The effective charges of fragments in other gases than oxygen but of comparable atomic number are about the same as those in oxygen. Thus our calculations indicate that the effective charge in argon will be about 2 percent larger than in oxygen when the effective charge >8; smaller for lower values of the effective charge. We may conclude that for a large range of atomic weights of stopping gases, the effective charge is essentially independent of the stopping gas.

From our cross sections, we may deduce the prob-

[13] J. H. Montague, Phys. Rev. **81**, 1026 (1951).

ability for a fragment of velocity v and nuclear charge 40 or 50 to have any arbitrary effective charge. For any definite velocity and nuclear charge of our fragment, we have a most probable value of fragment charge, call it z_0, such that $\sigma_c(z_0)\simeq\sigma_L(z_0)$, where $\sigma_c(z)$ is the cross section for capture of an electron by a fragment of effective charge z, and $\sigma_L(z)$ is the cross section for loss of an electron by a fragment of effective charge z. If $N(z)$ is the number of fragments having effective charge z, the equilibrium distribution of $N(z)$ will be such that the probability of going from z to $z+1$ will equal the probability of going from $z+1$ to z, or

$$N(z)\sigma_L(z)=N(z+1)\sigma_c(z+1). \tag{5}$$

To the extent to which $\sigma_c(z)$ and $\sigma_L(z)$ may be represented by curves of exponential form, $N(z)$ will have a Gaussian form about z_0.[14] Thus, if we set

$$\sigma_L(z)=\sigma_{L0}\exp[\beta(z-z_0)],$$
$$\sigma_c(z)=\sigma_{c0}\exp[\alpha(z-z_0)],$$

we find

$$N(z)=N(z_0)\exp[\tfrac{1}{2}(\beta-\alpha)(z-z_0)^2], \tag{6}$$

provided we set $\sigma_{L0}=\sigma_{c0}\exp[\frac{1}{2}(\alpha+\beta)]$.

From our cross sections and (5) we may also compute $N(z)$, and this has been done for a fragment of nuclear charge 40 and velocity $4.75c$. The results are indicated in Fig. 3 and compared with the Gaussian of Eq. (6) which is seen to be a good fit. We find that most probable, average, and rms values of z agree to within about 2 percent. It appears that for a wide range of fragments the equilibrium distribution $N(z)$ is roughly a Gaussian with width at half-maximum equal to one-third the most probable value z_0.

V. HYDROGEN AND HELIUM

The cross section for loss of an electron by a fragment interacting with a hydrogen atom presents no new problems, for this may be calculated using Born approximation with the perturbing potential of a bare proton. The results of Sec. III may be taken over with the z of the gas atom put equal to 1.

To obtain a simple picture of *capture* in hydrogen, we shall start by adapting our previous treatment of capture from a many electron atom. That is, we retain the notion that before liberation the electron moves in an unperturbed fashion, while after liberation it is aware only of the existence of the fragment. However, we take into account the velocity distribution of the hydrogen electron in detail instead of using the Fermi distribution. The probability that an electron in the hydrogen ground state has velocity between v_e and v_e+dv_e is

$$P(v_e)dv_e=\frac{32}{\pi}\frac{v_e^2}{(1+v_e^2)^4}dv_e. \tag{7}$$

[14] This Gaussian was suggested by Niels Bohr.

We then may multiply $P(v_e)dv_e$ by Eq. (1) and integrate over electron velocities to get a total capture cross section in terms of the liberation distance.

The velocity distribution for large v_e behaves as v_e^{-6}. This makes it very difficult for a fragment of high velocity to capture a hydrogen electron. A hydrogen electron will be liberated at a large distance from the fragment and must have a high velocity relative to its own nucleus, the proton, for capture to be possible; but such high velocities are rare.

To estimate a liberation radius one may extend some considerations introduced by Lamb.[4] By considering the saddle in the potential given by a fragment and a proton, it is easy to show that capture of a hydrogen electron is quite possible for proton-fragment separations of about $(2+4\sqrt{z})a_0$. As a liberation radius, however, we wish a separation for which it is probable that the electron will escape from the proton to the fragment in the order of 3×10^{-16} sec. By estimating barrier transparencies, solid angles subtended by the saddle of escape, and times required for an electron to get through the saddle, one finds that the liberation radius is of the order of $(2\sqrt{z})a_0$.

Fortunately, the total capture cross section is insensitive to the liberation radius. For example, a variation of 25 percent in the liberation radius produces only about a 2 percent change in the effective charge of a fragment.

The cursory character of these estimates is all too apparent, but we might hope that they would give the capture cross section within a factor of 2 or so, and we have used them to compute effective charges in hydrogen. The results are indicated in Fig. 4. The curves

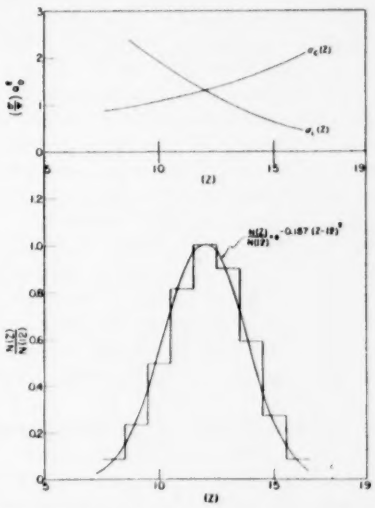

FIG. 3. Distribution of fragment charges about the most probable value, which is 12 for a fragment of nuclear charge 40 and velocity $4.75\alpha c$ in low density oxygen. The capture and loss cross sections are shown above.

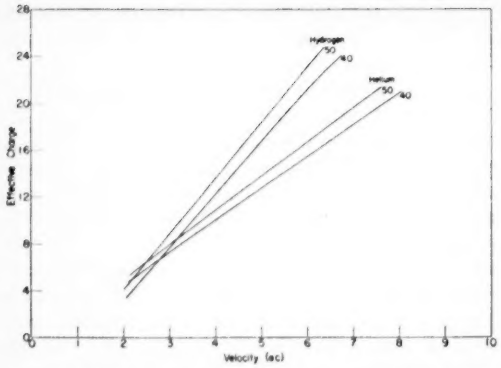

FIG. 4. Effective charges of fragments of nuclear charge $40e$ and $50e$ passing through low density hydrogen and helium; as functions of fragment velocity.

are considerably steeper, straighter, and higher than for fragments in oxygen. This is just a reflection of the difficulty which a fragment, especially a fast one, has in capturing a hydrogen electron. The curve is also, as will be seen in Sec. VI, in marked disagreement with experiment, being too high at least for high fragment velocities.

It may be that because of the smallness of the capture and loss cross sections, new effects will show up in the interactions of fragments with hydrogen atoms. In particular, the capture of liberated electrons through inelastic collisions with the fragment may be of importance. Thus a liberated electron may pass through the outer regions of a fragment and interact with a fragment electron so that in the final state (a) both electrons have been raised to the continuum and are free, (b) one electron is free and the other bound, or (c) both electrons are bound in the fragment. The first process would lead to loss but should be much smaller than proton-induced loss because of the low kinetic energy of the liberated hydrogen electron. The second process does not contribute to net capture or loss. The cross section for a capturing collision of type (c) may be a substantial fraction of the cross section for proton induced loss and thus lead to a large increase in the total capture cross section and a considerable lowering of the effective charge. To obtain a good idea of this effect one would like to consider the interaction between an electron bound in the fragment and a free electron and to calculate the probabilities of transitions to final states in which both electrons are bound. A time-dependent perturbation calculation would seem appropriate.

The above interactions will be of considerably less importance in capture from heavier gases. This is because in a heavier gas the regular capture and loss cross sections will be larger by about the square of the number of electrons liberated from the gas atom, while the cross section for inelastic capture of liberated electrons will go only linearly with this quantity.

We have also considered the possibility of capture of a liberated electron with the emission of radiation. This appears improbable. The natural cross section for measurement of bremsstrahlung is $z^2\alpha^5 a_0^2$. Even for fragment nuclear charge of the order of 50 and photon energies of the order of 100 ev, the relevant cross sections appear too small.

The capture of hydrogen electrons may be somewhat expedited by the diatomic nature of hydrogen. To estimate this effect we may consider the momentum distribution of an electron in a hydrogen molecule or molecular ion to be that of an electron around a "proton" of charge $1.2e$ [*viz.*, H. A. Bethe, *Handbuch der Physik* (J. Springer, Berlin), Vol. 24—1]. This considerably enhances the probability of capture but lowers the effective charge *vs* velocity curve by only about 5 percent.

These considerations have been applied to helium, taking both electrons in $1s$ states and ignoring the electron-electron interaction. The effective charge curve, Fig. 4, is much lower because high internal velocities are much more probable for helium electrons.

VI. COMPARISON WITH EXPERIMENT

To be able to compare our calculations with experimental values of the effective charge, we need to know the properties of fragments from the slow-neutron fission of U^{235}. In particular, we are interested in most probable initial energies, masses, and nuclear charges, and also the expected variations in these quantities.

Leachman[15] has recently completed time-of-flight measurements which give the most probable velocities of U^{235} fragments as $6.49\alpha c$ and $4.42\alpha c$ for light and heavy fragments. This gives most probable masses of about 96 and 140 and most probable energies of 100 and 68 Mev.

These energies are considerably higher than those which have been inferred from measurements of the total ionization produced by fragments.[16–19] For example, Brunton and Hanna obtained 94.5 and 60.2 Mev. However, in converting total ionization to energy loss, it had been assumed that ω, the number of electron volts per ion pair, is the same for fragments as for α particles. Knipp *et al.*[20,21] have recently pointed out that many of the recoiling gas atoms have low ionization efficiencies and that ω should be larger for fragments than α-particles. Agreement between the time-of-flight and ionization measurements is obtained if we assume the energy-ionization ratios ω of the most probable

[15] R. B. Leachman, Phys. Rev. **83**, 235 (1951), and private communication.
[16] W. Jentschke and F. Prankl, Z. Physik **119**, 696 (1942).
[17] Flammersfeld, Jensen, and Gentner, Z. Physik **120**, 450 (1943).
[18] M. Deutsch and M. Ramsey, U. S. Atomic Energy Commission Report MDDC-945, 1945 (unpublished).
[19] D. C. Brunton and G. C. Hanna, Can. J. Research **28**, 190 (1950).
[20] Knipp, Leachman, and Ling, Phys. Rev. **80**, 478 (1950).
[21] J. K. Knipp and R. C. Ling, Phys. Rev. **82**, 30 (1951).

light and heavy fragments to exceed ω of uranium α particles by factors of about 1.05 and 1.12, respectively. Leachman's higher energies appear to give better agreement with measured values of the total energy of fission[22] and fragment masses obtained from chemical analysis.[23]

The ionization measurements show that 15 percent variations in energy and mass are very common for both fragments.

The initial effective charges of fragments in low pressure gases have been measured by Lassen.[24] The fragments are deflected in the magnetic field of the Copenhagen cyclotron, and the effective charge is determined by combining the measured value of $H\rho$ with an estimate of the fragment momentum. When the deflecting chamber is filled with oxygen at a low pressure ($\sim$1 mm Hg), the effective charges of the light and heavy fragments are about $16.1\pm\sim0.5$ and $14.8\pm\sim0.5$, respectively. These numbers are somewhat larger than those given by Lassen himself since our value of the momentum exceeds his by about 6 percent. The corresponding numbers from our theory (Fig. 2) are about 15.5 and 13.5. In hydrogen the experimental values are about 16.7 and 13.3, while in helium they are about 14.9 and 12.2. The calculated values, from Fig. 4, are 22.5 and 16 for hydrogen and 16.5 and 12.5 for helium. Taking the molecular effect into account for hydrogen, we get about 21 and 15, so that a marked discrepancy remains. Theory and experiment agree that effective charges are higher in hydrogen than in helium, and in both gases there is a greater difference between the charges of the light and the heavy fragment than in heavier gases, the spread being greatest in hydrogen.

When the region of magnetic deflection is evacuated, it becomes possible to measure effective charges in the solid from which the fragments enter the vacuum. Lassen finds that initial effective charges in solids are about 30 percent higher than in gases. Bohr has noted that this is no doubt due to competition between the radiative decay of excited electronic states in the fragment and removal of the excited electrons by collision. It is observed that for fragments coming from solids, the heavy fragment has more effective charge than the light, contrary to the observation and theory in gases for initial fragment velocities. In general, the effective charge of a fragment increases with the pressure of the substance through which it passes.

Lassen also observes a wide distribution in value of $H\rho$ for both fragments emerging from solids. This should be and is roughly as in Fig. 3.

As a gas is introduced gradually into the deflection chamber, the fragments capture electrons from the gas atoms more or less rapidly depending on the gas pressure. It is of interest to calculate the average values of the effective charges of the most probable fragments as functions of the gas pressure. We take over the experimental values of the effective charges in solids and calculate the average values for the most probable fragments emerging from uranium into argon. Results are indicated in Fig. 5 for a path length of 20 cm and initial charges 21 and 23. There is general agreement with experiment. In particular, the equilibrium charge is approached much more rapidly by the heavy fragment.

Lassen[25] has also measured the specific ionization produced by a fragment in a gas as a function of its residual range. One may obtain information on the variation of effective charge with velocity from these measurements provided one has a theory for the specific ionization produced by such large charges. Such a theory has been developed by Bohr.[3] Using this theory and assuming that the fragment acts as a point charge, one calculates from the measured specific ionization an initial charge of about 22. The measurements were carried out at pressures between $\frac{1}{2}$ and $\frac{1}{10}$ atmosphere, but even admitting some increase of the effective charge with pressure, there is substantial disagreement with the magnetic deflection measurements and our predictions. However, if one multiplies all the charge values as obtained from specific ionization by a constant so as to give the initial effective charges in agreement with deflection experiments, one finds general agreement of the effective charge *vs* velocity with our curves of Fig. 2.

When we take into account the compound nature of the fragment, somewhat better agreement is produced. An actual fragment will lose energy more rapidly than a point charge equal to the effective charge because the actual field, which is stronger than the point Coulomb field within the fragment, will produce more ionization

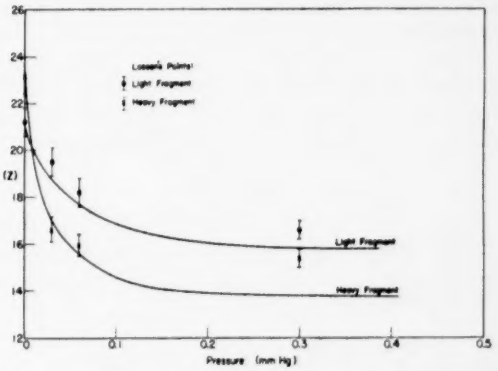

FIG. 5. Effective charges of most probable fission fragments emerging from uranium into low pressure argon as functions of pressure—measurements of Lassen described in reference 24.

[22] M. C. Henderson, Phys. Rev. **58**, 774 (1940).
[23] Plutonium Project, Revs. Modern Phys. **18**, 513 (1946).
[24] N. O. Lassen, Kgl. Danske Videnskab Selskab, Mat.-fys. Medd. **26**, No. 5 (1951). This article contains references to Lassen's several earlier papers on the subject.
[25] N. O. Lassen, Kgl. Danske Videnskab Selskab, Mat.-fys. Medd. **25**. No. 11 (1949).

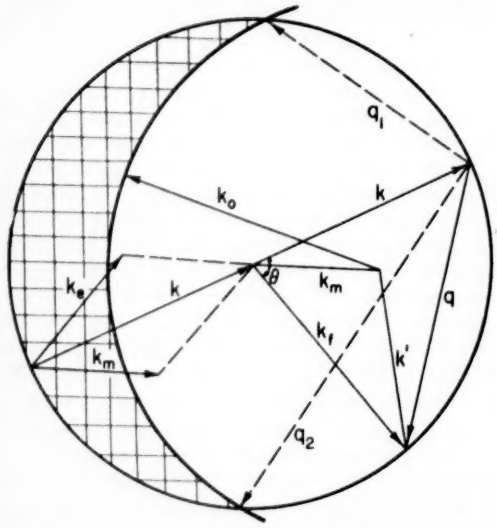

FIG. 6. Momenta used in the loss calculation: $\hbar k_e$ = initial electron momentum relative to fragment nucleus. $\hbar k_m$ = momentum of electron stationary in fragment relative to gas atom. $\hbar k$ = initial electron momentum relative to gas atom. $\hbar k_f$ = final electron momentum relative to gas atom. $\hbar q$ = momentum change, $2k\sin(\theta/2)$. $\hbar k_0$ = Minimum momentum relative to fragment which electron must have to be free. The integration is carried out over the crosshatched surface of the sphere. For $q \geq q_2$, loss is certain. For $q \leq q_1$, loss is impossible. For $q_2 > q > q_1$, there is a probability of loss between zero and one.

of the gas. This may add about 5 Mev per cm. Perhaps the most important new source of energy loss will arise from loss of electrons by the fragment itself. This is analagous to the charge exchange energy loss, recently discussed by Allison *et al.* for the passage of protons through hydrogen. It may amount to the order of 8–10 Mev per cm for initial fragments. Nevertheless, these two effects do not suffice to establish good agreemnnt between the specific ionization and magnetic deflection experiments.

It is a pleasure to thank H. A. Bethe for many valuable discussions. The author is also indebted to Niels Bohr, N. O. Lassen, and R. B. Leachman for communicating results in advance of publication.

APPENDIX

To get from Eq. (2) to Eq. (3), we must evaluate $\int q^{-4}d\Omega$ over all scattering angles and k consistent with fixed k_e, and k_m, and $(k^1)^2 \geq k_0^2$. (The k's are explained in Fig. 6.) We may write

$$Q = \int \frac{d\Omega}{q^4} = \frac{1}{k^2}\int_0^{2\pi} d\phi \int_{q_{\min}(\phi)}^{2k} \frac{dq}{q^3} = \frac{1}{2k^2}\int_0^{2\pi} d\phi \left(\frac{1}{q_{\min}^2(\phi)} - \frac{1}{4k^2}\right), \tag{A1}$$

where ϕ is the azimuthal scattering angle. We wish to express $q_{\min}(\phi)$ in terms of k_e, k_m, k, and ϕ. To do this we make use of the following equations:

$$(k^1)^2 = q^2 + k_e^2 + 2\mathbf{k}_e\cdot\mathbf{q},$$
$$\mathbf{k}_e\cdot\mathbf{q} = k_e q(\cos\theta_1\cos\theta_2 + \sin\theta_1\sin\theta_2\cos\phi), \tag{A2}$$
$$k_f^2 - k^2 - q^2 = 2kq\cos\theta_2, \quad k_f = k,$$

where θ_1 is the angle between $\mathbf{k}_e$ and $\mathbf{k}$, and θ_2 is the angle between $\mathbf{q}$ and $\mathbf{k}$. It follows that

$$(k^1)^2 = q^2 + k_e^2 + (k_e q/k)[-q\cos\theta_1 + (4k^2 - q^2)^{\frac{1}{2}}\sin\theta_1\cos\phi]. \tag{A3}$$

When $q = q_{\min}(\phi)$, $(k^1)^2 = k_0^2$, so that from Eq. (A3) we find

$$\frac{1}{q_{\min}^2} = \frac{k_e^2}{2k^2(k_0^2 - k_e^2)^2}\left[\frac{2k}{k_e}(k_0^2 - k_e^2)\left(-\cos\theta + \frac{k}{k_e}\right) + 4k^2\sin^2\theta\cos^2\phi\right] + b\cos\phi(e + f\cos^2\phi)^{\frac{1}{2}}, \tag{A4}$$

where b, e, and f are constants independent of ϕ. It is important that simply $\cos\phi$ multiplies the radical for this term gives zero upon integration. If we had taken $|(\cos^2\phi)^{\frac{1}{2}}|$, $q_{\min}^2(\phi)$ would not depend on the sign of ϕ, which is incorrect. When we express $\cos\theta_1$ in terms of k_e, k_m, and k, it follows that

$$Q = \pi\left[-\frac{1}{4(k_0^2 - k_e^2)^2} + \frac{1}{k^2}\left\{\frac{1}{2(k_0^2 - k_e^2)} + \frac{k_e^2 + k_m^2}{2(k_0^2 - k_e^2)^2}\right\} + \frac{1}{k^4}\left\{\frac{k_m^2 - k_e^2}{2(k_0^2 - k_e^2)} - \frac{k_e^4 + k_m^4 - 2k_e^2k_m^2}{4(k_0^2 - k_e^2)^2} - \frac{1}{4}\right\}\right]. \tag{A5}$$

To obtain the loss cross section per electron which is at distance r from the fragment nucleus, we must average Q over all velocities which the electron may have; these will be distributed isotropically and weighted proportional to $k_e^2dk_e$ up to a maximum value k_a. The average may be written

$$\frac{\sigma_L(k_m, k_a, k_0)}{4z^2/a_0^2} = \int\int Q\frac{k_e k}{k_m}dkdk_e \Big/ \left[2\int_0^{k_a} k_e^2 dk_e\right], \tag{A6}$$

where $\sigma(k_m, k_a, k_0)$ is the loss cross section per electron.

The limits on k and k_e must be considered with some care. We must have $k_m + k_e \geq k \geq |k_m - k_e|$, and for ionization to be possible we must have $k \geq k_0 - k_m$. It follows that there will be three cases involving different limits of integration, the first for $2k_m - k_0 < 0$, the second for $0 \leq 2k_m - k_0 \leq k_a$, and the third for $2k_m - k_0 > k_a$. However, it can be proved that the first two cases may be covered by the same formula. The proof makes use of Q being an even function of k_e. $\sigma_L = 0$, if $2k_m - k_0 < -k_a$.

By elementary if tedious integration we find that for

Case I.—$(2k_m - k_0 \leqslant k_a)$

$$\sigma_L(k_m, k_a, k_0) = A\int_{k_0-2k_m}^{k_a} k_e dk_e \int_{k_0-k_m}^{k_m+k_e} kQdk$$

$$= A\pi\left[\ln\left(\frac{k_m+k_a}{k_0-k_m}\right)\left[\frac{k_0^2+k_m^2}{4(k_0^2-k_a^2)}-\frac{1}{8}\right]\right.$$

$$\left.+\frac{1}{8}\frac{k_m}{k_m+k_a}-\frac{k_m}{4(k_0-k_a)}-\frac{1}{8}\frac{2k_m-k_0}{k_0-k_m}\right]. \quad \text{(A7)}$$

Case II.—$(2k_m - k_0 \geqslant k_a)$

$$\sigma_L(k_m, k_a, k_0) = A\int_0^{k_a} k_e dk_e \int_{k_m-k_e}^{k_m+k_e} kQdk$$

$$= \frac{A\pi}{4}\ln\frac{k_m+k_a}{k_m-k_a}\left\{\frac{k_m^2+k_0^2}{k_0^2-k_a^2}-\frac{1}{2}\right\}$$

$$-\frac{\pi k_a k_m}{2}\left\{\frac{1}{k_0^2-k_a^2}+\frac{1}{2(k_m^2-k_a^2)}\right\}, \quad \text{(A8)}$$

where $A = 6z^2/a_0^2k_a^3k_m$. This completes the derivation of Eq. (3).

PHYSICAL REVIEW VOLUME 90, NUMBER 4 MAY 15, 1953

Radiations from Selenium[75]

ERLING N. JENSEN, L. JACKSON LASLETT, DON S. MARTIN, JR.,
FRANCIS J. HUGHES, AND WILLIAM W. PRATT*
Institute for Atomic Research and Departments of Physics and Chemistry, Iowa State College, Ames, Iowa†

(Received January 23, 1953)

The radiations from 125-day Se^{75} have been examined by means of a thin lens spectrometer and absorption-coincidence techniques. Se^{75} was found to decay to As^{75} by orbital electron capture. The energies of ten transitions (0.066_8, 0.076_8, 0.098_3, 0.124_1, 0.138_4, 0.203_2, 0.268_8, 0.281_4, 0.307_8, and 0.405_6 Mev) were observed in the photoelectron and internal conversion spectra determined with the spectrometer. A decay scheme is proposed on the basis of the absorption-coincidence and spectrometer data. The multipole order of the 98.3-kev transition is discussed.

I. INTRODUCTION

A NUMBER of investigators[1–8] have examined the radiations from 125-day Se^{75}. From lead absorption measurements Burgus *et al.*[2] report two gamma-rays having energies of 0.18 and 0.335 Mev; Friedlander *et al.*[3] found a single gamma-ray having an energy of 0.4 Mev; Cowart *et al.*[5] report two gamma-rays with energies of 0.22 and 0.43 Mev; and Gest and Glendenin[6] found two gamma-rays having energies of 0.18 and 0.35 Mev. The three latter groups found x-rays corresponding to the K lines from arsenic, indicating that Se^{75} decays to As^{75} by orbital electron capture.

Ter-Pogossian *et al.*[7] examined the photoelectron spectra of Se^{75}, as obtained from lead and uranium radiators, in a 180° spectrometer. They report six, and possibly seven, gamma-rays with energies 0.076, 0.099(?), 0.123, 0.137, 0.267, 0.283, and 0.405 Mev. They did not obtain an internal conversion spectrum. Cork *et al.*[8] have examined the internal conversion spectrum of Se^{75} in spectrometers using photographic detection techniques. They report eleven gamma-rays with energies 0.0247, 0.0662, 0.0808, 0.0968, 0.1212, 0.1362, 0.1988, 0.2652, 0.2801, 0.3050, and 0.4019 Mev. They did not obtain a photoelectron spectrum.

DeBenedetti and McGowan[9] made a search for a metastable state in As^{75}, by means of delayed coincidences, and obtained a negative result in the range 10^{-6} to 10^{-3} sec.

Reports[10] have been made at various times on the decay and transition energies of Se^{75}, as determined

* Now at State University of Iowa, Iowa City, Iowa.

† Contribution from the Institute for Atomic Research and departments of physics and chemistry, Iowa State College, Ames, Iowa. Work was performed in the Ames Laboratory of the U. S. Atomic Energy Commission.

[1] Kent, Cork, and Wadey, Phys. Rev. **61**, 389 (1952).

[2] Burgus, Edwards, Gest, Stanley, and Williams, Plutonium Project Report CN-2839, p. 9 (June, 1945); cited by Seaborg and Perlman, Revs. Modern Phys. **20**, 585 (1948).

[3] Friedlander, Seren, and Turkel, Phys. Rev. **72**, 23, 888 (1947).

[4] H. H. Hopkins, Jr., and B. B. Cunningham, Phys. Rev. **73**, 1406 (1948).

[5] Cowart, Pool, McCown, and Woodward, Phys. Rev. **73**, 1454 (1948).

[6] H. Gest and L. E. Glendenin, Radiochemical Studies: The Fission Products (McGraw-Hill Book Company, Inc., New York, 1951), paper 327, National Nuclear Energy Series, Plutonium Project Record, Vol. 9, Div. IV.

[7] Ter-Pogossian, Robinson, and Cook, Phys. Rev. **75**, 995 (1949).

[8] Cork, Rutledge, Branyan, Stoddard, and Le Blanc, Phys. Rev. **79**, 889 (1950).

[9] S. DeBenedetti and F. K. McGowan, Phys. Rev. **74**, 728 (1948).

[10] Jensen, Laslett, and Pratt, U. S. Atomic Energy Commission Report AECD-1836, 1948; E. N. Jensen, Atomic Energy Commission Report AECD-2399, 1948; Progress Report in Physics, Iowa State College, ISC-46, 1949 (unpublished).

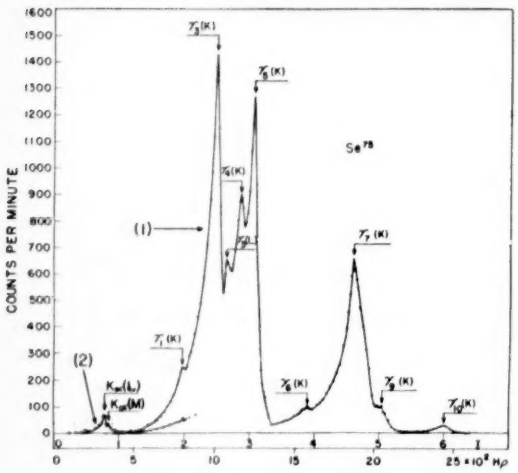

FIG. 1. Internal conversion spectrum of Se^{75}. Curves (1) and (2) were obtained with different counters. Curve (2) was determined from the same source as curve (1), but was obtained 2.3 half-lives later.

with a thin lens spectrometer. Nearly all of the transition energies so determined have been communicated privately to other workers and have subsequently been cited in several publications.[7,11,12] It is the purpose of this paper to present directly the evidence obtained here for the transition energies and decay scheme of Se^{75}.

The radioactive Se^{75} used in this investigation was produced by neutron bombardment of the metal in the Oak Ridge pile. The radiations were examined with a thin lens spectrometer[13] before it was modified to incorporate ring focusing.[14] The spectrometer was calibrated by means of the F conversion line of ThB and the annihilation radiation from Zn^{65}. All transition energies were calculated from the maximum counting rate of the respective lines, with corrections applied for the earth's magnetic field, the surface density of the source of electrons, and the resolution of the spectrometer.[13]

II. INTERNAL CONVERSION SPECTRUM

The source was mounted on 0.00025 inch aluminum which in turn was fastened to a Lucite holder. The surface density of the source was about 5 mg/cm². Such a thick source is of no great disadvantage in determining transition energies, since a correction can be made to take into account the surface density. There is a distinct advantage in that the counting rates are greatly increased, which enables the weaker transitions to be detected more readily.

The internal conversion spectrum of Se^{75} is shown in Fig. 1. Curve 1 was obtained with a Geiger counter having a Formvar window with a surface density of about 0.3 mg/cm². The pressure in the counter was 10 cm of mercury. Curve 2 was obtained from the same source as that used for curve 1, but was determined 286 days (2.3 half-lives) later than curve 1 and with a Geiger counter having a window of Formvar with a surface density of about 27 μg/cm². This window was supported between metal grids containing holes 0.040 inch in diameter and spaced 0.048 inch from center to center. The counter mixture was 33 percent alcohol and 67 percent argon, maintained at a pressure of 1.8 cm of mercury. For the curves shown in Fig. 1 the resolution of the spectrometer was 2.1 percent (half-width).

Curve 1 of Fig. 1 was redetermined 87 days later and, within experimental error, the intensities of all conversion electrons were found to have decreased by the same factor, indicating that the internal conversion lines shown in Fig. 1 are from the same activity.

It is apparent from Fig. 1 that no beta-rays are observed in the decay of Se^{75}. Furthermore the peaks labeled $K_\alpha(L)$ and $K_\alpha(M)$ are presumably attributable to Auger electrons. The corrected electron energy of $K_\alpha(L)$ is calculated to be 9.03 kev. The addition of the L binding energy of arsenic gives a value of 10.56±0.10 kev. This is in good agreement with the $K_{\alpha 1}$ and $K_{\alpha 2}$ values of 10.54 and 10.51 kev, respectively, for the As

TABLE I. Transition energies of Se^{75}.

Transition	Conversion shell	Energy Mev	Relative weight	Average energy Mev
1	As(K)	0.0666	2	0.066_6
2	Pb(L)	0.0765	3	
	Pb(M)	0.0768	3	0.076_6
3	As(K)	0.0987	10	
	As(L)	0.0968	3	0.098_3
4	As(K)	0.1239	5	
	Pb(K)	0.1216	3	
	Pb(L)	0.1271	3	0.124_1
5	As(K)	0.1384	10	
	Pb(K)	0.1366	10	
	Pb(L)	0.1399	10	
	Pb(M)	0.1397	3	0.138_4
6	As(K)	0.2032	3	0.203_2
7	As(K)	0.2688	10	
	Pb(K)	0.2677	10	
	Pb(L)	0.2700	10	0.268_8
8	Pb(K)	0.2814	5	0.281_4
9	As(K)	0.3078	3	0.307_8
10	As(K)	0.4052	5	
	Pb(K)	0.4029	10	
	Pb(L)	0.4070	10	0.405_0

[11] G. T. Seaborg and I. Perlman, Revs. Modern Phys. **20**, 585 (1948).
[12] *Nuclear Data*, National Bureau of Standards Circular 499 (1950).
[13] Jensen, Laslett, and Pratt, Phys. Rev. **75**, 458 (1949).
[14] Pratt, Boley, and Nichols, Rev. Sci. Instr. **22**, 92 (1951); Keller, Koenigsberg, and Paskin, Rev. Sci. Instr. **21**, 713 (1950).

x-rays.[15] It thus appears that the spectral lines designated $K_\alpha(L)$ and $K_\alpha(M)$ may be attributed to Auger electrons ejected from arsenic, following orbital electron capture in Se^{75} and possible subsequent internal conversion.

Stokes[16] has measured the x-rays emitted from the decay of Se^{75} by means of a Cauchois bent crystal spectrograph and finds that the x-rays of As are present and that the x-rays of Se are not observed. Our data on the Auger electrons are thus in agreement with the findings of Stokes.

The lines shown in Fig. 1 can be ascribed to eight nuclear transitions. The energies of these transitions, as determined from the data given in Fig. 1, are included in Table I and designated as conversions in As. The probable error in the energies is estimated to be less than one percent.

III. PHOTOELECTRON SPECTRUM

The photoelectron spectrum of Se^{75}, as obtained from lead foils, is shown in Fig. 2. The radioactive source was placed in a Lucite holder and covered with an aluminum cap of sufficient thickness (0.031 inch) to absorb the internal conversion electrons. The lead foils were fastened to the aluminum caps. Curves 1 and 2 of Fig. 2 were obtained with a spectrometer resolution of 2.3 percent (half-width), while all the inserts were obtained with a resolution of 2.1 percent. Curves 1 and 2 were determined with Geiger counters having mica windows of surface densities 3.8 and 1.0 mg/cm² respectively.

The lines shown in Fig. 2 can be ascribed to six gamma-rays, of which four are also included in the internal conversion spectrum of Fig. 1. The energies of the gamma-rays, as determined from the data given in Fig. 2, are listed in Table I as conversions in lead.

IV. ENERGIES OF NUCLEAR TRANSITIONS

The average energies of the ten transitions listed in Table I are in good agreement with those given by Ter-Pogossian *et al.*[7] In only one case is the percentage difference greater than the estimated probable error of one percent. Transitions 1, 6 and 9 are in addition to those reported by Ter-Pogossian *et al.*[7] These transitions are very weak and were observed only in the internal conversion spectrum, which was not obtained by Ter-Pogossian *et al.*[7]

The average energies of the transitions listed in Table I are also in fairly good agreement with those given by Cork *et al.*,[8] although for six of the transitions the discrepancies are greater than the estimated probable error of one percent. In one case, transition 2, the difference is 5.4 percent. Cork *et al.*[8] report a transition

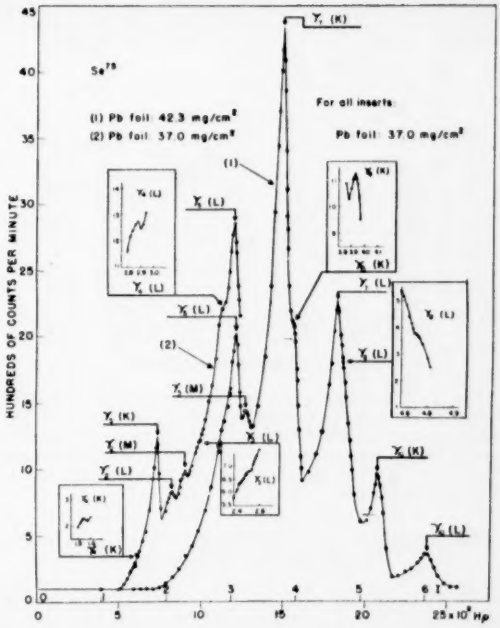

FIG. 2. Photoelectron spectrum of Se^{75}. Curves (1) and (2) were obtained with different counters. The inserts were obtained by more detailed examination of the regions indicated and with somewhat better resolution than used for curves (1) and (2).

having an energy of 0.0247 Mev, which is in addition to those given in Table I. We did not observe this transition. The internal conversion electrons from the K shell for a 0.0247-Mev transition would appear at a current value of 0.93 amp on curve 2 of Fig. 1. This is at a slightly larger current value than the peak labeled $K_\alpha(M)$ which has a value of 0.85 amp. There is no indication of a peak at 0.93 amp. Since Cork *et al.*[8] observed only the L and M electrons of this transition it is possible that the lines labeled $K_\alpha(L)$ and $K_\alpha(M)$ in curve 2 of Fig. 1 are due to the radiation which they have ascribed to a transition of energy 0.0247 Mev. However, since Se^{75} decays by orbital electron capture, presumably the Auger electrons should be observed. The peaks which we ascribe to Auger electrons, in curve 2 of Fig. 1, are in excellent agreement with the characteristic x-ray energies of As.

An additional gamma-ray, having an energy of 0.0103 Mev, has been reported by Stokes.[16,17] This gamma-ray, however, was apparently from an impurity present in the original sample, since the gamma-ray was not observed in a second sample of Se^{75} from which the impurities had been removed.[18] Radioactive impurities of Sb and Te were detected in the sample of Se^{75} from which Stokes' original source was prepared.

[15] A. H. Compton and S. K. Allison, *X-Rays in Theory and Experiment* (D. Van Nostrand Company, Inc., New York, 1935), second edition, p. 784.

[16] R. H. Stokes, U. S. Atomic Energy Commission Report AECD-1843, 1948 (unpublished).

[17] Progress Report in Physics, Iowa State College Report ISC-46, 1949 (unpublished).

[18] R. H. Stokes (private communication).

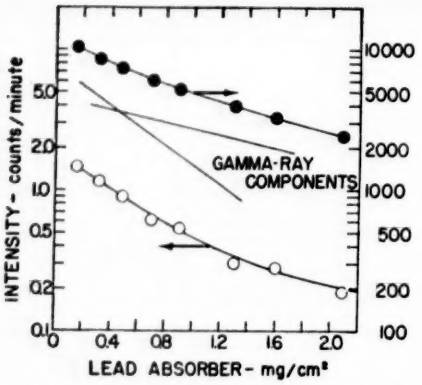

FIG. 3. Absorption curve for γ-γ coincidences with 225-mg Al/cm² in front of one counter and 225-mg Al/cm² plus varying lead absorbers in front of the other counter. θ = $\gamma-\gamma$ coincidence rate and $\bullet$ = γ-ray count for second counter. The γ-ray components were obtained from the extended lead absorption curve by the usual subtraction method.

V. INTENSITIES OF GAMMA-RAYS AND INTERNAL CONVERSION ELECTRONS

An attempt has been made to calculate the approximate ratios of the intensities of the gamma-rays and the internal conversion electrons from the maximum counting rate of the respective lines. Corrections have been applied for the photoelectric absorption coefficient, the transmission of the counter window, the momentum spread of the electrons due to the surface density of the source of electrons, and the transmission of the spectrometer. The photoelectric absorption coefficients were calculated by means of Gray's[19] empirical formula and the average spread in momentum produced by the lead foils and Se sources by means of a formula given by Heitler.[20] Electron scattering in the source has been neglected. The intensities of the internal conversion lines have been evaluated relative to that of γ_7 in Fig. 1. These values are given in Table II as e_i/e_7. The intensities of the gamma-radiations have been expressed relative to that of γ_7, which gave rise to the K and L photoelectron peaks $\gamma_7(K)$ and $\gamma_7(L)$ of Fig. 2. These relative intensities are given in Table II as q_i/q_7. These intensity ratios are of some help in constructing a decay scheme. It is estimated that the ratio e_x/e_7 is about 130, where e_x represents the intensity of Auger electrons as given by $K_\alpha(L)$ and $K_\alpha(M)$ of Fig. 1. The relative intensities given in Table II are only approximate values and are not reliable to better than a factor of about two.

VI. COINCIDENCE COUNTING MEASUREMENTS

Coincidence counting experiments were performed on several samples of Se^{75} using the counter arrangements and circuits described previously.[21] The selenium was precipitated as the element in a small drop on a thin mica sheet, 2 mg/cm² thick. After evaporation of the solution the mica sheet was mounted with the sample spot directly in front of a 3-mm hole in either a brass or lead plate which could be inserted between the two end-window Geiger counters. Samples were counted without absorber, with a paraffin absorber (148 mg/cm²), and with an aluminum absorber (225 mg/cm²). Counts obtained through the aluminum absorber were due to gamma-rays, counts through paraffin minus counts through aluminum were taken as the As K x-ray component, and counts with no absorber minus counts through paraffin gave the conversion electron contribution.

In agreement with DeBenedetti and McGowan[9] no delayed coincidences were found in the region of 0.3–10 μsec. Coincidence counts were obtained with several permutations of absorbers before the two counters. The usual subtractions for accidental coincidence counts and backgrounds were applied to the data. These results taken in conjunction with the spectrometer data, permit some conclusions regarding the decay scheme. Experimental values of the ratio of coincidence counting rates to the rates of individual counters are given in Table III.

In the treatment of the data the following symbols have been employed. Subscript "c" indicates a coincidence counting rate. Subscript numerals refer to transitions as listed in Table II. Superscripts ($'$) and ($''$) refer to channel or counter 1 and 2, respectively. e=an electron component. q=a photon component (γ-ray or x-ray). α=a conversion coefficient, e/q. n_i=a transition rate in As^{75}. n_0=a disintegration rate from Se^{75} directly to the ground state of As^{75}. n_t=total disintegration rate. E=a counter efficiency for detecting a particular radiation.

In accordance with the procedure described previously, E has been separated into three factors,

$$E=\omega A\epsilon,$$

where ϵ is the intrinsic efficiency for counting a par-

TABLE II. Approximate relative intensities of gamma-rays and internal conversion electrons from Se^{75}.

Transition	Energy, Mev	e_i/e_7	q_i/q_7
1	0.066_6	0.7	
2	0.076_6		0.2
3	0.098_3	9	~0.01
4	0.124_1	1	~0.03
5	0.138_4	4	0.3
6	0.203_2	0.06	
7	0.268_8	1	1
8	0.281_4		~0.07
9	0.307_8	0.05	
10	0.405_0	0.03	0.2

[19] L. H. Gray, Proc. Cambridge Phil. Soc. **27**, 103 (1931).
[20] W. Heitler, *The Quantum Theory of Radiation* (Oxford University Press, New York, 1944), second edition, p. 219.
[21] Martin, Jensen, Hughes, and Nichols, Phys. Rev. **82**, 579 (1951).

ticular radiation which penetrates the counter, A is the absorption (and scattering) factor of absorber material placed between the sample and counter, and ω is the effective solid angle or geometry factor.

An examination of intensities from the spectrometer data, Table II, reveals that effective contributions to electron or photon counting rates in these experiments could be attributed only to transitions 2, 3, 4, 5, 7, and 10. In addition, the K x-rays will contribute to the photon component. Only these transitions have been considered in the subsequent treatment.

In one experiment with sufficient lead before each counter to remove effectively the gamma-rays with an energy less than 0.15 Mev, no coincidences in excess of background or accidental counts were observed. Individual counter intensities were sufficiently high that it can be concluded that gamma-rays 7 and 10 cannot occur in cascade. Gamma-ray 7, being the most intense, is presumably a transition to the ground state. Further evidence in support of this conclusion is the fact that Smith *et al.*[22] found a weak 265-kev gamma-ray in the radiations from Ge^{75}, which decays by beta-emission to As^{75}. It is seen from the ratios of Table III that gamma-gamma coincidences did occur. Figure 3 shows the coincidence rate as a function of lead absorber thickness before one counter and indicates that the gamma-gamma-cascade must contain a "hard" and a "soft" transition. It appears therefore that transition 7 is in cascade with either transition 2, 5, or both. These two gamma-rays cannot be resolved by lead absorption measurements since they lie on opposite sides of the lead absorption edge and have approximately equal absorption coefficients. Cascade of transitions 7 and 5 appears likely because their energies add within the accuracy of the measurement of the energy of transition 10.

The ratio, $(e'-q_x'')_c/q_x''$, is very much less than ω' and indicates that conversion electrons can accompany only a few percent of the disintegrations, which is in agreement with the large ratio of e_x/e_7 given in Sec. V. The very low $(e'-e'')_c/e'$ ratio requires that at least one of the transitions in cascade must have a very low conversion coefficient.

TABLE III. Coincidence counting ratios for thin samples of Se^{75}.

Ratio	Experimental value	Calculated value from decay scheme, Fig. 4
$(e'-q_x'')_c/q_x''$	$1.34\pm0.04\times10^{-2}$	...
$(q_x'-q_\gamma'')_c/q_x''$	$3.7\ \pm0.5\ \times10^{-4}$	...
$(e'-q_x'')_c/e'$	$2.29\pm0.06\times10^{-3}$	$3.5\ \times10^{-3}$
$(q_\gamma'-q_x'')_c/q_\gamma'$	$1.2\ \pm0.2\ \times10^{-3}$	$1.7\ \times10^{-3}$
$(e'-q_\gamma'')_c/q_\gamma$	$2.27\pm0.02\times10^{-3}$	1.64×10^{-3}
$(e'-q_\gamma'')_c/e'$	$1.26\pm0.01\times10^{-4}$	1.07×10^{-4}
$(e'-e'')_c/e'$	$1.0\ \pm0.3\ \times10^{-3}$	$6.8\ \times10^{-4}$
$(q_\gamma'-q_\gamma'')_c/q_\gamma''$	$1.8\ \pm0.1\ \times10^{-4}$	2.04×10^{-4}

[22] Smith, Caird, and Mitchell, Phys. Rev. **88**, 150 (1952).

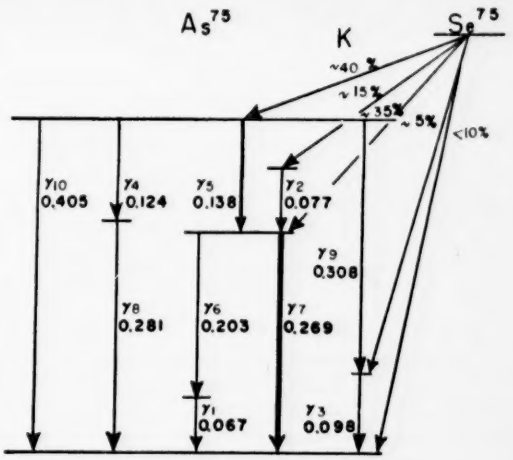

FIG. 4. Proposed decay scheme for Se^{75}. The energies are given in Mev.

VII. DECAY SCHEME

The decay scheme shown in Fig. 4 is consistent with the energies and relative intensities as given in Table I and II, respectively, and with the coincidence counting ratios of Table III. For this decay scheme the various counting rates could be calculated by the following equations:

$$q_\gamma'=\omega'\sum\frac{n_i\epsilon_{iq}}{1+\alpha_i}, \tag{1}$$

$$q_x''=\omega''\epsilon_{xq}''\left(\frac{1}{1+\alpha_x}\right)\left[\sum{}^{*}n_i+\sum\frac{n_i\alpha_i}{1+\alpha_i}+n_0\right]. \tag{2}$$

$\sum^{*}$ represents a summation of transitions in arsenic to the ground state. The disintegration rate $n_t=\sum^{*}n_i+n_0$.

$$e'=\omega'\sum\frac{n_i\alpha_iA_{ie}'}{1+\alpha_i}. \tag{3}$$

Coincidence rates are given by the following equations. Since $\alpha_i\ll1$ except for transition 3, a number of small terms can be omitted for simplicity:

$$(e'-q_x'')_c=\frac{\omega'\omega''\epsilon_{xq}''}{1+\alpha_x}\left[\frac{2n_bA_{be}'\alpha_b}{1+\alpha_b}+\frac{2n_7A_{7e}'\alpha_7}{1+\alpha_7}+\frac{2n_3A_{3e}'\alpha_3}{1+\alpha_3}+\frac{2n_4A_{4e}'\alpha_4}{1+\alpha_4}\right]. \tag{4}$$

$$(q_x'-q_\gamma'')_c=\frac{\omega'\omega''\epsilon_{xq}'}{1+\alpha_x}\sum_i\frac{n_i\epsilon_{iq}''}{1+\alpha_i}. \tag{5}$$

$$(q_\gamma'-q_\gamma'')_c=\omega'\omega''\left[\frac{n_2(\epsilon_{7q}'\epsilon_{2q}''+\epsilon_{2q}'\epsilon_{7q}'')}{(1+\alpha_7)(1+\alpha_2)}+\frac{n_5(\epsilon_{7q}'\epsilon_{5q}''+\epsilon_{5q}'\epsilon_{7q}'')}{(1+\alpha_7)(1+\alpha_5)}\right]. \tag{6}$$

$$(e'-e'')_c=\omega'\omega''\left[\frac{n_2\alpha_2\alpha_7(A_{7e}'A_{2e}''+A_{2e}'A_{7e}'')}{(1+\alpha_2)(1+\alpha_7)}+\frac{n_5\alpha_5\alpha_7(A_{7e}'A_{5e}''+A_{5e}'A_{7e}'')}{(1+\alpha_5)(1+\alpha_7)}\right]. \quad (7)$$

$$(e'-q_\gamma'')_c=\omega'\omega''\left[\frac{n_5(\alpha_5A_{5e}'\epsilon_{7q}''+\alpha_7A_{7e}'\epsilon_{5q}'')}{(1+\alpha_5)(1+\alpha_7)}+\frac{n_2(\alpha_2A_{2e}'\epsilon_{7q}''+\alpha_7A_{7e}'\epsilon_{2q}'')}{(1+\alpha_2)(1+\alpha_7)}\right]. \quad (8)$$

Counter characteristics used in these equations have been tabulated in Table IV. These equations were used with the relative intensities given in Table II which give the ratios of electron intensities, $n_i\alpha_i/(1+\alpha_i)$, and photon intensities, $n_i/(1+\alpha_i)$, compared to the corresponding quantities for transition 7. When the expression for $(e'-q_x'')_c/q_x''$ from Eqs. (2) and (4), including the numerical values from Tables II and IV, is set equal to the experimental ratio of 1.34×10^{-2}, the values of each electron component, $n_i\alpha_i/n_t(1+\alpha_i)$, can be calculated. Likewise a similar treatment using the ratio for $(q_x'-q_\gamma'')_c/q_x'$ was used to give values for $n_i/n_t(1+\alpha_i)$. From these two sets of data the intensity and conversion coefficient for each of the transitions were calculated and included in Table V. Transitions 3, 7, and 10 to the ground state account for more than 95 percent of the disintegrations. It was concluded that only a few percent of the orbital electron captures, at most, can lead directly to the ground state. With these results the remaining six coincidence counting ratios were calculated and appear in Table III. Support of the decay scheme shown in Fig. 4, is demonstrated by the satisfactory agreement between the calculated and observed values in every case.

TABLE IV. Counter characteristics used in Eqs. (1)–(8).

Quantity	Value	How estimated
ω'	0.115	From β-γ coincidences of Au^{198} and Co^{60}.[a]
ω''	0.135	
A_{xq}''	0.68	Calculated from mass absorption coefficient.[b]
α_x	0.92	Reference c.
A_{2e}'	0.0	From air and window absorber thickness assuming a linear absorption curve.[d]
A_{5e}'	0.6	
A_{4e}'	0.7	
A_{5e}'	0.75	
A_{7e}'	0.9	
ϵ_{xq}	33×10^{-3}	From β-γ coincidences of Au^{198} and counting efficiency ratios given by experimental curve for copper wall counters.[e]
ϵ_{2q}	6.6×10^{-3}	
ϵ_{5q}	3.0×10^{-3}	
ϵ_{7q}	2.0×10^{-3}	
ϵ_{10q}	2.5×10^{-3}	

[a] See reference 21.
[b] See reference 15, p. 800.
[c] See reference 15, p. 488.
[d] L. E. Glendenin, Nucleonics **2**, No. 1, 12 (1948).
[e] H. Saurer, Helv. Phys Acta No. 4, 381 (1950).

Similar computations were carried out for the alternative decay scheme in which transition 2 terminated in the ground state and was not in cascade with other transitions. For this case the ratio $(q_\gamma'-q_\gamma'')_c/q_\gamma'$ was 8.3×10^{-5}, disagreeing seriously with the experimental value of 1.8×10^{-4}.

Assuming that none of the orbital electron captures lead directly to the ground state, as is indicated by the coincidence data, it is possible to determine the conversion electron and photon intensities, the transition intensities, and the conversion coefficients from the decay scheme shown in Fig. 4, the relative intensities given in Table II, the ratio of Auger electrons to conversion electrons in transition 7 (i.e., e_x/e_7) and the fluorescent yield for arsenic x-rays (which is about 0.52) (see p. 488 of reference 15). These calculations make use of two equations, of which one gives the x-ray transition rate and the second gives the disintegration rate. The transition intensities (e_i+q_i) obtained in this way are in good axreement with those given in Table V. The conversion coefficients, α_i, calculated by this method are, however, approximately one-half of those given in Table V. This discrepancy is primarily due to the difference in the electron intensities, e_i. The ratio e_x/e_7 was not used in calculating the values given in Table V.

The intensity of transition 3 is appreciably greater than that of transition 9 and therefore requires that there be decay by orbital electron capture to the energy level 0.0983 Mev above the ground state of As^{75}. Similarly, there must also be decay by orbital electron capture to the energy level 0.269 Mev above the ground state of As^{75}.

Cork *et al.* have proposed a decay scheme which in many ways is similar to the one shown in Fig. 4. Two possible objections to their decay scheme might be mentioned, however. They have transition 3 precede and decay through the parallel transitions 9 and the 24.7-kev disintegration. As can be seen from Table II and Figs. 1 and 2, transition 3 is many times more intense than 9. As mentioned previously we have not found any evidence for the existence of the 24.7-kev gamma-ray or its internal conversion electrons. We would infer that, if it exists, it must be very weak. Hence, it appears improbable that transition 3 precedes 9. Cork *et al.*[8] also propose that the parallel transitions 1 and 2 precede and decay through 6. Our data, shown in Table II, indicate the e_1 is considerably larger the e_6 and that q_2 is also considerably larger than q_6 and hence it seems improbable that transitions 1 and 2 in parallel can precede and decay through 6.

It would be highly desirable to make coincidence measurements between individual transitions in order to verify the proposed decay scheme shown in Fig. 4.

VIII. DISCUSSION

There appears to be a real discrepancy between the K/L ratio and the apparently large internal conversion

coefficient for transition 3. A multipole order of the radiation cannot be assigned which is consistent with the K/L ratio, internal conversion coefficient, lifetime of the excited state, and the nuclear shell model. Most of the available evidence indicates magnetic dipole radiation. The evidence for this conclusion is given in the following discussion.

From the data shown in Fig. 1, a value of 11 is found for the K/L ratio of transition 3, for which the energy is 98.3 kev. The experimental curves of Goldhaber and Sunyar[23] indicate a K/L ratio of about 8 for both magnetic dipole and quadrupole radiation for $Z=33$ and $E=98.3$ kev, and a K/L ratio of about 4.3 and 3.0 for electric quadrupole and octupole radiation respectively. Hence the K/L ratio, although appreciably larger than the values given by the experimental curves of Goldhaber and Sunyar,[23] indicates magnetic dipole or quadrupole radiation with lifetimes of the excited state of 3×10^{-11} sec and 1×10^{-4} sec, respectively. These lifetimes are estimated from the formula of Weisskopf,[24] taking into account the internal conversion coefficients as determined from the tables of Hebb and Nelson[25] and the curves given by Axel and Goodrich.[26] The latter lifetime is in the region of 10^{-6} to 10^{-3} sec, within which DeBenedetti and McGowan[9] did not observe any delayed coincidences. Also, Feenberg and Hammack[27] and Nordheim[28] have pointed out that "islands of isomerism" exist for odd nuclei with $39 \leqslant (N \text{ or } Z) \leqslant 49$ and for $63 \leqslant (N \text{ or } Z) \leqslant 81$, where N and Z are respectively the number of neutrons and protons in the nucleus. As^{75}, with 33 protons and even N, does not fit into either one of these "islands." This would seem to indicate that transition 3 is magnetic dipole radiation.

The assignment of magnetic dipole radiation to transition 3 is inconsistent with the large internal conversion coefficient of 4 to 8, which is obtained from the data presented in this paper. From the curves given by Axel and Goodrich,[26] the relativistic K shell internal conversion coefficient for transition 3 in 0.07 for magnetic dipole radiation. It should be stated that the internal conversion coefficient for transition 3 as calculated from our data is a very approximate value, since, as can be seen in Fig. 2, the photoelectrons due to gamma-ray 3 had a very low intensity. This low intensity indicates, however, that the internal conversion coefficient must be fairly large.

TABLE V. Intensities and conversion coefficients for the transitions following the decay of Se^{75} as determined from coincidence data.

Transition	Energy Mev	Electron intensity e_i	Photon intensity q_i	Transition intensity e_i+q_i	Conversion coefficient e_i/q_i
1	0.066_6	0.005		0.005	
2	0.076_6		0.14	0.14	
3	0.098_2	0.058	~0.007	0.065	~8
4	0.124_1	0.006	~0.02	~0.03	~0.3
5	0.138_4	0.026	0.21	0.24	0.12
6	0.203_2	0.0004		0.0004	
7	0.268_8	0.0064	0.70	0.71	0.090
8	0.281_4		~0.05	~0.05	
9	0.307_8	0.0003		0.0003	
10	0.405_0	0.0002	0.14	0.14	0.0015
To ground state of As^{75}				0.03	

If one alternatively assumed magnetic octupole radiation for transition 3, the relativistic K shell internal conversion coefficient[26] would be about 5.7 and the K/L ratio given by the experimental curves of Goldhaber and Sunyar[23] would be approximately 6.0. The K/L ratio is appreciably smaller than the experimental value of 11. The lifetime[24–26] of the excited state expected for this radiation is about 3.5 min. This lifetime is inconsistent with the nuclear shell model. We have looked for a relatively long-lived metastable state in As^{75} by making a rapid (5 min) chemical separation of As from Se^{75}. About one percent of the total Se^{75} activity was observed in the separated As fraction, but this small activity could not be distinguished from the radiations of Se^{75} on the basis of half-life and absorption curves.

It should also be noted that the L and M electron lines of transition 2 were observed in the photoelectron spectrum of Fig. 2, but no internal conversion lines were observed in Fig. 1. This perhaps indicates that the internal conversion coefficient of transition 2 is small.

The authors wish to express their appreciation to Mr. J. H. Jonte for his help in preparing the sources, Messrs. R. T. Nichols and G. O. Pickens for their assistance in obtaining the data and making some of the calculations, and Mr. E. R. Rathbun, Jr., for construction of the Geiger counters.

[23] M. Goldhaber and A. W. Sunyar, Phys. Rev. **83**, 906 (1951).
[24] V. F. Weisskopf, Phys. Rev. **83**, 1073 (1951).
[25] M. H. Hebb and E. Nelson, Phys. Rev. **58**, 486 (1940).
[26] P. Axel and R. F. Goodrich, Internal Conversion Data (distributed privately).
[27] E. Feenberg and K. C. Hammack, Phys. Rev. **75**, 1877 1(949).
[28] L. W. Nordheim, Phys. Rev. **75**, 1894 (1949).

Measurement of the Transport Mean Free Path of Thermal Neutrons in D_2O by a Boron Poisoning Method*

S. W. KASH AND D. C. WOODS
Atomic Energy Research Department, North American Aviation, Inc., Downey, California
(Received December 22, 1952)

The transport mean free path of thermal neutrons in D_2O was experimentally determined by measuring the change in the relaxation length upon the introduction of known amounts of B_2O_3. The value found for 99.7 percent pure D_2O was 2.49 ± 0.04 cm. Upon correcting for the small hydrogen impurity, a value of 2.52 ± 0.04 cm was obtained for λ_{tr} in pure D_2O.

INTRODUCTION

THE transport mean free path λ_{tr} of thermal neutrons in D_2O was measured by an extrapolation method at the Montreal Laboratory of the Natural Research Council of Canada in 1946.[1] In this experiment the thermal neutron flux in the neighborhood of a plane cadmium boundary was measured and the distance d beyond the boundary at which the flux extrapolated to zero was determined. From the relationship $\lambda_{tr}=0.71d$, a value 2.31 ± 0.09 cm for the transport mean free path of 99.4 percent pure D_2O was obtained. Applying a correction for the mass spectrographically measured hydrogen impurity gave a value of $\lambda_{tr}(D_2O)=2.4\pm0.1$ cm for 100 percent pure D_2O. Because of the importance of $\lambda_{tr}(D_2O)$ in reactor calculations, it was desirable to measure this value by a different method. Accordingly, the relaxation length of thermal neutrons in a cylindrical column of D_2O was measured for various amounts of boron poisoning. From the variation of the relaxation length with boron concentration, the effective value of λ_{tr} and the hydrogen impurity content were determined for the particular D_2O used. The effective value was then corrected for the hydrogen impurity to give a value of 2.52 ± 0.04 cm for the transport mean free path of 100 percent pure D_2O.

THEORY

In a weakly absorbing, homogeneous medium, the diffusion length L, the macroscopic total cross section Σ, and the macroscopic absorption cross section Σ_a are related by

$$1/L^2=3\Sigma(1-\bar{\mu})\Sigma_a(1-k\Sigma_a/\Sigma), \tag{1}$$

where μ is the average value of the cosine of the angle through which a neutron is scattered in a single collision, and $k=0.80-\bar{\mu}(1-\bar{\mu})^{-1}$. In terms of the macroscopic scattering cross section Σ_s, Eq. (1) may be written as

$$1/L^2=3\Sigma_s(1-\bar{\mu})\Sigma_a+3\Sigma_a^2(1-\bar{\mu})(1-k). \tag{2}$$

The second term on the right side of this equation may often be neglected. In this experiment this term is at most about 0.1 percent of the first term. The first term may be written as $3\Sigma_a/\lambda_{tr}$, where

$$\lambda_{tr}=1/\Sigma_{tr}=1/[\Sigma_s(1-\bar{\mu})] \tag{3}$$

defines the transport mean free path for the medium.

For a cylindrical tank, with a neutron source at the bottom and bounded by cadmium on all the other sides, the thermal neutron flux is represented by

$$\phi=AJ_0(\mu r)\sinh\nu(h-z), \tag{4}$$

where z is measured from the bottom of the tank. The constants μ (not to be confused with $\bar{\mu}$ above) and ν will be referred to as the radial buckling and the reciprocal of the relaxation length, respectively. They are related to the diffusion length by

$$1/L^2=\nu^2-\mu^2. \tag{5}$$

Now ν^2 and μ^2 can be determined from the flux distribution, so if Σ_a is known, λ_{tr} can be determined. For D_2O, however, Σ_a is small and is very sensitive to impurities, in particular hydrogen, so that an accurate determination of λ_{tr} in this case is difficult. If a strong absorber such as boron is added, Σ_a may be considerably increased without measurably affecting λ_{tr}. Combining Eqs. (2), (3), and (5), and putting $\Sigma_a=\Sigma_a(D_2O)+\Sigma_a(B)$ gives

$$\nu^2-3\Sigma_a^2(1-\bar{\mu})(1-k)=3\Sigma_{tr}\Sigma_a(B)+3\Sigma_{tr}\Sigma_a(D_2O)+\mu^2. \tag{6}$$

The μ^2 term is determined by the radius of the tank and by λ_{tr} and so is essentially constant. Thus λ_{tr} can be determined from the slope of the straight line obtained by plotting the left side of Eq. (6) against $\Sigma_a(B)$.

If the D_2O solution contains a volume fraction r of H_2O, the effective value of the transport mean free

TABLE I. Summary of data.[a]

B_2O_3 concentration (mg/l)	Average temp. (°C)	$\Sigma_a(B)\times10^2$ (cm^{-1})	Average $\mu\times10^2$ (cm^{-1})	Average $\nu\times10^2$ (cm^{-1})	$(\nu^2-\Sigma_a^2)\times10^4$ (cm^{-2})
0	23.6	0	3.107 ± 0.016	3.291 ± 0.018	1.083 ± 0.012
46.9 ± 0.2	22.9	0.536 ± 0.008	3.100 ± 0.012	4.163 ± 0.018	1.733 ± 0.015
72.3 ± 0.1	23.3	0.827 ± 0.011	...	4.561 ± 0.022	2.079 ± 0.020
97.8 ± 0.2	23.3	1.119 ± 0.015	3.101 ± 0.010	4.938 ± 0.029	2.437 ± 0.029
123.5 ± 0.5	23.4	1.413 ± 0.020	3.082 ± 0.020	5.270 ± 0.019	2.775 ± 0.020
146.8 ± 0.5	26.1	1.671 ± 0.023	3.086 ± 0.016	5.573 ± 0.013	3.103 ± 0.014

[a] The errors listed are standard deviations.

* This report is based upon studies conducted for the U. S. Atomic Energy Commission.

[1] Auger, Munn, and Pontecorvo, Can. J. Research A25, 143 (1947).

path is given by

$$\frac{1}{\lambda_{tr}(\text{eff})}=\frac{1-r}{\lambda_{tr}(D_2O)}+\frac{r}{\lambda_{tr}(H_2O)}, \tag{7}$$

where $\lambda_{tr}(D_2O)$ and $\lambda_{tr}(H_2O)$ refer to 100 percent D_2O and 100 percent H_2O, respectively. This is easily verified by substituting in Eq. (3):

$$\Sigma_s=(1-r)\Sigma_s(D_2O)+r\Sigma_s(H_2O),$$

and

$$\bar{\mu}=(1/\Sigma_s)[(1-r)\Sigma_s(D_2O)\bar{\mu}(D_2O)+r\Sigma_s(H_2O)\bar{\mu}(H_2O)].$$

EXPERIMENTAL PROCEDURE

The measurements were made in the Atomic Energy Research Laboratory at North American Aviation, Inc. The D_2O was contained in a cadmium covered aluminum tank, 5 ft in diameter and 6 ft high. The tank was supported by a 5-ft diameter, 6-ft high graphite pedestal containing a water boiler reactor at its center. The reactor was operated at a power level of approximately $\frac{1}{2}$ watt and provided a flux of about 10^6 thermal neutrons per square centimeter per second at the base of the D_2O tank. Flux measurements were made along the axis of the tank and along a central diameter with indium foils 1 cm square and 0.005 cm thick (95 to 100 mg/cm^2). Bare and cadmium covered foil measurements were taken, and saturated foil activities were obtained using standard counting techniques. The foils were spaced at 5-cm intervals along the axis and at 4.9-cm intervals along the diameter.

Successive amounts of B_2O_3 were added to the D_2O. After each addition, the solution was thoroughly stirred in the aluminum tank, and samples were removed for analysis from at least four different parts of the tank. Flux measurements were then made for each B_2O_3 concentration. Six different concentrations were used, ranging from zero to approximately 150 mg of B_2O_3 per liter of solution. For each concentration a minimum of four radial and eight axial sets of foil exposures were made.

CALCULATIONS

1. Effective Values of λ_{tr} and $\Sigma_a(D_2O)$

A value of 750±10 barns was taken for the boron absorption cross section for 2200-m/sec neutrons.[2] Assuming the neutrons to have a Maxwellian velocity distribution at the temperature T of the D_2O solution, the effective absorption cross section was determined to be $\sigma(\text{eff})=(750\pm10)\times(\pi^{\frac{1}{2}}/2)\times(293/T)^{\frac{1}{2}}$ barns. For each boron concentration the macroscopic absorption cross section $\Sigma_a(B)$ was determined by multiplying $\sigma(\text{eff})$ by the average measured density of boron nuclei.

The radial buckling was determined by fitting each radial set of foil exposures to a zeroth-order Bessel function. Similarly, the relaxation length was determined by fitting each axial set of foil exposures to a hyperbolic sine function. The respective values of μ and ν thus obtained for each boron concentration were then averaged.

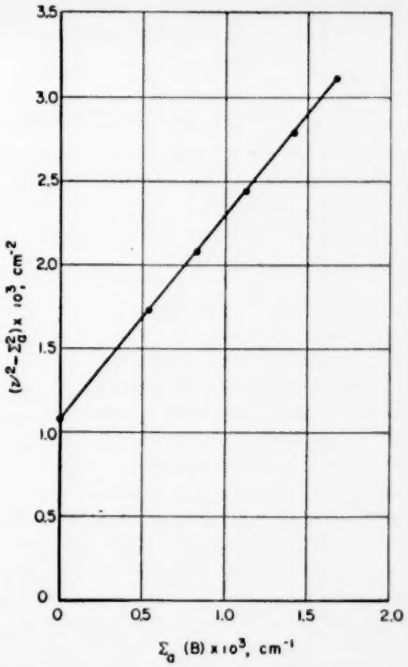

FIG. 1. Relaxation length as a function of the boron absorption. The slope of the line $(\nu^2-\Sigma_a^2)$ *vs* $\Sigma_a(B)$ determines the effective value of λ_{tr} for the D_2O. The effective absorption of the D_2O before the addition of any boron is obtained by subtracting μ^2 from the y intercept and dividing by $3\Sigma_{tr}$.

A summary of the measurements is presented in Table I. The first column gives the average value of the B_2O_3 concentration in milligrams per liter of solution. The second column gives the average temperature of the $D_2O-B_2O_3$ solution while the flux measurements were being made. The third column presents the computed macroscopic cross section of the B_2O_3 impurity; the absorption of the oxygen was neglected. The next two columns give the average values for the radial buckling and the reciprocal of the relaxation length. Note that the value of μ is constant within the accuracy of the measurements. The value of μ averaged over all concentrations is $0.03095+0.00010$ cm^{-1}. In the last column the values of $\nu^2-3\Sigma_a^2(1-\bar{\mu})(1-k)$ are tabulated. Since the term involving Σ_a^2 is small compared to ν^2, accuracy in $\bar{\mu}$ is not required here. With $\bar{\mu}=0.15$ (see below), $3(1-\bar{\mu})(1-k)=1.0$.

The values of $\nu^2-\Sigma_a^2$ are plotted against $\Sigma_a(B)$ in Fig. 1. From the slope and y intercept and the average value of μ the following effective values were deter-

[2] U. S. Atomic Energy Commission Report AECU-2040, May 15, 1952 (unpublished).

mined:

$$\lambda_{tr}(\text{eff}) = 2.49 \pm 0.04 \text{ cm},$$
$$\Sigma_a(D_2O) = (1.04 \pm 0.10) \times 10^{-4} \text{ cm}^{-1}.$$

2. Value of λ_{tr} for Pure D_2O

From the value of $\Sigma_a(D_2O)$ we can estimate the amount of hydrogen impurity in the D_2O and correct λ_{tr} accordingly. Converting the effective value of $\Sigma_a(D_2O)$ to the value for 2200 m/sec neutrons, we have

$$\Sigma_a(D_2O, 2200) = (1.2 \pm 0.1) \times 10^{-4} \text{ cm}^{-1}.$$

Of this the D_2O itself contributes about $0.4 \times 10^{-4} \text{cm}^{-1}$.[3] Attributing the remaining 0.8×10^{-4} cm^{-1} to H_2O requires a hydrogen to deuterium ratio of 0.0030 ± 0.0005.[4] This value is about twice the value normally obtained by some mass spectrograph analyses. However, since the effective absorption of the D_2O is very sensitive to the hydrogen impurity, the ratio of H to D computed by the above means should be more reliable. The contribution of other impurities in the D_2O to the macroscopic absorption is less than 0.01×10^{-4} cm^{-1} and has accordingly been neglected. The other impurities consist mainly of oxides of Si, Al, and Fe, and amount to less than 50 mg per liter of solution.

Some of the hydrogen will be in the form of H_2O, but most of it will be in the form of HDO. However, it may be shown that the transport cross section of HDO is equal to the simple average of the transport cross sections of H_2O and D_2O. Hence, we may take all the hydrogen to be in the form of H_2O and all the deuterium in the form of D_2O. Substituting in Eq. (7), the values $\lambda_{tr}(\text{eff}) = 2.49 \times 0.04$ cm, $\lambda_{tr}(H_2O) = 0.48 \times 0.01$ cm (see reference 4), and $r = 0.0030 \times 0.0005$, gives finally

$$\lambda_{tr}(100 \text{ percent pure } D_2O) = 2.52 \pm 0.04 \text{ cm}.$$

3. Value of $\bar{\mu}$

For D_2O we may take $\sigma_s = \sigma_t = (10.0 \pm 0.72E^{-\frac{1}{2}} \pm 0.3)$ barns, where the energy E is in electron volts.[5] Averaging over a Maxwellian collision distribution gives an effective $\sigma_s = 14.0 \pm 0.3$ barns, and so $\Sigma_s(D_2O) = 0.467 \pm 0.010$ cm^{-1}. Putting this value of Σ_s and the above value of λ_{tr} into Eq. (3) gives

$$\bar{\mu} = 0.15 \pm 0.03.$$

4. Comparison of the Two Measurements of λ_{tr}

The determination of λ_{tr} by the boron poisoning method has some definite advantages over its determination by the extrapolation method. The extrapolation method, while offering a more direct measurement of λ_{tr}, suffers from the fact that near the boundary the flux is small and the corrections for the depression of the flux by the detectors are neither negligible nor constant. In the boron impurity experiment such corrections are unimportant. Since in this case none of the foils need be less than several mean free paths from the D_2O surface, the depression of the flux at a foil due to the foil itself is essentially the same for all the foils. The depression of the flux at a foil caused by neighboring foils can be made small by adequately separating the foils; in any case, the exponential nature of the flux along the axis of the tank makes this depression the same constant factor for each foil. In the boron poisoning experiment the major source of error is caused by the uncertainty in the boron cross section.

Two small corrections should be applied to the value of λ_{tr} quoted in the extrapolation experiments of Auger *et al.* before comparing it with the value of this experiment. First, using a sinh function instead of a linear function and using transport theory instead of diffusion theory increases λ_{tr} by 0.25 cm. Second, using 0.48 cm for the transport mean free path of light water instead of 0.32 cm makes the hydrogen impurity correction only 0.07 cm. With these changes the value of λ_{tr} (100 percent D_2O) from the extrapolation experiment is 2.63 ± 0.12 cm. This is in reasonable agreement with the value obtained in the present experiment.

DISCUSSION

The scattering cross sections of boron and oxygen are approximately 4 barns each. At the maximum B_2O_3 concentration, the B_2O_3 macroscopic scattering cross section is approximately 3×10^{-5} cm^{-1}. Even with a factor of 2 or 3 for molecular effects, this is very small compared with Σ_{tr} which is approximately 0.4 cm^{-1}. Hence, the change in λ_{tr} upon the introduction of the B_2O_3 into the D_2O is negligible. A similar argument applies to the other nonhydrogen impurities present in the D_2O solution.

No measurable change in relaxation length with height was detected. The higher B_2O_3 concentrations showed what appeared to be hardening effects. However, this was traced to the scattering in of fast neutrons from the water-boiler reactor radiation shield and was completely eliminated by the addition of paraffin slabs across the top of the shield. The constancy of the relaxation length with height lent experimental justification to the assumption of a Maxwellian velocity distribution for the neutrons.

The authors wish to give thanks to Dr. A. T. Biehl who actively encouraged the experiment; to E. Martin, who assisted with the calculations, and to Dr. L. Silvermen, who supervised the introduction and removal of the boron.

[3] $\sigma_a(D_2O)$ was taken equal to 1.2 ± 0.1 millibarns; see Kaplan, Ringo, and Wilzbach, Phys. Rev. **87**, 785 (1952).

[4] F. J. Sisk, Oak Ridge National Laboratory Report ORNL-933, March 15, 1951 (unpublished). This unclassified report lists the following effective values for H_2O: $\sigma_a = 0.68 \pm 0.01$ barn, $\lambda_{tr} = 0.48 \pm 0.01$ cm.

[5] Rainwater, Havens, Dunning, and Wu, Phys. Rev. **73**, 733 (1948).

Gallium 67†

B. H. KETELLE, A. R. BROSI, AND F. M. PORTER
Chemistry Division, Oak Ridge National Laboratory, Oak Ridge, Tennessee
(Received January 29, 1953)

The electron capture decay of 78-hr Ga^{67} has been investigated with a magnetic lens spectrometer, a proportional counter spectrometer, scintillation spectrometers, and combinations of these spectrometers in coincidence. The experimental data indicate that electron capture occurs to 92-kev, 182-kev, 388-kev, and 880-kev levels in Zn^{67}. The lowest level at 92 kev is a metastable one with a half-life of 8.5 μsec. Branching ratios and conversion coefficients have been determined from which consistent spin and parity assignments have been made to the Zn^{67} levels.

INTRODUCTION

THE isotope now known to be 78-hr Ga^{67} was first produced by Livingood[1] using a d, n reaction on zinc. The studies of several workers, who produced the isotope by a variety of reactions, contributed to the assignment of the 78-hr period to gallium. Alvarez[2] assigned this decay period to mass number 67 on the basis of the reactions which had been used to produce it. Through a study of Ga^{67} Alvarez established that orbital electron capture occurs as a process of radioactive decay. His work on the Ga^{67} radiations also showed that internal conversion of gamma-radiation is an important process in the decay of artificially produced low Z radioisotopes.

In a magnetic spectrometer study of the Ga^{67} conversion electrons Valley and McCreary[3] were able to give a precise energy and K/L conversion ratio for the 92.5-kev gamma-ray. Helmholz[4] confirmed the work of Valley and McCreary and found two additional gamma-rays with energies of 180 kev and 297 kev. He proposed a decay scheme with electron capture to a level 570 kev above the ground state in Zn^{67}, followed by emission of 180-kev, 297-kev and 92.5-kev gamma-rays in sequence as written. Because of differences in gamma-ray intensities, he postulated independent electron capture to the 389-kev and 92.5-kev levels in Zn^{67}. Cork[5] confirmed the gamma-rays reported by Helmholz and reported an additional 174-kev gamma-ray.

Since previously unreported gamma-rays were found in some preliminary scintillation spectrometer measurements, and since earlier publications had not given relative intensities and conversion coefficients for all of the transitions reported, a detailed study of Ga^{67} was begun. This has included measurements with a thin lens spectrometer, scintillation spectrometers, and proportional counter spectrometers. Coincidence measurements have been made with various combinations of these spectrometers.

Since this work was completed, Mukerji and Preiswerk[6] have published a decay scheme for Ga^{67} which is in good agreement with the one reported here. We have found one additional level at 0.880 Mev in Zn^{67} and several transitions between levels which they did not report. In addition, some of our conversion coefficients are different from the ones they report and lead to different spin assignments for some of the levels in Zn^{67}. Meyerhof[7] has used NaI-Tl scintillation crystals with discrimination in coincidence in a study of Ga^{67}. He confirms the existence of a 0.88-Mev level and the metastability of the 0.092-Mev level reported here.

PREPARATION OF SOURCES

Ga^{67} was produced by a proton bombardment of zinc in the ORNL 86-inch cyclotron. The gallium was separated from the zinc target either by cation exchange[8] or isopropyl ether extraction.[9] A second isopropyl ether extraction was sufficient when thin samples were not required, since no evidence of radioactive impurities was found by following the decay for twelve half-lives.[10] In order to prepare thin sources for the lens spectrometer iron was precipitated as the hydroxide, and an additional ether extraction was made to remove the salts. A concentrated HCl solution of the Ga activity was then evaporated in an evacuated system, and the Ga activity was volatilized away from residual solids. The sources used to take the best conversion electron data were prepared by dissolving this volatilized activity in HCl and evaporating it on a platinum strip in a vacuum system. The Ga^{67} was then volatilized onto a masked conducting film by heating the platinum strip. Uniformly distributed sources containing 10 Mc of Ga^{67} and not more than a few micrograms of solids were prepared in this way.

† Under contract with the U. S. Atomic Energy Commission.
[1] J. J. Livingood, Phys. Rev. **50**, 425 (1936).
[2] L. W. Alvarez, Phys. Rev. **54**, 486 (1938).
[3] G. E. Valley and R. L. McCreary, Phys. Rev. **56**, 863 (1939).
[4] A. C. Helmholz, Phys. Rev. **60**, 415 (1941).
[5] Cork, Hadley, and Kent, Phys. Rev. **61**, 388 (1942).
[6] A. Mukerji and P. Prieswerk, Helv. Phys. Acta **25**, 387 (1952). See also K. Seigbahn, Arkiv Fysik **4**, 223 (1952); Fultz, Nash, Woodward, and Pool, Phys. Rev. **88**, 170 (1952).
[7] W. E. Meyerhof (private communication, September, 1952).
[8] R. E. Blanco and J. D. Perkinson, Jr., J. Am. Chem. Soc. **73**, 2696 (1951).
[9] N. H. Nachtrieb and R. E. Fryrell, J. Am. Chem. Soc. **71**, 4035 (1949).
[10] J. Tobailen, Compt. rend. **233**, 1360 (1951).

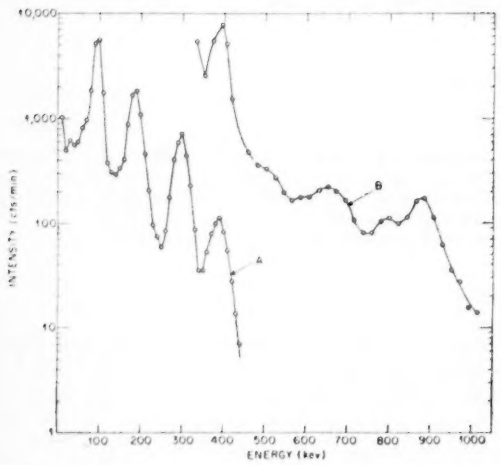

FIG. 1. Scintillation spectrometer pulse-height distribution of Ga^{67} γ-radiation. A. Low intensity source; B. Higher intensity source through 7-g/cm² Pb.

GAMMA-RAY MEASUREMENTS

The Ga^{67} gamma-radiation was studied using a scintillation spectrometer of the type described by Jordan and Bell.[11] The detector[12] was a selected 5819 photomultiplier and a selected Tl activated NaI crystal ground to fit the photosensitive end of the photomultiplier. The cylindrical crystal $1\frac{1}{2}$ in. in diameter and 2 in. long was sealed to the photomultiplier with silicone grease and covered with a 2-mm layer of powdered MgO. The assembly was made in a dry box and sealed in an aluminum can with Apiezon Q. The differential discriminator was the type described by Fairstein.[13]

Energy and intensity calibrations were made using Xe^{133}, Ce^{141}, Au^{198}, and Cs^{137} activities. A pulse-height distribution curve for Ga^{67}, taken with an assembly which had a resolution for the Cs^{137} gamma-ray of 9 percent full width at half-height, is shown in Fig. 1. This curve shows the presence of the previously reported gamma-rays with energies of 92 kev, 182 kev and 296 kev. In addition, peaks corresponding to 388-kev, 490-kev, 790-kev, and 880-kev gamma-rays are indicated. The shoulder on the 92-kev gamma-ray peak results to a large extent from the absorption of the 92-kev gamma-ray with escape of the 28-kev iodine x-ray rather than from the presence of a 65-kev gamma-ray. All points on these pulse-height distribution curves decay with the same half-life, showing that the higher energy peaks do not result from random coincidences of smaller pulses. This conclusion was supported by another experiment in which lead absorbers were placed between the sample and the detector. The counting rate of the low energy peaks was reduced relatively more than that of the high energy peaks. The relative intensities of these gamma-rays obtained from an intensity calibration curve are given in Table I.

TABLE I. Relative intensities and conversion coefficients of transitions in Ga^{67} decay.

Transition energy, kev	Relative N_γ	Relative N_K	Relative N_L	N_K/N_γ	Probable transition type	Theoretical N_K/N_γ	K/L
90	0.073	—		0.074	$M1$	0.072	
92	1.000	1.000	0.14	0.63	$E2$	0.71	7.0
182	0.81	0.014		0.011	$M1$	0.012	12.6
206	0.021	9.8×10^{-4}	7×10^{-5}	0.029			~14
296	0.54	2.5×10^{-3}	3.3×10^{-4}	2.9×10^{-3}	$M1$	3.5×10^{-3}	7.6
388	0.13	3.9×10^{-4}		1.9×10^{-3}	$M1$	1.9×10^{-3}	

The Ga^{67} gamma-radiation was also studied with a thin magnetic lens spectrometer. The photoelectron distributions from thin U, Os, Ta, and In radiators were measured using about 50-Mc Ga^{67} sources. These photoelectron distributions confirmed the presence of 92-, 182-, 296-, and 388-kev gamma-rays and indicated that a 206-kev gamma-ray was emitted in low intensity.

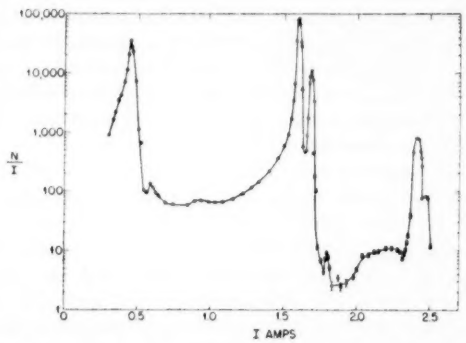

FIG. 2. Low energy conversion electron spectrum of Ga^{67}.

CONVERSION ELECTRONS

In measuring the energy distribution of conversion electrons a thin magnetic lens spectrometer with a momentum resolution of 1.5 percent full width at half-height was used. The detector was a proportional counter with a 10-μg/cm² window. The essentially weightless source was prepared as described above and was deposited on a 25 μg/cm² gold film which had been evaporated onto a 25 μg/cm² Formvar film. The intensity distribution at energies below about 180 kev is shown in Fig. 2 and at energies between 140 kev and 390 kev in Fig. 3. The K-conversion line of the 182-kev gamma-ray appears in each figure at 2.405 amperes. The log of N/I has been plotted rather than N/I because of the wide range of intensities encountered. The data for Fig. 3 were obtained with a somewhat more intense source and with somewhat poorer spectrometer resolution. At energies above 390 kev the conversion

[11] W. H. Jordan and P. R. Bell, Nucleonics **5**, 30 (October, 1949).
[12] C. J. Borkowski and R. L. Clark, Rev. Sci. Instr. (to be published).
[13] E. Fairstein, Rev. Sci. Instr. **22**, 761 (1951).

electron intensities were too low to measure with precision even when 10-Mc sources were used.

The conversion electron data confirm the presence of 92-kev, 182-kev, 296-kev, and 388-kev gamma-rays found with the scintillation spectrometer and also the 206-kev gamma-ray indicated by the photoelectron data. The relative intensities of the K- and L-conversion electron lines are given in Table I. The intensity data also show the presence of auger electrons at 7 kev and two sharp but low intensity peaks at 10 kev and 100 kev which may result from photoelectric absorption of the 92-kev and 182-kev gamma-rays, respectively, in the conducting gold film of the source. In addition, there are two rather broad low intensity distributions in the region of 140 kev and 325 kev. The relative intensities of these broad distributions were found to change from source to source. When an additional conducting film was placed behind the source, the number of electrons in these two energy regions was increased relative to the intensity of the conversion electron peaks. Because

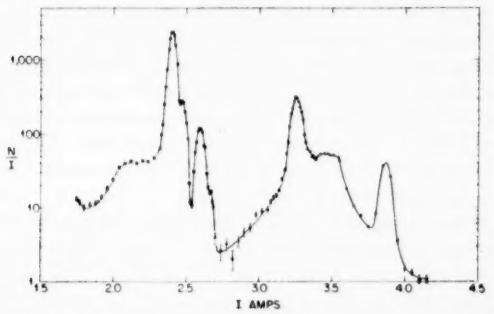

FIG. 3. Higher energy conversion electron spectrum of Ga^{67}.

of this it has been concluded that these electrons result from secondary processes.

COINCIDENCE MEASUREMENTS

Since the sum of the energies of the 92-kev and the 296-kev transitions reported by Helmholtz is the same as the energy of the 388-kev gamma-ray, this gamma-ray would be expected to be a cross-over transition, and coincidences between the 92-kev and the 296-kev gamma-rays should occur. Concidences were measured between the conversion electrons of the 92-kev gamma-ray on the magnetic lens spectrometer and the 296-kev gamma-ray on a scintillation spectrometer. Although true coincidences were found, the number of such coincidences was lower by an order of magnitude than would be expected from the counting yields of the two radiations. True coincidences also occurred when the 296-kev gamma-ray pulses were delayed several microseconds. A series of measurements with different delay lines showed that the 92-kev transition was from a metastable level which decayed with an 8.5-μsec half-life. The delayed coincidence data are shown in Fig. 4.

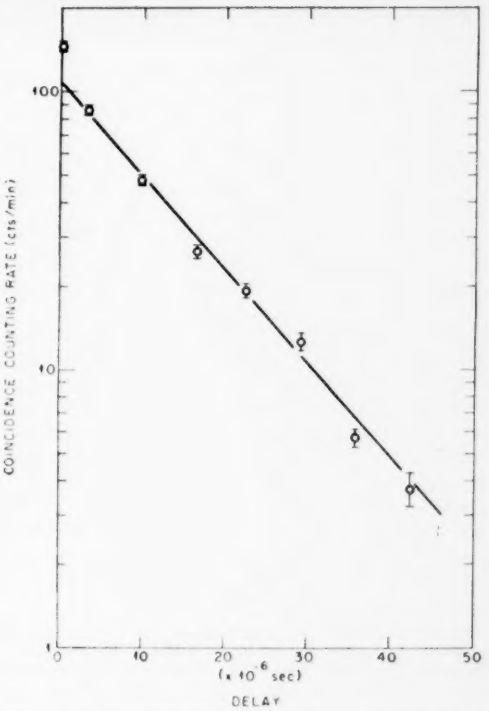

FIG. 4. Decay curve of the 92-kev metastable level of Zn^{67}.

In order to determine which gamma-transitions terminated at the metastable level, the pulses from two scintillation spectrometers were fed to a coincidence circuit. The two detectors were located about 1 cm apart with a Ga^{67} source placed between them. One spectrometer was set to accept pulses from the 92-kev gamma-ray and feed them directly to the coincidence circuit, while a 3.3-μsec delay line was placed between the second spectrometer and the coincidence circuit. Coincidence counting rates were then measured as a function of the pulse size accepted by the second spec-

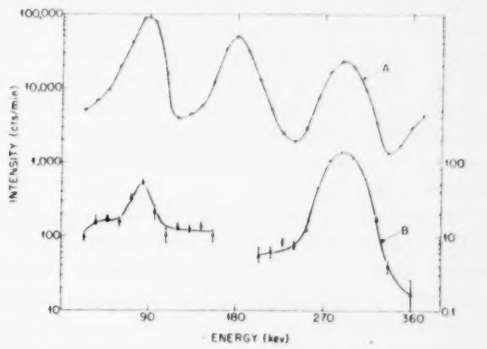

FIG. 5. Delayed pulse-height distribution coincident with 92-kev γ-ray. A. Single channel pulse-height distribution on left ordinate; B. Coincident pulse-height distribution on right ordinate.

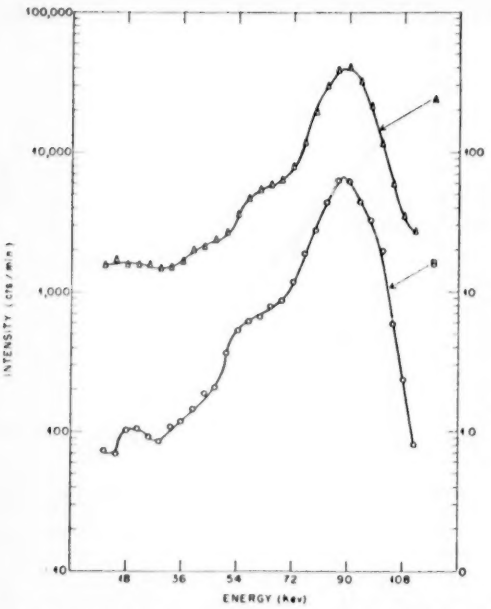

FIG. 6. Pulse-height distribution coincident with delayed 296-kev γ-ray. A. Single channel pulse-height distribution on left ordinate; B. Coincident pulse-height distribution on right ordinate.

trometer. Figure 5 shows the pulse counting rate of the second spectrometer and the coincidence counting rate, corrected for random events, as a function of the pulse height accepted by the second spectrometer. The data in Fig. 5 show that transitions with energies of 296 kev and 90 kev terminate at the metastable level. The relative intensity of these transitions was computed from the pulse counting rates and the intensity calibration curve of the second scintillation spectrometer.

To learn which transitions originate at the metastable level, pulses arising from the 296-kev gamma-ray were delayed. Coincidence counting rates were then measured as a function of the pulse height accepted by the other scintillation spectrometer. The pulse counting rates and the corrected coincidence counting rates are plotted in Fig. 6 as a function of pulse height. A 600-mg/cm^2 copper absorber was placed between the source and the detector counting the 296-kev pulses to prevent scattering of iodine x-rays into the other detector. The data in Fig. 6 show that pulse height peaks corresponding to energies of 92 kev and 21 kev originate at the metastable level.

The peak at 21 kev results from absorption of the 92-kev gamma-ray in the crystal by the Compton process with escape of the backscattered secondary gamma-ray from the crystal. This was shown by measuring the pulse-height distribution coincident with the 21-kev peak. The coincident gamma-rays had an energy of 70 kev and were found to originate in the crystal rather than the source. When the crystals were shielded from each other, the coincidence counting rate was reduced essentially to zero. In a similar manner apparent coincidences between 70-kev and 110-kev gammas were shown to result from Compton absorption of the 182-kev gamma-ray. Likewise, Compton absorption of the 296-kev gamma-ray leads to apparent coincidences between pulse height peaks corresponding to 140-kev and 150-kev gamma-rays.

Although Compton absorption of the 388-kev gamma-ray would lead to apparent coincidences between 182-kev and 206-kev radiations, it was shown that the 182-kev gamma-ray is in prompt coincidence with the 206-kev gamma-ray, since coincidences occurred when a lead absorber was placed between the crystals. As can be seen in Fig. 1, the resolution of our scintillation spectrometers was so low that pulses arising from neither the 182- nor the 206-kev gamma-ray could be counted with reasonable efficiency without accepting some pulses resulting from the presence of the other gamma-ray. The coincidence data shown in Fig. 7 were taken by accepting pulses from the low energy side of the 182-kev peak with one spectrometer while scanning with another spectrometer. When pulses from the high energy side of the 182-kev peak were accepted, the intensity of the coincident 90-kev peak was enhanced, and the position of the other peak was shifted to 182 kev. These measurements show that the 206-kev gamma-ray of Ga^{67} is in prompt coincidence with both a 90-kev and a 182-kev gamma-ray.

When pulses arising from either the 296-kev or the 388-kev gamma-ray were accepted, a peak was found in the coincident pulse height distribution corresponding to a 490-kev gamma-ray. Alternatively, when pulses corresponding to a 490-kev gamma-ray were accepted, the coincident pulse-height distribution had peaks

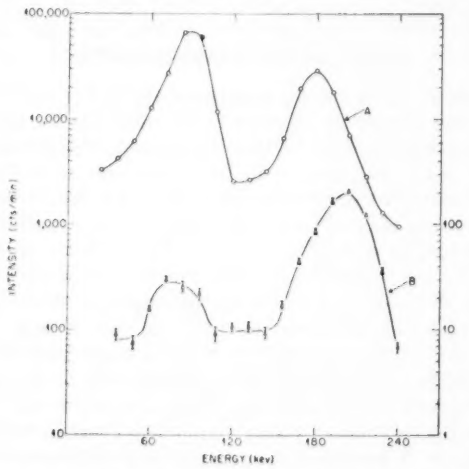

FIG. 7. Pulse-height distribution coincident with γ-rays in the 200-kev region. A. Single channel pulse-height distribution on left ordinate; B. Coincident pulse-height distribution on right ordinate.

arising from both the 296-kev and the 388-kev gamma-rays. These data show that both the 296-kev and the 388-kev gamma-rays are in prompt coincidence with a 490-kev gamma-ray.

Each of the Ga^{67} gamma-rays was found to be in coincidence with Zn x-rays when a proportional counter spectrometer was used as the detector for one channel of the coincidence counter. When the x-ray pulses were delayed several microseconds, only the 92-kev gamma-ray gave coincidences. This indicates that the 92-kev transition is the only transition which is delayed more than a few tenths of a microsecond.

In all of the coincidence measurements reported here when a coincident peak was found pulses from this peak were accepted, and the pulse height distribution in coincidence was scanned. This was done in order to establish that the coincidences were between two definite radiations and not between pulses arising from a particular radiation and a scattering process.

CONVERSION COEFFICIENTS AND BRANCHING RATIOS

Evidence has been presented for nine gamma-transitions in the decay of Ga^{67}. An energy level scheme for Zn^{67} which is consistent with the transition energies and the coincidence measurements is shown in Fig. 8. The relative intensities given in Table I can be used to compute conversion coefficients and branching ratios when the ratio of conversion processes to gamma-processes is known for a particular sample. This ratio was determined by measuring conversion electron intensities in a beta-spectrometer with calibrated transmission and gamma-intensities in a sample of known relative strength using a scintillation spectrometer with calibrated detection efficiency. The conversion coefficients are given in Table I, and the branching ratios are given in Table II and Fig. 8.

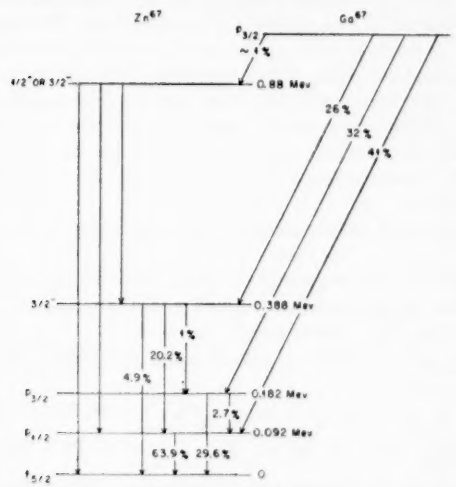

FIG. 8. Decay scheme of Ga^{67}.

TABLE II. Branching ratios in electron capture decay of Ga^{67}.

Energy of transition or level, kev	Percent of disintegrations giving transition	Percent of captures to level
90	2.7	
92	63.9	41
182	29.6	32
206	1	
296	20.2	
388	4.9	26
496	0.4	
790	0.2	
880	0.4	1

Since the 90-kev and 92-kev radiations were not resolved in either the conversion electron or the gamma-ray measurements, the conversion coefficients for these transitions were determined in the following manner. The intensity of the 90-kev gamma-ray relative to the 296-kev gamma-ray was found, from the delayed gamma 92-kev gamma coincidence data presented in Fig. 5, to be 0.135. The sum of the intensities of the 90-kev and the 92-kev gamma-rays relative to the 296-kev gamma-ray was found, from the scintillation spectrometer data presented in Fig. 1, to be 1.99. Therefore the ratio of intensity of the 90-kev gamma to the 92-kev gamma is 0.073.

In principle the ratio of intensities of the 90-kev and 92-kev conversion electrons could be determined by a method analogous to that used for the gamma intensity ratio. Since the method would involve low counting rates and would be subject to rather large errors, a different procedure was used. The coincidence counting rate between delayed 90-kev gamma-pulses and 92-kev conversion electron pulses is given by

$$C(\gamma_d-e)=\frac{Df'_{90}E_\gamma\alpha_{92}E_e}{(\alpha_{90}+1)(\alpha_{92}+1)}e^{-\lambda(t-\tau)}(1-e^{-2\lambda\tau}), \quad (1)$$

where $D=Ga^{67}$ disintegration rate, $f=$fraction of disintegrations giving the particular transition, $\alpha=$total conversion coefficient $(N_K+N_L)/N_\gamma$, $\tau=$resolving time of the coincidence counter, $t=$delay time, $\lambda=$decay constant of the 92-kev metastable level, $E_\gamma=$gamma-counting efficiency, $E_e=$conversion electron counting efficiency, and the subscripts refer to the transition energy. The coincidence counting rate between delayed 90-kev conversion electron pulses and 92-kev gamma-ray pulses is given by

$$C(e_d-\gamma)=\frac{Df_{90}\alpha_{90}E_\gamma}{(\alpha_{90}+1)(\alpha_{92}+1)}E_e e^{-\lambda(t-\tau)}(1-e^{-2\lambda\tau}), \quad (2)$$

where the notation is the same as in Eq. (1). When the slight difference in counting efficiencies of the 90-kev and 92-kev radiations is neglected, the ratio of the two coincidence counting rates gives the ratio of the total conversion coefficients of the 90-kev and 92-kev radia-

tions. The experimentally determined ratio α_{90}/α_{92} was found to be 0.12, showing that the 90-kev gamma-ray is internally converted to a much smaller extent than the 92-kev gamma-ray. Since the 90-kev gamma-ray intensity is only 0.073 of the 92-kev gamma-ray intensity, not more than 1 percent of the conversion electrons from these transitions is from the 90-kev gamma-ray. With this information the conversion coefficient of the 92-kev gamma-ray given in Table I was computed from the intensity data and the 90-kev coefficient was obtained from the ratio, α_{90}/α_{92}, determined above.

In order to check the 92-kev conversion coefficient determined by the above method, coincidences were measured between delayed 296-kev gamma-pulses and the 92-kev gamma-ray. The 296-kev gamma-count is given by

$$C_{296}=Df_{296}E_{296}/(\alpha_{296}+1), \tag{3}$$

and the 92-kev plus the 90-kev gamma-count is given by

$$C_{92}+C_{90}=\frac{Df_{92}E_{92}}{(\alpha_{92}+1)}+\frac{Df_{90}E_{90}}{(\alpha_{90}+1)}. \tag{4}$$

The coincidence counting rate is

$$C_{\gamma-\gamma}=\frac{Df_{296}E_{296}E_{92}}{(\gamma_{296}+1)(\alpha_{92}+1)}e^{-\lambda(t-\tau)}(1-e^{-2\lambda\tau}), \tag{5}$$

where the notation is the same as in Eq. (1). The product of the two gamma-counting rates divided by the coincidence counting rate is

$$\frac{C_{296}(C_{92}+C_{90})}{C_{\gamma-\gamma}}=\frac{Df_{92}}{e^{-\lambda(t-\tau)}(1-e^{-2\lambda\tau})}[1+C_{90}/C_{92}]. \tag{6}$$

Since the ratio of 90-kev and 92-kev gamma-counting rates was determined before and since the delay time, resolution time, and the decay constant of the 92-kev metastable level are known, this equation can be solved for Df_{92}, which is the rate of decay through the 92-kev level for the particular sample. When this rate is taken with the 92-kev conversion electron rate for the same sample, the 92-kev conversion coefficient obtained is in good agreement with that given in Table I.

Although the relative number of transitions of a given energy and the relative branching to excited levels is known, the relative number of orbital electron captures to the ground state remains to be determined. This was done by measuring prompt x-ray—182-kev gamma-coincidences. The K x-ray counting rate is given by

$$C_x=[Df_K+\Sigma K]E_x, \tag{7}$$

where the notation is the same as in previous equations and f_K = the fraction of electron captures which are K-electron captures, ΣK = the total K-conversion rate for all transitions, and E_x = the x-ray counting efficiency including the fluorescent yield. The gamma-counting rate is

$$C_{182}=Df_{182}E_{182}/(\alpha_{182}+1), \tag{8}$$

and the coincidence counting rate is

$$C_{x-\gamma}=\frac{Df_{182}f_KE_{182}E_x}{(\alpha_{182}+1)}. \tag{9}$$

The product of the two counting rates divided by the coincidence rate is

$$C_xC_{182}/C_{x-\gamma}=D+(\Sigma K/f_K). \tag{10}$$

Since ΣK, the total K-conversion rate of the sample, can be determined and since f_K can be obtained from theory,[14] this equation can be solved for D, the total electron capture rate. When this capture rate is compared with the capture rate to excited levels in Zn^{67}, as obtained from the transition intensities, the two rates are in good agreement, showing that not more than a few percent of electron captures occur directly to the ground state of Zn^{67}.

SPIN ASSIGNMENTS

On the basis of shell theory[15] and the data presented here, spin assignments can be made to the excited levels of Zn^{67}. The ground state spin of Zn^{67} has been measured and agrees with the shell theory assignment of $f_{5/2}$. The K-conversion coefficient of the 92-kev gamma-ray indicates[16] that it is an $M2$ or an $E2$ transition. The shell theory predicts a $p_{1/2}$ level which would give an $E2$ transition to the ground state, and, therefore, the 92-kev level is given a $p_{1/2}$ assignment. The transitions from the 388-kev and 182-kev levels, with the exception of the 206-kev gamma-ray, have conversion coefficients which indicate $M1$ transitions. Since there are no single particle assignments consistent with these observations, these levels are given $3/2^-$ assignments. No conversion coefficients were measured for transitions originating at the 880-kev level, but since the intensities of the transitions to the $p_{1/2}$ and $f_{5/2}$ levels are about the same, the most probable spin assignment for this level is also $3/2$.

The shell theory assignment for the ground state of Ga^{67} is $p_{3/2}$. This makes transitions to all of the levels of Zn^{67} except the ground state allowed. The transitions to the ground state with $\Delta l=2$ would fall into the class of l-forbidden transitions.[17]

It is a pleasure to acknowledge the help of H. D.

[14] M. E. Rose and J. L. Jackson, Phys. Rev. **76**, 1540 (1949).
[15] M. G. Mayer, Phys. Rev. **78**, 16 (1950).
[16] Rose, Goertzel, Spinrad, Harr, and Strong, Phys. Rev. **83**, 79 (1951).
[17] Mayer, Moszkowski, and Nordheim, Revs. Modern Phys. **23**, 315 (1951).

Bruner, M.D., of the Medical Division of the Oak Ridge Institute of Nuclear Studies whose interest and cooperation furnished the impetus for this work. We want to thank R. J. Hayes also of the Medical Division of the Institute, who furnished all of the Ga^{67} samples and made many special chemical separations; H. Zeldes of this Laboratory, who made many suggestions and helped with the preliminary work; and C. J. Borkowski and his co-workers for their help with the instrumentation.

PHYSICAL REVIEW VOLUME 90, NUMBER 4 MAY 15, 1953

Photomesonic Fission of Bismuth*

G. BERNARDINI, R. REITZ,† AND E. SEGRÈ‡
University of Illinois, Urbana, Illinois

(Received January 26, 1953)

The fission of bismuth by high energy photons is detected by a photographic plate technique and some measurements on the cross section as a function of the photon energy are reported.

These suggest that the mechanism for fission is the generation of pions inside of the bismuth nucleus, and their subsequent re-absorption in the same nucleus in which they have been produced. This re-absorption generates high energy nucleons which produce the fission.

THERE is a good amount of evidence that heavy nuclei absorb gamma-rays with a sort of broad resonance around 20 Mev and a decreasing cross section at higher energies,[1] but, besides this purely electromagnetic process of energy absorption, there is evidence for another mechanism of energy transfer from a photon to a nucleus operative from about 140 Mev; namely, through the intermediate "production" of a meson in the nuclear matter of the nucleus. This meson may be re-absorbed in the nucleus in which it has been produced and when this occurs it provokes a nuclear reaction corresponding to a liberation of energy much larger than what can be transferred by the photon directly through a simple electromagnetic interaction.

Evidence of this is shown, e.g., in the photostars,[2] in the photodisintegration of the deuteron and in the production of high energy protons or neutrons by gamma-rays.[3–6]

We have studied another fairly typical example of this phenomenon, namely, the photofission of bismuth. By exposing Ilford emulsions loaded with bismuth in the beam of the Illinois betatron we have found the following excitation curve, Fig. 1, for fission. The details of the exposure are as follows: Emulsion 200μ thick of D1-type contains, according to Ilford, 0.27 of a gram of bismuth per cm^3 of emulsion, 1600 r of bremsstrahlung *at the plate* (measured with a Victoreen thimble ionization chamber, behind a flat sheet of $\frac{1}{8}$ in. Pb). The plates were developed with the usual Occhialini temperature procedure, omitting however the pre-soaking. The procedure started directly with Amidol developer at 3°C. The fissions were counted and recognized as such from the length of the track (16–26μ) and from the density and aspect of the tracks. Equally exposed D1 plates not loaded with bismuth did not show any appreciable number of fission tracks. Six series of exposures at betatron energies of 100, 150, 200, 250, 290, 319 Mev were made, and the fission cross section per equivalent quantum was obtained (Fig. 1). The data were then further analyzed, using the theoretical bremsstrahlung spectrum[7] and the cross section for fission as a function of the photon-energy was determined. The results are shown in Fig. 2.

These measurements, although admittedly crude, deserve some comments. In the first place, the fission cross section becomes appreciable around 150 Mev, i.e., not far from the pion production threshold and increases rapidly with energy. The curve shape also seems to suggest that fission occurs mainly by the mechanism outlined at the beginning of this article, and probably

TABLE I. Fission cross sections of bismuth.

Particle	Energy in Mev	σ_f in 10^{-24} cm^2	$\Gamma_f/\Sigma\Gamma$
p	300	0.05–0.08	0.05
d	200	0.15	0.11
α	300	0.45	0.32
x-rays	300	0.009	0.25

* Supported by the joint program of the U. S. Office of Naval Research and U. S. Atomic Energy Commission.

† U. S. Atomic Energy Commission Predoctoral fellow.

‡ Now at the Department of Physics, University of California, Berkeley, California.

[1] See, e.g., J. M. Blatt and V. Weisskopf, *Theoretical Nuclear Physics* (John Wiley and Sons, Inc., New York, 1952), p. 651 ff.

[2] S. Kikuchi, Phys. Rev. **86**, 41 (1952).

[3] R. R. Wilson, Phys. Rev. **86**, 125 (1952).

[4] R. H. Huddlestone and J. V. Lepore, Phys. Rev. **87**, 207 (1952); W. S. Gilbert and J. W. Rosengren, Phys. Rev. **88**, 901 (1952).

[5] K. M. Terwilliger and L. W. Jones, Phys. Rev. **87**, 196 (1952).

[6] Kerst, Koester, Penfold, and Smith, Phys. Rev. **87**, 197 (1952).

[7] L. I. Schiff, Phys. Rev. **83**, 252 (1951); L. Katz and A. Cameron, Can. J. Phys. **29**, 518 (1951).

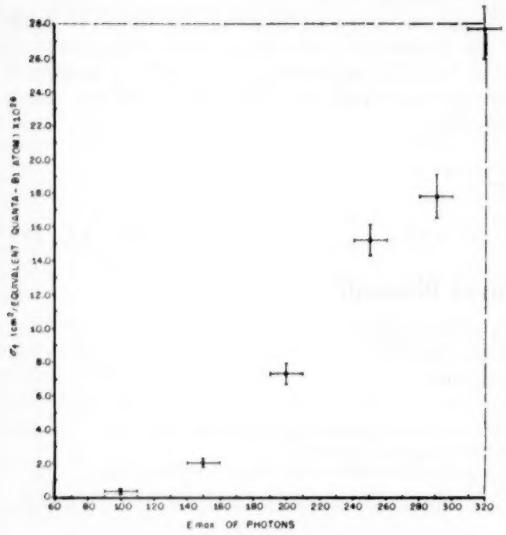

FIG. 1. Photofission excitation curve for bismuth.

with the contribution of the different kinds of mesons. The cross sections for the internal production of mesons is equal to σ'/p, where p is the escape probability of the meson from the nucleus, and σ' is the apparent production cross section, or the cross section for production of "free" mesons. If we try to make a more quantitative comparison, we may consider the point at maximum energy (310 Mev). The fission cross section σ_f can be estimated as

$$\sigma_f = A(\sigma_{\pi^0} + q\sigma_{\pi^\pm})(1-p)(\Gamma_f/\Sigma\Gamma),$$

where A is the mass number of bismuth (209), σ_{π^0}, $\sigma_{\pi^\pm}$ the cross sections for production of mesons on free nucleons, q is a correction factor which takes into account the fact that Pauli's principle, by preventing the nucleons to recoil into an occupied state, depresses the $\sigma_{\pi^\pm}$ meson production and $\Gamma_f/\Sigma\Gamma$ is the probability that the excited nucleus undergoes fission.

The values of σ_{π^0}, $\sigma_{\pi^\pm}$ are known roughly[8,9] and by integrating the differential cross sections, found by the investigations quoted above, we can estimate the σ_π. The factor q is near one as we can deduce from a comparison of photomeson production in carbon and hydrogen,[9,10] and p must be small as shown by the $A^{\frac{2}{3}}$ dependence of the photomeson production which indicates that photoproduction of mesons is a nuclear surface phenomenon.[10]

If we assume that the nucleus is fairly opaque ($p=0.2$) as suggested by the results of Littauer and Walker,[10] we arrive at the following crude estimate for σ_f:

$$\sigma_f = 209(1.5\times10^{-28}+0.55\times10^{-28})0.8(\Gamma_f/\Sigma\Gamma)\ \text{cm}^2.$$

The experimental value is $(5\div10)\times10^{-27}$, which would give $\Gamma_f/\Sigma\Gamma\sim0.25$. It is of interest to compare this number with the data on fission of bismuth induced by other high energy particles.[11]

Jungerman[11] finds the values reported in Table I for protons, deuterons, and α-particles. The geometrical cross section of bismuth is 2.35×10^{-24} cm^2 and σ_i(inelastic) for neutrons of 270 Mev is about 1.4×10^{-24} cm^2.[12] This last figure combined with σ_f, according to the relation $\sigma_f/\sigma_i=\Gamma_f/\Sigma\Gamma$, gives the numbers contained in the last column of Table I, except for the x-ray case.

We recognize that these evaluations of $\Gamma_f/\Sigma\Gamma$ are very crude indeed for several reasons, but we do not have, at present, better experimental data. For instance we lack reliable data on p, which seems to be considerably larger for 50-Mev mesons[13] than our assumption based on the direct results of Littauer and Walker.

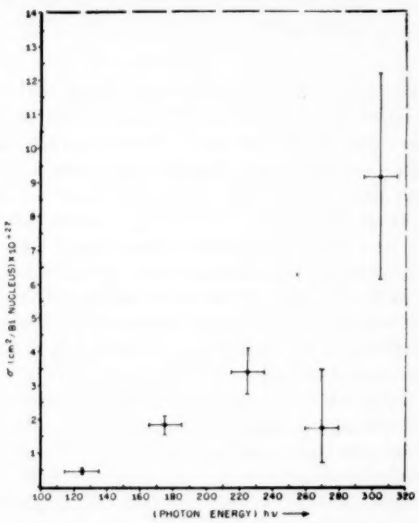

FIG. 2. Photofission cross section of bismuth as a function of the photon energy.

The order of magnitude of $\Gamma_f/\Sigma\Gamma$ for x-rays seems, though, to corroborate our interpretation of this effect, according to which the absorption of 300-Mev photons by bismuth is twofold: If it occurs on the surface it is often accompanied by meson-production, if it occurs in the interior, the mesons are mostly re-absorbed and accelerate a pair of nucleons to energies of the order of 100 Mev. The fission occurs when this pair of nucleons releases enough energy inside of the bismuth nucleus to produce fission with a mechanism similar to that accepted for fission produced by fast nucleons.[11]

[8] J. Steinberger and A. Bishop, Phys. Rev. **86**, 171 (1952).
[9] Steinberger, Panofsky, and Steller, Phys. Rev. **86**, 180 (1952); A. Silverman and M. Stearns, Phys. Rev. **88**, 1225 (1952).
[10] R. Littauer and D. Walker, Phys. Rev. **86**, 838 (1952).
[11] J. Jungerman, Phys. Rev. **79**, 632 (1950).
[12] J. DeJuren, Phys. Rev. **80**, 27 (1950).
[13] Byfield, Kessler, and Lederman, Phys. Rev. **86**, 17 (1952).

N^{14} Level Structure from the $C^{13}(p, n)N^{13}$ Reaction

J. K. Bair, J. D. Kington, and H. B. Willard
Oak Ridge National Laboratory, Oak Ridge, Tennessee
(Received January 26, 1953)

The neutron yield resulting from proton bombardment of C^{13} has been extended to a proton energy of 5 Mev. Maxima were found at bombarding energies of 3.78, 4.01, 4.10, 4.18, 4.52, and 4.8 Mev. The corresponding energies in the N^{14} compound nucleus are 11.05, 11.26, 11.35, 11.44, 11.74, and 12.0 Mev.

INTRODUCTION

THE threshold for the p, n reaction on C^{13} has been accurately measured by Richards, Smith, and Browne[1] to be 3.236 ± 0.003 Mev. Adamson, Buechner, Preston, Goodman, and Van Patter[2] have measured the neutron yield up to a bombarding energy of approximately 4 Mev. They found one maximum at 3.76 Mev followed by a rather rapid rise indicating that another level might exist at slightly higher energies than they were able to obtain. Blaser, Boehm, Marmier, and Scherrer[3] have investigated the excitation function to 6.8 Mev using a cyclotron and the stacked foil technique. The compound nucleus N^{14} has also been investigated in this energy region by means of the deuteron bombardment of C^{12}. The work of Bonner and the group at Rice Institute[4] and of Bailey, Freier, and Williams[5] yielded a number of levels in N^{14} at energies just above those reached by Adamson *et al.* As part of an effort to obtain further data on the relationship of levels in the same compound nucleus formed by different bombardments, the 5-Mev electrostatic generator at this laboratory has been used to extend the $C^{13}(p, n)N^{13}$ yield to higher energies.

EXPERIMENTAL PROCEDURE

An energy calibration of the magnetically analyzed proton beam was obtained as previously described,[6] and the reaction threshold was used as an additional calibration point. The beam energy determination is believed to be accurate to 0.2 percent relative to the $Li^7(p, n)Be^7$ threshold at 1.882 Mev. Resolution was also 0.2 percent or less. Targets consisted of thin (approximately 5 kev at threshold) carbon layers on platinum and were prepared by cracking methyl iodide vapor. The methyl iodide was obtained from Eastman Kodak Company with an enrichment of 61 percent. The targets were kindly prepared by Dr. H. E. Banta of this laboratory.

The neutron yield was measured by means of a "long counter" located at zero degrees with respect to the proton beam and placed 60 cm from the target. Neutron counts at each energy were measured for a fixed number of microcoulombs of beam as determined by a current integrator. Background, as determined by a run on a platinum target blank, was negligible. Since the $C^{12}(p, n)$ threshold is well above the beam energies used, no neutrons from that source should be produced.

RESULTS

Several runs were made over the energy region between threshold and 5 Mev. Figure 1 shows the unnormalized results not corrected for target thickness. The sharp rise at threshold is the geometrical peak. The rise at 3.78 Mev corresponds to the level found by Adamson *et al.*[2] Further well-defined maxima occur at 4.01, 4.18, 4.52, and 4.8 Mev corresponding to N^{14} excitation energies of 11.26, 11.44, 11.74, and 12.0, respectively. Blaser *et al.*[3] found maxima in our energy region at 4.0 and 4.9 Mev which, considering the 250 kev resolution of the foil technique used, agree well with our results. An unresolved peak was found at approximately 4.08 Mev. The resonances at 4.01 and 4.18 Mev were analyzed by fitting a Breit-Wigner curve to the data. When the effects of these two resonances were subtracted, the energy of the unresolved maximum was 4.10 Mev, corresponding to a N^{14} excitation energy of 11.35 Mev. For the levels at 4.01 and 4.18 Mev, a best fit was obtained using 20 and 30 kev, respectively, as the full widths at half maximum.

Table I lists in columns 1 and 2 our proton bombard-

TABLE I. Level structure of N^{14}: Columns 1, 2, and 3 list respectively the proton energy, width, and N^{14} excitation energy, as obtained from the $C^{13}(p, n)N^{13}$ reaction. Columns 4, 5, and 6 list the corresponding data from the reaction of $C^{12}+D^2$. Column 7 lists the products for which the deuteron-induced level has been observed.

	E_p Mev	$W_{\frac{1}{2}}$ kev	E_x Mev	E_d Mev	$W_{\frac{1}{2}}$ kev	E_x Mev	Type
1	3.78	100	11.05	0.91	100	11.04	$p\gamma n$
2	4.01	20	11.26	1.13	15	11.23	$p--$
3				1.16	100	11.26	$p\gamma-$
4	4.10	150	11.35				
5	4.18	30	11.44	1.30	50	11.38	$p\gamma n$
6				1.435	5.5	11.49	$p\gamma n$
7				1.62	100	11.65	$--n$
8	4.52	125	11.74	1.73	150	11.75	$-\gamma n$
9	4.8	100	12.0				

[1] Richards, Smith, and Browne, Phys. Rev. **80**, 524 (1950).
[2] Adamson, Buechner, Preston, Goodman, and Van Patter, Phys. Rev. **80**, 985 (1950).
[3] Blaser, Boehm, Marmier, and Scherrer, Helv. Phys. Acta **24**, 465 (1951).
[4] Bennett, Bonner, Richards, and Watt, Phys. Rev. **59**, 781 (1941); Bonner, Evans, Harris, and Phillips, Phys. Rev. **75**, 1401 (1949); Phillips, Bonner, and Richardson, Phys. Rev. **76**, 169 (1949); G. C. Phillips, Phys. Rev. **80**, 164 (1950); Farmularo, Thompson, and Bonner, Phys. Rev. **85**, 742 (1952).
[5] Bailey, Freier, and Williams, Phys. Rev. **73**, 274 (1948).
[6] Willard, Bair, Kington, Hahn, Snyder, and Green, Phys. Rev. **85**, 849 (1952).

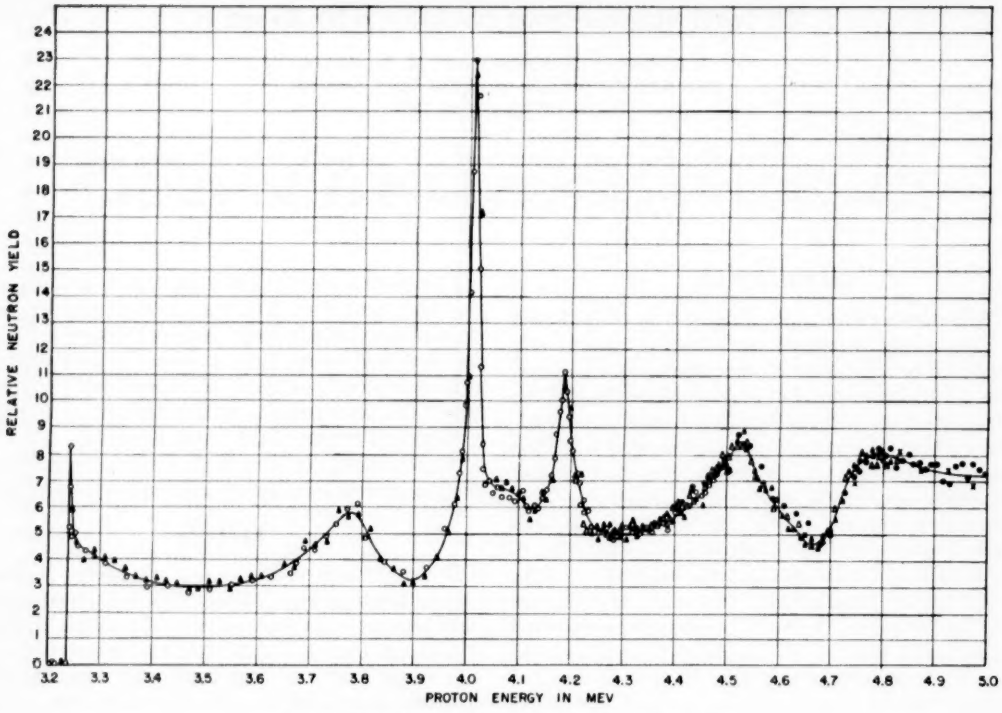

FIG. 1. $C^{13}(p, n)N^{13}$ yield curves in the forward direction.

ing energies and an estimate of the full width at half-maximum. Column 3 gives the excitation energies in N^{14}. Columns 4, 5, and 6 give corresponding data from the deuteron disintegration of C^{12}. Column 7 gives observed modes of disintegration of the deuteron induced reaction. The mass values of Li, Whaling, Fowler, and Lauritsen[7] were used to determine the excitation energies, $C^{13}+p-N^{14}=7.542$ Mev and $C^{12}+d-N^{14}=10.264$ Mev.

For maximum 1 of Table I, both the width and the excitation energies obtained by $C^{12}+d$ and $C^{13}+p$ are, as has been pointed out,[2] in good agreement. Although the excitation energy of our level at 4.01 Mev agrees best with that of the 1.16-Mev $d-p$ and $d-\gamma$ level, the width agrees much better with the 1.13 Mev $d-p$ level. Since the energy discrepancy is small (30 kev) and since the angular distribution can cause apparent energy shifts of this amount, we feel that it is more reasonable that our level at 4.01 Mev corresponds to that produced by 1.13-Mev deuterons. It would also appear that our maxima at 4.18 Mev and 4.52 Mev correspond to those produced by 1.30 and 1.73-Mev deuterons, respectively. It is possible that the wide unresolved maximum, number 4, at 4.10 Mev may correspond to the level excited by 1.16-Mev deuterons. A careful search over the region of proton bombarding energies from 4.2 to 4.5 Mev gave no indication of any maxima corresponding to those produced by 1.435- or 1.62-Mev deuterons. These measurements were made with the long counter at 0° with the proton beam, 60 cm from the target and also at 80° and 30 cm. The target thickness used was 4 kev (at threshold). No maximum in the deuteron data corresponds to that induced by 4.8-Mev protons; the next highest deuteron peak is at approximately 2.2 Mev, corresponding to a proton bombarding energy of about 5.0 Mev.

It is evident that the possibly expected correlation in N^{14} level structure as determined separately by proton and deuteron bombardment was not observed. It seems particularly interesting that at least two levels ($E_d=1.435$ and 1.62 Mev) appearing in the deuteron bombardments were not found in the present experiment. Apparently the explanation of the phenomena must await a more detailed description of the quantum states involved.

[7] Li, Whaling, Fowler, and Lauritsen, Phys. Rev. **83**, 512 (1951).

PHYSICAL REVIEW VOLUME 90, NUMBER 4 MAY 15, 1953

Geometrical Characterization of Nuclear States and the Theory of Angular Correlations

U. FANO
National Bureau of Standards, Washington, D. C.
(Received November 7, 1952)

Degenerate states of nuclei, atoms, or radiations are identified by their tensor properties, that is, by the mean values of a set of multipole operators. A treatment is outlined which serves to construct angular correlation functions on a geometrical basis and provides a geometrical interpretation of known correlation formulas; the dynamics of specific nuclear reactions influences only a final averaging procedure.

THE various degenerate states of a nuclear level with nonzero spin differ in geometrical properties loosely called "spin orientation" or "spin polarization." This note points out a geometrical characterization of the degenerate states of nuclei, atoms, or radiations, which serves to keep the geometrical elements of angular correlations separate from the dynamical elements.

The observation of the direction in which a nucleus has emitted a radiation provides *some* information about the "spin polarization" of the nucleus following the emission. This information, in turn, determines the directional distribution of radiations subsequently emitted by the same nucleus. Thus the data on the geometry of the intermediate nuclear state constitutes the central element of the angular correlation of successive nuclear radiations.

The correlation effect is but one example of problems in which the information available on a state amounts to less than the maximum afforded by quantum mechanics. States identified by less-than-maximum information are not described by a wave function but by a density matrix or, in an equivalent but more immediately operational manner, by the mean values $\langle U_\alpha \rangle$ of a complete set of operators U_α.[1]

The observable characteristics of a degenerate nuclear state that depend on its "spin polarization" include its coupling with anisotropic external fields. The coupling energies are the mean values of irreducible 2^k-pole tensor operators T_{kq} which transform under space rotations like the spherical harmonics Y_{kq}. The matrix elements of such operators in the (jm) scheme, $(j'm'|T_{kq}|jm)$, are known to consist of two factors. One factor depends on the angular momentum quantum numbers j', j and on the multipole order k as well as on the "spin orientation" and "multipole orientation" numbers m', m, and q. This factor may be expressed as a standard Wigner coefficient[2] $(kjj'm'|kjqm)$ or $(-1)^{j-m}(j'jm'-m|j'jkq)$. Being the same function of the quantum numbers for all different nuclei, it constitutes a purely geometrical element. The remaining factor, independent of the "orientation" quantum numbers m', m, and q, indicated by $(j'\|T_k\|j)$ or $(j'\|T^k\|j)$,[3] depends on the kind and strength of the interaction and on the nuclear structure, i.e., is different for different nuclei with equal j's.

A tensor operator, for which the second factor of the matrix element equals 1 for a specified pair of quantum numbers $(J'J)$ and zero otherwise, is a universal function of quantum numbers and therefore a purely geometrical element. Consider now a degenerate energy level of a nucleus, atom or radiation, which may include states with different angular momentum quantum numbers J, $J'\cdots$. Define the tensor operators $U_{kq}^{(J'J)}$ by the matrices

$$(j'm'|U_{kq}^{(J'J)}|jm) = (-1)^{j-m}(j'jm'-m|j'jkq)\delta_{j'J'}\delta_{jJ}, \quad (1)$$

where k runs from $|J-J'|$ to $J+J'$, q from $-k$ to k, and $(J'J)$ take all pairs of values pertaining to the energy level. This set of operators is "complete" in the sense that any matrix $(j'm'|T|jm)$ can be represented as a linear combination of matrices (1) and, particularly, that the density matrix of any state A of the energy level is completely determined by the set of mean values $\langle U_{kq}^{(J'J)}\rangle^{(A)}$. The irreducible tensors $\langle \mathbf{U}_k^{(J'J)}\rangle^{(A)} \equiv (\langle U_{kk}^{(J'J)}\rangle^{(A)}, \langle U_{kk-1}^{(J'J)}\rangle^{(A)} \cdots)$ may be called "state multipoles," owing to their relationship with multipole moments and interactions. For example, the state of spin j with fully random spin orientation ("natural spin polarization") is identified by the multipoles $\langle U_{kq}^{(J'J)}\rangle = (2j+1)^{-\frac{1}{2}}\delta_{jJ'}\delta_{j'J}\delta_{k0}\delta_{q0}$. The factor δ_{k0} indicates that all multipoles vanish in this unpolarized state (except the scalar $\langle U_{00}^{(JJ)}\rangle$, whose magnitude represents a trivial normalization constant). For a state of paramagnetic polarization, at least the dipole $\langle \mathbf{U}_1^{(JJ)}\rangle$ must be $\neq 0$.[4]

A technique based on the concept of "state multipoles" has been applied to the theory of angular correlations,[5] but its detailed publication has lagged pending

[1] See, for example, the application by L. Wolfenstein and J. Ashkin, Phys. Rev. **85**, 947 (1952), and especially the description of optical polarization by means of Stokes parameters, G. G. Stokes, Proc. Cambridge Phil. Soc. **9**, 399 (1852); U. Fano, J. Opt. Soc. Am. **39**, 859 (1949); D. L. Falkoff and J. E. Macdonald, J. Opt. Soc. Am. **41**, 861 (1951), which led to the ideas presented here.

[2] See, for example, E. U. Condon and G. Shortley, *Theory of Atomic Spectra* (Princeton University Press, Princeton, 1935), p. 71.

[3] G. Racah, Phys. Rev. **62**, 438 (1942), Sec. 3.

[4] For relativistic electrons and neutrinos a complete set of quantum numbers includes not only j and m but also $k=\pm(j+\frac{1}{2})$. Similarly for γ-rays one must add a quantum number of "electric" or "magnetic" multipolarity. Such quantum numbers must be treated like j's and one should actually write them alongside the j's, for example, $\langle \mathbf{U}_k^{(J'k'\,Jk)}\rangle$.

[5] National Bureau of Standards Report 1214 (1951).

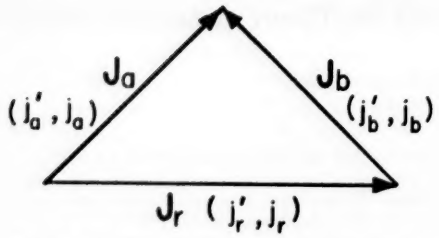

FIG. 1. Diagram of conservation of momentum and j quantum numbers.

improvements of the tensor operator algebra formalism in collaboration with G. Racah. An outline of the technique follows.

Consider the emission (or absorption) of radiation in the transition from a nuclear level a to a level b. The conservation of momentum in the transition is represented by the triangular diagram in Fig. 1. Each side of the triangle corresponds to one "reactant" (level a, level b, radiation). We also label it with a pair of quantum numbers $(j'j)$ which correspond to those of a set of state multipoles $\langle \mathbf{U}_k^{(j'j)} \rangle$. (When there is no degeneracy in j, i.e., when one reactant has a definite angular momentum j_0, there is only one pair of j's, namely, $(j_0 j_0)$.) The geometries of the three reactants are interdependent and the technique aims at expressing the "state multipoles" of any one of the three in terms of those of the other two. The usual situation is one in which (1) no information is available on the orientation of $\mathbf{J}_a$ so that

$$\langle \mathbf{U}_k^{(ja'ja)} \rangle^{(a)} = (2j_a+1)^{-\frac{1}{2}} \delta_{ja'j_0} \delta_{k0},$$

and (2) the emitted radiation has been detected by a polarization analyzer P in a direction $\mathbf{q}$, which determines the state multipoles $\langle \mathbf{U}_k^{(jr'jr)} \rangle^{(\mathbf{q}P)}$. Owing to the isotropic geometry of the state a, the state multipoles of b, $\langle \mathbf{U}_k^{(jb'jb)} \rangle^{(b)}$, are bound to be proportional to the radiation multipoles $\langle \mathbf{U}_k^{(jr'jr)} \rangle^{(\mathbf{q}P)}$. However, the radiation geometry would impress itself in full detail onto the geometry of b only if the angular momenta $\mathbf{J}_r$ and $\mathbf{J}_b$ were parallel, i.e., if $j_a = 0$. Otherwise the coupling through the randomly oriented $\mathbf{J}_a$ has a smearing effect which results in a "depolarization ratio"

$$\langle \mathbf{U}_k^{(jb'jb)} \rangle^{(b)} / \langle \mathbf{U}_k^{(jr'jr)} \rangle^{(\mathbf{q}P)} \leqslant 1. \qquad (2)$$

This ratio may be described as the transformation coefficient from a coupling scheme $\{[(j_a j_a)0, (j_r' j_r)k]k\}$ to $\{[(j_a j_r')j_b', (j_a j_r)j_b]k\}$ and is equal, to within a normalization constant, to the Racah coefficient $W(j_r' j_r j_b' j_b, k j_a)$.[3]

In a process of emission of two or more successive radiations, the diagram of conservation of momentum (Fig. 2) can be broken down into triangles. The "reactants" at the outer contour of the diagram are amenable to geometrical observation, in principle, but usually a correlation is established between the observations on two radiations only. Starting from the triangle containing the first observed radiation, one can "resolve" each triangle in succession, as for the triangle in Fig. 1 above. In this manner one constructs an expression for the expected multipoles $\langle \mathbf{U}_k^{(j_2 j_2)} \rangle^{(\exp)}$ of the second radiation. These multipoles equal the multipoles $\langle \mathbf{U}_k^{(j_1 j_1)} \rangle^{(\mathbf{q}_1 P_1)}$ of the first radiation, reduced by a depolarization ratio S_k which depends on the j's of all other "reactants." The detection of the second radiation by a detector $\mathbf{q}_2 P_2$ defines a different set of multipoles, $\langle \mathbf{U}_k^{(j_2 j_2)} \rangle^{(\mathbf{q}_2 P_2)}$. The predicted probability of detection by this detector is essentially the projection of the "expected" multipoles onto the detector's multipoles, that is, the sum of multipole scalar products

$$\Sigma_k \langle \mathbf{U}_k^{(j_2 j_2)} \rangle^{(\exp)} \cdot \langle \mathbf{U}_k^{(j_2 j_2)} \rangle^{(\mathbf{q}_2 P_2)} = \Sigma_k S_k \langle \mathbf{U}_k^{(j_1 j_1)} \rangle^{(\mathbf{q}_1 P_1)} \cdot \langle \mathbf{U}_k^{(j_2 j_2)} \rangle^{(\mathbf{q}_2 P_2)}. \qquad (3)$$

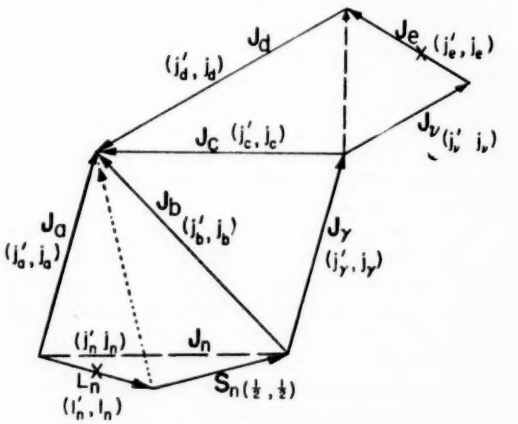

FIG. 2. Angular momentum diagram for the emission of a neutron in the transition from a to b, followed by an unobserved γ, from b to c, and by a β-process from c to d. "Reactants" whose geometry is observed are marked by a cross. The $\mathbf{J}_n$ vector is to be considered under conditions of strong spin-orbit coupling of the neutron, the dotted vector under conditions of strong spin-spin coupling with the nucleus. The spin-orbit coupling of electrons, neutrinos, and photons cannot be resolved, because of relativity (see reference 4).

This is a basic angular correlation function between $(\mathbf{q}_1 P_1)$ and $(\mathbf{q}_2 P_2)$, which depends only on quantum numbers j.[4] Therefore, it is a purely *geometrical* entity. This function pertains to a specified set of pairs of numbers $(j_a' j_a, j_1' j_1, j_b' j_b, \cdots)$ for each nuclear level and each radiation.

If various sets of j's have to be considered, a grand average must be performed over the corresponding correlation functions. Here is where the *dynamics* of the radiation emission by a specific nucleus enters into play; it determines the "weights" of the various elements in the average.

Formulas derived according to this procedure[5] are quite similar to formulas derived independently by F.

Coester and J. M. Jauch[6] and fully equivalent to those given by various authors, especially by Racah.[7]

[6] F. Coester, Helv. Phys. Acta, **26**, 3 (1953). Personal communication in advance of publication is gratefully acknowledged.

[7] G. Racah, Phys. Rev. **84**, 910 (1951). The scalar product $\langle U_k^{(j_1 j_2 j)}(q_1 P_1) \cdot \langle U_k^{(j_3 j_4 j)}(q_2 P_2)$ corresponds to the $\Sigma_{\rho\sigma} D^{(k)}{}_{\rho\sigma} C_{k\rho}{}^* C_{k\sigma}$ in Racah's Eq. (8), the depolarization ratio S_k to the product of W's. See also the general treatments of the angular correlations by L. C. Biedenharn and M. E. Rose, Revs. Modern Phys. (to be published); of the angular distribution of scattering and reaction cross sections by J. Blatt and L. C. Biedenharn, Revs. Modern Phys. **24**, 258 (1952); of the production of polarized particles in nuclear reactions by A. Simon and T. A. Welton, Phys. Rev. **89**, 886 (1953). The results of all these papers may be derived by the procedure outlined above.

The author is greatly indebted to G. Racah for a long series of discussions.

PHYSICAL REVIEW VOLUME 90, NUMBER 4 MAY 15, 1953

Nuclear Levels Associated with Zirconium 95 and Niobium 95†

J. M. Cork, J. M. LeBlanc, D. W. Martin, W. H. Nester, and M. K. Brice
Department of Physics, University of Michigan, Ann Arbor, Michigan

(Received February 9, 1953)

Using sources of zirconium 95, both as a fission product and as derived from neutron capture in enriched Zr^{94}, in magnetic spectrometers, a study has been made of the beta- and gamma-energies and of the half-lives associated with the radioactive decay. Zirconium 95 emits three beta-rays of energy about 910, 405, and 360 kev, each followed by a gamma-transition leading to a radioactive daughter product, niobium 95. The gamma-energies are 758, 725, and 235.2 kev. The niobium 95 decays by beta-emission, of energy 165 kev, to molybdenum 95 with accompanying gamma-energies of 753 and 768 kev. The observed transitions are found to fit a level scheme that is not incompatible with shell theory.

A LONG-LIVED radioactivity in zirconium, obtained as a fission product from uranium, was first observed[1] in 1940 by Grosse and Booth. Contemporary studies determined[2] the half-life of the activity to be 63 days and associated it with the isotope of mass 93. Subsequent investigations have shown that the activity is more likely in zirconium 95, which decays to radioactive daughter products in niobium 95. Many measurements have been made of the beta- and gamma-energies in the decay processes, with a rather wide divergence in the expressed values, as shown in Table I.

TABLE I. Previous data relative to Zr^{95} and Nb^{95}.

Item		Half-life	Energy in Mev PE[a]	RW[b]	MSK[c]	HL[d]	N[e]	F[f]	Z[g]
Zr^{95}	β_1	65 days	0.80			0.887	1.00		
	β_2		0.29			0.400	0.39		
	γ_1		0.85		0.91		0.92		
	γ_2					0.708	0.73		0.73
Nb^{95}	γ_3	90 hr				0.216	0.23		
Nb^{95}	β_1	35 days	0.14		0.14	0.146	0.15	0.163	
	γ_1		0.78	0.75	0.92	0.758	0.77	0.771	0.76

[a] M. Pool and J. Edwards, Phys. Rev. **67**, 60 (1945).
[b] W. Rall and R. Wilkinson, Phys. Rev. **71**, 321 (1947).
[c] Mandeville, Scherb, and Keighton, Phys. Rev. **74**, 888 (1948).
[d] J. Hugdens and W. Lyon, Phys. Rev. **75**, 206 (1949); *Radiochemical Studies: The Fission Products* (McGraw-Hill Book Company, Inc., New York, 1950), Paper No. 90.
[e] V. Nedzel, National Nuclear Energy Series, Plutonium Project Record, Vol. 9, Div. IV and earlier papers in Plutonium Project Reports.
[f] C. Fan, Phys. Rev. **81**, 300 (1951).
[g] Zucker, Mandeville, Shapiro, Mendenhall, and Conklin, Bull. Am. Phys. Soc. **28**, No. 1, 58 (1953).

† This investigation received the joint support of the U. S. Office of Naval Research and the U. S. Atomic Energy Commission.

[1] A. V. Grosse and F. Booth, Phys. Rev. **57**, 664 (1940).
[2] Sagane, Kojima, Miyamoto, and Ikawa, Phys. Rev. **57**, 1179 (1940).

In the present investigation specimens of Zr^{95} have been obtained both as a fission product and as produced in the pile by neutron capture in enriched (92 percent) zirconium 94. The gamma-energies have been determined from electron lines derived from internal conversion and from photoemission in lead radiators. Photographic magnetic spectrometers of high resolution have been employed and it is believed that the reported results are accurate to plus or minus 0.2 percent. The decay of Zr^{95} has been followed for more than a year and its half-life appears to be 65.2±1 days. A metastable state of niobium 95 with a half-life of 90

TABLE II. Electron energies associated with Zr^{95} and Nb^{95}.

Electron energy, kev	Interpretation	Energy sum, kev
216.1	*K* (41)	235.1
232.6	*L* (41)	235.3
235.0	*M* (41)	235.5
706.3	*K* (41)	725.3
722.7	*L* (41)	725.4
733.0	*K* (42)	753.0
739.6	*K* (41)	758.6
748.6	*K* (42)	768.6
765.8	*L* (42)	768.7
678	*K* (Pb)	766

TABLE III. Gamma energies due to transitions in Nb^{95} and Mo^{95}.

Nucleus	Energy, kev	*K*/*L* ratio
Nb^{95}	235.2	4.5±0.6
	725	5.0±1.0
	758	—
Mo^{95}	753	—
	768	7.6±0.6

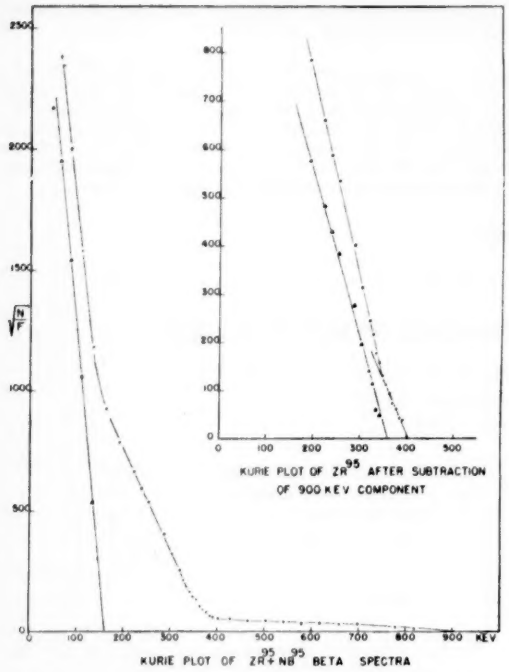

FIG. 1. Resolution of the beta-spectrum of zirconium 95.

hours had been reported. Beta-emission from the ground level of niobium leads to molybdenum 95. The half-life of this decay had been reported to be 35 days, and the radiation was believed to consist of a beta-ray followed by a single gamma.

The electron lines observed from the Zr^{95} source indicated the existence of more gamma-rays than had been previously reported. In order to identify the electron lines associated with the daughter product, a chemical separation of the niobium from the parent activity was kindly made by the Oak Ridge National Laboratory. Spectrograms obtained with this separated material allowed a complete resolution of the composite spectrum. The observed electron energies together with their interpretations are shown collected in Table II. The energies of the gamma-rays are given in Table III. The half-life of the separated niobium appears to be 35 ± 0.5 days.

It is of interest that of the many transitions assigned to the molybdenum 95 nucleus, from a study of the K-capture decay in technetium 95, only one, namely, the gamma-ray at 768 kev, is found to be present in the niobium radiation.[3]

The K/L ratios, shown in Table III, for three of the gamma-rays have been evaluated from densitometer traces of the photographic plates made with a Leeds and Northrup recording microphotometer. For the other two gamma-rays only the K lines were observed so the K/L ratios must be large compared to unity. It is apparent that absorption methods could never resolve the many gamma-rays with energies so nearly alike, nor could the proper assignments be made without the chemical separation.

In order to determine the proper arrangement of the three gamma-transitions in the niobium 95 nucleus a careful re-examination has been made of the beta-emission. The double focusing magnetic spectrometer of 40 cm diameter was employed in this study. The G-M tube was provided with a very thin zapon window and the metallized zapon backing of the source was as near massless as possible. The observed electron distribution is shown graphically on a "Kurie" plot in Fig. 1. The high energy component comprises only about two percent of the total number of electrons, and consequently is not subject to the best statistics.

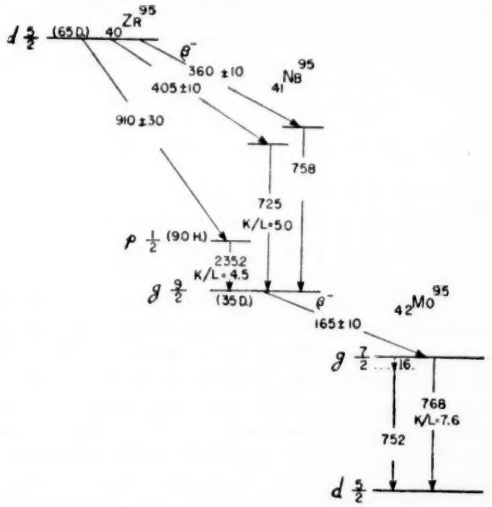

FIG. 2. Proposed nuclear level scheme for the radioactive decay of zirconium 95.

The upper energy limit appears to be about 910 ± 30 kev with a log ft value of 9.7. On the subtraction of this high energy component it seems quite certain that the resulting "Kurie" line is resolvable into two betas differing by about 40 kev at an energy around 400 kev. The exact end points and the relative percentage of each depend to some extent upon the choice of slope. The most probable energy values appear to be 405 and 360 kev, each with a log ft value of about 6.5. The beta-spectrum of niobium is also present as a low energy component, shown resolved in Fig. 1. The chemically separated source was also studied, confirming that the spectrum has an allowed shape with an upper energy limit of 165 ± 10 kev and a log ft of 5.0.

The gamma- and beta-energies may be arranged in a decay scheme as shown in Fig. 2. In the arrangement as shown, a low energy gamma-ray of about 16 kev might be expected. This energy is too low to produce

[3] Medicus, Preiswerk, and Scherrer, Helv. Phys. Acta **23**, 299 (1950).

conversion electrons observable in our spectrometers. There is evidence from an observation of the absorption in aluminum that some very low energy gamma-radiation is present.

The ground state of the molybdenum nucleus has been found to be $d_{5/2}$. For the first excited level of the odd-even nucleus with 53 neutrons, from shell theory, a $g_{7/2}$ level is expected. This is in good agreement with present observations if the 768-kev transition is magnetic dipole, and it also satisfies the allowed 165-kev beta-transition from a $g_{9/2}$ level. The 235-kev radiation in niobium is by virtue of its long radiation lifetime and its high conversion coefficient interpreted as an $M4$ transition. If, then, the upper level is a $p_{1/2}$ state and the initial zirconium level, like the molybdenum ground state, is characterized as $d_{5/2}$, it would follow that the 910-kev beta-transition would be forbidden, as observed. No transition from the initial $d_{5/2}$ level to the niobium $g_{9/2}$ level would be expected.

Note added in proof:—A recent report by V. Shpinel (USSR) Zhur. Eksptl. i Teort. Fiz. **21**, 1370 (1951), treats these radioactivities. Two gamma-rays are evaluated from photoelectrons and others are postulated to exist from differences in observed beta-energies. These are not in agreement with our observed energies.

PHYSICAL REVIEW VOLUME 90, NUMBER 4 MAY 15, 1953

Radiochemical Studies on the Photofission of Thorium*

DALE M. HILLER† AND DON S. MARTIN, JR.
Institute for Atomic Research and Department of Chemistry, Iowa State College, Ames, Iowa

(Received January 19, 1953)

The relative yields of thirteen products resulting from the photofission of Th^{232} have been determined radiochemically. Photofission was induced by a 69-Mev synchrotron bremsstrahlung beam. The photofission yield curve was shown by these data to have two peaks, occurring approximately at nucleon numbers 91 and 138 with values of 6.9 percent. The peak-to-valley ratio was 10 and the half-width of the peaks was 12. Symmetry of the curve about nucleon number of 114.5 indicated the average emission of approximately three neutrons. The results were compared with other photofission data and the yield curves of other fission processes.

I. INTRODUCTION

IN the photoexcitation of heavy nuclei at moderate energies, fission may occur in excited states of target nuclei. At higher energies, the fission may be preceded by the loss of one or more neutrons. In any event, the nuclei undergoing fission are generally different from those which are excited by neutron capture or by charged-particle bombardment. A study of photofission, therefore, extends the knowledge concerning the general fission process. This is of particular interest in the case of Th^{232} and U^{238} because neutron yields from spontaneous fission have been determined for the ground states of these two nuclides.[1–3]

Present information of photofission product yields from various fissionable materials is not nearly so comprehensive as that available for the yields from neutron fission reported by the Plutonium Project[4] and by subsequent workers.[5,6] Photofission yield curves have been estimated for Bi^{209} irradiated by 85-Mev x-rays[7] and for U^{235} irradiated by 22-Mev x-rays.[8] Also available are some preliminary results of a current study by Richter[9] and Coryell[10] involving the irradiation of natural uranium with 16-Mev x-rays.

In this paper are reported the radiochemically determined yields of thirteen nucleon (mass) numbers produced by the irradiation of thorium with 69-Mev bremsstrahlung. From the photofission cross section curve of thorium given by McElhinney[11] and Ogle[12] and the characteristics of the bremsstrahlung spectrum, it is apparent that the preponderant majority of fission events resulted from the relatively moderate excitation energies of 10–20 Mev. Therefore it is not surprising that a yield curve of the familiar "twin-peaked" form was produced. The data were sufficient to give a fairly reliable indication of the width of the peaks at half-height, the ratio of the yield of the most probable mode

* Contribution No. 225 from the Institute for Atomic Research and the Department of Chemistry, Iowa State College, Ames, Iowa. Work was performed in the Ames Laboratory of the U. S. Atomic Energy Commission. This paper was presented to the Division of Physical and Inorganic Chemistry at the 122nd National Meeting of the American Chemical Society in Atlantic City, New Jersey, September 17, 1952.

† Present address: Pigments Department, E. I. du Pont De Nemours Company, Inc., Newport, Delaware.

[1] Barclay, Galbraith, and Whitehouse, Proc. Phys. Soc. (London) **A65**, 73 (1952).

[2] D. J. Littler, Proc. Phys. Soc. (London) **A65**, 203 (1952).

[3] E. Segrè, U. S. Atomic Energy Commission Report AECD-3149, 1951 (unpublished).

[4] C. D. Coryell and N. Sugarman, *Radiochemical Studies: The Fission Products* (McGraw-Hill Book Company, Inc., New York, 1951), National Nuclear Energy Series, Vol. 9, Div. IV.

[5] A. Turkevich and J. B. Niday, Phys. Rev. **84**, 52 (1951).

[6] Steinberg, Seiler, Goldstein, and Dudley, U. S. Atomic Energy Commission Report MDDC-1632, 1948 (unpublished).

[7] N. Sugarman, Phys. Rev. **79**, 532 (1950).

[8] R. W. Spence, Brookhaven Conference Report BNL-C-9, p. 43, 1949 (unpublished).

[9] H. C. Richter, MIT Laboratory for Nuclear Science and Engineering Progress Report, No. 30, 1951, p. 30 (unpublished).

[10] C. C. Coryell (private communication, May 5, 1952). These results with minor revisions are available in U. S. Atomic Energy Commission Report AECU-2128 (unpublished).

[11] J. McElhinney and W. E. Ogle, Phys. Rev. **81**, 342 (1951).

[12] W. E. Ogle and J. McElhinney, Phys. Rev. **81**, 344 (1951).

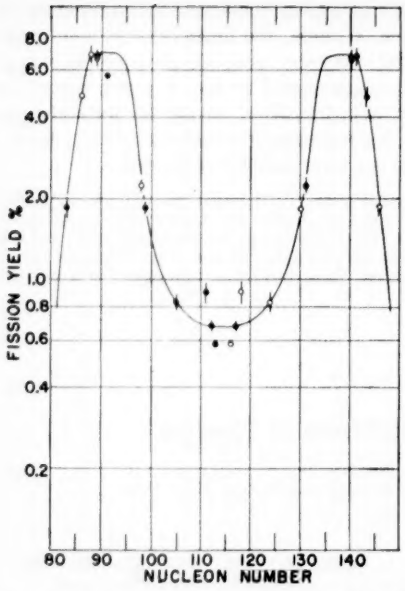

FIG. 1. Absolute yield curve from photofission of thorium with 69-Mev bremsstrahlung. Solid circles represent experimental data at nucleon number A. Open circles represent corresponding mirror images at (229-A).

of fission to that of the symmetrical mode (the peak-to-valley ratio) and the symmetry of the fission yield curve.

II. PROCEDURE

Thorium metal, weighing 13–20 grams, in the form of either pellets or powder, was placed in a glass tube having an 8 mm inside diameter. The sample was aligned with the x-ray beam, 24 cm from the tungsten target of the Iowa State College 69-Mev synchrotron. The specific activation of the sample in the tube decreased by a factor of two for every 7 grams of thorium. A standard irradiation lasted for five hours at an intensity of about 125 roentgens per minute as measured by a Victoreen thimble chamber enclosed in a 0.125-inch lead cylinder fitted with 0.125-inch base, placed one meter from the tungsten target. Deviations from the average intensity during any one bombardment, as monitored by a continuously-recording ionization chamber, were shown to be unimportant.

The freshly-irradiated thorium pellets were dissolved in hydrochloric acid, a small amount of fluosilicate ion being added as catalyst to aid in dissolving small quantities of thorium oxide and thorium carbide, and aliquots were taken for the determination of the various fission products. When powdered metal was irradiated, the target material was transferred to a dry flask and mixed thoroughly after which samples were weighed out and dissolved separately in hydrochloric or nitric acid plus fluosilicate catalyst. Determinations were made in duplicate for each element. In only two cases (strontium-barium and iodine-molybdenum) were analyses made for more than one element on the same aliquot.

A 10- or 20-mg portion of carrier of the element being measured was added to an aliquot of the acidic matrix solution and steps were taken to insure chemical exchange. The element was separated from the matrix solution, purified from all others, and precipitated as a weighable compound. Finally the precipitate, usually weighing from 5 to 30 mg, was filtered in an area of 2 cm^2 on a tared filter-paper disk which was then weighed, mounted on cardboard, and covered with Cellophane.

The chemistry was based on the fission product procedures reported by the Plutonium Project[4] and by Newton,[13] with modifications necessitated by the fact that aliquots of the matrix solution contained 3–5 grams of thorium. Specific modifications will be noted in the appendix which summarizes chemical procedures.

The radioactivity of the samples was measured with a thin mica end-window-type Geiger-Müller tube. The activity of the samples was generally too low to permit complete absorption curves to be taken. Therefore identification of isotopes was made almost exclusively by the interpretation of complete decay curves. Brief aluminum absorption curves were usually taken. These were then back-extrapolated to zero total absorber to correct the counting data for the absorption in the Cellophane, the counter window and the intervening air. Other corrections applied to the counting data were essentially those of Zumwalt,[14] except that because the samples were mounted on filter paper and cardboard, the corrections of Engelkemeir *et al.*[15] were applied for back-scattering, self-scattering and self-absorption. Using the refinements of Zumwalt, the maximum total

TABLE I. Absolute yields from the photofission of Thorium with 69-Mev bremsstrahlung.

Nucleon number	Nuclides isolated and measured	Yields, percent	Estimated reliability percent
83	2.4-hr Br^{83}	1.89	±0.15
89	53-day Sr^{89}	6.7	±0.1
91	9.7-hr Sr^{91}→51-min Y^{91}	5.7	±0.1
99	67-hr Mo^{99}	1.85	±0.10
105	4.5-hr Ru^{105}	0.83	±0.07
111	7.5-day Ag^{111}	0.90	±0.09
112	3.2-hr Ag^{112}	0.68	±0.02
113	5.3-hr Ag^{113}	0.58	±0.01
117	2.72-hr Cd^{117}→1.95-hr In^{117}	0.68	±0.02
131	30-hr Te^{131}→2.5-min. Te^{131}→ 8-day I^{131}	0.81	±0.06
	Total	2.25	±0.10
140	13.4-day Ba^{140}→41.4-hr La^{140}	6.6	±0.5
141	32.5-day Ce^{141}	6.8	±0.5
143	33-hr Ce^{143}	4.8$_5$	±0.5

[13] A. S. Newton. Numerous fission product separations from Thorium in U. S. Atomic Energy Commission Report AECD-2738, W. W. Meinke, Ed., 1949 (unpublished).

[14] L. R. Zumwalt, U. S. Atomic Energy Commission Report AECU-567, 1950 (unpublished).

[15] Engelkemeir, Seiler, Steinberg, and Winsberg, see reference 4, Paper 4, p. 56.

error is estimated to be 10 percent, most of which occurs in the backscattering corrections. In a few cases where interpolations of the data of Engelkemeir *et al.* were made, errors could have been even larger, but in this case the size of the error could not be confidently predicted.

Either Sr^{91} or Mo^{99} was isolated from each irradiated target and used as a comparative standard for the other isotopes. The yields of Sr^{91} and Mo^{99} were compared in two independent experiments.

III. RESULTS

The experimentally determined relative yields were plotted as a function of nucleon number and the relative yield curve was drawn. Then, since a negligible number of photofission events in thorium result in more than two major fragments,[16,17] the experimental yield points were multiplied by the necessary normalization factor to give an absolute yield curve with an integrated yield of 200 percent.

In drawing this curve, shown in Fig. 1, symmetry about some central nucleon number was assumed. It was further assumed that each peak was roughly symmetrical in the neighborhood of the most probable yield. The normalized fission yield values are shown in Table I.

The curve as drawn is symmetrical about nucleon number 114.5. In addition to the experimental data for nucleon numbers A, points corresponding to the mirror images at $229-A$ were plotted. Moving the line of symmetry to either 114 or 115 resulted in points which did not fit a smooth curve nearly so well. Therefore the curve seems to indicate that an average of 3 ± 0.5 neutrons was emitted from each thorium nucleus which underwent photofission.

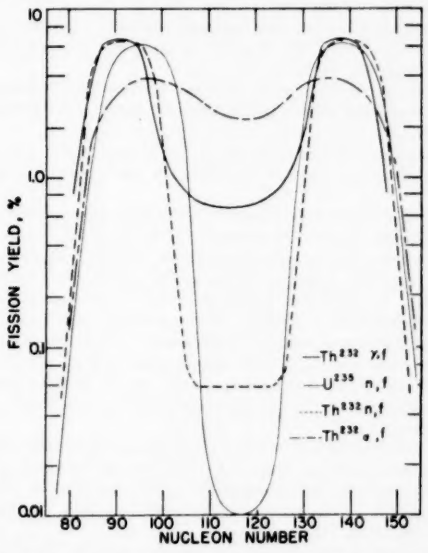

FIG. 2. Yield curves for thermal neutron fission of U^{235} (reference 19), and of thorium fission induced by 69-Mev bremsstrahlung, by pile neutrons (reference 5) and by 37.5-Mev α-particles (reference 18).

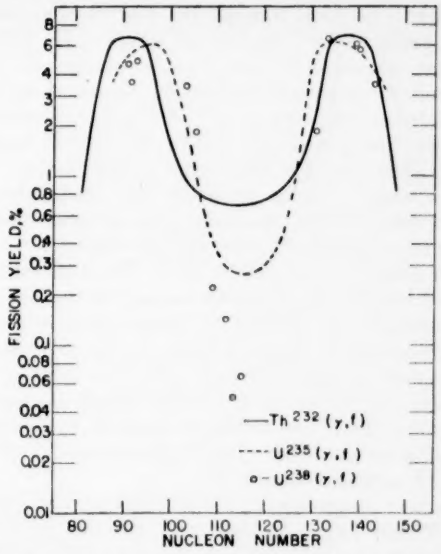

FIG. 3. Photofission yields of Th^{232}, U^{235} (reference 8), and U^{238} (references 9 and 10).

The most probable yields occurred with a magnitude of 6.9 percent at nucleon numbers 91 and 138, giving a value of 1.52 for the most probable mass ratio. The width of each peak at half-height is 12 nucleon units. The peak-to-valley ratio is 10.

IV. DISCUSSION

The yield curves for the fission of thorium by photons, by pile neutrons,[5] and by 37.5-Mev alpha-particles[18] are shown in Fig. 2 along with the well-known curve for thermal neutron fission of U^{235}.[19] The most noteworthy feature of this comparison is that symmetrical fission is ten times more probable in photofission than it is in pile neutron fission, but only about one-third as probable as in fission induced by alpha-particles.

Data are also available on the photofission of U^{238},[9,10] U^{235},[8] and Bi^{209}.[7] In all cases, including the present work, the number of points determined have been so few in number that the fission yield curves, when they can be drawn at all (see Fig. 3), are not sufficiently precise to be subject to fine interpretation. However certain trends can be detected which seem to justify some general statements.

The half-width of the photofission yield curve is 14 in the case of U^{235} and 12 in the case of Th^{232}. The thermal neutron fission yield peaks of U^{235} have a

[16] E. W. Titterton and T. A. Brinkley, Phil. Mag. **41**, 500 (1950).
[17] Goward, Titterton, and Wilkins, Nature **164**, 661 (1949).
[18] A. S. Newton, Phys. Rev. **75**, 17 (1949).
[19] E. P. Steinberg and M. S. Freedman, see reference 4, Paper 219, p. 1378.

half-width of 15.5, whereas the pile neutron fission yield peaks of Th^{232} have a half-width of 14. Thus it appears that, as in the case of neutron fission, the half-width increases with the mass of the compound nucleus. In addition, the cases of U^{238}, U^{235} and Th^{232} seem to indicate that photofission results in definitely smaller half-widths than does low energy neutron fission.

The most probable mode of Bi^{209} photofission is symmetrical.[7] The photofission peak-to-valley ratio is 10 in the case of Th^{232}, over 20 in the case of U^{235},[8] and much greater in the case of U^{238}.[9] The high ratio reported for U^{238} may be partly caused by the fact that photofission was induced by bremsstrahlung with a maximum energy of only 16 Mev, so that this result is not strictly comparable with others. In spite of this qualification, the above data seem to justify the general statement that the tendency towards symmetrical photofission decreases as the nucleon number of the excited nucleus increases.

Further comparison of the photofission yield curves of U^{235} and Th^{232} with their respective neutron fission yield curves reveals that in both cases the heavy peak of the curve predominantly is shifted in the light direction by an amount which, although small, appears to be too large to be accounted for merely by the difference of one neutron in the composition of the respective compound nuclei. The present preliminary data indicate that the photofission yield curve of U^{238} also follows this trend.

Previous reports that the Th^{232} photofission cross section has its peak at 17–18 Mev and practically vanishes above 30 Mev[12,20] led to the belief that in the present experiments the average amount of photo-excitation leading to fission was about 15 Mev, an excitation which is too low to cause emission of many neutrons from the excited nuclei prior to fission. This prediction is corroborated by the fact that the heavy branch of the radiochemically determined experimental yield curve is symmetrical with the light branch, which would not be the case if the neutron yield were high. In addition, comparison of the reported neutron yield of 2.6 per spontaneous Th^{232} fission event[1] with the value of 3 ± 0.5 neutrons per Th^{232} photofission event obtained in the present investigation, shows that the difference is small at most and may in fact not exist at all. If photofission actually does result in a higher neutron yield than does spontaneous fission, the increase is small and may be attributed to that fraction of fission events resulting from relatively high excitation. Further experiments would be required to resolve the doubt which remains as to whether or not photoexcitation ever causes Th^{232} to emit neutrons prior to fission.

This work is described in greater detail in the U. S. Atomic Energy Commission Report, ISC-227 (unpublished).

We are grateful to Dr. P. Chiotti and Dr. D. Peterson for their kind assistance in the preparation of the metallic thorium samples and to Dr. L. J. Laslett, Dr. D. J. Zaffarano and the entire synchrotron crew for their cooperation in performing the bombardment work.

[20] G. C. Baldwin and G. S. Klaiber, Phys. Rev. **71**, 3 (1947).

V. APPENDIX. CHEMICAL PROCEDURES

For each element listed below, the essentials of the chemistry involved in this investigation have been summarized. In the analytical procedures, the practice has been to repeat purification steps two or more times in order to achieve radiochemical purity.

Thorium—The metal sample was dissolved in HCl with a small amount of fluosilicate ion present to clear up the solution. If a minimum of three moles of HCl per mole of Th was present, a speed of solution was obtained which was much higher than that attainable with any other acid or combination of acids. The remaining acid necessary to dissolve the Th could equally well be HCl, $HClO_4$, or H_2SO_4.

Bromine—I_2 was extracted into CCl_4 after the oxidation of I^- to I_2 by dropwise addition of $2M$ cerium(IV). Further dropwise addition of $2M$ cerium(IV) oxidized Br^- to Br_2, which was then extracted into fresh CCl_4. Br_2 was then stripped from the CCl_4 with $NaHSO_3$ solution. AgBr was precipitated and weighed.

The samples decayed with the 2.4-hr half-life of Br^{83}.

Strontium—$Sr(NO_3)_2$ was precipitated with cold fuming HNO_3 after the HCl was displaced from the matrix solution by boiling with HNO_3. Separations of $BaCrO_4$ and $Fe(OH)_3$ were made. Sr was finally precipitated and weighed as $SrC_2O_4\cdot H_2O$.

Activities in the samples were resolved into the 9.7-hr decay of Sr^{91} in equilibrium with 51-min Y^{91}, the 53-day decay of Sr^{89} and the growth and subsequent decay of 57-day Y^{91}.

Molybdenum—Mo was extracted into ether from $6N$ HCl after Br_2 oxidation, precipitated with α-benzoinoxime from $3N$ HNO_3 containing $H_2C_2O_4$, oxidized to MoO_3 with HNO_3 and $HClO_4$, scavenged with $Fe(OH)_3$ and finally precipitated and weighed as $PbMoO_4$.

The samples decayed with the 67-hr half-life characteristic of Mo^{99} in equilibrium with its 6.0-hr Tc^{99} daughter.

Ruthenium—RuO_4 was distilled from the fuming $HClO_4$ into $6N$ NaOH containing Mo holdback carrier, precipitated as a lower oxide with EtOH, dissolved in weak HCl and precipitated as Ru^0 with Mg metal.

The decay curves resolved into the 4.5-hr decay characteristic of Ru^{105} and the growth and subsequent decay of its 37-hr Rh^{105} daughter.

Silver—Ag was precipitated as AgCl and Ag_2S, with intermediate scavengings with $Fe(OH)_3$. It was finally weighed as AgCl.

The decay curves were resolved into three components which were assigned to the 7.5-day Ag^{111}, 3.2-hr Ag^{112} and 5.3-hr Ag^{113}.

Cadmium—Cd was precipitated from cold HCl solution which was 1 percent in thiourea (shown as TH) as $Cd(TH)_2[Cr(NH_3)_2(SCN)_4]_2$ by adding a saturated solution of Reinecke's salt, $NH_4[Cr(NH_3)_2(SCN)_4]\cdot H_2O$. The precipitate was dissolved in weak HCl and precipitated as CdS and $Cd(OH)_2$, scavenged with $Fe(OH)_3$ and scavenged with basic indium acetate. 1.95-hr In^{117} was milked out as basic indium acetate, ignited to In_2O_3, slurried, dried and weighed. Cd was later quantitatively determined as the "Reineckate."

The decay curves of the counting samples resolved into the 1.95-hr decay characteristic of In^{117} and the 4.5-hr decay of In^{115}.

Tellurium—Te was precipitated as Te^0 by SO_2 in $3N$ HCl solution and scavenged repeatedly with $Fe(OH)_3$. The samples were weighed as Te^0.

The decay curves showed the presence of 77-hr Te^{132} in equilibrium with its daughter, 2.4-hr I^{132}, and 30-hr Te^{131} plus its 8.0-day I^{131} daughter.

Iodine—I_2 was extracted into CCl_4 after the oxidation of I^- to I_2 by dropwise addition of $2M$ cerium (IV). The I_2 was reduced to I^- and stripped from CCl_4 with aqueous $NaHSO_3$, and was finally precipitated and weighed as AgI.

The sample, separated 10 days after the end of the irradiation, decayed with the 8.0-day half-life characteristic of I^{131}.

Barium—$Ba(NO_3)_2$ was precipitated with cold fuming HNO_3 after the HCl was displaced from the matrix solution by boiling with HNO_3. Ba was precipitated as $BaCrO_4$ after scavenging with $Fe(OH)_3$, precipitated as $BaCl_2$ with HCl-ether mixture and redissolved in H_2O. The solution was milked of 41.4-hr La^{140} by a $La(OH)_3$ precipitation. The $La(OH)_3$ was filtered, ignited and counted. Ba was later quantitatively determined as $BaSO_4$.

The decay curve of the La sample was resolved to show a 40-hr decay attributed to La^{140}, as well as a 10.6-hr decay assigned to Pb^{212}.

Cerium—Th was extracted into mesityl oxide from the HCl matrix solution containing La, Y and Ce carriers and saturated with $Al(NO_3)_3$. The rare earths were precipitated as hydroxides with NaOH, extracted into tributyl phosphate from a 1*N* HNO_3 solution saturated with $Al(NO_3)_3$, stripped with H_2O and reprecipitated as hydroxides with NaOH. The Ce was oxidized with $HBrO_3$, precipitated as $Ce(IO_3)_4$, dissolved in HCl and H_2O_2 and scavenged with $Zr(IO_3)_4$. Ce was finally precipitated and weighed as $Ce_2(C_2O_4)_3 \cdot 10\ H_2O$.

The decay curves resolved into a 32.5-day decay characteristic of Ce^{141}, a 33-hr decay assigned to Ce^{143}, and an activity which demonstrated the growth and subsequent decay of Pr^{143}.

PHYSICAL REVIEW VOLUME 90, NUMBER 4 MAY 15, 1953

The Quadrupole Moment of Li^7

EDWARD G. HARRIS,* *Department of Physics, University of Tennessee, Knoxville, Tennessee*

AND

MICHEL A. MELKANOFF, *Department of Physics, University of California, Los Angeles, California*

(Received November 10, 1952)

The quadrupole interaction energy eqQ for Li^7 in Li_2 has been reported to be positive. In an attempt to determine $Q(Li^7)$ a calculation of q has been made using two approximate wave functions for Li_2. One of these is a Heitler-London function including inner shells and the other a twelve term variational function. The two functions lead to dissociation energies of 0.27 ev and 0.48 ev, respectively. The experimental value is 1.14 ev.

The results of the two calculations differ in sign. The more accurate variational function leads to a negative q and consequently a negative value of $Q(Li^7)$. Unfortunately, the electronic and nuclear parts of q are nearly equal in Li_2 so that the magnitude and even the sign are still uncertain.

I. INTRODUCTION

RECENT advances in experimental techniques have made possible the determination of the sign as well as the magnitude of the quadrupole interaction energy eqQ in diatomic molecules.[1,2] Unfortunately, in order to calculate the nuclear quadrupole moment from this data it is necessary to know q, the electric field gradient at the position of the nucleus.[3] This must be calculated from molecular wave functions. A calculation by Foley[4] using the Bartlett-Furry wave function[5] for Li_2 indicates that the quadrupole moment of Li^7 is about $+2\times10^{-26}$ cm^2. The Bartlett-Furry function is a Heitler-London-type wave function in which the inner shell electrons are neglected. James has shown that the good agreement that Bartlett and Furry found between their calculated value of the dissociation energy and the observed value is completely destroyed when the effect of the inner shell electrons is included.[6] Since the value of q calculated with this function is of doubtful accuracy, it was felt that the calculation should be repeated with more accurate wave functions.

II. CALCULATION OF q WITH THE HEITLER-LONDON TYPE WAVE FUNCTION

James has discussed a wave function of the Heitler-London type which leads to a dissociation energy of 0.27 ev.[6] The experimental value of the dissociation energy is 1.14 ev. All electrons are included in this wave function and are described by single particle functions of a form that was used in the treatment of the lithium atom problem. The electronic configurations of the molecule are represented by Slater determinants constructed from these functions. Terms representing the lowest ionic configurations are also considered, and the percentage admixture of these terms, as determined by the variational method, is about 3 percent for an internuclear distance of 2.98A.

For Li_2 the expression for q becomes

$$q=2eq'=2e\left[\frac{3}{R^3}-\frac{1}{2}\int\rho\frac{(3\cos^2\theta-1)}{r^2}d\tau\right],$$

where R is the internuclear distance and ρ is the elec-

TABLE I. Values of $q'(R)$ in Atomic Units.

R (A)	q' (atomic units)
2.49	$1/R^3-0.00388$
2.70	$1/R^3-0.00385$
2.91	$1/R^3-0.00375$

* U. S. Atomic Energy Commission Predoctoral Fellow.

[1] P. Kusch, Phys. Rev. **76**, 138 (1949).

[2] Logan, Coté, and Kusch, Phys. Rev. **86**, 280 (1952).

[3] The q used here corresponds to that used in reference 2.

[4] A calculation by H. M. Foley quoted in reference 1.

[5] J. H. Bartlett, Jr., and W. H. Furry, Phys. Rev. **38**, 1615 (1931).

[6] H. M. James, J. Chem. Phys. **2**, 794 (1934).

tron density calculated from the molecular wave function. This quantity should be averaged over the vibrational states of the molecule, but in our work this will not be done, since the effect is expected to be small.

The quantity q' was calculated for several values of R in the neighborhood of the equilibrium distance, $R=2.67$A. The results are given in Table I.

It was found that the inner shell electrons contributed very nearly $-2/R^3$ to q', so the first term in q' is the contribution of the nucleus shielded by its two inner shell electrons. The contribution of the remaining molecular charges is included in the second term. This term is primarily due to the functions representing valence electrons and all cross product terms which appear in the charge density. We shall refer to these terms as the nuclear term and the electronic term, respectively. q' is written in this form to facilitate comparison with the results obtained using the James variational wave function. It should be noted that the electronic term varies much more slowly with R than the nuclear term. It was found that including the ionic terms in the wave function increased the electronic term to 0.00394 for $R=2.70$A.

From these results the value of q' at $R=2.67$A is seen to be about $+0.0040$ atomic units. Using the experimental value of $eqQ/h=+0.060$ Mc/sec reported by Logan, Coté, and Kusch,[2] it is found that $Q(\mathrm{Li}^7)=+3.5\times10^{-26}$ cm^2.

III. CALCULATION OF q WITH THE JAMES VARIATIONAL WAVE FUNCTION

James has found a variational wave function for Li_2 which leads to a dissociation energy of 0.62 ev.[6] Although the discrepancy between this value and the experimental value of 1.14 ev is rather large, this wave function is the best that has been proposed. It consists of a linear combination of 18 Slater determinants, the coefficients of which were obtained by the variational method. The inner shell electrons were described by the same functions as were used in the Heitler-London treatment, and the valence electrons by function of the form $e^{-\gamma\lambda}\lambda^m\mu^j$, where λ and μ are the elliptic coordinates of the electron and the exponents m and j are integers. The chief defect of this wave function seems to be the absence of terms depending on the distance between the valence electrons.

Because of the labor involved in calculating q' with this function, a simpler 12-term function was found which yields a dissociation energy of 0.48 ev. The calculation of q' with this function was laborious but straightforward. Since the wave function was calculated for only one value of the internuclear distance, $R=2.98$A, q could be calculated for this distance only. The result was[7] $q'=1/R^3-0.0089=-0.0032$ atomic units.

[7] The second term in q' is the average of the values obtained independently by the authors whose results agreed to within 5 percent. This small discrepancy was attributed to small differences in the wave functions used.

If it is assumed that q' has about the same value at the equilibrium distance, $R=2.67$A, as it has at $R=2.98$A, then it is found that $Q(\mathrm{Li}^7)=-4\times10^{-26}$ cm^2. Because of the rapid variation of the nuclear term with R, this assumption is questionable.

Perhaps a more reasonable assumption is that the results of the last section are at least qualitatively correct and that the variation of the electronic term with R is negligible in the neighborhood of the equilibrium distance. Making this assumption it is found that $q'(R=2.67\text{A})=-0.0011$ atomic units and $Q(\mathrm{Li}^7)=-12\times10^{-26}$ cm^2.

IV. DISCUSSION

It is rather surprising that the two wave functions which differ so little in the predicted dissociation energy should lead to such greatly different values of q. It may be taken as an indication of the sensitivity of q to changes in the charge distribution in the molecule. In order to gain some insight into the reason for this difference, the charge density calculated with the variational wave function was plotted along the internuclear axis and compared with that calculated with the Heitler-London function. It was found that the two curves were similar, but that the variational function led to a charge density that was more than twice as great at the midpoint of the molecule and slightly less at the ends than the charge density calculated with the Heitler-London function.

Qualitatively, this is a reasonable result since the variational function is sufficiently flexible to take account of the polarization of each lithium atom by the other. In Nordsieck's work on the hydrogen molecule[8] it was found that the Heitler-London function underestimates the charge density at the midpoint of the molecule, but the error is much smaller than it is in the case of Li_2. This suggests that the Heitler-London function for Li_2 could be considerably improved by the addition of terms representing configurations in which one or both of the valence electrons were in $2p$ states in order to take account of polarization. Apparently the effect of polarization is much more important in the case of Li_2 than it is in H_2. This can perhaps be explained by the fact that in the limiting case of the united atom (i.e., when the nuclei coincide) two electrons of the lithium molecule must be promoted to the $2p$ shell. In the hydrogen molecule such promotion does not occur. It seems reasonable to believe that the effect of promotion would make the polarization terms more important in Li_2 than in H_2.

It may be concluded from these results that there is no longer any reason to believe that $Q(\mathrm{Li}^7)$ is positive. Since the variational wave function is more flexible than the Heitler-London function and gives a better value for the dissociation energy, our calculations tend to favor a negative value for $Q(\mathrm{Li}^7)$. It should be

[8] A. Nordsieck, Phys. Rev. **58**, 310 (1940).

pointed out that a negative quadrupole moment is in agreement with the predictions of all the simple nuclear models that have been proposed for Li^7. However the magnitude and even the sign of $Q(Li^7)$ must still be considered to be in doubt for the following reasons:

(1) The quantity q is the difference between two very nearly equal terms which represent, respectively, nuclear and electronic contributions. The electronic term in q is much more sensitive than the dissociation energy to changes in the wave function. Because of this sensitivity improved wave functions may lead to quite different values of q. One of us (M.A.M.) is repeating the calculations with the more accurate 18-term wave function.

(2) The variational wave function has been determined for only one internuclear distance, $R=2.98$A. The assumption made about the variation of q with R was based on calculations made with a simpler wave function.

(3) The experimental value of eqQ is rather uncertain, since the satellite maxima could not be resolved. There seems to be little doubt, however, about the sign.

(4) No average was made over the vibrational states of the molecule, and no account was taken of rotational distortion. The resulting errors are probably very small.

(5) In both of the wave functions used in these calculations, the $1s$ functions are of the form $e^{-\alpha r}$. No account has been taken of the shielding effect due to the quadrupole moment induced in the $1s$ shell. Sternheimer[9] has calculated a correction factor for this effect in atoms. He finds that for the excited lithium atom the observed nuclear quadrupole moment should be multiplied by the factor 1.148. Although our use of molecular wave functions for the valence electrons precludes a direct application of Sternheimer's result, it seems likely that the correction would be of the same order of magnitude.

It seems unlikely that $Q(Li^7)$ can be calculated with reasonable accuracy from the observed quadrupole interaction energy until a molecular wave function for Li_2 is developed which will compare in accuracy with the James-Coolidge function for H_2.

We are indebted to Dr. R. J. Finkelstein and Dr. R. D. Present for their valuable suggestions and discussions concerning this work and to Dr. H. M. James who kindly made available his manuscripts on the Li_2 molecule.

Note added in proof.—The calculations with the 18-term James function mentioned previously have been completed, and the following results were obtained: dissociation energy $=-0.51$ ev (James originally gave -0.62 ev due to a slight error in his calculations). Using $R=2.98$A: $q'=-0.0030$ atomic unit, $Q(Li^7)=-4.2\times10^{-26}$ cm^2.

[9] R. Sternheimer, Phys. Rev. **80**, 102 (1950); **84**, 244 (1951); **86**, 316 (1952).

PHYSICAL REVIEW VOLUME 90, NUMBER 4 MAY 15, 1953

Excited States of Even-Even Nuclei*

GERTRUDE SCHARFF-GOLDHABER
Brookhaven National Laboratory, Upton, New York

(Received January 20, 1953)

A general survey of excited states of even-even nuclei yields the following results: The nth excited state has usually a spin $I\leq 2n$. For $n=1$, the assignment $I=2+$ (even parity) is compatible with experimental results for 66 out of 68 nuclei investigated. For $n=2$, of 26 nuclei investigated, about one-third have $I=2+$, one-third $I=4+$, and one-third miscellaneous spins of both even and odd parities. The energy of the first excited state plotted against the number of protons or neutrons in the nucleus varies rather smoothly and reaches maxima at closed shells. Wherever the first excited state is very low, e.g., in the rare earths region and for the heavy elements from thorium up, the one-particle model for odd A nuclei is likely to break down except for the ground state. The lack of isomers of odd proton nuclei below magic number 82 may be due to this fact. The average energy of the first excited state of the even-even core in this region is of the order of 0.1 Mev, whereas this energy is of the order of 0.5 Mev for the core of the corresponding odd neutron nuclei ($N<82$). Isomerism in even-even nuclei is discussed. The results are compared with theoretical predictions derived from an extended j-j coupling model and from the liquid drop model of the nucleus.

I. INTRODUCTION

SINCE the strong spin orbit coupling model[1,2] implying a "shell structure" of the nucleus was suggested several years ago, nuclear physics has gravitated toward the study of odd A nuclei. This model, which received its first impetus from a consideration of the pronounced stability of certain nuclear species, soon scored a series of important successes wherever the prediction of spins and parities of nuclear states entered, e.g., in the fields of beta-decay and of isomeric states. However, at the same time a number of features became apparent which seemed to contradict a rigorous single particle picture, such as the large values found for the matrix elements of a number of $E2$ transitions, the sign and size of quadrupole moments, and the scarcity of odd-proton isomers for elements with $50<Z<82$. Also, the model in its present form does not provide a basis for quantitative prediction of energies of nuclear states.

Obviously, some interaction of the single particle with the even-even core has to be taken into account. Whether the whole core has to be considered[3,4] or, in first approximation, only the "loose" particles with the

* Work was supported by the U. S. Atomic Energy Commission.

[1] M. G. Mayer, Phys. Rev. **75**, 1894 (1949); **78**, 16 and 22 (1950).

[2] Haxel, Jensen, and Suess, Phys. Rev. **75**, 1766 (1949).

[3] J. Rainwater, Phys. Rev. **79**, 432 (1950).

[4] A. Bohr, Kgl. Danske Videnskab. Selskab, Mat.-fys. Medd. **26**, 14 (1952).

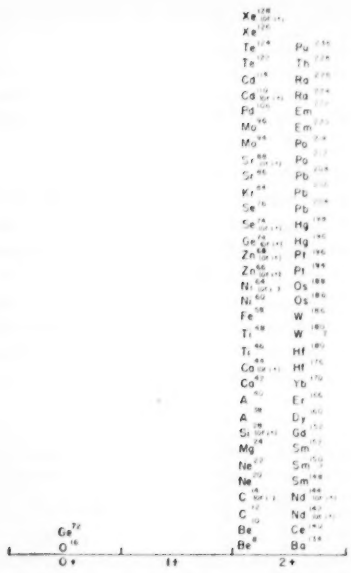

FIG. 1. Distribution of known spins and parities of first excited state of even-even nuclei. For methods of determination and references see Table I, columns 6 and 7. For 66 nuclei, a spin assignment of 2 and even parity is compatible with experimental results. In 53 of these cases a spin 2 and even parity can be assigned with certainty. For eleven more nuclei a spin of 2, even, seems probable, but the possibility that their first excited state has a spin 1, even, cannot be excluded. For two other cases, it can only be said that $I \leq 2$ for the first excited state. See Secs. II, 1 and III, 1 of text.

same quantum numbers (l, j) as those of the odd particle,[5,6] is not yet clear.

At this point, it seems of great interest to survey our empirical knowledge of even-even nuclei, for its own sake as well as to promote a better understanding of odd A nuclei.[7]

We restrict ourselves here to a survey of the spins and parities of the first 3 excited states of even-even nuclei and of the energy spacings between the ground state and these 3 excited states.

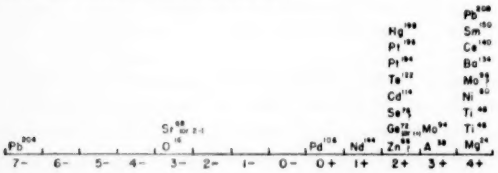

FIG. 2. Distribution of known spins and parities for the second excited state of even-even nuclei. The light nuclei show a preference of spin 4 and even parity for their second excited state. This is in agreement with theoretical expectations for nucleon pairs with low j. States with odd parity can be described as the result of "splitting up" of a pair of nucleons. See Secs. II, 2 and III, 2 of text. According to a private communication by F. Metzger, Os^{186} has also 2+ for its second excited state.

[5] D. Kurath, Phys. Rev. **87**, 218 (1952).

[6] B. H. Flowers, Phys. Rev. **86**, 254 (1952); Proc. Roy. Soc. (London) **215**, 398 (1952); and previous publications.

[7] Preliminary notes: G. Scharff-Goldhaber, Phys. Rev. **87**, 218 (1952); Physica **18**, 1105 (1952).

For the ground state of a nucleus, it is generally assumed that an even number of equivalent nucleons couple to zero angular momentum and, of course, even parity. Only a small number of nuclear spins of even-even nuclei have actually been measured,[8] but many experimental facts indicate that this assumption is correct. We therefore base our conclusions on spins and parities of excited states on the assumption that the ground state of an even-even nucleus has a total angular momentum (hereafter called spin) $I=0$ and even parity.

II. RESULTS OF THE SURVEY

1. Goldhaber and Sunyar[9] pointed out in 1951 that the first excited states of even-even nuclei have predominantly spin $I=2$ and even parity.[10] The summary of the first excited states with spin and parity known at that time yielded nineteen examples supporting this "2+ rule" and seven contradicting it. These seven cases consisted of two cases with spin 0, even, and five with spins 1 and 3, some of them with odd parity.

Meanwhile a great number of new spin assignments have been made, often with more accurate methods.

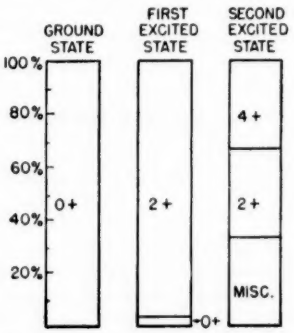

FIG. 3. Percentage distribution of spins and parities of ground state and first two excited states of even-even nuclei. See Secs. II, 3 and III, 3 of text.

Figure 1 shows the distribution of spins and parities of first excited states of even-even nuclei: *Apart from 2 nuclei, no sure exception from the 2+ rule for the first excited state exists.* The nuclei listed range from very light (Be^8) to very heavy (Pu^{238}). There are now altogether at least 66 nuclei for which a 2+ assignment is compatible with experimental results. Of these, 53 nuclei have 2+, 11 have either 2+ or 1+, and 2 have either 2+ or 1±.

The two exceptions, O^{16} and Ge^{72}, have spin zero and even parity in their first excited state. No γ-radiations are observed in these cases. The transition from the much investigated 6.05-Mev state of O^{16} takes place by pair emission with a half-life of 7×10^{-11} sec,[11] whereas the 0.68-Mev state[12] of Ge^{72} decays by means of internal

[8] J. E. Mack, Revs. Modern Phys. **22**, 64 (1950).

[9] M. Goldhaber and A. W. Sunyar, Phys. Rev. **83**, 906 (1951).

[10] Independently, Horie, Umezawa, Yamaguchi, and Yoshida [Prog. Theoret. Phys. **6**, 254 (1951)] discussed the spins and parities of first and second excited states of some even-even nuclei.

[11] Devons, Hereward, and Lindsey, Nature **164**, 586 (1949).

[12] Bowe, Goldhaber, Hill, Meyerhof, and Sala, Phys. Rev. **73**, 1219 (1948).

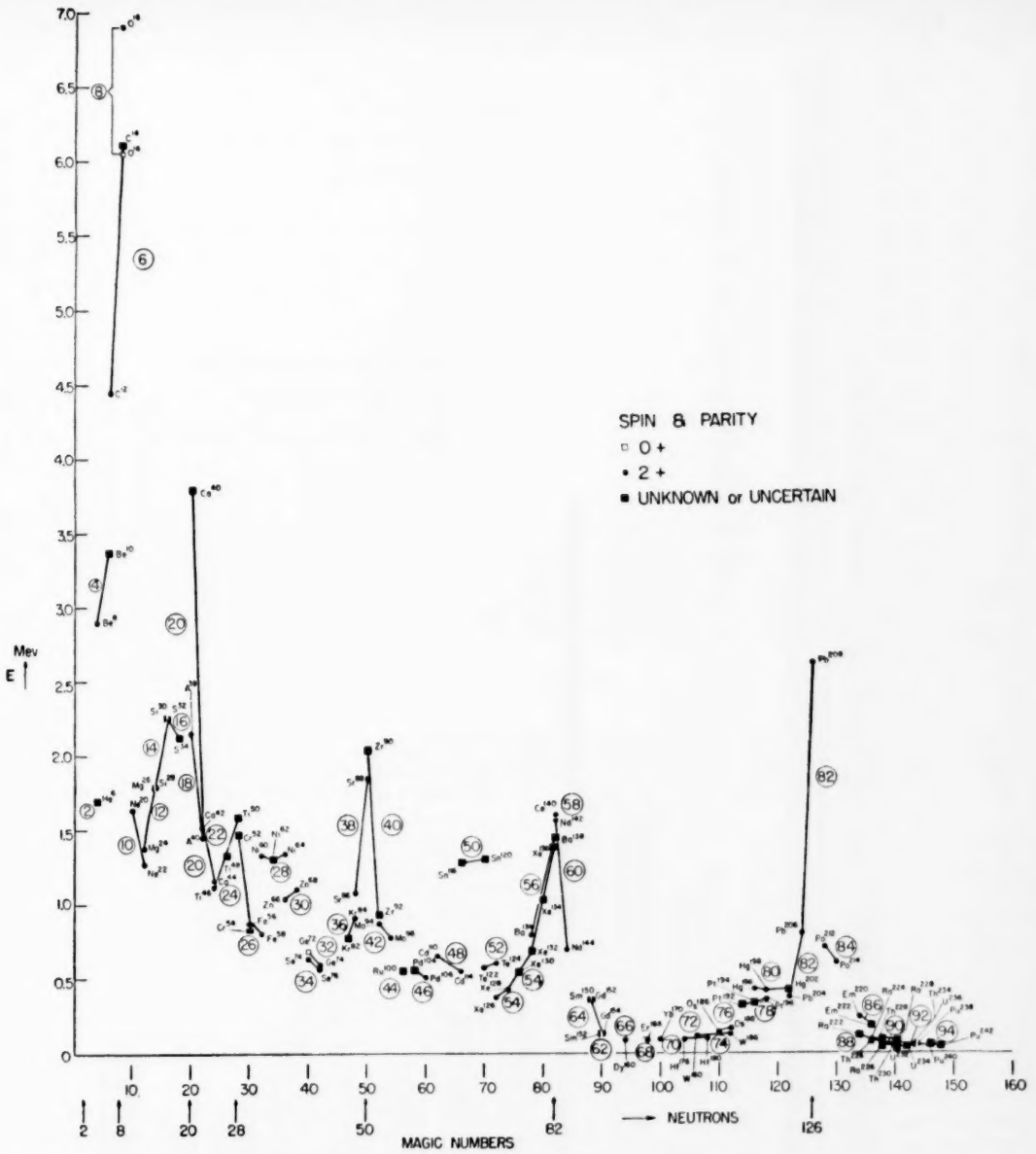

FIG. 4. Energies of first excited states of even-even nuclei plotted against number of neutrons. Points for isotopes of the same element are connected with straight lines. The corresponding proton number, encircled, appears next to the connecting lines. (See Secs. II, 4 and III, 4 of text.)

conversion with a half-life of 0.3 μsec. These lifetimes are in agreement with theoretical expectations.[13] Possible interpretations of these 0+ states will be given in Sec. III, 1.

2. *The distribution of spins and parities for the second excited state of even-even nuclei*, as represented in Fig. 2, *indicates that spin 2 or 4 and even parity is preferred.* Among the light nuclei spin 4 predominates. For medium heavy and heavy nuclei both possibilities appear. In addition, spins of 1 or 3 occur, and some second excited states have odd parity. Outstanding is again O^{16} with a spin of 3−, and Pb^{204}, with 7−.

It must be borne in mind that the identification of a state as a second excited state is not always certain, since a second excited state, e.g., of low spin 0 or 1, situated between a 2+ and a 4+ state may be poorly

[13] S. D. Drell, Oak Ridge National Laboratory Report ORNL-792 (unpublished).

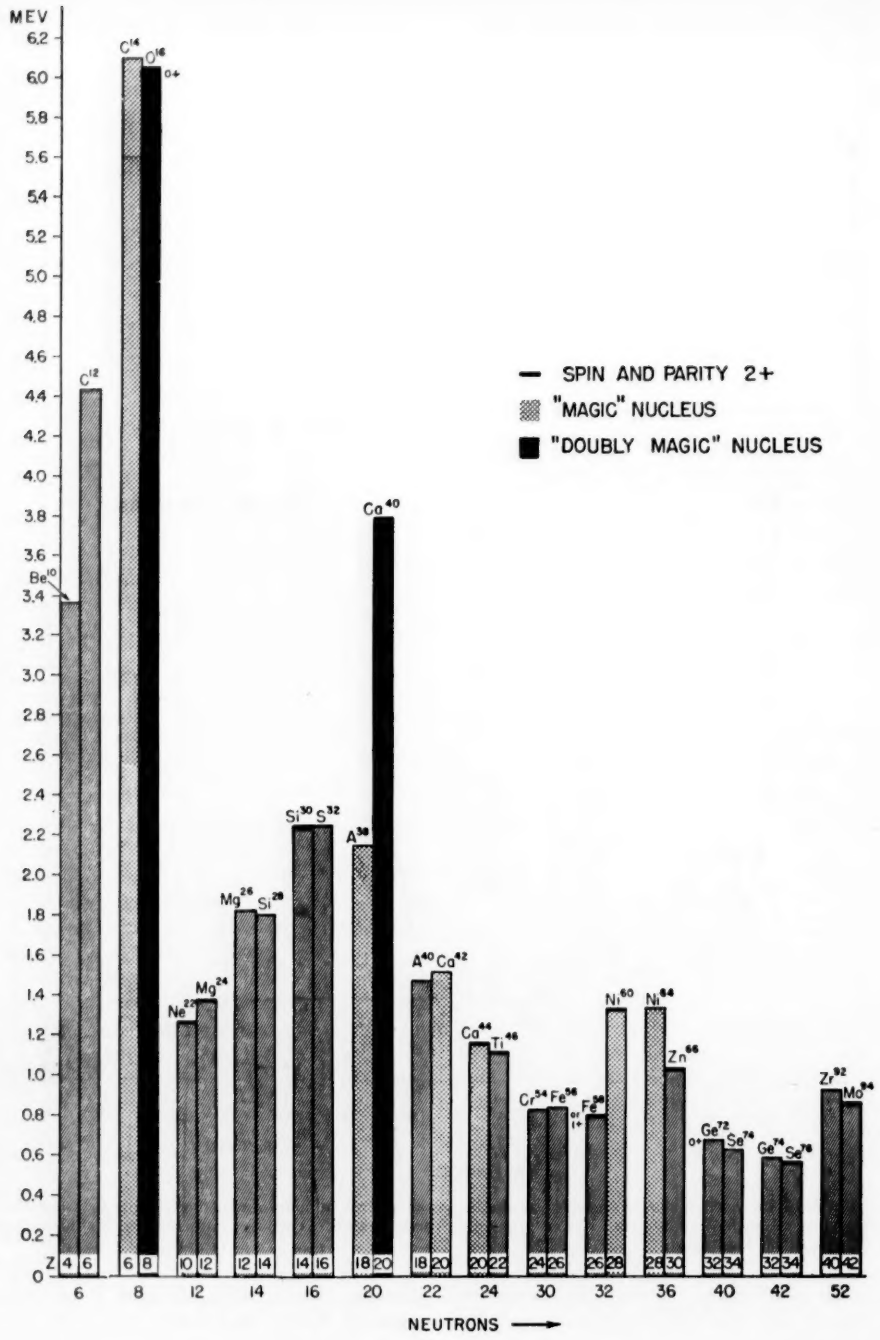

(a)

populated and hence be missed, if the 4+ state is mainly excited. It is much less likely that a first excited state is missed, unless it should turn out to have a very high spin. In that case it would be a metastable state. There is at present no evidence for the occurrence of low-lying, long-lived metastable states in even-even nuclei.

The spins of the second excited state will be further discussed in Sec. III, 2.

3. The percentage distribution of spin and parity of

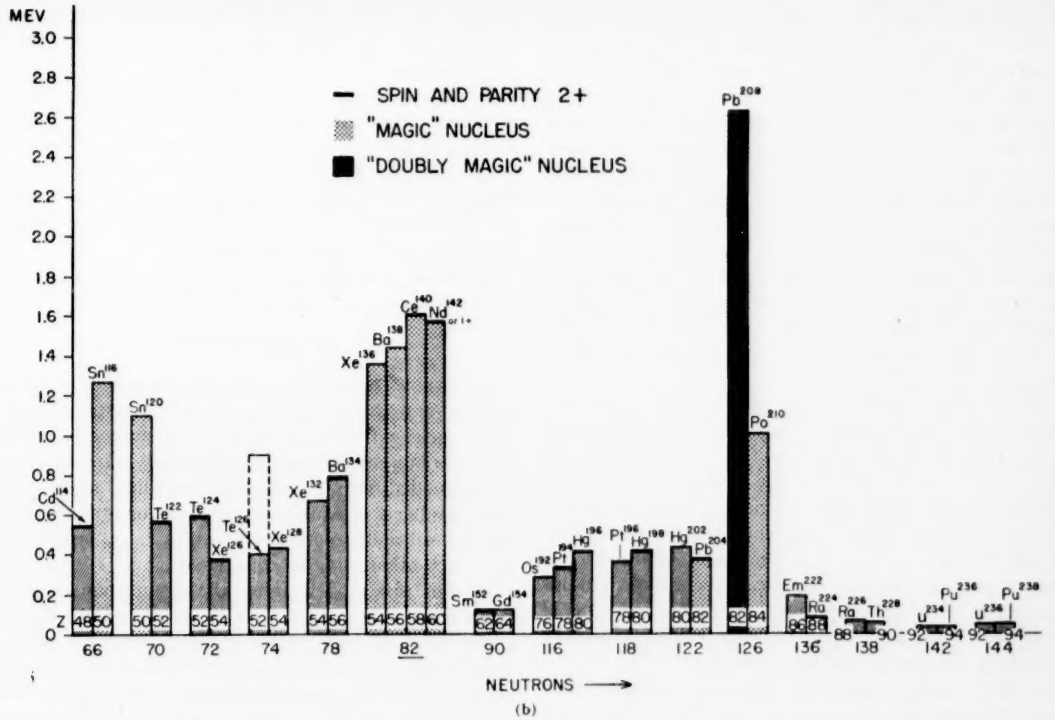

FIG. 5. Energies of first excited states of even-even nuclei are plotted against number of neutrons. (a) $N \leq 60$. (b) $N > 60$. Energies for nuclei differing by 2, 4, or 6, protons are compared, where possible. "Energy columns" for nuclei with either a magic neutron or proton number are cross hatched; energies of double magic nuclei are shown by black columns (see Sec. II, 4 of text).—For Te^{126} a value of 0.64 Mev should probably replace the 2 alternative energy values shown in the figure.

the ground state and the first two excited states is shown in Fig. 3. From this distribution and from the fact that very few long-lived even-even isomers exist, one can deduce that, as a rule, *$I \leq 2n$ for the nth excited state of an even-even nucleus.* Occurrence of an isomer would imply a spin change $\Delta I \geq 3$ between two successive states.

The only long-lived even-even isomers known at present are Pb^{204m} (68 min), Hf^{180m} (5.5 hr), and Pb^{202m} (5.6 sec). Pb^{204m} decays by means of a two step ($E5$-$E2$) isomeric transition.[14] Its isomeric state is the 7-state mentioned under II, 2. For Hf^{180m} and Pb^{202m},[15] spin and parity of the isomeric state are not known. Hf^{180m} emits a very complex γ-ray spectrum, suggesting that the isomeric state is probably the fourth excited state and that its spin $I \geq 7$.[14]

4. We come next to a consideration of the energy of the first excited state. Goldhaber and Sunyar[9] have already pointed out an interesting regularity: In the rare earth region first excited states of very low energy, of the order of 100 kev or less, occur, from which transitions to the ground state with matrix elements >1 (some with $|M|^2 \sim 150$) take place.

Meanwhile, a systematic survey of the energies of all reasonably well-assigned first excited states of even-even nuclei has been carried out.[7,16–18] The result is shown in Fig. 4. Here, the excitation energy is plotted against the number of neutrons in the nucleus. From this graph, the following conclusions may be drawn:

A. *The energy of the first excited state of even-even nuclei varies smoothly and decreases—in general—with increasing mass number. However, the curve has strong maxima for the "double magic" nuclei,* O^{16}, Ca^{40}, *and* Pb^{208}, *i.e., nuclei with a magic number of neutrons and a magic number of protons. Smaller maxima occur for nuclei with a magic number of neutrons and still less pronounced maxima for nuclei with a magic number of protons.* As mentioned above, a deep and smooth trough appears in the rare earth region between the neutron numbers 82 and 126 and the proton numbers 50 and 82. After having reached a maximum for Pb^{208}, the curve descends again in the heavy element region to an energy as low

[14] M. Goldhaber and R. D. Hill, Revs. Modern Phys. **24**, 179 (1952).
[15] N. J. Hopkins, Phys. Rev. **88**, 680 (1952).
[16] Independently, a similar survey was made by P. Preiswerk and P. Stähelin, Helv. Phys. Acta **24**, 623 (1952).
[17] For heavy elements, the dependence of the excitation energy of even-even nuclei on A has been considered by F. Asaro and I. Perlman, Phys. Rev. **87**, 393 (1952).
[18] A. H. Wapstra [Physica **18**, 799 (1952)] discusses the branching ratio for alpha-emission leading to the first excited state of an even-even nucleus.

as 40 kev. At the last point, which denotes the first excited state of Pu^{242}, no indication of an eventual rise is noticeable. On the whole, several remarkable regularities may be discerned in Fig. 4: e.g., a certain symmetry around the points for Sn stands out. The element lines for neighboring elements are frequently arranged in parallel, which would indicate, as Preiswerk and Stähelin[16] have pointed out, that it may be possible to construct the energy function for the first excited state as a sum of functions, of which one depends only on the number of protons and the other on the number of neutrons. However, in the environment of "doubly magic" nuclei, this rule seems to be broken: the lines for A(18) and Ca(20) intersect, and the point for Pb^{204} lies below that of Hg^{202}.

B. *In a large number of examples, addition of two protons to a nucleus hardly affects the energy of the first excited state.* This is emphasized by the representation in Fig. 5 (a) and (b), in which the excitation energies of nuclei with the same number of neutrons are compared. Strong differences appear only where the proton number of one of the two nuclei is "magic." Addition of a *neutron* pair to a nucleus seems to have a slightly more disturbing effect on the position of the first level, as is indicated by the slopes of the lines in Fig. 4 connecting points for isotopes of the same element.

C. If one adds a single nucleon to an even-even core and considers the excitation of the odd nucleon and that of the core in first approximation as independent, one would expect the excitation energy of an odd A nucleus to be at least as low as, or lower than, that of its even-even core. This expectation is found to be in excellent agreement with the facts.

5. In Table I the energies, spins and parities of the three lowest excited states of even-even nuclei are listed. The method of measurement used and the reference are given for each entry. The arrangement of the table and the symbols used are explained in the caption.

Wherever the energy of a first excited state is known with reasonable certainty from the knowledge of a decay scheme or the Q value of a reaction, it appears also in Fig. 4. In cases where it is known only that a γ-ray of a certain energy is emitted but the excited state from which it starts is not identified, the energy is given in parentheses in Table I and, as a rule, not included in Fig. 4. For the determination of spin and parity of an excited state a number of different criteria were used. The most prominent among these were: (1) Measurement of the K-conversion coefficient of the γ-ray in question, which allows identification of the order of transition by means of the table of Rose *et al.*[19] (2) Measurement of the ratio of K-conversion electrons to L-conversion electrons (K/L ratio) and comparison of this value with empirical curves given by Goldhaber and Sunyar.[9] (3) Measurement of γ-γ angular or polarization correlation. (4) Measurement of β-γ angular correlation. (5) Measurement of angular correlation of γ-rays and particles emitted in a nuclear reaction. (6) Intensity ratio of L-conversion lines.[20] (7) Wherever lifetimes were measured, the multipole order of a transition could usually be derived by means of Weisskopf's formulas[21] or empirical curves.[9] (8) For the case of β-decay a clue is furnished, if spin and parity of the mother nucleus as well as the character of the beta-spectrum leading to the excited state are known. (9) Measurement of angular distribution[22] and polarization[23] of γ-rays from aligned nuclei.

Wherever the lifetime of a first excited state has been measured, it is also given in the table.

III. DISCUSSION

Let us now compare the results of this survey on spins, parities, and energy spacings of excited states of even-even nuclei with conclusions which may be derived from various nuclear models. We shall start out with the extended strong spin-orbit coupling model: An even number n of equivalent neutrons or protons in an unfilled subshell (quantum numbers l, j), interacting with each other, may be considered.

(1) For this model, under the assumption of short range forces, the lowest state is always caused by the excitation of a single pair of nucleons, with a resulting nuclear spin of 2 and even parity.[5, 6] This result is clearly in agreement with most of the empirical data: the first excited states of the majority of nuclei are 2+. It also provides a possible explanation for the two certain exceptions: In O^{16} the neutron shell as well as the proton shell of 8 is filled. In order to excite this nucleus, we may have to transfer a neutron pair, say, from the $p_{1/2}$ to the $d_{5/2}$ shell, with resultant spin 0, even. Similarly, in Ge^{72} the $p_{1/2}$ neutron shell and the $p_{3/2}$ proton shell may be filled and excitation may take place by raising a proton pair or a neutron pair to a higher configuration.

However, if this model were strictly adhered to, we would not expect 2+ levels for nuclei with filled subshells. In this light the 2+ levels of nuclei like Ce^{140} ($h_{11/2}$ neutron shell and $g_{7/2}$ proton shell filled) seem to require additional explanation. On the other hand, this fact would help with the interpretation of spin 1 and even parity in a number of cases, if these assignments should prove to be right: e.g., for C^{14} this would correspond to the splitting of a proton pair, ending up with one $p_{3/2}$ and one $p_{1/2}$ proton. Similarly, a 1+ level in Si^{28} may be due to the splitting of a $d_{5/2}$ neutron pair, with one neutron being transferred to the $d_{3/2}$ shell.

In particular, on this basis doubly magic nuclei are not expected to have a lowest excited level with spin 2+. We have already seen that this is borne out for O^{16} which has a first excited state 0+. Spin and parity of the first level of Ca^{40} (20–20) are not yet determined.

[19] Rose, Goertzel, Spinrad, Harr, and Strong, Phys. Rev. **83**, 79 (1951).

[20] J. W. Mihelich, Phys. Rev. **87**, 646 (1952); Gellman, Griffith, and Stanley, Phys. Rev. **85**, 944 (1952).

[21] V. F. Weisskopf, Phys. Rev. **83**, 1073 (1951).

[22] Daniels, Grace, and Robinson, Nature **168**, 780 (1951); Gorter, Poppema, Steenland, and Benn, Physica **17**, 1050 (1951).

[23] Bishop, Daniels, Goldschmidt, Halban, Kurti, and Robinson, Phys. Rev. **88**, 1432 (1952).

Pb^{208} (82–126), however, is known to have $I=2$, even, in its first excited state, in disagreement with this rule. Pryce[24] has discussed this difficulty in some detail.

Another explanation for the 0+ level of O^{16} has been given on the basis of the alpha-particle model.[25]

The liquid drop model yields a spin of 2 and even parity for the first excited state of any even-even nucleus. Therefore, the spin of the first excited state of Pb^{208} is compatible with it. For light nuclei this model is, however, expected to break down.

On the whole, it may be said that the evidence concerning the spin of the first excited state does not allow a definite distinction between the various models to be made at present.

(2) For the second excited state of an even-even nucleus, the extended spin-orbit coupling model as defined in Sec. II, 1 predicts 4+ for 2 nucleons or 2 holes with $j=5/2, 7/2, 9/2, 11/2, \cdots$, if it is assumed that no change of configuration takes place.[26,27] For 4 nucleons with $j=7/2$ and 4 or 6 nucleons with $j=9/2$, however, a second 2+ state is possible. This fact may explain why light nuclei (low j values) have predominantly a second excited state with $I=4+$, whereas for medium heavy and heavy nuclei both possibilities appear. In this simplified model (no interaction between protons and neutrons) a 3+ state appears for the first time for 4 or 6 nucleons with $j=9/2$. At least one of the two 3+ states in Fig. 2, that of A^{38}, cannot be explained in this way. If one considers the interaction of 2 loose protons and 2 loose neutrons with the same j, one finds that a 3+ state may result. However, for A^{38} (filled neutron shell) this assumption does not apply. In addition, even under the assumption of the splitting up of a pair of nucleons a 3+ state cannot be explained for A^{38}. The 1+ state of Nd^{144} may be attributed to the coupling of the spin 2+ of a proton pair with that of a neutron pair. The $I=0+$ state of Pd^{106} may be due to the change of configuration of a neutron pair.

The odd parity states require a change of configuration of at least one nucleon in the j-j coupling model. The $I=3-$ state of O^{16} may be interpreted as due to the splitting up of a $p_{1/2}$ neutron pair, with one neutron changing over to a $d_{5/2}$ state. According to Dennison,[25] four alpha-particles can also be coupled to give a spin 3−. The $I=7-$ state of Pb^{204m} can be ascribed to the splitting up of an $i_{13/2}$ neutron pair with one neutron going to the $p_{1/2}$ shell.

The predictions made on the basis of the "liquid drop" model[4] for the second excited state of an even-even nucleus are: $I=0$, 2, or 4; even parity.

(3) For the higher excited states not too definite conclusions can be drawn in the framework of the "loose particle" picture. However, the rule derived empirically: $I\leq 2n$ for the nth excited state is in agreement with this model and also with the liquid drop model. The only well-studied case of an even-even isomer, that of Pb^{204m} which was discussed above, is an exception to the rule $I\leq 2n$. In this connection the isomer Mo^{93m} is of interest.[28] It can be explained as due to isomerism of the core (spins 2, 4, 8 for first, second, and third excited state, respectively), while the odd neutron probably does not change its configuration.

(4) The rather smooth variation with A of the energy of the first excited state of an even-even nucleus and the deep troughs between closed shells may speak for the existence of interconfigurational mixing.[29] The greatest amount of mixing takes place in the middle of a shell, which has the effect of lowering the level in question due to the interaction of various configurations.

The low energies of first excited states in the rare earth region may be responsible for the scarcity of odd-proton isomers for $50<Z<82$, which, as mentioned above, presents one of the difficulties for the strict single particle model: Since the even-even core is easily excited, the single proton may prefer to couple with the 2+ state of the core to form the first excited state. Thus, the requirement for isomerism, $\Delta I\geq 3$, will be very rarely realized. On the other hand, the core excitation energies for $50<N<82$ are of the order of 0.5 Mev, which is usually higher than the excitation energy for the single neutron. Hence, a great number of isomers appear for odd neutron isotopes.[14]

The generally smooth behavior of the energy function agrees well with the liquid drop picture, but the specific features of this function cannot be derived from it. However, it is possible to compare the distortion parameter β[4] derived from different nuclear properties, namely, from quadrupole moments and the variation of isotope shifts, with the same parameter β derived from the energies of the first excited states of even-even nuclei. This has been carried out by Ford.[30] The fit is fairly good in the rare earth region, where a liquid drop model seems to be most adequate, but differences appear for lighter nuclei. For the heaviest nuclei few data on quadrupole moments and isotope shifts exist.

SUMMARY

In conclusion, it may be stated that both the j-j coupling model and the "liquid drop model" of the nucleus can explain the regularities found for spins and parities of first and second excited states of even-even nuclei. The extended j-j coupling model can explain more specific features, but not all the spins of these low-lying states. The smooth variation of the energy spacing between the ground state and the first excited state may be understood on the basis of the liquid drop model, but not the shell structure aspects of the energy spacing. The assumption of interconfigurational mixing may be necessary for a qualitative understanding of both features. Apart from the theoretical interest the

[24] M. H. L. Pryce, Proc. Phys. Soc. (London) **A65**, 773 (1952).
[25] D. M. Dennison, Phys. Rev. **57**, 454 (1940).
[26] H. J. Maehly and P. Stähelin, Helv. Phys. Acta **25**, 624 (1952).
[27] D. C. Peaslee (unpublished).
[28] M. Goldhaber, Phys. Rev. **89**, 1146 (1953).
[29] A. de-Shalit and M. Goldhaber (unpublished).
[30] K. W. Ford, Phys. Rev. **90**, 29 (1953).

smooth variation found for the energy of the first excited state as a function of proton and neutron number has many experimental uses, e.g., in the studies of decay schemes and inelastic scattering of particles.

I should like to thank M. Goldhaber for frequent inspiring discussions, and A. de Shalit and J. Weneser for enlightening arguments of a theoretical nature.

REFERENCES TO TABLE I

(T1) J. T. Dewan *et al.*, Phys. Rev. **86**, 416 (1952).
(T2) F. Ajzenberg and T. Lauritsen, Revs. Modern Phys. **24**, 321 (1952).
(T3) V. L. Telegdi, Phys. Rev. **84**, 600 (1951).
(T4) Cohen, Schafroth, Class, and Hanna, Phys. Rev. **87**, 206 (1952).
(T5) R. Malm and W. W. Buechner, Phys. Rev. **81**, 519 (1951).
(T6) Hubbard, Nelson, and Jacobs, Phys. Rev. **87**, 378 (1952).
(T7) G. M. Lewis, Phil. Mag. **43**, 690 (1952).
(T7a) R. G. Thomas and T. Lauritsen, Phys. Rev. **88**, 969 (1952).
(T8) G. Harris and W. T. Davies, Proc. Phys. Soc. (London) **A65**, 564 (1952).
(T9) Devons, Hereward, and Lindsey, Nature **164**, 586 (1949).
(T10) D. E. Alburger, Phys. Rev. **88**, 1257 (1952).
(T11) D. E. Alburger, Phys. Rev. **76**, 435 (1949).
(T12) Hinman, Brower, and Leamer, Bull. Am. Phys. Soc. **28**, No. 1, 41 (1953).
(T13) D. E. Alburger and E. M. Hafner, Brookhaven National Laboratory Report BNL-T-9, July 1949 (unpublished).
(T14) E. L. Brady and M. Deutsch, Phys. Rev. **78**, 558 (1950).
(T15) S. D. Bloom, Phys. Rev. **88**, 312 (1952).
(T16) Hausman, Allen, Arthur, Bender, and McDole, Phys. Rev. **88**, 1296 (1952).
(T17) H. Slätis and K. Siegbahn, Arkiv Mat. Astron. Fysik **4**, 485 (1952).
(T17a) J. Ambrosen, Nature **169**, 408 (1952).
(T18) P. M. Endt *et al.*, Phys. Rev. **86**, 518 (1952).
(T19) J. E. May and B. P. Foster, Bull. Am. Phys. Soc. **28**, No. 1, 41 (1953).
(T20) R. W. King, *Beta Decay Schemes and Nuclear Structure Assignments*, Washington University, St. Louis, 1952 (unpublished).
(T21) H. H. Landon, Phys. Rev. **83**, 1081 (1951).
(T22) D. M. van Patter *et al.*, Phys. Rev. **83**, 212 (1951).
(T23) R. H. Dieke and J. Marshall, Phys. Rev. **63**, 86 (1943).
(T24) Arthur, Allen, Bender, Hausman, and McDole, Phys. Rev. **88**, 1292 (1952).
(T25) L. Ruby and J. R. Richardson, Phys. Rev. **80**, 760 (1950).
(T26) N. Hole and K. Siegbahn, Arkiv. Mat. Astron. Fysik. **33A**, No. 9 (1946).
(T27) R. M. Steffen, Phys. Rev. **80**, 115 (1950).
(T28) M. L. Good, Phys. Rev. **81**, 891 (1951).
(T29) P. Morrison, Phys. Rev. **82**, 209 (1951).
(T30) J. A. Harvey, Phys. Rev. **88**, 162 (1952).
(T31) K. Siegbahn, Arkiv. Mat. Astron. Fysik **34B**, No. 4 (1947).
(T32) J. R. Beyster and M. L. Wiedenbeck, Phys. Rev. **79**, 728 (1950).
(T33) J. A. Bruner and M. Langer, Phys. Rev. **79**, 606 (1950).
(T34) F. T. Porter and C. S. Cook, Phys. Rev. **81**, 640 (1951).
(T35) F. Metzger and M. Deutsch, Phys. Rev. **78**, 551 (1950).
(T36) G. F. Pieper, Phys. Rev. **88**, 1299 (1952).
(T37) P. S. Jastram and C. E. Whittle, Phys. Rev. **87**, 1133 (1952).
(T38) W. C. Peacock and M. Deutsch, Phys. Rev. **69**, 306 (1946).
(T39) B. Hamermesh, Phys. Rev. **87**, 528 (1952).
(T40) Robinson, ter Pogossian, and Cook, Phys. Rev. **75**, 1099 (1949).
(T41) Way, Fano, Scott, and Thew, *Nuclear Data* (National Bureau of Standards Circular 499, 1950).
(T42) M. Deutsch and L. G. Elliot, Phys. Rev. **65**, 211 (1944).
(T43) L. G. Elliot and M. Deutsch, Phys. Rev. **63**, 321 (1943).
(T44) K. Strauch, Phys. Rev. **79**, 487 (1950).
(T45) Bishop, Daniels, Goldschmidt, Halban, Kurti, and Robinson, Phys. Rev. **88**, 1432 (1952).
(T45a) Cheng, Pick, and Kurbatov, Phys. Rev. **88**, 887 (1952).
(T46) D. E. Alburger, Phys. Rev. **76**, 435 (1949).
(T47) M. Deutsch and K. Siegbahn, Phys. Rev. **77**, 680 (1950).
(T48) A. H. Williams and M. L. Wiedenbeck, Phys. Rev. **78**, 822 (1950).
(T49) Parmley, Meyer, and Lilly, Phys. Rev. **75**, 619 (1949).
(T50) Brower, Hinman, Lang, Leamer, and Rose, Phys. Rev. **86**, 1054 (1952).
(T51) G. Friedlander and D. E. Alburger, Phys. Rev. **84**, 231 (1951).
(T52) Roderick, Meyerhof, and Mann, Phys. Rev. **84**, 887 (1951).
(T53) A. Mukerji and P. Preiswerk, Helv. Phys. Acta **23**, 516 (1950).
(T54) Bowe, Goldhaber, Hill, Meyerhof, and Sala, Phys. Rev. **73**, 1219 (1948).
(T55) McGowan, deBenedetti, and Francis, Phys. Rev. **75**, 1761 (1949).
(T56) Johansson, Cauchois, and Siegbahn, Phys. Rev. **82**, 275 (1951).
(T57) J. J. Kraushaar and M. Goldhaber, Phys. Rev. **89**, 1081 (1953).
(T58) Siegbahn, Hedgran, and Deutsch, Phys. Rev. **76**, 1263 (1949).
(T59) C. M. Huddleston and A. C. G. Mitchell, Phys. Rev. **88**, 1350 (1952).
(T60) D. G. Karraker and D. H. Templeton, Phys. Rev. **80**, 646 (1951).
(T61) H. R. Muether and S. L. Ridgeway, Phys. Rev. **80**, 750 (1951).
(T62) D. T. Stevenson and M. Deutsch, Phys. Rev. **83**, 1202 (1951).
(T63) F. R. Metzger and H. C. Amacher, Phys. Rev. **88**, 147 (1952).
(T64) D. N. Kundu and M. L. Pool, Phys. Rev. **76**, 183A (1949).
(T65) P. Preiswerk and P. Stähelin, Helv. Phys. Acta **24**, 300 (1951).
(T66) Medicus, Preiswerk, and Scherrer, Helv. Phys. Acta **23**, 299 (1950).
(T67) P. Stähelin and P. Preiswerk (private communication from H. Medicus).
(T68) House, Colligan, Kundu, and Pool, Phys. Rev. **86**, 654 (1952).
(T69) G. E. Boyd (private communication).
(T70) D. Maeder and P. Preiswerk, Helv. Phys. Acta **24**, 625 (1951).
(T70a) F. A. Johnson, Proc. Roy. Soc. (Canada) **46**, A135 (1952).
(T71) M. Goldhaber and R. D. Hill, Revs. Modern Phys. **24**, 179 (1952).
(T72) Arfken, Klema, and McGowan, Phys. Rev. **86**, 413 (1952).
(T73) D. E. Alburger, Phys. Rev. **88**, 339 (1952).
(T74) M. Goodrich and E. C. Campbell, Phys. Rev. **85**, 742 (1952).
(T75) Johns, Cox, Donelly, and McMullen, Phys. Rev. **87**, 1134 (1952).
(T76) Johns, Cox, and McMullen, Phys. Rev. **86**, 632 (1952).
(T77) E. D. Klema and F. K. McGowan, Phys. Rev. **87**, 524 (1952).
(T78) Blaser, Boehm, and Marmier, Helv. Phys. Acta **24**, 623 (1950).
(T79) M. J. Glaubman and F. R. Metzger, Phys. Rev. **87**, 203 (1952).
(T80) F. R. Metzger, Phys. Rev. **86**, 435 (1952).
(T81) J. W. Barnes and A. J. Freedman, Phys. Rev. **84**, 365 (1951).
(T82) M. L. Perlman and G. Friedlander, Phys. Rev. **82**, 449 (1951).
(T83) D. T. Stevenson and M. Deutsch, Phys. Rev. **84**, 1071 (1951).
(T84) K. Siegbahn and N. Hole, Phys. Rev. **70**, 133 (1946).
(T85) Roberts, Elliot, Downing, Peacock, and Deutsch, Phys. Rev. **64**, 268 (1943).
(T86) A. P. Smith *et al.*, Phys. Rev. **87**, 454 (1952).
(T87) Maienschein, Bair, and Baker, Phys. Rev. **83**, 477 (1952).
(T88) Waggoner, Moon, and Roberts, Phys. Rev. **80**, 420 (1950).
(T89) S. Katcoff and M. McKeown (private communication).
(T90) M. M. Cransden and W. S. Boyle, Phys. Rev. **82**, 447 (1951).
(T91) B. L. Robinson and L. Madansky, Phys. Rev. **84**, 600 (1951).
(T92) L. M. Langer and R. B. Duffield, Phys. Rev. **89**, 907 (1953).
(T93) B. L. Robinson and L. Madansky, Phys. Rev. **84**, 1067 (1951).
(T94) E. N. Jensen *et al.*, Phys. Rev. **80**, 862 (1950).
(T95) D. E. Alburger *et al.*, Phys. Rev. **82**, 322 (1951).
(T96) D. E. Alburger and J. Kraushaar, Phys. Rev. **86**, 633 (1952).
(T96a) Hollander, Perlman, and Seaborg, UCRL 1928 (1952).
(T97) Hoff, Rasmussen, and Thompson, Phys. Rev. **83**, 1068 (1951).
(T98) Mack, Prickett, and Pool, Phys. Rev. **86**, 633 (1952).
(T99) Mack, Prickett, and Pool (verbal report).
(T100) J. K. Long and M. L. Pool, Phys. Rev. **85**, 137 (1952).
(T101) C. T. Hibdon and C. O. Muehlhause, Phys. Rev. **88**, 943 (1952).
(T102) H. B. Keller and J. M. Cork, Phys. Rev. **84**, 1079 (1951).
(T103) J. W. Mihelich (private communication).
(T104) M. Deutsch and W. E. Wright, Phys. Rev. **82**, 277 (1951).
(T105) R. Katz and M. R. Lee, Phys. Rev. **85**, 1038 (1952).
(T106) E. L. Church (private communication).
(T107) F. K. McGowan, Phys. Rev. **85**, 151 (1952).
(T108) F. K. McGowan, Phys. Rev. **85**, 142 (1952).
(T109) G. Wilkinson, University of California Radiation Laboratory Report UCRL-677 (unpublished).
(T110) F. K. McGowan, Phys. Rev. **80**, 923 (1950).
(T111) Scharff-Goldhaber, der Mateosian, and Mihelich, Phys. Rev. **85**, 734 (1952).
(T112) F. K. McGowan, Phys. Rev. **87**, 542 (1952).
(T113) G. Wilkinson, Phys. Rev. **80**, 495 (1950).
(T114) Brown, Bendel, Shore, and Becker, Phys. Rev. **84**, 292 (1951).
(T115) Muller, Hoyt, Klein, and DuMond, Phys. Rev. **88**, 775 (1952).
(T116) F. R. Metzger and R. D. Hill, Phys. Rev. **82**, 646 (1951).
(T116a) F. Metzger, private communication.
(T117) F. K. McGowan, Phys. Rev. **81**, 1066 (1951).
(T118) Richmond, Grant, and Rose, Proc. Phys. Soc. (London) **A65**, 484 (1952).
(T119) J. W. Mihelich (private communication).
(T120) T. C. Chu, Phys. Rev. **79**, 582 (1950).
(T121) Cork, LeBlanc, Stoddard, Childs, Branyan, and Martin, Phys. Rev. **82**, 258 (1951).
(T121a) Mihelich, de Schalit, and Gillon, (private communication).
(T122) J. M. Cork *et al.*, Phys. Rev. **83**, 222 (1951).
(T123) C. E. Whittle and P. S. Jastram, Phys. Rev. **87**, 203 (1952).
(T124) M. Lindner, Phys. Rev. **84**, 240 (1951).
(T125) R. M. Steffen and D. M. Roberts, Phys. Rev. **83**, 222 (1951).
(T126) P. Stähelin, Phys. Rev. **87**, 375 (1952).
(T127) L. G. Elliot and J. L. Wolfson, Phys. Rev. **82**, 333 (1951).
(T128) C. Y. Fan, Phys. Rev **87**, 252 (1952).
(T129) J. W. Mihelich, Phys. Rev. **87**, 646 (1952).
(T130) R. L. Graham and R. E. Bell, Phys. Rev. **84**, 380 (1954).
(T131) H. P. Israel and R. G. Wilkinson, Phys. Rev. **83**, 1051 (1951).
(T132) G. Wilkinson, Phys. Rev. **79**, 1014 (1950).
(T133) N. J. Hopkins, Phys. Rev. **88**, 680 (1952).
(T134) Sunyar, Alburger, Friedlander, Goldhaber, and Scharff-Goldhaber, Phys. Rev. **78**, 326 (1950).
(T135) M. Goldhaber and A. W. Sunyar, Phys. Rev. **83**, 906 (1951).
(T136) Sunyar, Alburger, and Friedlander, Phys. Rev. **78**, 326 (1950).
(T137) D. E. Alburger and G. Friedlander, Phys. Rev. **81**, 523 (1951).
(T138) S. deBenedetti and G. H. Minton, Phys. Rev. **85**, 944 (1952).
(T139) G. Lindström, Phys. Rev. **87**, 678 (1952).
(T140) H. E. Petch and M. W. Johns, Phys. Rev. **80**, 478 (1950).
(T141) H. Slätis and K. Siegbahn, Arkiv. Fysik **4**, 485 (1952).
(T142) D. G. E. Martin and H. O. W. Richardson, Proc. Phys. Soc. (London) **A62**, 223 (1950).
(T143) M. Miwa, S. Kazeyama, J. Phys. Soc. Japan **5**, 416 (1951).
(T144) Way, Fano, Scott, and Thew, *Nuclear Data*, National Bureau of Standards Circular 499, Supplement No. 3.
(T145) S. Rosenblum, Valadares, Guillot, Compt. rend. **234**, 1767 (1952).
(T146) S. Rosenblum and M. Valadares, Compt. rend. **234**, 2359 (1952).
(T147) Cork, Branyan, Stoddard, Keller, LeBlanc, and Childs, Phys. Rev. **83**, 681 (1951).
(T148) Victor, Teillac, Falk-Vairant, Boussières, J. phys. et radium **13**, 565 (1952).
(T149) F. Asaro and I. Perlman, Phys. Rev. **87**, 393 (1952).
(T150) S. Rosenblum and M. Valadares, Compt. rend. **235**, 238 (1952).
(T151) C. J. D. Jarvis and M. A. S. Ross, Proc. Phys. Soc. (London) **A64**, 535 (1951).
(T152) D. C. Dunlavey and T. Seaborg, Phys. Rev. **87**, 165 (1952).
(T153) J. Kyles, Edinburgh (private communication to Wapstra, Amsterdam).
(T154) J. Teillac, Compt. rend. **230**, 1056 (1950).
(T155) G. Scharff-Goldhaber, Brookhaven National Laboratory Report BNL-103, p. 17 (unpublished).
(T156) B. Zajac, Phil. Mag. **42**, 264 (1952).
(T157) G. Albouy and J. Teillac, Compt. rend. **234**, 829 (1952).
(T158) D. A. Orth and G. D. O'Kelley, Phys. Rev. **82**, 758 (1951).
(T159) A. Prohaska, University of California Radiation Laboratory Report UCRL-1395 (unpublished).
(T160) G. D. O'Kelley, UCRL 1243 (1951).

TABLE I. The known energies, spins and parities of the first three excited states of even-even nuclei are listed. Columns XX and XXI refer to the half-life of the first excited state and the corresponding reference. Under "Method" the method of production of the excited state as well as the method of measuring the excitation energy is given. Wherever the excited state has been produced by a nuclear reaction, the bombarded nucleus A, the incoming particle b and the outgoing particle c are indicated in the following fashion: $A+b-c$. If the energy of the state was determined by measuring the energy of the outgoing particle, this is indicated by the remark "c obs." If γ-rays have been observed, this is also stated. If the excited state of nucleus Z^A is reached by β decay, this is indicated by $(Z-1)^A\beta^-$; if it is reached by electron capture or positron emission, the notation used is $(Z+1)^A$ E.C. (and/or) β^+. For the methods of measurement of γ-ray energies the notation used by K. Way *et al.* in *Nuclear Data* (National Bureau of Standards Circular 499) and its three supplements has been adhered to. Measurements with a curved crystal gamma-ray spectrometer are indicated by "cryst; γ." As bases for the survey, Circular 499 and the article by M. Goldhaber and R. D. Hill [Revs. Modern Phys. **24**, 179 (1952)] were extensively used. The references usually refer to the latest papers which, in turn, give references to previous work.

Nucleus	First excited state						Second excited state						Third excited state							
I	II	III	IV	V	VI	VII	VIII	IX	X	XI	XII	XIII	XIV	XV	XVI	XVII	XVIII	XIX	XX	XXI
	E,[a] Mev	Method	Reference	Spin and parity	Method	Reference	E Mev	Method	Reference	Spin and parity	Method	Reference	E Mev	Method	Reference	Spin and parity	Method	Reference	Half-life of first excited state	Reference
$_2He^6$	1.71	$Li^7+t-\alpha$ α obs	(T1)																	
$_4Be^8$	2.94	$B^{11}+p-\alpha$ α obs	(T2)	2+	$C^{12}+\gamma$; energy distr. of α's measured	(T3)	4.05	$Li+d-n$	(T2)				4.9	$Li+d-n$	(T2)					
$_4Be^{10}$	3.37	Be^9+d-p p and γ obs	(T2)	2 +	$p-\gamma$ ang. correl. ang. distr. of protons	(T4) (T2)	6.3	Be^9+d-p	(T2)				7.38	Be^9+d-p	(T2)	3+		(T2)		
$_6C^{12}$	4.44	$N^{14}+d-\alpha$ α and γ obs	(T5)	2+	$B^{11}+p$ $\gamma-\gamma$ ang. correl.	(T6)	7.5	$Be^9+\alpha-n$	(T2)	0?	Internal pair formation coeff.	(T2)	9.62	$N^{14}+d-\alpha$	(T5)				$<3\times10^{-12}$ sec	(T7a)
					$p, \gamma, \gamma(\theta)$	(T7)	~7	$Be^9+\alpha-n$ pairs obs	(T8)											
$_6C^{14}$	6.110	$C^{13}+d-p$ γ obs	(T2)	1 or 2	Energy distr. of internally formed positrons	(T2)														
$_8O^{16}$	6.05	$F^{19}+p-\alpha$ α and pairs obs	(T2)	0+	pair emission; energy distr. of positrons and electrons; lifetime	(T2)	6.13	$F^{19}+p-\alpha$ other reactions	(T2)	3−	$\alpha-\gamma$ ang. correl.	(T2)	6.91	$F^{19}+p-\alpha$	(T2)	2+	$\alpha-\gamma$ ang. correl.	(T2)	7×10^{-11} sec	(T9)
$_{10}Ne^{20}$	1.631	$F^{20}\beta^-$ from $F^{19}+d-p$ sl; pe^-, Compt.	(T10)	2+ or 1+	decay argument	(T10)	2.2?	$Ne^{20}+p-p'$	(T2)				4.3	$F^{19}+d-n$ $Ne^{20}+p-p'$	(T2)					
$_{10}Ne^{22}$	1.277	$Na^{22}\beta^+$; sl: pe^-	(T11)	2+	From ft value of 0.542 Mev positron and shape: $I=2$. Odd parity excluded by lack of measurable lifetime.		3.4	$F^{19}+\alpha-p$	(T2)				4.5	$F^{19}+\alpha-p$	(T2)					
					K conv. coeff.	(T12)														

[a] Doubtfully assigned energy values for the first excited state are given in parentheses in the second column. The following is a comparison of these energies with the energy function represented in Fig. 4.
Se^{78}: None of the 3 energy values fits.
Mo^{92}: 1.5 Mev seems correct assignment.
Mo^{98}: 0.86 Mev seems too high.
Pd^{108}: 0.42 Mev seems correct assignment.
Xe^{130}: probably 0.537 state lowest as plotted in Fig. 4.

Ba^{132}: 1 Mev seems too high; about 0.7 Mev expected.
Ba^{136}: ~1.2 Mev seems more probable than 0.9 Mev.
Sm^{146}: 0.45 Mev seems too low. Better measurement of gamma-ray energy desirable.
Sm^{148}: 0.54 Mev seems slightly too high.
Gd^{156}: 0.0888 Mev fits well.
Gd^{158}: 0.0792 Mev fits well.
Dy^{162}: 0.1 Mev
Hf^{178}: 0.1 Mev } More accurate measurements seem desirable.

W^{182}: The two values given are chosen to fit the plot best.
Os^{190}: 0.17 Mev fits fairly well.
Os^{192}: 0.283 Mev probably correct.
Hg^{200}: 0.365 Mev fits best.
Pb^{202}: 0.89 Mev seems high. A lower energy γ-ray may follow this isomeric transition.
Po^{210}: 1 Mev seems reasonable.

TABLE I.—*Continued.*

Nucleus	First excited state						Second excited state						Third excited state							
I	II	III	IV	V	VI	VII	VIII	IX	X	XI	XII	XIII	XIV	XV	XVI	XVII	XVIII	XIX	XX	XXI
	E,[a] Mev	Method	Reference	Spin and parity	Method	Reference	E Mev	Method	Reference	Spin and parity	Method	Reference	E Mev	Method	Reference	Spin and parity	Method	Reference	Half-life of first excited state	Reference
$_{12}Mg^{24}$	(1.38)	$Mg^{24}+p-p'$ $Mg^{24}+n-n$ $Na^{24}-\beta^-$; γ obs	(T13)	2+	$\gamma-\gamma$ ang. correl. pair conv. coeff. shape of pair spectrum pair conv. coeff.	(T14) (T15) (T17)	4.14	$Mg^{24}+p-p'$ $Na^{24}-\beta^-$; γ obs	(T13)	4+	$\gamma-\gamma$ ang. correl. pair conv. coeff.	(T14) (T15) (T17)	5.51 4.24	$Mg^{24}+p-p'$ $Al+p-\alpha$	(T13) (T16)					
$_{12}Mg^{25}$	1.84	$Mg^{25}+d-p$ p obs	(T17a)				2.85	$Na^{23}+\alpha-p$ $Mg^{25}+d-p$	(T13)				4.0	$Na^{23}+\alpha-p$	(T13)					
	1.825	$Mg^{25}+d-p$ ppl γ obs, scin	(T18) (T19)				3.00	$Mg^{25}+d-p$ p obs γ obs, scin	(T17a) (T19)				4.00	$Mg^{25}+d-p$ γ obs, scin	(T17a) (T19)					
$_{14}Si^{28}$	1.8	$Al^{27}+d-n$; n obs $Al^{28}(\beta^-)$; γ obs	(T13)	2+ or 1+	Analysis of disint. scheme. Spin of Al^{28} is 3+, $\log ft=4.87$	(T20)	4.47	$Al^{27}+d-n$; n obs	(T13)				4.91	$Al^{27}+d-n$; n obs	(T13)					
$_{14}Si^{30}$	2.3	$Al^{27}+\alpha-p$ $p-\gamma$ coinc.	(T21)				3.6	$Al^{27}+\alpha-p$ $p-\gamma$ coinc.	(T21)				4.9	$Al^{27}+\alpha-p$ $p-\gamma$ coinc.	(T21)					
	2.25	$Si^{29}+d-p$ p obs	(T22)				3.5	$Si^{29}+d-p$ p obs	(T22)				3.8	$Si^{29}+d-p$ p obs	(T22)					
$_{16}S^{32}$	2.25	$S+p-p'$ p obs	(T23)				4.34 3.81	$S+p-p'$ $S+p-p'$	(T23) (T24)											
$_{16}S^{34}$	2.13	Cl^{34} E.C.; β^+ sl; ce$^-$; pe$^-$; Compt.	(T25)				3.30	Cl^{34} E.C.; β^+ sl; ce$^-$; pe$^-$	(T25)											
$_{18}A^{38}$	2.15	$Cl^{38}\beta^-$	(T26)	2+	$\gamma-\gamma$ ang. correl.	(T27)	3.75	$Cl^{38}\beta^-$	(T26)	3+	$\gamma-\gamma$ ang. correl.	(T27)								
$_{18}A^{40}$	1.459	K^{40} E.C.; s; pe$^-$; Compt.	(T28)	2+	Analysis of disintegr. scheme	(T29)														
$_{20}Ca^{40}$	3.8*	$Ca^{40}+p-p'$ p obs; a	(T30)																	
$_{20}Ca^{42}$	1.51	$K^{42}\beta^-$ $\beta^--\gamma$ coinc.	(T31)	2+	$\beta-\gamma$ ang. correl.	(T32)														
$_{21}Ca^{44}$	1.16	$Sc^{44}\beta^+$, E.C. sπ; ce$^-$; pe$^-$	(T33)	1+ or 2+	from shell model considerations and shape of β^+ spectrum	(T33)														
$_{22}Ti^{46}$	1.12	$Sc^{46}\beta^-$	(T34)	2+	K conv. coeff. $\gamma-\gamma$ ang. correl.	(T34) (T35)	2.01	$Sc^{46}\beta^-$	(T34)	4+	K conv. coeff. $\gamma-\gamma$ ang. correl.	(T34) (T35)								
$_{22}Ti^{48}$	1.33	$Ti^{47}+d-p$ p obs	(T36)	2+	$\gamma-\gamma$ ang. correl.	(T37)	2.31	$Sc^{48}\beta^-$ sl; pe$^-$, Compt. $V^{48}\beta^+$; sπ; pe$^-$, Compt.	(T38) (T40)	4+	$\gamma-\gamma$ ang. correl.	(T37)	3.29	$Ti+n-p$; β^- scin. 3γ's in cascade	(T39)					
$_{22}Ti^{50}$	1.58	$Ti^{49}-d-p$ p obs	(T36)				3.0	$Ti^{49}+d-p$ p obs	(T36)				4.14	$Ti^{49}+d-p$ p obs	(T36)					
$_{24}Cr^{52}$	1.46	Mn^{52}(5.8-day) E.C. β^+ sl; pe$^-$	(T38)				2.40	$Mn^{52}\beta^+$; E.C. s	(T41)				3.13	$Mn^{52}\beta^+$; E.C. s	(T41)					
	1.45	$V^{52}\beta^-$; a	(T41)				2.43	$Cr+p-p'$ p obs		(T16)			2.99	$Cr+p-p'$	(T16)					

* *Note added in proof:* According to a private communication by W. W. Buechner, the 3 lowest levels in Ca^{40} found by inelastic proton scattering have the following energies: 3.35, 3.74, and 3.90 Mev (Braams, Bockelman, Browne, and Buechner, Bull. Am. Phys. Soc., Washington Meeting, April 29–May 1, 1953).

TABLE I.—*Continued.*

Nucleus	First excited state						Second excited state						Third excited state							
I	II	III	IV	V	VI	VII	VIII	IX	X	XI	XII	XIII	XIV	XV	XVI	XVII	XVIII	XIX	XX	XXI
	E,[a] Mev	Method	Reference	Spin and parity	Method	Reference	E Mev	Method	Reference	Spin and parity	Method	Reference	E Mev	Method	Reference	Spin and parity	Method	Reference	Half-life of first excited state	Reference
$_{24}Cr^{54}$	0.835	Mn^{54} E.C. sl; pe^-	(T42)																	
$_{26}Fe^{56}$	0.845	$Mn^{56}\beta^-$, s $Co^{56}\beta^+$ sl; pe^-	(T41) (T43)				2.66	$Mn^{56}\beta^-$, s	(T41)				2.98	$Mn^{56}\beta^-$, s	(T41)					
$_{26}Fe^{58}$	0.805	Co^{58} E.C., β^+ sl; ce^-	(T44)	2+	γ ang. correl. for aligned nuclei K conv. coeff.	(T45) (T45a)														
$_{28}Ni^{60}$	1.332	$Co^{60}\beta^-$ sl; pe^-	(T46)	2+	$\gamma-\gamma$ polarization direction correl.	(T35) (T48)	2.507	$Co^{60}\beta^-$ sl; pe^-	(T46)	4+	$\gamma-\gamma$ pol. correl.	(T35)								
	1.338	$Co^{60}\beta^-$ sl; ce^-	(T47)				2.512		(T47)		$\gamma-\gamma$ ang. correl.	(T48)								
$_{28}Ni^{62}$	1.3	$Co^{62}\beta^-$; a	(T49)																	
$_{28}Ni^{64}$	1.34	Cu^{64} E.C., β^- sl; ce^-	(T50)	≤ 2	K conv. coeff.	(T50)														
$_{30}Zn^{66}$	1.044	$Cu^{66}\beta^-$ sl; ce^-	(T51)	2+ or 1+	derived from decay scheme	(T52)	2.762	Ga^{66} E.C.; β^+ sl; pe^- Compt.	(T53)	2+ (or 1+)	Analysis of disintegr. scheme									
$_{30}Zn^{68}$	1.10	$Ga^{68}\beta^+$ sl; pe^-, Compt.	(T53)	2+ or 1+	derived from decay scheme	(T53)														
$_{32}Ge^{72}$	0.68	$Ga^{72}\beta^-$ sl; ce^-	(T41)	0+	K conv. coeff. and lifetime	(T54)	0.84	$Ga^{72}\beta^-$ sl; pe^-	(T41)	1+ or 2+	derived from decay scheme								0.3×10^{-9} sec	(T55)
$_{32}Ge^{74}$	0.5963	As^{74} E.C. β^+ $s\pi\sqrt{2}$; pe^-	(T56)	2+ (or 1+)	derived from decay scheme	(T56)														
$_{34}Se^{74}$	0.6352	$As^{74}\beta^-$ $S\pi\sqrt{2}$; pe^-	(T56)	2+ (or 1+)	derived from decay scheme	(T56)														
$_{34}Se^{76}$	0.567	$As^{76}\beta^-$; s	(T41)	2+	$\gamma-\gamma$ ang. correl.	(T57)	1.21	$As^{76}\beta^-$, scint.	(T57)	2+	$\gamma-\gamma$ ang. correl.	(T57)	2.67	scint.	(T41)					
$_{34}Se^{78}$	(0.27) (0.046) (0.108)	$As^{78}\beta^-$, a Br^{78}, E. C., β^+; sc	(T41)																	
$_{36}Kr^{82}$	0.77	$Br^{82}\beta^-$; ce^-; s	(T58)				1.378	$Rb^{82}\beta^+$ sl; pe^-	(T59)											
	0.768	$Rb^{82}\beta^+$ sl; pe^-	(T59)																	
$_{36}Kr^{84}$	0.85	Rb^{84} E.C.; β^+ a	(T60)	2+	Analysis of disintegration scheme	(T59)														
	0.89	Rb^{84} E.C.; β^+ sπ; ce^-; scin.	(T59)																	
$_{38}Sr^{86}$	1.076	$Rb^{86}\beta^-$ sl; pe^-	(T61)	2+	$\beta-\gamma$ ang. correl.	(T62)														
$_{38}Sr^{88}$	1.853	$Rb^{88}\beta^-$ Y^{88} E.C., β^+ s	(T41)	2+ (or 1+)	K conv. coeff. Y^{88} K capt.	(T63)	2.76	$Rb^{88}\beta^-$ Y^{88} E.C., β^+	(T41)	3− (or 2−)	K conv. coeff.	(T63)								
$_{40}Zr^{90}$	(2.03)	$Nb^{90}\beta^+$; a	(T64)																	

TABLE I.—*Continued.*

Nucleus	First excited state						Second excited state						Third excited state							
I	II	III	IV	V	VI	VII	VIII	IX	X	XI	XII	XIII	XIV	XV	XVI	XVII	XVIII	XIX	XX	XXI
	E,[a] Mev	Method	Reference	Spin and parity	Method	Reference	E Mev	Method	Reference	Spin and parity	Method	Reference	E Mev	Method	Reference	Spin and parity	Method	Reference	Half-life of first excited state	Reference
$_{40}Zr^{92}$	0.930	Nb^{92} E.C. sl; pe^-	(T65)																	
$_{42}Mo^{92}$	(1.5)	Tc^{92} E.C., β^+	(T41)																	
$_{42}Mo^{94}$	0.87	Tc^{94} E.C., β^+ sl; Compt.	(T66)	2+	K conv. coeff.	(T66)	2.73	Tc^{94} E.C., β^+ sl; Compt.	(T66)	3+	derived from decay scheme	(T66)	3.27	Tc^{94} E.C. sl; Compt.	(T66)	2+	derived from decay scheme	(T66)		
$_{42}Mo^{96}$	0.770	Tc^{96} E.C. sl; ce^-, pe^-	T(66)	2+	K conv. coeff.	(T67)	1.60	Tc^{96} E.C. sl; ce^-, pe^-	(T66)	3+ or 4+	K conv. coeff.	(T67)	1.84	Tc^{96} E.C. sl; pe^-	(T65)					
$_{42}Mo^{98}$	(0.86)	Tc^{98} E.C.; a	(T68)																	
$_{44}Ru^{100}$	0.55	Tc^{100} β^-	(T69)																	
$_{46}Pd^{104}$	0.56	Rh^{104} β^-; scin.	(T70)																	
	0.555	Ag^{104} β^+	(T70a)																	
$_{46}Pd^{106}$	0.513	Rh^{106} β^-; sl; Ag^{106} β^+ sl; pe^-	(T71)	2+	$\gamma-\gamma$ ang. correl. K conv. coeff.	(T71) (T73)	1.137	Rh^{106} β^- Ag^{106} β^+ sl; pe^-	(T71)	0+	$\gamma-\gamma$ ang. correl.	(T71)	1.55	Rh^{106} β^- Ag^{106} β^+ sl; pe^-	(T71)	2+	$\gamma-\gamma$ ang. correl.	(T72)		
$_{46}Pd^{108}$	0.42 (0.19)	Ag^{108} E.C. scin.	(T74)																	
$_{48}Cd^{110}$	0.656	Ag^{110} β^- In^{110} β^+	(T71)	2+ (or 1+)	K conv. coeff.	(T71)	1.415	Ag^{110} β^- In^{110} β^+	(T71)				1.54	Ag^{110} β^- In^{110} β^+	(T71)					
$_{48}Cd^{114}$	0.550	In^{114} E.C. sl; pe^-	(T71)	2+	$\gamma-\gamma$ ang. correl.	(T71) (T76) (T77)	1.263	In^{114} E.C. sl; pe^-	(T71)	2+	$\gamma-\gamma$ ang. correl.	(T71) (T76) (T77)	1.856	In^{114} E.C. s; pe^-	(T75)	0 or 2	derived from decay scheme	(T75)		
$_{50}Sn^{116}$	1.274	In^{116} β^- sl; pe^-	(T71)				2.09	In^{116} β^- sl; pe^-	(T71)				2.36	In^{116} β^- sl; pe^-	(T71)					
$_{50}Sn^{120}$	1.30	Sb^{120} E.C.	(T78)				2.20	Sb^{120} E.C.	(T78)											
$_{52}Te^{122}$	0.568	Sb^{122} β^-	(T71)	2+	$(\beta-\gamma)+(\gamma-\gamma)$ ang. correl.	(T71)	1.24	Sb^{122} β^-	(T71)	2+	$\gamma-\gamma$ ang. correl.	(T71)								
					K conv. coeff. $\beta-\gamma$ ang. correl.	(T79)					K conv. coeff.	(T79)								
$_{52}Te^{124}$	0.607	Sb^{124} β^- I^{124} E.C.	(T71)	2+	K conv. coeff.	(T80)														
$_{52}Te^{126}$	0.64	I^{126} E.C. scin.	(T82)		(Sb^{124} β^-)															
	(0.4 or 0.9)	Sb^{126} β^- scin.	(T81)				1.3	Sb^{126} β^-	(T81)											
$_{54}eX^{128}$	0.382	I^{128} β^- sl; ce^-	(T82)	2+	$\beta-\gamma$ ang. correl.	(T83)														
$_{54}Xe^{128}$	0.428	I^{128} β^- sl; ce^-	(T84)	2+ (or 1+)	derived from beta spectra	(T84)														
$_{54}Xe^{130}$	(0.537 or 0.667 or 0.744)	I^{130} β^- sl; ce^-	(T85)																	
		No γ, Cs^{130} β^+ scin.	(T86)																	
$_{54}Xe^{132}$	0.68	I^{132} β^- scin.	(T87)																	

TABLE I.—*Continued.*

Nucleus	First excited state						Second excited state						Third excited state							
I	II	III	IV	V	VI	VII	VIII	IX	X	XI	XII	XIII	XIV	XV	XVI	XVII	XVIII	XIX	XX	XXI
	E,[a] Mev	Method	Reference	Spin and parity	Method	Reference	E Mev	Method	Reference	Spin and parity	Method	Reference	E Mev	Method	Reference	Spin and parity	Method	Reference	Half-life of first excited state	Reference
$_{54}Xe^{134}$	(1.03 or 1.17 ?)	Cs^{134} E.C.?	(T88)																	
$_{54}Xe^{136}$	1.38	$I^{136}\beta^-$ scin.	(T89)																	
$_{56}Ba^{132}$	(1.0)	$La^{132}\beta^+$ a	(T90)																	
$_{56}Ba^{134}$	0.794	$Cs^{134}\beta^-$ sl; ce^-, pe^-	(T41)	2+	$\gamma-\gamma$ ang. correl.	(T14)	1.36	$Cs^{134}\beta^-$ sl; ce^-, pe	(T41)	4+	$\gamma-\gamma$ ang. correl.	(T14)	1.93	$Cs^{134}\beta^-$ sl; ce^-, pe^-	(T41)	5	$\gamma-\gamma$ ang. correl.	(T91)		
$_{56}Ba^{136}$	(0.9) (1.2)	$Cs^{136}\beta^-$ a	(T41)																	
$_{56}Ba^{138}$	1.44	$Cs^{138}\beta^-$ scin., coinc.	(T92)				2.42	$Cs^{138}\beta^-$ scin.	(T92)				2.88	$Cs^{138}\beta^-$ scin.	(T92)					
$_{58}Ce^{140}$	1.6	$La^{140}\beta^-$ s; ce^-; scin.	(T41)	2+	$\gamma'-\gamma$ ang. correl.	(T93)	2.42	$La^{140}\beta^-$ s; ce^-; scin.	(T41)	4+	$\gamma-\gamma$ ang. correl.	(T93)								
$_{60}Nd^{142}$	1.576	$Pr^{142}\beta^-$ sl; pe^-	(T94)	2+ (or 1+)	derived from shape of β spectrum and decay scheme	(T94)														
$_{60}Nd^{144}$	0.695	$Pr^{144}\beta^-$ sl; pe^-	(T95)	2+ (or 1+)	$\gamma-\gamma$ ang. correl.	(T96)	2.185	$Pr^{140}\beta^-$ sl; pe^-	(T95)	1+	$\gamma-\gamma$ ang. correl.	(T96)								
$_{60}Nd^{146}$	(0.490)	$Pr^{146}\beta^-$ scin	(T96a)																	
$_{62}Sm^{146}$	(0.45)	Eu^{146} E.C. a	(T97)																	
$_{62}Sm^{148}$	(0.69)	Eu^{148} E.C. a	(T98)	(2+)	K conv. coeff.	(T99)														
	(~0.54)	$Pm^{148}\beta^-$ a	(T100)																	
$_{62}Sm^{150}$	0.3367	Sm^{149} neutron capt. sπ; ce^-	(T101)	(2+)	K/L ratio	(T101)	(0.777)	Sm^{149} neutron capt. sπ; ce^-	(T101)	4+	K/L ratio	(T101)								
$_{63}Sm^{152}$	0.122	Eu^{152} E.C. sπ; ce^-	(T102)	2+	K/L ratio	(T103)														
$_{64}Gd^{152}$	0.3441	$Eu^{152}\beta^-$ sπ; ce^-	(T102)	2+	K/L ratio	(T103)													$<3\times10^{-9}$ sec	(T104)
$_{64}Gd^{154}$	0.122	$Eu^{154}\beta^-$ sπ; ce^-	(T105) (T103)																	
$_{64}Gd^{156}$	(0.0888)	Gd+n sπ; ce^-	(T106)	2+	Rel. int. of L lines	(T106)														
$_{64}Gd^{158}$	(0.0792)	Gd+n sπ; ce^-	(T106)	2+	Rel. int. of L lines	(T106)														
$_{66}Dy^{160}$	0.085	$Tb^{160}\beta^-$ sl; ce^-	(T41)	2+	K conv. coeff.	(T107)													1.8×10^{-9} sec	(T108)
$_{66}Dy^{162}$	(~0.1)	Ho^{162} E.C.	(T109)																	
$_{68}Er^{166}$	0.080	$Ho^{166}\beta^-$ sπ; ce^-	(T71)	2+	K/L ratio lifetime	(T71)	1.44	$Ho^{166}\beta^-$ sl; pe^-	(T71)										1.7×10^{-9} sec	(T110)

TABLE I.—*Continued.*

Nucleus	First excited state						Second excited state						Third excited state							
I	II	III	IV	V	VI	VII	VIII	IX	X	XI	XII	XIII	XIV	XV	XVI	XVII	XVIII	XIX	XX	XXI
	E,[a] Mev	Method	Reference	Spin and parity	Method	Reference	E Mev	Method	Reference	Spin and parity	Method	Reference	E Mev	Method	Reference	Spin and parity	Method	Reference	Half-life of first excited state	Reference
$_{70}Yb^{170}$	0.084	Tm^{170} β^- sl; ce$^-$	(T41)	2+	K conversion coeff.	(T107) (T41)														
$_{72}Hf^{176}$	0.089	Lu^{176m} β^- sπ; ce$^-$	(T111)	2+	K/L ratio	(T111)													1.35×10^{-9} sec	(T112)
$_{72}Hf^{178}$	(~0.1)	Ta (9.35 min) E.C., β^+	(T113)																	
$_{72}Hf^{180}$	0.093	Ta^{180} E.C. sπ; ce$^-$	(T114)	2+	K/L ratio	(T114)														
$_{74}W^{180}$	0.102	Ta^{180} β^- sπ; ce$^-$	(T114)	2+?	K conv. coeff.	(T114)														
$_{74}W^{182}$	(0.100 or 0.113 or others)	Ta^{182} β^- cryst; γ	(T115)																	
$_{74}W^{184}$	0.123	Re^{184} E.C. sπ; ce$^-$, pe$^-$	(T116)	2+	K conv. coeff.	(T116)														
$_{76}Os^{186}$	0.137	Re^{186} β^- sπ; ce$^-$; pe$^-$	(T116)	2+	K conv. coeff. Lifetime	(T116) (T117)	0.764	Re^{186} β^- sl; pe$^-$	(T116)	2+	γ−γ ang. correl.	(T116a)							~0.8×10^{-9} sec	(T117)
$_{76}Os^{188}$	0.154	Re^{188} β^- sl; ce$^-$	(T118)	2+	K/L ratio	(T118)													$<5\times10^{-9}$ sec	(T104)
	0.1549		(T119)		K conv. coeff. $L_I L_{II} L_{III}$ int. ratios	(T119)														
$_{76}Os^{190}$	(0.17)	Ir^{190} E.C. a	(T120)																	
$_{76}Os^{192}$	(0.283)	Ir^{192} E.C. sl; ce$^-$	(T121)				0.4843	Ir^{192} E.C. sl; ce$^-$	(T121)				0.690	Ir^{192} E.C. sl; ce$^-$	(T121)					
$_{78}Pt^{192}$	(0.316 or 0.295)	Ir^{192} β^- sl; ce$^-$	(T121)				0.6115	Ir^{192} β^- sl; ce$^-$	(T121)				0.783	Ir^{192} β^- sl; ce$^-$	(T121)					
		Au^{192} E.C. sπ; ce$^-$	(T121a)																	
$_{78}Pt^{194}$	0.327	Ir^{194} β^- s; ce$^-$	(T122)	2 (or 1)	γ−γ ang. correl.	(T123)	1.81	Ir^{194} β^- a	(T41)	2	γ−γ ang. correl.	(T123)	2.1	Au^{194} E.C. s	(T41)					
		No γ	(T124)	2+	K/L ratio	(T119)		Au^{194} E.C. sl; ce$^-$												
	0.328	Au^{194} E.C. sl; ce$^-$	(T41)																	
$_{78}Pt^{196}$	0.358	Au^{196} E.C. sl; ce$^-$	(T41)	2+	γ−γ ang. correl.	(T115)	0.688	Au^{196} E.C. sl; ce$^-$	(T41)	2+	γ−γ ang. correl.	(T125)								
$_{80}Hg^{196}$	0.426	Au^{196} β^- s; ce$^-$	(T126)	2+	L conv. coeff.	(T126)														
$_{80}Hg^{198}$	0.411	Au^{198} β^- sl; ce$^-$	(T41)	2+	K conv. coeff. L_{II}/L_{III} ratio	(T127) (T128) (T129)	1.087	Au^{198} β^- sπ; ce$^-$	(T127)	2+	K conv. coeff. and β^- decay scheme	(T127)							$<0.08\times10^{-9}$ sec	(T130)
$_{80}Hg^{200}$	(0.365 or 0.577 or 0.622)	Tl^{200} E.C. scin.	(T131)																	
$_{80}Hg^{202}$	0.427	Tl^{202} E.C. s; ce$^-$	(T132)																	

TABLE I.—*Continued.*

Nucleus	First excited state						Second excited state						Third excited state							
I	II	III	IV	V	VI	VII	VIII	IX	X	XI	XII	XIII	XIV	XV	XVI	XVII	XVIII	XIX	XX	XXI
	E,[a] Mev	Method	Reference	Spin and parity	Method	Reference	E Mev	Method	Reference	Spin and parity	Method	Reference	E Mev	Method	Reference	Spin and parity	Method	Reference	Half-life of first excited state	Reference
$_{82}Pb^{202}$	(0.89)	Tl+p→Pb^{202m} (5.6 sec) Po^{206}→α(?)	(T133)																	
$_{82}Pb^{204}$	0.374	Pb^{204m} I.T. sl; ce$^-$ Bi^{204} E.C. sl: ce$^-$	(T134)	2+	K/L ratio K conv. coeff.; lifetime	(T135)	1.279	Pb^{204m} I.T. sl; ce$^-$	(T136)	7−	Lifetime Total conv. coeff. K/L ratio	(T135)							3×10^{-7} sec	(T134)
$_{82}Pb^{206}$	0.803	Po^{210} α Bi^{206} E.C. sl; ce$^-$	(T137)	2+	α−γ ang. correl.	(T138)														
$_{82}Pb^{208}$	2.614	Tl^{208}(ThC″) β^-	(T139)	2+	γ−γ ang. correl. pair formation coeff. γ−γ polarization correl.	(T140) (T141) (T57)	3.20	Tl^{208}(ThC″) β^-	(T41)	4+	γ−γ ang. correl. γ−γ polarization correl.	(T140) (T57)	3.48	Tl^{208} β^- [redacted]	(T41)					
$_{84}Po^{210}$	(1)	At^{210} E.C. a	(T41)																	
$_{84}Po^{212}$	0.729	Bi^{212}(ThC)β^-	(T115)	2+	K conv. coeff.	(T142)	0.83	Bi^{212} β^-	(T41)				1.60	Bi^{212} β^-	(T41)					
$_{84}Po^{214}$	0.606	Bi^{214}(RaC) β^- sπ; ce$^-$	(T41) (T144)	2+	K/L ratio	(T143)														
$_{86}Em^{220}$	0.241	Th^{224} α sπ; ce$^-$	(T145)	2+	K conv. coeff.	(T145)														
$_{86}Em^{222}$	0.188	$_{88}$Ra^{226}α α fine structure	(T41)	2+	Rel. int. of L lines, K conv. coeff. total conv. coeff. K/L ratio	(T146) (T147) (T148)														
$_{88}Ra^{222}$	0.117	Th^{226} α α fine structure	(T149)																	
$_{88}Ra^{224}$	0.0844	$_{90}$Th^{228}(RdTh)α α fine structure	(T150)	2+	L_{II}/L_{III} ratio total conv. coeff.	(T150) (T148)														
$_{88}Ra^{226}$	0.0678	$_{90}$Th^{230} α sπ; ce$^-$	(T145) (T151)	2+	Rel int. of L lines	(T146)														
$_{88}Ra^{228}$	0.055	$_{90}$Th^{232} α ce$^-$; ppl	(T152)																	
$_{90}Th^{226}$	0.070	U^{230} α α fine structure	(T149)																	
$_{90}Th^{228}$	0.060	U^{232} α ce$^-$; ppl	(T152)	2+	Rel. int. of L lines for γ from Ac^{228}→ β^-	(T153)														
	0.058	α fine struct.	(T149)																	
	0.058	Ac^{228}(MsTh$_2$)β^-	(T41)																	
$_{90}Th^{230}$	0.055	U^{234} α ce$^-$; ppl	(T154)				0.117 or 0.167*	U^{234} α scin.	(T155)											
	0.050	scin.	(T155)																	

* Bohr and Mottelson, Phys. Rev. (to be published) suggest that 0.167 Mev fits better, if both lowest levels of Th^{230} are interpreted as rotational states of a deformed nucleus.

TABLE I.—*Continued.*

Nucleus	First excited state						Second excited state						Third excited state							
I	II	III	IV	V	VI	VII	VIII	IX	X	XI	XII	XIII	XIV	XV	XVI	XVII	XVIII	XIX	XX	XXI
	E,[a] Mev	Method	Reference	Spin and parity	Method	Reference	E Mev	Method	Reference	Spin and parity	Method	Reference	E Mev	Method	Reference	Spin and parity	Method	Reference	Half-life of first excited state	Reference
$_{90}Th^{234}$	0.048	$U^{238}\alpha$ ce^-; ppl	(T156)																	
	~0.045	ce^-; ppl	(T152)																	
	0.050	ce^-; ppl	(T157)																	
$_{92}U^{232}$	0.045	$Pu^{236}\alpha$ ce^-; ppl	(T152)																	
$_{92}U^{234}$	0.040	$Pu^{238}\alpha$ ce^-; ppl	(T152)																	
	0.043	α fine structure	(T149)																	
$_{92}U^{236}$	0.044	$Pu^{240}\alpha$ α fine structure	(T149)																	
$_{94}Pu^{236}$	(0.150)*	$Np^{236}\beta^-$ $8\pi\sqrt{2}$; ce^-	(T158)																	
$_{94}Pu^{238}$	0.045	$Cm^{242}\alpha$ α fine structure	(T149)	2+	Rel. intensities of L conv. lines	(T159)	0.150	$Cm^{242}\alpha$ α fine structure	(T149)											
		ce^-; ppl	(T152)																	
$_{94}Pu^{240}$	0.045	$Am^{244}\alpha$ α fine structure	(T149)																	
$_{94}Pu^{242}$	0.038	Am^{242} E.C. $8\pi\sqrt{2}$; ce^-	(T71)																	
$_{96}Cm^{242}$	0.053	$Am^{242}\beta^-$ $8\pi\sqrt{2}$; ce^-	(T160)																	

* A re-interpretation of the conversion electron spectrum shown in (T160) suggests that the strongest gamma-ray line may have an energy of 0.04 Mev.

The Thermal Neutron Capture Cross Section of Hydrogen

B. HAMERMESH, G. R. RINGO, AND S. WEXLER
Argonne National Laboratory, Lemont, Illinois
(Received January 26, 1953)

The thermal neutron capture cross section of hydrogen has been measured to be 0.329±0.004 b at 2200 m/sec. This was done by measurement of the reduction in the neutron activation rate of NaI in a water solution when boron of a known absorption cross section was added to the solution.

I. INTRODUCTION

THE cross section for the thermal neutron capture of hydrogen (σ_H) is directly related to various parameters connected with the neutron-proton interaction potential. An accurate determination of this cross section might contribute to the resolution of questions concerning the shape of the *n-p* well[1] or might permit an evaluation of the effect of the Sach's type of magnetic interactions.[2] With these ideas in mind, a series of experiments was performed in order to determine σ_H to an accuracy of approximately one percent.

The method most commonly used for measuring σ_H is the integration technique of Frisch, Halban, and Koch.[3] This method requires the determination of the neutron density in an essentially infinite solution, at a series of distances from a source of neutrons located near the center of the tank which holds the solution. The solutions used are distilled water and distilled water containing a small amount of boric acid. The neutron density is measured by use of BF_3-filled chambers, boron-lined chambers, or manganese foils. In all of these cases, the effect of the detector is difficult to ascertain to the degree of accuracy which would lead to a one percent accuracy for σ_H.

Frisch, Halban, and Koch[3] obtained a value of σ_B/σ_H of 1940±100, whereas Fenning, Halban, and Seligman[4] obtained 2160±30. In each of these experiments, no correction was made for detector perturbations on the neutron density. In a similar experiment by Kubitschek,[5] this correction was made using manganese foils, and a value of 2380±70 was obtained. A value of 1954±24 has been reported by Schulz and Goldhaber.[6] The most recent result obtained by the integration technique is from the very careful experiment of Whitehouse and Graham.[7] Their result is 2270±30. However, an upper limit of three percent for the error caused by detector perturbation effects is not included in this estimate of accuracy.

In view of the wide variation in the value of σ_B/σ_H, we have sought a procedure which would lead to about a one percent accuracy in this ratio. Furthermore, since there are significant variations in the isotopic abundances[8] of boron, a careful determination of the capture cross section of the boron used in such an experiment was thought desirable.

Muehlhause[9] has recently determined σ_B/σ_H at this laboratory using the pile oscillator technique. He used a boron sample of known cross section and obtained a value for σ_H of 0.332±0.007. However, this method involves the use of certain pile constants which are difficult to evaluate.

II. METHOD

As has been implied, the present measurement consists of a comparison of the hydrogen capture cross section with that of a boron sample of known cross section. The method used for the boron to hydrogen comparison is similar in principle to that of references 3–7. It involves a study of the competition between capture in boron and hydrogen in a solution containing a neutron source. The activation of a constant amount of NaI in the solutions is used as a measure of the captures in hydrogen.

For purposes of understanding the experiment, assume that a constant source of neutrons is placed at the center of a large tank. The tank must be large enough so that when the appropriate solutions are added to the tank, all of the source neutrons are absorbed in the solutions, i.e., there is no leakage of neutrons from the tank. Two solutions are used: NaI in H_2O and $NaI+H_3BO_3$ in H_2O. Each solution is placed in the tank in turn and irradiated. The solution is continually stirred during irradiation, and a sample of it is later counted. If the irradiation time is the same in the two parts of the experiment, then the ratio of iodine activities in the two cases is

$$R=\frac{\left(\dfrac{N_I\sigma_I}{N_{NaI}\sigma_{NaI}+N_H\sigma_H}\right)}{\left(\dfrac{N_I'\sigma_I}{N_{NaI}'\sigma_{NaI}+N_H'\sigma_H+N_B'\sigma_B}\right)}. \quad (1)$$

[1] E. E. Salpeter, Phys. Rev. **82**, 60 (1951).
[2] N. Austern and R. G. Sachs, Phys. Rev. **81**, 710 (1951).
[3] Frisch, Halban, and Koch, Kgl. Danske Videnskab. Selskab, Mat.-fys. Medd. **15**, 1 (1938).
[4] Fenning, Halban, and Seligman, British Atomic Energy Project Report BR-135 (1943), unpublished.
[5] H. Kubitschek, Manhattan District Project Report CP-972 (1943), unpublished.
[6] L. G. Schulz and M. Goldhaber, Phys. Rev. **67**, 202 (1945); L. G. Schulz, Ph.D. thesis, University of Illinois (1945), unpublished.
[7] W. J. Whitehouse and G. A. R. Graham, J. Research **A25**, 261 (1947).
[8] Thode, Macnamara, Lossing, and Collins, J. Am. Chem. Soc. **70**, 3008 (1948).
[9] C. O. Muehlhause *et al.* (to be published).

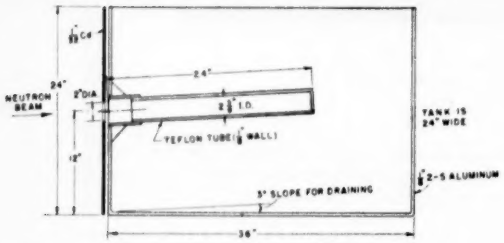

FIG. 1. A vertical cross section of the tank used in the neutron-proton capture experiment.

The various N's are the numbers of atoms/cm^3 of the different constituents, and the σ's are the capture cross sections. The unprimed N's refer to the no-boron experiment. The primed N's refer to the experiment with boron.

If N_I is made equal to N_I', then

$$R-1=\frac{N_B'\sigma_B+(N_H'-N_H)\sigma_H}{N_{NaI}\sigma_{NaI}+N_H\sigma_H}. \qquad (2)$$

$(N_H'-N_H)\sigma_H$ is relatively very small. The NaI concentration is so chosen that $N_{NaI}\sigma_{NaI}$ is small. Thus, with small corrections, Eq. (2) readily leads to σ_B/σ_H.

III. PROCEDURES AND RESULTS

A beam of neutrons from the thermal column of the Argonne heavy water-moderated reactor was used as a source. There are two advantgages of the beam technique compared with the point source (e.g., Ra−Be) method. First, since a thermal beam is used, one can perform Cd-difference experiments and thereby avoid problems associated with leakage of fast neutrons and neutron capture at other than thermal energies. Second, the difficulty associated with neutron capture in the source itself is eliminated.

The neutron beam was brought into the large tank (Fig. 1) through the attached Teflon tube. The dimensions of the tank were so chosen that leakage of neutrons through the tank walls was less than 0.1 percent. The incident neutron beam was monitored by matched gold foils which were supported at the center of the entrance hole of the tank and were later measured for the Au^{198} activity induced. During and for an eight-minute period after an irradiation, the solution was well mixed by electric stirrers. As a check on the thoroughness of the mixing, a test was made by taking samples of solutions from various parts of the tank after only four minutes of stirring. No difference in the counting rates of these samples was observed.

The two solutions used in the experiment were prepared by dissolving reagent grade NaI in approximately 700 liters of distilled water and then adding reagent grade H_3BO_3 to half of the iodide solution. The concentrations of the boric acid (as B_2O_3) and sodium iodide were accurately determined by chemical analysis to be 2.681 g/l and 41.48 g/l, respectively. NaI, rather than the ordinarily used manganese salts, served as the neutron detector because of the former's chemical compatability with boric acid in aqueous solutions. Each solution was made slightly basic with a small volume of NH_4OH in order to prevent air oxidation of iodide. The 25-min I^{128}, the predominant activity formed in the neutron irradiation, was counted in two glass-jacketed annular Geiger counters, each of which held approximately 20 cc of solution. The stability of the counters was checked by use of a standard 50-day In^{114} solution. Dead-time corrections were determined by means of two solutions of active NaF which differed by a factor of five in concentration. Care was taken to have the specific activity of the Na^{24} sufficiently high so that the densities of the two solutions were practically identical despite dilution. The dead-time corrections caused a 0.14 percent change in R.

A rigid schedule of irradiation, cooling and counting times was maintained in order to secure comparable data. An irradiation lasted 36 minutes, and stirring continued an additional eight minutes before withdrawal of the two samples of the solution for counting. Three 12-minute counts were taken, begun exactly 15 minutes after the irradiation and spaced by one-minute intervals. Appropriate background corrections were made by counting samples of the solution taken from the tank just before the irradiation. The two solutions were irradiated alternately.

A set of data from one complete experiment appears in Table I. A cadmium difference for each solution was obtained by irradiating with, and then without, a Cd cover over the entrance hole.

IV. CORRECTIONS

To obtain the ratio of the boron-to-hydrogen capture cross sections from the ratio of the activities of the two solutions, several corrections must be applied. The first is for neutrons absorbed in the Teflon tube. The effective absorption area of the tube was measured by comparison with cadmium wires, using the danger coefficient method[10] in a reactor. In addition, the neutron flux was measured at several points along the tube during an irradiation. From these two measurements the number of neutrons absorbed in the tube was calculated, and the measured activity of the solution corrected by the ratio of this number to the total number entering the tank (about 0.007). The effect of these changes in the activities was an increase of 0.1 percent in the activity ratio of the two solutions.

The second correction is for the loss of neutrons which leave the tank through the entrance hole. These neutrons were measured by a gold foil placed in the entrance hole and covered by cadmium on the side toward the reactor. Since the gold foil used for this measurement was essentially identical to the one used to monitor the

[10] Anderson, Fermi, Wattenberg, Weil, and Zinn, Phys. Rev. **72**, 16 (1947).

incident flux, the ratio of the activities of these two foils was a measure of the fraction of the neutrons escaping. The ratio of the activities was multiplied by the ratio of the areas of the entrance hole (the hole in the cadmium) and the escape area (an area slightly more than the area of the hole in the tank). This gave the ratio of leakage to absorbed neutrons. It turned out to be 0.016 for the solution without boron and so near to that for the other solution that the net effect on the ratio of the activities of the two solutions was only 0.06 percent.

As mentioned in the introduction, it was thought necessary to determine the capture cross section of the boron used in this experiment. This was done by comparing this boron with a standard whose absorption cross section had been measured absolutely. The standard used was another batch of boric acid whose absorption cross section had been determined by a transmission measurement[11] which was corrected for the rather small scattering cross section. The comparison of the borons was done by the danger coefficient method.

As can be seen from Eq. (2), a correction must be made for the absorption by the activator, NaI. Since

TABLE I. Sample data for one determination of R.

Solution in tank	Cd cover	Counter	Bkgd.	Counts per minute 1st	2nd	3rd
		A	51	1848	1417	1121
NaI	Yes	C	65	1913	1430	1077
		A	76	23 566	16 526	11 735
NaI	No	C	75	23 077	16 180	11 484
NaI+H_3BO_3	Yes	A	27	1178	877	691
		C	25	1117	859	703
NaI+H_3BO_3	No	A	50	9779	6975	4982
		C	49	9833	6925	4799

the amount of activator was chosen so that the absorption would be about 5 percent of that of the hydrogen, it would only be necessary to know it to about 5 percent to make the error it contributes negligible. The published values of the Na and I absorption cross sections,[12] however, vary rather widely; so a new measurement using the standard boron mentioned earlier as a standard was thought desirable. A value of 7.4 barns for the NaI absorption cross section was obtained by the pile oscillator method.[13]

In addition to the corrections which have been discussed, another possible source of error is the energy dependence of the absorption cross sections. It is implicit in Eq. (2) that the neutron spectra in the two solutions are the same or else that the absorption cross sections of iodine, hydrogen, and boron all have the same energy dependence. There is at least the possibility that the spectra differ slightly in the two solutions, so the other assumption had to be made. There is much experimental evidence that boron is a $1/v$ absorber, and there are good theoretical reasons for thinking hydrogen is also. However, iodine has resonances near the thermal region, and there is no direct evidence on the energy dependence of its capture cross section in the thermal region. Accordingly it was decided to test the dependence of the activation of the solution on the neutron spectrum. The solution containing boron was irradiated at 16.5°C and at 60°C. The solution activities, for a given incident neutron flux, were the same within the estimated accuracy of the experiment—two percent. The difference in the spectrum in the solution containing boron and that in the solution without boron is expected to be small compared to the difference in this heating experiment. Therefore this experimental result furnishes a reasonable confirmation of the assumptions in Eq. (2).

[11] Kimball, Ringo, Robillard, and Wexler (unpublished data).
[12] H. Pomerance, Phys. Rev. **83**, 643 (1951).
[13] Harris, Muehlhause, Rasmussen, Schroeder, and Thomas, Phys. Rev. **80**, 342 (1950).

V. RESULTS

The ratio of activity in the solution without boron to that in the solution with boron, corrected for the incident neutron flux, obtained from 9 runs, was 2.528 ± 0.016. Applying the corrections that have been discussed and using Eq. (2), we obtained a ratio of standard boron-to-hydrogen capture cross sections of 2292 ± 27. The measured standard boron cross section was 755 ± 3 b at 2200 m/sec; thus the neutron capture cross section of hydrogen is

$$0.329\pm0.004 \text{ b at } 2200 \text{ m/sec.}$$

The sources of error in this measurement are believed to be as shown in Table II.

VI. DISCUSSION

In general, these results are in good agreement with earlier work;[5,7,9] in better agreement, in fact, than would be expected in view of the known variations in boron isotopic ratios, which might spoil comparisons with some of these measurements. The error in the ratio of boron-to-hydrogen capture cross sections is not notably better than has been obtained earlier,[7] but this experiment has reduced the uncertainty in the cross section of the boron used in the comparison.

TABLE II. The sources of error in the experiment. The errors listed are the contributions to the error in the hydrogen cross section, not the error in the item listed.

Source	Error percent
Ratio of solution activities (based on statistics of 9 runs)	1.1
Standard boron	0.4
Comparison of borons	0.4
Analyses of boron	0.3
NaI capture cross section	0.2
Errors in other corrections	0.1
Total	1.3

It should be pointed out that this measurement and that of Muehlhause[9] are both dependent on the same standard boron cross section, so they only serve to check each other on the boron-to-hydrogen ratio. The standard boron cross section has as yet not been confirmed by other laboratories. Any change in the accepted value of this cross section will, of course, produce a proportionate change in the value of the capture cross section of hydrogen.

Because this experiment seems relatively free of uncertain corrections and the principal source of error appears to be the statistics of the activity ratio measurements of the two solutions, we believe that it would be entirely possible to reduce the error in σ_H to about $\frac{1}{2}$ percent. The effort involved in this would be warranted however only after there was more certainty in the capture cross-section standards.

It is a pleasure to express our gratitude to the following members of this laboratory: Dr. L. A. Turner for several suggestions on the method used in this experiment, to Dr. David Rose for his measurement of the NaI capture cross section, and to Mr. Ralph Bane and Mr. Ralph Telford for their careful boron and iodine analyses.

PHYSICAL REVIEW VOLUME 90, NUMBER 4 MAY 15, 1953

Inner Bremsstrahlung Associated with K Capture in A^{37}†*

CARL E. ANDERSON,‡ GEORGE W. WHEELER, AND W. W. WATSON
Yale University, New Haven, Connecticut

(Received February 2, 1953)

An investigation has been made of the inner bremsstrahlung accompanying K capture in A^{37}. The inner bremsstrahlung energy distribution was examined by absorption and scintillation spectrometer techniques and found to agree with that predicted by theory. A Kurie-type plot showed the maximum energy of the gamma-radiation to be 815±15 kev.

INTRODUCTION

THE theory of inner bremsstrahlung associated with beta-decay processes was extended to the case of K capture by Morrison and Schiff[1] in 1940. More recently, Jauch[2] has reviewed and improved the theory. The first experimental evidence for the existence of this inner bremsstrahlung was found by Bradt *et al.*[3] in the nucleus Fe^{55}. Later investigations on the same nucleus by Maeder and Preiswerk;[4] Jauch;[2] and Bell, Jauch, and Cassidy[5] have confirmed Bradt's conclusions and have also yielded further knowledge of the K capture transition energy and the gamma-radiation energy distribution. Up to the present investigation, Fe^{55} is the only nuclide shown to emit inner bremsstrahlung with K capture.

The theory shows, essentially, that the relative probability of photon emission per K capture is given by

$$\frac{dP}{P_0}=\frac{\alpha}{\pi m^2}\left(1-\frac{\omega}{W_0}\right)^2\omega d\omega \qquad (1)$$

and that the total number of photons emitted per K capture is given by

$$\int_0^{W_0}\frac{dP}{P_0}=\frac{\alpha}{12\pi}\left(\frac{W_0}{m}\right)^2. \qquad (2)$$

Here dP is the probability per unit time for photon emission, P_0 is the probability per unit time for K capture, ω is the energy of the photon, W_0 is the energy available for the transition, m is the rest energy of the electron, and α the fine structure constant. It has also been shown by Jauch[2] that it is possible to write (1) in such a form that a linear plot may be made of the experimental data. That is,

$$N(\omega)d\omega=C(\omega)\frac{\alpha}{\pi m^2}\frac{\omega}{W_0{}^2}(W_0-\omega)^2d\omega, \qquad (3)$$

where $N(\omega)$ is the number of photons having energy between ω and $\omega+d\omega$, and $C(\omega)$ is a slowly varying function (except at low energies) which is therefore treated as a constant. Upon simplification we have

$$K[N(\omega)/\omega]^{\frac{1}{2}}=W_0-\omega, \qquad (4)$$

where K is a constant. The intercept of this straight line on the energy axis will be W_0, the energy available for the transition.

HALF-LIFE

The A^{37} source was prepared by irradiating enriched argon gas for 30 days in the Brookhaven reactor. The

† This paper is part of a dissertation submitted in partial fulfillment of the requirements for the degree of Doctor of Philosophy in Yale University by C. E. A. A preliminary report on the results has appeared in Phys. Rev. **87**, 668 (1952).

* This work was supported by the U. S. Atomic Energy Commission.

‡ Now at the General Electric Research Laboratory, Schenectady, New York.

[1] P. Morrison and L. I. Schiff, Phys. Rev. **58**, 24 (1940).
[2] J. M. Jauch, Oak Ridge National Laboratory Report ORNL 1102, 1951 (unpublished).
[3] H. Bradt *et al.*, Helv. Phys. Acta **19**, 222 (1946).
[4] D. Maeder and P. Preiswerk, Phys. Rev. **84**, 595 (1951).
[5] Bell, Jauch, and Cassidy, Science **115**, 12 (1952).

argon had been enriched by means of thermal diffusion[6] to 96 percent A^{36}, 1 percent A^{38}, and 3 percent A^{40}. The irradiated gas was transferred from a quartz breakseal to a brass chamber having thin (9.7 mg/cm²) aluminum foil windows. This made it possible to observe the low energy gamma-rays and to be free of activities present in the quartz.

To verify that the observed gamma-ray continuum was indeed due to A^{37}, the half-life of this continuum was determined. The decay curve is shown in Fig. 1. The measured half-life of 32 days agrees, within statistics, with the value of 34.1 days found by Weimar *et al.*[7]

The theory developed by Morrison and Schiff and by Jauch applies only to allowed transitions, and consequently, it is necessary to show that the transition $A^{37} \rightarrow Cl^{37}$ is allowed before making use of the results of this theory. A calculation of the *ft* value of the process indicates that the transition is indeed allowed. For an allowed transition in this case $f_k^0(\epsilon_0) \cong 0.095$

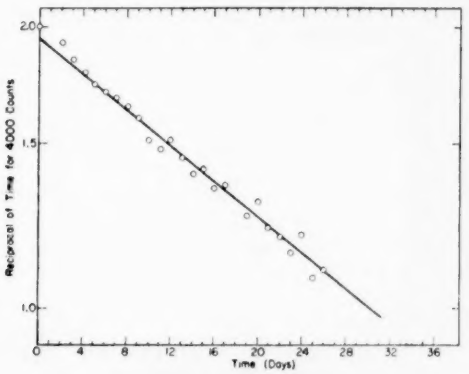

FIG. 1. Gamma-ray continuum half-life curve.

and for a first forbidden transition $f_k'(\epsilon_0) \cong 2.0 \times 10^{-3}$. From these *f* values the predicted half-lives are $t_{\frac{1}{2}} = 5.0 \times 10^5$ sec and $t_{\frac{1}{2}} = 2.4 \times 10^9$ sec, respectively. As the half-life is $t_{\frac{1}{2}} = 2.8 \times 10^6$ sec, the transition falls within the region of allowed transitions.

ENERGY DISTRIBUTION

Absorption Method

The absorption method consists in comparing an observed absorption curve with a curve calculated from the theoretical distribution curve, Fig. 2. To calculate the absorption curve the continuum was approximated by a set of mono-energetic gamma-rays whose intensities are proportional to the area of the energy region they represented. The individual absorption curves of these gamma-rays are then graphically added to obtain the complex absorption curve of the continuum.

[6] A. Zucker and W. W. Watson, Phys. Rev. **79**, 241 (1950).
[7] Weimar, Kurbatov, and Pool, Phys. Rev. **66**, 209 (1944).

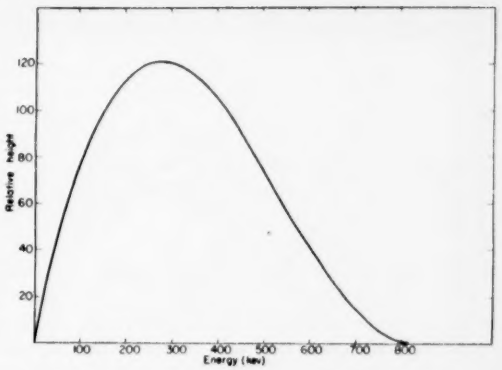

FIG. 2. Theoretical inner bremsstrahlung distribution, $W_0 = 816$ kev.

The observed absorption curve in lead was taken using an anthracene scintillation counter as detector. The theoretical absorption curve was calculated in the aforementioned manner after modification of the theoretical energy distribution for the variation of detector efficiency with energy (in this case, the percent transmission of the phosphor). The calculated and observed absorption curves are shown in Fig. 3. The agreement is good except at low absorber thickness. This is believed to arise from a compromise made between collimation and counting rate which allowed slightly more high than low energy gamma-rays to enter the detector.

Scintillation Spectrometer Method

Scintillation spectroscopy has been applied successfully to the measurement of continua by Madansky and

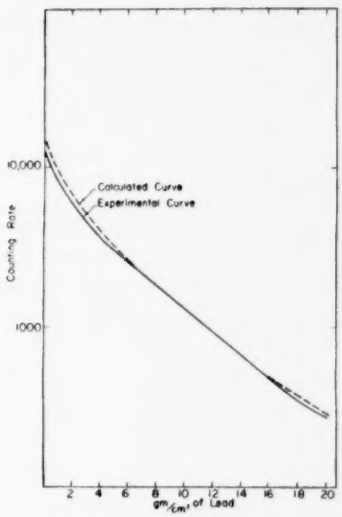

FIG. 3. Absorption curves in lead.

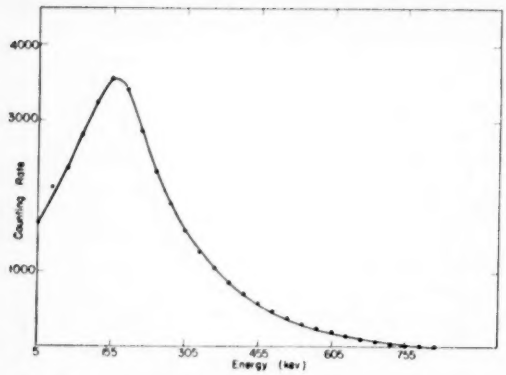

FIG. 4. Pulse-height distribution of gamma-ray continuum.

Rasetti;[8] Jauch;[2] Maeder and Preiswerk;[4] and Bell, Jauch and Cassidy.[5] Following the method used by Madansky and Rasetti, the effect of the finite resolution of the spectrometer was determined. This is done by assuming that only the photoeffect occurred and that the pulse spectrum of a mono-energetic gamma-ray can be represented by a Gaussian function. Therefore, the pulse-height distribution is given by

$$f(s)=(2\pi\sigma^2)^{-\frac{1}{2}}\int_0^1 f(\epsilon)\exp\left[-\frac{(s-\epsilon)^2}{2\sigma^2}\right]d\epsilon, \qquad (5)$$

where $f(\epsilon)$ is $(1-\epsilon)^2\epsilon$, the theoretical distribution, $\epsilon=\omega/W_0$, and σ is a width parameter. Assuming a resolution of 15 percent at 661 kev, we determined $f(s)$. Graphical comparison of $f(s)$ with $f(\epsilon)$ showed that no significant distortion occurred except at the end points of the distribution.

In all of the investigations mentioned above,[2-5,8] the maximum energy was low enough so that only photoelectric conversion was of importance in the phosphor and little distortion occurred from the presence of the Compton effect. This distortion is not readily susceptible to calculation. In the case of A^{37}, W_0 is about 800 kev, and thus significant distortion will occur. We can only say that the result will be to increase the maximum and shift it to lower energy, preventing a direct comparison of the experimental and theoretical distributions. However, by following the method of Jauch it is still possible to determine the maximum energy by means of a Kurie plot, because the distortion is small at the high energy end of the spectrum.

[8] L. Madansky and F. Rasetti, Phys. Rev. **83**, 187 (1951).

The photomultiplier used was an RCA 5819, while the phosphor was a $1\frac{1}{2}$ in. diameter$\times$1 in. thick NaI(Tl) crystal, roughly polished and imbedded in dry MgO powder. This arrangement gave a resolution of 11 percent at 661 kev. The spectrometer was calibrated with the following four sources: Cs^{137} (661 kev), Au^{198} (411 kev), Hg^{203} (285 kev), and W^{185} (135 kev).

The pulse-height spectrum obtained is shown in Fig. 4. This spectrum must be corrected for the variation of the counting efficiency with energy of the spectrometer. We have used as the most reasonable correction factor the variation of the percent absorption with energy of the 1-in. thick NaI crystal. This choice is only an approximation. Of course a very thick crystal would not require any correction. Perhaps a better correction could be deduced for our crystal from an analysis of the pulse-height distribution of a number of mono-energetic gamma-rays.

The corrected spectrum was then used to construct the Kurie plot shown in Fig. 5. For comparison, the

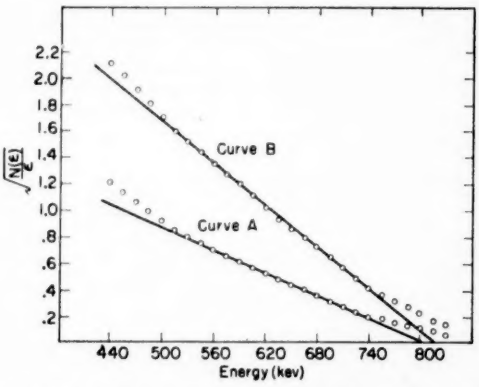

FIG. 5. "Kurie plots," curve A uncorrected data, curve B, after modification of data for detector efficiency.

Kurie plot of the uncorrected data is also shown. The maximum energy W_0 obtained from the Kurie plot is 815$\pm$15 kev. This value agrees well with that obtained from nuclear reaction data. Using the Q value of the reaction $Cl^{37}(p,n)A^{37}$, Richards, Smith, and Browne[9] obtain a value of 816$\pm$4 kev, while Schoenfeld, Duborg, Preston, and Goodman[10] obtain a value of 816$\pm$2 kev.

[9] Richards, Smith, and Browne, Phys. Rev. **80**, 524 (1950).
[10] Schoenfeld, Duborg, Preston, and Goodman, Phys. Rev. **85**, 873 (1952).

The Quadrupole Moment Ratio of I^{129} and I^{127} from Pure Quadrupole Spectra*

RALPH LIVINGSTON AND HENRY ZELDES
Oak Ridge National Laboratory, Oak Ridge, Tennessee

(Received January 30, 1953)

The pure quadrupole spectra for I^{129} and I^{127} have been observed in SnI_4 at 77°K and at 20°K. The nuclear quadrupole moment ratio has been determined to be $Q(I^{129})/Q(I^{127})=0.701213\pm0.000015$.

THE quadrupole moment ratio of long-lived fission I^{129} to stable I^{127} is known approximately from microwave measurements.[1] The frequencies of the direct quadrupole transitions for I^{129} and I^{127} in SnI_4 are reported in this paper. These measurements yield a more accurate value for the quadrupole moment ratio.

The compound selected for these measurements was SnI_4, since this substance gives very strong, sharp absorption lines, and it is easy to synthesize. A sample of SnI_4 was prepared from a solution containing about 40 mg of iodine as iodide. Although an isotopic analysis was not made on the sample, measurements on other similar samples consistently showed about 80 percent I^{129} and 20 percent I^{127}. The iodide was oxidized to iodine, extracted into CS_2, an excess of tin metal added, and the reaction allowed to go to completion by warming to about 50°C. This gave a solution of SnI_4 in CS_2 which was then evaporated to dryness. The solid product was sealed into a 2-mm diameter, thin-walled glass capillary. It is estimated that the capillary contained about 30 mg of I as SnI_4 (24 mg of I^{129} and 6 mg of I^{127}). The capillary fitted snugly into the spectrometer coil.

The spectrometer is a simple regenerative oscillator unit with a transmission line tuned circuit. The absorption lines were viewed on an oscillograph, and frequency measurements were made with a Gertsch FM-1B frequency meter. The Gertsch frequency meter contains a crystal oscillator, transfer oscillator, and interpolation oscillator. Improved accuracy was obtained by directly calibrating the interpolation oscillator at the settings used in each of the frequency measurements. A Signal Corps BC-221 frequency meter was used for this calibration. The FM-1B and BC-221 crystal oscillators were also compared with radio station WWV. The measured frequencies and assignments are given in Table I. The frequencies are the average of several determinations, and subsequent calculations indicate that the precision is substantially better than the estimated accuracy of about 0.001 percent.

There are two nonequivalent iodine lattice positions in SnI_4, and this gives rise to a pair of lines for each transition indicated by lattice type A or B in Table I.

Calculations were made using equations given by Bersohn[2] for the energy levels E_m. The parameters determining a given E_m value are the z component of the quadrupole coupling, the nuclear spin (5/2 for I^{127} and 7/2 for I^{129}) and the asymmetry parameter $\eta=[(\partial E_x/\partial x)-(\partial E_y/\partial y)]/(\partial E_z/\partial z)$, where the derivatives are components of the field gradient tensor in the principal axis system. The calculations are summarized in Table II. The magnitude of the asymmetry parameter was evaluated from the frequency ratio of the two transitions observed for I^{129}. A frequency ratio of 1.5 for these transitions corresponds to $\eta=0$, and within the accuracy of the frequency measurements this appears to be the case for the type B lattice positions (Table II). Further justification for $\eta=0$ will be given below. Although Bersohn has given the levels by perturbation theory to fourth-order in η, a second-order treatment proved adequate for the type A lattice positions because of the small magnitude of η. The η-values and the corresponding transition frequencies for the two isotopes were then used to calculate the quadrupole coupling values. The average of the four ratios in Table II gives

$$Q(I^{129})/Q(I^{127})=0.701213\pm0.000015.$$

The original microwave determination[1] of this ratio gave 0.7353. More recent and more extensive micro-

TABLE I. Observed frequencies and assignments for iodine in SnI_4.

Lattice type	Assignment: Isotope	Assignment: Transition ($\lvert m\rvert\rightarrow\lvert m+1\rvert$)	Frequency, Mc/sec: 77°K	Frequency, Mc/sec: 20°K
A	I^{129}	3/2→5/2	138.6783	139.2052
A	I^{129}	5/2→7/2	208.0254	208.8157
A	I^{127}	1/2→3/2	207.6855	208.4702
B	I^{129}	3/2→5/2	139.6604	140.2356
B	I^{129}	5/2→7/2	209.4924	210.3556
B	I^{127}	1/2→3/2	209.1324	209.9923

TABLE II. Summary of calculations and results for iodine resonances in SnI_4.

T°K	Lattice type	Freq. ratio, I^{129} $(5/2\rightarrow7/2)/(3/2\rightarrow5/2)$	$\lvert\eta\rvert$	$e(\partial E_z/\partial z)\times Q^{129}$	$e(\partial E_z/\partial z)\times Q^{127}$	Q^{129}/Q^{127}
77	*A*	1.5000573	0.00905	970.793	1384.446	0.701214
77	*B*	1.500013	0	977.627	1394.216	0.701202
20	*A*	1.5000568	0.00900	974.481	1389.678	0.701228
20	*B*	1.500016	0	981.654	1399.949	0.701207

* This work was performed for the U. S. Atomic Energy Commission.

[1] Livingston, Gilliam, and Gordy, Phys. Rev. **76**, 149 (1949).

[2] R. Bersohn, J. Chem. Phys. **20**, 1505 (1952).

wave measurements[3] by the same authors have given a ratio in much closer agreement. The crystal structure of SnI_4 is known,[4] and Dehmelt[5] has made and discussed higher temperature measurements of the I^{127} resonance. The lattice is cubic with two nonequivalent iodine lattice positions. One-quarter of the iodine atoms lie on C_3 axes of the unit cube and this symmetry requires $\eta=0$ for these atoms. The crystal symmetry does not require $\eta=0$ for the remaining three quarters of the iodine atoms. The type B lines for which $\eta=0$ are appropriately weaker than the corresponding type A lines in agreement with the crystal structure. Dehmelt's values for η, determined for I^{127} at room temperature, are the same as the lower temperature values for I^{129} given above. His quadrupole coupling value for I^{127} is appropriately lower than the above values because of the temperature difference.

We wish to acknowledge the help of Gordon Hebert and George Parker of the Chemistry Division, this Laboratory, for supplying the I^{129} which they isolated from fission material.

[3] R. Livingston *et al.* (unpublished results).
[4] R. W. G. Wyckoff, *Crystal Structures* (Interscience Publishers, New York, 1951).
[5] H. G. Dehmelt, Z. Physik **130**, 356 (1951).

PHYSICAL REVIEW VOLUME 90, NUMBER 4 MAY 15, 1953

Comparison of the Values of the Disintegration Constant of Be^7 in Be, BeO, and BeF_2*

J. J. KRAUSHAAR, ELIZABETH D. WILSON, AND KENNETH T. BAINBRIDGE†
Brookhaven National Laboratory, Upton, New York

(Received February 2, 1953)

The difference in the decay constants of Be^7 in Be, BeO, and BeF_2, have been measured using the differential ionization chamber technique. The results are $\lambda(Be)-\lambda(BeF_2)=(7.41\pm0.47)\times10^{-4}\lambda$, $\lambda(BeO)-\lambda(BeF_2)=(6.09\pm0.55)\times10^{-4}\lambda$, $\lambda(Be)-\lambda(BeO)=(1.31\pm0.51)\times10^{-4}\lambda$. These values are smaller than the results previously obtained by Leininger, Segrè, and Wiegand for the same compounds, but support their earlier work.

THE possibility of altering the decay rate of Be^7 by changing the electron density at the nucleus was suggested by Segrè[1] and by Daudel.[2] Experiments performed to determine the influence of different states of chemical combination of beryllium on the decay constant of Be^7 have given the results listed in Table I.

The present series of measurements was undertaken in order to compare $\lambda(Be)$, $\lambda(BeO)$, and $\lambda(BeF_2)$ in the same experiment, using the improved methods now available for the measurement of small currents and for the detection of source contaminants. The ionization currents were measured by a vibrating reed electrometer[3] used essentially as a null indicator, thus eliminating the effects of any variations in the gain or calibration of the instrument. The use of a scintillation counter,[4,5] not available in the earlier experiments,[6] is an aid in detecting and identifying radioactive contaminants.

* Work performed at the Brookhaven National Laboratory under the auspices of the U. S. Atomic Energy Commission and supported in part by the U. S. Office of Naval Research contract with Harvard University.
† On leave from Harvard University, Cambridge, Massachusetts.
[1] E. Segrè, Phys. Rev. **71**, 274 (1947).
[2] R. Daudel, Rev. sci. **85**, 162 (1947).
[3] Palevsky, Swank, and Grenchik, Rev. Sci. Instr. **18**, 298 (1947).
[4] H. Kallman, Phys. Rev. **75**, 623 (1949).
[5] R. Hofstadter, Phys. Rev. **74**, 100, 628 (1949).
[6] E. Segrè and C. E. Wiegand, Phys. Rev. **81**, 284 (1951); **75**, 39 (1949).

λ-values for different beryllium compounds were compared by the balanced ionization chamber method introduced in 1911 by Rutherford.[7] The particular ionization chambers and current measuring equipment for this experiment were those used by Bainbridge, Goldhaber, and Wilson[8] in the study of Tc^{99m}.

I. EXPERIMENTAL PROCEDURE

A. Preparation of the Sources

The Be^7 was obtained from a proton bombardment of cp metallic lithium with the 8.5-Mev proton beam from the cyclotron at the University of Pittsburgh. A radioautograph was taken of the bombarded target and the surface containing the Be^7 activity was scraped and dissolved in dilute hydrochloric acid. The solution was made 0.3N in hydrochloric acid, and 50 milligrams each of iron, nickel, cobalt, copper, zinc, and cadmium were added. The main contaminant, copper, was precipitated by hydrogen sulfide. The hydrogen sulfide was removed from the supernatant, and the active Be^7 was carried with $Fe(OH)_3$ precipitated by the addition of ammonium hydroxide. The $Fe(OH)_3$ was dissolved in dilute hydrochloric acid and again precipitated, in the presence of the hold back carriers, by ammonium

[7] E. Rutherford, Wien. Ber. **120**, 303 (1911).
[8] Bainbridge, Goldhaber, and Wilson, Phys. Rev. **90**, 430 (1953) [hereafter referred to as BGW].

hydroxide. This process was repeated three times, carefully washing the $Fe(OH)_3$ each time.

The $Fe(OH)_3$ solution was made 7.8*N* in HCl, and four iron extractions were made with isopropyl ether. The ether was evaporated from the aqueous phase and 62 milligrams of beryllium in the form of $Be(NO_3)_2 \cdot 3H_2O$ were added. On addition of ammonium hydroxide, $Be(OH)_2$ was precipitated and then washed three times with water. The $Be(OH)_2$ was dissolved in glacial acetic acid and taken to dryness several times in order to convert the hydroxide completely to the basic beryllium acetate. The basic acetate was extracted into chloroform and the chloroform layer thoroughly washed with water. The acetate was then taken to dryness and taken up with 10 cc of HNO_3. This compound was again taken nearly to dryness and diluted with water.

The purity of the Be^7 was determined from an aliquot of this solution. Zinc and copper carriers were added to 1 percent of the total solution and precipitated with hydrogen sulfide at a *p*H of 2–3. The precipitate was washed, dried, and saved for analysis. Two precipitations of $Be(OH)_2$ were then made from the same aliquot in the presence of the same hold back carriers, and the filtrate from this precipitation was dried and combined with the zinc and copper residues. The gamma-ray spectrum of these residues was analyzed by Mr. Michael McKeown with a NaI scintillation spectrometer. The only photoelectric peak observed was that of the 0.48-Mev gamma-ray associated with Be^7. The activity in the residues was 7×10^{-2} percent of the total Be^7 activity in that aliquot. Any contaminants emitting gamma-rays of energies differing by 0.06 or more Mev from the 0.48-Mev radiation of Be^7 could have been detected if present to one percent or greater of the Be^7 activity in the residues. Gamma-ray contaminants therefore did not exceed the negligible amount of 7×10^{-6} of the source activities. Another aliquot of 0.01 percent of the Be^7 solution was analyzed in the same way, and again only the peak associated with the 0.48 gamma-ray was observed.

The four sources used in the following measurements were then prepared from the remaining solution. Two identical sources of BeO were made by the ignition of $Be(OH)_2$ in platinum crucibles at 1000°C. The sources were housed in small brass capsules which had been lined with a thin layer of pure tin. Screw caps were then forced down on the oxides so as to prevent any mechanical movement during the measurements.

A beryllium fluoride source was prepared by the hydrofluorination of beryllium hydroxide. The hydroxide was held in a covered platinum boat and heated in a monel furnace for sixteen hours at a temperature of 200°C. The temperature was than raised to 500°C for five hours to sinter the beryllium fluoride. An x-ray analysis was performed by Mr. Otto F. Kammerer to determine the crystal structure of this fluoride and also of an earlier inactive sample of beryllium fluoride. The structure was found to be hexagonal with constants $a=4.72$A, $c=5.18$A. This result is in agreement with the observations by Novoselava *et al.*[9] and later by Leininger, Segrè, and Wiegand.[10] The fluoride was housed in a small brass capsule similar to those used for the oxides, with Apiezon wax packed around the source to prevent motion within the housing and also to prevent any moisture from coming in contact with the fluoride.

TABLE I. Relative differences, $\Delta\lambda/\lambda$, in the decay constant λ of Be^7 in different chemical compounds. Errors are standard deviations.

Item	Comparison	$10^4\Delta\lambda/\lambda$	References
1	$\lambda(Be)-\lambda(BeCl_2)$		
	$BeCl_2$ in solution	$50\pm\sim30$	a, b
2	$\lambda(Be)-\lambda(BeF_2)$		
	BeF_2 "noncrystalline"	100 ± 30	b, c, d
3	$\lambda(Be)-\lambda(BeO)$	0.69 ± 1.25	e
		2.38 ± 1.5	
	Weighted mean	$1.5\ \pm0.9$	
4	$\lambda(BeO)-\lambda(BeF_2)$	$6.9\ \pm0.3$	f
5 (3 plus 4)	$\lambda(Be)-\lambda(BeF_2)$	$8.4\ \pm1$	f

[a] Bouchez, Daudel, Daudel, and Muxart, J. phys. et radium **8**, 336 (1947).
[b] Benoist, Bouchez, Daudel, Daudel, and Rogozinski, Phys. Rev. **76**, 1000 (1949).
[c] Bouchez, Daudel, Daudel, and Muxart, Compt. rend. **227**, 525 (1948).
[d] Bouchez, Daudel, Daudel, Muxart, and Rogozinski, J. phys. et radium **10**, 201 (1949).
[e] E. Segrè and C. E. Wiegand, Phys. Rev. **81**, 284 (1951); **75**, 39 (1949).
[f] Leininger, Segrè, and Wiegand, Phys. Rev. **81**, 280 (1951); **76**, 897 (1949).

The metal was prepared by an elegant method developed by Dr. T. T. Magel of Massachusetts Institute of Technology.[11] A mixture of beryllium oxide and zirconium powder was heated by induction in a tantalum crucible under vacuum. At 1300°C the reduced beryllium metal distilled away from the zirconium and was collected on a cone shaped cold finger directly above the crucible. The metal was housed in another brass capsule and protected from motion and moisture with Apiezon wax. The four sources were then matched to within three divisions in 7000 by machining the capsule walls of the weaker sources and by adding absorber to the walls of the stronger sources.

B. Measurements of $\Delta\lambda/\lambda$

The apparatus and general technique used for the determination of $\Delta\lambda/\lambda$ for sources in different chemical states of combination have been described at length in BGW. Inasmuch as the same equipment and essentially the same method were used in this work, only points of difference between the two experiments will be discussed.

Since the balanced ionization chambers provide a means for measuring the relative strength of two sources, there are six possible combinations of the four

[9] Novaselava, Levina, Simanov, and Zhasmin, J. Gen. Chem (U.S.S.R.) **14**, 385–402 (1944).
[10] Leininger, Segrè, and Wiegand, Phys. Rev. **81**, 280 (1951); **76**, 897 (1949).
[11] We are indebted to Dr. A. R. Kaufmann of the same institution for suggesting the use of Dr. Magel's method.

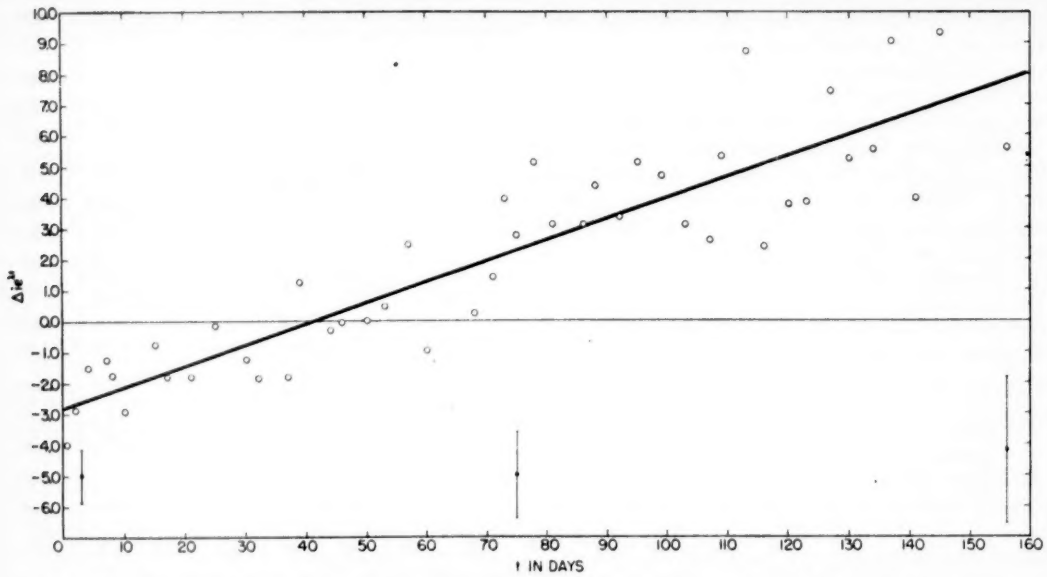

FIG. 1. $e^{\lambda t}\Delta i$ *versus* time for the BeF_2—Be source set. The errors to be associated with the individual points are indicated at three representative times and are standard deviations based on external consistency.

sources described above that can be measured. Data from all six sets of sources can be the basis of imposing constraints in the analysis of the final results, leading to more accurate values of $\Delta\lambda/\lambda$. Further, comparison of the two oxide sources provides a means for observing instrumental effects and possible physical change in the sources.

The experiment consisted then in the determination of the difference current, Δi, as a function of time for each of the six sets of sources. Δi was measured by allowing the charge to accumulate for 1200 seconds on the plates of the quartz-insulated, vacuum dielectric, 10^{-9} farad condenser. At the end of the 1200-second period the deflection as indicated on the chart of the recording potentiometer was matched by displacing the zero line. This displacement was produced by inserting a known voltage into the input of the vibrating reed electrometer by means of the potentiometer (Fig. 3, BGW).[8] The relationship $\Delta i = c\Delta v/\Delta t$ was then used to calculate Δi.

For each set of sources a 1200 second run was made with each of the two sources in a particular chamber. Immediately following the first run the sources were interchanged and the run repeated. A value of Δi was obtained by taking an average for the two runs.

The potential on the chambers was maintained by a pack of 45 volt batteries, with a provision for small adjustments. At the beginning of a run on a set of sources, the potentials on the two chambers were adjusted to a pre-selected value to within 1 part in 10 000. If after a 1200 second run they were found to have drifted as much as 5 parts in 10 000, they were readjusted. Since in any case the two battery packs stay close together as they drift, any induction effects cancelled and no error was introduced.

The sources were positioned in the chambers in a reproducible fashion as described in BGW.[8] The six sets of sources were measured using a routine that minimized their handling, and the sequence of operations remained the same for the length of the experiment. Measurements were taken twice a week over a five-month period (two mean-lives).

The currents were measured in units of 10^{-14} ampere. In order to present the data in a linear form, the values of Δi were multiplied by $e^{\lambda t}$, as was done by Segrè and Wiegand[6] and BGW. The data from the sets of sources that were used in obtaining the final results are shown in Figs. 1, 2, and 3. The solid lines are those calculated by a least squares procedure from the data.

In addition to the data obtained for the difference current as a function of time, other measurements were made to monitor the performance of the instrument and to obtain a value of the decay constant for Be^7. As in the case of BGW, the ionization current was measured with a weak radium source (about $5\mu c$) in one chamber and a blank source in the other. This measurement was made about once a week using two resistors of 10^{10} ohms, and the rms deviation from the average value was found to be 0.50 percent for one resistor and 0.76 percent for the other. Less frequently this current was measured using the 10^{-9} farad quartz-insulated condenser. In this way the values of R_1 and R_2 could be compared directly with the capacity of C.

The total ionization current at $t=0$, I_0, which enters directly into the calculation of $\Delta\lambda/\lambda$ from the slope of

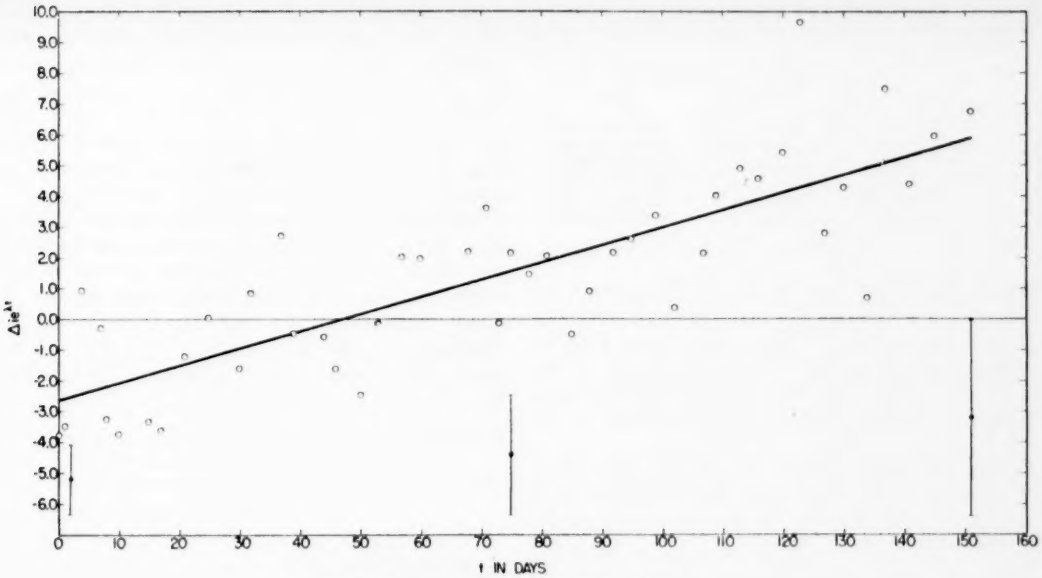

FIG. 2. $e^{\lambda t}\Delta i$ *versus* time for the BeF_2—BeO(1) source set.

the $e^{\lambda t}\Delta i$ plot, was determined from a series of measurements extending over a period of five months, using R_1 and R_2. These data from the metal source gave λ and I_0 for Be^7. By the comparison of R_1, R_2 and C with the weak radium source, the intensity I_0 could be expressed directly in terms of C, which was used for the Δi determinations.

Since R_1, R_2, and C were compared at about 480 divisions, and I_0 was 7133 divisions, it was important to establish the presence of any voltage coefficient of resistance for R_1 and R_2. Several times during the course of the experiment, a resistor calibration was carried out in the fashion described in BGW, and no measurable coefficient was found.

II. EXPERIMENTAL RESULTS

A. Determination of λ

The data on the direct measurement of the metal source with R_1 and R_2 were analyzed to determine the

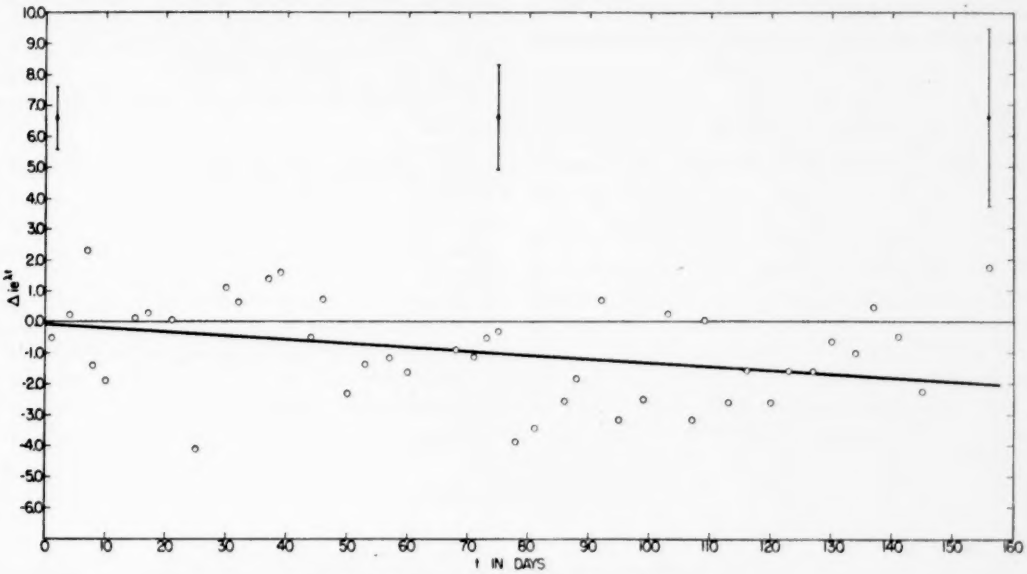

FIG. 3. $e^{\lambda t}\Delta i$ *versus* time for the Be—BeO(1) source set.

TABLE II. Results of the least squares analysis of the data for $e^{\lambda t}\Delta i$ *versus* t. The errors indicated are standard deviations based on external consistency.

No.	Sources	Intercept	Slope
1.	BeF_2-Be	-2.81 ± 0.29	0.0678 ± 0.0047
2.	$BeF_2-BeO(1)$	-2.67 ± 0.40	0.0568 ± 0.0064
3.	$Be-BeO(1)$	-0.08 ± 0.37	-0.0125 ± 0.0057
4.	$BeO(1)-BeO(2)$	1.30 ± 0.31	-0.0035 ± 0.0049
5.	$Be-BeO(2)$	0.78 ± 0.41	-0.0114 ± 0.0065
6.	$BeF_2-BeO(2)$	-2.26 ± 0.33	0.0630 ± 0.0053

decay constant. An analysis of the data using $\ln I = \ln I_0 - \lambda t$ as a basis for the least squares procedure gave $\lambda = 1.293\pm0.004\times10^{-2}$ day^{-1}. This result includes a correction of one part in 350 to take account of the effect of departure of the chamber characteristics from ideally complete saturation. The half-life is 53.61 ± 0.17 days.

Previous determinations of the half-life of Be^7 have been made by Hill,[12] 53 ± 2 days; by Bouchez *et al.*,[13] 54.3 ± 0.5 days; by Bonner,[14] 54.5 days; and by Segrè and Wiegand,[6] 52.93 ± 0.22 days.

B. Determination of $\Delta\lambda/\lambda$

The results of the least squares analysis of the data for the six sets of sources are shown in Table II. It can be seen that the comparison of the two oxide sources yielded no slope within the experimental error. Plots of the $BeF_2-BeO(2)$ measurements and others involving $BeO(2)$ indicated a change of slope at about 110 days. This was interpreted as a possible shift in the position of oxide (2) within the capsule. For this reason the data involving $BeO(2)$ were not utilized in computing the final results. It should be noted that the slopes of the $BeO(1)$ plots are not inconsistent with the $BeO(2)$ plots, and that if all of the data were included the final results would not be altered beyond the experimental errors.

[12] J. E. Hill, Phys. Rev. **57**, 567 (1940).
[13] Bouchez, Daudel, Daudel, and Muxart, J. phys. et radium **8**, 336 (1947).
[14] J. F. Bonner, Jr., Atomic Energy Commission Report AECU-107, unpublished.

The slope b is related to the desired quantity, $\Delta\lambda/\lambda$, by the relationship $\Delta\lambda/\lambda = b/I_0\lambda$. As previously stated, values of λ and I_0 were obtained by a measurement of the intensity of the metal source as a function of time. In terms of the capacity C of 10^{-9} farad, I_0 was found to be 7133 divisions (10^{-14} ampere per division). Values of $\Delta\lambda/\lambda$ have been calculated then for the three sets of sources involved and are shown in Table III.

The relationship that exists between the values of $\Delta\lambda/\lambda$ for the three source comparisons can be utilized to yield a more accurate knowledge of each of these values. A constraint fitting using a least squares procedure that followed the method of Deming[15] has been employed, and the new values of $\Delta\lambda/\lambda$ obtained as a result of this constraint fitting are also shown in Table III.

TABLE III. Relative differences in the decay constant of Be^7 in beryllium metal, oxide, and fluoride.

Sources	Values from data of Table II	Values adjusted by a constraint fitting
$\frac{\lambda(Be)-\lambda(BeF_2)}{\lambda}\times10^4$	7.37 ± 0.53	7.41 ± 0.47
$\frac{\lambda(BeO)-\lambda(BeF_2)}{\lambda}\times10^4$	6.15 ± 0.73	6.09 ± 0.55
$\frac{\lambda(Be)-\lambda(BeO)}{\lambda}\times10^4$	1.36 ± 0.63	1.31 ± 0.51

Our values of $\Delta\lambda/\lambda$ for $(BeO-BeF_2)$ and $(Be-BeF_2)$ are lower, by about twice the standard deviations, than those obtained by Leininger, Segrè and Wiegand,[6,10] but essentially these results confirm their earlier work.

The authors take pleasure in thanking Miss Jean Snover for carrying out the extensive calculations in this work. We also wish to thank J. A. Miskel for help in the preparation of the beryllium sources and R. Davis for aid in the preparation of the cyclotron target. The information contained in the notes of L. K. Nash and E. L. King was extremely useful in the purification of the Be^7.

[15] W. E. Deming, *Statistical Adjustment of Data* (John Wiley and Sons, Inc., New York, 1946).

The Total Neutron Cross Sections of Gold, Chlorine, and Phosphorus*

S. C. SNOWDON AND W. D. WHITEHEAD
Bartol Research Foundation, Franklin Institute, Swarthmore, Pennsylvania
(Received February 5, 1953)

The total neutron cross sections of gold, chlorine, and phosphorus have been measured over the energy range 100 to 700 kev using the mono-energetic neutrons from the $H^3(p,n)He^3$ reaction with an energy resolution of about 40 kev. Pronounced resonances were found in phosphorus, slight indications of resonances were found in chlorine, and no resonances were found in gold.

INTRODUCTION

PREVIOUS measurements[1] of the total cross section of phosphorus for fast neutrons have yielded only scanty information in the energy range available to us. The total cross section for chlorine has not been reported previously, while that for gold appeared in abstract form[2] during our investigation.

APPARATUS

A radiofrequency ion source has recently been installed in our small electrostatic generator, which together with suitable auxiliary focusing voltages yields a 15-μa resolved beam of protons in the energy range 500 to 1600 kev. The generator voltage is kept constant to within 1 to 2 kv by the use of a corona stabilizing circuit whose error signal is derived from a pair of insulated slits located at the output end of the analyzing magnet.

In order to measure the ion beam energy, work was initiated on a torsion balance with which the magnetic field of the analyzing magnet could be measured. Development work was under way at the time of these experiments, and the necessary stability and reproducibility of the torsion balance was achieved. However, since the completion of this work would have required more time than could reasonably be allotted to these experiments, it was decided to rely on the existing generating voltmeter. A careful investigation of the stability and reproducibility of the generating voltmeter revealed that after certain difficulties in the grounding of the rotor were eliminated, the only remaining variable was the temperature expansion of the generator column. When this was reduced as far as possible by the use of water cooling coils on the pressure tank, the reproducibility of the generating votmeter was generally about 2 kv. Thus, while the voltmeter left much to be desired, it was adequate for the present experiments and was then calibrated, using the $F(p;\alpha,\gamma)$ resonance at 873.5 kev, the $Al(p,\gamma)$ resonance at 993.3 kev, and the $H^3(p,n)$ threshold at 1.019 Mev.[3,4] In addition, the $H^3(p,n)$ threshold was checked after each 100-kev interval throughout the cross-section measurements.

The tritium targets were prepared by absorbing tritium gas at 1-mm Hg pressure into a zirconium film evaporated onto a wolfram backing.[5] Some difficulty was encountered in making uniform zirconium-tritium targets, as evidenced by the presence of fluctuations in the neutron counting rate of about two or three times the statistical fluctuations. To remove this source of trouble two pairs of crossed electrostatic deflecting plates were installed just after the output slits of the analyzing magnet. A 60-cycle per second ac voltage was applied across one pair of plates, and a 400-cycle per second ac voltage was applied across the other pair of plates in order to spread out the beam over the diaphragms near the target.

The target area was suitably diaphragmed to allow suppression of the secondary electrons from the target and thus permit the use of a beam current integrator in order to monitor the neutron yield. A conventional condenser and neon-glow tube was used in conjunction with a scale of 256 scalar for measuring the total charge accumulated on the target during each run.

The neutrons were detected by a conventional enriched $B^{10}F_3$ slow neutron counter[6] surrounded by paraffin with an outer layer of cadmium. The outside dimension of the counter with paraffin was 4 inches, and its effective length was 6 inches. Two checks of the stability of the neutron detector and its associated circuitry, using a 10 millicurie Ra-Be source, showed that electronic jitter and voltage drifts did not influence the counting rate more than one percent.

Finally, there was present in all the measurements a time dependent background of neutrons coming mainly from the region of the analyzing magnet chamber. This was reduced considerably by interposing a stack of five gallon cans filled with a saturated water solution of borax. In addition, the counting rate of these background neutrons was determined at frequent intervals while taking the data, and an attempt was made to correct the desired neutron counting rate for this source of neutrons. Since the amount of these background neutrons was never more than five percent, it is felt

* Assisted by the Joint Program of the U. S. Office of Naval Research the U. S. Atomic Energy Commission.
[1] R. K. Adair, Revs. Modern Phys. **22**, 249 (1950).
[2] Becker, Walt, and Okazaki, Bull. Am. Phys. Soc. **27**, No. 5, 19 (1952).
[3] Herb, Snowdon, and Sala, Phys. Rev. **75**, 246 (1949).
[4] Taschek, Jarvis, Argo, and Hemmendinger, Phys. Rev. **75**, 1268 (1949).
[5] A. B. Lillie and J. P. Conner, Rev. Sci. Instr. **22**, 210 (1951).
[6] Manufactured by N. Wood Counter Laboratory, 5491 Blackstone Avenue, Chicago 15, Illinois.

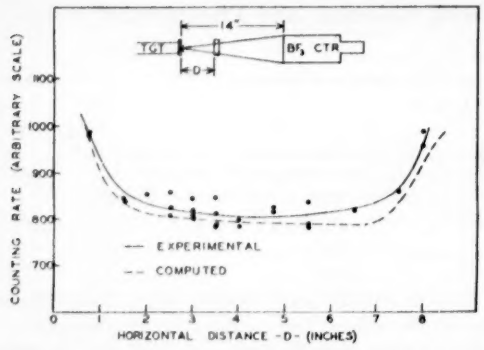

FIG. 1. Counting rate of neutron counter *versus* the distance of the gold scatterer from the target along the target-detector axis. The solid line is the average of the experimental points. The dashed curve was computed using the following parameters: counting rate without scatterer—1317, shadow cone background —130, cross section at 1.13 Mev—8.00 barns, counter diameter —4.00 inches, target-detector distance—16 inches.

that this source of fluctuation is adequately accounted for.

EXPERIMENTAL

Before measuring the total neutron cross sections the effect of the exact location of the scatterer was investigated. Figure 1 shows that the location of the scatterer along the target-detector axis is not very critical, and that the scattering-in correction can account for the observed variation of the counting rate. As the scatterer is moved nearer to the neutron source, the counting rate rises sharply and may be accounted for by the rapid increase of the solid angle subtended by the scatterer from the target. If the scatterer is moved toward the neutron counter, a sudden increase in counting rate occurs because in our set-up the diameter of the counter is larger than the diameter of the scatterer. As the scatterer passes inside the detector cone, some neutrons pass directly into the detector without passing through the scatterer. The entire effect can be computed from the parameters given in the caption to Fig. 1. Hence, it was felt that the correction which is due to the scattering of neutrons into the detector is adequately accounted for by the following formula:

$$\sigma nd = \ln[(1-f/(N/N_0-f)], \qquad (1)$$

where σ is the total cross section, n is the number of scattering nuclei/cm³, d is the thickness of the scatterer, N is the counting rate with the scatterer in place corrected for the paraffin shadow cone background, N_0 is the counting rate without the scatterer corrected for the shadow cone background, f is a geometrical measure of the scattering-in correction and is given by

$$f=[(4\pi/\sigma)(d\sigma/d\omega)]\cdot[(L/r)^2A/4\pi(L-r)^2], \qquad (2)$$

where $d\sigma/d\omega$ is the differential cross section in the direction of the detector, L is the target-detector distance, r is the target-scatterer distance, and A is the area of scatterer. The first bracket was taken equal to unity, since it is not exactly calculable but is expected to be near unity in our energy range according to the continuum theory of nuclear reactions.[7] In the geometry used the scattering-in correction f usually amounted to four percent.

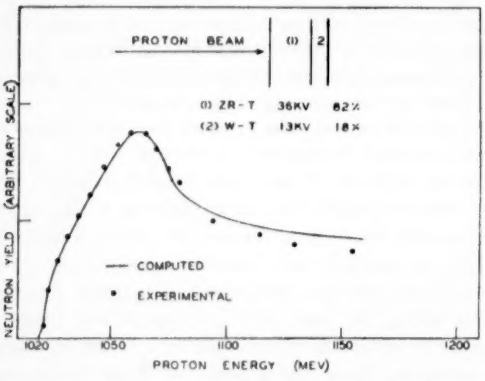

FIG. 2. Yield of neutrons in the forward direction from the $H^3(p,n)He^3$ reaction. The solid curve was computed by adding the yield predicted for a 36-kv thick target containing 82 percent of the tritium to the yield curve predicted for a 13 kv thick target containing 18 percent of the tritium but displaced in energy by 36 kv. The algebraic details are given in the Appendix.

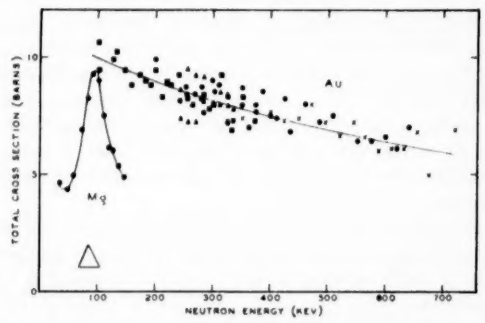

FIG. 3. Total cross section of gold for neutrons in the energy range 100–250 kev was measured with the detector 60° from the direction of the proton beam. The total cross section of magnesium was also measured in the 60° geometry.

The variation of the neutron counting rate as the scatterer was moved in a plane perpendicular to the target-detector axis was also investigated. A misalignment of about one-half inch gave a negligible change in the counting rate provided that the scatterer was aligned initially.

The energy spread of the neutrons was determined almost entirely by the thickness of the zirconium-tritium target. In order to measure this target thickness, careful measurements of the neutron yield in the forward direction were taken (see Fig. 2). In the Appendix the shape of the yield curve to be expected was calculated,

[7] Final Report of the Fast Neutron Data Project, NYO-636 (unpublished).

using several reasonable assumptions. If only one uniform target was employed, a departure of the experimental points from the calculated curve was observed in much the same fashion as that described by Bonner and Butler.[8] If, however, two different target layers were assumed to constitute the target, then much of the discrepancy was removed. In particular, if 82 percent of the tritium was assumed to be present in a 36-kv layer, and directly in back of this 18 percent of the tritium was assumed to be present in a 13-kv layer, then a unique fit was obtained within the accuracy of the assumptions involved. The second layer is thought to be due to an absorption of the tritium in the wolfram backing onto which the zirconium was evaporated. In any case the neutron energy spread is seen to be due to a 40–45 kv thick target.

As a check on this the narrow resonance in the total neutron cross section of magnesium at 85 kev reported by Fields and Walt[9] was measured with our source of neutrons. Figure 3 shows the observed neutron energy

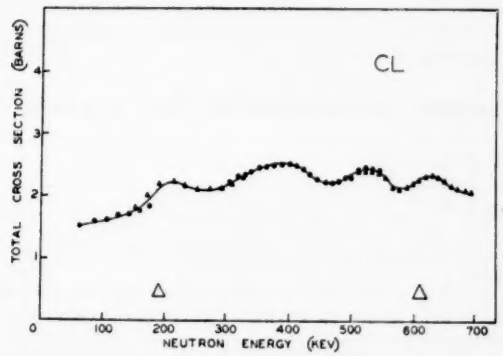

FIG. 4. Total cross section of chlorine for neutrons in the energy range 100–700 kev. The range 100–250 kev was measured in the 60° geometry.

width to be 45–50 kev in agreement with the target thickness prediction.

DATA

The gold scatterer consisted of a one-half inch thick cylinder of pure gold $1\frac{3}{4}$ inches in diameter. Figure 3 gives the results for gold, and it is to be noted that these data were taken before installing the beam spreaders and the water can absorbers. A comparison of the gold data with either the chlorine or phosphorus data shows the extent of the reduction in the fluctuations effected by the use of the beam spreaders and the water cans. (See Figs. 4 and 5.) Several check points were made on gold after the spreaders and the water cans were installed, and these repeat points fell right along the average line drawn through the points. From these results it is felt that the total cross section for gold does

[8] T. W. Bonner and J. W. Butler, Phys. Rev. **83**, 1091 (1951).
[9] R. E. Fields and M. Walt, Phys. Rev. **83**, 479 (1951).

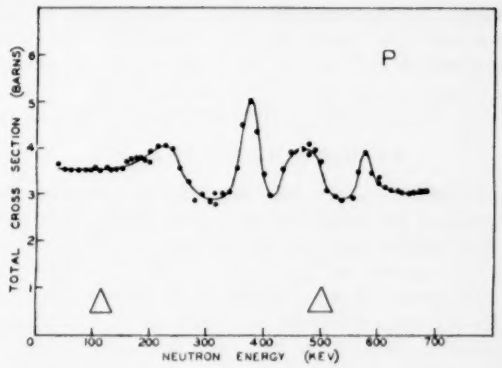

FIG. 5. Total cross section of phosphorus for neutrons in the energy range 100–700 kev. The range 100–250 kev was measured in the 60° geometry.

not have resonances in the energy range 100 to 700 kev. Furthermore, the magnitude of the cross section agrees well with those of neighboring atomic weight elements.

The total cross section for chlorine was measured using CCl_4 in a $1\frac{3}{4}$-inch diameter cylinder, 2 inches in length. The effect of the carbon was subsequently subtracted using the carbon cross section given by Adair.[1] Indications of resonances occur at several neutron energies and are separated by about 100 kev.

The total cross section for phorphorus was measured, using white phosphorus cast into a $1\frac{3}{4}$-inch diameter cylinder, $1\frac{1}{2}$ inches in length. There are several prominent resonances in this energy range, but higher resolution experiments, which we hope to be able to carry out, probably are needed to give any details concerning the nature of the resonances. The average value agrees well with that reported by Adair.[1]

The authors wish to acknowledge the continued interest of W. F. G. Swann, Director of the Bartol Research Foundation, in this work.

APPENDIX

The forward direction yield of the $H^3(p,n)He^3$ reaction from a target of finite thickness as measured by our finite sized counter (assumed to be a flat circular disk) is given by

$$Y=(N_0 n/4\pi)\int\int \eta(\theta)\sigma(E) \times(d\Omega\phi_1/d\Omega_0+d\Omega\phi_2/d\Omega_0)d\Omega_0 dx,$$

where N_0 is the number of protons striking the target per second, n is the number of tritium nuclei per cubic centimeter, θ is the laboratory angle measured from the proton beam direction, ϕ_1 and ϕ_2 are the two center-of-mass angles from which emergent neutrons contribute to the laboratory solid angle $d\Omega_\theta$, and $\eta(\theta)$ is the zonal efficiency of the detector. The differential cross section in laboratory coordinates has been calculated with the

assumption that the differential cross section in the center-of-mass coordinates is a constant. The total cross section $\sigma(E)$ is then only a function of the energy of the proton E in the layer dx of the target.

For convenience in integration, a parameter

$$k=(M_TM_R/M_BM_O)^{\frac{1}{2}}(1-E_0/E)^{\frac{1}{2}}$$

is introduced, where M_T, M_R, M_B, and M_O are the masses of the target, residual, bombarding, and outgoing particles, respectively. E_0 is the threshold energy of the reaction in laboratory coordinates. The total cross section of the reaction is assumed to vary as $(E-E_0)^{\frac{1}{2}}$ near threshold, and since the exact variation above threshold is not known, it is chosen for convenience in integrating to be such that $\sigma dx \sim k^2 dk$. The zonal efficiency of the counter $\eta(\theta)$ is also assumed to be a constant.

Using the dynamics of the $H^3(p,n)He^3$ reaction, the value of $d\Omega\phi/d\Omega_\theta$ may be found as a function of k and θ. The integration then may be carried out with the result that

$$Y=(N_0nA/3a)k_1^2 \text{ for } 0<k_1<\sin\theta_0,$$

$$Y=(N_0nA/3a)[k_1^3-\cos\theta_0(k_1^2-\sin^2\theta_0)^{\frac{1}{2}}] \text{ for } \sin\theta_0<k_1<(M_RM_T/M_BM_O)^{\frac{1}{2}} \times[1-E_0/(E_0+at)]^{\frac{1}{2}},$$

$$Y=(N_0nA/3a)[k_1^3-k_2^3-\cos\theta_0(k_1^2-\sin^2\theta_0)^{\frac{1}{2}}] \text{ for } 0<k_2<\sin\theta_0,$$

$$Y=(N_0nA/3a)[k_1^3-k_2^3-\cos\theta_0(k_1^2-\sin^2\theta_0)^{\frac{1}{2}} +\cos\theta_0(k_2^2-\sin^2\theta_0)^{\frac{1}{2}}] \text{ for } k_2>\sin\theta_0, \text{ but } k_1\leqslant 1.$$

In the formulas A is an unknown constant depending on the efficiency of the counter and other constants of the reaction, a is the energy loss per cm for the proton beam in the target, θ_0 is the half-angle subtended by the counter (7.50°), and t is the thickness of the target in cm. k_1 is the value of k at the front edge of the target, and k_2 is the value of k at the back edge of the target, each for an incident proton beam of energy E_B.

PHYSICAL REVIEW VOLUME 90, NUMBER 4 MAY 15, 1953

Total Cross Sections of Chlorine, Sodium, Titanium, and Bromine for Fast Neutrons*

H. R. Dvorak† and R. N. Little, Jr.
The University of Texas, Austin, Texas
(Received February 9, 1953)

Relatively new liquid scintillation counter methods were adapted to detect fast neutrons with a heretofore unattainable efficiency of about 19 percent. The geometry obtained was the so-called "good" geometry, which was a half-angle at the counter of 2.7°. With the more efficient counter reasonable counting times could be obtained with the detector subtending a half-angle of only 2.7° from the target.

The neutrons were obtained by using a modified Cockcroft-Walton linear accelerator of 100-kev bombarding energy. The neutron energy range was 2.15 to 2.82 Mev.

All the scatterers used were contained in almost identical glass "cells," and the effects of the glass cells were subtracted out by using an empty glass cell of the same type as a reference. The probable error, calculated statistically from the counting rates of the experiment, was 1.3 percent on total cross-section values. Actual reproducibility of each result was about 3 percent or better.

A carbon cross-section curve was obtained as a check on this method, and agreement with previously reported values was excellent. The chlorine and sodium cross sections were found to be about 3×10^{-24} cm², as determined indirectly by using carbon tetrachloride and sodium chloride. The titanium cross section was found to be about 4.1×10^{-24} cm² by using powdered titanium metal. The bromine cross section was found to be about 3.7×10^{-24} cm², by using a sample of liquid bromine. No large resonances were found in the energy region available.

Data were also taken on the angular distribution of the number of neutrons with respect to the forward direction of the incident deuteron beam, and they were found to agree well with theory except in the region where experimentally necessary geometric conditions dictated a deviation.

I. INTRODUCTION

In the past few years there has been much work done with regard to obtaining total cross sections of the elements for fast neutrons. In reviewing many articles, it has been found that there is still work to be done before all the total cross sections have been measured as accurately and with as good an energy resolution as the theoretical physicists would like. Hence, we have taken up a program of augmenting the available data with the apparatus being used here. Several elements were found that have not been reported as yet, and we are planning a systematic study of these elements as well as those elements that have only sparse data for our energy region. Wisconsin,[1,2] Aoki,[3] Argonne,[4] Stafford,[5] Los Alamos,[6,7] Oak Ridge,[8] MacPhail,[9] Ricamo,[10]

* This work has been assisted in part by the Research Institute of The University of Texas, the Air Research and Development Command and the U. S. Atomic Energy Commission.

† Part of a dissertation presented to the Faculty of the Graduate School of The University of Texas as partial fulfillment for the degree of Doctor of Philosophy.

[1] R. L. Henkel and H. H. Barschall, Phys. Rev. **80**, 145 (1950).
[2] Miller, Adair, Bockelman, and Darden, Phys. Rev. **88**, 83 (1952).
[3] H. Aoki, Proc. Phys.-Math. Soc. Japan **21**, 232 (1939).
[4] Hughes, Spatz, and Goldstein, Phys. Rev. **75**, 1781 (1949).
[5] G. H. Stafford, Proc. Phys. Soc. (London) **A64**, 388 (1951).
[6] Linenberger, Miskel, and Segrè, U. S. Atomic Energy Commission Report AECD-2458 (unpublished).

and Zinn[11] have studied a total of fifty-one elements either completely or partially in our energy region.

The results of these investigators were used as comparison values to correlate our data whenever possible.

Chlorine, sodium, and titanium are usually classified as lying below the so-called "heavy" nuclei and thus will probably not obey the sort of theory that tends to average over resonances such as the continuum theory of Feshbach, Peaslee, and Weisskopf.[12,13] However, the bromine data may be useful for this purpose.

II. EXPERIMENTAL PROCEDURE

A. Neutron Generator

A very brief description of the neutron generator being used by this group will be included here, since it has not previously been described.

This group is working with a modified Cockcroft-Walton linear accelerator similar to the Rice Institute accelerator.[14] The power supply is a special General Electric full-wave rectifier employing kenotrons, and it was primarily designed for x-ray work. It is capable of furnishing 100 000 volts at 100 milliamperes dc. The ion source power is provided by a transformer insulated for 100 000 volts dc, which is rated at 25 amperes at 20 volts ac. This power supply thus affords a voltage division along the four-element accelerator tube by using resistors instead of corona gaps. The current through the voltage divider is about 40 times larger than the ion beam current, giving very steady potentials on the accelerating electrodes. The available voltage limits the experiments here to the $D(d, n)$ and the $T(d, n)$ reactions.

A magnetic ion source similar to the one described by Kistemaker[15] is presently being used, and it delivers about 550 microamperes of beam about 1.5 centimeters in diameter at the target.

For this experiment a copper target 0.030 inch thick was used, and deuterium was "built up" on the copper[16] after a few hours bombarding which resulted in a neutron flux of about 2×10^6 neutrons per second. Deuterium target build-up has also been observed on aluminum and tungsten at this laboratory.

B. Neutron Counter

This "good" geometry experiment was made possible by the use of a liquid scintillation counter which consisted of a 51-millimeter diameter by 50-millimeter long glass cell filled with 5 grams of terphenyl in one liter of xylene[17] optically coupled with Dow Corning 200-Silicone fluid to an RCA 5819 photomultiplier. The scintillator was covered with a thin foil of highly reflecting aluminum which was crinkled to afford good reflection properties for the light pulses. The entire assembly was then made light tight by wrapping the foil and 5819 tube with black electrical Scotch tape. A mu-metal shield was placed over the assembly to further protect the photomultiplier from the earth's magnetic field and from extraneous magnetic fields, since it was operated in the vicinity of the accelerator. In this particular experiment, no quantitative energy resolution was necessary, since the energy range to be studied was not very great and the neutron energy in any given direction with respect to the incident deuteron beam was essentially monoergic. The scintillation counter was found to be about 19 percent efficient when compared to a long BF_3 counter that had been calibrated with a standard RaD-Be neutron source.

A cathode follower preamplifier was used to match the photomultiplier circuit to the coaxial cable, which in turn fed into an Atomic A-1 amplifier and thence to an Atomic 101M scaler.

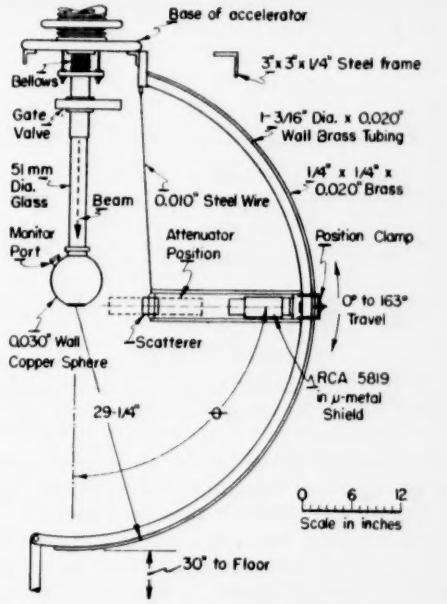

FIG. 1. Scale drawing of experimental apparatus used in measuring total cross section. The scatterer, attenuator, and alignment apparatus are held by a circular 0.020-in. aluminum clamp.

C. Counter Frame, Alignment Apparatus, and Scatterers

Figure 1 shows a scale drawing of the apparatus used to position the counter and scatterers with respect to the target. All the component parts were made of as

[7] D. H. Frisch, Phys. Rev. **70**, 589 (1946).
[8] Willard, Bair, and Kington (unpublished).
[9] M. R. MacPhail, Phys. Rev. **57**, 669 (1940).
[10] R. Ricamo, Nuovo cimento **8**, 383 (1951).
[11] Zinn, Seely, and Cohen, Phys. Rev. **56**, 260 (1939).
[12] Feshbach, Peaslee, and Weisskopf, Phys. Rev. **71**, 145 (1947).
[13] H. Feshbach and V. F. Weisskopf, Phys. Rev. **76**, 1550 (1949).
[14] Little, Long, and Mandeville, Phys. Rev. **69**, 414 (1946).
[15] Kistemaker and Douwes-Dekker, Physica **16**, 198 (1950).
[16] P. Baker, Jr., and A. Waltner, Phys. Rev. **88**, 1913 (1952).
[17] H. Kallman and M. Furst, Phys. Rev. **79**, 857 (1950).

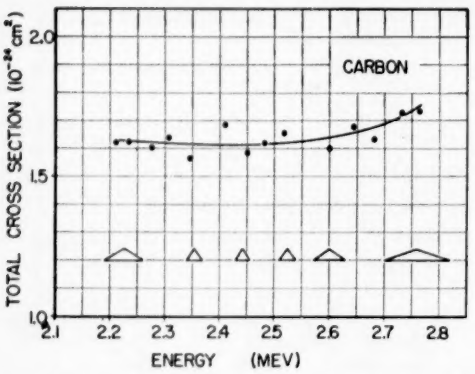

FIG. 2. Total cross section of carbon *vs* neutron energy in Mev. This curve was used as a check on the experimental procedure.

light a material as was believed possible without sacrificing rigidity of support for the 30-centimeter long by 51-millimeter diameter aluminum attenuator. Aluminum was used wherever possible, and no steel was used in the support apparatus proper except for the 0.010-inch diameter piano wire. The alignment apparatus was constructed as follows: A long thin-walled aluminum tube was machined to fit the key socket in the 5819 tube socket at one end, and a thin-walled aluminum cylinder with a diameter equal to the scatterer diameter was placed at the other end. A $\frac{1}{8}$-inch aluminum rod which extended to the target was fitted into the scatterer end of the aluminum tube, and the entire alignment apparatus was centered in a lathe to within 0.1 millimeters. The 5819 tube was removed from its socket key hole and secured at the scatterer clamp end. The crescent and steel wire were adjusted so that the end of the alignment apparatus touched squarely at the middle of the target area on the outside of the sphere. The alignment rig was taken out of the apparatus, the 5819 was plugged back into its socket, and the scatterers were clamped into their place in order. The alignment procedure was again checked after all the scatterers were run at each position to make sure that the relative positions of the mount, scatterer holder and target had not shifted.

All the samples except carbon were placed in glass cells that had been made to close tolerances. The inside lengths of the five glass containers were measured to be 1.7755±0.0084 inches, and the glass ends of the containers were all ground to be 0.0575±0.0010 of an inch thick. The cylinders of the glass cells were cut from standard 51-millimeter tubing. An empty glass cell was used to measure the incident intensity of the neutrons at the counter before and after the bottled samples were run. This incident intensity was used for our calculations of the total cross sections. The glass cells were found to produce about 5 percent attenuation of the incident neutron beam compared to the direct neutron beam with no glass cell between the target and counter. It was assumed that this effect of the glass cells was not great enough to affect the results in so far as multiple scattering was concerned.

The carbon sample used was 1.8811±0.0005 inches in diameter and 1.8865±0.0050 inches long. The material was machined from a large electric arc furnace type electrode. The incident neutron intensity used to compute the carbon cross-section data was taken without the empty glass cell.

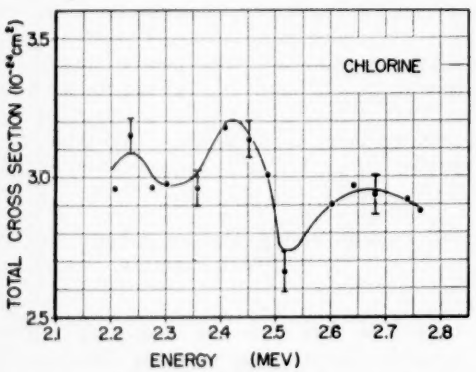

FIG. 3. Total cross section of chlorine *vs* neutron energy.

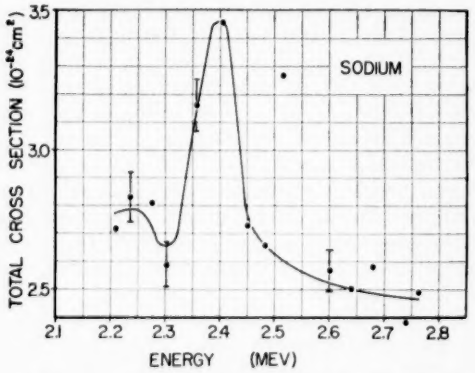

FIG. 4. Total cross section of sodium *vs* neutron energy.

All scatterers used were cylinders rather than properly truncated cones, since Poss *et al.*[18] found that a good geometry experiment was affected very little, if at all, by using the simpler cylindrical form. The scatterers were made slightly larger than absolutely necessary in order that some slight misalignment would not invalidate the results.

The counter was placed with its nearest face 55 centimeters from the target, and the scatterer was placed with its center 27 centimeters from the target. All scatterers were placed in the same position to within plus or minus two millimeters. The half-angle subtended by the active counter volume with respect to the target was 2.7°. The distance between the counter

[18] Poss, Salant, Snow, and Yuan, Phys. Rev. **87**, 11 (1952).

and target was not allowed to vary more than 5 millimeters, and the alignment was visually checked several times during each run to insure against gross errors in misalignment.

The transmission through the attenuator was calculated to be 1.1 percent, and this factor was neglected, since the statistical error for the number of counts that were used was calculated to be ±1.3 percent. The total number of counts accepted for any part of the experiment was at least 10 000 after the background had been subtracted out. With the long aluminum attenuator in position, the background was found to be about 26 percent of the total counts, and with no scatterer between the neutron source and the counter the background was 4.3 percent of the total counts. Each scatterer was run twice in each position, and the average value of the two separate calculations was taken as the best value. A histogram of the error differences was compiled for the entire experiment, and the average experimental error was determined to be ±1.7 percent.

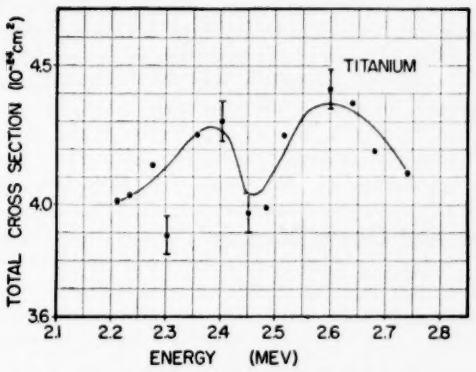

FIG. 5. Total cross section of titanium *vs* neutron energy.

III. RESULTS

A. Carbon

Carbon was used as the final experimental check on the method used in this experiment, and the results as seen in Fig. 2 agreed quite favorably with the results given by the Wisconsin group. The experimental error for the carbon total cross section was found to be ±1.7 percent and the energy resolution obtained in this experiment is shown by the bases of the triangles on Fig. 2 and is the same for the other elements discussed in this paper. Therefore, the experimental errors for the other elements are shown on subsequent figures, but the energy resolution is omitted.

B. Chlorine

The total cross section was measured for CCl_4,[19] and the total cross section for chlorine was obtained by subtracting out the total cross section for carbon. The CCl_4 used met ACS specifications for purity. The data in Fig. 3 indicate that no real resonances lie in this energy region. The experimental error was ±2.4 percent.

[19] Kiehn, Goodman, and Hansen, Bull. Am. Phys. Soc. **28**, 33 (1953).

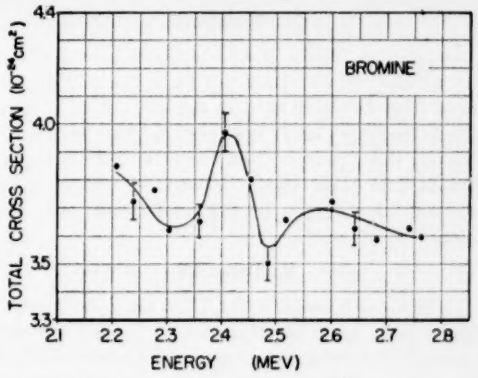

FIG. 6. Total cross section of bromine *vs* neutron energy.

C. Sodium

These data were obtained by using NaCl and subtracting out the total cross section of chlorine as determined from the above paragraph. The NaCl used met ACS specifications and was free of water of crystallization. The glass cell was loaded with the salt in a dry atmosphere. Aoki reported three points for the element sodium in our available energy region as follows: 3 barns at 2.85 Mev, 3.2 barns at 2.50 Mev, and 2.75 barns at 2.85 Mev. Argonne reported one point of 2.35 barns at 2.85 Mev. The data (Fig. 4) agree with Argonne at the high energy end, and we measured one point at 2.515 Mev which agrees with one of Aoki's points. There is a definite maximum at 2.40 Mev as shown by the data. We plan to study this curve using the element sodium in its metallic form more thoroughly in order to determine if there is another peak at about 2.5 Mev. The experimental error was ±2.7 percent.

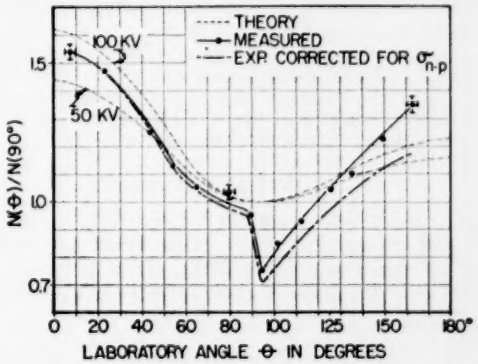

FIG. 7. Angular distribution of numbers of neutrons. Angle measured from forward direction of deuteron beam to direction of neutrons used. A "best fit" was taken in determining the experimental curve.

D. Titanium

The titanium was in the form of a powder and came to us marked 98 to 99 percent pure. No marked resonances were shown to exist in the data (Fig. 5), but it did not correlate Aoki's results. Aoki has reported the following three points: 1.83 barns at 2.23 Mev, 2.15 barns at 2.55 Mev, and 2.05 barns at 2.85 Mev. The experimental accuracy of the final results was ±1.7 percent.

E. Bromine

The element bromine in its liquid form was used, and it met the ACS specifications for purity. An indication of a peak was recorded at about 2.42 Mev. (Fig. 6). The experimental accuracy of the cross-section data was ±1.7 percent.

F. Angular Correlation of Number of Neutrons

The data recorded afforded an experimental check with respect to the angular correlation of number of neutrons in the laboratory system.[20,21] The heavy line in Fig. 7 is the angular distribution of numbers of neutrons with respect to the forward direction of the beam with no corrections. The heavy dotted line is our data corrected for the $n-p$ cross section[3] in the energy region used. This gives an indication that the counter being used at present has an energy sensitivity variation depending principally on the $n-p$ cross section. Plans are being made to do more work to find out more about the properties of this particular counter.

The sudden dip in the curve at 89° was found to be caused by the fact that the neutrons produced at the inside surface of the copper sphere had to pass through a relatively long section of copper to get to the outisde of the sphere. This geometrical consideration was found to exist for our particular apparatus up to about 120° with respect to the forward direction of the beam, and it is seen from the Fig. 7 that the correlation is relatively good on either side of the above-mentioned region. This should not affect the total cross-section data, since it was a constant effect for all readings taken at any given position.

The authors wish to express their gratitude to the following men for assisting them continuously in this work: Mr. N. M. Schaeffer for building the counter; Mr. P. C. Cadenhead for assisting in operation of the accelerator, as well as taking data; Mr. B. P. Leonard, Jr., for assistance in the operation of the accelerator, as well as the calculations; and Mr. G. H. Olewin for assistance in building the apparatus.

[20] C. E. Mandeville, J. Franklin Inst. **244**, 391 (1947).
[21] Bretscher, French, and Seidl, Phys. Rev. **73**, 815 (1948).

PHYSICAL REVIEW VOLUME 90, NUMBER 4 MAY 15, 1953

Mean Lifetimes of *V*-Particles and Heavy Mesons*

W. L. Alford† and R. B. Leighton
California Institute of Technology, Pasadena, California

(Received February 2, 1953)

A maximum-likelihood procedure for determining mean lifetimes of V-particles from cloud-chamber data is applied to samples taken from a group of 134 neutral V-particle decays. For 74 events which were consistent with a decay into a proton and a negative π-meson, a lifetime of $(2.5\pm0.7)\times10^{-10}$ sec is obtained. Dividing the data into "low Q" and "high Q" groups on the basis of the calculated energy release in the decay, a value of $\tau_L=(2.9\pm0.8)\times10^{-10}$ sec is found for those cases with $0\leq Q\leq 50$ Mev and a value of $\tau_H=(1.6\pm0.5)\times10^{-10}$ sec is found for those cases with $50<Q\leq 150$ Mev. While no significant difference exists between these two values, the difference is greater than for other plausible division schemes which are considered.

A qualitative discussion of lifetimes is given for the case of 23 charged V-particle decays. For the charged V-particles these data suggest either a lifetime less than that of the neutral V-particles, provided the sample is homogeneous, or, more likely, an apparent average lifetime less than that of the neutral V-particles, if the sample is a mixture of two or more types of particles. The possibility that κ- and/or χ-mesons make up a part of these decays is considered.

I. INTRODUCTION

SINCE the first report of the discovery of neutral and charged V-particles by Rochester and Butler[1] and the subsequent confirmation of the discovery by Seriff *et al.*[2] A number of cloud-chamber experiments[3–8] have been performed to make further studies of these particles. Although the findings have been more complex than one might have expected, and the need for a great deal more work has become apparent, certain definite conclusions have been reached and other possible results have been suggested.[7,8] All of these experiments

* Supported in part by the joint program of the U. S. Office of Naval Research and the U. S. Atomic Energy Commission.
† Now at Alabama Polytechnic Institute, Auburn, Alabama.
[1] G. D. Rochester and C. C. Butler, Nature **160**, 855 (1947).
[2] Seriff, Leighton, Hsiao, Cowan, and Anderson, Phys. Rev. **78**, 290 (1950).
[3] Armenteros, Barker, Butler, Cachon, and Chapman, Nature **167**, 501 (1951).
[4] Thompson, Cohn, and Flum, Phys. Rev. **83**, 175 (1951).
[5] W. B. Fretter, Phys. Rev. **82**, 294 (1951).
[6] Leighton, Wanlass, and Alford, Phys. Rev. **83**, 843 (1951).
[7] Armenteros, Barker, Butler, and Cachon, Phil. Mag. **42**, 1113 (1951).
[8] Leighton, Wanlass, and Anderson, Phys. Rev. **89**, 148 (1953).

point to the existence of two or more different types of neutral V-particles and one or more types of charged V-particles. This paper will be concerned principally with that type of neutral V-particle which decays with an energy release, Q, in a manner consistent with the scheme

$$V^0 \rightarrow P^+ + \pi^- + Q.$$

While there is no assurance that additional neutral particles as light as the π-meson are not among the decay products, the above decay scheme will be assumed to hold for those cases in which the visible decay products are consistent with a proton and a negative π-meson. This procedure is justified by the fact that the numerical results are not greatly changed if other decay schemes, consistent with the observed data, are assumed. Those events which are discussed as charged V-particle decays are cases in which a charged particle decays into a single charged particle plus one or more neutral particles. Only those events which can be shown to be inconsistent with known processes such as the decay of a π-meson into a μ-meson are included in the group of charged V-particles.

The average lifetime of V-particles is one characteristic quantity for which estimates have been made from the above experiments.[2,9] Although the cloud chamber can be used for lifetime determinations in principle, the difficulty of obtaining a sufficiently large unbiased sample of V-particle decays of a single type has prohibited accurate results. Although the information now available on the decay of neutral V-particles is considerably more extensive than in the previously reported experiments, this difficulty is still apparent in the present work, which treats the decay of 134 neutral V-particles and 23 charged V-particles.[10]

The method used is a maximum-likelihood procedure, which essentially involves finding the value of the mean lifetime which maximizes the probability of obtaining the observed distribution of decay points in the chamber.[11] This procedure is applied to the case of the neutral V-particle decays. Since it is apparent from the data that no significant treatment of the charged decays can be made, only a qualitative discussion of the mean lifetime is given in this case.

II. THE APPARATUS AND FIDUCIAL SURFACES

The apparatus used in this experiment[8] is shown schematically in Fig. 1. The lead blocks above and between the two chambers served to filter out the soft radiation and provided a region in which the production of V-particles could take place near the tops of the chambers. The trays of counters above and below the double chamber were used to select penetrating showers.

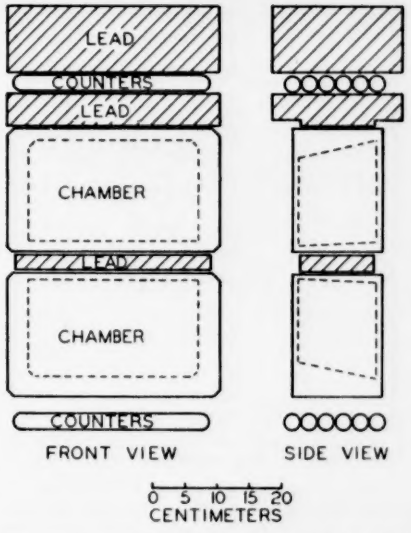

FIG. 1. The arrangement of the lead, counters, and cloud chambers. The dashed lines represent the fiducial surfaces.

Also shown in Fig. 1 are fiducial surfaces which are used in the measurement of certain geometrical quantities needed for the lifetime determination. These surfaces are drawn to include only well-illuminated regions of the cloud chamber within which all V-particle decays would be almost equally likely to be detected. They were located at distances ranging from $\frac{1}{2}$ cm to 5 cm from each of the inner walls of the chambers. One might wish to make this separation of the fiducial surfaces from the inner walls much greater so that any track originating within these surfaces would have sufficient visible length within the chamber to allow all necessary measurements to be made; however, the already critically small size of the chambers prohibits such a restriction on the usable volume. Although tracks and V-particle decays were often clearly visible in much of the region between the fiducial surfaces and the walls of the chambers, the terms "visible" or "illuminated" region will be used to refer to the volume within the fiducial surfaces.

III. THE DATA

The experimental quantities which were used in the determination of the lifetime of the neutral V-particle are listed as follows: x_i is the distance between the point of entrance of the ith V-particle into the visible region of the chamber and the point of decay. d_i is the distance between the point of entrance of this V-particle into the visible region and the point at which it would have left this region if it had not decayed. The term "gate length" or "potential path length" will be used

[9] Barker, Butler, Sowerby, and York, Phil. Mag. **43**, 1201 (1952).

[10] A rather extensive analysis of these same events has been made by other workers whose findings are given in reference 8. These reports describe the experimental techniques and discuss the experimental errors in more detail than will be done here. When information such as the mass of the neutral V-particle, decay schemes, etc., is needed for the purpose of a lifetime determination, the results given by these workers will be used.

[11] The maximum-likelihood procedure was used at the suggestion of Professor Leverett Davis, Jr. An independent treatment of the lifetime problem, also based upon the maximum-likelihood procedure, has recently been reported by J. G. Wilson and C. C. Butler, Phil. Mag. **43**, 993 (1952).

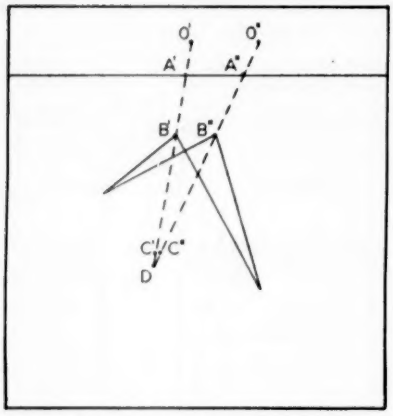

FIG. 2. A schematic diagram showing the superposition of the two stereoscopic views of a neutral V-particle decay.

to refer to this quantity. P_i is the momentum of the V-particle. t_i is the time taken to traverse the distance x_i. This time is given in the rest system of the V-particle. T_i is the time, measured in the rest system of the V-particle, taken to traverse the distance d_i. θ_i is the angle between the paths of the two charged decay products of the neutral V-particle. Q_i is the calculated energy release as given in reference 8. When a knowledge of the decay scheme of the neutral V-particle was required in order to determine some of the quantities given, a two-body decay into a proton plus a negative π-meson was assumed.

The distances, x_i and d_i, were measured from the predetermined fiducial surfaces which were shown in Fig. 1 and discussed in Sec. II. The values of x_i and d_i were obtained from the two stereoscopic photographs of the chamber. The two views were projected through a lens system identical to that of the camera onto a single screen following the procedure described in reference 8. The projection was such that points lying on the back plate of the chamber were superimposed upon the screen, while points which were forward in the chamber were separated by an amount dependent on their distance from the back plate. Figure 2 illustrates this for a V-particle which was produced in the lead plate between the two chambers. The particle had an origin determined from $0'$ and $0''$, a point of entrance through the top fiducial surface determined from A' and A'', a decay point determined from B' and B'', and a "potential point of exit" from the illuminated region at the back fiducial surface determined from C' and C''. The point D, at which the separation becomes zero, lies in the back plate. Figure 3 is a photograph showing one view of a decay in which the V-particle was following a trajectory of this kind.

P_i, the momentum of the V-particle, was determined in one of two ways depending on the available information. If the momenta of the two decay products could be determined, P_i was calculated as the vector sum of these momenta. If the momenta of the decay products could not be determined, P_i was found from θ_i under the assumptions: (1) that the energy release in the assumed two-body decay was 50 Mev and (2) that the decay products were emitted at right angles to the line of flight of the V-particle, in the center-of-mass system. Figure 4 shows that, if the decay products have a random angular distribution in the c.m. system of the V-particle, the second of these assumptions could lead to a considerable error in any one case but statistically should be a fair procedure. Also, it might be noted that P_i was quite large for most of the cases for which this procedure was used and, as shown later, such cases have very little weight in the determination of the lifetime.

The times, t_i and T_i, are given in the rest systems of the V-particles and are related to the distances, x_i and d_i, by the equations

$$t_i=(x_i/c)(M/P_ic) \quad \text{and} \quad T_i=(d_i/c)(M/P_ic).$$

M and P_ic are given in Mev so that P_ic^2/M is the product of the velocity of the V-particle and the time dilation factor. The mass of the neutral V-particle was taken to be 1120 Mev.[8]

In addition to the quantities mentioned above, one may feel that a knowledge of the time interval between the production of the V-particle and its entrance into the visible region of the chamber is necessary for a lifetime determination. However, it is assumed that the

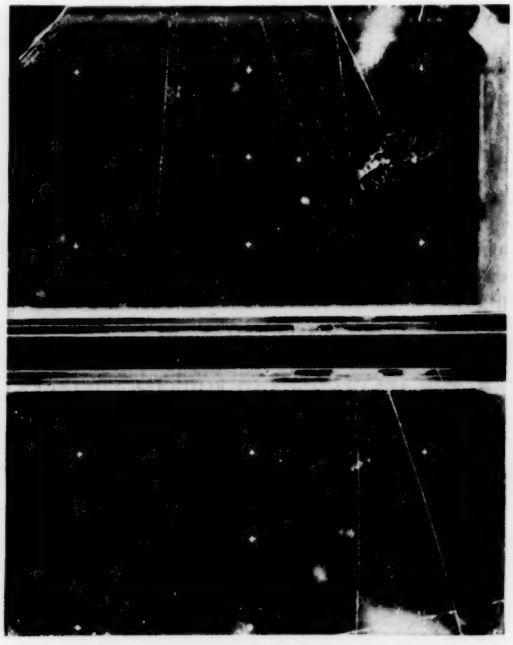

FIG. 3. Two examples of the decay of a neutral V-particle. The decay products are consistent with a proton and a negative pi meson. The trajectory of the V-particle in the lower chamber is described in part III.

probability of decay follows an exponential law, and this assumption implies that the decay is spontaneous and is independent of the past history of the V-particle. Thus one is justified in treating each particle as if it were created at its point of entrance into the visible region and in measuring t_i and T_i from the time at which the particle passed this point. This procedure has advantages in that: (1) it allows the use of many cases for which approximate points of entry into the chamber can be obtained, but for which no clearly identifiable origin can be found in the lead above the chamber, and (2) it eliminates the necessity for considering the unknown number of particles which decay before reaching the visible region or after passing through it. The only use which was made of the origins that were identified was in the determination of the direction along which to measure x_i and d_i. For those V-particles which had no identifiable origin, x_i and d_i were measured along the line determined by the vector sum of the momenta of the two decay particles. For fifteen percent of the events, for which neither an origin could be identified nor a momentum measurement made, the direction of flight of the neutral V-particle was taken to be along the line bisecting the angle between the paths of the two decay products. For most of the cases included in this last category the general direction of travel of the V-particle was clearly from the top of the chamber toward the bottom, and the angle between the paths of the decay products was small. These two conditions made the resulting error in x_i, d_i, and x_i/d_i quite small. Such would not be the case if the V-particle were traveling obliquely across the chamber or if the angle between the paths of the decay products were large.

IV. METHOD OF CALCULATING THE MEAN LIFETIME

In treating methods of determining the mean lifetime of the radioactive substances, Peierls[12] in 1935, Bartlett[13] in 1936, and Hole[14] in 1947, have discussed the application of the maximum-likelihood procedure[15] to counter experiments. The results given by these workers are almost immediately applicable to the present situation with the principal exception that each of these has treated the problem in which the gate time, T, is a constant, whereas the data obtained by use of the cloud chamber contain T_i's which vary over a rather wide range. The range in values of T_i is due to a difference in both the potential path lengths and the velocities of the V^0-particles. In spite of this difference the procedure with constant T_i is readily extended to cover the case in which T_i varies over a range of values.

A. The Maximum-Likelihood Procedure

An unstable particle, which follows an exponential decay law with mean lifetime τ and which is known to

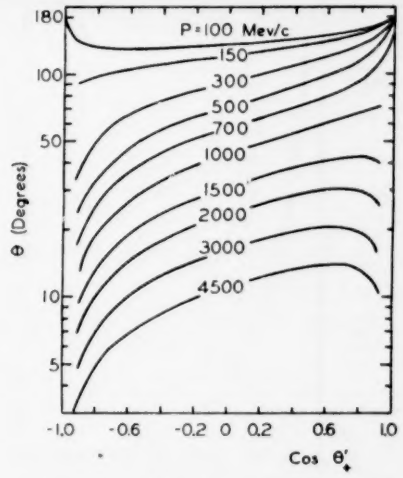

FIG. 4. Graph of θ *vs* θ_+' for various V-particle momenta. A two-body decay of a neutral V-particle into a proton and a negative pi meson with an energy release of 50 Mev is assumed. θ_+' is the angle, measured in the c.m. system of the V-particle, which the proton makes with the line of flight of the V-particle. P and θ are defined in Part III.

be "alive" at time $t=0$, has the probability

$$(dp)_i=(1/\tau)e^{-t_i/\tau}dt \tag{1}$$

of decaying at time t_i in the time interval dt. If the decay is known to have taken place within the time T_i, the probability of decay in that time can be normalized[16] to unity so that

$$(dP)_i=(1/\tau)\frac{e^{-t_i/\tau}}{(1-e^{-T_i/\tau})}dt. \tag{2}$$

For a set of N independent decays which follow the probability law of Eq. (2), the probability of having obtained the particular set of experimental data is proportional to

$$L=\prod_{i=1}^{N}(1/\tau)\frac{e^{-t_i/\tau}}{(1-e^{-T_i/\tau})}. \tag{3}$$

L will be referred to as the likelihood function. The maximum-likelihood procedure is based upon the assumption, much used in statistical methods, that the best value of a parameter on which the likelihood function depends is that value of the parameter which makes this function a maximum. Hence one wishes to find the value of τ for which L, or more conveniently $\ln L$, is maximum:

$$\partial \ln L/\partial\tau=0. \tag{4}$$

Carrying out the differentiation of $\ln L$ one obtains for

[12] R. Peierls, Proc. Roy. Soc. (London) **149**, 467 (1935).
[13] M. S. Bartlett, Proc. Roy. Soc. (London) **154**, 124 (1936).
[14] N. Hole, Arkiv Mat., Astron. Fysik **34B**, No. 12 (1947).
[15] R. A. Fisher, Trans. Roy. Soc. (London) **222**, 309 (1922).

[16] This normalization to unity essentially corrects for those particles which passed through the chamber and decayed after time T_i. Peierls does not proceed in this way but rather uses a procedure which requires assumptions as to the *a priori* probability of having had a given total number of decays for each particle which decayed in time T_i.

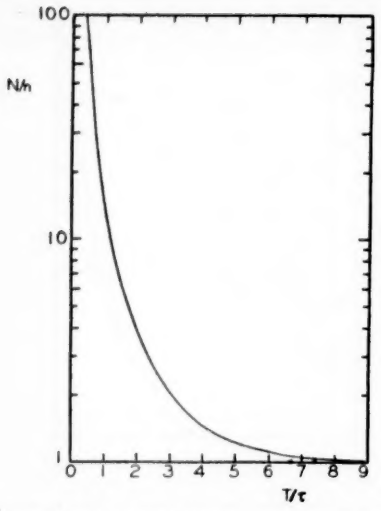

FIG. 5. The ratio N/n, as defined in Eq. (8), is plotted *versus* the ratio of the gate time to the mean lifetime.

the best value of the mean lifetime

$$\tau=\frac{1}{N}\sum_{i=1}^{N}\left(t_i+\frac{T_i}{e^{T_i/\tau}-1}\right). \tag{5}$$

Hence, in principle, the mean lifetime can be determined from data obtained in cloud chamber experiments. Given a set of t_i and T_i for the V^0 particle, Eq. (5) can be solved by iteration to find the best value of τ. The actual worth of such a determination will depend of course on the statistical and systematic errors involved. The next section will be devoted to a discussion of these errors.

B. Errors

Following Bartlett's discussion of the maximum-likelihood procedure, one is led to the statistical error in τ given by

$$\Delta\tau=1/\sqrt{I}, \tag{6}$$

in which I is defined by the equation

$$I=\frac{-\partial^2 \ln L}{\partial\tau^2}=\frac{1}{\tau^2}\sum_{i=1}^{N}\left[1-\frac{T_i^2}{\tau^2}\frac{e^{T_i/\tau}}{(e^{T_i/\tau}-1)^2}\right]. \tag{7}$$

Equation (6) is derived on the assumption that the estimates of the parameter, τ, are normally distributed as the variance of $\partial \ln L/\partial\tau$.[12] Although this condition is only approximately met in the present experiment because of the small sample available, this equation probably furnishes the best means of arriving at some estimate of the statistical error.

To gain some feeling for the effect of the finite gate time, it is interesting to consider the case for which all of the T_i are the same and to consider the quantity, n, which is given by

$$n=I\tau^2=N\left[1-\left(\frac{T}{\tau}\right)^2\frac{e^{T/\tau}}{(e^{T/\tau}-1)^2}\right] \tag{8}$$

and which is the number of decays with an infinite gate required to produce the same statistical accuracy as N cases with a given finite gate, T. The quantity N/n is plotted *versus* T/τ in Fig. 5.[17] As an example, if T/τ is equal to unity, N/n is found to be 12.5; so that 10 decays observed with T infinite would yield a lifetime with the same statistical accuracy as 125 decays for which T/τ was unity.

Since one assumes a knowledge of τ in using the quantity T/τ discussed above, the average value of the ratio t/T, which can be found directly from the experimental data, is more readily given as a measure of significance. For gate times which are small compared with τ one expects the decay points to be uniformly distributed throughout the chamber so that $\langle(t_i/T_i)\rangle_{Av}$ would be equal to one-half. Thus, one can hope to use the cloud chamber to measure mean lifetimes only if $\langle(t_i/T_i)\rangle_{Av}\neq\langle(x_i/d_i)\rangle_{Av}$ is significantly less than one-half.

Further uncertainty in the lifetime is due to the limitations of the experimental technique and to a lack of exact knowledge of the decay process or processes which are taking place. In each of the lifetime determinations which are given here, it is quite possible that the samples contain a mixture of particles of different lifetimes so that the "lifetime" calculated is actually some sort of an average value of two or more characteristic lifetimes. Efforts which were made to separate such possible mixtures will be discussed. Apart from the fact that the errors in the measurements of momentum prevent an accurate classification of the V-particle decays into homogeneous groups and may thereby prevent us from making a proper calculation, the errors in the quantities P_i, x_i, and d_i do not contribute very large errors to the mean life, τ. For most cases x_i and d_i can be measured with sufficient accuracy that the error can be neglected, and if selection criteria are used such that the momentum of each V-particle in the sample is measurable to within twenty or thirty percent, the resulting error in the mean lifetime should be small compared with the statistical error given by Eq. (6).[18]

V. THE MEAN LIFETIME OF NEUTRAL *V*-PARTICLES

In a series of 23 000 cloud-chamber photographs taken at Pasadena and on Mt. Wilson, 134 examples of the decay of neutral V-particles have been obtained. The distribution of the decays is shown in Fig. 6. Data on 74 of these examples which were consistent with the

[17] This graph was also quite useful in evaluating the terms in Eq. (7) to find the statistical error when T was allowed to take on many different values.

[18] Since such a selection might tend to discriminate against the decay of long-lived particles near the walls of the chamber, care must be taken that bias is not thus introduced into the sample.

decay scheme

$$V^0 \rightarrow P^+ + \pi^- + Q, \tag{9}$$

were used in the present calculation. The remaining 60 decays were eliminated from consideration for at least one of the following reasons:

(1) the decay occurred outside the fiducial surfaces,
(2) the total angle between the paths of the two decay products was $\leqslant 10°$, or
(3) the decay did not seem to fit the proton plus negative π-meson decay scheme.

These criteria were established in an attempt to obtain an unbiased sample of events for which maximum information was available. Nineteen decays between the walls of the chambers and the fiducial surfaces were discarded because of the nonuniform illumination and the reflections which made it doubtful that all of the V-decays in this region were detected. The arbitrary restriction on the total angle eliminated twenty-three cases for which the V-particle momentum was unmeasurably high and eliminated no case for which the V-particle momentum was accurately known. This restriction was chosen since the angle measurements are independent of the track length available and of the position of the decay point in the chamber. Thus there was no apparent discrimination against decays occurring near the bottom of the chamber. Such would not be the case if momentum measurements were required in making the selection.

More of the cases for which the momentum was not directly measureable could have been eliminated by throwing out those cases with $\theta \leqslant 20°$; however, this much greater restriction would have caused the loss of several events with known V-particle momentum. The final group of eighteen decays was removed because of the apparent inconsistency with the decay scheme given by Eq. (9). This group included such cases as those in which the positive decay particle was definitely lighter than a proton or in which the calculated energy release was greater than 150 Mev.

A mean lifetime was calculated for the remaining 74 examples from the t_i and T_i, assuming that these decays follow the two-body decay scheme given above. The average value of the ratio t_i/T_i was 0.30, with a statistical error of approximately 0.05, so that there was at least an indication of a result with some significance. Substitution of the numerical data into Eq. (5), gave a value of 1.6×10^{-10} sec for the average value of t_i. Since the second or correction term is always additive, this places a lower limit on the mean lifetime, subject only to the ordinary statistical fluctuations. Following an iterative procedure to solve Eq. (5), one obtains for τ the value

$$\tau = (2.5\pm0.7)\times10^{-10} \text{ sec.} \tag{10}$$

The statistical error has been computed by use of Eqs. (6) and (7). Although the effect of additional errors in the experimental quantities is difficult to determine, an attempt has been made to estimate the magnitude of the resulting error in τ. For three-fourths of the 74 cases the error in the V-particle momentum was approximately twenty percent or less, while for the remaining cases, whose momenta were determined solely from the value of θ_i, there was an appreciable probability of errors as large as one hundred percent. The errors in x_i and d_i were small compared with these errors in P_i. A consideration of these facts leads to an estimated probable error of about $\pm0.2\times10^{-10}$ sec in the value of the lifetime. If this error is assumed to be independent of the statistical error given above, the combined error is still given approximately as $\pm0.7\times10^{-10}$ sec.

FIG. 6. The distribution of the neutral V-particle decay points. A dot at the apex indicates production in the lead plate between the two chambers. A dashed track signifies a hidden apex.

This leaves to be considered the uncertainty due to the possibilities that the sample of 74 cases is a mixture of two or more types of particles with different lifetimes and that sources of bias are present in the data. Although it is impossible to reach any definite conclusions as to the actuality of these possibilities, the following checks were made in an effort to detect any such sources of error.

(1) A procedure was used which in effect reduced the volume enclosed by the fiducial surfaces.

(2) A separate lifetime determination was made for 32 decays occurring in the upper chamber and for 42 days occurring in the lower chamber.

(3) A separate lifetime determination was made for those V-particles with identifiable origins and for those without clearly identifiable origins.

(4) A comparison of the lifetime calculated for cases with an energy release between 30 Mev and 40 Mev was made with lifetime calculated for the remaining cases with Q either less than 30 Mev or greater than 40 Mev.

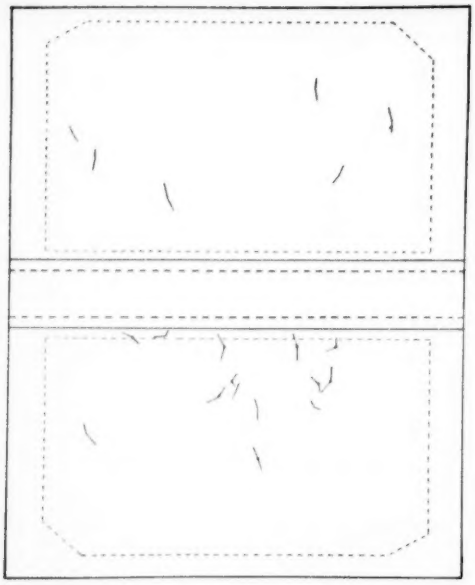

FIG. 7. The distribution of the charged V-particle decay points. A dot at the apex indicates production in the lead plate between the two chambers.

(5) Lifetimes were calculated for the two groups formed by placing those cases with Q less than or equal to 50 Mev in one group and those cases with Q greater than 50 Mev in a second group.

The first of these checks was aimed at testing whether or not the fiducial surfaces really eliminated bias due to observational difficulties in the region near the walls of the chamber. The method used was approximately equivalent to moving in the fiducial surfaces by reducing each gate time by ten percent.[19] The mean lifetime was then redetermined and found to agree within ten percent with the above value. The same result was found when each gate time was reduced by thirty-three percent.

The separate lifetime determinations for the 32 decays occurring in the upper chamber and for 42 decays occurring in the lower chamber were compared. Since the illumination improved slightly from top to bottom for the upper chamber and conversely for the lower chamber, it was felt that this check might indicate bias in the data. However, the two values of the lifetime fell within ten percent of the result given above for the combined data. Because of the distances of the principal source of V-particles in the lead above each chamber to the respective illuminated regions (Fig. 1), it was thought that this test might also indicate the presence of a mixture of two different lifetime particles with the upper chamber favoring the detection of the longer-lived particles and the lower chamber favoring the detection of the shorter-lived ones. The negative result which was found could mean, among many possibilities, that the V-particles were all or almost all of one kind or that different kinds, if present in comparable numbers, were of nearly the same lifetime.

There was no significant difference between the lifetime calculated for the decays with identifiable origins and that calculated for those without clearly identifiable origins.

The fourth point was checked because of the suggestion that part of the V-particles which were observed might follow the decay scheme of Eq. (9) with Q near 37 Mev, and the remainder the three-body scheme:

$$V^0 \rightarrow P^+ + \pi^- + \nu + Q, \tag{11}$$

with the apparent energy release calculated on the basis of the decay scheme of Eq. (9) varying over a range of values. Again the result was negative with no significant difference appearing in the two lifetimes.

The final division of the data arose from the analysis of the 134 neutral V-particle decays reported in reference 8. This analysis suggested the possible existence of two groups of V-particles which follow the decay scheme of Eq. (9), but with different values of the energy release, Q, and possibly with different lifetimes. There was a concentration of a number of decays with Q near 35 Mev and with Q near 75 Mev. This suggested a division of the data such that 37 cases with $Q \leqslant 50$ Mev were placed in a "low Q" group and 20 cases with 50 Mev $< Q \leqslant 150$ Mev, were placed in a "high Q" group. Substituting the data for the 37 low Q cases into Eq. (5), a lifetime of $\tau_L = (2.9 \pm 0.8) \times 10^{-10}$ was obtained. Again the error has been computed by using Eqs. (6) and (7) and does not include an estimate of the bias due to the failure to consider the remaining 17 cases for which Q could not be determined. If the 17 cases were added to the low Q cases but weighted by the factor 37/57,[20] the resulting lifetime was found to be $\tau_L = (3.0 \pm 0.8) \times 10^{-10}$ sec. A similar treatment of the high Q cases yielded a mean lifetime of $\tau_H = (1.3 \pm 0.5) \times 10^{-10}$ sec for the 20 cases of known Q-value and a mean lifetime of $\tau_H = (1.6 \pm 0.5) \times 10^{-10}$ sec when the 17 cases of unknown Q-value are added in but weighted by the factor 20/57. Other possible division schemes were tried in treatment of the 17 cases to determine the range of lifetime values which resulted from various ways of adding in these cases. If those divisions which give the greatest possible range of values consistent with the data are included, the values found in units of 10^{-10} sec were $1.3 < \tau_H < 2.3$ and $2.4 < \tau_L < 3.5$. Thus on the basis of these results and of the large statistical errors one would hesitate to place any real significance on the difference between the lifetimes of the low Q and high Q groups.[21]

VI. THE MEAN LIFETIME OF CHARGED V-PARTICLES

In the same series of 23 000 photographs which contained the 134 examples of neutral V-particles, 23 examples of charged V-particle decay were observed.

[19] Any event for which the decay time was then greater than the new gate time was removed from the sample.

[20] This weighting factor divides the cases in proportion to the number of known Q-values in each group.

[21] R. J. Finkelstein, Phys. Rev. **88**, 555 (1952).

For most of these cases, both the incident charged V-particle and the visible decay product had high momenta with the result that very few data could be obtained and no significant lifetime determination could be made. The distribution of decays as shown in Fig. 7 is suggestive of the existence of more than one type of particle in the group. The events shown in the figure with a dot at the apex to indicate their production in the lead plate between the chambers were decays which occurred predominantly near the top of the lower chamber. A qualitative comparison of these events with the neutral V-decays shown in Fig. 6 indicates a somewhat shorter mean free path for the charged V-particle.[22] Since ionization estimates show that P/M is, on the average, greater for the charged V-particles than for the neutral V-particles, a mean lifetime of less than 2.5×10^{-10} sec, possibly by a factor of from 2 to 4, is indicated for this particular type of charged V-decay. Also in support of this short lifetime is a consideration of the ratio of the number of V-particles produced in the lead between the two chambers to the number produced in the lead above the upper chamber. For the charged V-particles with identifiable origins this ratio is approximately unity, to be compared with one-half for neutral V-particles with identifiable origins. This comparison again points to a shorter average lifetime for the combined cases of charged V-particles than for the neutral V-particles.

On the other hand, the decays shown in Fig. 7 without a dot at the apex were apparently produced in the lead above the upper chamber and were distributed more uniformly throughout the chambers. Several of the particles decaying in the lower chamber traversed completely the upper chamber indicating a long lifetime, provided P/M is not too much greater for these particles than for the neutral V-particles. In addition, two examples, in which a relatively slow particle of estimated mass between that of the proton and the π-meson has been observed to decay into a particle consistent with a π- or μ-meson after a time greater than 10^{-9} sec, also suggest the presence of a comparatively long-lived particle of such mass accompanying penetrating showers. Thus it is felt that at least some of the charged V-particles are identical with these two examples and are probably κ- or χ-mesons[23,24] with a mean lifetime of 10^{-9} sec or greater.[25]

In addition to those events which have been described as charged V-decays and which may in part be κ- or χ-mesons decaying respectively into a μ- or π-meson plus one or more neutral particles, two examples have been obtained[23] of a charged particle decaying into three charged particles. Each of the three decay products in these two events has a mass consistent with that of a π-meson and the primary particle appears to be identical with the τ-mesons which have previously been observed in nuclear emulsions.[26] Although a reliable estimate of the lifetime of this particle cannot be made from only two cases, the relatively long paths of these τ-mesons in the chamber before decay and the estimates of P/M indicate a mean lifetime greater than that of the neutral V-particle, and perhaps greater than 10^{-9} sec.

VII. CONCLUSION

In the present attempt to determine the mean lifetime of V-particles, a worth-while numerical analysis is permitted only for those cases in which the decay is consistent with Eq. (9). Although the accuracy of this analysis is somewhat limited because of the present state of knowledge concerning the exact type of decay involved, assuming any one of several alternative decay processes, which are consistent with the data, should not greatly alter the given results. For example, the results would be changed very little if a three-body decay proved to be the actual process rather than the assumed two-body decay.

Apparatus which is now in operation should overcome many of the difficulties encountered here, because of the larger chambers which are used, the stronger magnetic field which is available, and other improvements which have been made in the apparatus and in the experimental techniques. It is likely that further investigation of lifetimes can be made, particularly for the neutral V-particle treated here and for the short-lived charged V-particle, if additional evidence of its existence is found. There should also be an opportunity for investigation of the one or more additional types of neutral V-particles which have been proved to exist[7,8] but which have essentially been ignored in this paper because of the small number of cases observed. For the apparently longer-lived κ-, χ-, and τ-mesons, the direct method here used in determining lifetimes is of doubtful value in obtaining good statistical accuracy since the gate times for useful events must be long and the frequency of observation of such decays has been quite low. Perhaps, however, even this difficulty will be eliminated by the use of these larger chambers or by the use of techniques which will increase the frequency of observing slow particles.

[22] The arguments based on this over-all comparison of neutral and charged V-particles are weakened somewhat because of the unequal efficiency of observing the two types of decay. A small deflection in the track of a very fast particle is often the only indication of a charged V-decay. Such a deflection is much more difficult to detect than is the inverted V which characterizes the decays of the neutral variety. This is especially true of events near the walls of the chambers.

[23] R. B. Leighton and S. D. Wanlass, Phys. Rev. **86**, 426 (1952).

[24] C. O'Ceallaigh, Phil. Mag. **42**, 1032 (1951).

[25] Approximately twice the amount of data discussed in this section is now available and these additional data lead to essentially the same conclusions as those given.

[26] Brown, Camerini, Fowler, Muirhead, Powell, and Ritson, Nature **163**, 82 (1949).

Impurity Diffusion and Space Charge Layers in "Fused-Impurity" *p-n* Junctions*

JOHN S. SABY, *Electronics Laboratory, General Electric Company, Syracuse, New York*

AND

W. C. DUNLAP, JR., *General Electric Research Laboratory, Schenectady, New York*

(Received October 29, 1953)

Fused-impurity *p-n* junctions have properties which depend upon alloying and diffusion of impurities. The inverse-voltage space charge distribution in such junctions is found to be such that nearly all the applied potential drop occurs within the base material. The barrier capacitance varies inversely as the square root of the applied voltage as expected for an abrupt transition junction. However, the diffusion of only 2×10^{12} acceptor atoms per cm² into *n*-type germanium is found sufficient to include the space charge layer (which includes the region of maximum dielectric stress) entirely below the diffused surface, in the relatively undisturbed base material.

Diffusion calculations are reported, based on the latest values of diffusion constants, for various impurities, heating times, and temperatures. These lead to the conclusion that even a few seconds diffusion time at very moderate temperatures (even below 500°C) is sufficient to result in the diffusion of more than 2×10^{12} atoms of any of the common donors or acceptors.

WHEN fused contact *p-n* junctions are formed by heating impurity elements of the proper type in contact with highly purified germanium,[1] several physical processes take place which determine the distribution of impurities in the junction region. It is the purpose of this paper to discuss quantitative aspects of the space charge region as related to the amount of solid impurity diffusion which has occurred.

When finite amounts of impurity are heated with germanium, the resulting structure, schematically represented in Fig. 1, contains an alloy region having a relatively high concentration of impurity. Beyond the alloy region is the diffusion zone whose thickness depends upon the extent to which impurity diffusion has been carried out. The inner boundary of the alloy region may consist of recrystallized germanium which may be deposited as a single crystal, as suggested by English,[2] upon the relatively undisturbed crystalline region. Such recrystallized material would contain a high concentration of the impurity used.

When an inverse voltage is applied to the junction, a charge dipole region is formed which contains virtually the entire potential drop. The thickness of this barrier region, the inverse breakdown voltages of the junction and its effective capacitance, are all determined by the impurity ion distribution in the junction region. We shall first express these relations explicitly and then examine the role played by impurity diffusion.

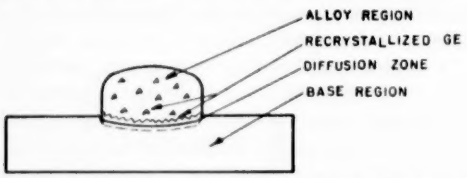

FIG. 1. Schematic representation of alloy-diffusion *p-n* junction.

Fused-impurity *p-n* junctions in germanium are characterized by a relatively rapid transition from *n*- to *p*-type as in Fig. 2(a). Let us consider specifically junctions formed by the diffusion of acceptor impurities into *n*-type germanium. Similar reasoning will apply to junctions formed by diffusing donors into *p*-type germanium, or to diffusion junctions in other semiconductors.

The space charge dipole region can be described approximately as in Fig. 2(b). The charge density is nearly constant and equal to the donor impurity density throughout the *n*-type portion of the dipole region, where nearly all the potential drop V occurs, as in Fig. 2(c). Under the assumption that the barrier

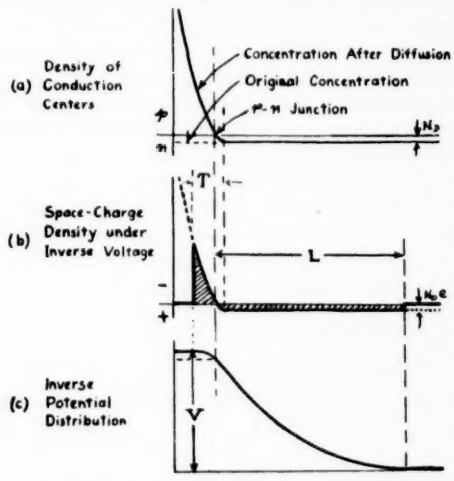

FIG. 2. Qualitative impurity concentration, space charge density, and inverse potential distribution in a *p-n* junction formed by impurity diffusion. Abscissa represents distance into germanium.

* The work of one of the authors (J.S.S.) was supported in part by the Air Materiel Command, the Signal Corps and the Bureau of Ships.

[1] R. N. Hall and W. C. Dunlap, Jr., Phys. Rev. **80**, 467 (1950).

[2] A. C. English (private communication to be published).

thickness L (cm) is large compared with the impurity transition distance T, Poisson's equation yields the following approximate relations for germanium, whose dielectric constant is $\epsilon/\epsilon_0=16$:

$$V=5.66\times10^{-8}N_DL^2 \quad \text{(i.e., } eN_DL^2/2\epsilon \text{ in mks units)}, \quad (1)$$

$$C=3.37\times10^{-6}N_D^{\frac{1}{2}}V^{-\frac{1}{2}} \quad \text{(i.e., } (\epsilon eN_D/2V)^{\frac{1}{2}} \text{ in mks units)}, \quad (2)$$

$$E_m=2VL^{-1}, \quad (3)$$

where N_D is the number[3] of donor atoms per cm^3, $C=dQ/dV$ is the barrier capacitance ($\mu\mu$f per mm^2) and E_m is the maximum field (v/cm) attained in the barrier region, i.e., at the junction.

These relations can be conveniently summarized in graphical form in the nomogram of Fig. 3, where it will be observed that C and E_m (and, hence, the Zener breakdown voltage, at which $E_m\doteq2\times10^5$ volts/cm is attained) here depend principally upon the underlying germanium, rather than upon the exact nature of the impurity diffusion region. This is in contrast to "graded" junctions described elsewhere[4,5] for which C, E_m and the Zener voltage depend directly upon the impurity concentration gradient in the transition region.

Capacitance-potential data plotted as shown in Fig. 3 lie on straight lines with slopes of approximately minus 0.5. Data for a typical junction are shown in the figure from which $N_D=3\times10^{14}$ cm^{-3} was inferred, which is consistent with that obtained from the measured resistivity (8 ohm cm) of the sample within the accuracy to which the effective area of this junction could be determined.

The shaded region of Fig. 3 should be regarded as inaccessible for germanium because of Zener breakdown. Junctions formed on germanium having impurity concentration much greater than 10^{16} cm^{-3} thus can be operated only at very low inverse voltages.

Diffused junctions as described above have many properties in common with theoretical "abrupt"[4] junctions formed between high resistivity n-type and low resistivity p-type germanium without any diffusion. However, they are not identical. When impurity diffusion is carried out to even a very small extent, the actual junction will be moved into the n-type material. Consequently, the maximum dielectric stress E_m then occurs in relatively undisturbed material rather than at a possibly imperfect impurity transition surface. Thus, in actual practice, the diffusion of impurities might have an important effect upon the properties of a junction, even if only a portion of the inverse charge dipole were so accommodated.

[3] This quantity, of course, actually represents the net number N_D-N_A for n-type material or N_A-N_D for p-type material.
[4] W. Shockley, Bell System Tech. J. **28**, 435 (1949).
[5] McAffee, Ryder, Shockley, and Sparks, Phys. Rev. **83**, 659 (1951).

If a sufficient number of acceptors has diffused into the germanium, the entire charge dipole will lie inside the impurity diffusion region and the undisturbed n-type germanium beneath, the field outside being zero. This required number of diffused acceptors (N^* per

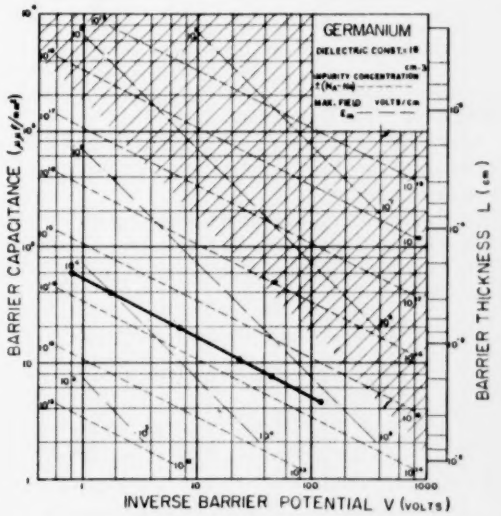

FIG. 3. Barrier capacitance, barrier thickness, and maximum field for alloy-diffusion junctions as functions of donor concentration in base germanium and applied voltage. Capacitance-voltage data are shown for a typical junction. The shaded region corresponds to E_m greater than the critical Zener field.

unit area of junction) is equal to the number of donor ions in the n-type side of the dipole, i.e., N_DL. It follows from Eqs. (1) and (3) that:

$$N^*=8.6\times10^6E_m \quad \text{(i.e., } \epsilon E_m/e \text{ in mks units)}. \quad (4)$$

If we restrict E_m to values below 2×10^5 (approximate Zener breakdown field for Ge), then less than 2×10^{12} acceptor atoms per cm^2 diffused into n-type germanium are sufficient to provide for the complete charge dipole of a diffused p-n junction, even at its maximum voltage. Rectifier junctions are usually operated well below the Zener breakdown voltage, so that a smaller number would ordinarily suffice.

From Eq. (4) it can be seen that N^* is independent of the resistivity of the germanium. For junctions with less diffusion, in which only a portion of the space charge dipole can be accommodated by the diffused region, the portion so accommodated will include the junction itself, which is the region of greatest dielectric stress.

For fused impurity junctions made under conditions implying negligible diffusion (e.g. low temperature, short diffusion time, or use of impurity or semiconductor having low diffusion constants) the space charge can be balanced by adsorption of N^* impurity ions per unit area. It is also possible that the charge dipole region may extend[2] into the alloy region, particularly if, as

TABLE I. Penetration of impurities into germanium for various temperatures and times.

D cm²/sec	Approximate temperature (°C) Sb, As	P	Zn	Ga	In	Penetration distance x_0 (angstrom) $t=1$ sec	10	100	1000	10 000
10^{-10}	875	925	—	—	—	8000	2.5×10^4	8×10^4	2.5×10^5	8×10^5
10^{-12}	700	725	800	900	875	800	2500	8000	2.5×10^4	8×10^4
10^{-14}	550	575	650	725	700	80	250	800	2500	8000
10^{-16}	450	475	550	600	575	8	25	80	250	800

mentioned above, this region contains a continuous redeposited crystalline region.

Next, consider the actual amount of diffusion to be expected for some of the donor and acceptor impurities of greatest interest.

When a source of impurities with impurity content N_0 is in contact with a piece of germanium, the diffusion (one-dimensional geometry) is governed by the following relation:

$$C(x,t)=N_0[1-\mathrm{erf}\{x/2(Dt)^{\frac{1}{2}}\}], \tag{5}$$

where C is the density of impurities (atoms/cm³) at any value of x and t, D is the diffusion coefficient (cm²/sec), and erf$x$ is the Gaussian error function. When $C\ll N_0$, the Gaussian integral can be replaced by the exponential:

$$\mathrm{erf}y=1-\exp(-y^2)/\pi^{\frac{1}{2}}y, \tag{6}$$

and the penetration x_0 of the p-n junction is given by

$$C_0/N_0=\exp(-y_0^2)/\pi^{\frac{1}{2}}y_0, \tag{7}$$

where $y_0=x_0/2(Dt)^{\frac{1}{2}}$, C_0 the density of impurities in the base germanium at $t=0$. To a first approximation when $C_0/N_0\sim10^{-5}$ to 10^{-8}, as is often the case with germanium, y varies from 3–4 and the penetration of the junction is approximately $8(Dt)^{\frac{1}{2}}$.

Latest values of the diffusion coefficients obtained by one of us[6] are, for 900°C: donors—antimony $D=2\times10^{-10}$ cm²/sec, arsenic 2×10^{-10}, and phosphorus 8×10^{-11}; acceptors—zinc 1×10^{-11}, gallium 2×10^{-12}, and indium 2×10^{-12}. This value for indium is tenfold greater than that previously published. The activation energy is about 2.5 ev (57 000 cal/mol). Table I gives values of x_0 for various temperatures, times, and impurities.

From Table I it is seen that the penetration of the p-n junction may range from a few angstroms to several thousands of angstroms in the temperature range 400°–920°C.

To apply these results to the calculation of the actual number of diffused impurity atoms per unit area, we need to integrate the concentration $\int_0^{x_0}C(x)dx$. The curve $C(x)$ depends critically upon the value N_0, the density of impurity in the alloy region. Determination of N_0 for all impurities has not been made, but N_0 appears to be greater than 10^{20} for indium, the element for which it appears to be the least. The integral $\int_0^{x_0}C(x)dx$ has been calculated for a number of cases. The number of diffused impurities $N^*=2N_0(Dt)^{\frac{1}{2}}/8\pi^{\frac{1}{2}}\sim N_0x_0/7$. Thus for junctions formed by all heating conditions where $x_0>10^{-8}$ cm (or one atomic distance), the entire dipole for all attainable voltages lies within germanium undisturbed by the alloying process.

Indeed, the number $N^*\doteq2\times10^{12}$ atoms/cm² corresponds to only about one percent of one monolayer of impurities. Diffusion of this small quantity of impurity ions is sufficient to accommodate the entire space charge dipole, thus relieving the alloy boundary from dielectric stress.

The maximum extent of the space charge layer into the diffusion zone is thus of the order of 10^{-8} cm. Deeper diffusion merely moves the barrier farther away from the recrystallization boundary. This also confirms the assumption $T\ll L$, since L is much greater than 10^{-5} cm for most junctions of interest (see Fig. 3).

Important problems remaining include experimental studies of effects upon p-n junction characteristics due to the slight gradation produced by diffusion, and the extension of the semiconducting region by recrystallization.

[6] W. C. Dunlap, Jr., Phys. Rev. **86**, 615 (1952). See also: W. C. Dunlap and D. E. Brown, Phys. Rev. **86**, 417 (1952); C. S. Fuller, Phys. Rev. **86**, 136 (1952); McAfee, Shockley, and Sparks, Phys. Rev. **86**, 137 (1952).

The High Energy Charged Particles from Targets Bombarded by 190-Mev Deuterons*

L. SCHECTER,† W. E. CRANDALL, AND G. P. MILLBURN, *Department of Physics, Radiation Laboratory, University of California, Berkeley, California*

AND

D. A. HICKS AND A. V. SHELTON, *California Research and Development Company, Livermore, California*

(Received January 30, 1953)

An investigation has been made of the angle and energy distributions of the high energy charged particles which emerge from beryllium, carbon, and uranium nuclei bombarded by 190-Mev deuterons. The results indicate that the yields can be explained as primarily due to two kinds of processes; nucleon-nucleon interactions, and stripping. Under this assumption, the total stripping cross section has been determined to be 0.35 ± 0.03 barn for the lighter elements and 2.6 ± 0.4 barns for uranium. These values suggest an $A^{\frac{1}{3}}$ dependence for this cross section.

I. INTRODUCTION

THE principal features of the inelastic processes which can be expected to occur, when nuclei are bombarded by high energy deuterons, have been described by the mechanisms of Bohr,[1] Serber,[2] Dancoff,[3] Goldberger,[4] Chew and Goldberger,[5] and Butler.[6] These features concern the various secondary particles whose angular and energy distributions are characteristic of the process which produces them. For deuterons whose incident energy is high, compared to the binding energy, it is convenient to consider a very loosely bound neutron-proton system. The effects to be described are then merely the results of high energy collisions of nucleons with the nucleus, modified by the relationship of the incident deuteron's constituent nucleons to each other.

When the incident nucleons have energy less than, roughly, 30 to 40 Mev (corresponding to an incident deuteron energy of less than 70 to 80 Mev, since the total energy is shared equally, on the average), the compound nucleus of Bohr describes one process. In this model, the mean free path of either incident nucleon within the nucleus is so short that its energy is quickly shared with other constituents of the nucleus, so that it is immediately captured. The resulting excited nucleus decays slowly, either by quantum emission, or, when sufficient energy becomes concentrated properly, by particle emission. These secondary particles will carry off most of the excitation energy, neutron emission being favored over charged particle emission because of the Coulomb barrier of the nucleus. The energy distribution will be, roughly, a decaying exponential, with substantially no particles carrying more than about 10 Mev. The angular distribution of these particles will be essentially isotropic.

When the incident deuteron has energy less than about 50 Mev, a particular process which we shall call Butler stripping is important. Since in the deuteron the nucleon separation is large and the binding energy low, just one of the incident nucleons may interact with the surface of the target nucleus. If its momentum is proper, it will be bound into the nucleus to form one particular state of a new nuclide, which may then decay to its ground state. The other nucleon, passing by, must conserve energy, parity, and angular momentum. This means that it may carry energy greater than its initial energy by the amount of the binding energy of the captured nucleon. Further, this "secondary" nucleon, instead of carrying just the momentum it had at the time of capture, will, in addition, possess additional angular momentum so that the conservation laws are satisfied. The resulting angular distribution is just a sum over those angular momentum states which are acceptable. Only a few of these are important, since the magnitude of each contribution is roughly inversely proportional to the angular momentum. The particles, then, are emitted in a pronounced forward direction, but the peak may be displaced from the axis of symmetry.

At higher deuteron energies, the Butler stripping becomes, in the limit, Serber stripping. In this mechanism the collision is "fast," so that the "secondary" particle, the nucleon which passes by, feels no reaction. In terms of the Butler theory, so many angular momenta are accepted that interference between them washes out the effect. The secondary's final momentum is the result of the motion of the deuteron center of mass and its motion with respect to the center of mass at the moment the other nucleon is stripped off by the edge of the nucleus. The resulting angular distribution is sharply forward, maximum in the direction of the axis of symmetry, with a half-width of about $3(\epsilon_d/T_d)^{\frac{1}{2}}$. The distribution of energies is centered around half the incident deuteron energy and has a half-width of about $2(T_d\epsilon_d)^{\frac{1}{2}}$, where ϵ_d is the deuteron binding energy, and T_d is the

* This work was performed under the auspices of the U. S. Atomic Energy Commission.

† Part of a dissertation submitted in partial satisfaction of the requirements for the Ph.D. degree.

[1] N. Bohr, Nature **137**, 344 (1936).
[2] R. Serber, Phys. Rev. **72**, 1008 (1947).
[3] S. M. Dancoff, Phys. Rev. **72**, 1017 (1947).
[4] M. L. Goldberger, Phys. Rev. **72**, 1269 (1948).
[5] G. F. Chew and M. L. Goldberger, Phys. Rev. **77**, 470 (1950).
[6] S. T. Butler, Phys. Rev. **80**, 1095 (1950).

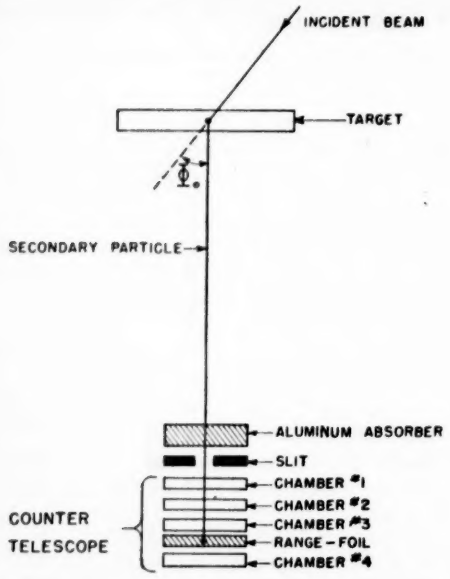

FIG. 1. Schematic diagram of the four chamber proportional counter telescope.

incident deuteron kinetic energy. The cross section for this process is proportional to the target nuclear radius.

Another effect which may occur is the "field stripping" described by Dancoff. It is the action of the Coulomb field of the target nucleus upon the incident deuteron. When the energy is low, this amounts to an orientation of the deuteron (because of Coulomb repulsion on the proton), which accounts in part for the high cross section for deuteron reactions. When the energy is sufficiently high, the transverse electric field seen by the moving deuteron may cause it to split up. The angular distribution from this process is narrower than that of the Serber stripping by a factor of two, but the total effect is predicted to be as important for heavy elements, since the cross section goes like the square of the charge of the target nucleus.

When the incident nucleon energy is as high as 90 Mev, the nucleus becomes somewhat transparent, because the nucleon-nucleon cross section decreases with energy. This makes the mean free path for nucleons in nuclear matter the order of the radius of the nucleus, so that if a collision occurs, one or more fast secondary particles may be emitted. The angular and energy distributions of the "knock-on" secondaries will depend upon the model chosen for the nucleus, but at least partial correlation is expected with the direction and energy of the incident nucleons, so that the secondaries will be emitted mainly forward, with energies equal to that of the incident nucleons, or less.

Chew and Goldberger have described a process by which deuterons, tritons, etc., may be produced. The nucleons within the nucleus are in motion, and when an incident nucleon penetrates, there is some probability that a pair may result in such a momentum relationship that, say, a deuteron is formed. If the total energy is high, so that the mean free path is long, this "pick-up" deuteron may escape as a secondary. Three-particle pick-up will result in a triton or He^3 secondary. These "pick-up" particles will be emitted strongly forward, and they will be peaked around some energy which gives the best compromise between the formation probability, which involves the internal nucleon momentum distribution, and the escape probability.

High energy fission can also occur when heavy nuclei are bombarded by nucleons. The secondary nucleons, mainly neutrons are emitted isotropically and with energy less than 10 Mev.

The aim of the present work was an investigation of the high energy charged secondary particles (proton energy >26 Mev, deuteron energy >35 Mev) from bombardment of beryllium, carbon, and uranium nuclei by 190-Mev deuterons. The information to be gained includes (a) the relative importance of the deuteron's binding energy in collisions with nuclei, (b) a measurement of the cross section for stripping, and (c) evidence for the existence of Dancoff field stripping.

II. EXPERIMENTAL METHOD

Consider an inelastic scattering process, defined to be one in which the particles emitted at a given mean angle Φ_0 include a more or less broad spectrum of energies. In such a case, the connection between the observation and the differential scattering cross section is given by

$$C(\Phi_0, T_0, T_0') = \int\int\int J(T')N\frac{d^2\sigma}{d\Omega dT}(\Phi, T, T') \times P(T, \Omega)d\Omega dT dT'. \quad (1)$$

$C(\Phi_0, T_0, T_0')$ = number of counts observed in the detector, when it is set to accept particles of mean energy T_0 at mean angle Φ_0, when particles of mean energy T_0' are bombarding the target.

$J(T')$ = number of incident particles whose energies lie between T' and $T'+dT'$. The integration is over all T'. $\int J(T')dT' = I$ = total number of particles incident upon the target. The beam particles are assumed to be independent of each other.

N = number of target nuclei per cm^2 in the beam direction and is assumed to be constant.

$\frac{d^2\sigma}{d\Omega dT}(\Phi, T, T')$ = differential scattering cross section in the laboratory system for producing particles of energy T at angle Φ when the target nuclei are bombarded with particles of energy T'.

$P(T, \Omega)$ = detector resolution probability function which describes how efficiently a particle of energy T emitted into a solid angle Ω will be detected.

If it is assumed that (a) the number of target nuclei remains constant, approximately, during bombard-

ment; (b) the incident beam particles are independent of each other; (c) the spread in energy of the incident beam particles is small compared to the nominal beam energy T_0'; (d) the differential scattering cross section varies only slowly over the range of incident beam particle energies and over the range of angles and energies accepted by the emitted-particle detecting system; and (e) the integral of the detector resolution function can be determined in terms of the accepted solid angle $\Delta\Omega_0$ and the accepted energy width $\Delta T(T_0)$, Eq. (1) can be written

$$C(\Phi_0, T_0, T_0') = I(T_0')N\frac{d^2\sigma}{d\Omega dT}(\Phi_0, T_0', T_0) \times \Delta\Omega_0 \Delta T(T_0). \quad (2)$$

For the purposes of the present experiment, it was sufficient to detect charged particles without trying to discriminate between them. It was already known that the secondary charged particles would be mainly protons, with some deuterons, and the numbers of other kinds of charged particles would be negligibly small, due to the small cross section for their production. Equation (1), generalized, becomes, in such a case,

$$C(\Phi_0, T_0^j, T_0') = \sum_j \int\int\int J(T')N\frac{d^2\sigma^j}{d\Omega dT^j} \times (\Phi, T^j, T')P(T^j, \Omega)d\Omega dT^j dT', \quad (3)$$

where the sum is over the j different kinds of secondaries. $d^2\sigma^j/d\Omega dT^j$ is the differential cross section for producing a type j secondary particle of energy T^j at angle Φ, when the incident energy is T'. Under suitable approximations, as explained, (3) becomes

$$C(\Phi_0, T_0^j, T_0') = I(T_0')N\Delta\Omega_0 \sum_j \frac{d^2\sigma^j}{d\Omega dT^j} \times (\Phi_0, T_0^j, T_0')\Delta T(T_0^j). \quad (4)$$

In the present investigation, the emitted charged particles were detected by a differential-range measuring device. These charged secondaries, in order to be counted were required to traverse the first three chambers of a proportional counter telescope (in coincidence) and stop in a thin range foil before reaching the fourth chamber (anticoincidence) (see Fig. 1). The secondary particle energies are measured by varying the thicknesses of aluminum absorbing foils placed in front of the counter telescope and applying the range-energy relationship.

Consider a specific proton which has been produced by a (d,p) reaction exactly at the midpoint of the target. Suppose this proton, moving at an angle Φ_0 (in the laboratory system) to the original beam direction, has energy just sufficient to carry it through (a) the remaining target thickness, (b) the air path between the target and the counter telescope, (c) the aluminum absorber, (d) the first three chambers of the telescope, and (e) exactly half the range-foil thickness.

Such a path defines a specific proton energy T_0. However, both the converter and the range foil have finite thicknesses, and even monoenergetic particles straggle in range. For this problem, we will assume that the final resolution of the detector is given by the fold function

$$P(T) = \int_{-\infty}^{\infty} p_c(T-E)\int_{-\infty}^{\infty} p_b(K)p_a(E-K)dKdE, \quad (5)$$

where $p_a(T)$ is a function which describes the effect of finite target thickness, $p_b(T)$ is a function which describes the effect of finite range foil thickness, and $p_c(T)$ is a function which describes the effect of range straggling.

An example of the fold is shown in Fig. 2 for a mean proton energy $T_0 \approx 155.7$ Mev. The fold was done graphically. While the detector resolution is 4 Mev wide at half-maximum, the integral of the resolution function is a bite in energy only about 1.5 Mev wide. The fold also indicated that the best resolution for a given counting intensity was to be obtained by making the range foil and target of equal range.

The lower limit to the energies of the secondary particles which can be detected is set by the minimum range which each particle must have in order to just reach the range foil in the detector. This minimum energy is 26 Mev for protons and 35 Mev for deuterons.

Regarding the incident deuteron as two essentially independent nucleons, the processes which will be observed in this experiment are the result of the incident proton interactions with the nucleus to yield (a) knock-on protons or (b) pick-up deuterons, and the incident neutron interactions with the nucleus to yield (a) stripped protons, (b) knock-on protons, and (c) pick-up deuterons. While the incident neutron interacts only with subnuclear protons to yield an observable particle (protons of energy >26 Mev, deuterons of

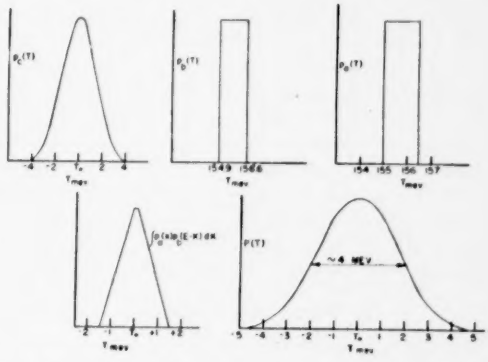

FIG. 2. The energy resolution of the detector, as the fold of the several detector functions. The fold was integrated graphically.

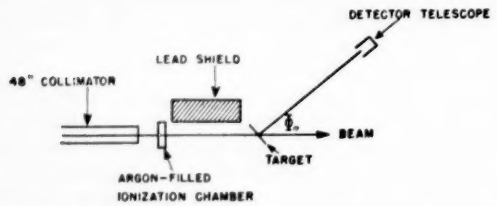

FIG. 3. Schematic diagram of the experimental arrangement.

energy >35 Mev), the incident proton can interact with either neutrons or protons. The counts observed when the detector is set at some mean angle Φ_0, and for particles of mean energy T_0', will be

$$C=IN\Delta\Omega_0\{\Sigma_p\Delta T_p+\Sigma_d\Delta T_d\}, \tag{6}$$

where

$$\Sigma_p=\frac{1}{A}\left\{(A-Z)\frac{d^2\sigma(p,n)}{d\Omega dT}+Z\frac{d^2\sigma(p,p)}{d\Omega dT}+Z\frac{d^2\sigma(n,p)}{d\Omega dT}\right\}+\frac{d^2\sigma(d,p)}{d\Omega dT},$$

$$\Sigma_d=\frac{1}{A}\left\{(A-Z)\frac{d^2\sigma(p,d)}{d\Omega dT}+Z\frac{d^2\sigma(n,d)}{d\Omega dT}\right\},$$

ΔT_p = energy bite taken by range foil for protons,

ΔT_d = energy bite taken by range foil for deuterons.

III. APPLICATION OF EXPERIMENTAL METHOD

A. General Procedure

The experimental arrangement is shown in Fig. 3. The collimated external deuteron beam of the 184-inch cyclotron was monitored by an argon-filled ionization chamber whose collected charge was integrated electronically. The targets were thin and larger in lateral extent than the beam. They were placed in the beam and the emitted charged secondary particles were detected by a proportional counter telescope. This detector was shielded with lead from any particles which might have scattered either from the mouth of the collimator or from the ionization chamber. The number of incident deuterons was determined from the charge collected in the ionization chamber, and the number of secondaries produced at mean angle Φ_0 into the solid angle defined by the slit was determined from the counts in the telescope. The range of each particle measured its energy. The effects of the air path of the incident beam and the general cyclotron background were removed by using no target on alternate runs. The target-blank difference thus measured the intensity of secondary particles which came from the target.

B. Beam and Alignment

The source of deuterons for the experiment was the full energy circulating beam from the 184-inch synchrocyclotron. These deuterons were multiply scattered[7] into the magnetic deflector channel and steered into a shielded enclosure where the experiment was carried out (Fig. 4). The beam pulse obtained this way is of about 40 microseconds duration, with a repetition rate of about 60 pulses per second. The deuteron energy is fixed by the path through the magnetic deflector channel and the steering magnet. This energy was determined from the curvature in the magnetic field and from the range in aluminum and corresponds to approximately 190 Mev. The variation in energy is thought to be less than ± 2 percent.

The beam was collimated by means of a four-foot brass plug so that it was about $\frac{1}{2}$ inch in diameter when it emerged from the shielding. The position and spread of this beam were measured by the blackening produced on x-ray films placed at several points along the beam path. The surface of the table which supported the apparatus was then oriented parallel to the plane containing the beam, target, and detector. The table was also adjusted so that fiducial marks inscribed for the purpose fell along the beam path as defined by the films. The alignment was checked frequently by means of films to insure that it was correct at each angular setting of the detector. The alignment is thought to be accurate to $\pm\frac{1}{2}$ degree.

In order to insure that the counts varied linearly with the number of deuterons incident, as indicated by Eq. (6), the beam intensity was adjusted so that the real coincidence counting rate per unit of collected charge was constant as a function of beam intensity. The beam intensity was always chosen so that the singles rate in any one chamber was about one count per beam pulse, since at this counting rate the number of accidental triple coincidences is negligible, as was shown by the beam plateau.

C. Beam Monitor

The deuteron beam was monitored with an argon-filled ionization chamber, whose multiplication factor for 190-Mev deuterons as determined by comparison with a Faraday cup, was 1525 charges collected per deuteron. The charge collected by the ionization chamber was placed on a low leakage condenser connected to the input grid of an integrating electrometer. The electrometer was of the 100 percent feedback type, and drove a continuous recorder which recycled itself after reaching a predetermined voltage. The recording circuit automatically calibrated itself periodically against a standard cell.

The condenser used was calibrated by means of an impedance bridge against a standard condenser whose capacitance is known to about 0.1 percent. The monitor system is believed to be accurate to ± 2 percent.

D. Targets

The beryllium, carbon, and uranium foil targets used in the experiment were all thin ($\sim$700 mg per cm^2) and

[7] C. E. Leith, Phys. Rev. **78**, 89 (1950).

cut from stock materials. These foils were mounted on a carriage which could be driven from a remote position. This arrangement made it simple to change targets with a minimum loss of running time, and a single no-target run sufficed to determine the background subtracted from all three targets for any one angle and energy determination. The targets were about 2 inches square, larger in lateral dimensions than the beam. This was checked photographically for the minimum and maximum angular positions of the target. The target carriage rotated upon a mount which also contained the detector telescope, and the target surface was at all times perpendicular to the line joining the target and the detector. The target thicknesses were made as nearly equal as possible, so that a change of target had a negligible effect upon the resolving power of the apparatus.

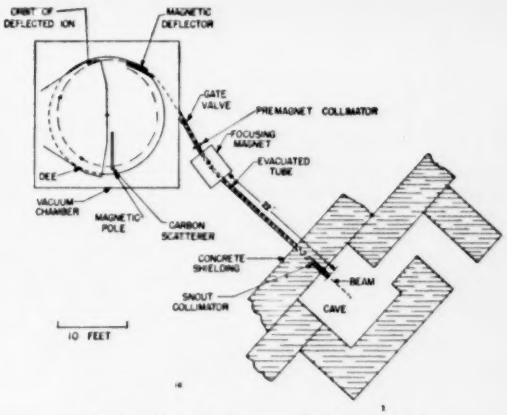

FIG. 4. Schematic diagram of cyclotron and shielded enclosure.

E. Absorber Correction

At the deuteron energy used in this experiment, the absorbers used to measure the emitted particle energies are so thick (up to several g/cm^2) that some particles which would otherwise pass through are removed by Rutherford scattering and nuclear absorption. The loss was ascertained as a function of aluminum absorber thickness by making an integral range determination using protons. The maximum correction used was of the order of 25 percent. An auxiliary experiment showed that the attenuation cross section for deuterons in aluminum is approximately twice that for protons.

F. Detector

In order to reduce the number of accidental coincidences due to background from the cyclotron and to define more sharply the direction from which the particles come, the detector consisted of a four-chamber proportional counter telescope, in front of which was placed a lead slit. The slit, two inches thick, had an opening one inch square which, at a distance of 30 inches from the target, defined the solid angle $\Delta\Omega_0$. The number of particles which have stopped in the range foil is then the number which traverse the first three chambers in coincidence, minus the number which traverse all four chambers in coincidence. In order to test that the counting rate varied linearly with solid angle as predicted by Eq. (6), a determination of counting rate was made as a function of the reciprocal of the square of the distance between the target and the slit. The dependence was found to be linear.

Each chamber of the telescope consisted of a multiwire, parallel-plate proportional counter, whose dimensions were 3 inches by 3 inches by $1\frac{1}{2}$ inches. The counter wires were made of 0.003-inch nickel, supported under spring tension by Teflon bars between brass frames. The spacing between wires was $\frac{3}{4}$ inch. The chamber volumes were defined by 0.0005-inch aluminum foils which were fastened across the brass frames. All the components were cleaned with chemicals and then rinsed with water. All four chambers were then mounted into a gas-tight box which was designed in such a way as to allow the range foil to be inserted between the third and fourth chambers from outside the box. A thin aluminum window allowed the particles to enter the telescope, and the electrical connections were brought out through Kovar seals in the roof of the box. After assembly, the box and its components were outgassed, flushed, and then filled with a mixture of 96 percent argon and 4 percent CO_2 to a pressure of one atmosphere.

The chambers were operated at about 2300 volts and the linear amplifier gains were adjusted so that the largest pulses were not quite overloading. Under these conditions, the typical plateau obtained by plotting the real coincidence rate against the discriminator bias setting on the first three chambers was adequate.

To test whether the fourth chamber was large enough in lateral dimensions to accept most of the particles from the one inch slit, the real coincidence rate was determined as a function of the amount of counter area open. This was done by putting a very thick shield in front of the fourth chamber and withdrawing it vertically. The main portion of the particles accepted by the slit lay well within the 3-inch by 3-inch face of the fourth chamber. The requirements placed on the detection system were found to be rather stringent, in that the telescope was required to detect charged particles over an extremely wide range of energies and hence, over an extremely wide range of ionization losses. In fact, the method of counting which was used introduces spurious counts which are the result of imperfect counting of particles in the fourth chamber and nuclear attenuation of particles in the range foil. The efficiency of the fourth chamber is less than unity because (a) particles which have energy sufficient to enter the fourth chamber may have been scattered enough to be missed, (b) the energy loss in the fourth chamber, being statistical, may fluctuate enough so that some particles

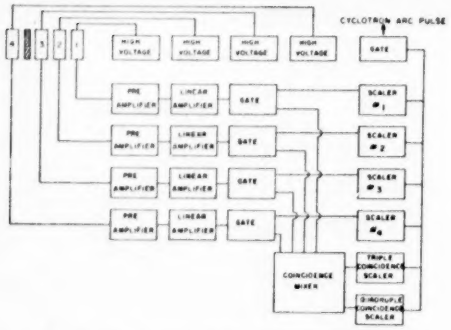

FIG. 5. Block diagram of the electronics associated with the detector.

are not counted, (c) the pulse from the fourth chamber may be delayed sufficiently (longer electron collection time in the counter, or electronic circuit delays) for some particles to be missed.

The range-foil material was tantalum, chosen because it was available in foil form in a variety of thicknesses, and because a material of high atomic weight was needed to give the most stopping power for the least nuclear absorption. The fourth chamber was large enough so that multiple scattering did not cause appreciable losses.

Correction runs were made for each experimental point to take account of the spurious events which the detector recorded because of its mode of operation. The correction to the data amounted to about 40 percent, at maximum, resulting in rather poor statistics for the real events at small angles.

G. Electronics

A block diagram of the electronic circuits associated with the operation of the counter telescope is shown in Fig. 5. Pulses from the first three chambers generated 2 microsecond gates, and pulses from the fourth chamber generated 3 microsecond gates which overlapped the others in time. The time delay in pulses from the fourth chamber relative to the pulses from the first three chambers was measured by the quadrupole coincidence rate, varying the delay on the gate from the fourth chamber. A small but finite contribution was missed, which was a contributing factor in making the fourth chamber efficiency less than unity. This jitter is believed to be the result not only of variation in ion collection time in the counter chambers, but also the effect of the response of the coincidence mixer circuits.

IV. RESULTS AND DISCUSSION

A. Presentation of Data

By the method indicated, the number of particles which stopped in the range foil per microampere of incident deuteron beam has been determined as a function of energy at laboratory angles of 7.5°, 10°, 15°, 20°, and 45°.

A set of composite curves, derived from both theory and experiment, with which to compare these points has been obtained by means of Eq. (6). The values used for the nucleon-nucleon differential cross sections $d^2\sigma(n,p)/d\Omega dT$, $d^2\sigma(p,n)/d\Omega dT$, and $d^2\sigma(n,d)/d\Omega dT$, were taken from the experiments of Hadley and York,[8] and Hoffmann and Strauch.[9] For the uranium target, the results of Hoffmann and Strauch were extrapolated from lead. As a first approximation, the differential cross section for producing protons by protons, $d^2\sigma(p,p)/d\Omega dT$, has been taken equal to that for producing protons by neutrons, $d^2\sigma(n,p)/d\Omega dT$, which has been verified in the case of scattering from hydrogen. The differential cross section for deuteron pick-up by protons $d^2\sigma(p,d)/d\Omega dT$ has been assumed equal to that for neutrons, $d^2\sigma(n,d)/d\Omega dT$. Finally, the shape of the stripping cross section, $d^2\sigma(d,p)/d\Omega dT$, has been computed from the theory of Serber and normalized to fit the observed points. This theory predicts the differential cross section to be

$$\frac{d^2\sigma(d,p)}{d\Omega dT}=\frac{CT_0^{\frac{1}{2}}}{[\frac{1}{2}\epsilon_d+T_1+T_0-2(T_1T_0)^{\frac{1}{2}}\cos\Phi_0]^2}, \quad (7)$$

where T_1 is one-half the incident deuteron kinetic energy, ϵ_d is the deuteron binding energy, Φ_0 is the angle between the beam direction and the emergent nucleon, and T_0 is the kinetic energy of the emergent nucleon.

An example of the construction of a resultant composite yield curve is shown in Fig. 6. The variation of the composite curves with angle is shown in Fig. 7 for the case of carbon.

Figures 8, 9, and 10 show the data, together with the appropriate composite curves. In these figures the composite curves have been corrected for absorber attenuation. The data have been normalized to counts per microcoulomb of incident deuterons and has been corrected for cyclotron background and detector effciency. The ranges of aluminum used in the experiment have been converted to energies on the proton scale by means of the curves of Aron *et al.*,[10] for both protons and deuterons which the counter telescope detected, so that a single energy scale suffices for both kinds of particles. The standard deviations shown are due to counting statistics only. The energy resolution of the detector for each point was determined by a graphical integration of Eq. (5), using the appropriate parameters at each energy.

B. Results

By fitting curves of the shape given by Eq. (6) to the experimental points at each angle, centered around 90

[8] J. Hadley and H. York, Phys. Rev. **80**, 345 (1950).
[9] K. Strauch and J. A. Hoffmann, Phys. Rev. **86**, 563 (1952).
[10] Aron, Hoffman, and Williams, U. S. Atomic Energy Commission Report AECU-663 (unpublished).

Mev, values of the proportionality constant C in Eq. (7) were determined. This enabled the total cross section for stripping to be computed by integrating Eq. (7). In view of the fact that stripping has a relatively small dependence upon atomic weight, the beryllium and carbon targets give the same cross sections, within the accuracy of the experiment. For this reason the cross sections determined from these two elements have been lumped together and averaged. The results are given in Table I. The weighted averages are:

beryllium or carbon $(0.35\pm0.03)\times10^{-24}$ cm^2,
uranium $(2.6\pm0.4)\times10^{-24}$ cm^2.

The standard deviations were computed from external consistency by assigning a standard deviation to the proportionality constant which was consistent with those attributed to the experimental points. It is felt that this procedure is justified, since the constant cannot be varied over wider limits and still have the composite curve fit the data so well.

In addition to the data shown, the charged particle yield was investigated as a function of energy in preliminary experiments at laboratory angles of 90° and 135°. The yields were low and dropped off rapidly with increasing energy and angle.

C. Conclusions

From the comparison of the experimental points and the composite curves, it can be said that the assumed interactions are indeed the principal collision mechanisms, at least to a first approximation. It is, of course, to be expected that the deuteron can be considered as a system of two independent nucleons, since the binding energy (~2.2 Mev) is small compared to the total kinetic energy (~190 Mev).

Beryllium and carbon were chosen as target nuclei in the hope that the loose neutron in beryllium might produce a large effect, compared to a nucleus with a closed structure, like carbon. No such effect was observed.

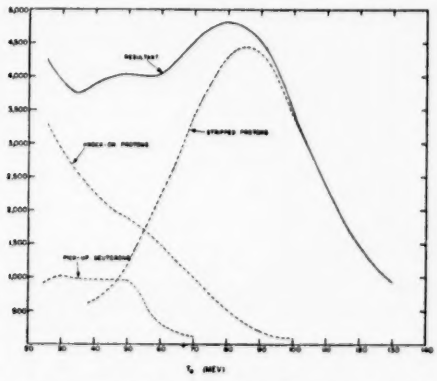

FIG. 6. Example of the construction of a composite yield curve from its components. The case shown is for the carbon target at $\Phi=10°$.

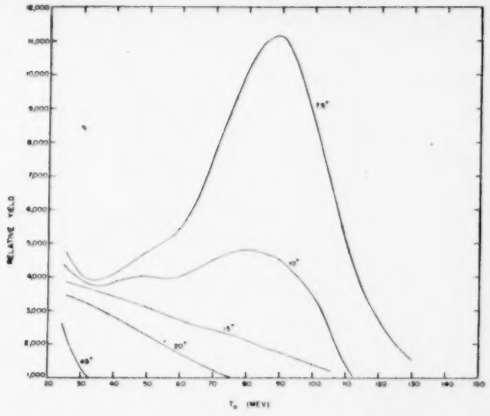

FIG. 7. A complete set of composite curves for the angles investigated experimentally. The case shown is for the carbon target.

With respect to the magnitude of the stripping cross section, the values 0.35 barn and 2.6 barns are much larger than the values of 0.12 barn and 0.43 barn which are to be expected from the Serber stripping theory for beryllium and uranium, respectively. Further, this theory predicts an $A^{\frac{1}{3}}$ dependence for the total stripping cross section. However, the values determined in this experiment indicate an $A^{\frac{1}{2}}$ dependence, shown in Fig. 11. This discrepancy in magnitude and dependence is not wholly unexpected, in view of the fact that the Serber theory does not include the large contribution to stripping which must result from the transparency of nuclear matter. For example, if the projected deuteron separation is such as to allow both nucleons of the deuteron to fall within the area defined by the nuclear diameter, it would be possible for one nucleon to be removed by collision, while the other passed through the transparent nucleus. For such collisions, the stripping cross section would more closely approximate the geometrical cross section, and a dependence faster than $A^{\frac{1}{3}}$ would result. Of course, the nucleus is not perfectly transparent, and the diameters of the heavy nuclei are of the order of several mean free paths for the nucleons with which we are concerned. This means that the shape of the differential cross section which was used to fit the data is certainly not correct. However, the shape cannot differ too much from the form used, and still permit a good fit to the data. The accuracy of the experiment does not permit a more detailed description of this enlarged differential stripping cross section.

The large cross section for uranium can be used to explain qualitatively the results of Helmholtz *et al.*,[11] in observing the angular distribution of neutrons from deuterons bombarding uranium targets. Their angular distribution fitted the shape predicted by the Serber theory alone. Now the Dancoff cross section for electric

[11] Helmholz, McMillan, and Sewell, Phys. Rev. **72**, 1003 (1947).

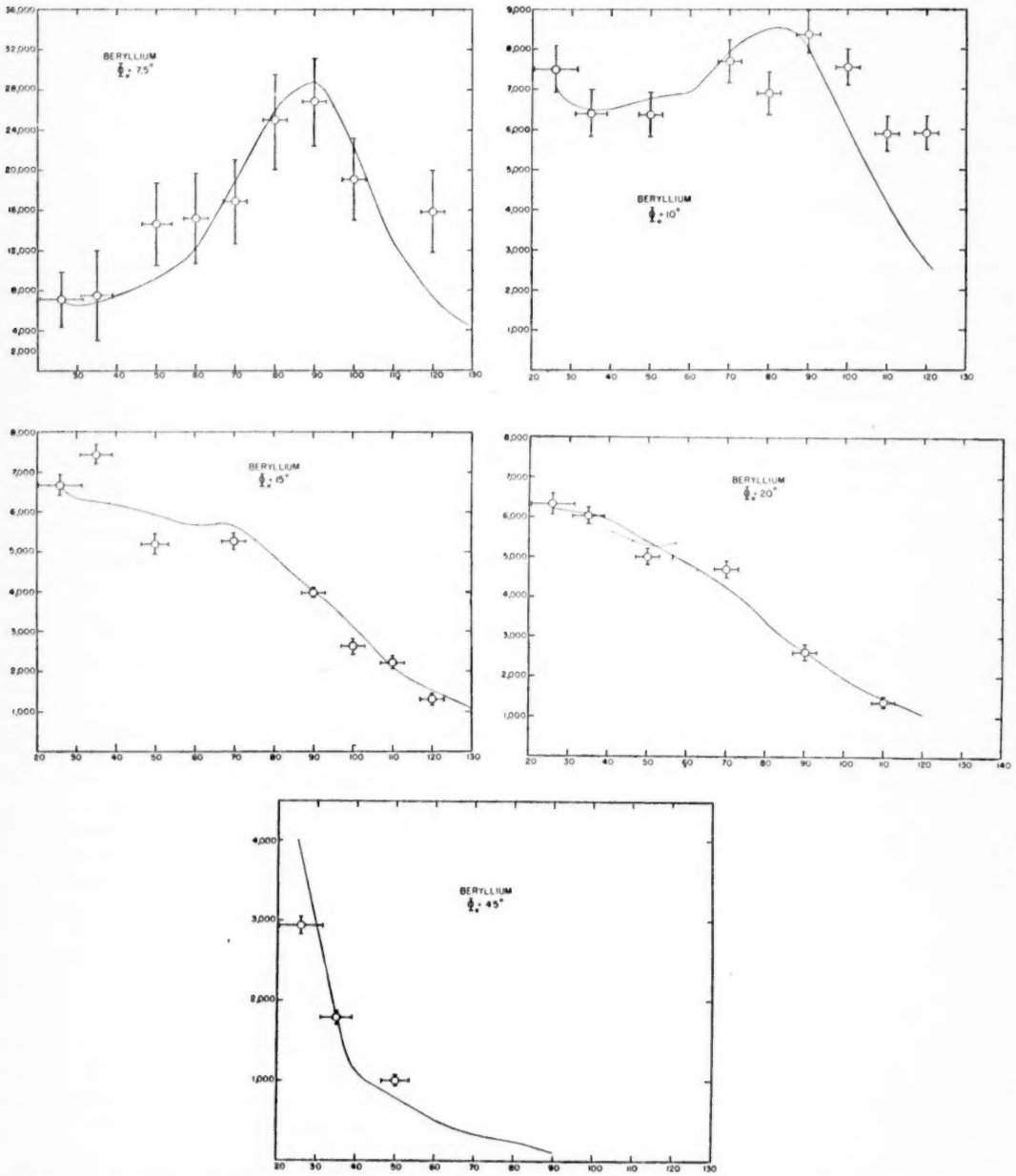

FIG. 8. The energy distributions of secondary charged particles from a thin beryllium target at laboratory angles of 7.5°, 10°, 15°, 20°, and 45°. The abscissas are in Mev on the proton energy scale. The ordinates are in number of counts detected per microcoulomb of incident deuterons.

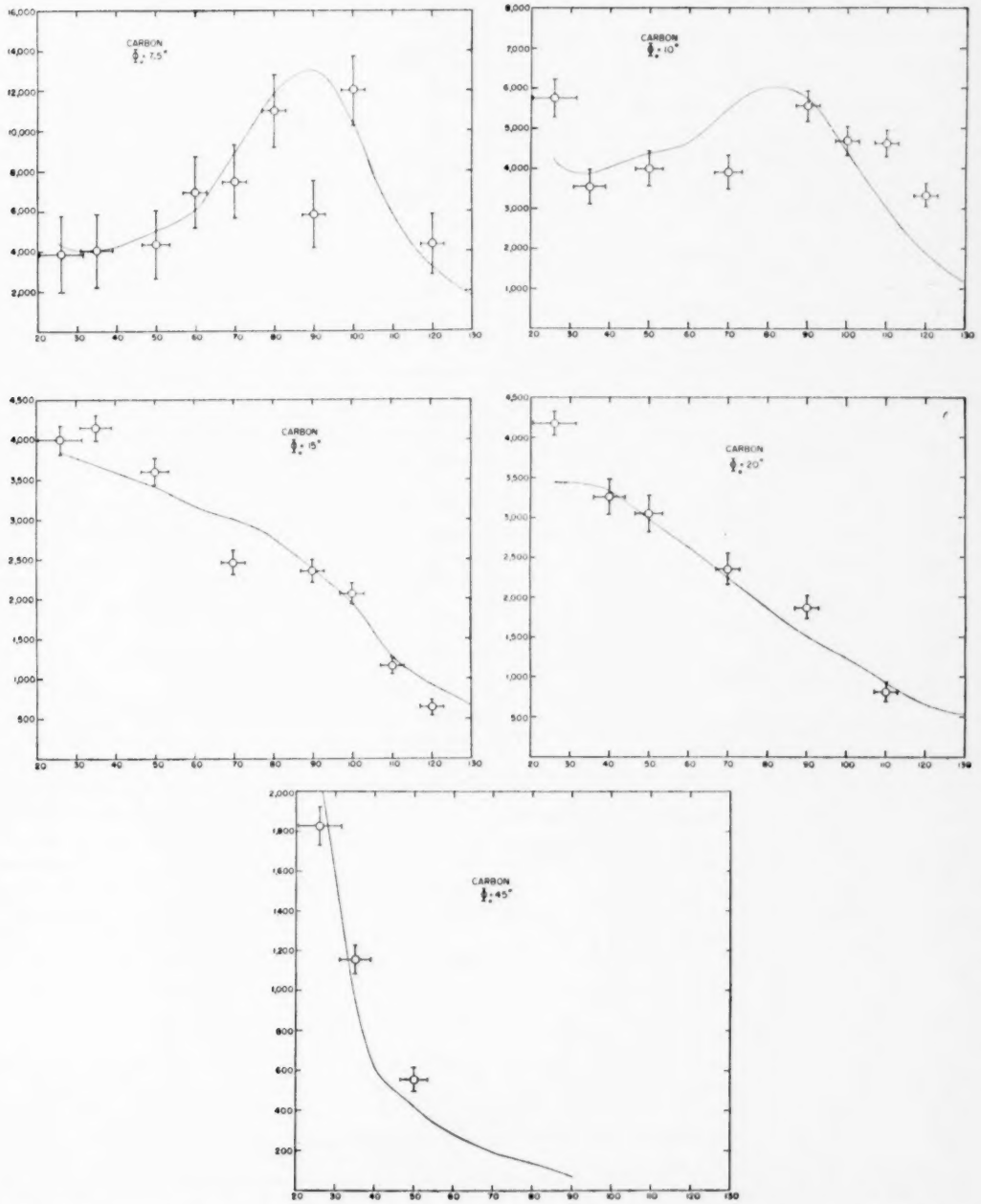

FIG. 9. The energy distributions of secondary charged particles from a thin carbon target at laboratory angles of 7.5°, 10°, 15°, 20°, and 45°. The abscissas are in Mev on the proton energy scale. The ordinates are in number of counts detected per microcoulomb of incident deuterons.

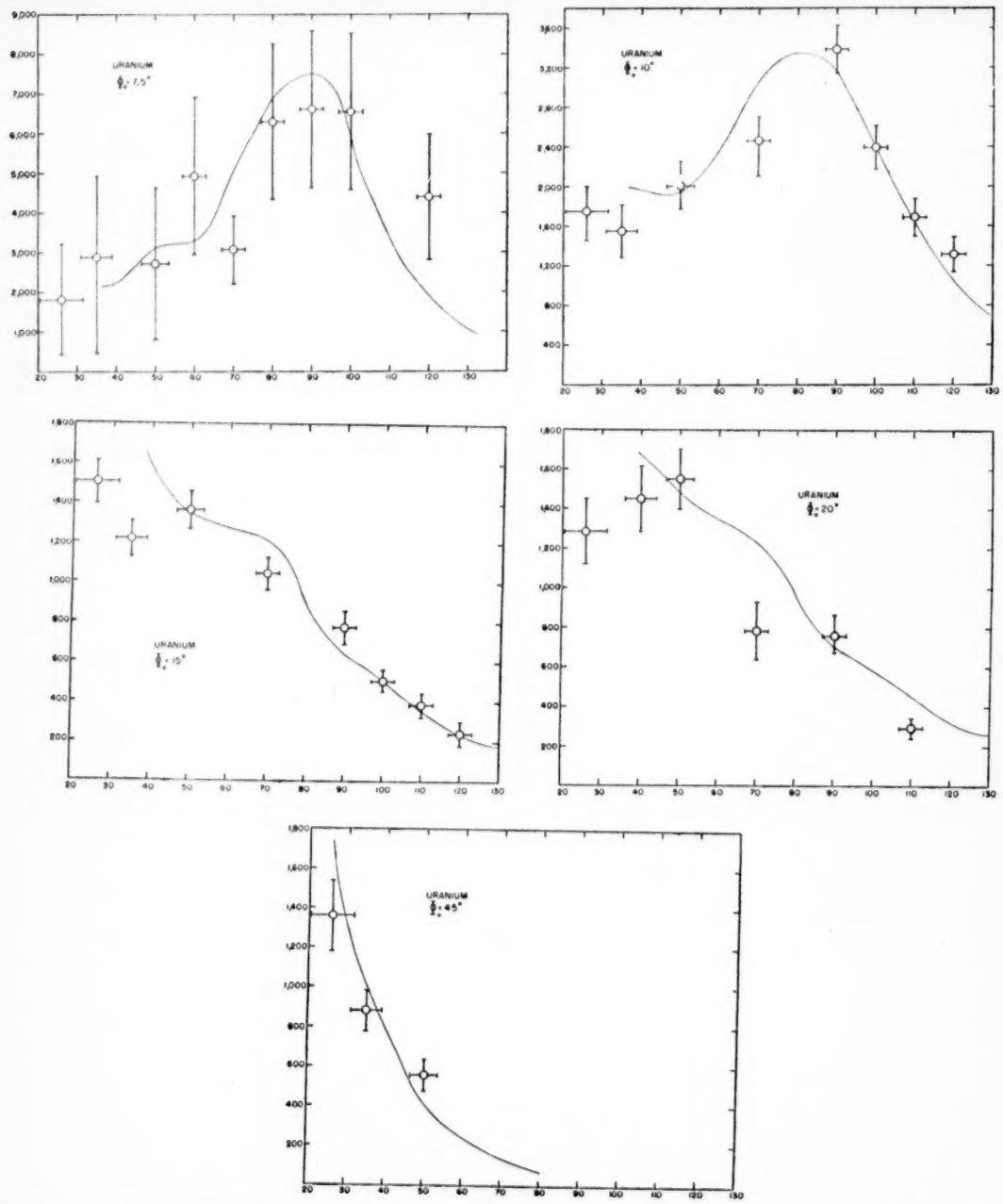

FIG. 10. The energy distributions of secondary charged particles from a thin uranium target at laboratory angles of 7.5°, 10°, 15°, 20°, and 45°. The abscissas are in Mev on the proton energy scale. The ordinates are in number of counts detected per microcoulomb of incident deuterons.

field stripping was predicted to be about 0.1 barn in uranium, compared to 0.43 barn for the Serber process. Therefore, since the angular distribution from electric stripping is much narrower than that from the Serber theory, a total angular distribution is to be expected that is somewhat narrower than was observed, corresponding to a superposition of these two effects. This was hard to understand, as long as the Serber process was the only expected one. However, comparing the 0.1 barn for electric stripping in uranium to the enlarged

TABLE I. The measured cross sections and their weighted averages.

$$\Sigma=\int\int\frac{d^2\sigma}{d\Omega dT}dTd\Omega=2\pi C\int_0^\infty\int_0^\pi\frac{T_0^{\frac{1}{2}}\sin\phi_0 d\phi_0 dT_0}{[\frac{1}{2}\epsilon_d+T_0+T_1-2(T_1T_0)^{\frac{1}{2}}\cos\phi_0]^2}=\frac{4\pi^2C}{(2\epsilon_d)^{\frac{1}{2}}}.$$

Target	Angle	Σ (barns)	
Be	7.5°	0.40±0.03	
	10°	0.26±0.02	
	15°	0.34±0.01	
	20°	0.58±0.05	
C	7.5°	0.33±0.06	Σ_{Av}(Be or C) = (0.35±0.03) barn
	10°	0.36±0.03	
	15°	0.38±0.02	
	20°	0.64±0.07	
U	7.5°	2.9±0.8	
	10°	2.9±0.1	
	15°	1.6±0.2	Σ_{Av}(U) = (2.6±0.4) barns
	20°	4.6±0.7	

stripping cross section of 2.6 barns, with its angular distribution similar to that of Serber, the results of the neutron angular distribution measurements are quite reasonable.

The high total yield of neutrons observed by Knox[12] can also be qualitatively explained by the values of the enlarged stripping cross sections without invoking contributions from the electric stripping, which appears to be negligible in comparison.

D. Comparison with Theory

Although it was expected that the nuclear transparency should allow some contribution to stripping from the central portion of the nucleus, that contribution cannot be calculated easily. However, a few simple considerations can give some ideas concerning the quantities measured in this experiment.

Let σ_S be the Serber stripping cross section, σ_D be the Dancoff electric stripping cross section, τ_S be the transparency factor for 90-Mev nucleons near the edge of the nucleus, τ be the transparency factor for 90-Mev nucleons which pass through the main body of the nucleus, and R be the nuclear radius. The total stripping cross section can then be roughly represented by

$$\sigma=\sigma_S+\sigma_S\tau_S+(\pi R^2-\sigma_S)\tau+\sigma_D. \quad (8)$$

That is, σ_S is the cross section for the proton missing the nucleus, while the neutron hits the edge; $\sigma_S\tau_S$ is the cross section for the neutron missing the nucleus while the proton hits the edge, but traverses with probability τ_S; $(\pi R^2-\sigma_S)$ is the probability that both the incident nucleons strike the nucleus, and, when multiplied by τ, gives the cross section for the proton emission.

As a rough approximation, we can take τ_S equal to unity; it is probably somewhat larger than τ. A value for τ can be inferred from the analysis of neutron scattering made by Fernbach, Serber, and Taylor.[13] They find that the absorption cross sections for 90-Mev nucleons in beryllium and uranium are 0.55 and 0.88 of the geometric cross sections, respectively. This means that the respective transparency factors in these nuclei are 0.45 and 0.12, which lead to total stripping cross section values of approximately 0.33 barn for beryllium and approximately 1.3 barns for uranium. Comparing these with the measured values, it would seem that while the agreement in the case of beryllium is excellent, this simple mechanism does not account for the high uranium value. If, on the other hand, the theory is roughly correct, the measurement implies a nuclear transparency of about 0.6 for uranium, which is clearly in disagreement with absorption cross-section measurements. Part of the discrepancy in the uranium case can be accounted for by using a radius in Eq. (8)

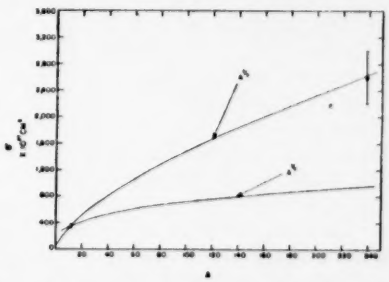

FIG. 11. The enlarged stripping cross section as a function of atomic weight.

which is enlarged to include the range of nuclear forces, as has been necessary to explain other nuclear collision processes. Probably the main reason for the disagreement is to be found in our neglect of the opaqueness of the uranium nucleus, in which case the agreement within a factor of two with the simple theory is mainly fortuitous. This is to be expected from the breakdown of the impulse approximation at the larger angles, rendering Eq. (7) invalid.

The authors wish to express their sincere gratitude to Professor A. C. Helmholz for his valuable guidance and support in all phases of the work. The assistance and the continued encouragement of Dr. C. M. Van Atta are gratefully acknowledged. The authors are also indebted to Dr. Warren Heckrotte for enlightening discussions concerning the interpretation of the results. Finally, thanks are due the members of the cyclotron crew, the accelerator technicians, and the electronics maintenance group, whose combined efforts made the investigation possible.

[12] W. J. Knox, Phys. Rev. **81**, 687 (1951).

[13] Fernbach, Serber, and Taylor, Phys. Rev. **75**, 1352 (1949).

Time Distribution of Positron Annihilation in Liquids and Solids

R. E. Bell and R. L. Graham
Physics Division, Atomic Energy of Canada Limited, Chalk River Laboratory, Chalk River, Ontario, Canada
(Received January 12, 1953)

The time distribution of the annihilation radiation emerging from liquids and solids, following the absorption by the samples of fast positrons, has been studied by the delayed coincidence method. The mean life of positrons in metals is found to be about 1.5×10^{-10} sec, nearly independent of the metal chosen. Some simple crystals behave similarly, but many amorphous substances, both solid and liquid, show a complex time decay in which about $\frac{3}{4}$ of the positrons annihilate with mean life a few times 10^{-10} second, and the remaining $\frac{1}{4}$ with mean life from 0.45×10^{-9} sec to 3.5×10^{-9} sec, depending on the substance. This longer lifetime is shown to decrease, in general, as the sample is cooled. Placing the sample in moderate electric and magnetic fields has no detectable effect. The long-delayed radiation is shown to be similar in energy and angular distribution to the more prompt component. Tentative interpretations of these facts are given, but some points still await a full explanation.

I. INTRODUCTION

A STUDY is being made of the time distribution of the annihilation radiation emerging from samples of condensed materials (solids and liquids) following the absorption by the samples of fast positrons. The time intervals measured thus include the time required for the positrons to slow down to the low energy at which most of the annihilations are generally supposed to take place, as well as the life of the positrons after reaching that energy. The measurements are made by the delayed coincidence method, using scintillation counters and a coincidence circuit[1] of resolving time $2\tau_0\sim2\times10^{-9}$ sec. Results have been obtained for a number of metals, nonmetallic crystals, liquids, and amorphous solids. Many of the materials in the latter two categories show a complex time decay curve which has two distinct components of comparable intensity with different mean lives. Preliminary reports of some of the results described in this paper were given at the 1952 Washington Meeting of the American Physical Society and at the 1952 Quebec Meeting of the Royal Society of Canada.[2]

Following the work of Deutsch and his collaborators[3] on the time decay of the annihilation radiation from positrons absorbed in gases, leading to the discovery of positronium, a number of workers[4–6] have attempted to measure the mean life of positrons in solids and liquids. The lifetimes in liquids and solids are expected to lie in the 10^{-9} to 10^{-10} sec range and hence are more difficult to measure than in the case of gases. Moore[4] has obtained a value of τ (mean life) of positrons in stilbene of $(1.0\pm0.5)\times10^{-9}$ sec. Millett's[5] results on Plexiglas suggest $\tau=1.4\times10^{-9}$ sec. An extensive series of comparison measurements by DeBenedetti and Richings[6] has shown that the difference in positron mean life between various metals is $(0\pm0.5)\times10^{-10}$ sec, but that mean lives in certain amorphous materials and liquids are longer than those of the metals by (2 to 4)$\times10^{-10}$ sec. The actual values of τ were not measured. De Benedetti and Richings did not carry their measured curves out to sufficiently long delays to detect the complex time behavior reported here for some of the same amorphous materials.

II. EXPERIMENTAL ARRANGEMENTS AND RESULTS

(a) Lifetime Measurements

The first measurements in this study were made by a method using a pair of lens beta-ray spectrometers placed end to end,[7] as shown in Fig. 1. The left-hand scintillation counter, shown enlarged in Fig. 1(b) consisted of a stilbene crystal, a short Lucite light-pipe, and a 1P21 photomultiplier, all enclosed in an iron block for magnetic shielding. The stilbene crystal, which was $\frac{1}{4}$ inch in diameter and 50 mg/cm^2 thick, covered a small hole in the Lucite light pipe in which was inserted a source of the positron emitter, Na^{22}. Thus each positron entering the spectrometer from the source had already passed through the stilbene crystal and given a zero of time to the coincidence circuit to which the two scintillation counters were connected. The positrons passed through the left-hand spectrometer, Fig. 1(a), and were focused onto a $\frac{1}{2}$-in. hole in the baffle separating the two spectrometers. The positrons passing through the hole were already selected in energy and trajectory, so that the right-hand spectrometer was not provided with a baffle. The scintillation counter for the right-hand spectrometer used a 1 cm^3 crystal of diphenylacetylene over which the sample under test was placed, as shown in Fig. 1(c). Thus positrons entering the right hand spectrometer could strike no material other than the sample under test. With the sample removed, the focused positrons fell directly on the right-hand scintillation crystal, and the two counters of Fig. 1 then supplied the coincidence circuit with

[1] Bell, Graham, and Petch, Can. J. Phys. **30**, 35 (1952).
[2] R. E. Bell and R. L. Graham, Phys. Rev. **87**, 236 (1952); June Meeting, Quebec, Royal Society of Canada (1952).
[3] J. W. Shearer and M. Deutsch, Phys. Rev. **76**, 462 (1949); M. Deutsch, Phys. Rev. **82**, 455 (1951); **83**, 207 (1951); **83**, 866 (1951).
[4] D. C. Moore, Phys. Rev. **82**, 336 (1951).
[5] W. E. Millett, Phys. Rev. **82**, 336 (1951).
[6] S. DeBenedetti and H. J. Richings, Phys. Rev. **85**, 377 (1952).
[7] R. E. Bell and R. L. Graham, Phys. Rev. **86**, 212 (1952).

coincidences that were prompt, except for the fixed transit time of the positrons through the pair of spectrometers. When the sample was in place, the positrons were absorbed in it and the diphenylacetylene counter detected a fraction of the annihilation quanta emerging from the sample. The coincidence circuit then received coincidences having delays equal to the lifetimes of the positrons in the sample. The measurement of the lifetime properties of positrons absorbed in any particular sample material consisted of a comparison of sample-out (prompt) and sample-in (delayed) conditions by the usual delayed-coincidence method. The methods used for analysis of the coincidence resolution curves so obtained have been described in a previous paper.[1]

The positron energy selected by the spectrometers was 220 kev, kept constant throughout the measurements. The selected positrons had already dissipated about 150 kev in the 50 mg/cm^2 stilbene crystal of the source counter, Fig. 1(b), and so must have left the source with an energy around 370 kev, a point of favorable intensity in the 575-kev β^+ spectrum of Na^{22}. With the sample out the full positron energy, 220 kev, was dissipated in the diphenyacetylene crystal of the sample counter, Fig. 1(c). With the sample in place, this counter registered the Compton recoil electron distribution of a 511-kev gamma-ray, extending from 0 to 341 kev. Since the discriminator for this counter was biased to reject pulses of size corresponding to less than ~150 kev, the average pulse height when counting gamma-rays with the sample in (150–340 kev) was approximately equal to that when counting positrons directly with the sample out (220 kev). Diphenylacetylene was chosen as a phosphor for this counter in preference to stilbene because preliminary measurements showed that the mean time delay for the appearance of the first photoelectron in the photomultiplier ($\dot{t}$, in the notation of reference 1) is smaller by a factor of about 2 for diphenylacetylene than for stilbene. The difference in time delay caused by inequality of the pulse sizes between the sample-out and sample-in conditions is estimated to be less than 2×10^{-11} sec.

The method just described has the disadvantage of requiring the sample under test to be placed in the vacuum of the spectrometer. It has, however, a number of advantages over simpler arrangements. It gives the value of the mean life absolutely, and not merely by comparison with that of another sample. The method does not depend on the nuclear properties of the source. It is nearly free of chance coincidences, since nearly every true count in the sample counter corresponds to a coincidence event. Unwanted genuine counts due to annihilation in materials other than the sample are negligible because of the double spectrometer arrangement.

The samples used in this method were in the form of disks 1-inch or more in diameter and at least thick enough to stop 220-kev positrons. Finely divided materials were either pressed into the required form or held together by adding about 1 percent by weight of plastic binder.

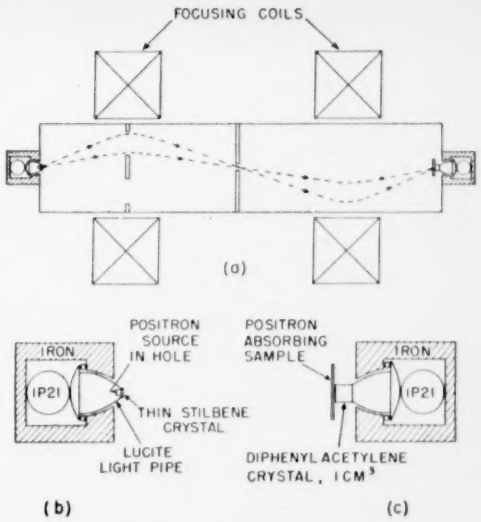

FIG. 1. Pair of identical end-to-end β-ray spectrometers which are operated with the coils in series. Positrons emerging through the stilbene crystal of the left scintillation counter, shown enlarged in (b), are selected in energy and trajectory by the left spectrometer. Positrons, which pass through the hole in the central diaphragm into the right spectrometer, can strike only the sample placed in front of the right hand, γ-sensitive scintillation counter, shown enlarged in (c) or the diphenylacetylene crystal of the counter directly if the sample is removed. The scintillation counters are connected to a coincidence circuit (not shown) of resolving time $2\tau_0=2\times10^{-9}$ sec.

The results for the first sample, aluminum, are shown in Fig. 2, in the form of a pair of coincidence resolution curves. The procedures used in recording these curves were those of reference 1, the inserted time delay x being provided by the motor-driven helical delay unit described there. The prompt curve $P(x)$ (sample out) yielded a counting rate at its peak of several hundred counts per minute, and was recorded during the daytime hours. The delayed curve, marked "aluminum sample" in Fig. 2, yielded a counting rate about 5 percent as great, and was recorded overnight, the prompt curve being repeated the next day as a check. The two curves have been plotted to the same included area in Fig. 2. The same procedure was followed for all the samples measured by this method. In all cases the $P(x)$ curve was separately determined for each sample and not merely repeated from Fig. 2.

The displacement of the centroid of the aluminum curve (Fig. 2) to the right of that of the prompt curve shows that 220-kev positrons entering aluminum have a mean life τ of about 1.5×10^{-10} sec. The resolution is not sufficient to prove that the time decay is exponential; the result is, however, consistent with this assumption.

A run with a gold sample gave a result similar to that for aluminum, the indicated value of τ being 1.2×10^{-10}

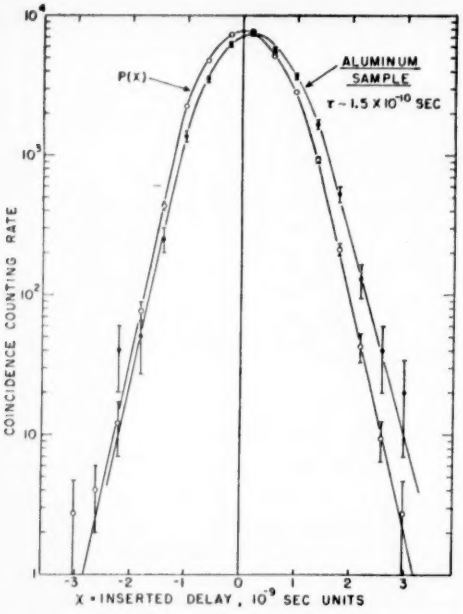

FIG. 2. Coincidence resolution curves. The delayed curve (solid circles) was obtained when the positrons were absorbed in a sample of aluminum, and the prompt curve $P(x)$ was obtained when the sample was removed and positrons were detected directly by the crystal of the right counter in Fig. 1. In this and in Figs. 3 to 8 $P(x)$ is an average of the prompt runs taken immediately before and after the run with sample in position. The standard deviations are shown by vertical bars.

sec. These results and others reported later in this paper support the findings of DeBenedetti and Richings on the near consistency of τ with different metals. The probable error in these values of τ, due to statistics and the uncertainty in $\bar{t}$ mentioned above, is about 0.3×10^{-10} sec, and it is therefore not possible to say definitely whether the mean life in Au is slightly shorter than that in Al.

Figure 3 gives the results for a single crystal of α-quartz (SiO_2).[8] Again we have an apparently simple time decay with $\tau=(2.0\pm0.3)\times10^{-10}$ sec. Proceeding to Fig. 4, the sample has been changed from the crystalline quartz of Fig. 3 to fused quartz (a piece of fused quartz laboratory ware). The delayed resolution curve is now seen to split naturally into two components, one of mean life $\tau_1=(3.5\pm0.5)\times10^{-10}$ sec, and the other an apparently exponential decay of mean life $\tau_2=(1.8\pm0.2)\times10^{-9}$ sec. These values were obtained in the following manner. Taking the value of τ_2 from the slope of the tail and knowing the shape of $P(x)$ the part of the resolution curve due to τ_2 alone was numerically calculated and is shown in Fig. 4 as a broken line; the τ_1 component is obtained by subtraction. The areas under the two separate curves give the relative proportions of positrons annihilating with mean lives τ_1 and τ_2 as (71±5) percent and (29±5) percent, respectively.

This complex time-decay phenomenon is observed in a large number of substances, usually, but not always, amorphous or liquid in structure. Figure 5, for example, gives the curve for a polystyrene sample, which yields the result $\tau_1=(3.7\pm0.5)\times10^{-10}$ sec (64±5) percent, and $\tau_2=(2.3\pm0.2)\times10^{-9}$ sec, (36±5) percent. Behavior similar to that of polystyrene has been observed in paraffin wax, cellulose nitrate, polyethylene, Teflon [polytetrafluoroethylene, $(CF_2)_n$], water, ice, methyl alcohol, and isopropyl alcohol. Not all of these have been measured in great detail and not all by the present method. Further results on some of them are given later.

The three forms of carbon—diamond, "amorphous" carbon, and graphite—were examined, and results are shown in Fig. 6 for the first two. The diamond was in the form of powder and the amorphous carbon was low temperature sugar charcoal. Each shows only a single mean life, and the graphite result (not shown) was similar. The indicated values of τ for diamond, amorphous carbon, and graphite are, respectively, $(1.3\pm0.3)\times10^{-10}$, $(4.3\pm0.4)\times10^{-10}$, and $(3.0\pm0.3)\times10^{-10}$ second, and are roughly inversely proportional to the densities of the substances. No indication of a longer-lived component is seen on any of the carbon curves. The very weak tail on the right-hand part of

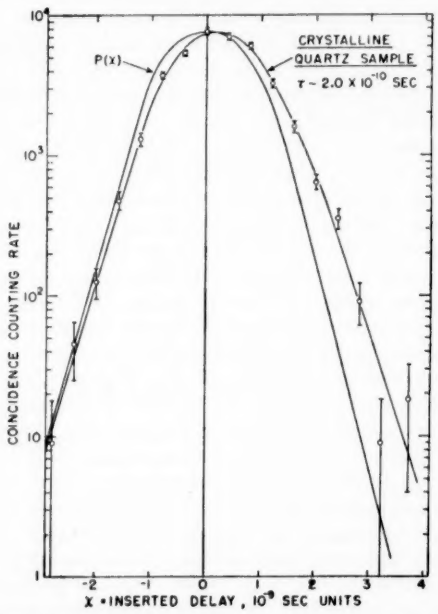

FIG. 3. Coincidence resolution curve obtained with a sample of crystalline α-quartz with a prompt curve $P(x)$ for comparison. Since the prompt curve was always better determined statistically than the delayed curve, the experimental points have been omitted from $P(x)$ here and also in Figs. 4–8. The standard deviations of the points in the delayed curve are shown by vertical bars.

[8] The α-quartz sample was kindly supplied by Dr. D. G. Hurst.

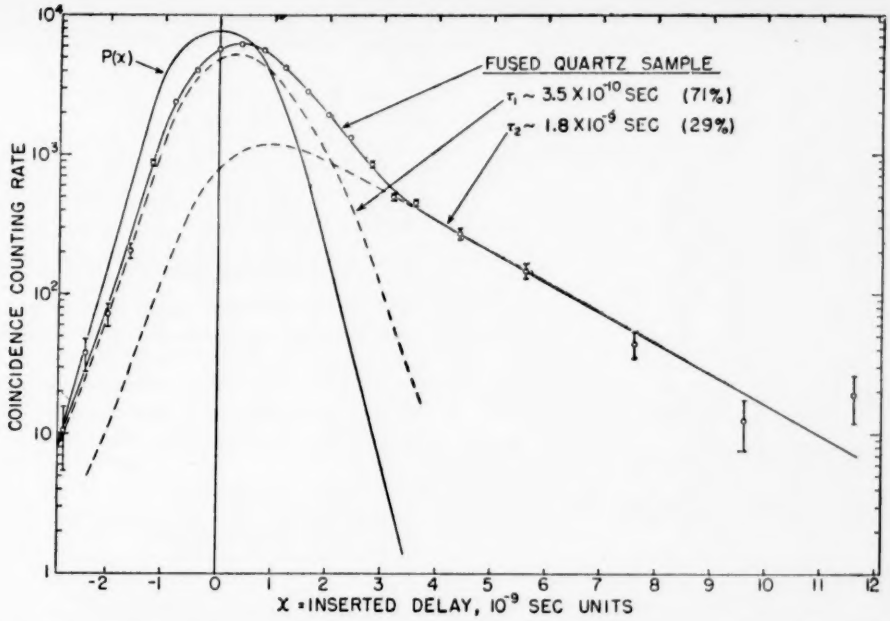
P(x)
FUSED QUARTZ SAMPLE
$\tau_1 \sim 3.5 \times 10^{-10}$ SEC (71%)
$\tau_2 \sim 1.8 \times 10^{-9}$ SEC (29%)
COINCIDENCE COUNTING RATE
X = INSERTED DELAY, 10^{-9} SEC UNITS

FIG. 4. Coincidence resolution curve obtained with a sample of fused quartz laboratory ware, with a prompt curve $P(x)$ for comparison. The standard deviations are shown by vertical bars.

the curve for diamond can be attributed to the plastic binder used to hold the diamond powder together.

A comparison of monoclinic crystal sulfur with plastic sulfur is shown in Fig. 7. The plastic sulfur was prepared by pouring sulfur heated nearly to its boiling point into cold water. (Plastic sulfur prepared in this way probably contains some sulfur crystals.) It is interesting to see in Fig. 7 that while the crystalline sulfur result is consistent with a single $\tau = 2.1 \times 10^{-10}$ sec, the plastic sulfur curve is inconsistent with the assumption of any single

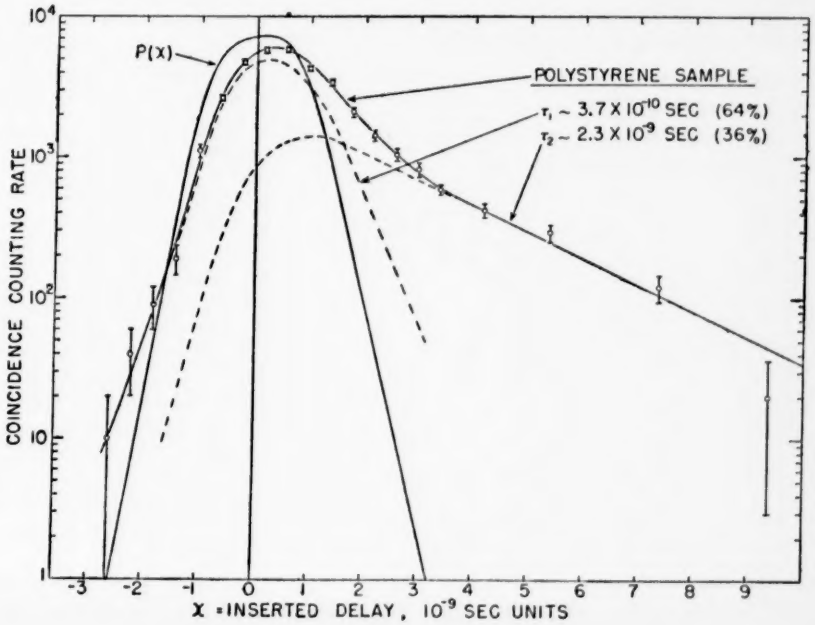
P(x)
POLYSTYRENE SAMPLE
$\tau_1 \sim 3.7 \times 10^{-10}$ SEC (64%)
$\tau_2 \sim 2.3 \times 10^{-9}$ SEC (36%)
COINCIDENCE COUNTING RATE
X = INSERTED DELAY, 10^{-9} SEC UNITS

FIG. 5. Coincidence resolution curve obtained with a sample of polystyrene with a prompt curve $P(x)$ for comparison. The standard deviations are shown by vertical bars.

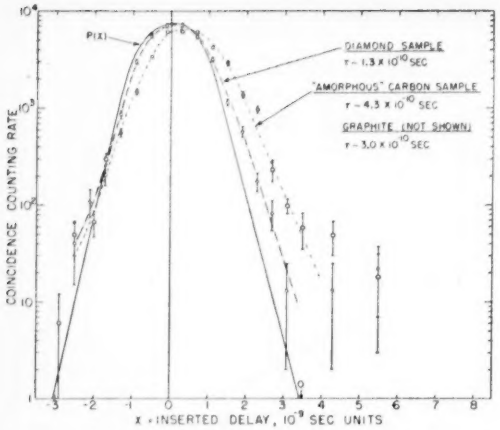
P(x)
DIAMOND SAMPLE
τ ~ 1.3 × 10^-10 SEC
"AMORPHOUS" CARBON SAMPLE
τ ~ 4.3 × 10^-10 SEC
GRAPHITE (NOT SHOWN)
τ ~ 3.0 × 10^-10 SEC
COINCIDENCE COUNTING RATE
x = INSERTED DELAY, 10^-9 SEC UNITS

FIG. 6. Coincidence resolution curves obtained with a sample of diamond powder, and a sample of amorphous carbon (low temperature sugar charcoal) together with a prompt curve $P(x)$ for comparison. The standard deviations are shown by vertical bars.

mean life. The curve fails to have its maximum at its intersection with $P(x)$,[9] and the shift of its centroid is inconsistent with the slope of its tail.[1] The plastic sulfur curve could be fitted, as mentioned in Fig. 7, by two components having mean lives $\tau_1 = 1.5 \times 10^{-10}$ sec and $\tau_2 = 4.5 \times 10^{-10}$ sec, the latter decay being at least roughly exponential. These values must be regarded as estimates only, but this observation on the two forms of sulfur is of value as a parallel to the results on the two forms of quartz. Plastic sulfur is the only elementary substance so far tried that shows signs of the longer-lifetime phenomenon.

Figure 8 shows the results for a sample of vitreous $Na_2B_4O_7$ made by melting borax with a glassblowing

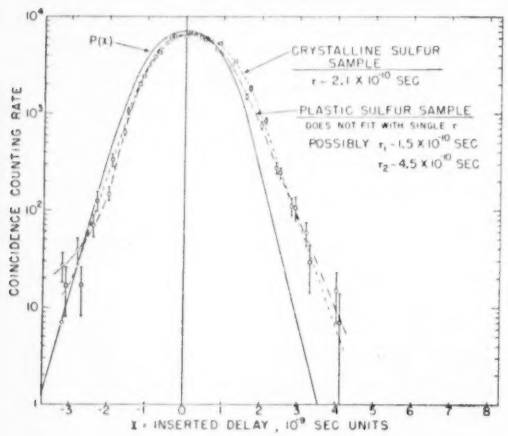
P(x)
CRYSTALLINE SULFUR SAMPLE
τ ~ 2.1 × 10^-10 SEC
PLASTIC SULFUR SAMPLE
DOES NOT FIT WITH SINGLE τ
POSSIBLY τ1 ~ 1.5 × 10^-10 SEC
τ2 ~ 4.5 × 10^-10 SEC
COINCIDENCE COUNTING RATE
x = INSERTED DELAY, 10^-9 SEC UNITS

FIG. 7. Coincidence resolution curves obtained with a sample of monoclinic crystal sulfur and a sample of plastic sulfur together with a prompt curve $P(x)$ for comparison. The standard deviations are shown by vertical bars.

[9] T. D. Newton, Phys. Rev. **78**, 490 (1950) and reference 1.

torch. Here the longer lifetime is clearly present, yielding $\tau_2 = (8.7 \pm 1.2) \times 10^{-10}$ sec, but it is not as long as in the polystyrene and fused quartz cases. The intensity of the τ_2 component, 32 percent, is comparable with that for the previous cases.

A sample of crystalline NaCl gave a result similar in appearance to that for aluminum, the indicated mean life being $(2.3 \pm 0.3) \times 10^{-10}$ sec, with no sign of any longer-lived component.

(b) Factors Influencing the Lifetimes

In order to make the samples more readily accessible, a series of measurements was next made in an arrangement similar to that of De Benedetti and Richings,[6] illustrated in Fig. 9. Here a thin source of Na^{22} sealed between two 2 mg/cm² Al foils is sandwiched between layers of the sample material, or immersed in it if it is

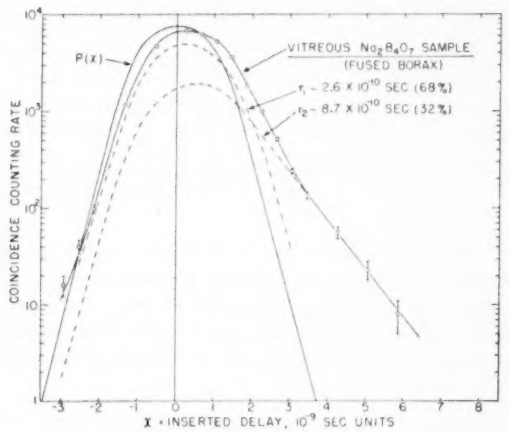
P(x)
VITREOUS Na2B4O7 SAMPLE
(FUSED BORAX)
τ1 ~ 2.6 × 10^-10 SEC (68%)
τ2 ~ 8.7 × 10^-10 SEC (32%)
COINCIDENCE COUNTING RATE
x = INSERTED DELAY, 10^-9 SEC UNITS

FIG. 8. Coincidence resolution curve obtained with a sample of vitreous $Na_2B_4O_7$ and a prompt curve $P(x)$ for comparison. The standard deviations of the points are shown by vertical bars.

a liquid. Under these conditions most of the positrons from the source enter the sample material and are stopped there, but a certain fraction of them will be annihilated in the aluminum source envelope. Since this fraction may be expected to vary with the atomic number and density of the sample material, this arrangement is not as suitable for absolute measurements of the intensity of the longer-lived component as the previous one. In addition, it is not convenient in such an arrangement to measure absolute lifetimes, and the result will consist of comparisons of the lifetimes for different substances.

Simple arrangements, not shown in Fig. 9, were made to allow the source and sample assembly to be cooled to dry ice or liquid nitrogen temperature, in order to study the effect of temperature on the phenomena already found.

In Fig. 9, stilbene counter 1 is biased so as to count only the 1.28-Mev nuclear gamma-ray accompanying

the emission of each positron from the Na^{22} source. Stilbene counter 2 is biased to count annihilation gamma-rays from the sample, and coincidences between counters 1 and 2 can be analyzed for delayed events in the same way as previously, except that now a comparison sample (usually aluminum) must be used in addition to the sample under study.

A series of results for four metals is shown in Fig. 10. The results are all very similar for beryllium, aluminum, copper, and liquid mercury. The latter shows no sign of the long-lifetime effect in spite of the fact that it is a liquid. Small arrows in Fig. 10 mark the centroids of the resolution curves. The centroids shift to the right by about 0.5×10^{-10} sec as we go from mercury to beryllium. This shift is hardly outside the limits of error, but if it is real it would suggest that the mean life of positrons in light metals is very slightly longer than that in heavier metals. The outstanding feature of Fig. 10, however, is the similarity of the four curves, and we summarize the results with metals by saying that the mean life for metals is constant ±25 percent, independent of the metal chosen.

Results with water are shown in Fig. 11. Here we have plotted the curves for water at room temperature,

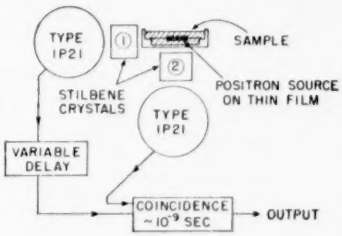

FIG. 9. Arrangement of scintillation counters for examining liquid as well as solid samples.

brine (saturated NaCl solution) at room temperature, ice at -7°C, and ice at -196°C, with an aluminum curve for comparison. One might have expected water and ice to yield results similar to those obtained for fused and crystalline quartz. In fact, however, all the forms of water and ice show the long-lived effect, the value of τ_2 changing from 1.7×10^{-9} sec (water, room temperature) to 1.2×10^{-9} sec (ice, -7°C), to 0.85×10^{-9} sec (ice, -196°C). The intensity does not seem to be altered much by temperature changes. The brine result, $\tau_2=1.5\times10^{-9}$ sec, shows that any slight impurity of the water used is unlikely to introduce any serious error in the result for water, and is interesting because crystalline NaCl has already been shown not to display the longer lifetime.

The effect of variation of temperature of a sample of fused quartz is shown in Fig. 12. It may be seen that there is little difference in either lifetime or relative intensity of the longer lived component between 20°C and -196°C. In Fig. 13 a similar set of curves is shown for a teflon sample, which has the longest τ_2 at room temperature of any substance so far tested. Teflon shows a marked variation in τ_2 with temperature, the

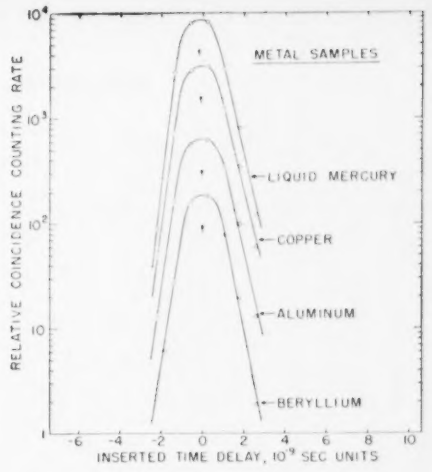

FIG. 10. Coincidence resolution curves obtained with metal samples.

values being $\tau_2=3.5\times10^{-9}$ sec at 20°C, $\tau_2=2.5\times10^{-9}$ sec at -78°C and $\tau_2=1.6\times10^{-9}$ sec at -196°C. The intensity of the τ_2 component remains unchanged at about 33 percent throughout these temperature changes. Polystyrene shows a temperature effect intermediate between fused quartz and Teflon; the measurements, not shown in a diagram, give $\tau_2=2.3\times10^{-9}$ sec at 20°C and $\tau_2=1.5\times10^{-9}$ sec at -196°C, the intensity again being roughly independent of temperature.

In further experiments using apparatus similar to that of Fig. 9, it was shown that the τ_2 component in Teflon and polystyrene is not markedly affected by the application to the sample of either an electric field of 15 kv/cm or a magnetic field of 3500 gauss.

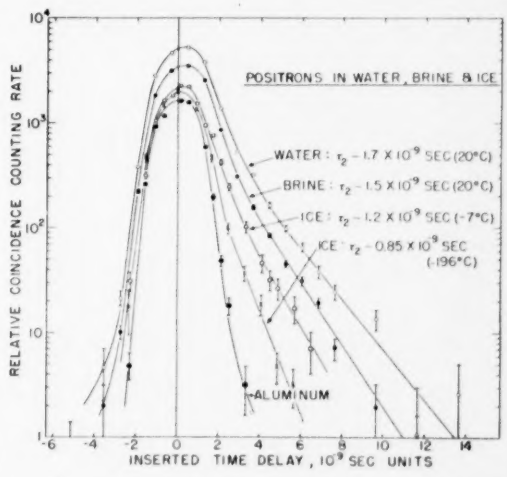
POSITRONS IN WATER, BRINE & ICE
WATER: τ₂ - 1.7 X 10⁻⁹ SEC (20°C)
BRINE: τ₂ - 1.5 X 10⁻⁹ SEC (20°C)
ICE: τ₂ - 1.2 X 10⁻⁹ SEC (-7°C)
ICE: τ₂ - 0.85 X 10⁻⁹ SEC (-196°C)
ALUMINUM
RELATIVE COINCIDENCE COUNTING RATE
INSERTED TIME DELAY, 10⁻⁹ SEC UNITS

FIG. 11. Coincidence resolution curves obtained with samples of water brine and ice. The standard deviations are shown by vertical bars.

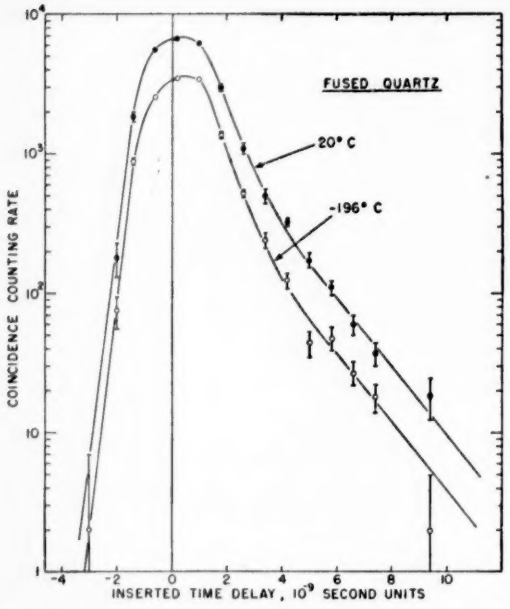

FIG. 12. Comparison of the coincidence resolution curves obtained with a fused quartz sample at two temperatures. The standard deviations are shown by vertical bars.

(c) Properties of the Delayed Annihilation Radiation

An experiment was next performed to compare the spectral distribution and angular distribution of the long-delayed (τ_2) annihilation radiation with those of the more prompt (τ_1) component. The apparatus, shown in Fig. 14, is similar to that of Fig. 9, with the addition of the sodium iodide counter 3, connected to a single-channel pulse-height analyzer whose output is placed in slow coincidence (resolving time = 1 μsec) with the output of the 10^{-9} sec coincidence circuit. As before, stilbene counter 1 detects 1.28-Mev nuclear gamma-rays from the Na^{22} source, and counter 2 detects the annihilation radiation from positrons decaying in the sample material. Now, however, in the interests of higher counting rate, the discriminator bias on counter 1 was lowered, so that it counted more of the 1.28-Mev gammas and hence also annihilation quanta. This meant that counters 1 and 2 were equivalent so far as the fast coincidence circuit was concerned, since annihilation quanta and 1.28-Mev gamma-rays were counted by both and the resulting resolution curves showed the τ_2 component on both sides, when it occurred. The τ_2 component on the right-hand side, however, still corresponded to detection of 1.28-Mev gamma-rays by counter 1 and of annihilation quanta by counter 2, as before. For normal annihilation radiation, in which the two quanta are strongly correlated at 180°, counter 3 will detect a large fraction of the coincident partners of the annihilation quanta whose delay is being measured by counter 2. The apparatus of Fig. 14 allows us to measure the delay of one member of a pair of annihilation quanta detected by counter 2 and the pulse-height spectrum of its coincident partner detected by counter 3. This complex arrangement could be avoided if a phosphor material were available which had both the absorption coefficient and light output of NaI and the speed of the organic phosphors.

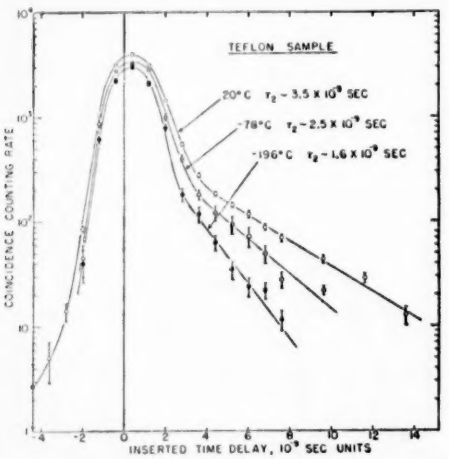
TEFLON SAMPLE
20° C $\tau_2 \sim 3.5 \times 10^{-9}$ SEC
-78° C $\tau_2 \sim 2.5 \times 10^{-9}$ SEC
-196° C $\tau_2 \sim 1.6 \times 10^{-9}$ SEC
COINCIDENCE COUNTING RATE
INSERTED TIME DELAY, 10^{-9} SEC UNITS

FIG. 13. Comparison of the coincidence resolution curves obtained with a sample of Teflon at three temperatures. The standard deviations of the points are shown by vertical bars.

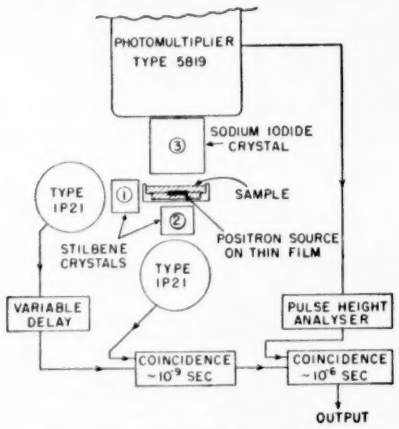

FIG. 14. Arrangement of scintillation counters used to compare the spectral and angular distributions of the long-delayed (τ_2) annihilation with those of the more prompt (τ_1) component.

The results of an experiment with an Al sample are shown in Fig. 15(a) and (b). Here (b) shows the resolution curve observed in the usual way for coincidences between counters 1 and 2. The delay chosen for pulse-height selection is indicated by an arrow in Fig. 15(b), and is near the peak of the aluminum curve. For these conditions Fig. 15(a) shows the total and coincidence pulse height spectra observed in counter 3. The spec-

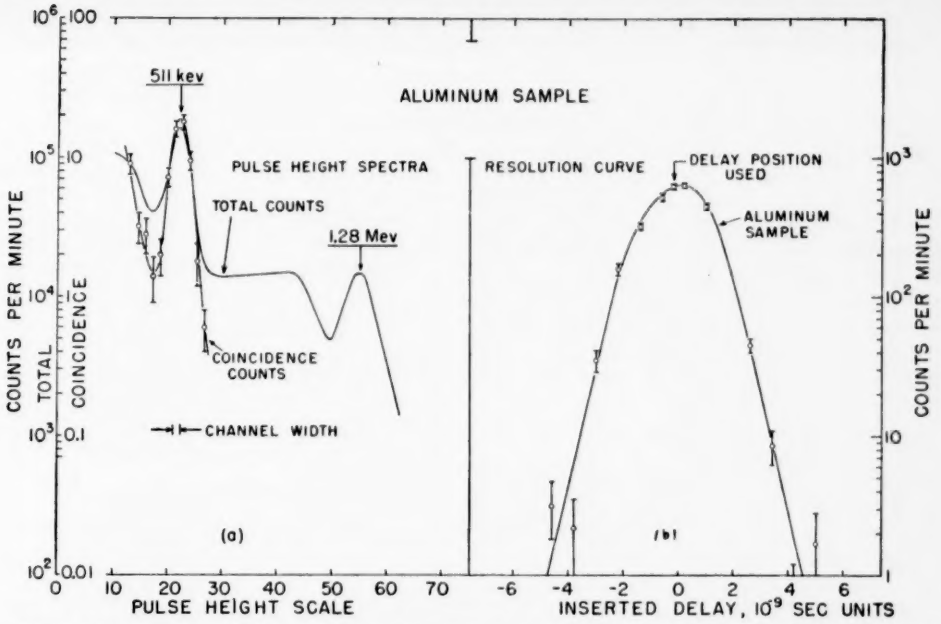

FIG. 15. (a) Comparison of the gross pulse-height spectrum (solid line) obtained in counter 3, Fig. 14, with that (open circles) obtained in coincidence with the prompt decay component using a sample of aluminum. (b) Coincidence resolution curve obtained with counters 1 and 2 Fig. 14. Standard deviations are shown by vertical bars.

trum of total counts shows peaks at 1.28 Mev and 0.511 Mev, while the coincidence spectrum shows only the peak at 0.511 Mev, as expected.

The results for polystyrene are shown in Fig. 16(a) and (b). Here (b) shows the resolution curve for the polystyrene sample, with the previously observed

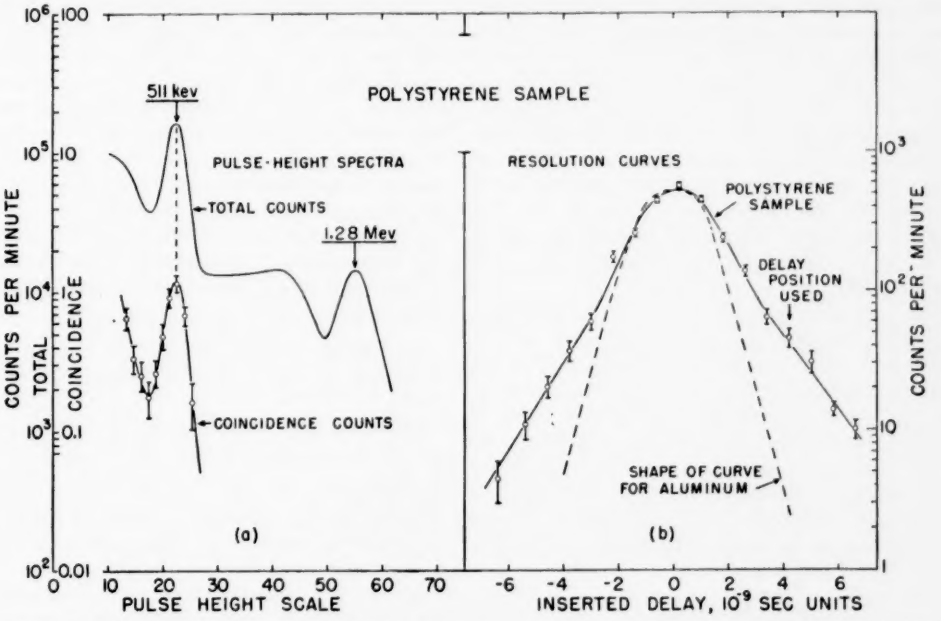

FIG. 16. (a) Comparison of the gross pulse-height spectrum in counter 3, Fig. 14, with that part of it which coincides with the longer lived (τ_2) component using a sample of polystyrene. (b) Coincidence resolution curve obtained with counters 1 and 2, Fig. 14. Standard deviations are shown by vertical bars.

TABLE I. Mean lives of positrons in condensed materials.

Material	°C	τ_1 (sec)	%	τ_2 (sec)	%
Li[a]	20	$(1.5\pm0.6)\times10^{-10}$	(100)		
Be	20	$(1.7\pm0.5)\times10^{-10}$	100		
B "amorphous"	20	$(1.7\pm0.4)\times10^{-10}$	100		
C "amorphous"	20	$(4.3\pm0.4)\times10^{-10}$	100		
C graphite	20	$(3.0\pm0.3)\times10^{-10}$	100		
C diamond	20	$(1.3\pm0.3)\times10^{-10}$	100		
Na[a]	20	$(1.5\pm0.6)\times10^{-10}$	(100)		
Al	20	$(1.5\pm0.3)\times10^{-10}$	100		
S monoclinic crystal	20	$(2.1\pm0.3)\times10^{-10}$	100		
S "plastic"	20	$(1.5\pm0.4)\times10^{-10}$	~70	$(4.5\pm0.6)\times10^{-10}$	~30
K[a]	20	$(1.5\pm0.6)\times10^{-10}$	(100)		
Cu	20	$(1.2\pm0.5)\times10^{-10}$	100		
Ag[a]	20	$(1.5\pm0.6)\times10^{-10}$	(100)		
Au	20	$(1.2\pm0.3)\times10^{-10}$	100		
Hg	20	$(1.2\pm0.5)\times10^{-10}$	100		
Pb[a]	20	$(1.5\pm0.6)\times10^{-10}$	(100)		
water	20			$(1.7\pm0.2)\times10^{-9}$	~30
ice	−7			$(1.2\pm0.2)\times10^{-9}$	~30
ice	−196			$(0.85\pm0.15)\times10^{-9}$	~30
brine (NaCl)	20			$(1.5\pm0.2)\times10^{-9}$	~30
NaCl crystal	20	$(2.3\pm0.3)\times10^{-10}$	100		
quartz, α-crystal	20	$(2.0\pm0.3)\times10^{-10}$	100		
quartz, fused	20	$(3.5\pm0.5)\times10^{-10}$	71±5	$(1.8\pm0.2)\times10^{-9}$	29±5
Polystyrene	20	$(3.7\pm0.5)\times10^{-10}$	64±5	$(2.3\pm0.2)\times10^{-9}$	36±5
Polystyrene	−196			$(1.7\pm0.3)\times10^{-9}$	~30
cellulose nitrate	20			$(2.3\pm0.4)\times10^{-9}$	~30
teflon	20			$(3.5\pm0.4)\times10^{-9}$	~30
teflon	−78			$(2.5\pm0.4)\times10^{-9}$	~30
teflon	−196			$(1.6\pm0.4)\times10^{-9}$	~30
polyethylene	20	$(3.0\pm0.5)\times10^{-10}$	71±5	$(2.4\pm0.3)\times10^{-9}$	29±5
borax crystals	20			$(9.0\pm2.0)\times10^{-10}$	~30
fused borax	20	$(2.6\pm0.5)\times10^{-10}$	68±5	$(8.7\pm1.2)\times10^{-10}$	32±5
mica	20	$(2.2\pm0.5)\times10^{-10}$	100		
isopropyl alcohol	20			$(2.3\pm0.4)\times10^{-9}$	~30

[a] Lifetimes for these metals are deduced from the comparison measurements of DeBenedetti and Richings (reference 6) and the absolute lifetime in Al obtained here.

aluminum curve for comparison. At the selected delay position shown in Fig. 16(b), the coincidence counting rate is down by a factor of 15 from its peak value, and the coincidences are at least 95 percent due to the τ_2 component in polystyrene. The corresponding pulse-height spectra in counter 3 are shown in Fig. 16(a). The coincidence spectrum again shows the clean peak at 0.511 Mev, with an intensity lower than that in the aluminum case, Fig. 15(a), by a factor of 15. The yield of triple coincidences per recorded double coincidence is therefore equal for the aluminum and polystyrene samples.

We conclude from these results that the long-delayed (τ_2) annihilation quanta have an energy equal to that of the more prompt (τ_1) annihilation quanta, to an accuracy estimated at ±3 percent, and that the long-delayed (τ_2) component consists mainly of pairs of quanta strongly correlated at 180°; the angular resolution with which this observation was made was about ±20°. There is therefore no evidence from this experiment that the long-delayed component of the annihilation radiation differs from the more prompt component in anything but mean life.

III. DISCUSSION

A summary of the lifetime measurements of positrons in various materials is presented in Table I. Where the simple experimental arrangement of Fig. 9 was used and the resolution curve was found to be complex, only the longer τ_2 mean life is reported; estimates of the relative intensities of the two components and hence of τ_1 are unreliable as remarked above. In all such cases, however, the intensity of the τ_2 component is consistent with the figure of ~30 percent found in the double spectrometer experiments. Absolute lifetimes of positrons in five metals not tried here are deduced from the comparison measurements of DeBenedetti and Richings[6] and the absolute lifetime of Al found here.

Two main sets of experimental facts have appeared in this study:

(i) The mean life of positrons in a metal is, within ±25 percent, independent of the metal chosen, and is near 1.5×10^{-10} sec.

(ii) Some substances, usually, but not always, liquid or amorphous, show a longer-lived component whose mean life τ_2 can be as long as 3.5×10^{-9} sec, and whose relative intensity is always about $\frac{1}{3}$, in addition to a shorter-lived component having a mean life τ_1 equal to a few times 10^{-10} sec and an intensity about $\frac{2}{3}$. The value of τ_2 varies from substance to substance over wide limits, and it is possible that all substances including the metals would show the double lifetime effect if the time resolution of the apparatus were

sufficiently good. In most cases the value of τ_2, but not the intensity of the τ_2 component, is reduced by lowering the temperature of the sample. Moderate electric and magnetic fields do not seem to have a detectable effect. The annihilation radiation emitted with the longer delay is similar in energy and angular distribution to the more prompt component.

In order to try to explain result (i) we may attempt to predict the mean life of positrons in a metal from the Dirac cross section[10] for the annihilation of slow positrons by a free electron,

$$\sigma=\pi r_0^2 c/v, \tag{1}$$

where r_0 is the classical electron radius and v is the velocity of the positron relative to the electron. The mean life of slow positrons in a medium of free electron density D is given by

$$\tau=[\pi r_0^2 cD]^{-1}. \tag{2}$$

The total electron density of a material of mass density ρ, atomic number Z, and mass number A is

$$D_e=(N_0\rho Z/A)\ \text{cm}^{-3}, \tag{3}$$

where N_0 is Avogadro's number. Thus if all the electrons in a substance are regarded as free, the predicted mean life for positrons in it is

$$\tau=[\pi r_0^2 c\rho N_0 Z/A]^{-1}=2.2\times10^{-10}(A/\rho Z)\ \text{sec}. \tag{4}$$

The results of DeBenedetti *et al.*[11] on the angular correlation suggest that only valence electrons or conduction electrons take part appreciably in the annihilation process. In that case, instead of Z, the effective number of electrons per atom is N_e, a number lying perhaps between 1 and 4, depending on the valence of the atom. Equation (4) now becomes

$$\tau=2.2\times10^{-10}(A/\rho N_e)\ \text{sec}. \tag{5}$$

Taking N_e for Al as 3, for example, we get

$$\tau_{\text{Al}}(\text{calc})=7.5\times10^{-10}\ \text{sec}, \tag{6}$$

a value five times greater than the observed one. If N_e is taken to be less than 3, the magnitude of the disagreement is increased. The fact that all the metals tried showed the same value of τ within ±25 percent, means that on the above analysis $A/\rho N_e$ should be constant to the same degree. If we take N_e as the number per atom of electrons having binding energy less than, say, 15 ev, the quantity $A/\rho N_e$ varies widely for different metals, being 2.44 for Be and 23.7 for Na, for example. The above simple analysis therefore is unable to account for either the shortness of the mean life in metals, or its constancy from metal to metal.

It now appears that the present picture of the slowing down and annihilation of positrons in metals is in need of revision. Positrons were formerly supposed to slow down to thermal energies and spend some time diffusing through the metal before being annihilated.[11] The mean time for slowing down has been calculated by DeBenedetti *et al.*[11] as 3×10^{-10} sec for metallic gold. Both the fact that the total mean life of fast positrons in gold is only about 1.2×10^{-10} sec, and the fact of the nonappearance of thermal positrons in the experiment of Madansky and Rasetti[12] suggest that most of the positrons are annihilated in a metal before they have slowed down to thermal energies. It seems likely that fast positrons in a metal slow down rapidly to energies of a few ev, where they have a high probability of forming singlet positronium, whose mean life is 1.25×10^{-10} sec.[13] In support of this idea, no sample has shown an experimental mean life shorter than 1.25×10^{-10} sec within experimental error.

Turning to result (ii), the appearance of two distinct mean lives in some substances means not only that two different annihilation processes are present, but also that these two processes are mutually exclusive. Positrons decaying with the longer mean life are somehow prevented from participating in the faster process. The effect is reminiscent of that observed by Deutsch *et al.*,[3] in which a fraction of the positrons absorbed in a gas forms triplet positronium decaying with a mean life of 1.5×10^{-7} sec (extrapolated to zero gas pressure). This fraction has been measured by Pond[14] for various gases, the result varying with the gas from 0.11 (N_2) to 0.19 (H_2) in the presence of a magnetic field. Using the dependence upon magnetic field found by Pond and Dicke,[15] we find that the fraction to be expected with zero magnetic field is from 0.16 (N_2) to 0.26 (H_2), which is slightly less than the intensity of the longer lived component found here. Deutsch[16] found that in freon 12 (CCl_2F_2) the mean life of triplet positronium could be represented by

$$\tau=(6.8\times10^6+0.3\times10^6 p)^{-1}\ \text{sec}, \tag{7}$$

where p is the gas pressure in atmospheres, and the second term of (7) represents a shortening of the mean life due to collisions with gas atoms. If we now regard one of our amorphous condensed materials as equivalent to a gas at, say, 1000 atmospheres, the value of τ deduced from (7) is

$$\tau\sim3\times10^{-9}\ \text{sec}, \tag{8}$$

agreeing in order of magnitude with the values found for τ_2.

A possible explanation of the τ_2 component found in the experiments is then as follows: Positrons slowing down in the sample form triplet positronium in some

[10] W. Heitler, *The Quantum Theory of Radiation* (Oxford University Press, London, 1944), p. 208.
[11] DeBenedetti, Cowan, Konneker, and Primakoff, Phys. Rev. **77**, 205 (1950).
[12] L. Madansky and F. Rasetti, Phys. Rev. **79**, 397 (1950).
[13] A. Ore and J. L. Powell, Phys. Rev. **75**, 1696 (1949).
[14] T. A. Pond, Phys. Rev. **85**, 489 (1952).
[15] T. A. Pond and R. H. Dicke, Phys. Rev. **85**, 489 (1952).
[16] M. Deutsch, Phys. Rev. **83**, 866 (1951).

fraction of the cases, according to our results about $\frac{1}{3}$. This triplet positronium is destroyed mainly by conversion to the short-lived singlet state[13] ($\tau = 1.25 \times 10^{-10}$ sec) in collisions with atoms of the sample material. The triplet positronium thus has its own lifetime shortened, as suggested by (7) and (8), by a factor of 50 or more. On this view, less than 2 percent of the τ_2 component observed in the experiments would consist of three-photon annihilations, a fraction which would have escaped detection in any of the experiments reported here. The absence of an observable τ_2 component in metals and some crystals might then be explained by assuming that electrons in energy bands determined by the crystal structure are effectively free so far as positrons or positronium are concerned. These electrons would rapidly convert the triplet positronium to the singlet state by collision, in much the same way that the odd electron in NO destroys triplet positronium in a gas.[14,16]

This explanation is not free of objections. In the first place if the magnitude of τ_2 is determined mainly by "gas collisions," it might be expected to increase as the temperature is reduced, whereas the opposite is observed. Secondly, the intensity of the τ_2 component formed here, $\sim\frac{1}{4}$, is somewhat greater and more constant than the values measured for the formation of triplet positronium in gases.[14,16] On the other hand, the above picture is consistent with the independence in the observed effect of moderate fields. Certainly the rate of conversion of triplet positronium to singlet positronium due to the magnetic fields used here is expected[14,15] to be much less than that previously estimated due to collisions.

Some light may be thrown on the temperature variation of τ_2 by noting that in all the samples a connection seems to exist between regularity of structure and shortness of τ_2. Generally speaking, lowering the temperature of a substance tends to make its structure more regular. The observations presented on the various forms of water, Fig. 11, show that τ_2 shortens with increase of regularity of structure. Ice is not completely regular,[17] being "crystalline only in the position of its molecule . . . glass-like in their orientation,"[18] but is more so than water. Brine is also more regular than water because the presence of small ions in solution increases the regularity of the water solvent.[18] Ice at a low temperature may be expected to be more regular than ice near room temperature. There is a suggestion in these remarks that experiments of the kind reported here might form a useful tool in the experimental study of the solid and liquid state. Before this is possible, however, the interpretation of the effects observed must be placed on firmer ground.

If the analysis given here is substantially correct, a sample showing a long τ_2 would yield substantially more three-quantum events than one not showing an appreciable τ_2. Thus, in an experiment designed to detect the three-quantum effect, such as those reported by Rich[19] or DeBenedetti and Siegel,[20] the replacing of a metal sample by a Teflon sample would give a large increase in the three-quantum counting rate. An experiment of this kind is now being planned in this laboratory.

The authors have been greatly assisted in this work by discussions with many persons, including Drs. B. N. Brockhouse, L. G. Elliott, E. P. Hincks, D. G. Hurst, J. D. Jackson, W. B. Lewis, T. D. Newton, and N. K. Pope. We also thank Mr. W. F. Merritt for preparing the Na^{22} sources.

[17] Wollan, Davidson, and Shull, Phys. Rev. **75**, 1348 (1949).
[18] J. D. Bernal and R. H. Fowler, J. Chem. Phys. **1**, 515 (1933).
[19] J. A. Rich, Phys. Rev. **81**, 140 (1951).
[20] S. DeBenedetti and R. Siegel, Phys. Rev. **85**, 371 (1952).

Fluctuations and Latitude Effect of Cosmic Rays at High Altitudes and Latitudes*

H. V. Neher, V. Z. Peterson, and E. A. Stern
California Institute of Technology, Pasadena, California
(Received December 22, 1952)

Using a newly developed ionization chamber, which transmits its information by radio, simultaneous balloon flights were made from widely separated stations in the summer of 1951. Bismarck, North Dakota (geomagnetic latitude, λ_m, 56°N) was used as a base station. Four flights were made from shipboard going north from Boston and five were made from Thule, Greenland ($\lambda_m = 88$°N), simultaneous with those at Bismarck. In all, 28 successful flights were made by the two expeditions. In seeking to determine the geomagnetic effects on the low energy primaries, considerable information was gathered on the radiation that fluctuates from day to day. The following are the chief experimental findings together with some of the conclusions that may be drawn.

(1) The fluctuations in the primary radiation at 90 000 feet were as much as 10 percent in a few days. (2) These were simultaneous (except as noted in the text) and very close to the same amount at the two stations. (3) The magnitude of the fluctuations at high altitudes was considerably larger than the geomagnetic effect between Bismarck and Thule. (4) The radiation that fluctuated contained both high (>15 Bev/c) momentum and low (down to 1.5 Bev/c) momentum particles. (5) There was a good correlation between the fluctuations in the radiation at high altitudes and the fluctuations in the neutron and meson components at ground level. (6) The fact that no particles fluctuated at Thule that did not also fluctuate at Bismarck leads us to conclude that there are few, if any, low energy particles coming in at Thule that are not also present at Bismarck, otherwise they too would be expected to vary. (7) From the manner in which the fluctuating radiation is absorbed in the atmosphere, it is concluded that the fluctuations cannot be due to heavy primaries alone. Rather it appears that the particles that fluctuate are of the same nature as the other incoming particles but have somewhat less energy per particle. (8) Varying magnetic fields of the geomagnetic axially symmetrical type are discarded as being able to produce the kind of fluctuations observed. A more satisfactory mechanism appears to be varying electric fields. (9) There was a negative latitude effect in the total ionization at intermediate altitudes (30 000 to 50 000 feet) at high latitudes. This we attribute to the greater importance of μ-meson decay in the warmer air of the stratosphere which exists at the more northerly latitudes. The temperature coefficient arrived at is −0.19 percent °C^{-1}. (10) There was a positive latitude effect in the total ionization above 60 000 feet at high latitudes. Evidence is presented to show that this is not likely to be due either to atmospheric effects or to low energy particles admitted by the earth's magnetic field above 66°N. We attribute this increase to the shadow effect of the earth. (11) The absence of particles with momenta in the range 1.5 to 0.6 Bev/Ze (0.8 to 0.14 Bev for protons), shown by (a) a lack of increase of ionization at very high altitudes between geomagnetic latitudes 58° and 66°N, (b) the absence of an increase of area under the ionization-depth curve at latitudes north of $\lambda_m = 58$°N, and (c) the absence of any particles that fluctuate at Thule that do not also fluctuate at Bismarck, indicates a cutoff of the primary particles. (12) This cutoff we attribute to a general solar magnetic field. The magnetic moment required is 0.65×10^{34} gauss-cm^3 corresponding to a field at the solar equator of 19 gauss. (13) Any diurnal effect on cosmic rays due to such a magnetic moment would normally be hidden by the daily fluctuations of the primary particles.

I. INTRODUCTION

A. The Latitude Effect at High Latitudes

IN studying the geomagnetic latitude effect in cosmic rays in the hope of being able to determine the energy distribution of the primary radiation at intermediate and high latitudes, it became evident a number of years ago[1] that simultaneous balloon flights would have to be made at two stations, because of the fluctuations in the primary radiation that take place from day to day. While not completely fulfilling this requirement, the B-29 airplane flight[2] made in 1948 from geomagnetic latitude 64°N[3] to the equator at 30 000 feet elevation did cover the high latitudes in the space of a few hours, and it was known that the fluctuations are usually not important in this period of time. This flight made it possible to normalize our former balloon flight curves, taken with counter telescopes, to agree with the airplane data at 310 g cm^{-2} air pressure. After so doing, an 8 percent increase in intensity at the maxima of the curves and a 2.2 percent increase in area was shown in going from Omaha (geomagnetic latitude, $\lambda_m = 51$°N) to Saskatoon ($\lambda_m = 60$°N).

Among earlier attempts to measure the latitude effect near the "knee" of the curve may be mentioned that of Cosyns[4] in 1935. He allowed a counter telescope, carried by a balloon, to drift at 204 g cm^{-2} air pressure over the range of geomagnetic latitude 47° to 51°N. The curve he obtained of intensity *vs* geomagnetic latitude showed a leveling off at 50°N.

In 1937 Carmichael and Dymond[5] made two good balloon flights near the geomagnetic pole; one with a counter telescope and another with an ionization chamber. Not having made comparison flights, the telescope data were fitted to those of Pfotzer[6] taken at $\lambda_m = 49$°N at ground level. The ionization data were fitted at 125 g cm^{-2} air pressure to those of Bowen, Millikan, and Neher,[7] taken also with ionization chambers at 60°N ten days later. After so fitting, each of

* Assisted by the joint program of the U. S. Office of Naval Research and the U. S. Atomic Energy Commission.

[1] Biehl, Montgomery, Neher, Pickering, and Roesch, Revs. Modern Phys. **20**, 366 (1948).

[2] Biehl, Neher, and Roesch, Phys. Rev. **76**, 914 (1949).

[3] In all cases in this paper only geomagnetic latitudes will be used.

[4] Max Cosyns, Nature **135**, 313 (1935).

[5] H. Carmichael and E. G. Dymond, Proc. Roy. Soc. (London) **A171**, 321 (1939).

[6] G. Pfotzer, Z. Physik **102**, 41 (1936).

[7] Bowen, Millikan, and Neher, Phys. Rev. **53**, 855 (1938).

their curves was about 6 percent higher than the corresponding reference curve at the maxima.

A more recent attempt to determine the latitude effect at high latitudes has been made by Pomerantz.[8] Counter telescope balloon flights, using a 7.5-cm lead absorber, were made at Swarthmore, Pennsylvania ($\lambda_m = 52°$N). A trip was next made to Churchill, Canada ($\lambda_m = 69°$N), and two months later further data were taken at Swarthmore. Using no absorber, only data taken at Churchill and on the return to Swarthmore have been reported. In each case a 40 to 60 percent increase in the intensity at very high altitudes was found in comparing the two sets of data.

In attempting to determine the number of primary particles alone, Van Allen and Singer[9] have used rockets carrying either single Geiger counters or counter telescopes beyond the atmosphere. Aside from the fact that only a few minutes are available for measurement, these experiments suffer from the same disadvantage as others where simultaneous flights are not made from some base station. Since, as will be shown later, the fluctuation in the ionization at 90 000 feet is from 5 to 10 percent from day to day, this also means that there will be a change in the numbers of primary rays. In fact, the percentage change in ionization at 90 000 feet should be approximately the same as the percentage change in the number of primaries.

In evaluating the experiments above summarized, it must be borne in mind that, as pointed out many times before,[1,10–12] rather large fluctuations occur in the primary radiation and the agreement of flights made at a given location at different times may be fortuitous and that considerable caution must be used in drawing conclusions from data taken at different times at different locations, especially when the geomagnetic effects are expected to be of the same order of magnitude as the fluctuations themselves.

The importance of determining accurately the energy distribution of the primary radiation at the lower end of the energy spectrum lies in the implications involved from the standpoints of (a) the mechanism or mechanisms of origin of the radiation, and (b) the bearing on the problem of the general magnetic field of the sun. If it should be established that few if any primary cosmic-ray particles reach the earth with momenta less than a certain value, a cut-off mechanism would need to be found. This might exist either during the acceleration process or subsequently, but before they reach the influence of the magnetic field of the earth. One such mechanism, first suggested by Janossy,[13] is that a general solar magnetic field would, if its strength were of the proper magnitude, prohibit particles whose momenta were less than a certain value from reaching the vicinity of the earth. The bearing upon this problem of the experiments, to be described, will be discussed later.

B. The Role Played by Fluctuations

Considerable information on fluctuations that exist in the primary radiation has been accumulated over the years. Forbush[14] in 1938, in analyzing ground level data, drew attention to the world-wide character, not only of the large changes in cosmic rays that occur during magnetic storms, but also to the small changes that take place from month to month. There is also a correlation between these smaller changes and fluctuations in the earth's magnetic field. In each case the algebraic sign of the ratio of the change of cosmic-ray intensity to the change in the magnetic field is positive and of approximately the same value, thus indicating that the mechanism giving rise to the changes is the same in each case.

Recently, Simpson *et al.*[15] have reported the results obtained from monitoring neutron intensities at several stations. It was shown by Neher and Forbush[16] that these fluctuations were well correlated with the changes in the penetrating component as measured by ionization chambers at Cheltenham, Maryland and Huancayo, Peru, the ratio between the fluctuations of the neutrons and mesons being approximately 3 to 1.

Fluctuations at high altitudes have been measured with both ionization chambers[10–12] and counter telescopes.[1] For the series of flights made in 1947 using counter telescopes (reference 1) the fluctuations as measured at the maxima of the curves were compared with Forbush's sea level data. The ratio of the fluctuations at the peaks of the curves then found was 10 to 1. For the series of flights with ionization chambers made from Bismarck, North Dakota, in the summer of 1951, the ratio between the fluctuations found from day to day at 50 g cm^{-2} air pressure (about 70 000 feet) to the meson component at sea level was approximately 7 to 1.[16] This increase of the fluctuations with altitude indicates that the average energy of the particles (if singly charged) responsible for the changes is somewhat less than the average energy of the total radiation, yet sufficiently great to get through the earth's magnetic field at the equator and give changes of about the same amount as are found at the higher latitudes. This is in keeping with the behavior reported by Forbush[14] who found that the percentage change at mountain altitudes was somewhat greater than at sea level. Jesse[17] also has reported fluctuations in the primary radiation as measured with ionization chambers carried up by balloons from Chicago. The ratio of the fluctuations

[8] M. A. Pomerantz, Phys. Rev. **77**, 830 (1950); M. A. Pomerantz and G. W. McClure, Phys. Rev. **86**, 536 (1952).
[9] J. A. Van Allen and S. F. Singer, Phys. Rev. **78**, 819 (1950).
[10] R. A. Millikan and H. V. Neher, Phys. Rev. **56**, 491 (1939).
[11] R. A. Millikan and H. V. Neher, Proc. Am. Phil. Soc. **83**, 409 (1940).
[12] Millikan, Neher, and Pickering, Phys. Rev. **66**, 295 (1944).
[13] L. Janossy, Z. Physik **104**, 430 (1937).
[14] S. E. Forbush, Phys. Rev. **54**, 975 (1938).
[15] Simpson, Fonger, and Wilcox, Phys. Rev. **85**, 366 (1952).
[16] H. V. Neher and S. E. Forbush, Phys. Rev. **87**, 889 (1952).
[17] W. P. Jesse, Phys. Rev. **58**, 281 (1940).

shown by his data to that obtained by the Carnegie instrument at Huancayo, Peru, as determined from his published data, was about 6 to 1.

In addition to the above discussed fluctuations that occur from day to day in the high energy radiation, sudden increases have been measured by a number of observers[18] at or near sea level which are apparently due to lower energy particles. These increases are characterized by (1) they do not occur at the geomagnetic equator,[19] (2) the increase in the neutron component is many times the increase in the ionizing component,[18] (3) the increase is much more pronounced at mountain altitudes than at sea level,[19] and (4) there seems to exist a "spottiness" in that for about the same geomagnetic latitude but different longitudes the increase measured by different observers varies over wide ranges.[18]

It is particularly important to study these fluctuations at high altitudes because (1) atmospheric effects play a much less prominent role, (2) some of the radiation that fluctuates does not extend its influence to sea level, and (3) considerable information about the composition of the primary radiation that fluctuates may be obtained by the way in which it is absorbed in the atmosphere.

To gain information on the true latitude effect these fluctuations need to be taken into account. Consequently, a series of simultaneous flights was carried out at Bismarck, North Dakota (geomagnetic latitude, $\lambda_m = 56°$N) and Thule, Greenland ($\lambda_m = 88°$N). Four intermediate latitude flights were also made from shipboard going north. All of these latter flights and five of those made in Greenland were made simultaneously with similar flights at Bismarck.

C. Discussion of Instruments

Of the various types of instruments that can be used to attack the problem of fluctuations at high altitudes, the field is narrowed immediately by the following requirements: (1) Since the fluctuations are usually of the order of 5 to 10 percent, errors in measurement should be no more than $\frac{1}{10}$ of this at the most. (2) A large number of flights need to be made, and this demands a simple instrument. While the ionization chamber is omnidirectional and yields no direct information on the kinds of particles, it does have the advantage of measuring a quantity proportional to the energy per unit area falling on the atmosphere at the location where it is used, it is light in weight and simple to construct.

The ionization chamber may be compared with Geiger counters that are sent above the atmosphere in rockets as follows: First let us estimate the average ionization per particle at high altitudes. The curve given in Fig. 4 for Bismarck on August 3, 1951 becomes nearly horizontal at the lowest pressures of 15 to 30 g cm^{-2}. Assume the intersection of this curve with the axis is at $I = 400$ ions cm^{-3} sec^{-1} atmos^{-1} of air, and take Van Allen's and Singer's data for the numbers of incident particles at about this latitude, namely, 0.28 particle cm^{-2} sec^{-1} sterad^{-1}. For 2π solid angle we would expect a number $J = 1.8$ particles cm^{-2} sec^{-1}. If $\bar{\sigma}$ is the average specific ionization per particle, then the ionization will be

$$I = \bar{\sigma} J$$

or

$$\bar{\sigma} = 400/1.8 = 220 \text{ ions cm}^{-1} \text{ atmos}^{-1} \text{ of air.}$$

This is to be compared with 180 arrived at for the average ionization throughout the atmosphere in comparing counter telescope and ionization chamber flights at Saskatoon.[20] Bursts and stars should be relatively unimportant in this connection.

Next, consider the ionization chamber at 10 to 20 g cm^{-2} down into the atmosphere. If we assume the same value of $\bar{\sigma}$ as before for the particles that change from day to day, then the percentage change in the ionization at these altitudes will be the same as the change in the numbers of primary particles. In this case stars and showers will give some contribution at large zenith angles, but it is evident from the way the curve flattens off at high altitudes that any such contributions are balanced by the effect of new particles as one goes to lower pressures.

The possibility that the fluctuations in the primary radiation are due only to particles of large atomic number should be considered. In such a case the changes as measured by Geiger counters in rockets would be much smaller than those observed with ionization chambers. It will be shown later that if one takes the number distribution given by Kaplon, Peters *et al.*[21] for particles of all atomic numbers Z and assumes that the constants by which the number distributions are multiplied are the quantities that change, then it is unlikely that Z can be larger than three times that for the average of all primaries. It is perhaps more reasonable to assume that the mechanism that causes the fluctuations affects all incoming particles.

We thus arrive at the conclusion that the ionization chamber, compared with the rocket-borne Geiger counter, will show a relative change at least as large for changes in the primaries. The advantages of using the balloon-borne ionization chamber are (1) for equal times the ion chamber gives much better statistics, and (2) the length of time available for measurement is the order of hours compared with minutes when rockets are used.

[18] See *Progress in Cosmic-Ray Physics* (North-Holland Publishing Company, Amsterdam, 1952), pp. 502–510 for summary.
[19] Forbush, Stinchcomb, and Schein, Phys. Rev. **79**, 501 (1950).
[20] See reference 18, p. 260.
[21] Kaplon, Peters, Reynolds, and Ritson, Phys. Rev. **85**, 295 (1952).

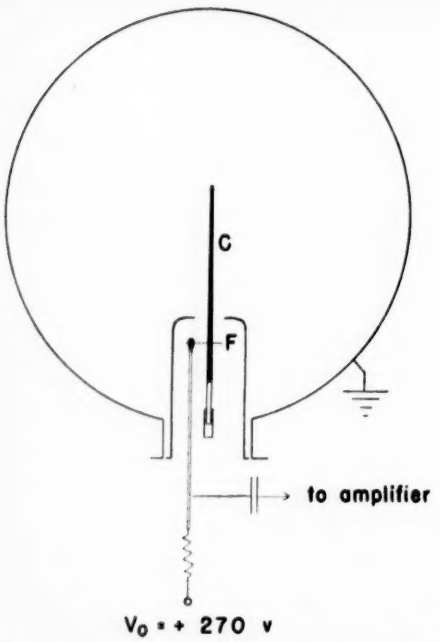

FIG. 1. Schematic drawing of the automatic ionization chamber. Ion collector C is a quartz rod made conducting by a coating of graphite except at the lower end, where the bare quartz serves as an insulator. Quartz fiber F recharges C when the potential of the collector reaches a definite value.

II. INSTRUMENTS AND EXPERIMENTAL PROCEDURES

A. The Ionization Chamber

In planning for flights near the geomagnetic pole an instrument was devised whose information could be transmitted by radio since the problem of recovery was a serious one.

The ionization chamber, described in detail elsewhere,[22] consisted of a steel spherical shell, 25 cm in diameter, having a wall thickness of 0.5 mm (0.4 g cm^{-2}), and filled to a pressure of 8 atmos of argon. The ion collector was a conducting quartz rod, the lower end of which was left uncoated for insulation purposes. A small conducting quartz fiber automatically touched the collector when the potential of the latter dropped to a definite value of about $V_0/1.5$, where V_0 was the potential applied to the quartz fiber. When contact was thus made a pulse was generated across a series resistor and this pulse was amplified and transmitted.

The device is represented schematically in Fig. 1. The fiber F is normally maintained at a potential of 270 volts. As the collector C loses charge by collecting negative charges from the ionized gas, the fiber moves closer until it becomes unstable due to image forces, rapidly touches C, charging it again, and flies away. The process is then repeated. At the maximum rate of ionization during a balloon flight, this recharging occurs every 15 to 20 seconds.

The rate of recharging for a constant ionization depends on the potential V_0 applied to the fiber. In practice this dependence was about 0.7 percent $volt^{-1}$ change of V_0. The battery used was the commercial 300-volt unit. To determine the potential of the batteries for the standard instruments, a potentiometer was used which was sensitive to less than 0.1 volt. Tests were made on the constancy of this potential for the current drains used and for the temperature changes expected. In each case the changes of potential were negligible. (The temperature coefficient determined was +0.02 percent $°C^{-1}$.)

For calibration purposes one instrument was chosen as a standard and two others as secondary standards. Before leaving Pasadena a comparison was made between these new instruments and the older photographically recording balloon ionization chambers used in past years to gather data in various regions of the world.[23] The walls of both instruments were steel and very close to the same thickness. In comparing the two, an ionization of approximately the maximum value to be expected during a flight was used. The source of radiation consisted chiefly of the gamma-rays from thorium C'' filtered through 3.7 cm of steel. This procedure should then tie our new results in with those obtained in past years.

Each group, the one that went to Bismarck, North

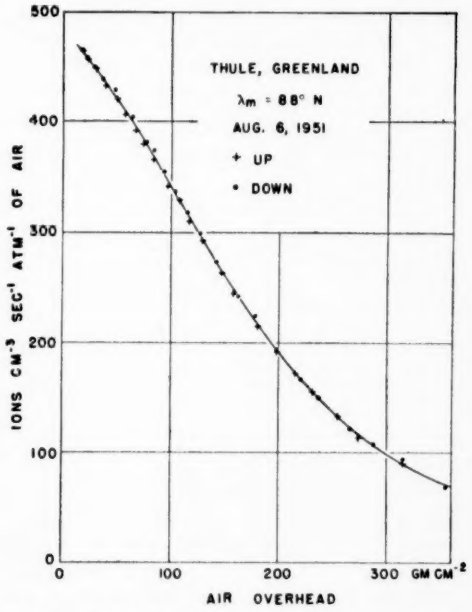

FIG. 2. Example of a single flight using the automatic ionization chamber showing the consistency of the individual points as well as the agreement between the flight going up and coming down.

[22] H. V. Neher, Rev. Sci. Instr. **24**, 99 (1953).

[23] Bowen, Millikan, and Neher, Phys. Rev. **53**, 855 (1938).

TABLE I. Data for the four flights at Thule, Greenland at definite atmospheric pressures (columns a) have corrections applied for the fluctuations as measured during simultaneous flights at Bismarck, North Dakota (columns b). The resulting corrected data (columns c) show a consistency better than ±0.5 percent from flight to flight.

	20 g cm^{-2}			40 g cm^{-2}			60 g cm^{-2}			80 g cm^{-2}			100 g cm^{-2}		
Date	a	b	c	a	b	c	a	b	c	a	b	c	a	b	c
Aug. 3, 1951	424	+24	448	406	+23	429	380	+20	400	351	+18	369	321	+15	336
Aug. 4, 1951	437	+15	452	414	+15	429	387	+10	397	358	+11	369	326	+12	338
Aug. 5, 1951	457	−10	447	435	− 6	429	404	− 8	396	372	− 6	366	342	− 7	335
Aug. 6, 1951	455	− 6	449	430	+ 1	431	400	− 2	398	367	0	367	334	+ 2	336
Average			449±1			430±1			398±1			368±1			336±1

Dakota, and the one that went to Thule, Greenland, took a standard and two secondary standards. These were used to calibrate the instruments sent aloft. In so doing an ionization about equal to the maximum expected was again used.

The group that went to Bismarck, for example, using 2 cm of steel as a filter for the gamma-rays, found that the intensity for the geometry there was 1.1 percent greater than for the arrangement in Pasadena. For the geometry at Thule, Greenland, the calibration intensity was 1.3 percent less than in Pasadena before leaving. In Pasadena the calibration intensity was 566 ions cm^{-3} sec^{-1} per atmosphere of air. Hence, at Bismarck it was 572 and at Thule, 559.

As a further check on the calibration rates, the rate at Thule was carefully noted just before leaving and was then compared with the standard used at Bismarck after returning to Pasadena. A calculation of the intensity at Thule, assuming the Bismarck instrument correct, gave 561 ions cm^{-3} sec^{-1} instead of 559 given above.

We therefore believe that the relative calibration intensities at Bismarck and Thule are known to one percent or better.

The instrument to be used was checked, just prior to being sent aloft, with the battery employed during the flight.

B. The Barometer Unit

The measurement of barometric pressure, giving the mass of air overhead, is a most important quantity. Where the curve of ionization *vs* air mass is the steepest, an error of 1 mm of mercury pressure is approximately equivalent to an error of 0.6 percent in ionization. The barometer unit used on these flights has been described elsewhere.[24] Briefly, it consists of a good commercial, three-section bellows whose expansion is measured by a series of contacts. No mechanical magnification is used, and friction is such that no effect due to it may be detected. Approximately 20 barometer signals are received for a change of one atmosphere pressure.

In calibrating the barometer unit the pressure was changed at about the rate to be expected during a flight, both for decrease and increase of pressure. This tends to make the hysteresis effect in the bellows nearly the same in the two cases.

[24] H. V. Neher, Rev. Sci. Instr. **24**, 97 (1953).

A temperature effect was looked for in the barometer unit. No detectable effect was found between 0° and 25°C.

The slightly larger value for the acceleration of gravity near the pole, *viz.*, 980.6 at Bismarck *vs* 982.6 cm sec^{-2} at Thule, introduces a slight correction amounting to 0.1 percent in the value of the ionization at 100 g cm^{-2} pressure. This increases to 0.4 percent at 300-g cm^{-2} and to 0.7 percent at 500-g cm^{-2} pressure. This correction, because of its small size at the higher altitudes, has not been taken into account.

C. Performance of the Equipment

In Fig. 2 the results of a single flight are given as measured at Thule, Greenland (geomagnetic latitude 88°N) on August 6, 1951. The ordinates, in ions cm^{-3} sec^{-1} atmos^{-1} of air, are in terms of our old ionization measurements[23] and may be directly compared. The rates of ascent and descent on this flight were approximately the same, and a good record was obtained throughout.

Perhaps the best indication of the consistency of the flights at the two locations is afforded by the following comparison. On August 3, 4, 5, and 6 simultaneous flights were made at the two stations. The Greenwich times when the flights reached their maximum height are given in Tables V and VI. If it is assumed that the absolute values of the fluctuations are the same at the two stations, then the measured values at Thule may be corrected for the fluctuations as measured at Bismarck simply by adding or subtracting from the Thule flights the change measured at Bismarck. The flight of July 17 at Bismarck is arbitrarily taken as a reference and the departures of the other flights at Bismarck from the flight of July 17 are then applied to the corresponding flights at Thule.

The data given in Table I are taken from the smooth curves drawn through the points for the different flights at Thule, Greenland ($\lambda_m = 88°$N).

The column designated "a" gives the ionization at the indicated depth in the atmosphere for that particular day. Column "b" gives the correction as determined from the corresponding flight at Bismarck as explained above. Column "c" gives the corrected values at Thule.

If the fluctuations are actually simultaneous and if the instruments are functioning relative to one another as they should, then one would expect agreement

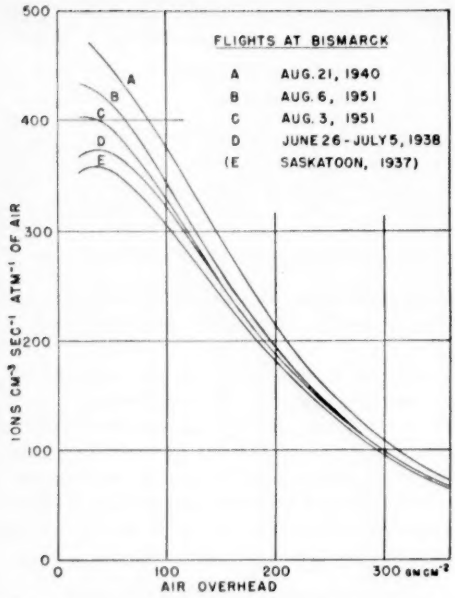
FLIGHTS AT BISMARCK
A AUG. 21, 1940
B AUG. 6, 1951
C AUG. 3, 1951
D JUNE 26 - JULY 5, 1938
(E SASKATOON, 1937)
IONS CM⁻³ SEC⁻¹ ATM⁻¹ OF AIR
AIR OVERHEAD
300 GM CM⁻²

FIG. 3. Extremes of ionization *vs* depth in the atmosphere measured thus far at Bismarck, North Dakota. Curve *E* taken at Saskatoon is included since Bismarck at the same time should in no case have been higher.

between the various flights as given in column "c." It is seen that the corrections are not small, amounting at 20 g cm^{-2} to a plus 5.5 percent correction on August 3 and a minus 2.2 percent on August 5. Yet when the corrections are made for the fluctuations as measured at Bismarck, the corrected Thule values agree to less than 0.3 percent. The errors given are merely determined by the scatter of the corrected data and do not in any way represent the estimated error in the absolute value of the numbers.

In evaluating the results given in Table I, it should be borne in mind that not only errors in the calibration, both of the ionization chambers and barometers, together with errors in the individual flights, enter at the one station but similar errors enter for the corresponding instrument sent up at the other station.

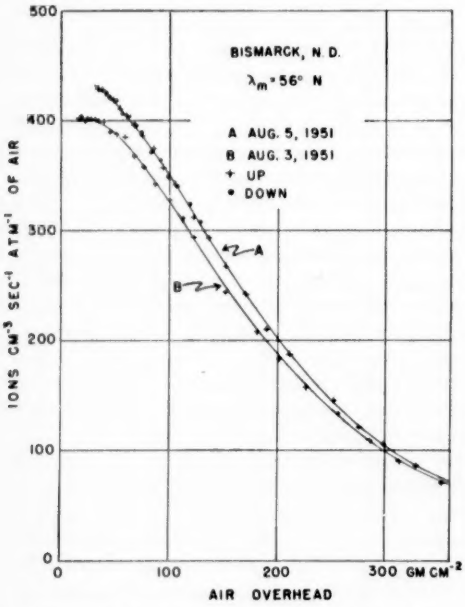

FIG. 4. Representative curves for two particular days at Bismarck, geomagnetic latitude, λ_m, 56°N.

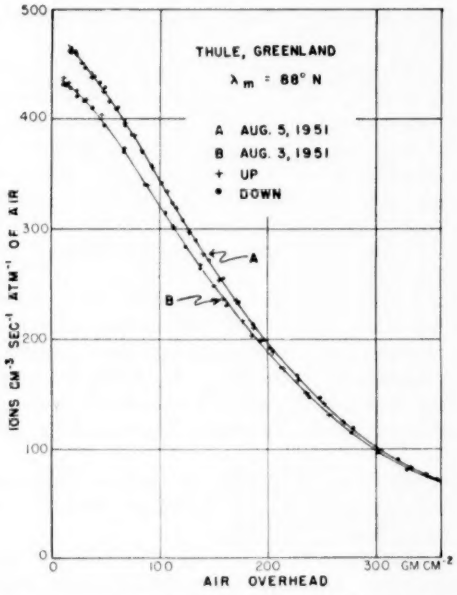

FIG. 5. Curves at Thule, Greenland ($\lambda_m = 88°$N) for the same two days as those at Bismarck in Fig. 4. Note the similarity in the change that took place at the two stations.

III. EXPERIMENTAL RESULTS

A. Fluctuations

As pointed out previously, before the latitude effect can be determined at high latitudes, it is first necessary to determine the fluctuations. Since data had been obtained at Bismarck in past years, we shall first compare two typical flights, using the present equipment on different days, with flights made with our older, photographically recording ionization chambers. These old and new chambers have very closely the same wall thickness (0.5 mm of steel) and were compared with each other in the laboratory with hard gamma-rays using an intensity of radiation about equal to the maximum to be expected during a flight.

Figure 3 shows how radically different the atmospheric absorption curves can be at a given location at

different times. Curve A is the average of three flights[25] made on the same day on August 21, 1940. Curves B and C are flights made on August 6 and 3 of 1951 with the present equipment. Curve D is the average of four flights[26] made during the period June 26 to July 5, 1938. In addition to these four curves, curve E is given which is the average of 3 flights[7] at Saskatoon ($\lambda_m = 60°$N) on August 14, 16, and 17, 1937. Since the intensity due to geomagnetic effects should in no case decrease with increasing latitude, the fact that curve E falls below D is taken to mean a real increase took place in the primary intensity between 1937 and 1938 for the times the flights were made. Curves A to E represent then, the extremes of the fluctuations at Bismarck as measured thus far and, from arguments given in the Introduction, represent a change in the numbers of primary particles of about 30 percent.

TABLE II. Data from ionization-depth curves for each simultaneous flight from the U.S.S. Wyandot (column W) and Bismarck (column B). Ionization is in terms of ions cm^{-3} sec^{-1} $atmos^{-1}$ of air. Values given in parentheses are extrapolated, based on the other, similar flights. July, 1951.

g cm^{-2}	July 17 W 55°N	July 17 B 56°N	July 22 W 58.5°N	July 22 B 56°N	July 23 W 62.5°N	July 23 B 56°N	July 24 W 68°N	July 24 B 56°N
15	···	(430)	409	···	434	402	421	412
20	418	429	408	···	430	401	420	412
30	418	427	407	···	421	393	417	411
40	416	423	402	397	411	385	412	406
50	408	415	395	390	400	375	403	397
60	395	401	384	381	388	363	391	386
80	366	375	357	353	360	339	360	360
100	336	344	328	323	328	312	328	332
120	···	313	298	294	298	282	297	302
140	···	282	268	265	269	254	267	272
160	···	252	241	237	242	226	240	242
180	···	224	216	210	216	202	214	216
200	···	198	191	185	191	178	190	191
220	···	175	168	164	168	158	167	167
240	···	154	148	145	146	139	146	147
260	···	136	131	128	128	121	129	130
280	···	120	115	112	111	105	113	113
300	···	106	100	99	98	92	101	99
340	···	81	74	76	76	70	79	76
380	···	60	56	57	60	54	61	59
420	···	46	44	44	48	42	46	45
460	···	35	···	34	···	32	36	35
500	···	26	···	27	···	···	···	26

It is of interest that the ionization-depth curve obtained near Thule by Carmichael and Dymond[5] in 1937 passed through a maximum as did also our own curves taken at Saskatoon ten days later. Whether or not such a curve passes through a maximum will depend on the ratio of the numbers of particles that do not multiply appreciably as they strike the atmosphere to those that do. In other words, the presence of a sufficient number of primary nuclei of momenta around 1 Bev/c will explain the difference between the upper parts of curves A and E.

[25] Millikan, Neher, and Pickering, Phys. Rev. **66**, 295 (1944).
[26] R. A. Millikan and H. V. Neher, Proc. Am. Phil. Soc. **83**, 409 (1940).

TABLE III. Data from ionization-depth curves for each simultaneous flight at Thule, Greenland (T), 88° geomagnetic north and Bismarck, (B) at 56°N. Ionization in terms of ions cm^{-3} sec^{-1} $atmos^{-1}$ of air. Values given in parentheses are extrapolated but based on other similar flights. August, 1951.

g cm^{-2}	August 2 T	August 2 B	August 3 T	August 3 B	August 4 T	August 4 B	August 5 T	August 5 B	August 6 T	August 6 B
15	448	401	427	405	442	···	461	···	461	438
20	445	401	424	405	437	414	457	(439)	455	435
30	436	401	416	404	426	411	447	(436)	443	431
40	427	398	406	400	414	408	435	429	430	423
50	416	394	394	393	401	401	421	419	416	414
60	404	383	380	381	387	391	404	409	400	403
80	375	361	351	357	358	364	372	381	367	375
100	343	334	321	329	326	333	342	352	334	343
120	310	304	290	298	295	300	307	320	301	309
140	281	274	260	268	267	271	277	289	269	278
160	252	244	232	236	242	243	248	257	241	248
180	224	216	207	210	214	216	220	228	213	220
200	198	193	185	188	189	190	193	202	187	193
220	175	171	164	166	166	167	170	178	164	169
240	154	153	145	148	145	144	150	157	143	147
260	135	135	127	131	127	127	132	137	125	131
280	121	119	112	115	111	112	115	120	109	115
300	106	105	98	101	97	99	101	105	96	101
340	81	82	76	77	74	76	79	81	74	78
380	62	64	59	60	58	57	60	62	57	59
420	47	50	46	45	44	42	46	47	44	44
460	36	···	35	···	33	31	35	···	34	···
500	28	···	26	···	27	···	27	···	25	···

It is significant that while curve A as compared with D or E shows the presence of radiation that is rapidly absorbed in the upper part of the atmosphere, there was also present on August 21, 1940, more penetrating radiation as compared with July of 1938. In fact, curve A continues to lie above the others throughout the atmosphere. A more complete discussion of the character of the radiation at high altitudes and latitudes that fluctuates from day to day will be given later.

Figures 4 and 5 give the data obtained for August 3 and 5 at Bismarck and Thule. The curves given hereafter will not, in general, contain the plotted points but only the smooth curves or the data taken therefrom will be given. For most of the flights, records were obtained for both the descent as well as the ascent, and in most cases agreed very well. A particular case where the two did not agree will be discussed later.

The data taken from the individual curves are given for each of the simultaneous flights in Tables II and III. In Table IV are given the results after correcting the data taken from shipboard and at Thule for the fluctuations as measured at Bismarck, using the data at the latter station on July 17 as a reference.

In Tables V and VI are given the times when the instruments reached their maximum height, the minimum pressures and the locations where the flights were made. While the Greenwich times for launching were not identical, it will be seen from the tables that the times when the instrument reached the maximum height did not usually differ by more than 1 hour. The fact that the points on the descent nearly always agreed with those taken on the ascent means that, in general,

TABLE IV. Corrected values of ionization for shipboard and the four simultaneous flights at Thule, using July 17 at Bismarck as a base. Column b gives corrections as obtained from departures of the particular Bismarck flight from that on July 17. Column c gives the corrected values of ionization in ions cm^{-3} sec^{-1} $atmos^{-1}$ of air.

g cm^{-2}	July 17 W 55°N	July 17 B 56°N	July 22 58.5°N b	July 22 58.5°N c	July 23 62.5°N b	July 23 62.5°N c	July 24 68°N b	July 24 68°N c	Aug. 3, 4, 5, 6 88°N c (Av)
15	···	(430)	···	···	(28)	462	(17)	438	454
20	418	429	(27)	435	27	457	17	437	449
30	418	427	(26)	433	34	455	16	433	441
40	416	423	26	428	38	449	17	429	430
50	408	415	25	420	40	440	18	421	417
60	395	401	20	404	38	426	15	406	398
80	366	375	22	379	36	396	15	375	368
100	336	344	21	349	32	360	12	340	336
120	···	313	19	317	31	329	11	308	304
140	···	282	17	285	28	297	10	277	274
160	···	252	15	256	26	268	10	250	247
180	···	224	14	230	22	238	8	222	218
200	···	198	12	203	19	210	7	197	193
220	···	175	10	178	16	184	7	174	170
240	···	154	9	157	15	161	7	153	151
260	···	136	8	139	15	143	6	135	132
280	···	120	8	123	15	126	7	120	116
300	···	106	7	107	14	112	7	108	102
340	···	81	5	79	10	86	5	84	79
380	···	60	3	59	6	66	2	63	59
420	···	46	2	46	4	52	1	47	46
460	···	35	1	···	3	···	0	36	36
500	···	26	−1	···	···	···	0	···	···

the radiation did not change appreciably in a period of 1 to 2 hours.

To give a better idea of where the various flights were made, Fig. 6 is given showing a map of the regions of interest. Three of the four flights from shipboard were made in foggy weather. The flight of July 17 was incomplete because of radio interference from equipment on the ship.

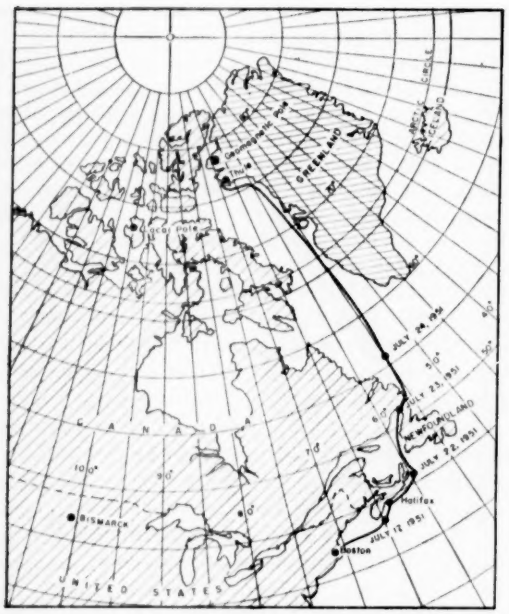

FIG. 6. Map of the region where simultaneous flights were made.

At Thule, the flights during the first week of August were made in very good weather. Toward the middle and end of August more fog and clouds were present. The winds at both the surface and at high altitudes were in general low. The result was that only on one occasion was any difficulty experienced in filling and launching the balloons even though this was done out-of-doors. The winds above 30 000 feet during the month of August were low and variable. The total distance of drift of the instruments during a 4 to 5 hour flight was from 30 to 150 miles. A summary of the weather observations at both surface level and high altitudes at Thule may be obtained from the U. S. Weather Bureau.[27]

To illustrate the simultaneity of the fluctuations at Bismarck and Thule, Fig. 7 is given. Here the ionization

TABLE V. Data for individual flights at Bismarck, North Dakota, geomagnetic latitude 56°N.

	Time at p_{min} GCT	p_{min}		Time at p_{min} GCT	p_{min}
July 17	14:22	22 g cm^{-2}	Aug. 2	15:38	23 g cm^{-2}
July 22	16:37	45	Aug. 3	14:24	17
July 23	14:08	12	Aug. 4	14:20	25
July 24	13:57	21	Aug. 5	13:38	33
			Aug. 6	14:35	23

TABLE VI. Data for individual flights from shipboard and at Thule.

	λ_m	Time at p_{min} GCT	p_{min}		Time at p_{min} GCT	p_{min}
July 17	55°N	13:14	22 g cm^{-2}	Aug. 2	13:40	16 g cm^{-2}
July 22	58.5°	12:54	17	Aug. 3	13:08	10
July 23	62.5°	12:55	11	Aug. 4	13:20	8
July 24	68°	12:55	9	Aug. 5	13:25	16
				Aug. 6	13:05	13

for certain pressures as taken from Table III for August 3, 4, 5, and 6 are plotted for these stations. The data for August 2 will be discussed later.

In addition to the fact that for these particular days, the intensity of the radiation went up and down simultaneously at these two stations that are 2300 miles apart, two other characteristics are apparent from an examination of the values given in Fig. 7. These are (1) the relatively large difference between Thule and Bismarck in the ionization at 20 g cm^{-2} and (2) the reversal of the intensities at the intermediate pressures. These effects are brought out more fully in curves to follow.

Not only do the fluctuations near the north geomagnetic pole appear to be simultaneous with fluctuations at Bismarck but it also appears to be true that these

[27] *Climatological Summary*, Thule, Greenland, U. S. Weather Bureau, Washington, D. C.

are simultaneous with changes in the ionizing component and neutron intensities as measured at ground level. For completeness we reproduce in Fig. 8 a series of curves already published[16] showing these changes during the period of July 17 to August 14, 1951. The balloon flight data are taken at 50 g cm^{-2}, or about 70 000 feet, primarily because some of the flights did not go above this altitude.

These data emphasize the fact pointed out before by Forbush[14] that these changes are world wide. The present experiments which demonstrate the simultaneous nature of the fluctuations in the radiation at high altitudes between the north geomagnetic pole and intermediate latitudes together with the correlation of changes at high altitudes and ground elevations at both intermediate and equatorial latitudes, gives added support to Forbush's suggestion and places on a firmer basis the world-wide character of these fluctuations.

The ratio of the percentage change in ionization at 70 000 feet to that found at sea level from these data is about 7 to 1. It is obvious that the mean energy of the particles responsible for these fluctuations is less than for the total radiation, since, if the total radiation changed by a given amount, the percentage change would be independent of altitude. Nevertheless, these changes are measured at the equator, although, as Forbush has pointed out,[14] the percentage variation there is somewhat less than at Cheltenham ($\lambda_m = 50°$N).

The ratio of 7 to 1 between changes in the ionizing component at 70 000 feet to those at sea level here found may be compared with the ratio of 10 to 1

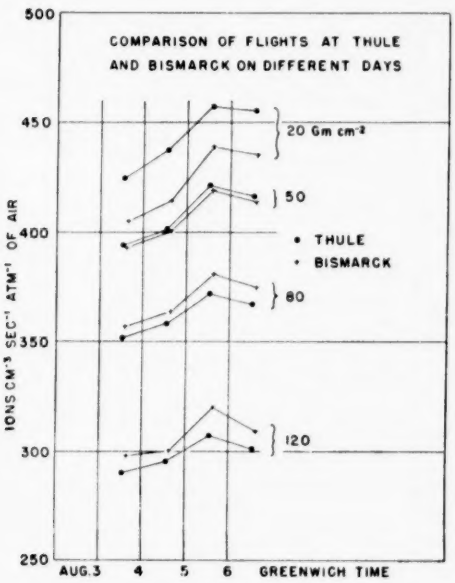

FIG. 7. At given depths in the atmosphere at Thule and Bismarck the ionization changed very close to the same amount for these particular days.

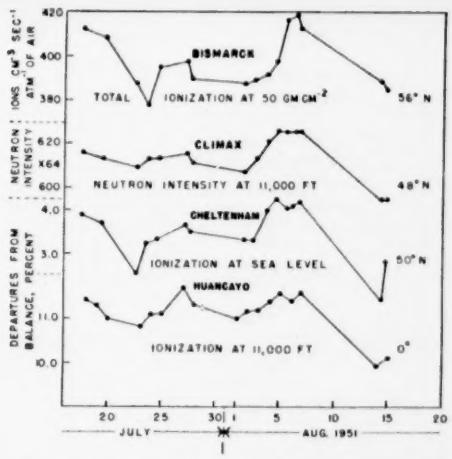

FIG. 8. During July and August, 1951, there was a good correlation between the ionization as measured at 70 000 feet at Bismarck, the neutron intensity at Climax, Colorado, the ionization at Cheltenham, Maryland, and the ionization at Huancayo, Peru.

found by Biehl *et al.*[1] with counter telescopes at about 50 000 feet and a ratio of 6 to 1 found by Jesse.[17] Some further information bearing on the ratio of changes in ionization at high altitudes as compared with sea level is as follows. On July 27, 1946 (data unpublished) a balloon flight was made from Ft. Worth, Texas with our photographically recording ion chambers. This was two days after the large solar flare of July 25 which caused an oft-cited increase in cosmic rays. By July 27 the cosmic-ray intensity at Mt. Wilson had dropped to 5.5 percent below its pre-flare value, while the ionization at 70 000 feet over Texas was 22 percent less than its pre-flare value. This gives a ratio of about 4 to 1. These data indicate that as one proceeds toward the equator, i.e., as the average energy of the primaries increases, the ratio between the fluctuations at high to low altitude decreases.

Since fluctuations in the ionizing component of the order of 1 percent at ground level, which are not attributable to atmospheric effects, are quite common, we conclude from this information that fluctuations of 7 to 10 percent in the ionization are just as frequent at high altitudes and latitudes. From the arguments given in the Introduction, we conclude that the corresponding change in the numbers of primary particles is also of the order of 10 percent.

The percentage change in neutron intensity at Climax, Colorado is roughly three times the change in ionization at Cheltenham. As pointed out previously,[16] the fluctuations shown in Fig. 8 are not due to solar flares such as that which occurred on November 19, 1949. On this occasion the change in neutron intensity at Manchester, England[28] was 60 times the change in

[28] N. Adams, Phil. Mag. **41**, 503 (1950).

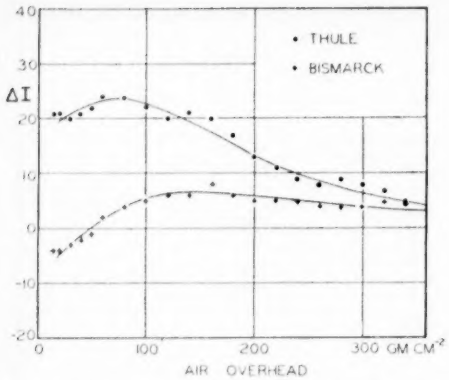

FIG. 9. Differences at Bismarck and at Thule, August 2–August 3, 1951. August 2, 1951 appeared to be anomalous in that the change measured at Thule compared with August 3 was not the same as at Bismarck.

ionizing particles, both measurements being made at ground level.

While it seems reasonable to assume from the above discussion that the fluctuations, at such widely separated stations as Bismarck and Thule, are usually simultaneous, there are some important exceptions to this rule.

A study of Table III will show some of these differences. Comparing the difference between Thule and Bismarck on August 2 with those on August 3, 4, 5, and 6 it is seen that while the former difference tends to disappear at the higher atmospheric pressures, the difference at the low pressures is very much larger than for the other simultaneous flights. We do not believe the difficulty is instrumental. The most likely instrumental failure is that the constant by which the rate of recharging is multiplied, to convert to ions cm^{-3} sec^{-1} $atmos^{-1}$ of air, somehow changed. If this were so, one would not expect the Bismarck and Thule curves to agree at pressures around 300 g cm^{-2}. Furthermore, the points coming down for both flights agreed with those taken going up. Plotted in Fig. 9 are the curves of the differences between August 2 and 3 at both stations.

The above indicates that on August 2 there was present at Thule radiation that was not present at Bismarck. Further, the manner in which it is absorbed in the atmosphere indicates that the particles should have had sufficient momentum to get through the earth's magnetic field at Bismarck.

A further indication that the radiation changes may be different at two widely separated stations is afforded by the flight from shipboard on July 23, 1951. Not allowing for any fluctuations as measured at Bismarck, the upper parts of the three curves taken on July 22, 23, and 24 while proceeding north by ship from Boston are plotted in Fig. 10. These curves show very well what can happen to the shape of the curve at high altitudes from one day to the next. It is evident that on July 23 there were present low energy particles that were not present in such copious numbers on July 22 or July 24. The effect of these particles seems to die out completely in the first 50 g cm^{-2}.

The corresponding Bismarck flight was made about one hour after the July 23 flight from shipboard. The upper part of the curve from this flight we give in Fig. 11. Two facts stand out when this flight is compared with other flights and the July 23 flight from shipboard. (1) The points coming down, in the upper part of the atmosphere, do not agree with those going up. (2) The whole curve is lower than the flight from shipboard.

The "hysteresis" effect shown by the Bismarck curve is interpreted as being due to a more intense incoming radiation while the instrument was coming down than when going up. Since the points coming down agree with those going up at depths greater than 100 g cm^{-2}, we conclude that these particles, if protons, had energies of not more than 0.6 Bev. A search for solar phenomena which may have been present at this time indicates that a flare of magnitude 1 occurred at 1130 Greenwich time. This time is to be compared with 1255 and 1408 when the flights from the ship and at Bismarck reached their maximum heights, respectively. It appears that the effect of the solar flare, while present over Newfoundland was delayed in arriving at North Dakota, its influence being felt only while the instrument was going down.

Spatial dependence on increases in cosmic rays have been reported previously. The increase of February 28,

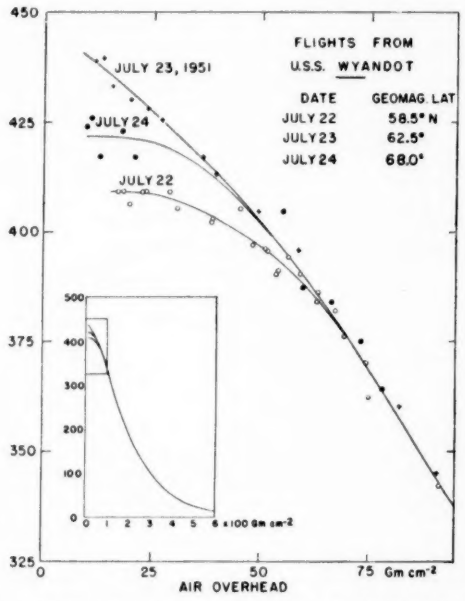

FIG. 10. On July 23 considerably more absorbable radiation was present at high altitudes near Newfoundland than on July 22 or July 24.

1942 amounted to 7 percent at Cheltenham, Maryland,[29] but only a one percent increase in London[30] was observed. The cosmic-ray flare of November 19, 1949 was of different magnitude also at different locations. At Ottawa,[31] Rose reported a 70 percent increase in the ionizing component, while only a 3.6 percent increase was noted by Dauvillier[32] in France. Furthermore, differences in times of an hour for the increase to reach its maximum are reported by various observers.

The indications from the present data are that even small solar flares may give rise to increases in low energy charged particles, whose effects never reach down to sea level and that there are spatial and time differences, which, at the present time, are not well understood.

B. The Geomagnetic Effect at High Latitudes

Having made simultaneous flights at Bismarck and Thule and at points in between, and having eliminated the effect of fluctuations by so doing, it now becomes possible to determine a true geomagnetic effect in going north from 55° geomagnetic latitude, to essentially the geomagnetic pole.

In Fig. 12 the resultant ionization-depth curves are plotted for Bismarck and Thule. The Bismarck curve is that obtained for July 17, 1951, while the Thule curve is the average of the four coincident flights (August 3, 4, 5, and 6) at Thule after having been corrected for the fluctuations as measured at Bismarck, using the flight of July 17 as reference. These two curves cross at about 60 g cm^{-2} (65 000 feet) and also at about 400 g cm^{-2} (25 000 feet). In between these two pressures the maximum difference is about 2.5 percent.

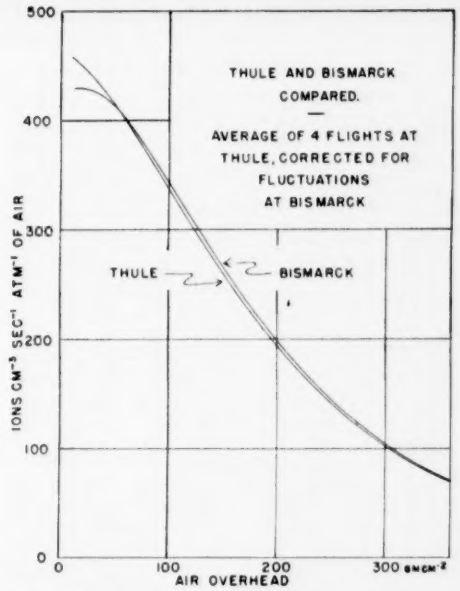

FIG. 12. When the Thule flights are corrected for the fluctuations as measured at Bismarck the resultant ionization-depth curves at the two stations can be compared. The increase of Thule over Bismarck at low pressures is attributed primarily to the shadow effect of the earth. The decrease of Thule over Bismarck at intermediate pressures is ascribed to a temperature effect.

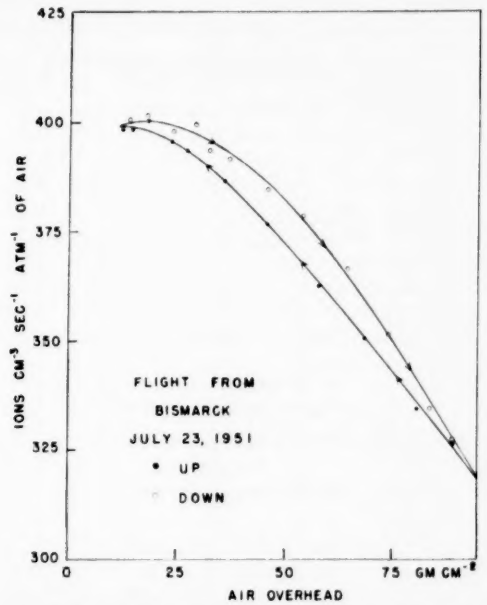

FIG. 11. Flight from Bismarck on July 23 showed an interesting "hysteresis" loop. There is a possible connection of this behavior with that exhibited in Fig. 10.

To determine the manner in which the ionization changes with latitude, the flights from shipboard are used. Figure 13 illustrates the necessity of correcting for fluctuations. Here we have plotted the ionization for given depths in the atmosphere for each of the flights as a function of geomagnetic latitude. The points for a given pressure have arbitrarily been connected by straight lines. The uncertainties given at Thule ($\lambda_m = 88°$N) are merely the extremes of the four flights made on August 3, 4, 5, and 6.

In Fig. 14 we plot the same data as in Fig. 13 but now corrected for the fluctuations as measured at Bismarck, again using the flight of July 17 at Bismarck as a reference. The flight of July 23 at $\lambda_m = 62.5°$N, as discussed previously, is considered anomalous and is omitted. The uncertainties indicated at 88°N are the remaining extremes of the four simultaneous flights after having been so corrected. The somewhat larger disagreement between the Thule flights at pressures greater than 100 g cm^{-2} may be due to variable atmospheric conditions from day to day. The meteorological data for Thule show considerably larger day-to-day fluctuations in temperature for August 3, 4, 5, and 6

[29] I. Lange and S. E. Forbush, Terr. Mag. Atm. Elec. **47**, 331 (1942).
[30] A. Duperier, Proc. Phys. Soc. (London) **57**, 473 (1945).
[31] D. C. Rose, Can. J. Phys. **29**, 227 (1951).
[32] A. Dauvillier, Compt. rend. **229**, 1096 (1949).

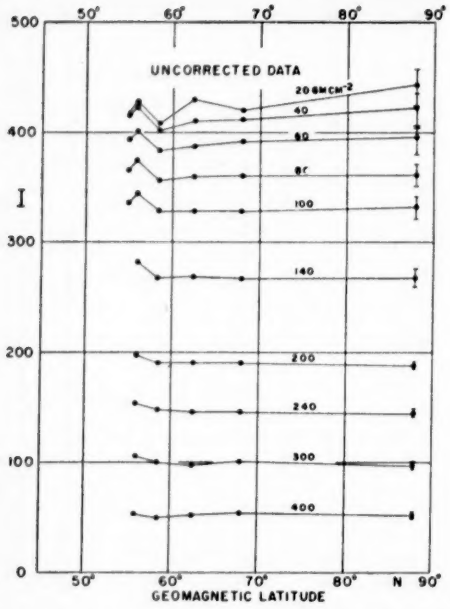

FIG. 13. Ionization for given depths in the atmosphere for each flight as a function of geomagnetic latitude. Before corrections are made to the data obtained at intermediate latitudes and at Thule for the fluctuations measured at Bismarck, very little consistency is evident when ionization at given depths is plotted against geomagnetic latitude.

at the intermediate altitudes compared with those at the higher altitudes. The data for the different flights should then become more consistent at high altitudes and this they appear to do.

The present results may be compared with some previous data taken by Biehl and Neher[33] with an unshielded ionization chamber while on a B-29 airplane flight at 30 000 feet from 64° geomagnetic north to the equator, along longitude 80°W. This ionization chamber had an average wall thickness of 8 mm of steel. The contribution of showers from this amount of material plus additional matter close by, due to its location in the plane, probably accounts for the somewhat larger value of ionization shown in Fig. 14 as compared with the present data, taken with thin-walled ionization chambers (0.5-mm steel), for the same atmospheric pressure. However, the agreement as to the slopes of the lines seems to be quite satisfactory.

The two outstanding characteristics, evident from both Figs. 12 and 14 are (1) the negative latitude effect at intermediate latitudes and altitudes and (2) the positive latitude effect at very high altitudes.

Effect (1) appears to be due to the influence of the warmer atmosphere over northern Greenland in the summer compared with that over North Dakota. Weather data, furnished by the U. S. and Danish Weather Bureaus, show that the average temperature for August 3, 4, 5, and 6, 1951 at the 100-mb level at Thule was −42°C and at Bismarck −63°C. At the 50-mb level the temperatures were −41°C and −54°C, respectively (see Fig. 15). In the warmer, and hence more attenuated, atmosphere the μ-mesons will decay, on the average, with more kinetic energy than in the denser atmosphere and hence more energy, on the average, will go into the two resulting neutrinos. Assuming that no new particles get through the earth's magnetic field between Bismarck and Thule, whose influence can penetrate to these intermediate altitudes, we calculate a temperature coefficient on the above basis, assuming an effective temperature difference of 16°C,

$$\alpha=(1/I)(dI/dT)=-0.19 \text{ percent } ^\circ\text{C}^{-1},$$

for altitudes of 30 000 to 50 000 feet. The value found at sea level by various observers is close to this for intermediate latitudes but it is not clear just how they are related.

At high altitudes the atmospheric temperature situation becomes somewhat different. Studies of Kellogg and Schilling[34] indicate that in the summertime the temperature from about 30 to 50 km altitude should be lower over northern Greenland than over Bismarck. At a height of about 30 km (100 000 feet) their analysis indicates

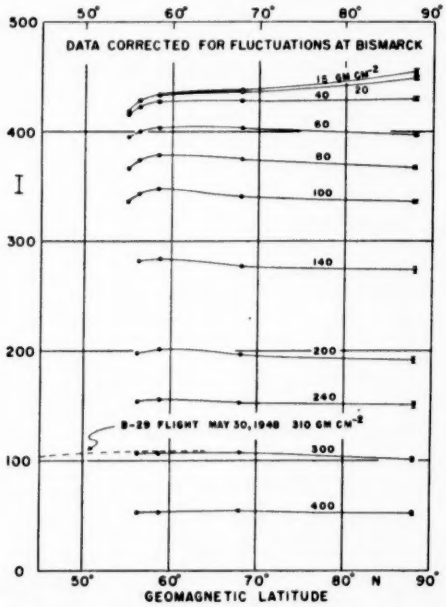

FIG. 14. After corrections are made to the flights at intermediate latitudes and at Thule, the data show much more consistency than is evident in Fig. 13. The uncertainties indicated at 88°N are the resultant extremes of the 4 simultaneous flights after corrections are made.

[33] A. T. Biehl and H. V. Neher, Phys. Rev. **78**, 172 (1950).

[34] W. W. Kellogg and G. F. Schilling, J. Meteorol. **8**, 222 (1951); also, W. W. Kellogg, *Physics and Medicine of the Upper Atmosphere* (The University of New Mexico Press, New Mexico, 1952), Chap. IV, page 71.

that there is little, if any, change of temperature with latitude, during the summer months, from intermediate latitudes on to the pole. The actual situations for August 3, 4, 5, and 6, as determined from the weather data, for the two stations, are shown in Fig. 15. The solid lines give the average temperatures for these four days. The dashed parts represent the probable extensions of these curves to higher altitudes from the analysis of Kellogg and Schilling. We infer, then, that the effects of decay, in causing a difference in the ionization at Bismarck compared with points north, should disappear for pressures of 10 to 15 g cm^{-2}.

As to the increase in ionization with increasing latitude at very high altitudes mentioned above as effect (2), it will be noticed from Fig. 14 that an increase of 5 percent in the ionization occurs at 15 g cm^{-2} between 66° and 88°N. The minimum energy allowed by the Stoermer cone for protons at 66°N is approximately 140 Mev. Protons of this energy have a range in air of about 16 g cm^{-2} and hence would just penetrate to the instrument. The increase from 66° to 88° should then not be due to new particles let in by the opening of the Stoermer cones.

At a given geomagnetic latitude only part of the sky is accessible to particles of a given momentum. The boundary that separates the accessible from the forbidden regions, forms what is known as the Stoermer cone. An application of Liouville's theorem implies that over the accessible region, particles of this momentum come in with uniform intensity. At latitudes where the Stoermer cone has opened up completely for particles of a given momentum, one might expect the whole sky to be uniformly illuminated by these particles. The presence of the earth, however, prevents some of the particles from arriving due to the fact that their trajectories have intersected the earth elsewhere.

Schremp[35] has calculated this shadow effect and has presented his results in the form of orthogonal projections for every 10° of latitude. For positive particles in the northern hemisphere, the boundaries to these shadow cones are at zenith angles greater than 45° and extend from the northwest quadrant around toward the southeast. The theory indicates that particles of high momentum are affected most. Thus at 70°N even some particles of momentum 14 Bev/Zc are not present near the eastern horizon due to the fact that they have struck the earth before reaching the point of observation.

Using Schremp's calculations and the energy distribution of the primary radiation given in a previous paper,[36] the effect of these shadow cones has been determined by graphical integration. The results show (1) that the magnitude of the increase calculated between geomagnetic latitudes 56° and 88° is about 4 times that observed and (2) that the increase in the numbers of particles between 66° and 88° should be about four times that between 56° and 66°. As far as the discrepancy in magnitude is concerned, some of it can be explained by the greater length of path for the particles coming in at the large zenith angles which will result in secondaries that lose a considerable portion of their energy in neutrinos. More work needs to be done, however, both from the experimental and theoretical points of view.

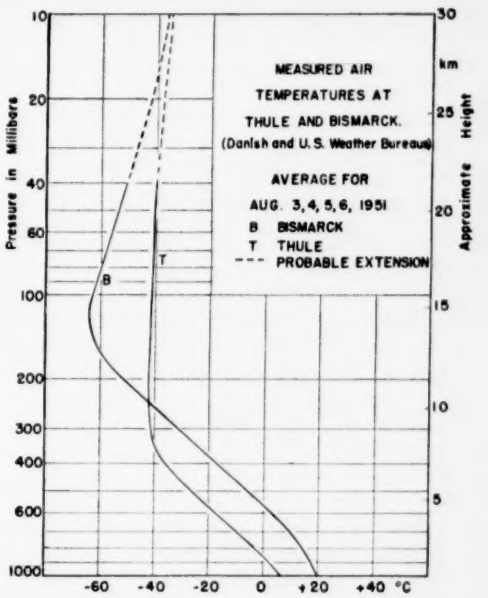

FIG. 15. Temperature data at the two stations were furnished by the U. S. and Danish Weather Bureaus. The extensions indicated are based on the analysis of Kellogg and Schilling. (See reference 34.)

We may, then, divide the distance, at very high altitudes, between Thule and Bismarck, into two regions, (1) that between 56° and 66°N where the increase in ionization at 15 g cm^{-2} may be due to both the increase in the number of low energy particles admitted by the earth's magnetic field and the decrease of the shadow cones, and (2) that between 66° and 88° where the increase must be due to the shadow effect alone since new low energy particles admitted above 66° cannot reach down to the instrument. We may then take the increase from 66° to 88°N as an experimental determination of the shadow effect at these latitudes. The increase in ionization between these latitudes is 4 percent, at 15 g cm^{-2}, from Fig. 14. Assuming the latitude dependence as calculated for the shadow cones as correct we would then expect a 1 percent increase in the ionization due to the shadow effect between 56° and 66°. From Fig. 14 it will be seen that the increase in ionization is about 1 percent between 58° and 66°N. We therefore conclude that the shadow effect can account for all the increase measured, at the highest

[35] E. J. Schremp, Phys. Rev. **54**, 158 (1938).
[36] H. V. Neher, Phys. Rev. **83**, 649 (1951).

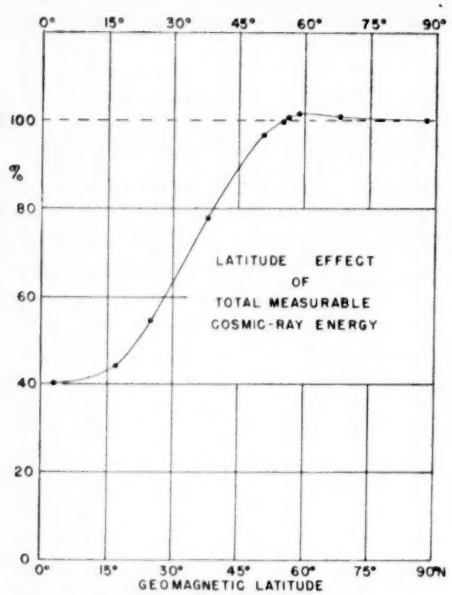

FIG. 16. The latitude effect of the total measurable cosmic-ray energy per unit area dissipated in the atmosphere.

altitudes, from about geomagnetic latitude 58°N to the pole.

The latitude effect may be defined also in terms of the energy dissipated in the atmosphere per unit of horizontal area as a function of latitude. It is easily shown that, except for loses in particles, such as neutrinos, which never reappear in the form of ionizing radiation, the area under the ionization-depth curve gives the total energy dissipated in a vertical column of air of unit cross section. If we call the total area under the Thule curve 100 percent, then the areas at the other latitudes may be expressed in terms of this. In so doing we arrived at the values given in Fig. 16.

In determining the area at 55°N, some interpolation was necessary in drawing the curve, since the data extended down only to 100 g cm^{-2}. The curve was completed by running it into the corresponding Bismarck curve at a somewhat higher pressure. To extend the curve of Fig. 16 to lower latitudes our data taken in past years were used. The point at 51°N was obtained from the data taken at Saskatoon and Omaha[7] in 1937. A decrease in area of 4.7 percent was found at that time[37] in going from 60°N to 51°N, and this is the difference between the Omaha point and the value at 60°N in Fig. 16. The point at 38°N is at San Antonio, Texas and is taken from our data[7] of 1936. The point at 3°N is from our balloon flights in India in 1936 which agreed with those made[38] in 1940. That at 17°N is from the Agra flights in December, 1939. The above flights were all made with similar, carefully compared, photographically recording ionization chambers. The point at 25°N is for Peshawar, India from data obtained with single Geiger counters. Single counter flights were also made at 17°N and 3°N and a comparison made with our ionization chambers at these latitudes.

While the points from 51°N to the equator in Fig. 16 were not taken simultaneously the few percent error that might have been introduced into this relative comparison will not alter the principle features of this curve.

It should be pointed out that the lower three points of Fig. 16 were taken at longitudes 70° to 77°E while all the other points were taken at about 95°W. The effect of change of longitude on the area is such[39] that approximately 16 percent should be added to the values at 70°E longitude near the equator to obtain the expected values at 90°W. It should further be pointed out that all of these data at the intermediate and higher latitudes were taken in the summer months and may not quite represent the conditions prevailing during the winter.

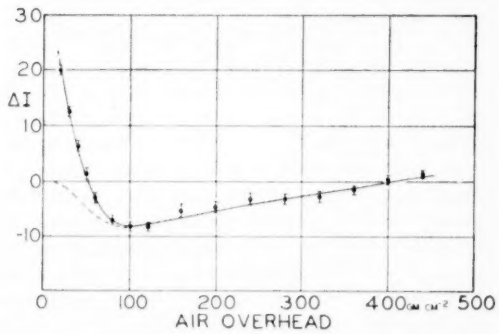

FIG. 17. Difference between Thule and Bismarck as shown in Fig. 12. (Average of four flights.) The dashed line represents an estimate of the temperature effect extended to higher altitudes.

The behavior of the curve of Fig. 16 from 56° on north is determined by the same effects discussed previously, namely, (1) any new particles that are permitted to enter by the earth's magnetic field, (2) new particles admitted by the closing of the shadow cones, and (3) differences in losses in neutrinos throughout the atmosphere because of the different density of the air. To gain an estimate of the magnitudes of these effects on the areas under the ionization depth curves, we have plotted Fig. 17 giving the difference between the curves of Fig. 12 which are the averages obtained for Bismarck and Thule. The negative part of the curve we have attributed to μ-meson decay effects in the middle part of the atmosphere. As pointed out

[37] Reference to the Cheltenham data of the Carnegie Institution of Washington shows that the ground level ionization was very close to the same for these Saskatoon and Omaha flights. [See I. Lange and S. E. Forbush, Carnegie Institution of Washington Publication No. 175, p. 130, 1948.]

[38] H. V. Neher and W. H. Pickering, Phys. Rev. **61**, 408 (1942).

[39] H. V. Neher, Phys. Rev. **78**, 674 (1950).

previously, this difference should disappear at the higher altitudes where the temperature of the air becomes nearly equal at the two stations. We have drawn a dashed line in Fig. 17 to represent what seems to be a reasonable extension to lower pressures for this temperature effect. The sharp upturn of the curve we attribute primarily to new particles admitted by the disappearance of the shadow effect at Thule, although there may be some effect of added particles let in by the opening of the Stoemer cones. The negative area of Fig. 17, which we assume is due to the temperature effect, is 2 percent of the total area under the ionization-depth curve. The positive area added is 1 percent. Since some of this must be due to the shadow effect, it is evident that very little can be due to the addition of lower energy particles. It appears from Fig. 16, however, that there is an increase in energy up to about geomagnetic latitude 58°N. This is consistent with the ionization shown by the top curve of Fig. 14.

Recapitulation on the latitude effect at high altitudes and latitudes: We have shown (1) that any new particles admitted by the earth's magnetic field, if protons, should reach down to our instrument at least up to a latitude of 66° geomagnetic north, (2) that at these altitudes (90 000–100 000 feet) the temperature of the atmosphere should be approximately independent of latitude and hence temperature differences should not affect the relative ionization at these altitudes at latitudes above 56°N because of losses due to neutrinos, (3) that the shadow effect alone can account for all new particles that appear at very high altitudes from 58° to 88° geomagnetic north, and (4) that the temperature and shadow effects will account for the difference in the areas under the ionization-depth curves from 58° to 88°N.

In addition to the above experimental evidence for a cutoff of primary particles, another argument can be made in terms of the fluctuations measured at Bismarck and Thule. When corrections are made to the Thule flights for fluctuations as measured at Bismarck, it is found that on 4 out of the 5 days when simultaneous flights were made, the corrected values at Thule showed a remarkable consistency from day to day. This is illustrated in Table I. The interpretation we placed on this is that no radiation fluctuates at Thule that does not also fluctuate at Bismarck. If any low energy primary particles were present at Thule which were not also present at Bismarck, one would expect them to fluctuate also. From Table I the corrected data for the 4 flights are consistent with each other to less than ±0.5 percent down to an atmospheric depth of at least 100 g cm^{-2}. Hence, within rather narrow limits, there are no lower energy particles, which could penetrate the atmosphere down to our instrument and which would be admitted by the earth's field, from geomagnetic latitude 56° to 88°N.

Giving somewhat less weight to this latter argument than those given previously, we conclude that a real cutoff of the primary particles exists and we place the latitude at which this occurs at 58°±1° geomagnetic north. Because of the omnidirectional character of our instrument, particles of a given momentum will be effective until the allowed cone is nearly completely open. We shall take a zenith angle of the allowed cone of 45°E in the E-W plane and assume that any further opening will not appreciably affect our results. The limiting momentum at this angle at 58° is found to be[39] 1.5±0.2 Bev/Zc, which for protons represents an energy of 0.8±0.2 Bev. The errors indicated in the energy and momentum give the estimated uncertainties arising from both the experimental errors and those in estimating the effective opening of the allowed cone.

IV. DISCUSSION

A. The Fluctuating Radiation

In Fig. 3 we have given the curves obtained at Bismarck and at Saskatoon on various occasions. In Fig. 18 we have plotted the difference between Bismarck in August, 1940 and Saskatoon in August, 1937. This latter curve represents the absorption in the atmosphere of the radiation present in 1940 that was not there in 1937. At the highest altitudes reached the ionization in 1940 was about 33 percent higher than in 1937, corresponding to a similar increase in the number of primary particles. A reasonable extension of the original curves to higher altitudes would certainly increase this number.

The additional radiation present in 1940 consisted mostly of low energy particles that were rapidly absorbed in the atmosphere. In addition, however, there were also present particles whose effects extended down through the whole atmosphere. If we compare the increase, as measured at 50 g cm^{-2}, of the 1940 Bismarck data over that at Saskatoon in 1937 with similar data at Cheltenham and Huancayo[40] for the

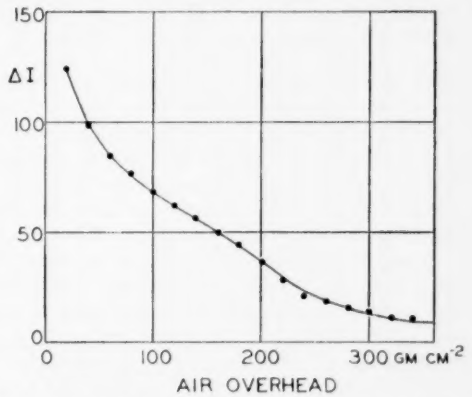

FIG. 18. The difference between curves *A* (Bismarck, Aug. 21, 1940) and *E* (Saskatoon, Aug. 14, 1937) of Fig. 3. This curve represents the way in which the additional radiation at Bismarck in August, 1940 over that present in 1937 is absorbed in the atmosphere.

[40] I. Lange and S. E. Forbush, Carnegie Institution of Washington Publication No. 175, 1948.

same days, we find a ratio of about 10 to 1, if we take the average shown by these two ground stations. This is consistent with the ratios previously determined for this latitude. (The reason for taking the average for Huancayo and Cheltenham is that over a period of years there seems to be a gradual drift of the instruments which is different at the two stations.)

A similar curve is obtained by taking the difference between August 6 and August 3, 1951. In Fig. 19 this difference for both Thule and Bismarck has been plotted. This curve emphasizes again the usual similarity in the fluctuations at the two locations. There is a striking resemblance of this curve with that given in Fig. 18 and discussed above. The chief difference is in the magnitude of the ordinate. We shall assume that the same agency is at work in causing these changes in each case.

As pointed out in the Introduction, a clue as to the nature of the particles that fluctuate may be obtained

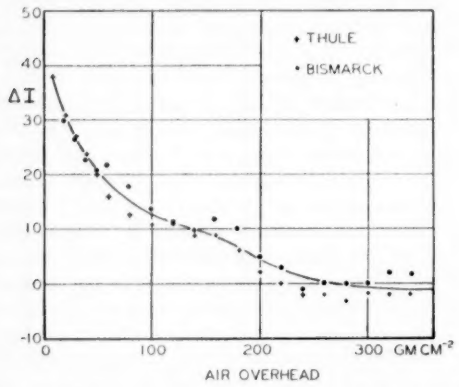

FIG. 19. Differences at Bismarck and at Thule, August 6–August 3, 1951. The difference at Thule on August 6 compared with August 3 is quite similar to the difference shown at Bismarck for the same two days.

by comparing the change in ionization at very high altitudes with the change in area that they produce. For the total incoming particles, as obtained from Fig. 3 curve C, the ratio of the ionization at very high altitudes to the total area they produce is 4.2×10^{-3} g^{-1} cm^2. With a reasonable extrapolation to zero pressure, the average for this quantity as obtained from Figs. 18 and 19 is 12×10^{-3} g^{-1} cm^2. We interpret this to mean, that for these occasions, either the average particle that fluctuated ionized 3 times as much along its path as the average for all cosmic-ray particles, or that the particles that fluctuated were essentially the same as the total but that their average energy was one-third as great. There might, of course, have been a mixture of these two possibilities.

It is evident, however, that the fluctuations could not have been in heavy nuclei alone. Kaplon *et al.*[21] found that the dependence of the number distribution on the energy per nucleon is approximately the same for all atomic numbers Z. The ionization of a high velocity nucleus varies as Z^2, while the energy brought in by a nucleus of a given momentum (pc/Z) varies as Z. The ratio of these two is Z. It is clear then that if the energy distribution of the particles remains unaltered, and the fluctuations were only in particles heavier than protons, that their average Z could not have been greater than three times that for the average of all primaries. We think it more likely that, whatever the mechanism causing the fluctuations, it affects particles of all Z but alters the energy distribution, so that particles of low energy are changed more than those with higher energy.

In seeking an explanation for these fluctuations, one may assume (1) that the source itself fluctuates and/or (2) that the fluctuations are due to some agency between the source and the earth.

If the intensity changes at the source, then the number of sources must be small and near at hand. The reason for the small number of sources is as follows: Suppose the number were large and scattered throughout the galaxy. Then one would hardly expect any one or even a few to predominate in their effects on the earth. Since the fluctuations are large we conclude, from probability considerations, that if the sources fluctuate their number must be small and, from energy considerations, they must be relatively close.

The other possibility, that the fluctuations are due to some agency between the source and the earth, has been treated by a number of authors. One such agency discussed by Meixner[41] might be a fluctuating solar magnetic field. The effect of such a varying field has been discussed by Alfven.[42] Briefly, the arguments are as follows. The effect of a general magnetic field of the sun whose dipole moment is in the neighborhood of 0.5×10^{34} gauss-cm^3 is to eliminate all particles whose momentum is less than about 1 Bev/Zc from arriving at the earth. However, no changes would be expected at the equator if only particles with momentum of less than a few Bev/Zc were so affected. This is contrary to the world-wide changes in cosmic rays that appear to exist.

Another possible agency that has often been discussed is a fluctuating magnetic field set up by a ring current surrounding the earth. Although such a mechanism has many attractive features from the point of view of interpreting magnetic fluctuations, serious objections have been raised by those attempting to explain cosmic-ray fluctuations by any such ring current. Johnson long ago[43] pointed out that the changes in cosmic rays were many times greater than could be expected from the measured change in the magnetic field during a magnetic storm. Furthermore, the calculations of Hayakawa[44] indicate that if the radius of this

[41] W. Heisenberg, Editor, *Cosmic Radiation* (Dover Publications, New York, 1946), p. 178.
[42] H. Alfven, Nature **158**, 618 (1946).
[43] T. H. Johnson, Revs. Modern Phys. **10**, 193 (1938).
[44] See S. Hayakawa, reference 18, p. 496 for discussion.

ring current is greater than 1.3 earth radii, the effect on incoming cosmic-ray particles of 15 Bev/Zc momentum is opposite to that observed.

A further objection to the ring current as explaining cosmic-ray fluctuations seems to be as follows: The axis of the ring presumably coincides with that of the geomagnetic axis. Along this axis all directions should be allowed for all energies of incident particles. For an isotropic distribution at great distances, this means the sky at the geomagnetic north pole should be equally illuminated with particles of all energies in all directions. A changing magnetic field should have no effect on this intensity. At the equator or at intermediate latitudes, changes in intensity would, however, occur. This is contrary to the experimental fact that changes are definitely observed near the pole.

Another mechanism suggested by Alfven[42,45] is that of electrical fields being built up in the ionized streams ejected from the sun. Cosmic-ray particles passing through these streams would not only lose or gain energy, changing the energy dissipated in the atmosphere, but the latitude for cutoff for particles of a given original momentum would also change.

Nagashima[46] has investigated the effect of changing electric fields on the distribution in numbers of particles arriving at the earth at various latitudes when Liouville's theorem is applied in the generalized form to apply to electric as well as magnetic fields.[47] He finds that changing potentials, at some distance from the earth, of the order of 0.1 Bev can cause changes in the ionization at high altitudes of a few percent at the equator and 5 to 10 percent at the higher latitudes. This proposed mechanism has the advantage of giving changes at the equator as well as at the poles which are roughly in agreement with experiment.

In seeking an explanation for these fluctuations in the primary cosmic rays, any proposed mechanism or mechanisms must satisfy the requirement first, that, in general, the changes are world wide; second that the changes in the ionizing component at sea level are nearly independent of latitude; third, that the changes in the ionizing component increase with increasing latitude; fourth, that the fluctuations in the ionizing component at high altitudes are larger than at intermediate altitudes or at ground level; fifth, that the changes in the neutron component are several times those in the ionizing component.

B. The Latitude Effect at High Altitudes and Latitudes

We have presented experimental evidence to show that there is a cutoff of the primary cosmic-ray particles at about 58° geomagnetic north. Briefly, this conclusion is based on the following arguments: (1) The small increase in ionization (Fig. 14) of one percent at 15-g cm^{-2} air pressure from 58° to 68°N can be accounted for entirely by shadow effects due to the interception of particles of relatively high energy by the earth. (2) The behavior of the curve (Fig. 16) giving the total energy dissipated in the atmosphere *vs* geomagnetic latitude from 58° to 88°N can be accounted for entirely by atmospheric temperature and shadow effects. (3) No particles fluctuate at 88°N, in general, that do not also fluctuate at 56°N. We interpret this to mean that, with certain exceptions, no low energy particles are present at the one station that are not also present at the other. We have given more weight to the first two arguments and have set the cut-off latitude at 58°±1°. Because of the omnidirectional character of our apparatus the cut-off momentum is not that for the vertical direction. Taking as an effective zenith angle, 45°E, we found the cut-off momentum to be 1.5±0.2 Bev/Zc. This corresponds to an energy for protons of 0.8±0.2 Bev.

In a recent discussion of their own measurements with rockets compared with the results of Pomerantz,[8] and Van Allen and Singer[48] have shown that within experimental errors their rocket flight at 58°N shows the same primary flux as Pomerantz's balloon flights with Geiger counters at 69°N. The experimental errors are given by Van Allen and Singer as ±10 percent for their own measurements and ±8 percent for those of Pomerantz. These two sets of experiments were performed at different times. Those of Pomerantz were in August, 1949, while Van Allen and Singer made their rocket flight in January, 1950. In view of the fluctuations discussed above one must add to the experimental uncertainties those due to possible changes in the radiation also, since no monitoring station was used. On the basis of the fluctuations given in Figs. 7 and 8, we conclude that in each case the uncertainties for each set of experiments would need to be increased to ±15 or 20 percent. Thus, barring any large changes, such as occurred at Bismarck and given in Fig. 3, there could be a 30 to 40 percent increase in the numbers of primary particles in going from 58° to 69°N at any given time and a comparison of these two experiments would stand a good chance of not revealing such an increase.

Several mechanisms have been invoked to account for the cutoff of low energy particles in cosmic rays. Janossy's[13] suggestion that the general magnetic field of the sun turns away particles below a certain momentum from the earth is still a distinct possibility. Alfven's[49] discussion of the effect of turbulence in the photosphere of the sun on the Zeeman pattern for such a weak field, has thrown some doubt on the interpretation of such measurements as a means of arriving at the general magnetic field of the sun. The magnetic moment of the sun that would cause a cutoff of cosmic-ray particles in the neighborhood of 58° geomagnetic

[45] H. Alfven, Phys. Rev. **75**, 1732 (1949).
[46] K. Nagashima, J. Geomag. Geoelec. **3**, 100 (1951).
[47] W. F. G. Swann, Phys. Rev. **44**, 224 (1933).
[48] J. A. Van Allen and S. F. Singer, Nature **170**, 62 (1952).
[49] H. Alfven, Nature **168**, 1036 (1951).

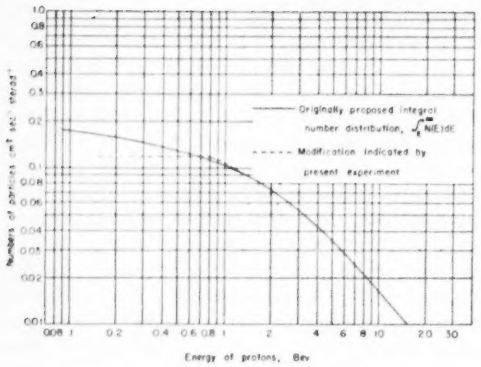
Originally proposed integral number distribution, $\int_E^\infty N(E)dE$
Modification indicated by present experiment
Energy of protons, Bev

FIG. 20. The present experiments indicate a cutoff of the primary radiation at 58°±1° geomagnetic north. A modification to the number distribution proposed previously (see reference 36) is here indicated.

north is 0.65×10^{34} gauss-cm³. This corresponds to an equatorial solar magnetic field at the photosphere of 19 gauss.

The diurnal effects to be expected from such a dipole of the sun have been discussed by Epstein,[50] Kane, Shanley, and Wheeler,[51] Dwight,[52] and Singer.[53] On the basis of Epstein's and Dwight's calculations one might expect a diurnal effect at geomagnetic latitude 51° for the above solar dipole moment. The expected magnitude would be 5 to 8 percent, depending on the energy distribution of the primary particles, with a maximum at about 6 A.M. and a minimum at 6 P.M. Bergstralh and Schroeder[54] made two balloon flights at 56°N which were intended primarily to test for a diurnal effect. None was found, either in the total ionizing radiation, the low energy gamma-rays or the fast neutrons at high altitudes. It is evident, however, that if the solar magnetic field keeps any new particles from coming to the earth above 58°N that only a small diurnal effect might be found at 56°N. A more appropriate geomagnetic latitude would be 51° to 53°N.

On the other hand, while no serious attempts have apparently been made to detect any systematic differences at different times of the day, it is difficult to understand how such large changes from 6 A.M. to 6 P.M. could have escaped detection. Alfven[55] proposed a mechanism which would decrease the expected diurnal effect, and the detailed calculations of Kane, Shanley, and Wheeler[51] have shown that this mechanism would result in a maximum diurnal change of only a few percent of that calculated by Epstein. Alfven considered the scattering of incoming particles by the magnetic field of the earth. Depending on the magnitude of the solar magnetic field, particles within a certain momentum range that came within the influence of the earth's magnetic field but did not hit the earth would be deflected into trapped orbits about the sun. Eventually these would hit the earth but would come from directions that were initially prohibited. It seems reasonably certain that the absence of a large diurnal effect is not an argument against a solar cutoff.

The residual systematic diurnal effect found by Kane *et al.* would be difficult to establish in view of the much larger random diurnal effects discussed earlier in this paper.

Unsöld[56] has proposed that the cutoff is due to low energy charged particles being stopped by losing their energy through ionization in passing through interstellar matter which, on the average, he estimates at 50 g cm^{-2}. If there is a uniform distribution in the energies of the initial primaries, one would expect that by this same mechanism other particles with slightly higher energies would end up in the lower energy group and thus no cutoff would occur.

With the present information it is now possible to revise the number spectrum proposed by one of us.[36] In Fig. 20 the originally proposed integral spectrum derived from balloon-borne ionization chamber and counter telescope data is represented by a solid line while the modification indicated by the present experiments is given by the dashed line. The cutoff of the primary radiation we have placed at 0.8 Bev for protons as discussed above.

V. SUMMARY

Using a new type of integrating ionization chamber, whose information is transmitted readily by radio, a series of balloon flights was made from shipboard going north from Boston in the summer of 1951. These were made from geomagnetic latitudes 55°, 58.5°, 62.5°, and 68°N. Another series of flights was made from Thule, Greenland at geomagnetic latitude 88°N. Five of these latter and the 4 shipboard flights were made at approximately the same Greenwich time as similar flights from Bismarck, North Dakota (56°N) made by another expedition. The major experimental results and conclusions drawn therefrom may be stated as follows:

1. The ionization-depth curves at Bismarck in July and August, 1951 did not pass through a maximum as was the case in 1938. They were, in fact, intermediate between the 1938 flights and those obtained in 1940.

2. The fluctuations in the radiation at high altitudes, measured during the present series of flights, were simultaneous at the two stations. Two of the nine simultaneous flights were exceptions to this statement. On at least one of these occasions, a small solar flare may have been responsible for this difference.

3. During the period of observation, the magnitude

[50] P. S. Epstein, Phys. Rev. **53**, 862 (1938).
[51] Kane, Shanley, and Wheeler, Revs. Modern Phys. **21**, 51 (1949).
[52] K. Dwight, Phys. Rev. **78**, 40 (1950).
[53] S. F. Singer, Nature **170**, 63 (1952).
[54] T. A. Bergstralh and C. A. Schroeder, Phys. Rev. **81**, 244 (1951).
[55] H. Alfven, Phys. Rev. **72**, 88 (1947).
[56] A. Unsöld, Phys. Rev. **82**, 861 (1951).

of the fluctuation in the ionization from day to day amounted to from 5 to 10 percent at the highest altitudes.

4. The fluctuations at high altitude in the ionizing component showed a good correlation with ground level measurements of the ionizing component both at 50°N and at the geomagnetic equator. The changes at 70 000 feet were approximately 7 times as large as the changes in penetrating component at sea level. Since changes of the order of 1 percent at sea level are quite common, that are not ascribable to atmospheric effects, we conclude that changes of 7 to 10 percent at very high altitudes and high latitudes are also common.

5. There was a similar correlation between the ionization at 70 000 feet and the neutron component as measured at ground level at intermediate latitudes. The ratio of the fluctuations in this case was about 2 to 1.

6. On only 2 occasions out of a total of 14 at the two stations, where such an effect should have been detected, was the curve obtained on the down flight significantly different than on the up flight. Since the time spent at the high altitudes was from 1 to 2 hours, we conclude that changes in the radiation are not likely to occur in this period of time.

7. The particles that fluctuate cannot be those of high atomic number only. This we deduce from the ratio of the change in the ionization at very high altitudes to the change in area under the ionization-depth curve they produce, compared with a similar ratio for all cosmic-ray particles. If the fluctuations are due to particles with atomic number Z, larger than 1, evidence is cited to show that Z is probably not larger than 3. We conclude that the most reasonable explanation for the factor 3 is that some mechanism affects the energy distribution of the primary particles in such a manner that the average energy of the particle that fluctuates is about $\frac{1}{3}$ of the average for all primaries.

8. A negative latitude effect in the ionization at high latitudes and intermediate altitudes was found. This we have ascribed to a temperature effect due to the warmer air above Thule as compared with Bismarck for that time of year. The coefficient obtained is -0.19 percent per degree Centigrade for altitudes around 40 000 feet.

9. At pressures less than 40 g cm^{-2} we find a positive latitude effect at high latitudes. This we have ascribed to the disappearance of the earth's shadow cones as one goes north. The increase beyond 66°N at the highest altitudes reached (about 15 g cm^{-2}) cannot be due to new low energy particles being admitted by the earth's magnetic field, since their energy is too low to penetrate the residual atmosphere above the instrument.

10. At altitudes corresponding to 15 g cm^{-2} there appears to be no latitude effect in the total ionization between 58° and 66° geomagnetic north. Arguments are presented to show that differences in ionization cause by temperature differences between these two latitudes and at this altitude should be small. The sum of the effects due to the earth's shadow and new particles appears to be less than 1 percent. We therefore conclude that the number of new low energy particles whose energy, if protons, lies between 0.8 and 0.14 Bev must be less than 1 percent of the total number of incident particles.

11. A similar conclusion is drawn from the areas under the ionization curves *vs* geomagnetic latitude. The slightly smaller area at 88°N compared with 58°N is assigned to a difference in energy loss due to neutrinos, while the absence of a significant change from 58° to 66°N is interpreted as meaning that no new particles come to the earth in the above energy interval.

12. The simultaneous nature of the fluctuations at Bismarck and Thule, together with the fact that they usually were closely of the same amount, shows that, in general, no particles fluctuated at Thule that did not also fluctuate at Bismarck. We interpret this to mean again that no new particles were entering north of Bismarck, since if there were, they too would have fluctuated. Weighing the experimental evidence we have placed the latitude of cutoff of the primary particles at 58°$\pm$1° geomagnetic north.

13. To account for this cutoff of low energy particles, which for protons is about 0.8 Bev, we think a general solar magnetic field is the most reasonable mechanism. If so, the magnetic moment necessary would be 0.65×10^{34} gauss-cm^3. This would correspond to 19 gauss at the solar equator.

In conclusion, we want to acknowledge the aid and cooperation of persons and agencies who made the carrying through of these experiments possible. The local Pasadena U. S. Office of Naval Research as well as the main ONR office in Washington were of great assistance in making many of the arrangements. The U. S. Navy and the Military Air Transport Service we wish to thank for furnishing the necessary transportation. We are also grateful to Captain F. W. Laing and the officers of the U. S. S. Wyandot for their cooperation in making the flights from shipboard in going north from Boston.

We are particularly grateful to the U. S. Weather Bureau for the assistance rendered. Through Chief of the Bureau, Dr. F. W. Reichelderfer, arrangements were made for helium supplies at Bismarck, Thule and on shipboard. Also through his office arrangements were made for accommodations at the Weather Bureau station at Thule. We also want to thank Mr. Robert B. Sykes, Jr., Chief of the Arctic Operations Project, Mr. J. Glenn Dyer, Assistant Chief, and Mr. George Rabbitt, all of the Weather Bureau, for much needed assistance. The help of Mr. John T. Crowell, Officer in charge of the Weather Bureau station at Thule, and of Mr. F. J. Bavendick, in charge of the Bismarck Office, is gratefully acknowledged.

We want also to express our appreciation to the Danish Government for permission to go to Greenland to make these flights. The assistance of the Thule Colony Manager, Mr. Krough in enlisting the help of the Eskimos and Danish residents in locating instruments is also appreciated. By this means, two instruments were found, one, 150 miles north of Thule on the ice cap.

Finally we want to thank Dr. Robert A. Millikan who assisted in making the arrangements and who was greatly interested in the project. Also we are grateful for the able assistance of Dr. Bernard Steenson and Mr. Alan Johnston in making the equipment, in its calibration, and in carrying out the flights. Our thanks are also due Dr. Oliver Wulf for valuable discussions on the properties of the upper atmosphere.

PHYSICAL REVIEW VOLUME 90, NUMBER 4 MAY 15, 1953

Nuclear Interactions of 210-Mev π^- Mesons in Emulsions

A. H. MORRISH
Radiation Laboratory, McGill University, Montreal, Canada
(Received December 11, 1952)

A study has been made of the interactions of 210±20-Mev π^- mesons with the nuclei of photographic emulsions which were exposed to the University of Chicago synchrocyclotron. Detailed classification of the events into elastic and inelastic scatterings, stops and stars, permitted some discussion of the mechanisms involved. The mean free path for a nuclear interaction was found to be 25.7 cm, as determined from an examination of 2823 cm of track. The increase in this mean free path over that observed at lower energies at Columbia appears to be primarily due to a decrease in the probability for π^- meson absorption in a nuclear collision.

INTRODUCTION

AT Bristol,[1] analysis of photographic emulsions exposed to the cosmic radiation has permitted investigation of the nuclear interactions of π-mesons in the energy interval 50 to 1100 Mev. In such studies, the number of observations in any given energy interval is small, and the events examined are usually confined to stars with at least 2 or 3 heavy (or black) prongs. The production of fairly intense, monoenergetic, well-collimated π-meson beams by the large accelerators, now permits a more detailed study in the lower energy region. At Berkeley,[2] observations on 35-Mev π^- mesons and 45-Mev π^+ mesons have been made, while at Columbia,[3] more extensive experiments up to energies of 110 Mev have been performed. Further, many complementary experiments using pure materials instead of emulsion have been carried out at Berkeley, Cornell, Columbia, and Chicago.[4]

This communication reports on a study of 227-Mev (nominal value) π^- meson interactions in emulsions. A stack of Ilford G5 plates, 400 microns thick, and 6 in.×3 in. was placed in the high energy pion beam from the University of Chicago synchrocyclotron. A description of the channels, analyzing magnet, and the scintillation counter detection system has been published by Martin.[5] The plates were exposed one foot from the pole pieces of the analyzing magnet, with the emulsion plane roughly parallel to the beam. They were developed with an amidol bisulfite solution using the well-known temperature method.

TECHNIQUE

An individual meson track was followed from the point the meson entered the emulsion to the point where either it left the emulsion, left the scan area, or produced an interaction. Observations showed that about 95 percent of the mesons entered the emulsion from the glass surface; it was therefore considered desirable and convenient to restrict the observations to the tracks of these mesons. Further selection was made by requiring that the mesons enter the emulsion within 10° (in horizontal projection) of the mean incident direction; in practice it was found that the vast majority entered within 3° of this direction. Finally, in order to reduce the possibility of large energy loss, no scanning was performed further than 3 cm from the edge of the plate that faced the beam during the exposure. The average length of individual meson tracks in the emulsion was about 7 mm. In all, 4483 tracks were followed, for a total track length of 3003.4 cm.

Scattering and grain density measurements were made on about 1 percent of the tracks selected at

[1] W. O. Lock and G. Yekutieli, Phil. Mag. **43**, 231 (1952).
[2] H. Bradner and B. Rankin, Phys. Rev. **87**, 547, 553 (1952).
[3] Bernardini, Booth, Lederman, and Tinlot, Phys. Rev. **80**, 924 (1951), and **82**, 105 (1951); Bernardini, Booth, and Lederman, Phys. Rev. **83**, 1075, 1277 (1951); G. Bernardini and F. Levy, Phys. Rev. **84**, 610 (1951).
[4] See, for example: M. Skinner and C. Richman, Phys. Rev. **83**, 217 (1951). Camac, Corson, Littaver, Shapiro, Silverman, Wilson, and Woodward, Phys. Rev. **82**, 745 (1951). Chedester, Isaacs, Sachs, and Steinberger, Phys. Rev. **81**, 958 (1951). Fermi, Anderson, Lundy, Nagle, and Yodh, Phys. Rev. **85**, 935 (1952).
[5] R. L. Martin, Phys. Rev. **87**, 1052 (1952).

random. It was found that the π^- meson's average energy was about 210±20 Mev, somewhat below the 227-Mev nominal value, presumably caused mainly by loss of energy by ionization in the glass-emulsion assembly. (At 210 Mev, a calculation shows that this loss is about 20 Mev per 3 cm of emulsion.) The grain density of π^- meson tracks at this energy is close to the minimum value. A check on the possibility that some tracks were produced by high energy singly charged particles from the cosmic-ray flux was made by scanning for minimum ionization tracks in a direction perpendicular to the π^- meson tracks. It was concluded that less than 2 percent, and probably less than 1 percent of the tracks originated from this source. However, some of the tracks were produced by μ-mesons which originated from π-μ decays in flight. A consideration of absorption curves obtained with the scintillation counter system showed that 5±2 percent of the beam was contaminated with μ-mesons. The total length of π^- meson track was therefore about 94 percent of that scanned, i.e., 2823.3 cm.

For the purposes of analysis, events were classified according to the following definitions:

(1) *Elastic scatterings.*—Events in which the incoming π^- meson is scattered by 5° or more, with a grain density change of less than 4 percent. This corresponds to a maximum energy loss of about 25 Mev.

(2) *Inelastic scatterings.*—Events in which the meson survives; either a large angle scattering with an energy loss greater than 25 Mev, or a nuclear disintegration with one or more black or gray prongs.

(3) *Stops.*—Events in which the π^- meson disappears in flight with no visible disintegration products.

(4) *Stars.*—Events in which the π^- meson disappears and produces a nuclear disintegration with one or more black or gray prongs.

ELASTIC SCATTERINGS

A histogram of the elastic scattering events in 5° intervals is shown in Fig. 1. Figure 2 is a microprojection drawing of one of the backward scattering events. Occasionally one or more slow electrons were observed at the point of scattering.

A calculation shows that only two or three π-μ decays are to be expected for this length of track and at this energy. Also, the maximum angle possible for a π-μ decay is about 12°. Therefore, one may neglect this process in analyzing Fig. 1.

The solid curve in the figure is the calculated expected number of Coulomb scatterings. At least below 20°, it is reasonable to assume that almost all of the excess of the number of elastic scatterings is due to diffraction scattering. Calculations were made for the expected number of diffraction scatterings assuming a total cross section of πR^2, where R was a mean for the nuclei of the emulsion, excluding the hydrogen nuclei. On comparing the result with the experimental data, it was concluded that

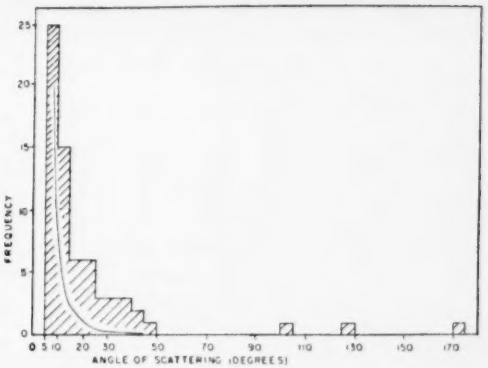

FIG. 1. A frequency histogram of the elastically scattered events in 5° intervals. The solid curve is the expected number of Coulomb scatterings.

the cross section for diffraction scattering is about 33 percent of the geometrical value. Further, most of the scatterings >20° are probably due to a nuclear interaction, i.e., about 19 out of the 21 observed events. Bernardini *et al.*[3] consider only scatterings greater than 30° as a result of nuclear interaction; we observe 12 such events in this experiment. However, since the Coulomb and diffraction scatterings are expected to be confined to smaller angles at higher meson energies, probably the former results are to be compared with those of Bernardini. The mean free paths, both from this work at 210 Mev, and from the work of other authors[2,3] at lower energies, are given in the first two rows of Table I. Except possibly at very low energies, it is questionable if the variation of the mean free path with energy is significant.

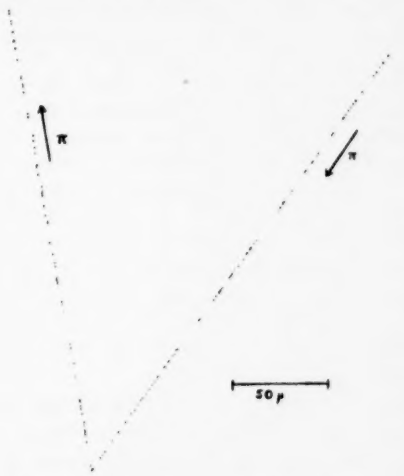

FIG. 2. Elastic backward scattering of a 210-Mev π^- meson. Note that in the drawing the grain density of the outgoing meson track is less than that of the incoming one. This is due to fluctuations, since the average grain density for the total length of each track in the emulsion is the same.

TABLE I. Interaction mean free paths, in cm.

Energy	20–35 Mev[a]	30–50 Mev[b]	60–90 Mev[b]	100–110 Mev[b]	190–230 Mev
Elastic scatterings					
$>30°$	50.6	110	196	131	236
$>20°$					149
Inelastic scatterings	225	318	123	81.8	94.2
Stops	180	239	246	145	282
Stars	82	39	31	34	55
Stars plus stops	56	34	28	28	46
All interactions, incl. scatterings $>30°$	23.8	24.0	20.4	18.0	27.4
scatterings $>20°$					25.7
Geometrical $\left[N\pi\hbar^2\left(\frac{A^{\frac{1}{3}}}{\mu c}+\frac{1}{p}\right)^2\right]^{-1}$		15.6	19.1	20.4	21.8
Geometrical (including hydrogen) $(N\pi R^2)^{-1}$					27.2

[a] See reference 2.
[b] See reference 3.

INELASTIC SCATTERINGS

If of sufficient length, inelastically scattered meson tracks were identified by grain density and multiple scattering measurements. Identification was also possible for short tracks if the grain density was less than twice minimum; in such a case a proton would have an energy higher than the total energy of the incoming meson. Table II lists the inelastic scatterings observed, including the energy of the emergent π, its angle with the incident meson, the number of heavy prongs, and the number of gray tracks (protons>30 Mev) associated.

The maximum energy a 210-Mev π-meson can impart to a nucleon in an elastic collision is about 35 Mev. The very large loss of energy observed in some events can be explained by this model only if one assumes that the incident meson frequently makes more than one collision inside the target nucleus. Six of the interactions are accompanied by a proton with energy >30 Mev. At least one of these was an elastic meson-proton collision, thus illustrating one inadequacy of the method of classification used in this experiment.

One of the inelastic scattering events is shown in Fig. 3. The energy of the incident and ejected mesons was found to be 205 and 40 Mev, respectively. Also, a 45-Mev proton was ejected in the nuclear explosion. The five charged heavy prongs had a total kinetic energy of about 35 Mev. Also, four to six neutrons were probably ejected during the explosion. In order to conserve energy, one of the neutrons must have had an energy of about 50 Mev.

In ten other events, unambiguous identification of a gray track could not be made. Three of these, if protons, had an energy greater than the kinetic energy of the primary meson. Since this seems an improbable process in negative meson absorption, it appears that these events were inelastic meson scatterings. Further, from considerations of the relative numbers of identified π-mesons and fast protons it is reasonable to assume that another four of the remaining seven events were inelastic scatterings. This is a total of 30 such events. The variation of cross section with energy is given in Table I; it increases with energy up to 100 Mev, and is about the same at 210 Mev. The average number of mesons ejected in events with at least one black prong (including stars) is 0.24 ± 0.08; this is to be compared with the Bristol results of 0.21 ± 0.15 ($N_h \gtrsim 3$).

STOPS AND STARS

Ten π^- meson tracks disappeared in the emulsion. It is possible that two or three were meson scatterings into a direction almost perpendicular to the emulsion. However, it seems certain that most of the disappearances are real, being either neutron stars, or charge exchange interactions.

TABLE II. Inelastic scattering events.

Event	π energy Mev	$\theta°$	N_{heavy}	N_{gray}
1	200	58	2	0
2	180	28	1	0
3	165	168	0	0
4	160	35	0	0
5	140	113	1	0
6	125	25	0	0
7	100	154	0	0
8	100	89	0	0
9	90	140	0	1
10	85	69	1	0
11	80	88	0	1
12	80	121	0	1
13	80	150	4	0
14	70	58	0	0
15	65	112	0	1
16	60	33	2	0
17	60	120	1	0
18	55	88	1	0
19	50	85	0	1
20	50	92	2	0
21	40	94	5	1
22	35	36	1	0
23	6	100	1	0

There were 48 stars. In addition, three of the seven events with unidentified gray prongs were probably stars, giving a total of 51. The black prong size distribution, normalized to 100 events, is given in Table III ($E_{\text{prong}}<30$ Mev only), for (a) the star and inelastic scattering events, and (b) the stars alone. In each case the "unidentified gray track" and stop events are included. Some of the zero prong events are probably just π^- meson interactions with hydrogen nuclei. Comparison with the Columbia results at 50–100 Mev confirms the expected star size increase with energy. Most of these ejected particles were protons; however, an exact estimate of the other particles is difficult with the electron-sensitive emulsions employed. One Li^8 ejection was observed (hammer track).

Of the 48 stars, only 6 had proton tracks of energy greater than 30 Mev. Two of these were emitted from

stars in a backward direction ($\theta > 90°$), an observation in agreement with the Bristol findings. Such tracks cannot, of course, be explained by single-nucleon collisions.

Also, it follows that most of the energy in the stars was carried away by one or more neutral particles, either a neutron or neutrons in an absorption process, or a π^0 meson in a charge exchange process. At Columbia, comparison with the interactions of π^+-mesons showed that the absorption process prevailed. It follows that the decrease in the cross section for stars and stops (Table I) at 210 Mev is primarily caused by a decrease in the probability for absorption. This conclusion is supported by Lock and Yekutieli's observations, who found indications that charge exchange predominates over absorption at energies above 160 Mev.

CONCLUSIONS

The mean free path for an interaction of π^--mesons at 210 Mev in G5 nuclear plates is given in Table I, including first, the number of elastic scatterings $>20°$, and second, the number $>30°$. It is approximately equal to that implied by the geometrical value of πR^2 for the emulsion nuclei, and significantly longer than found by Bernardini at lower energies. In addition, the mean free path for a geometrical model which includes the effect of the wavelength, $\lambda(=\hbar/p)$ of the incident meson, is tabulated. Comparison with this model gives a transparency of 15 to 20 percent, depending on how many elastic scatterings are included.

TABLE III. Black prong frequency.

No. of prongs	0	1	2	3	4	5	6
Columbia 50–100 Mev	18	35	25	16	4	2	0
(a) 210 Mev	26	19	21	9	14	9	2
(b) 210 Mev	19	15	23	12	18	10	3

Bethe and Wilson[6] have computed curves of the diffraction scattering as a function of the opacity of the nucleus for various values of the change of the propagation vector inside a nucleus. This is, of course, related to the average nuclear potential V_0 for π^- mesons. The diffraction scattering was found to be 33 percent of "geometrical" from the elastic scattering results. This, in combination with a value for the opacity of about 80 percent, as determined from the data assuming the "geometrical" cross section to be $\pi(R+\lambda)^2$, gives a value of 0 ± 10 Mev for the average nuclear potential. Cornell experiments on 45-Mev π^- meson interactions in carbon give $V_0=11\pm11$ Mev.

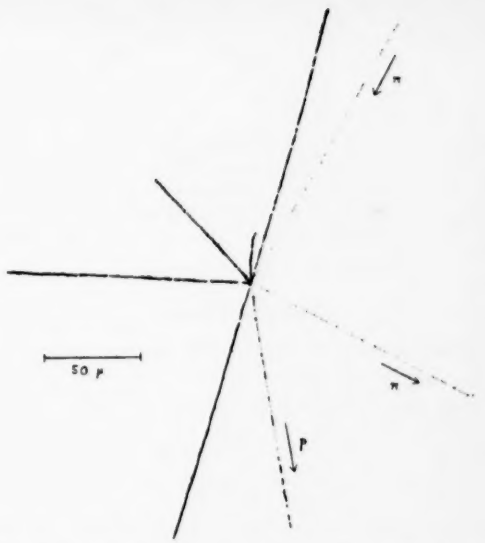

FIG. 3. An inelastic π^- meson scattering. The emergent meson has an energy of 40 Mev, and is accompanied by a fast proton of energy about 45 Mev.

I am greatly indebted to H. L. Anderson for the exposure to the 227-Mev negative pion beam from the University of Chicago synchrocyclotron. I wish to acknowledge several helpful discussions with J. D. Jackson, and also to thank J. S. Foster for his interest in this experiment. Finally, I am grateful to the Ottawa Cosmic Ray Group, particularly L. Voyvodic, for some assistance and discussion.

[6] H. A. Bethe and R. R. Wilson, Phys. Rev. **83**, 690 (1951).

Positron-Electron Scattering at 1.3 Mev*

HORACE A. HOWE† AND K. R. MACKENZIE
University of California, Los Angeles, California
(Received December 15, 1952)

Using an incident beam energy of 1.3 Mev, the ratio of electron to positron scattering on atomic electrons has been determined for the case where one-half the incident energy is transferred to the atomic electron. The measured ratio is 1.82 ± 0.11, which agrees with the theoretical ratio of 1.83, calculated from the expressions given by Møller and Bhabha when exchange effects are included. The theoretical ratio, excluding exchange effects, is 1.36.

INTRODUCTION

THE theory of electron-electron scattering, published by Møller[1] in 1932, has been checked experimentally several times in recent years[2] and appears to be correct. However, the theory of positron-electron scattering, published by Bhabha[3] in 1936, has had very little in the way of confirmation. Several experiments using cloud chambers[4] have given indecisive results because of the difficulty of obtaining enough tracks to give good statistics. Recently, using counters, Ashkin and Woodward[5] were able to measure the ratio of positron-electron to electron-electron scattering for 600-kev particles and obtained good agreement with theory. This ratio is easier to measure than the absolute cross section and is the quantity measured in this work.

The Møller formula for electron-electron scattering and the Bhabha formula for positron-electron scattering are reproduced below, where the differential cross-section is given as a function of the fractional energy ϵ imparted to the stationary particle.

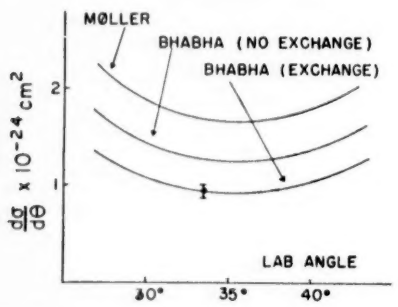

FIG. 1. Theoretical differential scattering cross section in aboratory system as a function of laboratory angle. Experimental point is shown at 33.5°.

Møller [p. 569, reference 1, with $A=\epsilon$ and $Q=mc^2(\gamma-1)\epsilon$]:

$$\left(\frac{d\sigma}{d\epsilon}\right)_M=\frac{2\pi e^4}{m^2c^4}\frac{\gamma}{(\gamma-1)^2\epsilon^2}G(\gamma,\epsilon),$$

where

$$G(\gamma,\epsilon)=\frac{\gamma}{\gamma+1}\left[1+\frac{\epsilon^2}{(1-\epsilon)^2}-\frac{\epsilon}{(1-\epsilon)}+\left(\frac{\gamma-1}{\gamma}\right)^2\left(\epsilon^2+\frac{\epsilon}{(1-\epsilon)}\right)\right].$$

Bhabha:

$$\left(\frac{d\sigma}{d\epsilon}\right)_B=\frac{2\pi e^4}{m^2c^4}\frac{\gamma}{(\gamma-1)^2\epsilon^2}F(\gamma,\epsilon),$$

where

$$F(\gamma,\epsilon)=\frac{1}{\gamma(\gamma+1)}\left[\{1+2(\gamma-1)(1-\epsilon)+(\gamma-1)^2(1-\epsilon+\tfrac{1}{2}\epsilon^2)\}+\left(\frac{\gamma-1}{\gamma+1}\right)^2\epsilon^2\times\{3+2(\gamma-1)+(\gamma-1)^2(\tfrac{1}{2}-\epsilon+\epsilon^2)\}-\frac{\gamma-1}{\gamma+1}\epsilon\{3+4(\gamma-1)(1-\epsilon)+(\gamma-1)^2(1-\epsilon^2)\}\right].$$

$$\gamma=\frac{1}{(1-v^2/c^2)^{\frac{1}{2}}},$$

$$F_0(\gamma,\epsilon)=\frac{1}{\gamma(\gamma+1)}[1+2(\gamma-1)(1-\epsilon)+(\gamma-1)^2(1-\epsilon+\tfrac{1}{2}\epsilon^2)].$$

The quantity $F_0(\gamma,\epsilon)$ is the first term in the expression for $F(\gamma,\epsilon)$ and refers to what Bhabha calls ordinary scattering, or the scattering that would take place if the electron and positron could not annihilate. The second term is the "exchange" term representing the possibility of annihilation and re-creation of a new pair, and the third term is the interference term between the first two. Bhabha plots $F(\gamma,\epsilon)$ and $F_0(\gamma,\epsilon)$ against ϵ for various

* Supported in part by the joint program of the U. S. Office of Naval Research and the U. S. Atomic Energy Commission.
† Now at Reed College, Portland, Oregon.
[1] C. Møller, Ann. phys. **406**, 531 (1932).
[2] L. Page, Phys. Rev. **81**, 1062 (1951); Scott, Hanson, and Lyman, Phys. Rev. **84**, 638 (1951); Groetzinger, Leder, Ribe, and Berger, Phys. Rev. **79**, 454 (1950).
[3] H. J. Bhabha, Proc. Roy. Soc. (London) **A154**, 195 (1936).
[4] Ho Zah-Wei, Compt. rend. **226**, 1083 (1948); Von O. Ritter *et al.* Z. Naturforsch. **6a**, 243 (1951); G. R. Hoke, Phys. Rev. **87**, 285 (1952).
[5] A. Ashkin and W. M. Woodward, Phys. Rev. **87**, 236 (1952).

values of γ. The experimental ratio of positron-electron to electron-electron scattering is to be compared with the ratios F/G and F_0/G.

In order to distinguish between these ratios it is desirable to choose values of γ and ϵ which maximize or minimize the ratio of F/F_0. The maximum value of 2 occurs at $\gamma=\infty$ and $\epsilon=1$ (180° scattering in the center-of-mass system). However, high values of γ and ϵ are rather unfavorable experimentally, since the cross section decreases rapidly as γ approaches ∞ and as ϵ approaches 1, with the added difficulty that the impinging positron is not left with much energy in the laboratory system. At low incident energy, the ratio F_0/F has a broad maximum of about 1.4, for $\gamma=2.4$ (700 kev) and $\epsilon=0.5$. Since coincidence counting of both particles is very desirable to eliminate nuclear scattering and other background, a value of $\epsilon=0.5$, where both particles are scattered through equal angles, is very convenient. The incident energy chosen in this experiment was 1.3 Mev, for which $F_0/F=1.34$. The scattered particles thus have an energy of 650 kev each, which allows discrimination against the 0.51-Mev pulses from annihilation radiation.

Since no distinction is made between positron and electron in a coincidence counting arrangement, the significant ratio is

$$\left\{\frac{1}{\epsilon^2}F(\gamma,\epsilon)+\frac{1}{(1-\epsilon)^2}F(\gamma,(1-\epsilon))\right\}\Big/\left\{\frac{1}{\epsilon^2}G(\gamma,\epsilon)\right\}.$$

These expressions are in terms of ϵ, but since the experimental arrangement described below selects the particles according to their angle of emission from the scatterer, the cross sections must be expressed as a function of angle (Fig. 1), using the relation $\epsilon=\{(\gamma+1)\sin^2\theta\}/\{2+(\gamma-1)\sin^2\theta\}$. The particles scatter symmetrically at $\epsilon=0.5$, making an angle of 33.5° with the axis, but due to the relativistic distortion of angles, the minimum counting rate for a given solid angle is obtained at approximately 35°.

EXPERIMENTAL EQUIPMENT

The experimental arrangement is shown in Fig. 2. An electron or positron beam of energy up to 2 Mev was produced by a magnetic lens spectrometer 7 feet in length. Such a spectrometer has the advantage that the beam and the source are very far apart. Particles emerging from a source rod 0.08 in. in diameter between the angles of 5° and 10° from the axis were focused into a beam 2 cm in diameter with an angular divergence of 1.5° from the axis. The energy spread was 7 percent as determined from the Cs^{137} line. Helical baffles were used to exclude particles of the wrong sign. The trajectories were determined by means of a light current-carrying wire.

The scattering chamber shown in Fig. 2 was connected to the same vacuum as the spectrometer. The pairs of

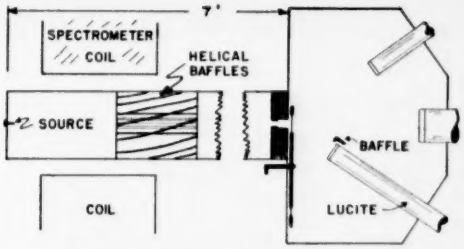

FIG. 2. Spectrometer and scattering chamber.

particles scattered from various foils (mounted on a wheel), were counted in coincidence by high resolution scintillation detectors.

The electron source was Y^{90}, daughter of 25-year Sr^{90} with an end-point energy of 2.2 Mev. It was prepared by evaporating thirty millicuries of the chloride salt on the end of a glass rod 0.08 in. in diameter. A thin film of polystyrene was then sprayed over the rod to lessen the hazard of contamination. The positron source was Ga^{66} with a 9.4-hr half-life and an end point of 3.9 Mev. It was produced in the UCLA cyclotron by bombarding the end of a 0.08 in. Zn rod with 16-Mev protons. Self-absorption in the Zn made the shape of the gallium spectrum almost indistinguishable from the spectrum of Y^{90} in the region around 1.3 Mev.

Three sodium iodide crystals were used as counters. Although inferior to anthracene for this experiment because of higher sensitivity to gamma-radiation, sodium iodide was used as it happened to be on hand in sufficient quantity. The incident beam was recorded by a crystal 5 cm in diameter and 7 mm thick. The side counters were 2.7 cm in diameter and 4 mm thick. The crystals were mounted on Lucite light pipes of the same diameter, which extended through the vacuum walls and were then cemented to the 5819 photomultiplier tubes. The crystals were first carefully polished, then wiped with a thin coat of mineral oil to prevent absorption of moisture and covered with a very thin Al foil.

One crystal, at 35°, was used as a defining counter and was placed 14.7 cm from the scattering foil, thus defining an angular spread of 10.5° from a point scatterer, and an "effective" angle of 13°, when the size of the source and angular spread of the beam are considered. This angular spread was necessary in order to increase intensity and reduce the effects of multiple scattering. As seen from Fig. 1, the counting rate is very insensitive to angle in this region. The other counter was set at an angle of 33°, and a distance of 6.8 cm from the foil, thus subtending over four times the solid angle. Both solid angles were defined by the edges of the crystals. It was considered undesirable to determine the solid angle with diaphragms, since gamma-ray pairs, produced by positrons striking the diaphragms, might give false coincidences. However a thin baffle between the crystals was considered necessary in order to prevent particles from being scattered by one crystal into the other.

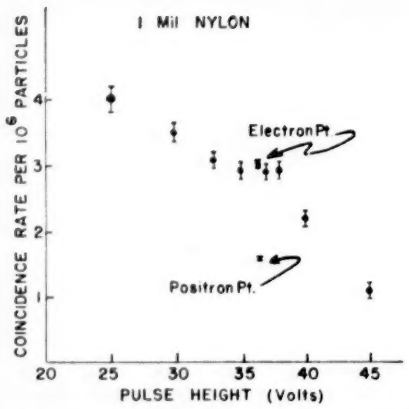

FIG. 3. Number of scattering events recorded per 10^6 incident particles on 1-mil Nylon foil as a function of discriminator bias.

Pulses in each side channel were fed through a cathode follower to a wide band amplifier, then to a discriminator, a coincidence circuit and register. Two scalers and registers recorded the pulses in each side counter. The main beam pulses were recorded after going through a wide band amplifier and a scaler with a resolution time of 0.4 microsecond.

EXPERIMENTAL PROCEDURE

Scattering runs were made with 1-mil and 2-mil Nylon foils. The results after making the necessary corrections are shown in Fig. 3. The runs with 2-mil Nylon foil (Fig. 4) were exploratory, and the statistics were poor, but the data are presented to show that the ratio is not very sensitive to discriminator bias. Most of the counting was done with the 1-mil foil so that the multiple scattering corrections would be smaller.

Theoretically a definite plateau should be observed for coincidences against discriminator bias (varied simultaneously in both channels). Since the counters and the scattering foil are relatively large compared with their separations, the scattered electrons recorded by the defining counter have an energy spread from 0.44 to 0.88 Mev, corresponding to an angular spread of 16.5° as measured from extreme edges of the foil and defining crystal, plus 3° for the spread in the incident beam. Therefore coincidences should first be observed when the bias is lowered to a value corresponding to about 0.65 Mev, since only below this setting will both members of the pair have sufficient height to record a coincidence. As the bias is lowered the coincidence rate should rise until 0.44-Mev particles are admitted, and then it should remain constant, but only on the assumption that there is an exact correspondence between pulse height and energy. The actual distribution in pulse height was measured by setting the spectrometer to produce a monochromatic beam of 0.65-Mev electrons. The half-width of the curve so obtained was 12 percent for the monitor and 9 percent for the defining counter with a tail on the low pulse-height side. This variation in pulse height was presumably due to imperfections in the crystals and light pipe system and possibly to a non-uniform oil film covering the crystals.

Consequently the bias must be reduced essentially to zero in order that all coincidences be recorded and the onset of the theoretical plateau is replaced by a knee in the curve. Many of the coincidences at very low bias are undoubtedly due to scattering events at angles widely different from 35°, in which the high energy electron is recorded by the wide angle monitor and the low energy particle is multiply scattered into the defining counter. To eliminate such events, most of the counting time was used in comparing the positron-electron, electron-electron scattering ratio for a bias which was just over this knee in the curve. This point is also a compromise between maximum discrimination against false coincidences resulting from annihilation quanta, and minimum variation of counting rate due to fluctuations in pulse height caused by changes in either the discriminator bias or high voltage on the photomultiplier tubes.

Since the number of "extra" coincidences at low bias is unknown, it is possible that over 50 percent of the true coincidences were lost by counting near the knee of the curve. This makes an absolute determination of the cross section rather difficult, but does not affect the ratio which depends only on the constancy of the equipment. Great pains were taken to insure this constancy of equipment. In addition to the usual precision regulation of power supplies (less than $\frac{1}{8}$ percent for the photomultipliers), a special circuit "blocked" all registers whenever excessive transients were detected on the ac line.

The runs were made by first warming up the equipment for four or five hours and then making an electron run for a few hours, during which time a positron source was being prepared in the cyclotron. Then the positron source was inserted and counted for some 20 hours. To insure that the equipment had not changed, the electron source was immediately put back and counted again. Counting rates for the electron source were 0.13 coincidence per second with a beam of 44 000 particles per second. The positron rate was 0.013 per second for an initial beam of 8000 particles per second. Several such runs were made until some 1000 positron counts and 5000 electron counts had been recorded.

CORRECTIONS

The counter and foil geometry (Fig. 2) was such that the monitor counter subtends over four times the solid angle seen by the defining counter. With an incident beam of particles $\frac{1}{2}$ cm in diameter, and a thin foil (as originally planned), this geometry was such that the monitor counter would receive a particle for almost every particle that reached the defining counter. However, to obtain sufficient intensity, the beam was widened to 2-cm diameter and the foil thickness in-

creased to 1 mil. The new geometrical factors introduced by the wide beam caused the monitor counter to miss 16 percent of the events that were registered by the defining counter. With a 1-mil Nylon foil, multiple scattering caused another loss estimated to be around 20 percent, based on extrapolation to very thin foils of the curves given by Snyder and Scott.[6] The 16 percent figure is common to both the electron and positron cases, but since the multiple scattering is reported as 10 percent less for positrons than for electrons,[7] a correction of 2 percent was subtracted from the positron counting rate.

As can be seen from Fig. 1, the apparent ratio of electron-electron scattering to positron-electron scattering will be somewhat reduced by the above angular spread. The effect was graphically estimated to be 2 percent; hence the measured ratio was increased by 2 percent.

The positron source produced a large background of annihilation radiation. The coincidence counters were biased so that they were very insensitive to this radiation, but the main beam counter was not so biased, since it was desirable that all the incident positrons and electrons be recorded. A 12 percent correction was necessary for this gamma-background. It was determined by recording the gamma-ray background when the main beam was stopped at the entrance to the lead collimator.

In addition to the above corrections, there were several processes which could give false coincidences. The single counting rates for electrons were 20 counts per second in the defining counter and 28 in the other. Practically all of these counts were stray electrons, scattered primarily from the edges of the lead collimator. This was shown by noting that the single counting rates were not reduced more than the statistical counting error of 1.5 percent when the foil was removed. With a coincidence resolving time of 1 microsecond, the accidental rate was negligible compared with the true coincidence rate of 0.13 count per second. For positrons, the initial rates were about 40 and 50 counts per second, mostly because of annihilation quanta from the source. The order of magnitude of the total number of accidental counts was calculated from a simple integral formula involving the resolving time, the individual rates and the half-life. For the first few hours the relation was integrated numerically because of the presence of the 48- and 68-minute activities resulting from Ga^{64} and Ga^{68}. The correction was approximately 10 percent of the total recorded coincidences.

Another correction must be applied in the case where a positron stops in one counter and one of the annihilation quanta is absorbed in the other. Taking into account the number of positrons striking the counters, the solid angles seen by each counter relative to the other, and the approximate efficiency of the counters for

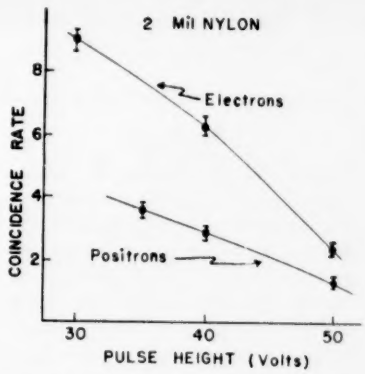

FIG. 4. Number of scattering events recorded per 10^6 incident particles on 2-mil Nylon foil as a function of discriminator bias.

0.51 gamma-rays, the correction was estimated to be around 4 percent.

Since the individual counting rates did not change (within statistical limits) when the foil was removed, it was possible to subtract false coincidences due to both the above causes by making runs with and without the foil in place. The total correction was 15 percent, which was very close to the calculated estimate.

False coincidences, which cannot be subtracted experimentally, can be recorded in the following way: When a positron is absorbed in either the defining or monitor crystal, there is a certain probability that one of the annihilation quanta will be absorbed in the same crystal. For such a gamma-ray the average path length in the crystal, for all positions of the impinging positron, is of the order of 0.4 cm. For 0.51-Mev gamma-rays in NaI, the fractional loss of photons per cm, resulting from the photoelectric effect, is 0.057.[8] For a path length of 0.4 cm, the probability of conversion is then 2.3 percent, giving a total probability of 4.6 percent, since there are two annihilation quanta. Consequently some small pulses, which would normally be rejected by the high bias setting, would have their heights increased by 0.51 Mev and be recorded, whereas the corresponding small pulses in the electron-electron scattering case would not. This effect was estimated by noting the increase in coincidence rate in the electron-electron scattering case when the discriminator bias was lowered an amount corresponding to 0.5 Mev (approximately zero bias) in one side channel at a time. The average increase for such a procedure in both channels was 47 percent. Thus the correction to be subtracted from the positron coincidence rate is 4.6 percent of 47 percent, which is 2.2 percent. There are also Compton electrons which are four times as numerous as the photoelectrons, but have an average energy of only 0.2 Mev. Lowering the bias in one channel by an amount corresponding to 0.2 Mev

[6] H. S. Snyder and W. T. Scott, Phys. Rev. **76**, 220 (1949).
[7] Groetzinger, Humphrey, and Ribe, Phys. Rev. **85**, 78 (1952).
[8] National Bureau of Standards Report NBS-1003 (unpublished).

increased the rate 20 percent. Hence the amount subtracted is four times 4.6 percent of 20 percent, which is 3.7 percent. When this is added to the above 2.2 percent, the total correction is about 6 percent.

RESULTS

The ratio of electron-electron to positron-electron scattering is shown in Figs. 1 and 3 after all corrections have been applied. The theoretical ratio at 33.5° is 1.83 (with exchange), and 1.36 (no exchange). The experimental ratio is 1.82 ± 0.11. Most of this error is due to uncertainties in the corrections. The Bhabha theory with exchange is thus very definitely favored.

The coincidence rates quoted above are only 0.35 times the rates expected from absolute cross section calculations. When the theoretical rate is reduced by the previously mentioned factors of 16 percent and 20 percent successively, a counting rate for electrons of 0.22 coincidence/sec is obtained. The absolute experimental coincidence rate lies somewhere between 0.27 count/sec, which is the rate just above the noise level near zero bias, and 0.13 count/sec, which is the rate at the knee of the curve. Hence no conclusions can be drawn regarding absolute cross sections.

The authors wish to express thanks to H. Keller, R. LeLevier, and R. Schrack who designed and built the spectrometer, and to G. Jones and S. Plunkett for assistance with electronic equipment.

PHYSICAL REVIEW VOLUME 90, NUMBER 4 MAY 15, 1953

The Radiation of a High Energy Electron in a Constant Magnetic Field

MAURICE NEUMAN
Radiation Laboratory, University of California, Berkeley, California
(Received January 14, 1953)

The quantum-mechanical radiation formula for an electron in a constant magnetic field—rigorous within the approximation of the first power of the fine structure constant—is derived. With it, the quantum effects for energies $E_{\text{Bev}}<4(10^4/H_{\text{gauss}})$ are analyzed and their importance assessed. The electron and the photon severally are subject to fluctuations which produce effects that are quite significant relative to the difference between the velocity of light and that of the electron, the decisive quantity at high energies. The net result however is that they are inconsequential in the domain investigated and that in its radiative aspects the system behaves—for all practical purposes—classically.

I. INTRODUCTION

A CALCULATION is here presented to show that there are no quantum corrections (in the practical sense) to the radiation of an electron in a constant magnetic field up to energies $E<4(10^4/H)$ Bev. The magnetic field H in the formula (as elsewhere in this article) is to be expressed in gauss.

A detailed inquiry into a domain, where an elementary application of the correspondence principle renders it plausible that the classical results are valid, seems to require an explanation. It was not undertaken with the thought that this principle could somehow be circumvented. Nor was it deemed necessary or feasible to verify its operation in detail for systems of considerable complexity. In view, however, of persistent reports[1] that significant quantum corrections have been deduced from the theory, a possibility seemingly not inconsistent with the principle, as it has hitherto been applied, suggested itself.

As the electron energy assumes very high values, the difference between its velocity and the velocity of light becomes increasingly important in the description of the frequency spectrum and the angular distribution of the radiation. It is therefore perhaps not entirely fair to gauge the importance of quantum fluctuations by considering their effect on the group velocity of the particle. A relevant quantity in this very high energy domain might also be the difference between the two velocities.

It turned out in the course of the work that elements of competition are present between the quantum uncertainty in the velocity and the difference mentioned, and the result is quite sensitive to the relative magnitude of these two quantities. In the domain investigated, however, the latter quantity is overwhelmingly larger. The possibility that the situation may change at much higher energies, but still well within the range of correspondence of the two theories, cannot be ruled out completely on the basis of the present investigation, but it seems rather unlikely that such effects play any important role in this particular context.

On the practical side, the somewhat remote possibility of such effects had to be weighted against the important consequences their presence would have on future accelerator design. It was concluded that a detailed search for them was not an altogether unreasonable precaution.

In order to exhibit the quantum aspect of the problem

[1] See for example, L. Schiff, Am. J. Phys. **20**, 474 (1952), reference 9.

with some clarity relative to the classical theory, the calculation was based on the Lorentz force law rather than the more usual Hamiltonian scheme. The wave functions of the electron were constructed in a representation to which the operational methods recently emphasized by Feynman[2] may readily be applied. Thus the bulk of analytic operations—which are apparently difficult to handle—has been dispensed with and this computational aspect of the problem reduced to a few elementary manipulations. Inessential complications have been avoided by completely neglecting spin effects —which do not matter here—and by carrying out the calculation within the framework of the Schrödinger-Gordon theory. Moreover, an average over the polarization of the emitted photons is carried out at an early stage since information of this type is not of particular interest.

The investigation is limited to the energy range $0.1\times(10^4/H)$ Bev$<E<4\times(10^4/H)$ Bev. It is unncesessary to consider lower energies, since there the validity of the classical theory has already been established by Judd, Lepore, Ruderman, and Wolff,[3] and by Olsen and Wergeland.[4] Higher ones are avoided in order to remain at a safe distance from the analytic morass of an asymptotic transition region.[5] It was felt in this connection that a more definite statement limited to a narrower domain may be more useful than a vague one covering a broader range. Unlike the effects in the lower energy range considered in reference 3 and 4, a more subtle effect involving light quanta has to be taken into account here in order to establish the substantial identity of the two theories.

It is believed that the following may fairly be said. There are no corrections, in the practical sense, for $E<4\times(10^4/H)$ Bv. From this one may reasonably infer that no significant correction will come into play at energies that are of interest in connection with present or immediate future accelerator design. Because of the mathematical fact that an asymptotic transition region sets in above these energies, one may perhaps suspect that some corrections are called for well above the energies of present experimental interest but below the limit sometimes assigned to the validity of the classical radiation formula.[1] These suspicions should be considerably allayed by the fairly convincing wave packet arguments offered by Schiff[1] and mildly sharpened by the possibility mentioned earlier.

II. QUANTUM-MECHANICAL RADIATION FORMULA

This formula will now be derived within the approximation of the first power of the fine structure constant. The conservation law for the stress tensor $\theta_{\mu\nu}$ of the dynamical part of the electromagnetic field,

$$\partial_\mu\theta_{\mu\nu}+(1/c)F_{\nu\lambda}j_\lambda=0, \tag{1}$$

implies that the field gains momentum

$$P_\nu(\sigma)=(1/c)\int_\sigma d\sigma_\mu\theta_{\mu\nu} \tag{2}$$

in a time interval T contained between two space like surfaces σ_1 and σ_2 at an average rate of

$$\Delta P_\nu/\Delta T=-(1/Tc^2)\int_{\sigma_1}^{\sigma_2} d^4xF_{\nu\lambda}j_\lambda. \tag{3}$$

The limits of integration in (3) may be extended from $+\infty$ to $-\infty$ with the understanding that an infinite time factor in the form of a redundant delta-function will subsequently be canceled against T.

The operators in (3) are specified in the Heisenberg representation. The current $j_\lambda(x)$ is therefore in part maintained by an external agency (the constant electromagnetic field) and in part induced by the vacuum fluctuations of the dynamic field. The two may effectively be separated by transforming to a bound state representation.[6] In it, the expectation value of (3) in a state with one electron and no photons appears as

$$(\Delta P_\nu/\Delta T)_{1,0}=-(i/\hbar c^2T)\int_{-\infty}^{+\infty}dx\int_{-\infty}^{\sigma}dx'$$
$$\times\langle 1,0|[j_\alpha(x)A_\alpha(x),F_{\nu\lambda}(x')j_\lambda(x')]|1,0\rangle, \tag{4}$$

where only the first nonvanishing term of an expansion has been retained. The momentum transfer in (4) due to radiation is separated from self-energy effects by employing an idea of Dirac,[7] which implies that the former quantity is given by the right side of (4) if the finite limit of integration is extended to infinity and a factor (1/2) appended.

The photon operators in (4) obey the free Maxwell equations and their expectation value in the vacuum state is readily expressed in the form[8]

$$(\Delta P_\nu/\Delta T)_{1,0}{}^R=(1/c^3T)\int_{-\infty}^{+\infty}dx\int_{-\infty}^{+\infty}dx'$$
$$\times\langle 1|j_\lambda(x)j_\lambda(x')|1\rangle\partial_\nu D^+(x-x'). \tag{5}$$

Because of the time average incorporated in (3) transient effects were removed in going from (4) to (5) by the simple device of partial integration. It will be noticed that (5) is formally almost identical with the corresponding classical expression. For the case of commuting current operators only the odd part of $D^+(x)$, namely $\frac{1}{2}D(x)$, is effective, thus reducing (5) to its classical form.

[2] R. Feynman, Phys. Rev. **84**, 108 (1951).
[3] Judd, Lepore, Ruderman, and Wolff, Phys. Rev. **86**, 123 (1952).
[4] H. Olsen and H. Wergeland, Phys. Rev. **86**, 123 (1952).
[5] F. Tricomi, Ann. Mat. **28**, 263 (1949).
[6] W. Furry, Phys. Rev. **81**, 115 (1951).
[7] P. Dirac, Proc. Roy. Soc. (London) **167**, 148 (1938).
[8] J. Schwinger, Phys. Rev. **75**, 651 (1949).

The average power radiated, $\mathcal{P}$ is given by the time-like component of (5) multiplied by c:

$$\mathcal{P}=-(1/c^2T)\int_{-\infty}^{+\infty}dx\int_{-\infty}^{+\infty}dx' \times\langle 1|\,j_\lambda(x)\,j_\lambda(x')\,|1\rangle\partial_0 D^+(x-x'). \quad (6)$$

Even though more elegant representations of the one-particle expectation value in (6) are available, we shall express it as an infinite sum over final states. These are denoted by $n-\lambda$, l'. The initial state is assigned hte letters n, $-n$. (This—still somewhat vacuous—labelling scheme is introduced at the present point to save rewriting formulas.) Representing $D^+(x)$ by means of a Fourier integral and eliminating the time-like component of the current with the aid of the conservation law, we obtain from (6):

$$\mathcal{P}=(1/c^2T)(1/(2\pi)^3)\int d^3k\langle 1|\,\mathbf{n}\times\mathbf{j}(-\mathbf{k})\cdot\mathbf{n}\times\mathbf{j}(\mathbf{k})\,|1\rangle, \quad (7)$$

where

$$\mathbf{j}(\mathbf{k})=\int_{-\infty}^{+\infty}d^4x\,\exp(-ikx)\mathbf{j}(x);\quad k=[\mathbf{k},\,i|\mathbf{k}|];\quad \mathbf{n}=\mathbf{k}/|\mathbf{k}|. \quad (8)$$

For a Schrödinger-Gordon current $\mathbf{j}(\mathbf{k})$ is given by

$$\mathbf{j}(\mathbf{k})=(e/2m)\int_{-\infty}^{+\infty}d^4x\bar{\phi}(x)\{\pi(x),\exp(-ikx)\}\phi(x)\}. \quad (9)$$

The curly bracket in (9) denotes an anticommutator and $\Pi=p-(e/c)A$. Equation (7) assumes the form

$$\mathcal{P}=(1/T)(e/mc)^2(2\pi)^{-3}\sum_{l,\lambda}\int d^3k \times\left|\int d^4x\bar{\phi}_{n,\,-n}(x)\mathbf{n}\times\pi(x)\,\exp(-ikx)\phi_{n-\lambda,\,l}(x)\right|^2. \quad (10)$$

The wave function $\phi(x)$ obeys the equation:

$$(\Pi^2+m^2c^2)\phi=0. \quad (11)$$

A transformation of the wave function,

$$\phi(x)\rightarrow\exp\left[(ie/\hbar c)\int_0^1 d\lambda A_\mu(\lambda x)x_\mu\right]\phi(x), \quad (12)$$

changes

$$\Pi_\mu\rightarrow p_\mu+(e/c)\int_0^1 d\lambda\cdot\lambda F_{\mu\nu}(\lambda x)x_\nu, \quad (13)$$

leaving (10) and (11) otherwise unaltered. In this new gauge, in the presence of a constant electromagnetic field,

$$\Pi=p+(e/2c)Fx. \quad (14)$$

[The F and A in Eqs. (12)–(14) are parameters referring to the external field and are not to be confused with the photon operators used previously.] If in addition we specialize to a frame in which the electric field vanishes and the magnetic field has the z direction and is sensed upward, (11) may be written

$$[(p_1^2+p_2^2)+m^2c^2\kappa_L^2(x_1^2+x_2^2) -2mc\kappa_L L+p_3^2-p_0^2+m^2c^2]\phi=0, \quad (15)$$

where

$$L=x_1p_2-x_2p_1 \quad (16)$$

is a constant of motion for the system. The quantity κ_L is a relativistic invariant which in this frame reduces to

$$\kappa_L=eH/2mc^2, \quad (17)$$

(within a multiplicative constant) the Larmor frequency. Choosing $\phi(x)$ to be an eigenfunction of p_3 and p_0, we may write

$$\phi(x)=(\kappa_C/K_0)^{\frac{1}{2}}(1/Z)^{\frac{1}{2}}\exp[i(K_3x_3-K_0x_0)]\psi(x_1,x_2). \quad (18)$$

Here $\kappa_C=mc/h$, Z is the length of the magnetic field in the Z direction and the factor $(\kappa_C/K_0)^{\frac{1}{2}}$ has been chosen to normalize the charge to unity.

Equation (18) is now substituted in (10), and the integrations over x_3 and x_0 are carried out. This gives rise to some redundant delta-functions which are canceled against Z and T. The components of the vector $\mathbf{n}$ are then expressed in spherical coordinates, with the Z direction chosen as a polar axis. A short calculation shows that (10) may be put in the following form:

$$\mathcal{P}=2c(e/mc)^2(1/4\pi)\sum_{\lambda,\,l}\int d^3k\delta(K_0{}^n-|\mathbf{k}|-K_0{}^{n-\lambda}) \times R_n(\lambda,l). \quad (19)$$

The function $R_n(\lambda,l)$ may be expressed in terms of two quantities $A_\pm{}^n(\lambda,l)$ which are defined as

$$A_\pm{}^n(\lambda,l)=\int dx_1dx_2\bar{\psi}_{n-\lambda,\,l}(x_1x_2) \times\exp[-i(k_1x_1+k_2x_2)]\Pi_\pm\psi_{n,\,-n}(x_1x_2), \quad (20)$$

where

$$\Pi_\pm=(1/2)(\Pi_1\pm i\Pi_2), \quad (21)$$

the explicit expression being

$$R=(1+\cos^2\theta)[\bar{A}_+A_++\bar{A}_-A_-] -\sin^2\theta[\exp(2i\phi)\bar{A}_+A_-+\exp(-2i\phi)\bar{A}_-A_+]. \quad (22)$$

We neglected to write out corresponding indices on both sides of (22). The assumption was made that $K_3=0$ in the initial state.

Going back to (15) and (16) it is seen that a change of variables

$$x_i=(2^{\frac{1}{2}}\kappa)^{-1}(a_i+a_i{}^*);\quad p_i=-ih\kappa 2^{-\frac{1}{2}}(a_i-a_i{}^*); \quad [a_i,a_j{}^*]=\delta_{ij};\quad i=1,2, \quad (23)$$

followed by a transformation

$$a_1=2^{-\frac{1}{2}}(a_-+a_+);\quad a_2=+i2^{-\frac{1}{2}}(a_--a_+);\qquad [a_+, a_+^*]=[a_-, a_-^*]=1, \quad (24)$$

where

$$\kappa=(\kappa_C\kappa_L)^{\frac{1}{2}}, \quad (25)$$

leaves them in the form

$$[4\kappa^2 a_+^* a_+ + K_3^2 - K_0^2 + \kappa_C^2]\psi=0, \quad (26)$$

$$L=\hbar(a_-^* a_- - a_+^* a_+). \quad (27)$$

The eigenfunction may then be written as

$$\psi_{n,l}=[n!(n+l)!]^{-\frac{1}{2}} a_+^{*n} a_-^{*n+l}\phi_0, \quad (28)$$

where ϕ_0 is the vacuum state. The degeneracy has been classified according to the eigenvalues of L. Thus

$$L\psi_{n,l}=\hbar l\psi_{n,l};\quad -n\leqslant l<\infty, \quad (29)$$

where it is understood that only integers enter the inequality in (29). By (26), the physical parameters are constrained through

$$4\kappa^2(n+\tfrac{1}{2})+K_3^2-K_0^2+\kappa_C^2=0. \quad (30)$$

It is not too difficult to see that $l=-n$ corresponds to a classical orbit centered about the origin of coordinates; a state with $-n<l<0$ to a family of orbits with the origin as an interior point; for one with $l>0$ the origin is exterior to the orbits.[9] The significance of the labeling scheme introduced earlier is now clear.

Substituting (23), (24), and (28) into (20) and using the relations $\Pi_+=-i\hbar\kappa a_+$, $\Pi_-=i\hbar\kappa a_+^*$, the quantities in question become

$$A_+^n(\lambda, l)=-i\hbar\kappa S_{n-\lambda+l} \times\{\psi_{n-\lambda}, \exp[-i\alpha(a_+^* \exp(i\phi) + a_+ \exp(-i\phi))]a_+\psi_n\}, \quad (31a)$$

$$A_-^n(\lambda, l)=i\hbar\kappa S_{n-\lambda+l}\{\psi_{n-\lambda}, \exp[-i\alpha(a_+^* \exp(i\phi) + a_+ \exp(-i\phi))]a_+^*\psi_n\}, \quad (31b)$$

where

$$S_{n-\lambda+l}=\{\psi_{n-\lambda+l}, \exp[-i\alpha(a_-^* \exp(-i\phi) + a_- \exp(i\phi))]\phi_0\}, \quad (32)$$

and

$$\alpha=\tfrac{1}{2}(k/\kappa)\sin\theta. \quad (33)$$

In going from (21) to (31) the product space of a_+ and a_- has been factored. The a_- operators have been absorbed in the $S_{n-\lambda+l}$, the a_+, into the factor by which they are multiplied. An essential simplification is now achieved by observing that the representation of the a_+ and a_- operators is only determined to within a phase factor. The transformation,

$$a_\pm\rightarrow a_\pm \exp(\pm i\phi), \quad (34)$$

without altering the algebraic relations among them, will free the exponentials in (31) of its dependence on the angle and, in addition, induce a transformation on the products:

$$\bar{A}_\pm A_\pm\rightarrow\bar{A}_\pm A_\pm, \quad (35a)$$

$$\bar{A}_\pm A_\mp\rightarrow\exp(\mp 2i\phi)\bar{A}_\pm A_\mp. \quad (35b)$$

These are precisely the phase factors needed to free R [Eq. (22)] of its dependence on ϕ. Thus ϕ may effectively be put equal to zero.

The radial integration in (20) is now carried out. The delta-function in the integrand together with (30) implies that

$$k(\lambda)=k^m[1-(1-2k^C(\lambda)/k^m)^{\frac{1}{2}}]. \quad (36)$$

The symbols appearing on the right side of (36) denote:

$$k^m=K_0/\sin^2\theta, \quad (37)$$

$$k^C(\lambda)=2(\kappa/K_0)\kappa\lambda. \quad (38)$$

The quantity $k^C(\lambda)$ is harmonic to the classical rotation frequency of the electron and it may be inferred from its dependence on λ that it corresponds to the classical radiation frequency. If we let

$$(2k^C(\lambda)/k^m)^{\frac{1}{2}}=\text{arc}\sin\delta(\lambda), \quad (39)$$

then (36) may be written as

$$k(\lambda)=k^C(\lambda)\sec^2(\delta(\lambda)/2). \quad (40)$$

A short calculation shows that single term of the sum over λ in Eq. (19) is given by

$$\frac{d\wp(\lambda)}{d\Omega}=ce^2\frac{4\kappa^2[n(n+1)]^{\frac{1}{2}}}{K_0^2}\cdot\frac{k^2(\lambda)}{2\pi}\cdot\frac{1-k(\lambda)/K_0}{1-\sin^2\theta k(\lambda)/K_0}H(n,\lambda), \quad (41)$$

where the angular integration has been represented in differential form. The explicit appearance of the n's is accounted for by the use of the well-known relations, $a^*\psi_n=(n+1)^{\frac{1}{2}}\psi_{n+1}$ and $a\psi_n=n^{\frac{1}{2}}\psi_{n-1}$, to reduce (31) to a standard form, which will soon be indicated. The fractional expression preceding the still undefined quantity $H(n,\lambda)$ arises from the evaluation of the derivative of the argument of the delta-function, *qua* function of k, at the relevant zero of the function. Finally $H(n,\lambda)$ may, after some rearrangements, be put in the form

$$H(n,\lambda)=P_1\{\cos^2\theta\mathfrak{L}_{n,\lambda}^{(+)2}(\alpha^2)+\mathfrak{L}_{n,\lambda}^{(-)2}(\alpha^2) +\tfrac{1}{2}[\{n/(n+1)\}^{\frac{1}{2}}-\{(n+1)/n\}^{\frac{1}{2}}] \times\mathfrak{L}_{n,\lambda}^{(+)}(\alpha^2)\mathfrak{L}_{n,\lambda}^{(-)}(\alpha^2)+\tfrac{1}{4}[\{n/(n+1)\}^{\frac{1}{2}} +\{(n+1)/n\}^{\frac{1}{2}}-2](1+\cos^2\theta) \times[\mathfrak{L}_{n,\lambda}^{(+)}(\alpha^2)+\mathfrak{L}_{n,\lambda}^{(-)}(\alpha^2)]\}, \quad (42)$$

where $\mathfrak{L}_{n,\lambda}^{(\pm)}$ are contractions for

$$\mathfrak{L}_{n,\lambda}^{(\pm)}=\tfrac{1}{2}[\mathfrak{L}_{n-\lambda}^{\lambda-1}\pm\mathfrak{L}_{n-\lambda}^{\lambda+1}]. \quad (43)$$

[9] For a discussion of other representations of the eigenfunctions see M. Johnson and B. Lippman, Phys. Rev. **77**, 702 (1950).

The quantities $\mathfrak{L}$ and P_1 denote:[10]

$$\mathfrak{L}_{n-\lambda}{}^{\lambda}(\alpha^2)=i^{\lambda}\{\psi_{n-\lambda},\exp[-i\alpha(a+a^*)]\psi_n\}, \tag{44}$$

$$P_1=\sum_l|\{\psi_{n-\lambda+l},\exp[-i\alpha(a+a^*)]\phi_0\}|^2, \tag{45}$$

the symbols having been chosen appropriate to familiar objects in still unrecognized form. Thus, $\mathfrak{L}_{n-\lambda}{}^{\lambda}$ will turn out to be the well-known normalized Laguerre function (after some reduction). The distinction between a_+ and a_- is no longer necessary and has therefore been abandoned in the notation.

The only remaining task in this section is the evaluation of (44) and (45). These are of the form to which the Feynman methods[2] apply and are readily handled with the aid of two equalities:

$$\exp(\mu_1 a+\mu_2 a^*)\equiv\exp(\mu_1\mu_2/2)\exp(\mu_2 a^*)\exp(\mu_1 a),$$
$$\exp(\mu_1 a)\exp(\mu_2 a^*)\equiv\exp(\mu_1\mu_2)\exp(\mu_2 a^*)\exp(\mu_1 a).$$

The manipulations are trivial and only the result will be stated. The right side of (44) is what the symbol on the left alleges it to be.[11] In evaluating (45) it is found that

$$|\{\psi_{n-\lambda+l},\exp[-i\alpha(a+a^*)]\phi_0\}|$$
$$=\exp(-\alpha^2/2)[(n-\lambda+l)!]^{-\frac{1}{2}}\alpha^{n-\lambda+l}.$$

Squaring and summing with respect to l, we obtain[12]

$$P_1\equiv 1. \tag{46}$$

With due regard to (46), Eqs. (41) and (42) represent the rigorous quantum-mechanical radiation formula (within the approximation of the first power of the fine structure constant). In the range of energies that will be considered here, it is permissible to neglect terms whose coefficients are $O(n^{-1})$ and $O(n^{-2})$ relative to those of order $O(1)$. Equation (42) therefore simplifies to

$$H(n,\lambda)=\cos^2\theta\,\mathfrak{L}_{n,\lambda}{}^{(+)2}(\alpha^2)+\mathfrak{L}_{n,\lambda}{}^{(-)2}(\alpha^2). \tag{47}$$

III. THE CORRESPONDENCE DOMAIN

Before comparing the radiation formulas[13] (41) and (42) with the one deduced from classical theory,[14] we should like to delineate, with some precision, the domain in which the comparison is to be made. A general orientation in the orders of magnitudes involved is helpful:

$$\kappa_L=2,93(H/10^4)\ \text{cm}^{-1},$$
$$\kappa=2,76\times10^5(H/10^4)\ \text{cm}^{-1},$$
$$\kappa_C/\kappa_L=0.88\times10^{10}(10^4/H).$$

Thus κ_L is for most fields of interest of order unity and κ —the geometric mean of the reciprocal Compton and Larmor lengths—is of the order of the reciprocal wavelength of visible light. From these relations one readily sees that

$$n=\tfrac{1}{4}\beta^2(E/mc^2)^2(\kappa_C/\kappa_L)=2.2\beta^2(E/mc^2)^2\times(10^4/H)\times10^9. \tag{48}$$

We shall now attempt to define a domain of correspondence of classical and quantum theory in this particular problem. This is not to be construed to imply substantial identity. Quantum effects here may be of some importance, but they are only corrections to an essentially classical theory. The frequency of the emitted radiation may be taken as a fairly sensitive indicator. Classically the emitted frequency is harmonic to the rotational frequency

$$\omega=2c(\kappa_C/K_0)\kappa_L \tag{49}$$

of the electron, thus being proportional to $k^C(\lambda)$ in (40). More quantitatively, expression (36) should be adequately represented by the first nonvanishing term obtained after expanding the square root. Numerically $(k/k_m)=0.500$ corresponds to $(k^C/k_m)=0.375$, hardly a close approximation. The ratio $(k/k_m=0.100$ calls for $(k^C/k_m)=0.095$, still a significant difference. The number $(k/k_m)=0.0100$ gives a more comfortable result $(k^C/k_m)=0.00995$. Thus a ratio of 1/137 is about the right order of magnitude. With this (not entirely unique) choice of an integer, the classical principal harmonic

$$k_p{}^C=3\kappa_L(K_0/\kappa_C)^2 \tag{50}$$

is situated comfortably within the range if

$$K_0/\kappa_C<\tfrac{1}{3}\kappa_B/\kappa_L, \tag{51}$$

where $\kappa_B=2\times10^8$ cm^{-1} has the magnitude of a reciprocal Bohr length. In terms of practical parameters this reads

$$E_{\text{Mev}}<1\times10^7(10^4/H). \tag{52}$$

Thus an argument based on the frequency of the emitted quanta rather than the electron energy seems to lead to a somewhat lower upper limit (by a factor of about 10^2) for the validity of the classical radiation formula.[1] That such frequency shifts $\delta(\lambda)$ must be taken into account in this very high energy domain will soon become apparent. The limit (52) should not be pushed much higher; otherwise radiation whose principal harmonic has a sizeable $\delta(\lambda)$ correction will be included.

The asymptotic behavior of Laguerre functions is too involved[5] in the entire range (52) to permit an easy comparison of the results of the two theories. A further

[10] The reader will overlook for a moment a notational inconsistency in (44).

[11] A normalized Laguerre function may be represented by the series $\mathfrak{L}_n{}^{\lambda}(x)=(n!/(n+\lambda)!)^{\frac{1}{2}}x^{\lambda/2}\exp(-x/2)\sum_s\binom{n+\lambda}{n-s}(1/s!)(-x)^s$.

[12] This has been shown, within a good approximation, in a less trivial analytical context in references 3 and 4. Equality (46) asserts that the specific effect then under discussion is not only immaterial to a particular energy range, but nonexistent. An effect P_2, unrelated to P_1, will be studied in the next section. It occurs within the framework of the correct radiation formula and turns out, on examination, to be insignificant, but is none the less extant.

[13] Some of its features have been recognized by G. Parzen, Phys. Rev. **84**, 235 (1951). References 3 and 4 should also be consulted.

[14] See, for example, J. Schwinger, Phys. Rev. **75**, 1912 (1949).

restriction,

$$\alpha^3/n^{\frac{1}{2}}<1, \tag{53}$$

is therefore imposed for reasons of purely mathematical convenience. Within the limitation of (53) the substantial identity of the two theories will be established.

Before doing this, however, we shall indicate the physical implications of this inequality. It may be written with the aid of (33) as

$$\beta^3(\lambda/2)^3(1/n^2)\sin^3\theta<1, \tag{54}$$

or, expressed differently,

$$k^C(\lambda)/K_0<(\beta/\sin\theta)(1/n^{1/3}). \tag{55}$$

A glance at (48) makes clear the numerical significance of (55). The electron indeed loses only a very small fraction of its energy. The principal harmonic will be located in this range if

$$E/mc^2<[(4/27)\beta(\kappa_c/\kappa_L)^2\sin^{-3}\theta]^{1/5}, \tag{56}$$

or, numerically,

$$E_{\text{Mev}}<4\times10^3(10^4/H)^{2/5}\sin^{-3/5}\theta. \tag{57}$$

These formulas have been written with a somewhat greater care than the circumstances call for in order to exhibit the fact that if the breakdown of the asymptotic representation should imply the appearance of significant quantum effect, then these would make themselves first felt in the neighborhood of the orbital plane.

Within this domain, a normalized Laguerre function may be approximated by[5]

$$\mathfrak{L}_n{}^{\alpha}(x)\cong J_\alpha[2(n_1x)^{\frac{1}{2}}];\quad n_1=n+(\alpha+1)/2. \tag{58}$$

With the aid of the sum and difference rule for Bessel functions (47) can be represented as

$$H(n,\lambda)=\cot^2\theta[J_\lambda(\lambda\beta P_2\sin\theta)/\beta P_2]^2 +[J_\lambda'(\lambda\beta P_2\sin\theta)]^2, \tag{59}$$

where

$$P_2=(1-\lambda/2n)^{\frac{1}{2}}\sec^2(\delta(\lambda)/2). \tag{60}$$

In writing down (59) the numbers 1 and 2 were neglected relative to n and $n-\lambda$. In terms of classical parameters [$R=(n+1)^{\frac{1}{2}}/\kappa$, ω defined in (49)] Eq. (41) may be written as

$$d\mathcal{P}(\lambda)/d\Omega=(e^2/R)\omega\beta^3(\lambda^2/2\pi)\sec^4(\delta(\lambda)/2) \times[1-\beta^2(\lambda/2n)\sec^2(\delta(\lambda)/2)] \times[1-\beta^2(\lambda/2n)\sec^2(\delta(\lambda)/2) \times\sin^2\theta]^{-1}H(n,\lambda). \tag{61}$$

Looking back at the numbers quoted earlier it is seen that (61) is adequately approximated by

$$dP(\lambda)/d\Omega=(e^2/R)\omega\beta^3(\lambda^2/2\pi) \times\{\cot^2\theta[J_\lambda(\lambda\beta P_2\sin\theta)/\beta]^2 +[J_\lambda'(\lambda\beta P_2\sin\theta)]^2\}, \tag{62}$$

an expression identical with the classical radiation formula except for the presence of P_2. The importance of this quantity will now be assessed.

IV. THE QUANTUM EFFECT

The decisive variable in the behavior of Bessel functions in this asymptotic range is the difference between order and argument, or

$$1-\beta P_2\cong\tfrac{1}{2}(1-\beta^2)+(1-P_2)-\tfrac{1}{2}(1-P_2)(1-\beta^2) +\tfrac{1}{8}(1-\beta^2)^2, \tag{63}$$

where we have confined ourselves to the orbital plane. As noted in the introduction, $1-P_2$ is being compared here with the difference between the velocity of the particle and that of light as expressed in $1-\beta^2\sim10^{-8}$. If indeed $1-P_2$ were significant relative to this small magnitude, the classical radiation formula would break down. According to (60), P_2 consists of a factor

$$(1-\lambda/2n)^{\frac{1}{2}}\cong1-\lambda/4n-\lambda^2/32n^2 \tag{64}$$

arising from the lack of precision in the definition of the orbit, and of a factor

$$\csc^2(\delta(\lambda)/2)\cong1+\beta^2\lambda/4n+\beta^4\lambda^2/8n^2 \tag{65}$$

expressing a very slight shift in the frequency of the photon relative to the classical frequency. Their product is

$$1-P_2\cong-\lambda^2/32n^2+(\lambda/4n)(1-\beta^2), \tag{66}$$

and (63) becomes

$$1-\beta P_2\cong\tfrac{1}{2}(1-\beta^2)-\lambda^2/32n^2+(\lambda/4n)(1-\beta^2) +\tfrac{1}{8}(1-\beta^2)^2. \tag{67}$$

(Some numbers to keep here in mind are $E\sim5\times10^3\,mc^2$, $1-\beta^2\sim4\times10^{-8}$, $\lambda/n\sim2\times10^{-6}$; the terms in (67) are roughly 10^{-8}, -10^{-13}, 10^{-14}, 10^{-16}.) The second term in (67) is about a hundred thousand times smaller than the first (classical) term and the third (the hopeful one) a million. A physically *un*interesting observation in this connection is that the sign of the leading quantum term is negative. Thus because of (insignificant) quantum effects the particle has an effective velocity (insignificantly) closer to that of light and radiates (insignificantly) more, contrary to some expectations.

It should be noted in this connection that had only the electron term (64) been taken into account, the quantum correction would have been $\lambda/4n\sim10^{-7}$; a quantity larger than the classical term $1-\beta^2\sim10^{-8}$. Unlike in the lower energy range, both of these effects must be considered, in order to establish the substantial identity of the two theories. This, admittedly crude, argument will now be put on a more quantitative basis.

It is convenient for this purpose to write (62) in the form

$$d\mathcal{P}(\lambda)/d\Omega=(e^2/R)\omega(\lambda^2/2\pi)\{[J_\lambda'(\lambda\beta_e)]^2 +\tan^2\psi[J_\lambda(\lambda\beta_e)]^2\}, \tag{68}$$

where

$$\beta_e=\beta P_2\cos\psi \tag{69}$$

and

$$P_2=2[1+(1-\beta^2\cos^2\psi\lambda/n)^{\frac{1}{2}}]^{-1}(1-\lambda/2n)^{\frac{1}{2}}. \quad (70)$$

A change of variable $\psi=\pi/2-\theta$ has also been introduced. The interesting part of the spectrum,

$$\lambda\sim(1-\beta_e)^{-\frac{3}{2}}, \quad (71)$$

is dominated by the Nicholson asymptotic formulas:

$$J_\lambda(\lambda\beta_e)\cong(2/\lambda)^{\frac{1}{3}}\,\mathrm{Ai}(\xi), \quad (72a)$$

$$J_\lambda'(\lambda\beta_e)\cong-(2/\lambda)^{\frac{2}{3}}\,\mathrm{Ai}'(\xi), \quad (72b)$$

$$\xi=(\lambda/2)^{\frac{2}{3}}2(1-\beta_e). \quad (72')$$

Airy functions appearing in (72) may be defined by the integral

$$\mathrm{Ai}(x)=(1/\pi)\int_0^\infty d\tau\,\cos(\tau^3/3+x\tau), \quad (73)$$

and the expressions can be regarded as first terms of asymptotic expansion[15] with $(1-\beta_e)$ as a parameter of smallness. In the neighborhood of (71) Eq. (68) is then approximated by

$$d\mathcal{P}(\lambda)/d\Omega=(2/\pi)(e^2/R)\omega(\lambda/2)\times[(2/\lambda)^{\frac{1}{3}}\,\mathrm{Ai}'^2(\xi)+\tan^2\psi(\lambda/2)^{\frac{1}{3}}\,\mathrm{Ai}^2(\xi)]. \quad (74)$$

The effect of P_2 will now be studied in two limiting cases when the argument of the Airy function is much smaller and much larger than unity. Physically these correspond to the spectral ranges of subcritical and supercritical harmonics, respectively.

Case I. $\lambda\ll 2[2(1-\beta_e)]^{-3/2}$

With the aid of the expansions,

$$\mathrm{Ai}(x)\cong(1/2\pi)[3^{-1/6}\Gamma(\tfrac{1}{3})-3^{1/6}\Gamma(\tfrac{2}{3})x], \quad (75a)$$

$$\mathrm{Ai}'(x)\cong-(1/2\pi)[3^{1/6}\Gamma(\tfrac{2}{3})-(\tfrac{1}{2})3^{-1/6}\Gamma(\tfrac{1}{3})x^2], \quad (75b)$$

(74) may be written as

$$d\mathcal{P}(\lambda)/d\Omega=(e^2/R)\omega(2/\pi)\{(1/4\pi^2)3^{\frac{1}{3}}\Gamma^2(\tfrac{2}{3})(\lambda/2)^{\frac{1}{3}}+(1/4\pi^2)\tan^2\psi 3^{-\frac{1}{3}}\Gamma^2(\tfrac{1}{3})(\lambda/2)^{4/3}-(1/2\pi)3^{-\frac{1}{3}}(\lambda/2)^2[2(1-\beta_e)]^2-(1/\pi)3^{-\frac{1}{3}}(\lambda/2)^2\tan^2\psi[2(1-\beta_e)]\}. \quad (76)$$

Expression (76) was calculated under the assumption that ψ is not too large. With this in mind,

$$2(1-\beta_e)\cong 4\sin^2(\psi/2)+\cos\psi(1-\beta^2)+(\lambda/2n)\times\cos\psi(1-\beta^2\cos^2\psi)-(\lambda^2/16n^2)\cos\psi. \quad (77)$$

For the special case of radiation in the orbital plane, (76) and (77) may be combined to yield

$$d\mathcal{P}(\lambda)/d\Omega=(e^2/R)\omega(2/\pi)\{(1/4\pi^2)3^{\frac{1}{3}}\Gamma^2(\tfrac{2}{3})(\lambda/2)^{\frac{1}{3}}-(1/2\pi)3^{-\frac{1}{3}}(\lambda/2)^2(1-\beta^2)^2+(1/16\pi)3^{-\frac{1}{3}}(\lambda/2)^2(1-\beta^2)(\lambda^2/n^2)-(1/2\pi)3^{-\frac{1}{3}}(\lambda/2)^2(1-\beta^2)^2(\lambda/n)\}. \quad (78)$$

The first two terms in the curly bracket of (78) are of classical, the last two of quantum origin. The latter are seen to represent small corrections to the leading energy independent classical term and are quite insignificant in practice. Expansion (78) being a limiting form of (74) valid mainly in the neighborhood of (71) was checked by expression (68) directly in terms of a Meissel series which constitutes a more appropriate representation for the subcritical range of the spectrum.

For other angles to which (76) is applicable the expressions are more involved but the conclusions the same. The case of very large angles of emission, $\beta_e\sim 0$, requires special treatment. This may be carried out with the aid of the formula

$$J_\lambda(\lambda\beta_e)\cong(2\pi\lambda)^{-\frac{1}{2}}(\beta_e/2)^\lambda\exp\lambda. \quad (79)$$

Quantum effects are here even less impressive and the details will therefore be omitted.

Case II. $\lambda\gg 2[2(1-\beta_e)]^{-3/2}$

The asymptotic expressions,

$$\mathrm{Ai}(x)\cong\tfrac{1}{2}\pi^{-\frac{1}{2}}x^{-\frac{1}{4}}\exp[-\tfrac{2}{3}x^{\frac{3}{2}}], \quad (80a)$$

$$\mathrm{Ai}'(x)\cong-\tfrac{1}{2}\pi^{-\frac{1}{2}}x^{\frac{1}{4}}\exp[-\tfrac{2}{3}x^{\frac{3}{2}}], \quad (80b)$$

substituted in (74) yield

$$d\mathcal{P}(\lambda)/d\Omega=(e^2/R)\omega(\lambda/4\pi^2)\{[2(1-\beta_e)]^{\frac{1}{2}}+\tan^2\psi[2(1-\beta_e)]^{-\frac{1}{2}}\}\exp\{-\tfrac{2}{3}\lambda[2(1-\beta_e)]^{\frac{3}{2}}\}. \quad (81)$$

Expanding the exponential we obtain

$$d\mathcal{P}(\lambda)d\Omega=(d\mathcal{P}(\lambda)/d\Omega)^c\exp\{\tfrac{1}{16}(1-\beta^2+\psi^2)^{\frac{1}{2}}(\lambda^3/n^2)-(1-\beta^2+\psi^2)^{\frac{3}{2}}(\lambda^2/2n)\} \quad (82)$$

for angles close to the orbital plane. The approximate expressions that were employed in obtaining this formula are

$$P_2\cong 1+\tfrac{1}{32}(\lambda/n)^2-\tfrac{1}{4}(\lambda/n)(1-\beta^2+\psi^2), \quad (83)$$

$$\beta_e\cong 1-\tfrac{1}{2}(1+\lambda/2n)(1-\beta^2+\psi^2)+\tfrac{1}{32}(\lambda/n)^2. \quad (84)$$

It is clear from (81) that large angles need not be considered. The exponential factor for $\beta_e\ll 1$ is powerful enough to suppress practically all radiation. The unfamiliar symbol in (82) is defined by

$$(d\mathcal{P}(\lambda)/d\Omega)^c=(e^2/R)\omega(\lambda/4\pi^2)\times\{(1-\beta^2+\psi^2)^{\frac{1}{2}}+\psi^2(1-\beta^2+\psi^2)^{-\frac{1}{2}}\}\times\exp\{-\tfrac{2}{3}\lambda(1-\beta^2+\psi^2)^{\frac{3}{2}}\}, \quad (85)$$

and is equal to the classical expression for the radiated

[15] Expansions of this type have recently been obtained by F. W. J. Olver, Proc. Cambridge Phil. Soc. **48**, 414 (1952). The mathematical material used in this section will be found in Watson, *Bessel Functions* (The Macmillan Company, New York, 1945).

power in the supercritical range. Its multiplying factor in (82) represents the quantum effect.

Looking back to (54) we see that even for $\lambda^3/n^2 \sim 8$, when the Bessel function representation of Laguerre functions becomes somewhat doubtful, the quantum factor is still only $\sim\exp(10^{-4})$. This strongly suggests that the classical theory is valid for energies considerably higher than the range in which it has been here explicitly shown to hold. Before this suggestion is taken seriously, however, it is necessary, in view of (71), to show that the "safety factor" $(1-\beta^2+\psi^2)^{\frac{1}{2}}$ is not incidental to the limiting form of the particular asymptotic representation that has been employed.

This point may be checked by verifying that the Debye forms,

$$J_\lambda(\lambda\beta_e)\cong(2\pi\lambda)^{-\frac{1}{2}}(1-\beta_e^2)^{-\frac{1}{4}} \times\{\beta_e[1+(1-\beta_e^2)^{\frac{1}{2}}]^{-1}\exp(1-\beta_e^2)^{\frac{1}{2}}\}^\lambda, \quad (86a)$$

$$J_\lambda'(\lambda\beta_e)\cong(2\pi\lambda)^{-\frac{1}{2}}(1-\beta_e^2)^{-\frac{1}{4}}\{\beta_e^{-1}-\beta_e[1+(1-\beta_e)^{\frac{1}{2}}]^{-1}\} \times\{\beta_e[1+(1-\beta_e^2)^{\frac{1}{2}}]^{-1}\exp(1-\beta_e)^{\frac{1}{2}}\}^\lambda, \quad (86b)$$

which are applicable to the supercritical frequency range irrespectively of the electron energy (the Nicholson forms can be used only when the energy is very high), yield expression (82) in the relativistic limit. Substituting (86) into (62) we obtain

$$d\mathcal{P}(\lambda)/d\Omega=(e^2/R)\omega(\lambda/4\pi^2)\beta^3(1-\beta_e^2)^{-\frac{1}{2}} \times\{[\beta_e^{-1}-\beta_e(1+(1-\beta_e^2)^{\frac{1}{2}})^{-1}]^2+\beta^{-2}\tan^2\psi\} \times\{\beta_e[1+(1-\beta_e^2)^{\frac{1}{2}}]^{-1}\exp(1-\beta_e^2)^{\frac{1}{2}}\}^{2\lambda}, \quad (87)$$

a formula valid even if the velocity of the electron is not very high. It is easy to show with a few elementary manipulations that this more rigorous expression reduces to (82) in the limit $(1-\beta_e^2)^{\frac{1}{2}}\ll 1$.

The radiation formula in the intermediate frequency range cannot be expressed in terms of elementary functions. A cursory examination of the numerical tables[16] of Airy functions readily convinces one that the quantum effects in this region are even less significant than in Case II considered previously.

V. SUMMARY

In the domain of ultrarelativistic energies the difference between the velocity of light and that of the particle is decisive in the determination of its radiative properties. Here the classical results may cease to be valid, not only because the electron radiates so intensely that its final state falls into a region where quantum fluctuations count but also because quantum uncertainties may be large relative to this difference.

Quantum effects manifest themselves in the lack of precision in the definition of the orbit and in a shift of the frequency of the emitted radiation. The first effect, though exceedingly small relative to the total velocity of the electron, is sufficient at these energies to produce a considerable diminution in the radiated intensity; the second to give rise to an appreciable increase. If both, however, are properly taken into account, the net result is entirely nugatory.

The author is grateful to Dr. David Judd and Dr. J. V. Lepore for illuminating discussions of various phases of this problem. He also wishes to thank Professor L. I. Schiff for some valuable comments and criticisms.

The work was performed under the auspices of the U. S. Atomic Energy Commission.

[16] Advancement of Sci., Math. Tables, *The Airy Integral* (Cambridge University Press, Cambridge, 1946). Part—, Vol. B.

Fredholm Theory of Scattering in a Given Time-Dependent Field

ABDUS SALAM, *St. John's College, Cambridge, England, and Government College, Lahore, Pakistan*

AND

P. T. MATTHEWS,* *Cavendish Laboratory, Cambridge, England*

(Received October 27, 1952)

It is shown that Feynman's relativistic solution for the scattering of an electron (or pair creation) by a given external field is the Fredholm resolvent of the related integral equation and is thus the unique and absolutely convergent solution for any strength of field.

INTRODUCTION

THE Fredholm theory of integral equations has been applied to the nonrelativistic theory of scattering by Jost and Pais.[1] We here consider the extension of this theory to the interaction of the quantized electron-positron field with a prescribed external electromagnetic field. This problem has been considered by Feynman.[2] Feynman's solution is most simply derived from the S matrix in the form given by Dyson.[3] The appropriate matrix element for electron scattering or pair creation is obtained as an expansion in the external field and is normalized by multiplying by the vacuum expectation value of the S matrix. We show that this is identical with the Fredholm resolvent of a related integral equation and is thus absolutely convergent for any strength of the external field, for which the cross section has any meaning.

In the first section the Fredholm theory is stated in a form given by Plemelj,[4] which exhibits the Fredholm solution in terms of the iterations of the kernel and its traces. These quantities have the advantage over the usual form of the theory[5] that they are either the same as, or closely related to, expressions occurring in the S matrix and can be written down directly by Feynman's graphical methods. The relation of the Fredholm solution to the solution by iteration is discussed. The problem of scattering in a pure external field is then treated in Secs. 2 and 3, with the result stated above. The case of a static field is related to the work of Jost and Pais.[1]

1. FREDHOLM THEORY

Consider Fredholm's integral equation

$$x(s)=y(s)+\lambda\int K(s,t)x(t)dt, \tag{1.1}$$

$$(\text{or } x=y+\lambda Kx),$$

where the integration may be over a fixed interval, finite or infinite. Smithies[6] has shown that, if $K(s,t)$ is a measurable function of s and t, and

$$C_1\equiv\int\int|K(s,t)|^2dsdt<\infty, \tag{1.2}$$

then (1.1) has the unique solution

$$\begin{aligned}x(s)&=d^{-1}(\lambda)\int D(\lambda,s,t)y(t)dt,\\&=d^{-1}(\lambda)\Delta(\lambda,s),\end{aligned} \tag{1.3}$$

for all λ for which $d(\lambda)\neq 0$. Here

$$d(\lambda)=\sum_{n=0}^{\infty}d_n\lambda^n, \tag{1.4}$$

$$D(\lambda,s,t)=\sum_{n=0}^{\infty}D_n(s,t)\lambda^n \tag{1.5}$$

[$D(\lambda,s,t)$ is called the Fredholm resolvent], where $d_0=1$,

$$d_n=\frac{(-1)^n}{n!}\begin{vmatrix}\sigma_1 & n-1 & 0 & \cdots & 0\\ \sigma_2 & \sigma_1 & n-2 & \cdots & 0\\ \cdot & & & & \\ \cdot & & & & \\ \cdot & & & & \\ \sigma_n & \sigma_{n-1} & & \cdots & \sigma_1\end{vmatrix}, \tag{1.6}$$

$$D_n(s,t)=\frac{(-1)^n}{n!}\begin{vmatrix}\delta(s-t) & n & 0 & 0 & \cdots & 0\\ K(s,t) & \sigma_1 & n-1 & 0 & \cdots & 0\\ K^2(s,t) & \sigma_2 & \sigma_1 & n-2 & \cdots & 0\\ \cdot & & & & & \\ \cdot & & & & & \\ \cdot & & & & & \\ K^n(s,t) & \sigma_n & \sigma_{n-1} & & \cdots & \sigma_1\end{vmatrix} \tag{1.7}$$

$$\begin{aligned}K^n(s,t)&=\int K^{n-1}(s,u)K(u,t)du\\&=\int K(s,u)K^{n-1}(u,t)du,\end{aligned} \tag{1.8}$$

* Now at Department of Mathematical Physics, University of Birmingham, Birmingham, England.

[1] R. Jost and A. Pais, Phys. Rev. **82**, 840 (1951).

[2] R. P. Feynman, Phys. Rev. **76**, 749 (1949).

[3] F. J. Dyson, Phys. Rev. **75**, 486, 1736 (1949).

[4] J. Plemelj, Monatsch. Math. **15**, 93 (1904).

[5] See, for example, E. T. Whittaker and G. N. Watson, *Modern Analysis* (Cambridge University Press, Cambridge, 1940), fourth edition, Chapter XI.

[6] F. Smithies, Duke Math. J. **8**, 107 (1941).

and

$$\sigma_n = \mathrm{Trace} K^n = \int K^n(s,s)ds. \tag{1.9}$$

If $x(s)$ is a spinor function, the trace in (1.9) is also taken over the spinor suffixes of K. The function $d(\lambda)$ is proved to be convergent for all complex values of λ, so that it is an integral function of λ; the resolvent, $D(\lambda, s, t)$, is also uniformly convergent for all λ, so the solution (1.3) is valid for the whole complex λ-plane (except for λ satisfying $d(\lambda)=0$). This formulation is shown to be identical with the usual formulation by Smithies.[6]

As already stated in the introduction, an advantage of this form is that for any field theoretic equations, the expressions $K^n y$ are just those appearing in the solution by iteration[7] and can be calculated directly by the Feynman-Dyson[2,3] method. The σ_n are closely related to the vacuum graphs of the S matrix, and Feynman's methods are again immediately applicable.

From the definition (1.6),

$$d_n = -\frac{1}{n}\sum_{m=1}^{n-1}\sigma_m d_{n-m}, \tag{1.10}$$

so that

$$\sum_{n=0}^{\infty}(n+1)d_{n+1}\lambda^n = -\left(\sum_{n=0}^{\infty} d_n\lambda^n\right)\left(\sum_{q=0}^{\infty}\sigma_{q+1}\lambda^q\right). \tag{1.11}$$

Thus

$$d^{-1}\frac{\partial d}{\partial \lambda} = -\sum_{q=0}^{\infty}\sigma_{q+1}\lambda^q.$$

Hence

$$d(\lambda) = \exp\left[-\sum_{n=1}^{\infty}\sigma_n\lambda^n/n\right]. \tag{1.12}$$

From the definition (1.7),

$$D_n = \sum_{m=0}^{n} K^m d_{n-m} \left(= Id_n + KD_{n-1}\right). \tag{1.13}$$

Hence

$$D(\lambda) = d(\lambda)(1+\lambda K+\lambda^2K^2+\cdots). \tag{1.14}$$

The relation between the Fredholm solution and the solution by iteration is brought out clearly by substituting (1.14) into (1.3). The Fredholm solution then reduces to

$$x = \frac{D(\lambda)y}{d(\lambda)} = \frac{d(\lambda)(1+\lambda K+\lambda^2K^2+\cdots)y}{d(\lambda)}, \tag{1.15}$$

which is just the solution by iteration if the $d(\lambda)$ term is canceled. The Fredholm solution is exhibited as an analytic continuation of the iterated solution; the function $d(\lambda)$ is an integral function such that its zeros cancel the poles of the solution by iteration,[8] $(1+\lambda K+\lambda^2K^2+\cdots)y$, thus making $D(\lambda)y$ also an integral function. Fredholm's work shows not only that such a function exists but provides a method for actually calculating it.

The proof of the convergence of the Fredholm solution is based on the inequality

$$|\sigma_n| \leqslant |C_1|^{n/2} \quad (n=2,3,\cdots). \tag{1.16}$$

The condition (1.2) does not require that σ_1 be finite, and in fact the solution is unaltered by replacing σ_1 by zero in (1.6) and (1.7), whatever its actual value. However, if σ_2 diverges the condition (1.2) cannot be satisfied.

It may happen that $C_1, \cdots, C_{m-1}$ are not bounded, but that C_m is, where, by definition

$$C_m \equiv \int\int |K^m(s,t)|^2 dsdt. \tag{1.17}$$

One can still obtain a convergent solution to the equation by first iterating m times. Thus, in operator notation,

$$\begin{aligned} x &= y+\lambda Kx \\ &= (1+\lambda K+\lambda^2K^2+\cdots+\lambda^{m-1}K^{m-1})y+\lambda^m K^m x. \end{aligned} \tag{1.18}$$

This equation has a solution, since

$$C_m < \infty,$$

namely,

$$\begin{aligned} x = \frac{D_m(\lambda)y}{d_m(\lambda^m)} &= \frac{d_m(\lambda^m)}{d_m(\lambda^m)}\cdot(1-\lambda^m K^m)^{-1} \\ &\quad \times(1+\lambda K+\cdots+\lambda^{m-1}K^{m-1})y \\ &= \frac{d_m(\lambda^m)}{d_m(\lambda^m)}\cdot(1+\lambda K+\lambda^2K^2+\cdots)y, \end{aligned} \tag{1.19}$$

where

$$d_m(\lambda^m) = \exp\left\{-\left[\lambda^m\sigma_m+\frac{\lambda^{2m}}{2}\sigma_{2m}+\cdots\right]\right\}. \tag{1.20}$$

[7] The solution by iteration is known as the Neumann-Liouville solution. This is the Born approximation in nonrelativistic scattering theory and is the "weak coupling" expansion of relativistic field theory.

[8] This result has been established quite rigorously in the literature. Just to clarify the structure of the Fredholm solution, we can cast $d(\lambda)$ in a different form by the following nonrigorous argument. This was pointed out to the authors by Professor R. E. Peierls.

The solution by iteration is the binomial expansion of

$$x = \frac{1}{1-\lambda K}y.$$

The poles of this solution are given by the eigenvalues of the homogeneous equation

$$(1-\lambda_\alpha K)x_\alpha = 0.$$

The eigenvalues of K^n are $(1/\lambda_\alpha)^n$, and the trace σ_n is thus

$$\sigma_n = \Sigma_\alpha\,(1/\lambda_\alpha)^n.$$

Hence, by Eq. (1.12),

$$\begin{aligned} d(\lambda) &= \exp\left[-\sum_{n=1}^{\infty}\sum_{\alpha}\frac{1}{n}\left(\frac{\lambda}{\lambda_\alpha}\right)^n\right] \\ &= \exp\left[\Sigma_\alpha \log(1-\lambda/\lambda_\alpha)\right] \\ &= \Pi_\alpha(1-\lambda/\lambda_\alpha), \end{aligned}$$

which is just the form required for $d(\lambda)$ to cancel the poles of the solution by iteration.

This solution is reducible, and one can factor an integral function from the numerator and the denominator. Poincare[9] has shown the irreducible solution is given by Eqs. (1.3)–(1.9) with $\sigma_1, \sigma_2, \cdots \sigma_{m-1}$ replaced by zero.

2. THE EXTERNAL FIELD

Consider the problem of the quantized Dirac field in interaction with a given external field, which is time dependent and may create pairs. The field produced by the electrons themselves is neglected. The S matrix for the system is

$$S=\sum_n \frac{(-i)^n}{n!}\int\cdots\int dx_1\cdots dx_n \times P(H^e(x_1),\cdots H^e(x_n)), \quad (2.1)$$

where

$$H^e(x)=-i\lambda\bar{\psi}(x)\boldsymbol{A}^e(x)\psi(x), \quad (2.2)$$

$$\boldsymbol{A}^e(x)=A^e{}_\mu(x)\gamma_\mu, \quad (2.3)$$

and λ is a constant which determines the strength of the field.

We consider the cross section for scattering of an electron from a state $u(q)$ to a state $u(p)$, where both momentum and spin are specified. The transition amplitude obtained from the S matrix is written as $(p|S|q)$. From Dyson's theory[3] applied to (2.1) it follows that

$$(p|S|q)=(0|S|0)(p|R|q); \quad (2.4)$$

where $(0|S|0)$ is the vacuum expectation value of the S matrix, represented by vacuum graphs, while $(p|R|q)$ is, by definition, represented by the connected graphs for the scattering process itself.[10] Because we are dealing with a time-dependent external field the vacuum-to-vacuum transition probability $|(0|S|0)|^2$ is not unity, and so $(0|S|0)$ is not a mere phase factor and has to be expressly considered.

To calculate $(p|R|q)$ define $M(p,q)$ such that

$$(p|R|q)=\bar{u}(p)M(p,q)u(q). \quad (2.5)$$

From the S matrix an integral equation for $M(p,q)$ can readily be derived. For weak external fields (λ small), where an expansion in field strength is permissible we have, by Feynman-Dyson methods,

$$M(p,q)=\lambda\boldsymbol{A}^e(p-q)-2\pi\lambda^2\int\boldsymbol{A}^e(p-k)S_F(k) \times\boldsymbol{A}^e(k-q)d^4k,+\cdots, \quad (2.6)$$

where

$$S_F(k)=\frac{1}{2\pi i}\frac{i\gamma_\mu k_\mu-\kappa}{k^2+\kappa^2-i\epsilon}, \quad \epsilon>0. \quad (2.7)$$

[9] H. Poincare, Acta Math. **33**, 57 (1910).

[10] Dyson's treatment is a restatement in more conventional terms of Feynman's solution. $(p|S|q)$ is called the "absolute" probability amplitude and $(p|R|q)$ the "relative" probability amplitude by Feynman.

Write $M_I(p,q)$ for the right-hand side of (2.6) and define

$$(p|R_I|q)=\bar{u}(p)M_I(p,q)u(q). \quad (2.8)$$

Now $M_I(p,q)$ is the solution by iteration (hence the suffix I) of the integral equation[11]

$$M(p,q)=\lambda\boldsymbol{A}^e(p-q)-2\pi\lambda\int\boldsymbol{A}^e(p-k)S_F(k) \times M(k,q)d^4k, \quad (2.9)$$

which defines $M(p,q)$ for any strength of field. This is an equation for $M(p,q)$, (q constant) of the Fredholm type and we can consider the application of the theory of the previous section.[12]

The kernel of the equation is

$$K(p,k)=\boldsymbol{A}^e(p-k)S_F(k)(-2\pi). \quad (2.10)$$

This is a measurable function for reasonable $A^e(p-k)$ provided the limit $\epsilon\to 0$ is not taken until the end of the calculation.[13]

The Fredholm traces σ_n can be looked at graphically, as stated in the introduction. For this particular integral equation, the σ's happen to be precisely the expressions represented by the vacuum graphs of the S matrix theory. Define

$$L=\sum_{n=1}^{\infty}\frac{\sigma_{2n}\lambda^{2n}}{2n} \quad (2.11)$$

so that the Fredholm determinant [Eq. (1.12)] is

$$d(\lambda)=\exp(-L). \quad (2.12)$$

From (2.11), L is the sum of all vacuum graphs taken singly.[14] With this definition of L, Feynman has shown that

$$(0|S|0)=\exp(-L), \quad (2.13)$$

[11] This equation has already been considered by M. Neuman, Phys. Rev. **83**, 1258 (1951); **85**, 129 (1952).

[12] Since $S_F{}^A(x,y)$, the electron propagator in a given field, satisfies

$$\left[\gamma_\mu\frac{\partial}{\partial x_\mu}-\kappa-ie\boldsymbol{A}(x)\right]S_F{}^A(x,y)=-2i\delta(x-y),$$

$$S_F{}^A(x,y)=S_F(x-y)-\frac{e}{2}\int S_F(x-z)\boldsymbol{A}(z)S_F{}^A(z,y)dz.$$

This is the same equation and can be solved by the same methods.

[13] We refer here to the standard procedure for calculating Feynman integrals for σ_n and K^n, in terms of which the answer is expressed [formulas (1.3)–(1.9)]. This procedure has been demonstrated for particular examples by R. P. Feynman [Phys. Rev. **76**, 769 (1949); see particularly the penultimate paragraph of Sec. 7] and discussed generally by R. J. Eden, Proc. Roy. Soc. (London) **A210**, 388 (1952).

For $\epsilon>0$ the momentum integrals are all taken along the real axis. After completing these integrals, it is, in general, necessary to keep $\epsilon>0$ in order to define the analytic continuation of these functions round the branch points which occur at creation thresholds. Only after this can the limit $\epsilon\to 0$ be taken, to give the physical answer.

[14] Note that $\sigma_{2n+1}=0$ by Furry's theorem. The factor $(1/2n)$ in the nth term comes from $(2n!)^{-1}$ in (2.1) multiplied by $(2n-1)!$, the number of permutations of the $2n$ points round the closed loop of the graph for σ_{2n}.

and, therefore,[15]

$$(0|S|0)=d(\lambda). \tag{2.14}$$

Let us now consider the σ's for convergence. The expression for σ_2 is

$$\sigma_2=(2\pi)^2\int\int dpdk \times \mathrm{Tr}[\boldsymbol{A}^e(p-k)S_F(k)\boldsymbol{A}^e(k-p)S_F(p)]. \tag{2.15}$$

By a change of variable,

$$\sigma_2=(2\pi)^2\int dtA_\mu^e(t)A_\nu^e(-t)\int dk \times \mathrm{Tr}[\gamma_\mu S_F(k)\gamma_\nu S_F(t-k)]. \tag{2.15'}$$

The integral over k is the expression which occurs in the vacuum polarization and is divergent. (This is obvious from the graph of σ_2, which is the well-known loop of two electron lines.) Thus, σ_2 diverges for any choice of A^e. By (1.16) it follows that

$$C_1>\infty, \tag{2.16}$$

and Fredholm theory is not immediately applicable to the equation in this form. This difficulty can be overcome by the device of Poincare,[8] stated at the end of the previous section. Fredholm theory can be applied in a slightly modified form to our equation, provided[16]

$$C_2<\infty. \tag{2.17}$$

For the moment we will assume this condition to be satisfied and will show in the next section how all fields of physical interest can be included.

Assuming (2.17), the unique convergent solution for any strength of field is given by replacing σ_2 by zero in the general formulas of Sec. 1. By (1.3), (2.8), and (2.12) this is

$$(p|R|q)=\{\bar{u}(p)\Delta_q(\lambda, p)u(q)\}/\exp(-L'), \tag{2.18}$$

where

$$L'=\sum_{n=2}^{\infty}[\sigma_{2n}\lambda^{2n}/2n], \tag{2.19}$$

and Δ is defined by (1.7) applied to (2.10). The suffix q on Δ_q denotes that it is also a function of q. By (2.11) and (2.13)

$$(p|S|q)=\exp(-L)\{\bar{u}(p)\Delta_q(\lambda, p)u(q)\}/\exp(-L') =\{\bar{u}(p)\Delta_q(\lambda, p)u(q)\}\exp[-\sigma_2\lambda^2/2]. \tag{2.20}$$

The factor in curly brackets is essentially the resolvent of the Fredholm solution of (2.9) and is thus an integral function of λ. The σ_2 which occurs in the other term is infinite, but its real part is finite,[17] and it thus contributes a finite numerical factor to the probability $|(p|S|q)|^2$. Our final expression for $|(p|S|q)|^2$ is thus an infinite series in λ, each term of which is finite, and which is absolutely and uniformly convergent for any value of λ, that is, for any strength of field.

But according to the form of $\Delta(\lambda)$ given by (1.15),

$$\Delta_q(\lambda, p)=\exp(-L')M_I(p, q). \tag{2.21}$$

Thus, the Fredholm solution, Eq. (2.20), can be written

$$(p|S|q)=(p|R_I|q)\exp(-L). \tag{2.22}$$

This is precisely the solution by iteration, properly normalized, which is derivable from (2.1) by standard methods and was originally given by Feynman.[2] This is a rather surprising result, since the iteration $(p|R_I|q)$ has, in general, a finite radius of convergence, and from Feynman's point of view the term $\exp(-L)$ is introduced simply as a normalizing factor. This identity of the normalized iterated solution and the Fredholm solution is a special property of the system under discussion and is a direct consequence of the relation (2.14) between the Fredholm determinant and the vacuum expectation value of the S matrix. The identity is not true for static external fields, which, for reasons which will be made clear in the next section, cannot be regarded as a particular case of the time dependent field.

We remark finally that the above theory can equally well be applied to the calculation of pair creation. Also, since electrons interact with each other explicitly only through the exclusion principle on the initial and final states, we can consider any number of electrons or positrons. This has been shown by Feynman.[2]

3. FREDHOLM CONDITION AND THE STATIC FIELD

A. The Fredholm Condition

We have yet to establish the condition (2.17), which justifies the application of the Fredholm theory to (2.9). From (1.17) and (2.10),

$$C_2=\int dk_1dk_2dldm \times|\boldsymbol{A}(l-k_1)S_F(k_1)\boldsymbol{A}(k_1-m)S_F(m) \times\boldsymbol{A}(l-k_2)S_F(k_2)\boldsymbol{A}(k_2-m)S_F(m)|. \tag{3.1}$$

[15] This result was obtained previously by M. Neuman. See reference 11.

[16] We are actually employing a generalization of Poincare's result, which has been proved by numerous authors [F. Smithies (private communication)].

[17] This has been calculated directly by J. Schwinger and others. The result in our notation is quoted by R. Karplus and N. M. Kroll, Phys. Rev. **77**, 536 (1950). That the real part is finite can be inferred, however, from the unitarity of the S matrix. Let

$$S=1+eS_1+e^2S_2+\cdots.$$

Since S is unitary,

$$S_2+S_2^*=-S_1S_1^*.$$

Therefore,

$$\mathrm{Rl}[2\sigma_2]=(0|S_2+S_2^*|0)=-\sum_{p,q}|(0|S_1|p, q)|^2,$$

where the right-hand side is the total probability of creating one pair, calculated to lowest order. This is finite.

It must be shown that this is convergent. It is not true of C_2 as it was of C_1, that by a change of variables one can produce a divergent factor, independent of $A(k)$. Dyson has shown that the convergence of such integrals can be estimated by counting powers. On this basis it can be seen that C_2 converges, provided $A(k)$ falls off faster than k^{-3} for large k.

Consider the expression

$$E=\int J_\mu(k)A_\mu(k)d^4k=\int k^2A_\mu(k)A_\mu(-k)d^4k, \quad (3.2)$$

where J_μ is the current producing the external field. By a Fourier transformation this is equal to the energy density of the field, integrated over all space and time.

Now the transition probability

$$\omega_\infty=|(p|S|q)|^2 \quad (3.3)$$

is the probability for the whole of time and the whole of space. For purely general fields this is infinite and there is, in fact, no physically significant cross section that one can consider for such a field. We consider now the space extension only. In most cases the field will be defined throughout space, but will be effectively nonzero only over a finite region. In such a case the probability for the whole of space gives the probability for the whole field, which is the physically significant quantity. Alternatively the field may have some general periodicity in a lattice with some cell volume v. One may then ask for the cross section per cell. This may be calculated by considering the probability for all space for a field equal to the given field over a large but finite volume $V(\gg v)$ and zero elsewhere. The boundary should be made smooth and taken large enough for surface effects to be negligible.

The treatment of the time is exactly analogous. Either the field is defined for all time in such a way that it is effectively nonzero only for a finite period (in this case ω_∞ is, directly, the physically significant expression) or it has a periodicity τ. In this latter case the probability per period τ can be calculated from ω_∞, for the field switched on for a long, but finite time $T(\gg\tau)$.

In any significant case, the field considered is nonzero only over a finite region and for a finite time. For such fields the energy integral E is finite. But this integral is only convergent if $A(k)$ falls off faster than k^{-3} for large k.[18a] Therefore, for any time-dependent field for which a physically reasonable cross section can be considered, we have

$$C_2<\infty, \quad (3.4)$$

and Fredholm theory is applicable.

B. The Static Field

For a static field the expression of physical significance is not ω_∞, but ω, the probability per unit time. To derive this exactly from the S matrix, Eq. (2.1), it is necessary to consider the field to be on for an infinite time. Since the argument above depended essentially on the fact that the field was only "on" for a finite time, the static field requires special consideration.

A static field is

$$A_\mu(k)=A_\mu(\mathbf{k})\delta(k_0), \quad (3.5)$$

where $\mathbf{k}$ is the space part of k. Energy is conserved in any real process, so that

$$|(0|S|0)|^2=1.$$

Thus, $(0|S|0)$ is simply an (infinite) phase factor and probability amplitudes are given directly by $(p|R|q)$. Define $M'(\mathbf{p},\mathbf{q})$ by

$$M(p,q)=M'(\mathbf{p},\mathbf{q})\delta(p_0-q_0). \quad (3.6)$$

The solution by iteration for $M'(\mathbf{p},\mathbf{q})$ and hence $(p|R_I|q)$ is obtained by substituting (3.5) and (3.6) into (2.6).[18] The integral equation for $M'(\mathbf{p},\mathbf{q})$ is, from (2.9),

$$M'(\mathbf{p},\mathbf{q})=\lambda A^e(\mathbf{p}-\mathbf{q})-2\pi\lambda^2\int A^e(\mathbf{p}-\mathbf{k})S_0(\mathbf{k})\times M'(\mathbf{k},\mathbf{q})d\mathbf{k}, \quad (3.7)$$

where

$$S_0(\mathbf{k})=S_F(\mathbf{k},p_0) \quad (3.8)$$

is given by (2.7) with k_0 replaced by p_0. The Fredholm solution of (3.7) can be performed analogously to the solution of (2.10). The condition for the applicability of Fredholm theory is the convergence of the three-dimensional analog of (3.1). This can be deduced from the convergence of

$$\int|\mathbf{k}|^2A_\mu(\mathbf{k})A_\mu(-\mathbf{k})d\mathbf{k}. \quad (3.9)$$

This is the integral of the energy density over all space (but not time), which must converge for any physically reasonable field, as in the previous section.

From (3.6),

$$(p|R|q)=\bar{u}(\mathbf{p})M'(\mathbf{p},\mathbf{q})u(\mathbf{q})\delta(p_0-q_0)=(\mathbf{p}|\mathbf{R}|\mathbf{q})\delta(p_0-q_0). \quad (3.10)$$

Thus,

$$\omega_\infty=|(\mathbf{p}|\mathbf{R}|\mathbf{q})|^2\delta(p_0-q_0)\delta(0). \quad (3.11)$$

This is, of course, infinite, but the final factor is

$$\delta(0)=\lim_{T\to\infty}\lim_{x\to0}\frac{1}{2\pi}\int_{-T/2}^{T/2}e^{ixt}dt=\lim_{T\to\infty}(T/2\pi), \quad (3.12)$$

where T is the time for which the field is on. The probability per unit time is

$$\omega=\lim_{T\to\infty}(\omega_\infty/T)=\frac{1}{2\pi}|(\mathbf{p}|\mathbf{R}|\mathbf{q})|^2\delta(p_0-q_0). \quad (3.13)$$

[18a] This is not true if $A(x)$ is singular at the origin, but such cases may be included by introducing a suitable factor to smooth out the singularity.

[18] R. H. Dalitz, Proc. Roy. Soc. (London) **A206**, 509 (1951).

Note that owing to the extraction of a δ-function factor in the derivation of (3.7) from (2.10), it is *not* true that the Fredholm determinant $d(\lambda)$ of (3.7) is equal to $(0|S|0)$. Consequently, for a static field, the iterated solution, $(\mathbf{p}|\mathbf{R}_I|\mathbf{q})$, (Born approximation) is *not* the same as the Fredholm solution. This is in agreement with the conclusion of Jost and Pais.[1]

The authors are indebted to Dr. N. Kemmer for numerous discussions and particularly Dr. F. Smithies for much help with the theory of integral equations. One of us (A.S.) would like to thank the Education Department of the Punjab Government, Pakistan for a grant enabling him to stay at St. John's College, Cambridge.

PHYSICAL REVIEW VOLUME 90, NUMBER 4 MAY 15, 1953

Spherically Symmetric Solutions in Nonsymmetrical Field Theories. I. The Skew Symmetric Tensor*

P. C. VAIDYA
Vallabh Vidyanagar, Anand, India
(Received August 1, 1952)

The spherically symmetric form of the skew tensor g_{ik}, given by Papapetrou, is not sufficiently general. A more general form is found. This necessitates a reconsideration of the program of spherically symmetric solutions in nonsymmetrical field theories initiated by Papapetrou. The present paper makes a beginning in this direction.

The new form of the spherically symmetric tensor g_{ik} is derived from a consideration of the infinitesimal rotation of a sphere about a diameter. It is hoped to use this form to obtain nonstatic solutions in nonsymmetrical field theories which will correspond to solutions of a radiating star in general relativity.

I. INTRODUCTION

PAPAPETROU[1] initiated the study of rigorous (nonapproximate) solutions in the various unified field theories by showing that the skew symmetric tensor g_{ik} with only $g_{14}=w(r,t)$ and $g_{23}=v(r,t)\sin\theta$ as the surviving components, is spherically symmetric. This form of the tensor was the starting point for a number of investigations in this direction. Papapetrou himself worked out the solutions of the field equations of Schrödinger.[2] Rigorous solutions of the field equations of Einstein and Strauss[3] were given by Wyman.[4] Bandyopadhyaya[5] gave a simple solution of the latest unified field theory of Einstein.[6] Recently Bonner[7] has satisfactorily solved the problem of finding static spherically symmetric solutions in Einstein's unified field theory. All these investigations began with the form of g_{ik} found by Papapetrou.

A nonsymmetrical tensor field can be split up into its symmetrical and skew symmetrical parts. We write

$$g_{ik}=g_{\underline{ik}}+g_{\underset{\smile}{ik}},$$

the bar or the hook below the suffixes distinguishing the two parts, respectively.

For spherically symmetric solution the form of $g_{\underline{ik}}$ is well known from general relativity. In order to find the spherically symmetric form of $g_{\underset{\smile}{ik}}$, Papapetrou considered the rotation of a sphere about a diameter POP' and compared the values of the various components of $g_{\underset{\smile}{ik}}$ before and after the rotation at the point P on the sphere and the axis of rotation. Since a rotation through a right angle will interchange the components perpendicular to OP, these would vanish at a point on the axis of rotation. Hence Papapetrou's method will naturally give the components of $g_{\underset{\smile}{ik}}$ along the radial direction only. That is why only $g_{\underset{\smile}{14}}$ and $g_{\underset{\smile}{23}}$ (which correspond to the radial components of magnetic and electric field, respectively) survived in his tensor. In what follows we consider an infinitesimal rotation of a sphere and compare the values of $g_{\underset{\smile}{ik}}$ at a point not on the axis of rotation. We shall, of course, recover Papapetrou's components; but we shall also find that there are some other components of $g_{\underset{\smile}{ik}}$ which are nonzero.

II. INFINITESIMAL ROTATIONS OF A SPHERE

In this section we shall be interested in the two-dimensional geometry of the surface of a sphere of radius a. The fundamental quadratic form ψ on this surface is given by

$$\psi=a^2d\theta^2+a^2\sin^2\theta d\varphi^2=g_{22}(dx^2)^2+g_{33}(dx^3)^2. \quad (2.1)$$

The contravariant components ξ^μ, $(\mu=2,3)$ of an infinitesimal transformation which would represent a motion of the sphere into itself, satisfy the following

* This work was done under the Springer Research Scholarship of the University of Bombay, Bombay, India.

[1] A. Papapetrou, Proc. Roy. Irish Acad. **A52**, 69 (1948).
[2] For field theory of Schrödinger, see E. Schrödinger, Proc. Roy. Irish Acad. **A51**, 163 (1947).
[3] A. Einstein and E. G. Strauss, Ann. Math. **47**, 731 (1946).
[4] M. Wyman, Can. J. Math. **2**, 427 (1950).
[5] G. Bandyopadhyaya, Nature **167**, 648 (1951).
[6] A. Einstein, *Meaning of the Relativity* (Methuen, London, 1950), Appendix II.
[7] W. B. Bonner, Proc. Roy. Soc. (London) **A209**, 353 (1951); **A210**, 427 (1952).

equations of Killing:[8]

$$\cos\theta\xi^2+\sin\theta(\partial\xi^3/\partial\varphi)=0,$$
$$\sin^2\theta(\partial\xi^3/\partial\theta)+(\partial\xi^2/\partial\varphi)=0, \qquad (2.2)$$
$$\partial\xi^2/\partial\theta=0.$$

From the third of these equations, we have $\xi^2=X_3$, where X_3 is a function of φ alone. Indicating by primes derivatives with respect to the arguments, from the first two we have

$$\partial\xi^3/\partial\varphi=-X_3\cot\theta, \quad \partial\xi^3/\partial\theta=-X_3'\operatorname{cosec}^2\theta, \qquad (2.3)$$

for which the condition of consistency is

$$X_3''+X_3=0, \quad \text{or} \quad X_3=A\cos(\varphi+B). \qquad (2.4)$$

We thus arrive at the following final form of the contravariant components ξ^μ of an infinitesimal rotation of a sphere about a diameter:

$$\xi^2=A\cos(\varphi+B), \qquad (2.5)$$

$$\xi^3=-A\sin(\varphi+B)\cot\theta+C, \qquad (2.6)$$

A, B, and C being arbitrary constants.

III. SPHERICALLY SYMMETRIC TENSOR FIELDS

The condition for a spherically symmetric tensor field is the following: there is a frame of reference such that, after an arbitrary rotation around the center of symmetry, the new components g'_{ik} are the same functions of the new coordinates x'^μ as the g_{ik} are of x^μ. Taking the center of symmetry as the origin, let x^μ be a set of polar coordinates r, θ, φ and the time coordinate t. Consider an infinitesimal rotation given by

$$x'^\mu=x^\mu+\xi^\mu\delta\epsilon, \qquad (3.1)$$

where

$$\xi^1=0, \quad \xi^2=A\cos(\varphi+B),$$
$$\xi^3=-A\sin(\varphi+B)\cot\theta+C, \quad \xi^4=0, \qquad (3.2)$$

and $\delta\epsilon$ is an infinitesimal. It is clear from general considerations that arbitrary transformations of the coordinates r and t will leave the spherical symmetry of a tensor expression undisturbed, and so in (3.2) transformations of the coordinates θ and φ alone are considered by stipulating $\xi^1=\xi^4=0$. The criterion of spherical symmetry of a tensor field g_{ik} is

$$g'_{ik}(x'^\mu)=g_{ik}(x'^\mu). \qquad (3.3)$$

Substituting from (3.1) the values of x'^μ in the right-hand member of (3.3), applying Taylor's theorem, and retaining terms only up to the first power of $\delta\epsilon$, we can write this criterion in the form

$$g'_{ik}(x'^\mu)=g_{ik}(x^\mu)+g_{ik,\mu}\xi^\mu\delta\epsilon. \qquad (3.4)$$

Applying the tensor law of transformation to $g_{ik}(x^\mu)$, we find, again correct to the first power in $\delta\epsilon$, that

$$g'_{ik}(x'^\mu)=g_{ik}(x^\mu)-[\xi^\alpha{}_{,i}g_{\alpha k}+\xi^\alpha{}_{,k}g_{i\alpha}]\delta\epsilon. \qquad (3.5)$$

With the help of Eq. (3.5), the criterion (3.4) for the spherical symmetry of the field can be written in the form,

$$\xi^\alpha{}_{,i}g_{\alpha k}+\xi^\alpha{}_{,k}g_{i\alpha}+g_{ik,\alpha}\xi^\alpha=0. \qquad (3.6)$$

The first two terms in the left-hand member of this equation arise out of the tensor law of transformation of g_{ik}, while the third term may be called the "transport term." It arises because the value of g_{ik} at a point x^μ is compared with the transformed g_{ik} at the point which after the transformation possesses the coordinates x^μ (and therefore, originally had the coordinates $x^\mu-\xi^\mu\delta\epsilon$).

We now split up the g_{ik} field into its symmetrical and skew parts,

$$g_{ik}=\underset{\frown}{g_{ik}}+\underset{\smile}{g_{ik}}.$$

The general form of the spherically symmetric $\underset{\frown}{g_{ik}}$, known from general relativity, is

$$\underset{\frown}{g_{ik}}=\begin{bmatrix}-\alpha & 0 & 0 & a\\ 0 & -\beta & 0 & 0\\ 0 & 0 & -\beta\sin^2\theta & 0\\ a & 0 & 0 & \gamma\end{bmatrix}, \qquad (3.7)$$

where α, β, γ, and a are functions of r and t. We now obtain the form of $\underset{\smile}{g_{ik}}$ which will satisfy the criterion (3.6).

It is easy to verify that, as a result of the Eq. (3.6) both $\underset{\smile}{g_{14}}$ and $\underset{\smile}{g_{23}}\operatorname{cosec}\theta$ have to satisfy only one equation of the form

$$z_{,\alpha}\xi^\alpha=0, \quad \text{or} \quad \xi^2(\partial z/\partial\theta)+\xi^3(\partial z/\partial\varphi)=0. \qquad (3.8)$$

This is a differential equation for z in terms of the variables θ and φ, and with ξ^2 and ξ^3 given by (3.2), its general solution would be

$$z=f(w, r, t), \qquad (3.9)$$

$$w=A\sin(\varphi+B)\sin\theta+C\cos\theta, \qquad (3.10)$$

f being an arbitrary function of its arguments. We assume this arbitrary function to be expressed as a product of a function of (r, t) and a function of (θ, φ). Since in spherically symmetric fields the transformation of the variables r and t can be studied independently of the transformations of the variables θ, φ, this assumption will not contradict the requirements of spherical symmetry. Further, we shall find that under this assumption we shall be able to obtain an expression for the spherically symmetric g_{ik} which will be more general than that found by Papapetrou. This assumption introduces a good deal of simplification in the procedure of solving the field equations. The form of the functions of (θ, φ) will now be determined by the criterion (3.6) of spherical symmetry, while the form of the function of (r, t) will be decided by the field equations which

[8] See L. P. Eisenhart, *Riemannian Geometry* (Princeton University Press, Princeton, 1949), pp. 241, 242.

govern the $g_{\underset{\sim}{ik}}$ field. Therefore, from (3.8) we can write

$$g_{\underset{\sim}{14}}=H(r,t)h(w);\quad g_{\underset{\sim}{23}}=E(r,t)\sin\theta k(w).$$

H, E, h, and k are arbitrary functions of their arguments.

Writing the remaining components of $g_{\underset{\sim}{ik}}$ as products of a function of (r,t) and a function of (θ,φ), it will be found that criterion (3.6) gives the following forms for these components:

$$g_{\underset{\sim}{12}}=p(r,t)v(\theta,\varphi),\quad g_{\underset{\sim}{13}}=-p(r,t)u(\theta,\varphi)\sin\theta;$$
$$g_{\underset{\sim}{24}}=q(r,t)v(\theta,\varphi),\quad g_{\underset{\sim}{34}}=-q(r,t)u(\theta,\varphi)\sin\theta.$$

Of course, all the functions of (r,t) will be arbitrary; but $u(\theta,\varphi)$ and $v(\theta,\varphi)$ have to satisfy the equations

$$-A\sin(\varphi+B)\operatorname{cosec}\theta u+\xi^2(\partial v/\partial\theta)+\xi^3(\partial v/\partial\varphi)=0, \quad (3.11)$$

$$A\sin(\varphi+B)\operatorname{cosec}\theta v+\xi^2(\partial u/\partial\theta)+\xi^3(\partial u/\partial\varphi)=0. \quad (3.12)$$

We can combine these two equations to obtain

$$\xi^\alpha[\partial(u^2+v^2)/\partial x^\alpha]=0, \quad (3.13)$$

and

$$\xi^\alpha[\partial(\tan^{-1}(u/v))/\partial x^\alpha]+A\sin(\varphi+B)\operatorname{cosec}\theta=0. \quad (3.14)$$

From Eq. (3.13) we immediately find that

$$u^2+v^2=f^2, \quad (3.15)$$

where $f=f(w)$ is an arbitrary function of w. Equation (3.14) can be integrated to yield

$$v/u=A\cos(\varphi+B)\{\partial w/\partial\theta\}^{-1},$$

so that we ultimately find

$$v=A\cos(\varphi+B)(A^2+C^2-w^2)^{-\frac{1}{2}}\cdot f(w), \quad (3.16)$$

$$u=(A\sin(\varphi+B)\cos\theta-C\sin\theta)\times(A^2+C^2-w^2)^{-\frac{1}{2}}\cdot f(w), \quad (3.17)$$

where w is given by the Eq. (3.10). Thus the final expression for the tensor field $g_{\underset{\sim}{ik}}$ which satisfies the criterion (3.6) is

$$g_{\underset{\sim}{ik}}=\begin{bmatrix} 0 & pv & -pu\sin\theta & Hh \\ -pv & 0 & Ek\sin\theta & qv \\ pu\sin\theta & -Ek\sin\theta & 0 & -qu\sin\theta \\ -Hh & -qv & qu\sin\theta & 0 \end{bmatrix}, \quad (3.18)$$

p, q, E, H are arbitrary functions of r and t, h and k are arbitrary functions of w, and u, v, w are given by (3.17), (3.16), and (3.10), respectively. It should be noted that (3.18) is not the most general solution of (3.6), because of the assumption which separated the variables (r,t) and (θ,φ).

IV. THE POLARIZATION OF THE $g_{\underset{\sim}{ik}}$ FIELD

We shall now consider in detail the dependence of these components on the variables θ and φ. This dependence is mainly given by the functions u, v, and w. Consider first the function

$$w=A\sin(\varphi+B)\sin\theta+C\cos\theta. \quad (4.1)$$

If the point P, (r,θ,φ), of the sphere of radius r, at which these components of $g_{\underset{\sim}{ik}}$ are evaluated, has the usual Cartesian coordinates (x,y,z), then (4.1) can be written in the form

$$w=(ax+by+cz)/r, \quad (4.2)$$

where the constants a, b, c can be easily expressed in terms of the earlier constants A, B, C. If OQ is the diameter of the sphere (center O) with direction-cosines proportional to a, b, c, from (4.2) w is seen to be proportional to the cosine of the angle POQ. The occurrence of the arbitrary functions of this variable w in spherically symmetric tensors can now be easily understood, if we realize that OQ was the axis about which the infinitesimal rotation was given to the sphere to derive the criterion (3.6). This interpretation of w also points out a marked difference between the two factors $E(r,t)\sin\theta$ and $k(w)$ of $g_{\underset{\sim}{23}}$, or between the factors $H(r,t)$ and $h(w)$ of $g_{\underset{\sim}{14}}$. Let us choose our Cartesian axes of coordinates in such a way that OZ is along the axis of rotation OQ. Then we have $A=0$, $B=0$, and

$$w=C\cos\theta. \quad (4.3)$$

If, however, the coordinate axes are oriented in such a way that OY is along the axis of rotation, we would get $B=0$, $C=0$, and

$$w=A\sin\theta\sin\varphi. \quad (4.4)$$

Thus the functional form of w (as a function of θ and φ) depends on the orientation of the axis of rotation. Further, the *form* (4.3) of w will remain the same for rotations round OZ only, while the form (4.4) of w will remain invariant for all rotations round OY only. We say that w is an invariant spherically symmetric expression with a polarization. For w given by (4.3) we may say that "the axis of polarization" is the z axis, while in (4.4) it is the y axis. It is now easy to see that

$$g_{\underset{\sim}{14}}=H(r,t)\quad\text{and}\quad g_{\underset{\sim}{23}}=E(r,t)\sin\theta \quad (4.5)$$

are spherically symmetric unpolarized components of $g_{\underset{\sim}{ik}}$, while

$$g_{\underset{\sim}{14}}=H(r,t)h(w),\quad g_{\underset{\sim}{23}}=E(r,t)\sin\theta k(w),$$

are spherically symmetric with a polarization. The $g_{\underset{\sim}{ik}}$, with only nonvanishing components given in (4.5), was first obtained by Papapetrou.

Now consider the functions u and v. They also show a polarization. If $A=0$, $B=0$ we find

$$u=f(\cos\theta),\quad v=0. \quad (4.6)$$

If, however, $B=0$, $C=0$, we find

$$u=\sin\varphi\cos\theta(1-\sin^2\theta\sin^2\varphi)^{-\frac{1}{2}}\cdot f,$$
$$v=\cos\varphi(1-\sin^2\theta\sin^2\varphi)^{-\frac{1}{2}}\cdot f. \tag{4.7}$$

For u and v given by (4.6), we find that

$$g_{12}=0,\quad g_{13}=-pf\sin\theta,$$
$$g_{24}=0,\quad g_{34}=-qf\sin\theta. \tag{4.8}$$

If we accept the interpretation of g_{ik} as given by the first ordered solution,[7] we see that (4.8) will represent a polarized spherical wave with the electric vector in the plane of the point P and the z axis. In our notations (4.8) gives a spherically symmetric tensor field which is polarized, the axis of polarization being the z axis.

We would like to put down together the conclusions that we have drawn from the discussions of this section. Tensor fields may satisfy our criterion of spherical symmetry, (3.6), in two different ways. Some of them satisfy (3.6) for all possible values of the parameters A, B, C of the infinitesimal transformations. An illustration of such a field is Papapetrou's tensor field with two nonvanishing components, $g_{14}=H(r,t)$, $g_{23}=E(r,t)\sin\theta$. Such tensor fields are spherically symmetric without any polarization. On the other hand, there are some other tensor-fields which satisfy the criterion (3.6) through the appearance of the parameters A, B, C in the very expressions of the components of the fields. Thus the functional forms of the various components carry, as it were, an impression of the axis about which the infinitesimal rotation was given to derive the criterion (3.6). Such fields are spherically symmetric and polarized. We have called the particular axis of rotation the "axis of polarization" of the field. An illustration of such a field is the electromagnetic tensor $F_{\alpha\beta}$ used to describe the spherically symmetric field of a radiating star in general relativity.[9] We have found above a general spherically symmetric skew tensor field with any arbitrary axis of polarization. Both the above illustrations are particular cases of the field found here.

Since we are at liberty to choose the orientation of our coordinate axes, we shall not be specializing our g_{ik} in any way if we take the axis of polarization of g_{ik} as the z axis. We put $A=0$, $B=0$, $C=1$ and find our g_{ik} to be of the form,

$$g_{14}=H(r,t)h(\theta),\quad g_{23}=E(r,t)\sin\theta k(\theta),\quad g_{12}=0,\quad g_{24}=0,$$
$$g_{13}=-p(r,t)\sin\theta f(\theta),\quad g_{34}=-q(r,t)\sin\theta f(\theta).$$

This is the simplest and, at the same time, the most general form of g_{ik} which is spherically symmetric and which exhibits polarization about the z axis.

[9] See V. V. Narlikar and P. C. Vaidya, Nature **159**, 642 (1947); Proc. Natl. Inst. Sci. (India) **14**, 53 (1948).

V. THE SYMMETRIC TENSOR g_{ik}

In Eq. (3.7) we have written down the spherically symmetric form of g_{ik} which is used in general relativity. From the discussion of the last section on the polarization of tensor-fields, we can now see that the general relativity form (3.7) of g_{ik} is its general spherically symmetric unpolarized form. The question now arises: What is its general polarized form? This question never arose in general relativity, because there g_{ik} is the metric tensor of space-time and polarization of a metric tensor has no physical meaning. In nonsymmetrical field theories, g_{ik} need not be the metric tensor of space-time. Though all the previous authors (Papapetrou,[1] Wyman,[4] Bonner[7]) have tried to interpret their static spherically symmetric solutions on the assumption that g_{ik} is the metric tensor, doubts have been raised by many (including Wyman) as regards this assumption. Wyman has actually put forward alternative suggestions for the metric tensor. In his letter Infeld states that Einstein's theory gives no interaction of a moving charged mass-particle with the electromagnetic field.[10] This may be taken to mean that the identification of the metric tensor with g_{ik} cannot be true even at sufficiently large distances from the center of the particle. As a matter of fact, this is the view taken by Kurşunoğlu,[11] who has suggested an alternative set of field equations to replace those given by Einstein, which explicitly recognize a metric tensor b_{ik} distinct from the field-tensor g_{ik}.

It is obvious that the tensor g_{ik} must be connected in some way with the metric tensor b_{ik}. However, at the present stage of development of nonsymmetric field theories, it does not seem possible to say definitely that g_{ik} is identical with the metric tensor b_{ik}. We are, therefore, specifying here the general form of g_{ik} which is spherically symmetric with a polarization. By working systematically with the equations obtained from the criterion (3.6), it will be found that this general form of g_{ik} can be expressed in terms of the functions u, v, and w defined earlier, in the following way:

$$g_{11}=-\alpha(r,t)F(w),\quad g_{14}=a(r,t)F(w),\quad g_{44}=\gamma(r,t)F(w),$$
$$g_{22}=-[\beta(r,t)+B(r,t)v^2]G(w),$$
$$g_{23}=+B(r,t)uvG(w)\sin\theta,$$
$$g_{33}=-[\beta(r,t)+B(r,t)u^2]G(w)\sin^2\theta,\quad g_{12}=\lambda(r,t)v,$$
$$g_{13}=-\lambda(r,t)u\sin\theta,\quad g_{24}=\mu(r,t)v,\quad g_{34}=-\mu(r,t)u\sin\theta.$$

F and G are arbitrary functions of w. In putting down the same function $F(w)$ as a factor in each of the three components g_{11}, g_{14}, and g_{44}, we have used the fact that these components are interconnected by arbitrary transformations of the coordinate r and t.

[10] L. Infeld, Nature **166**, 1075 (1950).
[11] B. Kursunoğlu, Proc. Phys. Soc. (London) **A65**, 81 (1952).

The Construction of Potentials in Quantum Field Theory*

K. A. BRUECKNER AND K. M. WATSON
Department of Physics, Indiana University, Bloomington, Indiana
(Received January 26, 1953)

An inductive method, based on the formal solution of the Schrödinger equation in the form given by Lippmann and Schwinger, is used to construct scattering potentials in quantum field theories of various types. The method is applied to a linear theory without nucleon pair production, to a general nonlinear theory without pair production, and finally to a general nonlinear theory with pair production. The nth order potential is obtained by the solution of a Schrödinger type equation involving the potential of lower order; the series of potentials so obtained is, however, not a power series in the coupling constant. Rough estimates indicate that some of the problems of convergence associated with the usual perturbation expansion are obviated by this method. Simple illustrative examples are given for the linear and nonlinear theories.

I. INTRODUCTION

THE most straightforward attempts to calculate scattering cross sections in field theory have involved power-series expansions of the scattering matrix in the coupling constant. In the case of meson theories, at least, there seems to be little hope that the power series method will lead to useful results. Other methods such as the radiation damping theory of Heitler[1] also do not appear promising.

On the other hand, the usefulness and validity of the approaches of Bethe and Salpeter[2] and of Tamm[3] and Dancoff[4] remain to be determined. These methods have been applied primarily to problems of the scattering of two particles without the creation of new particles. The interaction between the two particles is obtained as a power series in the coupling constant which is used to solve a Schrödinger equation. This in turn gives the scattering matrix.

In the present work, a new approach is used to obtain the interaction potential between two particles. The method makes use of the integral-equation expression for the Schrödinger equation given by Lippmann and Schwinger[5] and of the algebraic techniques for handling this developed by Chew and Goldberger[6] and by Watson.[7] The method is related to that of Tamm and Dancoff in that it leads to an interaction potential which is diagonal in particle occupation numbers but nondiagonal in the momentum states of the interacting particles. Just as in the Tamm-Dancoff and Bethe-Salpeter methods, the potential is obtained as a sum of an infinite number of terms. However, in contrast to these theories, the series is not a power-series in the coupling constant.[8] In particular, the nth term in the series for the potential is obtained in terms of the solution of the "Schrödinger equation" which results from using for the "interaction potential" the first $(n-1)$ terms in the series. Because the successive potentials are diagonal in particle occupation numbers, these successive "Schrödinger type" equations do not involve the complications of field theory and can in principle be considered soluble. (We note that there are several powerful variational methods available for the handling of such problems.)

The present study was initiated as a result of the work of Chew[9] on the scattering of mesons by nucleons. Chew has applied the Tamm-Dancoff method to obtain the g^2 potential. His calculation of the scattering with pseudovector coupling in the pseudoscalar meson theory was in not unsatisfactory agreement with present experimental results.[10]

To simplify the presentation of the material we shall first derive the potential for a coupling linear in the meson field variables and without nucleon pair production. The results will then be extended to general nonlinear interactions (still without nucleon-pair production). Finally the production of nucleon pairs will be taken into account. We further remark that although we have meson theory most specifically in mind, the results are generally applicable to other field theories such as electrodynamics.

We shall not in this paper consider the renormalization problem; preliminary considerations indicate, however, that the usual renormalization procedures may be applicable. The detailed investigation of this problem will be the content of a later paper.

II. PRELIMINARY CONSIDERATIONS

We begin the discussion by presenting some formal relations which will be repeatedly used. We suppose the Schrödinger equation to have the form

$$(H_0+H')\psi=E\psi, \tag{1}$$

where E is the energy of the system, H_0 is the energy of two uncoupled fields under consideration, and H' is

* Supported in part by a grant from the National Science Foundation.
[1] W. Heitler, Proc. Cambridge Phil. Soc. **37**, 291 (1941).
[2] E. Salpeter and H. Bethe, Phys. Rev. **84**, 1232 (1951).
[3] I. Tamm, J. Phys. (U.S.S.R.) **9**, 449 (1945).
[4] S. M. Dancoff, Phys. Rev. **78**, 382 (1950).
[5] B. Lippmann and J. Schwinger, Phys. Rev. **79**, 469 (1950).
[6] G. F. Chew and M. L. Goldberger, Phys. Rev. **87**, 778 (1952).
[7] K. M. Watson, Phys. Rev. **89**, 575 (1953).
[8] M. Lévy [Phys. Rev. **88**, 72 (1952)] has also devised a (different) method of constructing successive interactions by means of integral equations.
[9] G. F. Chew, Phys. Rev. **89**, 591 (1953).
[10] Anderson, Fermi, Nagle, and Yodh, Phys. Rev. **86**, 793 (1952).

the coupling between the fields. For instance H_0 operating on a state containing mesons in momentum states $k_1, k_2, \cdots k_n$ with the wave function $\chi(k_1, \cdots, k_n)$, gives

$$H_0\chi=[\omega_1+\omega_2+\cdots+\omega_n]\chi, \tag{2}$$

where $\omega_1=(k_1^2+\mu^2)^{\frac{1}{2}}$, etc. ($\mu$ is the meson rest mass and we use units in which $\hbar=c=1$).

We suppose ψ in Eq. (1) to describe a scattering event which originates in an eigenstate of H_0, say χ_a. In terms of the Møller[11] wave matrix Ω, we write

$$\psi=\Omega\chi_a, \tag{3}$$

where Ω satisfies the Lippmann-Schwinger[5] equation,

$$\Omega=1+\frac{1}{E+i\eta-H_0}H'\Omega, \tag{4}$$

which is supposed to operate on the state χ_a. (In this expression η is a small positive parameter used to specify the contour of integration which is set equal to zero after the integration is done.) Chew and Goldberger[6] have introduced the solution

$$\Omega=1+\frac{1}{E+i\eta-H_0-H'}H' \tag{5}$$

to Eq. (4), which may be readily verified by using the operator relation

$$A^{-1}-B^{-1}=A^{-1}(B-A)B^{-1}=B^{-1}(B-A)A^{-1}. \tag{6}$$

We shall need a straightforward generalization of Eqs. (4) and (5). Let a and q be matrix operators and suppose that a has an inverse. Then the unique solution to

$$\omega=1+(1/a)q\omega \tag{7}$$

is

$$\omega=1+\frac{1}{a-q}q, \tag{A}$$

where "1" is the identity operator and it is supposed that relation (A) has a well-defined meaning. We shall frequently use the converse to relation (A); namely, that ω as defined in relation (A) satisfies the integral Eq. (7).

We shall encounter and require a prescription for evaluating quantities such as

$$P\equiv Q_1\frac{1}{a-q}Q_2, \tag{8}$$

where Q_1 and Q_2 are two other matrix operators. Using Eq. (6), P can be written as

$$P=Q_1\left[\frac{1}{a}+\frac{1}{a-q}q\frac{1}{a}\right]Q_2$$

$$=Q_1\omega(1/a)Q_2, \tag{B}$$

[11] C. Møller, Kgl. Danske. Videnskab. Selskab, Mat.-fys. Medd. **23**, No. 1 (1945).

where ω is the solution to Eq. (7). In general q and a will be functions of field variables and consequently non-diagonal in particle occupation numbers. Our primary task will be to express all such quantities P in terms of an operator q which is *diagonal* in occupation numbers and an operator a which has the form

$$a=E+i\eta-H_0.$$

Equation (7) is then reduced to a scattering-type problem and for present purposes will be considered soluble. If the matrix elements of Q_1 and Q_2 are known, then P will be considered as evaluated.

Our next general relation is

$$\frac{1}{a-q}q=\frac{1}{a-L}q+\frac{1}{a-L}L, \tag{C}$$

where

$$L=q(1/a)q. \tag{9}$$

Relation (C) can be proved by expanding $(a-L)^{-1}$ in a power series in L and $(a-q)^{-1}$ in a series in q, then comparing both sides of Eq. (C) term by term with L expressed in terms of q by Eq. (9). The proof can also be carried out more elegantly by adding the identity operator to both sides of Eq. (C) and showing that both sides satisfy the same integral Eq. (7).[12]

Our final formal relation is obtained by setting $q=q_1+q_2$ (where q_1 and q_2 are both matrix operators) in the left side of Eq. (C). Then

$$\frac{1}{a-q_1-q_2}(q_1+q_2)=\frac{1}{a-q_2-M}(q_2+M)$$

$$+\frac{1}{a-q_2-M}q_1\left[1+\frac{1}{a-q_2}q_2\right], \tag{D}$$

where

$$M=q_1\frac{1}{a-q_2}q_1. \tag{10}$$

Relation (D) is obtained from relation (C) as follows:

$$\frac{1}{a-q_1-q_2}(q_1+q_2)=\frac{1}{(a-q_2)-q_1}q_1+\frac{1}{(a-q_2)-q_1}q_2$$

$$=\frac{1}{a-q_2}q_2+\frac{1}{(a-q_2)-q_1}q_1\left[1+\frac{1}{a-q_2}q_2\right], \tag{11}$$

using Eq. (6). By relation (C), we have

$$\frac{1}{(a-q_2)-q_1}q_1=\frac{1}{a-q_2-M}(q_1+M), \tag{12}$$

on identifying $(a-q_2)$ and (q_1) with a and q of relation

[12] Relations (C) and (D) are special forms of a solution to the Schrödinger equation given in Appendix (B) of reference (7), where methods of deriving such equations are considered in more detail.

(C). Simplifying with the use of Eq. (6), relation (D) follows.

In what follows, we shall show how to construct a potential in quantum field theories by sequential application of relation (D).

III. LINEAR COUPLING WITHOUT NUCLEON PAIR PRODUCTION

The interaction H' in Eq. (1) is assumed to be a homogeneous linear polynomial in the meson field variables ϕ_σ ($\sigma=1, 2, \cdots N$) and it is supposed that H' is diagonal in nucleon occupation numbers so no nucleon pairs can be created. The index "σ" on ϕ_σ may refer to isotopic spin components, vector components, field variables evaluated at the position of different nucleons, etc.

Defining

$$a \equiv E+i\eta-H_0,$$

Eq. (4) has the solution (5):

$$\Omega=1+\frac{1}{a-H'}H'$$

$$=1+\frac{1}{a-\Delta_0}H'+\frac{1}{a-\Delta_0}\Delta_0. \tag{13}$$

The last step follows from relation (C) and the definition

$$\Delta_0=H'(1/a)H'. \tag{14}$$

We shall now develop some general theorems relating to expressions of the type of Eq. (13) which will allow us to express the part of Ω which refers to scattering without particle creation or annihilation in terms of operators which themselves are diagonal in occupation numbers.

We note the following self-evident lemma.

Lemma I

A homogeneous polynomial $G(\phi)$ of degree r in the field variable ϕ (by ϕ we mean the set "ϕ_σ") has only matrix elements for the production or absorption of a net number of mesons which is even or odd depending upon whether r is even or odd.

It follows from Lemma I that the term

$$\frac{1}{a-\Delta_0}H'$$

in Eq. (13) does not contribute to a scattering event in which no particles are produced or absorbed, since this quantity is odd in H' and thus in ϕ. Thus for calculating such a scattering, we need only (the diagonal part of)

$$\Omega_S(0)=1+\frac{1}{a-\Delta_0}\Delta_0. \tag{15}$$

Comparing with relation (A) and Eq. (7), we see that $\Omega_S(0)$ satisfies a Schrödinger equation with Δ_0 as a potential.

We now split Δ_0 into two parts:

$$\Delta_0=V_0+U_0, \quad V_0=\mathrm{DP}\Delta_0, \quad U_0=\mathrm{NDP}\Delta_0, \tag{16}$$

where the symbol $\mathrm{DP}\Delta_0$ means the diagonal part of Δ_0 with respect to meson occupation numbers and "$\mathrm{NDP}\Delta_0$" means the nondiagonal part of Δ_0 with respect to meson occupation numbers. (This notation will be used frequently in what follows.)

If we were to approximate Eq. (15) by setting $U_0=0$, then V_0 would be the potential in the Schrödinger equation which then has the form used by Chew[9] to discuss meson-nucleon scattering.[13]

To proceed, we define by induction from Eq. (16):

$$\begin{aligned}
&\Delta_n=U_{n-1}\frac{1}{a-\mathfrak{V}_{n-1}}U_{n-1},\\
&U_n=\mathrm{NDP}\Delta_n,\\
&V_n=\mathrm{DP}\Delta_n,\\
&\mathfrak{V}_n=\mathfrak{V}_{n-1}+V_n=\sum_{e=0}^{n}V_e.
\end{aligned} \tag{17}$$

We wish to show that in the limit as n approaches infinity that $\mathfrak{V}_n$ is the desired interaction potential to be used in the Schrödinger equation which describes the scattering event (if the series defining $\mathfrak{V}_n$ converges).

Since the $\mathfrak{V}_n$'s are diagonal in meson occupation numbers, we may suppose the matrix elements of $\mathfrak{V}_n$ to have been evaluated as numbers and to be *no longer functions* of the field variables. Then U_n is a homogeneous polynominal of degree 2^{n+1} in the field variables. This follows by induction since U_n contains twice as many ϕ's as does U_{n-1} and since U_0 is of second degree in ϕ.

Lemma II

For some value of n let us suppose that U_{n-1} can only produce (or absorb) a net number of meson pairs equal to 2^{n-1}; i.e., we suppose the difference between the number n_p of creation operators and the number n_a of annihilation operators is

$$\tfrac{1}{2}|n_p-n_a|=2^{n-1}.$$

Then U_n can only produce or absorb a net number of 2^n meson pairs (that is, it has no other matrix elements).

The proof follows immediately from the form of Δ_n in Eq. (17). Since by definition U_n cannot be diagonal in occupation numbers, it follows that each of its factors of U_{n-1} must either produce or absorb 2^{n-1} meson pairs. Then U_n produces or absorbs twice this number of pairs (or 2^n pairs).

[13] The present method has been employed in reference 7 to derive the potential in the "optical model" for meson-nucleus scattering when meson absorption can occur.

Theorem I: U_n (for all n) can actually only produce or absorb a net number of meson pairs equal to 2^n.

The proof goes by induction from Lemma II since U_0 can obviously only produce or absorb one meson pair (i.e., $2^\circ=1$).

A useful theorem for the evaluation of the U_n's is the following:

Theorem II: In U_n all the field variables must either produce or absorb mesons. There are no virtual emissions and reabsorptions in U_n. (Remembering that we have considered the $\mathfrak{V}_n$'s to be evaluated, so that they are no longer functions of the field variables.)

The proof follows from counting the number of ϕ's occurring in U_n. As remarked above, U_n is a degree 2^{n+1} in ϕ. Since U_n must create or absorb 2^n *pairs* of mesons (i.e., 2^{n+1} mesons), there are no ϕ's left over to perform virtual creations and reabsorptions.

The importance of this theorem is that for the evaluation of V_n all the 2^n emission operators must stand on the right of the 2^n absorption operators (except for the smallest value of n, where the order can be inverted).

Lemma III

All functions of a given U_n which do not otherwise contain the field variables and which are odd in U_n contain no matrix elements which are diagonal in the meson occupation numbers.

The proof is trivial: Each U_n absorbs or emits only 2^n pairs of mesons and can be considered as a single emission or absorption operator for this number of meson pairs. By the argument of Lemma I an odd number of such emission or absorption operators must lead to a net emission or absorption of mesons.

We are finally led to the following theorem.

Theorem III: The potential to be used in the Schrödinger equation which describes the original scattering event is

$$\mathfrak{V}=\lim_{n\to\infty}\mathfrak{V}_n=\sum_{e=0}^{n}V_e, \tag{18}$$

assuming proper convergence.

The proof proceeds by induction. Assume that the scattering is described by

$$\Omega_S=\mathrm{DP}[\Omega_S(n)],$$

where

$$\Omega_S(n)=1+\frac{1}{a-\mathfrak{V}_n-U_n}[\mathfrak{V}_n+U_n]. \tag{19}$$

We use relation (D), identifying q_2 with $\mathfrak{V}_n$ and q_1 with U_n. Then

$$\Omega_S(n)=1+\frac{1}{a-\mathfrak{V}_n-\Delta_{n+1}}[\mathfrak{V}_n+\Delta_{n+1}]+\frac{1}{a-\mathfrak{V}_n-\Delta_{n+1}}U_n\left[1+\frac{1}{a-\mathfrak{V}_n}\mathfrak{V}_n\right]. \tag{20}$$

The last term may be discarded by Lemma III, since it is of odd order in U_n and can give no contribution to the scattering cross section (we are assuming scattering without creation or absorption of mesons). Writing [by Eq. (17)] $\Delta_{n+1}=V_{n+1}+U_{n+1}$, the scattering is also given by

$$\mathrm{DP}[\Omega_S(n+1)]=\Omega_S,$$

where

$$\Omega_S(n+1)=1+\frac{1}{a-\mathfrak{V}_{n+1}-U_{n+1}}[\mathfrak{V}_{n+1}+U_{n+1}], \tag{21}$$

which has the form of Eq. (19) with n increased by unity. Since $\Delta_0=V_0+U_0$, Eq. (15) has the form of Eq. (19) with $n=0$. Proceeding step by step to sufficiently large values of n, if the matrix elements of U_n decrease to zero with sufficient rapidity that the series defining $\mathfrak{V}_n$ converges, we obtain in the limit

$$\mathfrak{V}=\sum_{e=0}^{n\to\infty}V_e \tag{22}$$

and

$$\Omega_S=1+\frac{1}{a-\mathfrak{V}}\mathfrak{V}. \tag{23}$$

Now Ω_S contains all matrix elements of Ω which are diagonal in occupation numbers and so contains all the information required to completely describe the desired scattering cross section.

By relation (A) Ω_S satisfies the Lippmann-Schwinger equation,

$$\Omega_S=1+\frac{1}{E+i\eta-H_0}\mathfrak{V}\Omega_S. \tag{24}$$

For the evaluation of the V_n's as well as the U_n's we use relation (B),

$$\Delta_{n+1}=U_n\frac{1}{a-\mathfrak{V}_n}U_n=U_n\omega_n(1/a)U_n, \tag{25}$$

where ω_n satisfies

$$\omega_n=1+(1/a)\mathfrak{V}_n\omega_n. \tag{26}$$

This describes the scattering of the virtual and real mesons in an "intermediate state." Because in the definition of V_n Eq. (17) the first U_n contains only creation operators (except for the smallest n value, as remarked previously, where the order can be inverted) and the second U_n only absorption operators, the structure of the V_n's (and U_n's) is relatively simple compared (for instance) to the complexity of the Feynman diagrams for a high order process. Thus the matrix elements of V_n can be written directly in terms of the ω_n's and integrals over virtual meson states by only enumerating the order of reabsorption for a given order of emission. Also, because of the large number of

meson states upon which $(a-\mathfrak{V}_n)$ operates ($\simeq 2^{n+1}$), except for small n values, a will be quite large in magnitude and a reasonable approximation might be to neglect $\mathfrak{V}_n$ entirely for all but the lowest n-values in Eq. (25). This would make the evaluation of the V_n's relatively simple. Also, in this case $\mathfrak{V}$ becomes a power series in g^2, but of the form

$$\mathfrak{V}=O(g^2)+O(g^4)+O(g^8)+O(g^{16})+O(g^{32})+\cdots. \quad (26')$$

In this approximation, the terms contributing to $\mathfrak{V}$ are particularly simple. Making use of the defining equation for V_n, we find

$$V_n=a[(1/a)H']^{2^n}[(1/a)H']^{2^n},$$

where by theorem II, the first 2^n operators H' must create mesons, the last 2^n operators annihilate mesons. It is interesting to note that the operators $1/a$ which appear in this expression will contribute factors roughly of the form

$$1/(2^n!)^2$$

multiplied by dimensionless factors depending on the convergence of the integrals over the momenta of the virtual mesons. In evaluating the contribution to V_n, we will in general be able to create the 2^n particles in $2^n!$ ways corresponding to the ways of permuting the creation operators. A corresponding factor will come from the annihilation operators, neglecting cancellations due to reordering of noncommuting spin and isotopic spin matrices. Accordingly, aside from other factors, the factorial dependence of the V_n arising from the multiplicity of contributions in high order is at least cancelled by the behavior of the energy denominators.

Aside from this approximation the form (25) is surprisingly simple. This is to be compared, for instance, with the greater complexity of the perturbation or Tamm-Dancoff methods, which do not lead to a decomposition into the U_n's and the V_n's. The simplification results from considering explicitly the "scattering" of virtual mesons before reabsorption. It is also of interest to note from Eq. (17), that the difference between the power of g occurring in the numerator and the combined powers of g in the denominators is just g^2 in every Δ_n (and thus $\mathfrak{V}_n$). This suggests that, as the coupling becomes larger, the successive terms may not increase with g as rapidly as might otherwise be indicated (if the quantities $(a-\mathfrak{V}_n)^{-1}$ had no singularities, then every term in $\mathfrak{V}$ would be of order g^2 in the strong coupling limit).

The effect just mentioned is apparent in the calculation of the first two terms of Eq. (22) for the nuclear forces, as is done in the Appendix. Here, the multiple scattering of the virtual exchanged meson is shown to arise from V_1. The second term is of order g^4 for weak coupling but becomes of order g^2 for large values of g. The nuclear force problem discussed in the Appendix is given to illustrate techniques of handling the formal algebraic expressions which have been used above.

Problems of meson production and absorption may also be easily handled by the present techniques. In this case, it is of course necessary to keep some of the off-diagonal terms in Ω which were discarded in analyzing processes which are diagonal in occupation numbers (actually, only a small finite number of these terms need be kept in any case of practical importance). By repeating inductive arguments such as those given previously, one may easily show that [Eq. (13)]

$$\Omega=\Omega_S[1+(1/a)F],$$

where Ω_S is given by Eq. (24). F is a non-diagonal operator, which may be broken into parts for producing (or absorbing) one meson, two mesons, etc. For instance, for the production of a single meson when no meson is initially present (i.e., by nucleon-nucleon collisions) we have directly from Eq. (13)

$$\frac{1}{a-\Delta_0}H'=\Omega_S(0)\frac{1}{a}H'. \quad (27)$$

It therefore follows that

$$F^{(1)}=H', \quad (28)$$

where $F^{(1)}$ is that part of F which has matrix elements for the production of just one meson. Equation (28) results since H' must obviously produce a meson. Since we wish just one meson produced, the remaining factor, $\Omega_S(0)$, must be diagonal. But $\mathrm{DP}[\Omega_S(0)]=\Omega_S$ so Eq. (28) follows. For single meson production by the collision of a meson with a nucleon, we must generalize Eq. (28):

$$F^{(1)}=\left[1+U_0\frac{1}{a-V_0}\right]H'. \quad (28')$$

It is of course implied that we keep only those matrix elements on the right-hand side of this equation which refer to the production of a single meson. Equation (28') obviously reduces to Eq. (28) for those initial states which do not contain a meson. The general expression for $F^{(1)}$ may easily be worked out. The absorption of mesons may be obtained from the above using the detailed reversibility theorem,[14] or directly by re-expressing the above quantities with the nondiagonal operators to the left rather than to the right of the scattering operators. The generalizations of the above arguments to the nonlinear and nucleon pair theories are straightforward and will not be given in detail.

IV. NONLINEAR INTERACTIONS

Nonlinear interactions such as those obtained by Berger *et al.*[15] or by Drell and Henley[16] by transforming

[14] J. M. Blatt and V. F. Weisskopf, *Theoretical Nuclear Physics* (John Wiley and Sons, New York, 1952), p. 528.
[15] Berger, Foldy, and Osborn, Phys. Rev. **87**, 1061 (1952).
[16] S. Drell and E. Henley, Phys. Rev. **88**, 1053 (1952).

the linear pseudoscalar interaction may also be handled by the methods here employed. If the matrix elements of the interaction term can be evaluated by some such method as Glauber's,[17] then it is not necessary to expand the interaction in powers of g. We again assume that the interaction is diagonal in nucleon occupation numbers, so no nucleon pairs are formed.

In the Schrödinger Eq. (1) H' will be assumed to be nonlinear in ϕ. We first break H' into two parts.

$$H'=H_1+H_2, \tag{29}$$

where H_1 is odd in ϕ and H_2 is even in ϕ. Thus the wave matrix Ω satisfies [see Eq. (4)]

$$\begin{aligned}\Omega&=1+\frac{1}{E+i\eta-H_0}(H_1+H_2)\Omega\\&=1+\frac{1}{a-H_1-H_2}(H_1+H_2)\end{aligned} \tag{30}$$

(where again $a=E+i\eta-H_0$). We use relation (D), identifying H_1 with q_1 and H_2 with q_2 to express Ω as

$$\begin{aligned}\Omega=1&+\frac{1}{a-H_2-D_0}(H_2+D_0)\\&+\frac{1}{a-H_2-D_2}H_1\left[1+\frac{1}{a-H_2}H_2\right],\end{aligned} \tag{31}$$

where

$$D_0=H_1\frac{1}{a-H_2}H_1. \tag{32}$$

Now, by Lemma I, since H_1 is odd in ϕ, H_1 produces (or absorbs) a net odd number of mesons. Furthermore H_2, being even in ϕ, produces (absorbs) an even number of mesons only. Since the last term of Eq. (31) is odd in H_1, it contains an odd number of production events, each producing an odd number of mesons, plus any number of events producing an even number of mesons (because of H_2). The net number of produced mesons arising from this term is therefore odd and it consequently cannot be diagonal in meson occupation numbers. It will not contribute to a scattering event in which no particles are produced and may be dropped. We may thus calculate the scattering from

$$\Omega_S(0)=1+\frac{1}{a-H_2-D_0}(H_2+D_0). \tag{33}$$

The "potential," H_2+D_0, in Eq. (33) has only diagonal matrix elements or matrix elements for the production of mesons in multiples of two. Since the interaction, H_1+H_2, with which we started in Eq. (30), had diagonal matrix elements or matrix elements for the production of one meson, two mesons, three mesons, etc., we have increased the minimum multiplicity of virtual mesons present. It is clear that this process may be iterated, each step increasing the multiplicity of mesons in the *off diagonal* matrix elements of the interaction.

To proceed more generally, we first define

$$\begin{aligned}v_0&=\mathrm{DP}(H_2+D_0),\\U_0(e)&=\mathrm{NDP}(e2)(H_2+D_0),\\U_0(o)&=\mathrm{NDP}(o2)(H_2+D_0).\end{aligned} \tag{34}$$

The notation DP and NDP is as used before. The symbol "(em)" is interpreted to mean the matrix elements which produce (or absorb) *even multiples* of m-mesons. The symbol "(om)" likewise is to be interpreted as those matrix elements which produce (or absorb) *odd multiples* of m mesons. Thus in Eq. (34), where $m=2$, $U_0(e)$ produces (or absorbs) only even multiples of two mesons (except zero) and $U_0(o)$ produces (or absorbs) only odd multiples of two mesons.

As in the last section, we define by induction an infinite set of such quantities as those in Eq. (34). Let us suppose that we have already defined three quantities (for some value of n) $\mathfrak{V}_n$, $U_n(o)$ and $U_n(e)$. $\mathfrak{V}_n$ is assumed to be a scattering interaction (that is, diagonal in meson occupation numbers). The U's are supposed by hypothesis to be only nondiagonal in meson occupation numbers and $U_n(o)$ is a quantity of the type $(o2^{n+1})$ and $U_n(e)$ is of the type $(e2^{n+1})$. This means that $U_n(o)$ can produce (or absorb) mesons only in odd multiples of the number 2^{n+1} whereas $U_n(e)$ can produce (or absorb) mesons only in even multiples of 2^{n+1}. Now define

$$\begin{aligned}D_{n+1}&=U_n(o)\frac{1}{a-\mathfrak{V}_n-U_n(e)}U_n(o),\\K_{n+1}&=U_n(e)+D_{n+1}.\end{aligned} \tag{35}$$

Lemma IV

The quantity K_{n+1} can produce (or absorb) mesons only in multiples of 2^{n+2}.

It follows from its definition that $U_n(e)$ can produce only in multiples of 2^{n+2} mesons. From the structure of D_{n+1} in the definition (35) it also follows that D_{n+1} can also produce (or absorb) mesons only in multiples of 2^{n+2}. Thus the Lemma IV is proven. We can therefore define

$$\begin{aligned}v_{n+1}&=\mathrm{DP}K_{n+1},\\U_{n+1}(e)&=\mathrm{NDP}(e2^{n+2})K_{n+1},\\U_{n+1}(o)&=\mathrm{NDP}(o2^{n+2})K_{n+1},\\\mathfrak{V}_{n+1}&=\mathfrak{V}_n+v_{n+1}.\end{aligned} \tag{36}$$

If we define

$$\mathfrak{V}_0=v_0,$$

and start with Eq. (34), we can now construct by induction all the quantities in Eq. (36) to any order in

[17] R. J. Glauber, Phys. Rev. **84**, 395 (1951).

n. In particular,

$$\mathfrak{V}_n=\sum_{e=0}^{n} v_e. \tag{37}$$

The following theorem finally gives the potential $\mathfrak{V}$.

Theorem IV: Assuming suitable convergence, the interaction potential is

$$\mathfrak{V}=\lim_{n\to\infty}\mathfrak{V}_n=\sum_{e=0}^{\infty} v_e. \tag{38}$$

We proceed by induction. Let us assume for some n that $\Omega_S(n)$ has the form

$$\Omega_S(n)=1+\frac{1}{a-\mathfrak{V}_n-U_n(e)-U_n(o)}\times[\mathfrak{V}_n+U_n(e)+U_n(o)]. \tag{39}$$

Using relation (D), in which q_2 is interpreted as $\mathfrak{V}_n+U_n(e)$ and q_1 as $U_n(o)$, we have

$$\Omega_S(n)=1+\frac{1}{a-\mathfrak{V}_n-U_n(e)-D_{n+1}}[\mathfrak{V}_n+U_n(e)+D_{n+1}]+\frac{1}{a-\mathfrak{V}_n-U_n(e)-D_{n+1}}\times U_n(o)\left[1+\frac{1}{a-\mathfrak{V}_n-U_n(e)}(\mathfrak{V}_n+U_n(e))\right]. \tag{40}$$

The last term may be dropped, since it corresponds to an odd number of productions in odd multiplicities of 2^{n+1} mesons and therefore has no matrix elements diagonal in meson occupation numbers. From the definitions (35) and (36) we write

$$U_n(e)+D_{n+1}=v_{n+1}+U_{n+1}(e)+U_{n+1}(o),$$

so the first two terms in Eq. (40) have the form

$$\Omega_S(n+1)=1+\frac{1}{a-\mathfrak{V}_{n+1}-U_{n+1}(e)-U_{n+1}(o)}\times[\mathfrak{V}_{n+1}+U_{n+1}(e)+U_{n+1}(o)]. \tag{41}$$

Since the first Eq. (33) has the form of Eq. (39) with $n=0$ [by the definitions (34)], we obtain Eq. (41) after n iterations of the process just described. If for sufficiently large n, the matrix elements of the U's become negligible and if the series for $\mathfrak{V}$ converges, we obtain finally

$$\Omega_S=1+\frac{1}{a-\mathfrak{V}}\mathfrak{V}, \tag{42}$$

which satisfies the Schrödinger equation,

$$\Omega_S=1+(1/a)\mathfrak{V}\Omega_S. \tag{43}$$

Since $\mathfrak{V}$ is diagonal in meson occupation numbers, it is a potential in the ordinary sense and Eq. (43) can be considered soluble.

Our problem is still solved only in the formal sense, however, since the definitions of the D_{n+1}'s as given in Eq. (35) contain the nondiagonal operators $U_n(e)$ in the energy denominator. To complete the solution we note that by relation (B) D_{n+1} can be written as

$$D_{n+1}=U_n(o)\omega_n(1/a)U_n(o), \tag{44}$$

where ω_n satisfies

$$\omega_n=1+(1/a)[\mathfrak{V}_n+U_n(e)]\omega_n. \tag{45}$$

To solve this equation we must proceed just as we did in the solution to Eq. (30), etc. The process here is clearly much more complicated than was that of Sec. III in which the linear theory was studied, but still leads to a means of constructing the potentials in terms of integral equations which do not involve emissions or absorptions. In any actual problem, one will cut off the series defining $\mathfrak{V}$ at a certain multiplicity of virtual mesons. The V_n's occurring in $\mathfrak{V}$ can be defined to the same order in virtual mesons. Since the multiplicities increase with n as 2^n, the calculation is not as complicated as might appear, if only low multiplicities are kept. We illustrate this by developing the method of evaluating

$$v_0=\mathrm{DP}\left[H_2+H_1\frac{1}{a-H_2}H_1\right]. \tag{46}$$

Defining

$$H_d=\mathrm{DP}H_2$$

and

$$H_2=H_d+H_2', \tag{47}$$

it is apparent that H_2' must create at least two mesons. Using relation (D) we obtain

$$H_1\frac{1}{a-H_2}H_1=H_1\frac{1}{a-H_d-R}H_1+H_1\frac{1}{a-H_d-R}H_2'\frac{1}{a-H_d}H_1, \tag{48}$$

where

$$R=H_2'\frac{1}{a-H_d}H_2'. \tag{49}$$

The quantity R is clearly calculable in terms of the solution to an integral equation with H_d as a potential by means of relation (B). The NDP(R) creates at least four mesons. If, for instance, we do not permit such high multiplicities this can be neglected and we need keep only

$$\mathrm{DP}[R]\equiv R_d,$$

and the expression (48) can be evaluated using relation (B). The calculation can obviously be extended to higher multiplicities.

To give a specific illustration, we calculate the potential which results from applying the Dyson transformation[18] to the symmetric pseudoscalar coupling term in pseudoscalar meson theory. To order g^2 the interaction H' is

$$H'=\frac{g}{2M}\boldsymbol{\sigma}\cdot\nabla\boldsymbol{\tau}\cdot\boldsymbol{\phi}+\frac{g^2}{2M}\boldsymbol{\phi}\cdot\boldsymbol{\phi}. \tag{50}$$

If we compare this result with the defining equation (29) for H_1 and H_2 and make use of Eq. (46), we find

$$v_0=\mathrm{DP}\left[\frac{g^2}{2M}\boldsymbol{\phi}\cdot\boldsymbol{\phi}+\frac{g^2}{4M^2}\boldsymbol{\sigma}\cdot\nabla\boldsymbol{\tau}\cdot\boldsymbol{\phi}\times\frac{1}{a-(g^2/2M)\boldsymbol{\phi}\cdot\boldsymbol{\phi}}\boldsymbol{\sigma}\cdot\nabla\boldsymbol{\tau}\cdot\boldsymbol{\phi}\right]. \tag{51}$$

Consistent with the approximation just discussed, we shall restrict ourselves to diagonal elements of $\boldsymbol{\phi}\cdot\boldsymbol{\phi}$ in evaluating the integral operator $[a-(g^2/2M)\boldsymbol{\phi}\cdot\boldsymbol{\phi}]^{-1}$. If we evaluate the second term of v_0 for p-state mesons, then the s-state potential $(g^2/2M)\mathrm{DP}[\boldsymbol{\phi}\cdot\boldsymbol{\phi}]$ cannot scatter the incoming meson or the virtual mesons created in p-states by the first operator $\boldsymbol{\sigma}\cdot\nabla\boldsymbol{\tau}\cdot\boldsymbol{\phi}$ if nucleon recoil is neglected. For s-state mesons, the two operators $\boldsymbol{\sigma}\cdot\nabla\boldsymbol{\tau}\cdot\boldsymbol{\phi}$ can create and absorb a virtual p-state meson, the s-state meson being scattered by the potential $(g^2/2M)\mathrm{DP}[\boldsymbol{\phi}\cdot\boldsymbol{\phi}]$.

This process gives a contribution to the s-state interaction of the same form and sign as the first term of v_0. Accordingly we have approximately

$$v_0=\mathrm{DP}\left[\lambda\frac{g^2}{2M}\boldsymbol{\phi}\cdot\boldsymbol{\phi}+\frac{g^2}{4M^2}\boldsymbol{\sigma}\cdot\nabla\boldsymbol{\tau}\cdot\boldsymbol{\phi}\frac{1}{a}\boldsymbol{\sigma}\cdot\nabla\boldsymbol{\tau}\cdot\boldsymbol{\phi}\right], \tag{52}$$

where λ is of the order of 2. The second term of this is the p-state potential considered by Chew[9] which gives strong scattering in the isotopic spin $\frac{3}{2}$ and spin $\frac{3}{2}$ state; the first term is a strongly repulsive potential which gives a rather smaller s-wave scattering (roughly 50 millibarns at 100 Mev).[19]

V. NUCLEON PAIR PRODUCTION

We suppose the interaction H' to be in general nonlinear in both the meson field variables and in the pairs of nucleon field variables. We may formally obtain the "interaction potential" from the results of the previous section by either of two methods: First, we may ignore the nucleon field variables and diagonalize the interaction in meson occupation numbers only, just as was done in Sec. IV. The operator $\mathfrak{V}$ obtained in this manner is now a nonlinear operator in the nucleon field variables and is the type discussed in Sec. IV. This operator is a gain broken into parts even and odd in the production (or absorption) of *nucleon pairs*. We can proceed to diagonalize it in nucleon states just as was done for the meson states.

A more straightforward method for calculation is to formally include in out set of field variables ϕ_σ ($\sigma=1, 2, \cdots N$) each pair of nucleon field variables $\bar{\psi}O\psi$ (where O is a matrix operating on the components of ψ). This can be done since we have not made use of the commutation rules for the ϕ's. For purposes of argument we can say that a "particle" is emitted when either a nucleon pair or a meson is created. Splitting H' into parts even and odd in "particle" creation we can develop the potential as in Sec. IV. There is no point in a detailed development, since it follows the methods used in Sec. IV.

We shall illustrate the method by showing how to proceed for an H' which is linear in ϕ and linear in $\bar{\psi}O\psi$ (i.e., of the usual sort).

We set

$$H'=H_e'+H_o' \tag{53}$$

where H_e' produces (or absorbs) one meson and one nucleon pair (even in "particle" creation) and H_o' produces (or absorbs) one meson and no nucleon pairs. Using relation (D)

$$\begin{aligned}\Omega&=1+\frac{1}{a-H'}H'\\&=1+\frac{1}{a-H_e'-D_o}[H_e'+D_o]\\&\quad+\frac{1}{a-H_e'-D_o}H_o'\left[1+\frac{1}{a-H_e'}H_e'\right],\end{aligned} \tag{54}$$

where

$$D_o=H_o'\frac{1}{a-H_e'}H_o'. \tag{55}$$

The second term in Eq. (2) can be discarded and $H_e'+D_o$ can be broken into a "diagonal part," a part producing an even number of pairs of "particles" and a part producing an odd number of pairs of "particles." The process can now be repeated, etc. The terms in the "potential" can be defined by means of integral equations as in the previous sections.

VI. DISCUSSION

We have seen that potentials can be obtained in a straightforward manner in quantum field theories. Since the potential is given as an infinite series of terms the question of convergence remains to be studied. It is evident that the potentials of the type discussed here will always converge if a strict power series expansion (in the coupling constant) converges, since each term in the potential series can be expanded into a power series in g^2. It is also quite possible that the series given here may converge even when the power series expansion is not convergent.

[18] F. J. Dyson, Phys. Rev. **73**, 929 (1948).

[19] G. F. Chew (private communication) has called our attention to this small value of the s-wave scattering.

The results of our studies strongly suggest that a great deal of the apparent complexity of the S matrix in field theory is associated with the scattering of real and virtual particles in intermediate states. When these effects are identified and isolated, the complexity of the analysis is strikingly reduced.

It is to be noted that the potential $\mathfrak{V}$ will be hermitean when and only when true absorption and emission of particles is not energetically possible. When creation or absorption is possible some of the energy denominators will be singular and the $i\eta$ term will contribute an anti-hermitean part to $\mathfrak{V}$. Otherwise $i\eta$ is redundant for the construction of the potentials and may be neglected. In this case bound state problems may be handled by dropping the additive identity operator on the right-hand side of Eq. (26) and (43) and solving the resulting eigenvalue problem.

Finally, although meson theory has been most specifically considered, the results are of course applicable to other types of field theories.

We are indebted to Professor G. F. Chew and Professor F. Low for several interesting discussions concerning problems related to the present one.

APPENDIX

Nuclear Forces in the Isotopic Spin Zero State for the Symmetric Scalar Theory

We consider this case explicitly to illustrate the development of the method for a simple problem. For the two nucleon system, the coupling term of Eq. (1) is

$$H'=H'(1)+H'(2), \tag{A1}$$

where $H'(i)$ is the coupling term for the ith nucleon. For simplicity we shall in this problem treat the nucleons as infinitely heavy so that their energy is unchanged by the emission of mesons. The operator

$$-a=-E+H_0 \tag{A2}$$

will then give just the sum of the energies of the virtual mesons present.

The first two terms in the potential series are [Eq. (17)]

$$\begin{aligned} V_0&=H'\frac{1}{a}H'^*+H'^*\frac{1}{a}H', \\ V_1&=H'\frac{1}{a}H'\frac{1}{a-V_0}H'^*\frac{1}{a}H'^*, \end{aligned} \tag{A3}$$

where the starred operators create mesons, the unstarred annihilate mesons. The sum of these is particularly simple if in the term

$$H'\frac{1}{a-V_0}H'^* \tag{A4}$$

appearing in V_1 we retain in V_0 only that part which first annihilates a meson; this is equivalent to restricting the number of mesons present to two or less. If this approximation is made, then it is easily shown that

$$\begin{aligned} H'\frac{1}{a-V_0}H'^*&=V_0'+V_0'\frac{1}{a-V_0'}V_0' \\ &\equiv T, \end{aligned} \tag{A5}$$

where

$$V_0'=H'(1/a)H'^* \tag{A6}$$

and T is the scattering matrix associated with V_0'. With this result we obtain for the first two terms in the nuclear potential,

$$V^{(1)}=V_0+V_1=H'\left(1+\frac{1}{a}T\right)\frac{1}{a}H'^*. \tag{A7}$$

This result differs from the lowest order potential V_0' in that the meson created by H'^* goes into the scattering state

$$\omega_S=1+(1/a)T, \tag{A8}$$

which describes the scattering of the meson by the two nucleons Only if the scattering is small and we can set $\omega_S=1$ is the lowest order potential an adequate approximation. The principal difficulties of evaluating $V^{(1)}$ are now those of solving the multiple scattering equation for ω_S.

In terms of the potentials v_1 and v_2 which scatter the meson at nucleons (1) and (2), the equation for ω_S is

$$\omega_S=1+(1/a)(v_1+v_2)\omega_S. \tag{A9}$$

The solution to this equation can be given in terms of the set of equations discussed by Watson[7] and Brueckner:[20]

$$\omega_S=1+(1/a)(T_1\omega_1+T_2\omega_2), \tag{A10}$$

where

$$\omega_1=1+(1/a)T_2\omega_2, \quad \omega_2=1+(1/a)T_1\omega_1, \tag{A11}$$

and T_i is the scattering matrix for the potential v_i. These coupled integral equations are difficult in general to solve; under a reasonable qualitative approximation we can, however, obtain exact solutions. For the symmetric scalar theory, the potential for the scattering of a meson is

$$(\mathbf{k}|v|\mathbf{k}_0)=-\tfrac{1}{2}g^2(1+\boldsymbol{\tau}_1\cdot\mathbf{I})e^{i(\mathbf{k}_0-\mathbf{k})\cdot\mathbf{r}_1}/[(\omega\omega_0)^{\frac{1}{2}}(\omega+\omega_0)], \tag{A12}$$

where $\mathbf{I}$ is the isotopic angular momentum operator for the meson and $\boldsymbol{\tau}$ is the nucleon isotopic spin operator. In this form the integral equation relating v_1 to T_1 is not easily solved; if, however, we make the replacement

$$\omega+\omega_0\rightarrow(\omega\omega_0)^{\frac{1}{2}}, \tag{A13}$$

then we obtain directly

$$(\mathbf{k}|T_1|\mathbf{k}_0)=-\sigma_1 e^{i(\mathbf{k}_0-\mathbf{k})\cdot\mathbf{r}_1}/(\omega\omega_0), \tag{A14}$$

[20] K. A. Brueckner, Phys. Rev. **89**, 834 (1953).

where

$$\sigma_1=\tfrac{1}{2}g^2(1+2\Delta+\boldsymbol{\tau}_1\cdot\mathbf{l})/[(1-2\Delta)(1+\Delta)] \quad \text{(A15)}$$

and

$$\Delta=\tfrac{1}{2}g^2(2\pi)^{-3}\int d\mathbf{k}/\omega_k{}^3. \quad \text{(A16)}$$

Substituting this result into the coupled equations of Eq. (A11) we find

$$\begin{aligned} G_1&=e^{i\mathbf{k}_0\cdot\mathbf{r}_1}/\omega_0+\sigma_2 I(r)G_2,\\ G_2&=e^{i\mathbf{k}_0\cdot\mathbf{r}_2}/\omega_0+\sigma_1 I(r)G_1, \end{aligned} \quad \text{(A17)}$$

and

$$\begin{aligned}(\mathbf{k}|\,\omega_S\,|\mathbf{k}_0)&=(2\pi)^3\delta(\mathbf{k}_0-\mathbf{k})\\ &\quad+(1/\omega)(\sigma_1 G_1 e^{-i\mathbf{k}\cdot\mathbf{r}_1}+\sigma_2 G_2 e^{-i\mathbf{k}\cdot\mathbf{r}_2}) \end{aligned} \quad \text{(A18)}$$

where

$$G_i=(2\pi)^{-3}\int\frac{(\mathbf{k}|\,\Omega_i\,|\mathbf{k}_0)}{\omega}e^{i\mathbf{k}\cdot\mathbf{r}_i}d\mathbf{k} \quad \text{(A19)}$$

and

$$I(r)=(2\pi)^{-3}\int\frac{e^{i\mathbf{k}\cdot\mathbf{r}}}{\omega^3}d\mathbf{k}. \quad \text{(A20)}$$

Eliminating G_2 in Eq. (A17) we obtain for G_1

$$(1-I^2\sigma_2\sigma_1)G_1=(1/\omega_0)e^{i\mathbf{k}_0\cdot\mathbf{r}_1}+(\sigma_2 I/\omega_0)e^{i\mathbf{k}_0\cdot\mathbf{r}_2}, \quad \text{(A21)}$$

with a similar result for G_2. The construction of the inverse of the operator $(1-I^2\sigma_2\sigma_1)$ is in general rather complicated; for the case of total isotopic spin zero, however, the operators σ_2 and σ_1 are diagonal with the matrix elements

$$\begin{aligned}\sigma_1=\sigma_2&=-\tfrac{1}{2}g^2/(1+\Delta)\\ &\equiv\rho. \end{aligned} \quad \text{(A22)}$$

With this result the wave matrix ω_S is

$$\begin{aligned}(\mathbf{k}|\,\omega_S\,|\mathbf{k}_0)&=(2\pi)^3\delta(\mathbf{k}_0-\mathbf{k})-\frac{1}{\omega^2\omega_0{}^2}\frac{\rho}{1-I^2\rho^2}\\ &\quad\times\{e^{i(\mathbf{k}_0-\mathbf{k})\cdot\mathbf{r}_1}+e^{i(\mathbf{k}_0-\mathbf{k})\cdot\mathbf{r}_2}\\ &\quad-\rho I[e^{i(\mathbf{k}_0\cdot\mathbf{r}_1-\mathbf{k}\cdot\mathbf{r}_2)}+e^{i(\mathbf{k}_0\cdot\mathbf{r}_2-\mathbf{k}\cdot\mathbf{r}_1)}]\}. \end{aligned} \quad \text{(A23)}$$

Finally the potential is

$$\begin{aligned}V^{(1)}=\frac{-3g^2}{(2\pi)^6}\int&\frac{d\mathbf{k}_0 d\mathbf{k}}{2\omega_0(\omega_0\omega)^{\frac{1}{2}}}(e^{i\mathbf{k}\cdot\mathbf{r}_1}-e^{i\mathbf{k}\cdot\mathbf{r}_2})\\ &\times(\mathbf{k}|\,\omega_S\,|\mathbf{k}_0)(e^{-i\mathbf{k}_0\cdot\mathbf{r}_1}-e^{-i\mathbf{k}_0\cdot\mathbf{r}_2}), \end{aligned} \quad \text{(A24)}$$

where we have set $\boldsymbol{\tau}_1=-\boldsymbol{\tau}_2$ (for the singlet state) and $\boldsymbol{\tau}_1\cdot\boldsymbol{\tau}_1=3$. In evaluating the integrals over $\mathbf{k}_0$ and $\mathbf{k}_1$ we encounter expressions of the form of

$$\frac{1}{(2\pi)^6}\int\frac{d\mathbf{k}d\mathbf{k}_0}{(\omega\omega_0)^{5/2}}e^{i\mathbf{k}\cdot(\mathbf{r}_a-\mathbf{r}_b)}e^{i\mathbf{k}_0\cdot(\mathbf{r}_c-\mathbf{r}_d)}. \quad \text{(A25)}$$

Consistent with the approximation [Eq. (A13)] we have already made in obtaining the scattering matrices, we shall approximate this integral very roughly by

$$\begin{aligned}\frac{1}{(2\pi)^6}\int&\frac{d\mathbf{k}d\mathbf{k}_0}{\omega^2\omega_0{}^2}e^{i\mathbf{k}\cdot(\mathbf{r}_a-\mathbf{r}_b)}e^{i\mathbf{k}\cdot(\mathbf{r}_c-\mathbf{r}_d)}\\ &=Y(\mathbf{r}_a-\mathbf{r}_b)I(\mathbf{r}_c-\mathbf{r}_d), \end{aligned} \quad \text{(A26)}$$

where

$$Y(r)=(1/4\pi)e^{-\mu r}/r \quad \text{(A27)}$$

is the Yukawa potential and $I(r)$ is defined by Eq. (A20).

With this approximation we obtain for the potential:

$$\begin{aligned}V^{(1)}=3g^2Y(r)&\left[\frac{1-2\rho I(r)}{1-\rho I(r)}\right]\\ &-3g^2Y(0)\left[\frac{1-\rho I(r)-\rho I(0)}{1-\rho I(r)}\right]. \end{aligned} \quad \text{(A28)}$$

The second term contains mass renormalization effects since it remains finite as $r\to\infty$; if we subtract these as self energies and replace $I(r)Y(0)$ by $I(0)Y(r)$ as was done in Eq. (A26), we obtain, using Eq. (A22) for ρ,

$$\begin{aligned}V^{(1)}=3g^2Y(r)&[\{1+\tfrac{1}{2}g^2I(0)\}\\ &\times\{1+\tfrac{1}{2}g^2I(0)-\tfrac{1}{2}g^2I(r)\}]^{-1}. \end{aligned} \quad \text{(A29)}$$

The dependence on $g/[1+\frac{1}{2}g^2I(0)]$ which appears in this result is probably a charge renormalization effect although the identification as such is not unambiguous; if we replace

$$g/(1+\tfrac{1}{2}g^2I(0))\to g', \quad \text{(A30)}$$

then

$$V^{(1)}=3g'^2Y(r)[1-gg'I(r)]^{-1}. \quad \text{(A31)}$$

This potential increases more rapidly with decreasing r than does the Yukawa potential; the denominator is always positive, however, so that it does not introduce new singularities.

Letters to the Editor

PUBLICATION of brief reports of important discoveries in physics may be secured by addressing them to this department. The closing date for this department is five weeks prior to the date of issue. No proof will be sent to the authors. The Board of Editors does not hold itself responsible for the opinions expressed by the correspondents. Communications should not exceed 600 words in length and should be submitted in duplicate.

Temperature, Current, Magnetic Field Phase Diagram of Superconductivity*

W. MEISSNER, F. SCHMEISSNER, AND H. MEISSNER
Kommission für Tieftemperaturforschung, Bayerische Akademie der Wissenschaften, Herrsching bei München, Germany
(Received March 30, 1953)

MENDELSSOHN, Squire, and Teasdale[1] conclude from their measurements that the so-called "paramagnetic effect" studied by us[2,3] can be only a dynamical one. But the fluxmetric recording made by us has shown[4] that the increased flux can be maintained permanently if current, field, and temperature are constant. The experiments of Mendelssohn *et al.* also agree with our results concerning the minimum of current-strength necessary to get a flux increase. Figure 1 gives the minimum of current as a

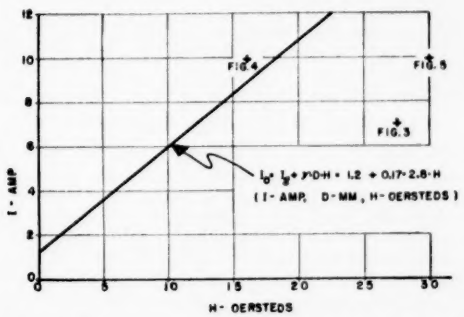

FIG. 1. Minimum current as function of the longitudinal magnetic field H for the Sn-sample used by Mendelssohn *et al.*

function of the longitudinal field for the Sn sample of Mendelssohn *et al.* The crosses represent the values of current and field for the beginning of the drop in the diagrams of Figs. 3, 4 and 5 of the paper in question. It may be seen that the paramagnetic effect is impossible for the observation represented in Figs. 3 and 5. In the case of Fig. 4, a small increase may be expected from our figure, if the right temperature is taken. Indeed, Fig. 4 shows a small increase of the flux, but it is taken as an experimental error by the authors. It should be taken into account that the temperature must be fixed to within about one thousandth of a degree to gain the maximum flux increase.

Furthermore, the following may be mentioned: Mendelssohn *et al.* intend to screen the magnetic field of the return lead of the current by a lead tube. However, the screening current flows on the inside of the lead tube in a direction opposite to that of the primary current. On the outside of the tube we have a current equal to the primary current, giving the same field on the outside of the tube as the primary current would give without the lead shield. It is best to use a tube containing the sample as the return lead, as we have done.

[1] Mendelssohn, Squire, and Teasdale, Phys. Rev. **87**, 589 (1951).
[2] Meissner, Schmeissner, and Meissner, Z. Physik **130**, 521, 529 (1951).
[3] Meissner, Schmeissner, and Meissner, Z. Physik **132**, 529 (1952).
[4] Reference 3, p. 531, lines 1 and 2.

The Paramagnetic Effect in Superconductors

TOM S. TEASDALE* AND H. E. RORSCHACH, JR.
Rice Institute, Houston, Texas
(Received March 30, 1953)

ON receiving the Letter of Meissner, Schmeissner, and Meissner,[1] measurements were made in a region where their note indicates that a large flux increase should be observed with our apparatus. A temperature was chosen such that the superconducting transition occurred for $I=11.5$ amp, and $H=5$ oersteds. (See Fig. 1 of reference 1.) Two modifications of the equipment described in our previous paper[2] were made: (1) following the suggestion of Meissner *et al.*, a brass tube concentric with the specimen was used as the return current lead; and (2) the current supplies were obtained from a bank of Edison cells. The first measurements indicate that the prediction of a flux increase in reference 1 is correct.

Figure 1 shows the galvanometer deflections as a function of the current in the sample. The temperature and external magnetic field are held constant. The deflections of the ballistic galvanometer (proportional to the flux in the tin) show a pronounced

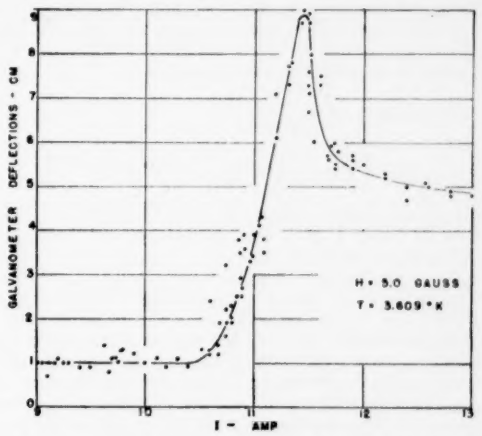

FIG. 1. Galvanometer deflection as a function of current in the specimen. The coil is dropped from the tin to the lead section of the sample.

increase before the transition into the superconducting state. In the immediate neighborhood of the peak in the curve, the galvanometer shows spontaneous fluctuations of 5 to 10 mm. These random deflections appear when the coil is held stationary around the tin. They do not occur at other points of the curve. In appearance they are similar to critical point fluctuations.

* Shell Oil Company Fellow.
[1] Meissner, Schmeissner, and Meissner, preceding Letter [Phys. Rev. **90**, 709 (1953)].
[2] Mendelssohn, Squire, and Teasdale, Phys. Rev. **87**, 589 (1952).

Annealing of Bombardment Damage in Solids

W. L. BROWN, R. C. FLETCHER, AND S. MACHLUP
Bell Telephone Laboratories, Murray Hill, New Jersey
(Received April 1, 1953)

IT has been found possible to obtain an analytical expression for the annealing of isolated interstitial vacancy pairs, N, which are presumably introduced by bombardment with particles having energies just slightly higher than threshold. This expression is neither exponential nor hyperbolic as has been previously suggested,[1,2] but is the sum of three different types of terms, $N=N_M+N_L+N_B$, as discussed below.

Under the influence of thermal excitation the interstitial will jump to adjacent interstitial sites with an average jump time

given by $\tau=\nu_0^{-1}\exp(E/kT)$, where ν_0 is the average lattice frequency (ca 10^{13} sec^{-1}), and E is the potential barrier between the sites. In the region close to the vacancy there is elastic deformation of the lattice which results in progressively smaller potential barriers and shorter jump times as one approaches the vacancy. In this region the interstitial has a preference for jumps toward the vacancy. Thus, the time required for recombination will be approximately the time in which the interstitial will jump out of its initial site in the deformed region. This gives rise to the N_M (M for monomolecular) term of the annealing, $N_M=\Sigma_1 N_i\exp(-t/\tau_i)$, where N_i is the number of interstitials located initially at the ith site, τ_i is the corresponding average jump time towards the vacancy, and the summation Σ_1 is over all sites within the deformed region.

For those interstitials which are located outside this deformed region, which we will assume extends out to radius r_c, the probability of jumping in any direction is the same. Thus these atoms wander according to a random walk process, some wandering back within r_c where they are subsequently captured, and the rest wandering off through the crystal. The interstitials which are thus liberated can eventually be captured by other vacancies. If we neglect capture at surfaces and dislocations, the liberated atoms will recombine by a bimolecular process. These two processes give rise to the N_L (L for liberation) and N_B (B for bimolecular) terms of the annealing expression:

$$N_L=\Sigma_2 N_i\frac{r_c}{r_i}\operatorname{erf}\left[\frac{r_i-r_c}{(2\langle b^2\rangle)^{\frac{1}{2}}}\left(\frac{\tau}{t}\right)^{\frac{1}{2}}\right],$$

$$N_B=\Sigma_2 N_i\left(1-\frac{r_c}{r_i}\right)\Big/\left[1+4\pi r_c^2\langle b\rangle\left(\frac{t}{\tau}\right)\Sigma_2 N_i\left(1-\frac{r_c}{r_i}\right)\right],$$

where r_i is the distance of the ith interstitial site from the vacancy, b is the magnitude of the change in this distance for each jump, the brackets $\langle\ \rangle$ indicate the average over all possible jumps, and Σ_2 is the summation over-all sites outside r_c. In order of time, N_M will vanish before N_L because $\tau_i<\tau$ and because the atoms in the N_L mechanism require many jumps of time τ before capture. N_L will vanish before N_B if r_c is less than the separation between adjacent vacancies, as it will be except with extremely heavy bombardments. By defining r_c we have assumed that there is a sharp division between the N_M and the N_L stages. Since actually there is a smooth transition between these stages, the given expression for the annealing is only approximately correct for those centers initially near r_c. The expression for N will be the same if vacancies are considered to jump instead of interstitials, τ now being the jump time of a vacancy.

It should be noted that the annealing time t appears only in the ratio, t/τ. By comparing the times at which the same degree of annealing occurs for different temperatures, the barrier energy can be determined without an actual fit of the theoretical expression to experimental data. The barrier energy, so determined, will be constant in the stages of the annealing governed by N_L and N_B, but will decrease with decreasing time (or temperature) in the stage governed by N_M. The actual fit yields additional information about the capture radius r_c an the initial distribution of interstitials N_i.

[1] G. L. Pearson and W. H. Brattain, Phys. Rev. **80**, 846 (1950).
[2] K. Lark-Horovitz, *Reading Conference Report* (Butterworths Publications, London, 1951), p. 59.

The Extra-Resistivity Owing to Vacancies in Copper

P. JONGENBURGER*
Technical University of Delft, Delft, Holland
(Received April 2, 1953)

THE scattering of the conduction electrons by vacancies in copper is calculated using the well-known method of Faxén and Holtsmark.[1] This is a rather elaborate method, as the radial differential equation must be integrated numerically to obtain the asymptotic phase shifts α_l for the electrons at the top of the Fermi-distribution; but it must be used, as the scattering field of a vacancy is too large for these slow electrons to permit the use of Born's approximation.

In order that the vacancy may be neutral after the removal of the Cu^+ ion, one free electron must be displaced from the vacancy; thus according to Friedel[2] the following relation between the phase shifts α_l must hold:

$$-(2/\pi)\,\Sigma_l(2l+1)\alpha_l=1.$$

We do not know very much about the scattering field of a vacancy. Therefore we shall take a suitable starting field and adjust its parameters until Friedel's equation holds.

We have done this for two different fields, but the results appear to be about the same.

(a) We suppose that the removal of an ion with its field is equivalent to adding a field of opposite sign. Therefore we take for the scattering field the negative of the field of a free Cu^+ ion, which can be found from Hartree and Hartree's[3] effective nuclear charge $Z_p(r)$. Of course, this cannot be absolutely correct, since in the metal the field will be somewhat deformed, but it is taken as a first approximation.

One free electron must be displaced from the vacancy, so that there is a spherical hole with radius r_s in the electron gas. The corresponding reduced effective nuclear charge Z_p' can be found by subtracting from Z_p the quantity z_p given by:

$$z_p=\tfrac{1}{2}r(3r_s^2-r^2)/r_s^3, \qquad r<r_s;$$
$$z_p=1, \qquad r\geq r_s.$$

$Z_p'=Z_p-z_p$ can be represented very well by $Z_p'=24e^{-2.5r}$ (note, that $24\neq Z_{Cu}$), and the scattering field by $V=(24/r)e^{-2.5r}$ in atomic units.

The phase shifts α_l, calculated by using this field, are

$$\alpha_0=-0.73, \qquad \alpha_1=-0.233, \qquad \alpha_2=-0.013.$$

Friedel's equation gives $-(2/\pi)\,\Sigma_l(2l+1)\alpha_l=0.95$; this is sufficiently good. The solution could be somewhat improved by calculating the new free electron distribution from the wave functions; this would give a better z_p and thus a better field, etc. However, in view of our rather crude assumptions, the small improvement which might result is not thought to be of significance.

The above values of α_l give an effective scattering area of 2.2A^2, and the extra-resistivity due to vacancies appears to be:

$$\rho_0=1.25\times10^{-6}\ \Omega\text{ cm per atomic percent vacancies.}$$

(b) Now we suppose the scattering field to be constant $=U_0$ for $0\leq r<r_s$ and zero for $r\geq r_s$. U_0 must be chosen of such magnitude, that the phase shifts α_l obey Friedel's equation. For $U_0=6.35$ ev we find:

$$\alpha_0=-0.796, \qquad \alpha_1=-0.229, \qquad \alpha_2=-0.028.$$

Friedel's equation gives $-(2/\pi)\,\Sigma_l(2l+1)\alpha_l=0.99$. The effective scattering area is 2.42A^2, and the extra-resistivity is given by:

$$\rho_0=1.35\times10^{-6}\ \Omega\text{ cm per atomic percent vacancies.}$$

We see that both fields give about the same result.

The relaxation of the lattice is estimated, using the ion-ion interaction $U=Be^{-r/\rho}$, and assuming that only nearest neighbors are displaced. Their shift is found to be about 1.5 percent of their distance. The influence of this displacement is roughly estimated by comparison with the temperature resistance, and is about 3 percent of the vacancy resistance; so it can be neglected.

Recently Dexter[4] has published his calculations on the scattering of electrons from point singularities in metals; his result ($\sim0.4\times10^{-6}$ Ω cm per atomic percent vacancies) is, however, much smaller than ours.

To summarize, the extra-resistivity due to vacancies in copper is calculated to be $\rho_0\approx1.3\times10^{-6}$ Ω cm per atomic percent vacancies, and is of the same order of magnitude as the extra-resistivity due to Ni in copper.

A detailed article will be published shortly in *Applied Science Research.*

This work was carried out at the Technical University of Delft, Holland. I am indebted to Professor R. Kronig for his valuable help, and to Professor M. J. Druyvesteyn for suggesting the problem.

* Now at Philips Research Laboratories, N. V. Philips' Gloeilampenfabrieken, Eindhoven, Netherlands.

[1] H. Faxén and J. Holtsmark, Z. Physik **45**, 307 (1927); see N. F. Mott and H. S. W. Massey, *Theory of Atomic Collisions* (Clarendon Press, Oxford, 1949), second edition, chap. II.

[2] J. Friedel, Phil. Mag. **43**, 153 (1952), form. 2, p. 157.

[3] D. R. Hartree and W. Hartree, Proc. Roy. Soc. (London) **A157**, 490 (1936).

[4] D. L. Dexter, Phys. Rev. **87**, 768 (1952).

Paramagnetic Resonance in Manganese Formate

D. J. E. Ingram
University of Southampton, Southampton, England
(Received March 31, 1953)

THE paramagnetic resonance spectra of two salts of manganese have been studied in detail by Bleaney and Ingram,[1] and an analysis of the five groups of six hyperfine structure lines made in terms of the electronic splitting and crystalline field symmetries. Measurements are reported here on the spectra obtained from crystals of diluted manganese formate, and are of interest in that the electronic splitting is considerably greater than usual, being twice that observed in any inorganic salt so far.

All the measurements were made at room temperature and at a wavelength of 1.25 cm, the magnetic field being calibrated by means of normal proton resonance methods, and a modulating sweep being used for detection and display. The crystals of $Zn(HCOO)_2 \cdot 2H_2O$ and $Mn(HCOO)_2 \cdot 2H_2O$ are both monoclinic prismatic with very nearly equal axial angle and ratio; $\beta = 97°19'$ and 97°38′, respectively.[2] The paramagnetic absorption spectra show that there are two ions per unit cell, as in the case of the Tutton salts.[1]

Rotation in the plane of crystallographic symmetry (i.e., xz plane), in which the spectra of the two ions coincide, showed that the electronic splitting remains small in all directions, indicating that the crystalline field axes of the two ions must lie near the y axis. A maximum occurs at an angle of $+7°$ to the z axis, and, in order to establish whether this direction was K_1 or K_2, the crystal was rotated in the two planes (a) through the y axis and $+7°$ to z, and (b) through the y axis and $+97°$ to z.

Rotation in the first plane gives an electronic splitting which has a maximum along the y axis, with a subsidiary one at right angles, and this shows that it is the K_2K_3 plane. Hence K_1 makes an angle of $+97°$ to z in the xz plane.

Rotation in the second plane (K_1K_3) gives two maxima, corresponding to the largest electronic splittings obtained in the crystal, at angles $\alpha = \pm 62°$ to K_1. This explains why the separation along K_1 is small, as the electronic splitting goes through a minimum at about 60° to the crystalline field axis.

The separations between the centers of the five groups along the three crystal axes, and the axis of the crystalline field of the Mn^{++} ion, are listed in Table I.

The hyperfine structure separation remains constant with a splitting of 98 gauss between successive lines. In analyzing the spectra the usual Hamiltonian,

$$\mathcal{H} = g\beta \mathbf{H} \cdot \mathbf{S} + D\{S_z^2 - \tfrac{1}{3}S(S+1)\} + E(S_x^2 - S_y^2) + F(a) + AS_zI_z + B(S_xI_x + S_yI_y),$$

is used, and from the expressions[1,2] for the separation between successive groups along the field axis, one obtains for the coefficients, in units of 10^{-4} cm^{-1}:

$$A = B = 91, \qquad D = 485, \qquad E = 110, \qquad a = 9.5.$$

The accuracies are to within 1 percent for A, B, and D, but since evaluation of E depends on second-order effects its accuracy is much smaller. E can also be estimated from the splitting obtained along different directions at right angles to the field axis. These vary from 1060 gauss to 2950 gauss, measured between the extreme groups, and give 85 ± 40 as a probable value of E.

TABLE I. Electronic splittings along different axes.

Direction	Separation of groups (gauss)			
x axis	280	290	285	280
y axis	860	630	650	475
z axis	355	420	480	480
Field axis	1105	1020	1010	1065

The g value was determined by means of a free-radical marker and, allowing for the second-order corrections, was evaluated as $g = 1.999 \pm 0.0015$.

It is of interest to compare these results with those obtained from other manganese results,[1,3-5] as is shown in Table II.

TABLE II. Comparison of splittings in different salts. The coefficients are given in units of 10^{-4} cm^{-1}.

Salt	D	A	a	E	Reference
$Mn(COOH)_2 \cdot 2H_2O$	485	91	9.5	110	—
$Mn(CH_3COOH)_2 \cdot 4H_2O$	412	87	8	56	4
$Mn(NH_4)_2(SO_4)_2 \cdot 6H_2O$	243	91	5	100	1
$Mn(NO_3) \cdot 2Bi(NO_3)_2 \cdot 24H_2O$	80 64	90 88	10 10	—	5
$Mn(CH_3COOH)_2 \cdot 3H_2O$	252	—	—	27	3
$MnSiF_6 \cdot 6H_2O$	197	96	7	—	1

The first four salts all have two ions per unit cell, and it is seen that D decreases as the number of waters of crystallization increases; as is also the case for the last two, which have only one ion per unit cell.

This confirms the fact that the symmetry of the crystalline field round the paramagnetic ion is probably mainly due to the water molecules in all the salts investigated.

[1] B. Bleaney and D. J. E. Ingram, Proc. Roy. Soc. (London) **A205**, 336 (1951).

[2] P. Groth, *Chemische Krystallographie* (Leipzig, 1910), Vol. 3, p. 18.

[3] Kumagai, Ono, Hoyahi, and Kambe, Phys. Rev. **87**, 374 (1952).

[4] D. J. E. Ingram, Proc. Phys. Soc. (London) **A66**, 412 (1953).

[5] R. S. Trenam, Proc. Phys. Soc. (London) **A66**, 118 (1953).

An Excitation Curve for Photomesons from Beryllium*

David Luckey†
Newman Laboratory of Nuclear Studies, Cornell University, Ithaca, New York
(Received March 25, 1953)

THE yields of 54-Mev π^- and π^+ mesons at 90° were obtained as a function of the maximum energy of the Cornell synchrotron. A double-focusing magnet deflects the mesons through 90° into a proportional counter telescope. The solid angle and energy resolution of the magnet were determined by means of a current-carrying wire. The full width at half-maximum was 25 Mev. The angular aperture was $\pm 7°$ horizontally and $\pm 3.5°$ vertically. Agreement was found with the strong energy dependence of the π^-/π^+ ratio observed by Littauer and Walker at 135°.[1] The following ratios were obtained.

Maximum gamma-ray energy (Mev)	310	275	250	225
Ratio π^-/π^+	1.65 ± 0.05	2.0 ± 0.1	2.4 ± 0.3	3.3 ± 0.5

The maximum energy of the bremsstrahlen was varied by turning off the accelerating rf at the appropriate part of the magnetic cycle. The beam was monitored by an ionization chamber behind 1 inch of copper. The response of the chamber is nearly proportional to the total energy in the gamma-ray beam in the region from 200- to 300-Mev maximum energy.[2] By the subtraction of the yields normalized to the same number of "equivalent quanta"

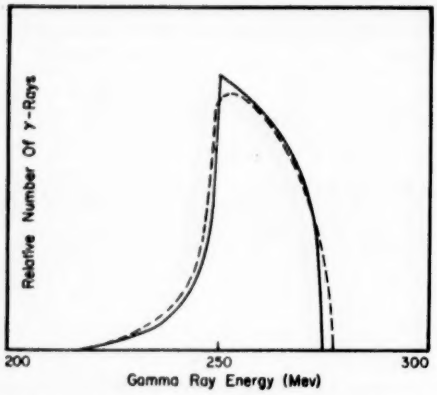

FIG. 1. Difference spectrum resulting from subtraction of 275- and 250-Mev spectra. Dotted curve shows approximate spectrum due to the experimentally used spectra.

one can obtain the yield due to "monochromatic" gamma-rays. Figure 1 shows a typical difference spectrum resulting from the subtraction of two bremsstrahlen spectra of different maximum energy. Because the beam was slightly spread out in time to reduce background, there was a slight spread in the maximum energy of the beam. This introduces more spread to the difference spectrum. It was assumed that all the meson production from the 225-Mev maximum gamma-rays was due to the band of gamma rays between 200 and 225 Mev. A run at lower energy yielded no mesons within the statistics. Figure 2 shows the cross sections for

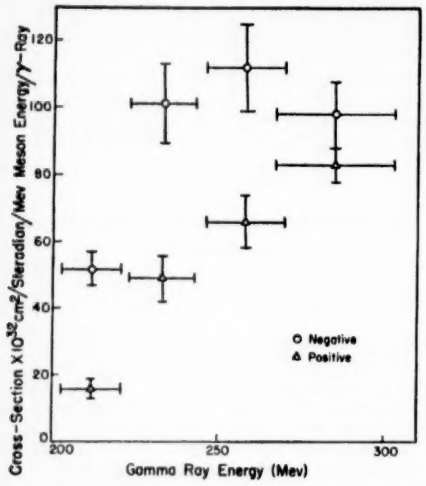

FIG. 2. Cross sections for production of 54-Mev π^- and π^+ mesons from beryllium *vs* γ-ray energy.

the production of 54-Mev charged mesons *vs* gamma-ray energy. The errors indicated are those due to counting statistics. Other systematic errors may have occurred due to errors in determination of the maximum energies.

The results of the experiment are consistent with the following interpretation: the difference in positive and negative production is due mainly to the "extra loosely bound" neutron of Be^9. Figure 3 shows the production due to the extra neutron. It was assumed that neutrons in the core are 1.0 times as efficient as protons in the core (from the plus-minus ratio of carbon). The solid curve is the approximate shape expected if the neutron were free and had a

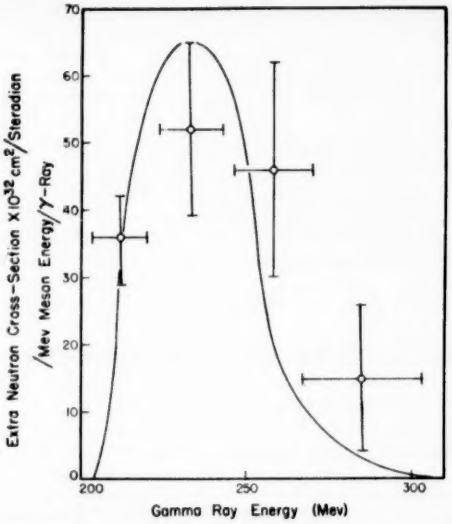

FIG. 3. Extra-neutron of beryllium cross section *vs* γ-ray energy.

cross section equal to the free proton cross section. The width of the free particle curve is mainly due to the resolving power of the magnet and the asymmetry on the high energy side to the long low energy tail of the difference spectra. For a bound neutron, one would expect the width to be increased because of the momentum distribution. Hence the extra neutron acts approximately as if it were free, in agreement with other experiments[3] and with what one would expect from shell structure theory and the small binding energy of the extra neutron.

The author wishes to thank Thomas Palfrey, Thomas Jenkins, and Professor R. R. Wilson.

* Supported by the U. S. Office of Naval Research.
† General Electric Fellow.
[1] R. M. Littauer and D. Walker, Phys. Rev. **86**, 846 (1952).
[2] J. DeWire and A. Perry (private communication).
[3] J. C. Keck and R. Littauer have studied the photomeson production from the extra neutron by requiring a correlated proton in coincidence with the meson (private communication).

Differential Cross Section for Elastic *p-p* Scattering at 435 Mev*

W. E. MOTT, R. B. SUTTON, J. G. FOX, AND J. A. KANE
Carnegie Institute of Technology, Pittsburgh, Pennsylvania
(Received March 23, 1953)

THE differential scattering cross section for elastic collisions of high energy protons with protons as a function of the angle of scattering in the center-of-mass system has been measured using the external beam of the Carnegie Institute of Technology synchrocyclotron.

Figure 1 gives a general picture of the cyclotron, deflecting magnet, collimators, the path of the particles in the external beam, and the scattering arrangement, including target, counters, and ionization chamber.

The protons which emerge from the cyclotron without the aid of deflecting mechanisms have an intensity 10 meters from the machine of the order of 2×10^5 cm^{-2} sec^{-1}. The beam was monitored by integrating the current of an argon-filled ionization chamber similar to the one described by Chamberlain, Segrè, and Wiegand.[1] A knowledge of the energy loss per proton per cm of argon[2] and the energy necessary to produce one ion pair in this gas[3] made an absolute calibration of the monitoring device possible. A nuclear emulsion technique is now being investigated as

an alternate, and perhaps more accurate, method of calibrating the chamber. Absorption and time of flight measurements have indicated that the proton energy is approximately 435 Mev.

The scattered and recoil protons were detected simultaneously in scintillation counters (*trans*-stilbene crystals viewed by 5819 photomultipliers). The associated coincidence circuit had a resolving time of 2×10^{-9} sec.

Foils of polyethylene varying in weight from 643 to 110 mg/cm² were used as targets. The cross sections were obtained by taking polyethylene-carbon differences, where each polyethylene target was matched with a carbon target of equal stopping power. The effect from hydrogen has been calculated using the formula

$$H=(CH_2-b)-z(C-b),$$

where CH_2, C, and b are the number of coincidence counts obtained when using a polyethylene target, a carbon target, and no target; and z is the ratio of the carbon surface density of the polyethylene target to the surface density of the carbon target. In each case the counts were recorded for a given integrated beam. This method of subtracting the carbon has been checked by comparing cross sections taken under different conditions of beam intensity and target thickness. In all cases the cross sections have agreed to within the counting statistics.

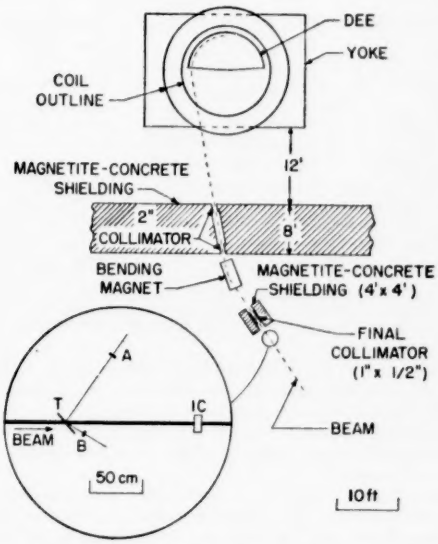

FIG. 1. Diagram of the cyclotron, bending magnet, collimators and scattering area. The inset shows the target, T; defining counter, A; monitoring counter, B; argon ionization chamber, IC.

Previously[4] the ratios of the cross sections were reported for the scattering angles of 90°, 65.3°, and 36.4° in the center-of-mass system. Measurements have now been improved and extended to include the angle at 25.2°. The results indicate a definite deviation from isotropy in contrast to the investigations[1,5-7] in the energy range 100–345 Mev which suggested an isotropic cross section over the same angular region.

TABLE I. Differential scattering cross section $\sigma(\theta)$ in center-of-mass coordinate system in 10^{-27} cm²/sterad. Errors indicated are standard deviations from counting statistics only.

θ	$\sigma(\theta)$	$\sigma(\theta)/\sigma(\theta=90°)$
25.2°	4.49±0.25	1.32
36.4°	4.16±0.14	1.23
65.3°	3.59±0.10	1.06
90°	3.39±0.10	1

Table I gives the differential scattering cross section $\sigma(\theta)$ at the center-of-mass angle θ, and the ratios of $\sigma(\theta)/\sigma(\theta=90°)$.

The errors quoted in Table I are standard deviations due to counting statistics only. To obtain the uncertainty in the cross section an error due to other factors, estimated to be 8 percent for the point at $\theta=25.2°$ and 6 percent for the other points, should be superimposed on the errors in the table. A 6 percent error is assigned to the values of $\sigma(\theta)/\sigma(\theta=90°)$.

Complete details of the experiment and additional results will follow with the completion of small angle measurements.

* Supported in part by the U. S. Atomic Energy Commission.

[1] Chamberlain, Segrè, and Wiegand, Phys. Rev. **83**, 923 (1951).
[2] Aron, Hoffman, and Williams, U. S. Atomic Energy Commission Report AECU-663 (unpublished).
[3] C. J. Bakker and E. Segrè, Phys. Rev. **81**, 489 (1951).
[4] W. E. Mott and R. B. Sutton, Bull. Am. Phys. Soc. **28**, No. 10 (1953).
[5] C. L. Oxley and R. D. Schamberger, Phys. Rev. **85**, 416 (1952); O. A. Towler, Phys. Rev. **84**, 1262 (1951).
[6] Birge, Kruse, and Ramsey, Phys. Rev. **83**, 274 (1951).
[7] Cassels, Pickavance, and Stafford, Proc. Roy. Soc. (London) **214**, 262 (1952).

Constancy of Cosmic-Ray Flux over the Past 30 000 Years*†

J. LAURENCE KULP AND HERBERT L. VOLCHOK
Lamont Geological Observatory, Columbia University, Palisades, New York
(Received March 27, 1953)

THE carbon-14 method of age determination[1] which has been used to date archeological and geological samples[1-3] is based on two major assumptions. (1) The integrated cosmic-ray flux is constant. (2) The C^{14} atoms produced in the upper atmosphere by the $N^{14}(n,p)C^{14}$ reaction are rapidly mixed into the carbon reservoir of the atmosphere, biosphere, and hydrosphere. The time scale for these assumptions is on the order of centuries since the average life of C^{14} atoms is approximately 8000 years, and the present maximum C^{14} dating accuracy is ±100 years.

The second assumption has been verified by the observation that the concentration of C^{14} in living organisms at widely different latitudes and in the carbon dioxide of the air at various locations and altitudes is essentially constant. The first assumption has been verified for the period of written history by showing that the carbon-14 ages on archeological specimens are correct. Since this agreement was established for the last 4000 years, and since the

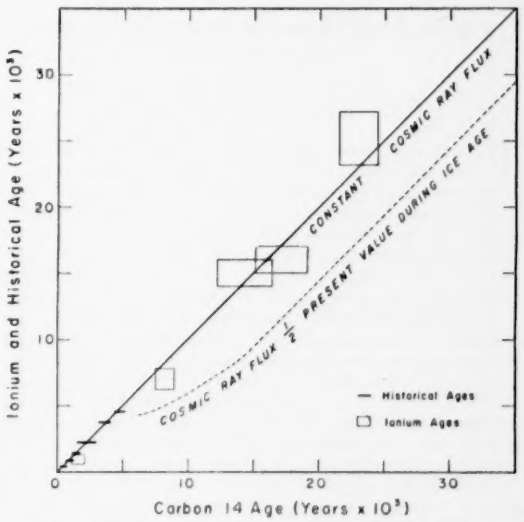

FIG. 1. Correlation of carbon-14 age of various samples with age determined by written history or the ionium method.

carbon-14 atoms now found in modern wood are 8000 years old on the average, the integrated cosmic-ray flux seems to have been essentially constant for the last 12 000 years.

Unfortunately this takes us back only to the end of the last great glacial period. A method was devised to show constancy from the present back to about the maximum of the last phase of the Wisconsin glaciation (estimated at 30 000–40 000 years ago). This span of recent earth history displays about one-half of the greatest mean annual temperature fluctuation since the Cambrian period (500 000 000 years ago). Thus if the cosmic-ray flux was constant in this interval, and if it is related in any way to the total energy received by the planet, the integrated cosmic-ray flux would appear to have remained constant over most of geologic time.

An attempt was made to determine the possible variation in the cosmic-ray flux by dating layers of mud in a deep sea core by both the carbon-14 and ionium[4] ($_{90}Th^{230}$) methods. For the ionium ages, the radium concentration in homogeneous cores as a function of depth was obtained. For the carbon-14 ages, the carbon in the precipitated calcium carbonate of the same core was used.

Figure 1 shows the results of both methods obtained for several of these deep sea core samples as well as some of the carbon-14 ages on specimens whose age could be determined by written history. The errors are indicated by the size of the box or, in the case of the historical samples, by the length of the line. Although these errors are rather large, it seems certain that the cosmic-ray flux has not varied by more than 10–20 percent over the last 35 000 years. A hypothetical curve shows the relation if the cosmic-ray flux was half of its present value during the ice age. The errors in the carbon-14 ages are large because the samples were very small. Additional cores of much larger diameter will be taken next summer on one of the scientific cruises under the direction of Professor Maurice Ewing. This should make it possible to reduce considerably the probable error of these measurements.

The assistance of B. J. Eckelmann, S. O. Harris, and W. A. Snell with the carbon-14 measurements is greatly appreciated.

* Lamont Geological Observatory Contribution No. 81.
† This work resulted from projects supported by the National Science Foundation and the U. S. Office of Naval Research.
[1] W. F. Libby, *Radiocarbon Dating* (University of Chicago Press, Chicago, 1952).
[2] Kulp, Feely, and Tryon, Science **114**, 565–568 (1951).
[3] Kulp, Tryon, Eckelmann, and Snell, Science **116**, 409–414 (1952).
[4] C. S. Piggot and W. D. Urry, Bull. Geol. Soc. Am. **53**, 1187– 0 (1942)

Angular Distributions of Elastically Scattered 1-Mev Neutrons*

M. Walt† and H. H. Barschall
University of Wisconsin, Madison, Wisconsin
(Received March 30, 1953)

FESHBACH, Porter, and Weisskopf[1] have accounted for the observed regular variations of total fast neutron cross sections with energy and atomic weight[2] by using a model in which nuclear matter is assigned a fixed refractive index and absorption coefficient. Since this theory should also predict angular distributions of elastically scattered neutrons, differential cross sections for the elastic scattering of 1-Mev neutrons were measured for several elements in order to obtain a further check on the theory.

1-Mev neutrons with an energy spread of about 100 kev were produced by bombarding a Li target with protons from an electrostatic accelerator. In order to distinguish between elastically and inelastically scattered neutrons a biased recoil counter was used as a detector. It was operated at two biases, one to give a threshold of about 750 kev, the other about 850 kev. After correction for energy loss of the neutrons in elastic collisions, results obtained at the two biases showed no significant differences. It was, therefore, assumed that only elastically scattered neutrons were detected. Differential cross sections were measured at 15° intervals from 30° to 150° scattering angles with an angular resolution of about 15°.

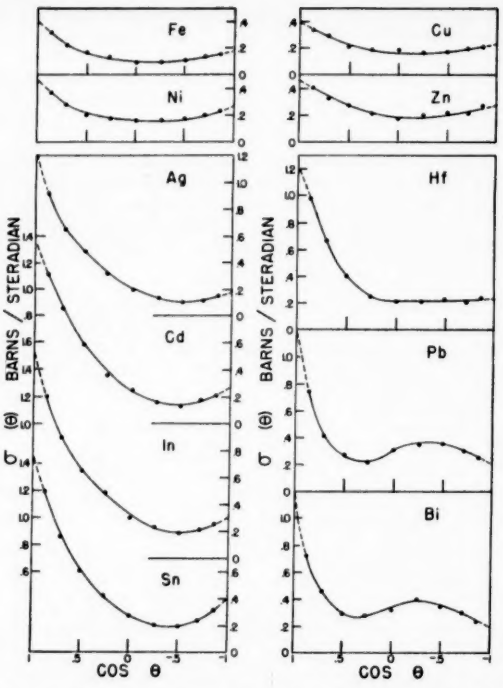

FIG. 1. Differential cross sections for the elastic scattering of 1-Mev neutrons as a function of the cosine of the scattering angle in the laboratory system. The data are still subject to a correction for multiple scattering.

The results of the measurements are shown in Fig. 1. It may be noted that the angular distributions of neutrons scattered by neighboring elements are similar, while the angular distributions for elements in different parts of the periodic table have varying characteristic shapes. Such a behavior might be expected on the basis of Weisskopf's theory.

Since the scattering samples had thicknesses comparable to a mean free path, the data have to be corrected for the attenuation of the primary neutron beam in the sample, and for multiple scattering. The cross sections shown in Fig. 1 have been corrected for the attenuation of the primary neutrons in the sample but not for multiple scattering. A calculation of the multiple scattering effect is in progress and will tend to increase both the anisotropy and the areas under the curves.

The difference between the total cross section and the integral over all angles of the elastic scattering cross section is the inelastic collision cross section. Preliminary values of these cross sections are shown in Table I. In the last column tentative values of the

TABLE I. Preliminary values (in barns) of elastic and inelastic collision cross sections for 1-Mev neutrons.

Element	Total cross section	Area under curves in Fig. 1	Difference between two preceding columns	Estimate of inelastic collision cross section
Fe	2.5	2.0	0.5	0.4
Ni	2.9	2.8	0.1	0.1
Cu	3.2	2.9	0.3	0.3
Zn	3.6	3.3	0.3	0.3
Ag	6.6	4.2	2.4	2.1
Cd	6.9	5.2	1.7	1.4
In	6.7	6.1	0.6	0.4
Sn	6.8	6.0	0.8	0.7
Hf	7.2	4.7	2.5	2.1
Pb	4.9	4.6	0.3	0.3
Bi	4.9	4.8	0.1	0.1

inelastic collision cross sections are given, based on an estimate of the effect of multiple scattering. The accuracy of the integrated elastic cross sections shown in the third column is about fifteen percent apart from the effects of multiple scattering. The estimate of the inelastic collision cross section is, therefore, uncertain by at least fifteen percent of the values given in the third column.

The observed angular distributions are in qualitative agreement with results obtained with pile neutrons.[3]

Measurements on other elements are in progress, and final results will be reported after the calculations of the corrections are completed.

* Work supported by the U. S. Atomic Energy Commission and the Wisconsin Alumni Research Foundation.
† U. S. Atomic Energy Commission Predoctoral Fellow.
[1] Feshbach, Porter, and Weisskopf, Phys. Rev. **87**, 188 (1952) and private communication.
[2] H. H. Barschall, Phys. Rev. **86**, 431 (1952).
[3] E. T. Jurney and C. W. Zabel, Phys. Rev. **86**, 594 (1952).

The Elastic Scattering of Pions in Deuterium*

K. A. Brueckner
Indiana University, Bloomington, Indiana
(Received April 2, 1953)

RECENT experiments by Arase, Goldhaber, and Goldhaber[1] on the elastic scattering of pions in deuterium have shown a considerable discrepancy with the results of a straightforward application[2] of the impulse approximation[3] to the problem. It is the purpose of this note to show that inclusion of the effects of the multiple scattering of the mesons by the two nucleons in the deuteron leads to a considerable improvement of the agreement of experiment with theory. The method used has been developed in a recent paper[4] (to be referred to as I) by the author and there applied to the evaluation of the total cross section. The results obtained can be easily extended to the determination of the elastic cross section.

The approximations made in I were (a) the usual impulse approximation[3] of neglecting both the binding effects in the deuteron on the scattering matrices and the off-the-energy-shell dependence of the scattering matrices; (b) the adiabatic approximation for the treatment of the nucleon motion, i.e., treating the nucleons as very heavy.[5] It was not necessary, however, to make the additional approximation of neglecting the rescattering of the outgoing meson waves from one nucleon by the other nucleon in the deuteron. The coupled algebraic equations obtained could be solved exactly by straightforward methods to give the cross sections. The result for the total cross section for π^+ mesons on deuterons was

$$\sigma_{\text{total}}=4\pi\lambda\,\text{Im}\int f_R(0)\,|\psi_D(R)|^2 d\mathbf{R}. \tag{1}$$

The elastic cross section is given by[6]

$$\frac{d\sigma_{\text{elastic}}}{d\Omega}=\left|\int f_R(\theta)\,|\psi_D(R)|^2 d\mathbf{R}\right|^2. \tag{2}$$

In both of these results $f_R(\theta)$ is the scattered amplitude into the isotopic spin singlet state with the two nucleons at a separation R. In I, $f_R(\theta)$ was evaluated for P-wave scattering with isotopic spin dependence; for scattering in the isotopic spin state 3/2 state alone, which is a quite good approximation to the experimental results for scattering on free nucleons,[7] $f_R(\theta)$ is given by

$$f_R(\theta)=\frac{2b\lambda}{1-b^2f^2}\Big\{\cos\theta\big[e^{i(\mathbf{k}_0-\mathbf{k})\cdot\frac{1}{2}\mathbf{r}}+e^{i(\mathbf{k}_0+\mathbf{k})\cdot\frac{1}{2}\mathbf{r}}\big]$$
$$+\frac{(\mathbf{k}\cdot\mathbf{R})(\mathbf{k}_0\cdot\mathbf{R})}{R^2}\lambda^2bg\big[b(f+h)e^{i(\mathbf{k}_0-\mathbf{k})\cdot\frac{1}{2}\mathbf{r}}-(1+b^2fh)e^{i(\mathbf{k}_0+\mathbf{k})\cdot\frac{1}{2}\mathbf{r}}\big]\Big\}$$
$$+\text{a term in which }\mathbf{R}\text{ is replaced by }-\mathbf{R}, \tag{3}$$

where $b=e^{i\delta}\sin\delta$, $f=(1/x)(d/x)(e^{ix}/x)$, $g=xdf/dx$, $h=f+g$, and $x=R/\lambda$. The neglect of multiple scattering is equivalent to the retention of terms linear in b only.

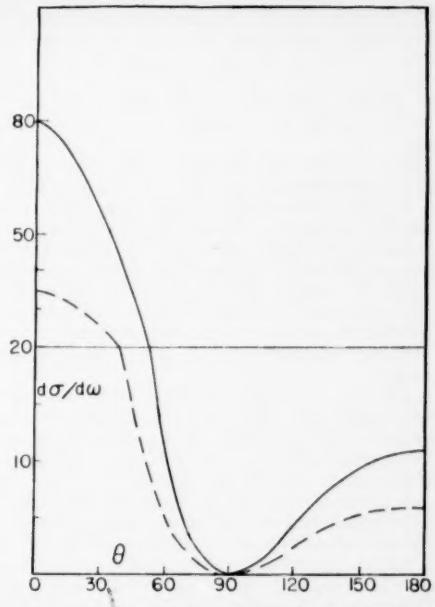

FIG. 1. Elastic P-wave scattering of pions by deuterons at 140 Mev for a phase shift of 45°. The solid curve gives the impulse approximation neglecting multiple scattering; the dashed curve includes the effects of multiple scattering. The curves are in the center-of-mass system for the meson and one nucleon. Note the change in scale at $d\sigma/d\omega=20$ mb/steradian.

The differential cross sections calculated from Eqs. (2) and (3) are given in Figs. 1 and 2, together with the result obtained if the multiple scattering is neglected. In evaluating the integrals over the deuteron wave function, the Hulthén wave function has been used. The cases given are for phase shifts of 45 degrees at 140

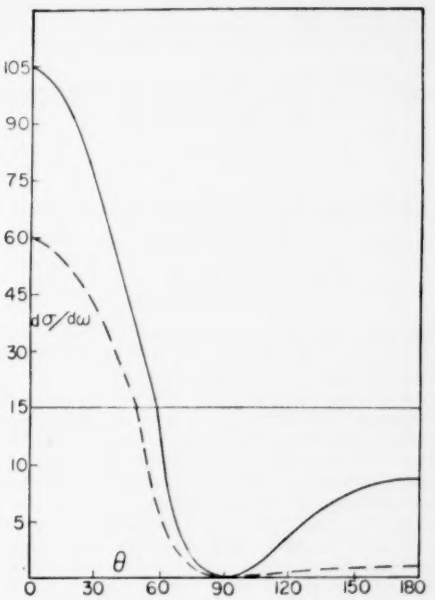

FIG. 2. Elastic scattering at 200 Mev for a phase shift of 90°. The notation is the same as in Fig. 1. Note the change in scale at $d\sigma/d\omega=15$ mb/steradian.

Mev and 90 degrees at 200 Mev; the former gives approximately the correct total cross sections for π^+, π^-, and charge exchange scattering, and roughly the correct angular distribution for π^+ scattering on protons. The actual scattering is of course spin dependent and also includes strong even wave interference so that these results can serve only to illustrate the effects of the multiple scattering.

It is clear from Figs. 1 and 2 that a very marked departure from the impulse approximation results if multiple scattering is included. This is particularly apparent for phase shifts as large as 90 degrees for which the backward elastic scattering is almost entirely eliminated. These results reflect the strong depression of the scattering which sets in when the two scatterers are at distances less than roughly twice the scattering length, the effect when the phase shifts are large being particularly marked for large momentum transfers (large angle scatterings) where the small distance contributions to the cross section are especially important.

It is possible to conclude from these results that the elastic scattering is probably considerably overestimated by the usual impulse approximation and that the angular distribution is also given incorrectly when the phase shifts are large, with strong interference effects reducing the backward scattering. Both of these conclusions are in qualitative agreement with experiment.[1] It is quite possible that the cross sections may be further altered by additional effects such as scatterings which do not conserve energy and the nonadiabatic motion of the nucleons. The correct treatment of these, however, is quite difficult since coupled integral equations are encountered[5] and in addition knowledge of the scattering matrices off the energy shell is required. It is expected that a more detailed treatment of these points will be contained in future papers.

The author is indebted to Dr. Arase, Dr. G. Goldhaber, and Dr. S. Goldhaber for information on their experimental results in advance of publication and to Dr. T. Green for information on his theoretical interpretation.

* This work was supported by a grant from the National Science Foundation.

[1] Arase, Goldhaber, and Goldhaber, Phys. Rev. **90**, 160 (1953).
[2] Fernbach, Green, and Watson, Phys. Rev. **82**, 980 (1951).
[3] G. F. Chew, Phys. Rev. **80**, 196 (1950); G. F. Chew and G. C. Wick, Phys. Rev. **85**, 636 (1952).
[4] K. A. Brueckner, Phys. Rev. **89**, 834 (1953).
[5] The validity of this approximation is discussed in some detail in reference 2.
[6] Compare, for example, reference 2.
[7] Anderson, Fermi, Nagle, and Yodh, Phys. Rev. **86**, 793 (1952).
[8] A related problem is discussed in the Appendix of the article by K. A. Brueckner and K. M. Watson, Phys. Rev. **90**, 699 (1953).

High Energy Nuclear Interactions in Lead and Light Elements*

M. F. KAPLON, D. M. RITSON, AND W. D. WALKER
University of Rochester, Rochester, New York
(Received April 3, 1953)

IN order to extend previous measurements[1] on nuclear interactions in the energy region 10^{12}–10^{14} ev, an emulsion cloud chamber consisting of a "block" of emulsion 6 in.×4 in.×2 in. placed on top of an emulsion cloud chamber of 25 alternate 3-mm lead plates and 250-micron G-5 emulsion was flown for six hours at White Sands. The "block" of emulsion consisted of 92 G-5 stripped emulsions, 6 in.×4 in.×400μ, which were separated after flight and processed by the NRL technique[2] (emulsions attached to glass backing prior to development).

Figure 1 shows the results for interactions observed starting in the lead. The multiplicity observed on the plate directly below the lead absorber in which the interaction occurred is plotted against the distance back to the point of interaction. The line of the graph which appears to represent the data is calculated assuming an initial production of 20 charged particles and ten neutral π mesons decaying into two photons with a laboratory lifetime less

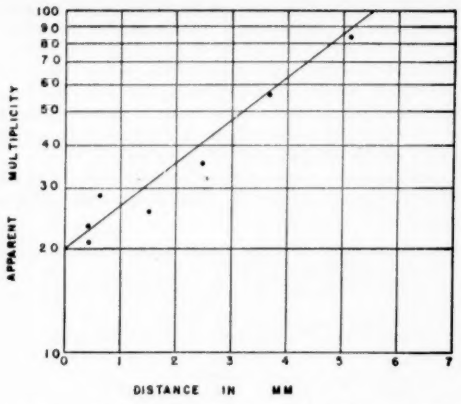

FIG. 1. Apparent multiplicity of showers vs distance in lead.

than 3×10^{-12} sec.[3] (For 3×10^{-12} sec, the mean decay distance of 0.9 mm is short compared to the radiation conversion length in lead.) The calculated line seems to fit the data well and accordingly in the majority of showers the initial multiplicity of charged particles would appear to be about 20. The median energy of this group of interactions was about 2×10^{12} ev as estimated from the median angle of the shower particles.

Seven primary interactions were found in emulsion. Table I[9,10] gives the value of N_s, the number of minimum ionizing particles, and N_h, the number of gray plus black prongs, occurring in the interaction. The median energy for this group was $\sim10^{13}$ ev. The multiplicity appears to be independent of N_h with an average value of about 16. If the interaction cross section for primaries of these energies is geometric, approximately half the collisions in emulsion would occur in Ag or Br and the rest in C, N, O, and H. Though the division of interactions on the basis of the number of star prongs is not certain, it seems likely that the cases with $N_h=0$ occur in light elements, and the case with $N_h=15$ must have arisen from an interaction in an Ag or Br nucleus. If the dividing line between the light and heavy elements is taken to be $N_h\approx4$ or 5, then our data are consistent with half the interactions occurring in light elements and half in heavy elements. It is seen that the mean number of shower particles for interactions with $N_h<4$ and $N_h>4$ is 16 for both cases.

If we now utilize previous results[1] and correct for the differences in median energies on the assumption that the multiplicity varies as $E^{\frac{1}{4}}$, we can compare multiplicities of shower particles in various elements for primary energies of $\sim5\times10^{12}$ ev. For lead the multiplicity is ~24, brass~18, Ag and Br~14, and light elements~14. It would appear that the multiplicity in this energy region is almost independent of the target nucleus. There have been cases found in which the multiplicity of shower particles is much higher than those considered above.[4]

TABLE I. High energy stars in emulsion.

No. of evaporation prongs N_h	No. of shower particles N_s
0	10
0	16
2	19
4	12
6	15
15	16
1	15[a]
7	18[b]
Secondary interaction	
1	15

[a] See reference 9.
[b] See reference 10.

Our observations can be explained by a theory in which the particles are produced multiply in the initial interaction.[8] The multiplicity apparently does not seem to increase by a large factor through subsequent interactions inside the target nucleus; this is probably because the shower particles do not interact individually inside the nucleus because of their extreme collimation.[1,6,7] The fluctuations from the average behavior as noted above could be the result of large fluctuations in the angular distribution of the shower particles. A few shower particles of the first or possibly the second generation projected at angles considerably greater than the average could be effective in starting independent cascades inside the nucleus, which could increase the observed multiplicity by a considerable factor.

We have also noted the occurrence of both high and low energy pairs of charged particles produced by neutral radiation, in observing the passage of the high energy showers through the block of stripped emulsions. The most reasonable assumption is that these pairs are electron-positron pairs produced by photons; though our statistics are too low to draw any definite conclusion, the contribution of bremsstrahlung according to Schiff's theory[9] seems to be too low to account for the low energy pairs.

We are indebted to the Aero Medical Field Laboratory, Holloman Air Force Base for their cooperation in obtaining successful balloon flights. We wish to thank Miss Barbara Hull and Miss Katherine Merry for their assistance in scanning the plates.

* This research has been supported in part by funds from the Department of the Air Force.

[1] M. F. Kaplon and D. M. Ritson, Phys. Rev. **88**, 386 (1952).
[2] Stiller, Shapiro, and O'Dell, Phys. Rev. **85**, 712 (1952).
[3] A lifetime of 3×10^{-13} sec in the laboratory system corresponds approximately to a mean life of $\sim10^{-15}$ sec in the rest system of the π^0 meson.
[4] Daniel, Davies, Mulvey, and Perkins, Phil. Mag. **43**, 753 (1952). Recently in this laboratory a proton induced star of about sixty shower particles has also been observed.
[5] E. Fermi, Phys. Rev. **81**, 683 (1951).
[6] U. Haber Schaim, Phys. Rev. **84**, 1199 (1951).
[7] F. C. Roesler and C. B. A. McCusker, Nuovo cimento **10**, 127 (1953).
[8] L. Schiff, Phys. Rev. **76**, 89 (1949).
[9] This case was obtained by Lord, Fainberg, and Schein, Phys. Rev. **80**, 972 (1950).
[10] A. Gerosa and P. Levisetti, Nuovo cimento **8**, 601 (1951).

Nonuniform Track Shrinkage in Nuclear Emulsions*

JOHN R. HORAN
American Cyanamid Company, Atomic Energy Division, Idaho Falls, Idaho
(Received February 20, 1953)

SEVERAL Eastman NTA and NTB nuclear track plates have been exposed to monoenergetic alpha-particles from Po^{210} plated silver foils, and a study has been made of the resulting alpha-tracks as a function of the angle of incidence.

Observation of the tabulated data indicated that the average track length increased as a function of the dip angle θ. Experiments by Rotblat and Tai[1] with lithium-loaded emulsions showed that shrinkage was uniform at all depths of the emulsion. Also the shrinkage factor for alpha-tracks was a function of both the gelatin content and the dip angle. They concluded that the shrinkage factor remained fairly constant with angles of dip up to 25–30°. Roberts,[2] in studying $n-\alpha$ reactions, measured tracks with values of θ up to 40° and found that resolution was considerably improved by limiting θ to $\leq 20°$.

Figure 1 is a plot of the average track range in microns *versus* the angle of dip in the processed emulsions. The empirically determined shrinkage factor 2.7 ± 0.3 was used in these calculations. Both NTA and NTB plates show substantially the same results with the average range of the particles continuing to increase with increasing angles of dip. Extrapolation of the curve to zero yields the range of the alpha particles without shrinkage error. This value, 21.3μ, agrees within experimental error with Steigert's[3] empirical value of 21.2μ as well as his theoretical value of 21.3μ for NTA plates.

Thus, the usual method of correcting for emulsion shrinkage by multiplying the vertical track projection by the shrinkage factor should be restricted to angles of dip less than 6° for heavily ionizing particles if the error of measurement is to be less than 2 percent.

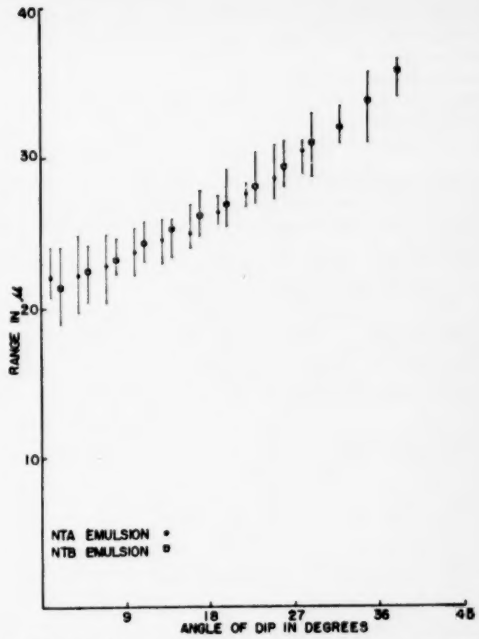

FIG. 1. Average alpha-track range *vs* angle of dip in processed emulsions.

The final criterion for selection was that each alpha track should lie entirely within the depth of focus of the microscope which was approximately 0.5μ, which is equivalent to a variation of less than 2° in the angle of dip. The maximum error introduced by measuring only the horizontal component, with the above limitation, is 0.1μ. This modified procedure resulted in histograms having a maximum dispersion of 5μ and a half-width at half-maximum of 0.5μ.

* Work performed at the Oak Ridge Institute of Nuclear Studies, Oak Ridge, Tennessee.
[1] J. Rotblat and C. T. Tai, Nature **164**, 835 (1949).
[2] J. H. Roberts, U. S. Atomic Energy Commission Report AECU-1381, 1950 (unpublished).
[3] Steigert, Toops, and Sampson, Phys. Rev. **83**, 474 (1951).

Rotational States in Even-Even Nuclei

AAGE BOHR AND BEN R. MOTTELSON*
Institute for Theoretical Physics, Copenhagen, Denmark
(Received March 24, 1953)

IN a recent note,[1] an interpretation of the short-lived $E2$ isomers has been suggested in terms of rotational states of the deformed nucleus. Empirical evidence is rapidly accumulating on the low energy spectra of even-even nuclei;[2-4] the purpose of the present note is to call attention to the extensive support which exists in these data for the above interpretation, and to suggest its usefulness in the analysis of decay schemes.

In the model describing the nucleus in terms of the coupled particle motion and surface oscillations, low-lying rotational states are associated with the large deformations expected in regions with many particles outside of closed shells. In such regions, the rotational spectrum is expected to be given rather accurately by the simple expression[1]

$$E_I=\frac{\hbar^2}{2\mathcal{I}}I(I+1), \quad I=0,2,4,6, \quad \text{even parity} \tag{1}$$

where the moment of inertia $\mathcal{I}$ is proportional to the square of the deformation. The relative order of magnitude of the deviations from this formula is rotational energy divided by the potential energy of the deformed surface.[5] Typical among the correction terms is the vibration-rotation interaction, which contributes a term of the form

$$\Delta E_I = -\text{const}\, I^2(I+1)^2, \qquad (2)$$

well known from molecular spectra. In the vicinity of closed shells, such correction terms may essentially modify the spectrum, and a more detailed treatment of the coupled particle surface system is required.

The following points summarize some of the relevant evidence on the excited states of even-even nuclei.

I. Energy trends of first excited states.—Figure 1 shows the excitation energies[6] in the region of the rather heavy elements, which is dominated by the doubly closed shell at $Z=82$ and $N=126$. The evidence is consistent with a (2+) assignment for all the states in the figure.[4] The decreasing energy as we move

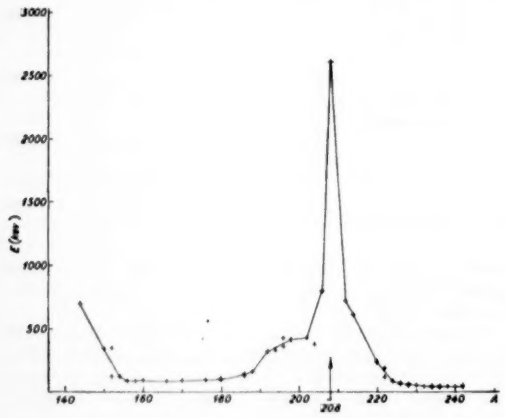

FIG. 1. First excited state in even-even nuclei with $A>140$. The data are taken from references 3 and 4. The reported 374-kev state in Pb^{204} falls somewhat off the regular curve. [A. H. Wapstra, Physica **18**, 799 (1952).] It may be of a different type from the rest, as is also indicated by its excessively long comparative half-life. (See Wapstra, above, and reference 1.) Some uncertainty exists regarding the mass assignment of this activity. (We are indebted to Dr. P. Stähelin for comments on the Pb^{204} activity.)

away from closed shells is an immediate consequence of the increasing deformation produced by the extra particles and also observed in the quadrupole moments.[7] The rapid decrease for the first few particles added to closed configurations, which develops into a rather flat minimum, can be understood from the fact that the particle states with large deformative power are the first to be filled, while in the middle of shells the last added particles are less coupled to the deformation. The minimum in the very heavy elements is lower by a factor of two than that in the rare earth region. This is accounted for by the variation with A of the mass parameter B in the moment of inertia,[1] and implies similar deformations in the two regions.

II. Lifetimes.—The transition probabilities, more than a hundred times larger than single particle estimates,[1] which are observed for the levels in the rare earth region, furnish direct evidence for the collective nature of the excitation. The interpretation of the states as rotational levels permits one to calculate from the lifetimes the intrinsic quadrupole moments of the deformed surface, which are found to be just of the magnitude of those deduced from spectroscopic data.[1]

III. Higher rotational states.—In regions of large deformations, one expects a number of higher members of the rotational spectrum (1). Table I lists evidence on such higher states for the nuclei of Fig. 1. It is seen that in the regions where Eq. (1) is expected to hold, there is indeed evidence for higher rotational states with the predicted energies. The minor deviations of the energy ratios from the limiting strong coupling values (1) show a systematic behavior which may be attributed to a term of the form (2), but the empirical data are not yet sufficiently accurate to warrant a detailed analysis of the effect.

TABLE I. Higher rotational states in even-even nuclei with $A>140$. The table lists the energies (in kev) of the (2+) states and of the tentatively suggested (4+) and (6+) states. In many cases, the available empirical evidence for the character of the states in columns three and five is inconclusive and the suggested assignment is based largely on the energy ratio of the observed gamma-rays.

Nucleus	E_2	E_4	$E_4:E_2$	E_6	$E_6:E_2$	Ref.
$_{62}Sm^{150}$	337	777	2.3			4
$_{72}Hf^{176}$	89	270	3.0	540	6.1	2
$_{72}Hf^{180}$	93	307	3.3	637	6.9	2
$_{82}Pb^{208}$	2614	3200	1.2			4
$_{88}Ra^{226}$	70	215	3.1	450	6.4	a
$_{90}Th^{228}$	58	187	3.2	371	6.4	b
$_{90}Th^{230}$	50	167	3.3			3
$_{94}Pu^{238}$	43	146	3.4			3
Eq. (1)			3.33		7.00	

[a] I. Curie, J. phys. et radium **10**, 381 (1949); F. Rasetti and E. C. Booth, Phys. Rev. **90**, 388 (1953).
[b] D. H. Black, Proc. Roy. Soc. (London) **A106**, 632 (1924).

For $_{62}Sm^{150}$, and especially for $_{82}Pb^{208}$, the small $E_4:E_2$ ratios as well as the large value of E_2 confirm the major deviations from the strong coupling situation expected in the neighborhood of closed shells.

It is characteristic of the rotational spectrum given by (1) that the excitation of a high member is followed by a cascade of $E2$ gamma-transitions with energy values in the ratio $3:7:11:15\cdots$, with no cross-overs. Examples of such cascades are given in Fig. 2.

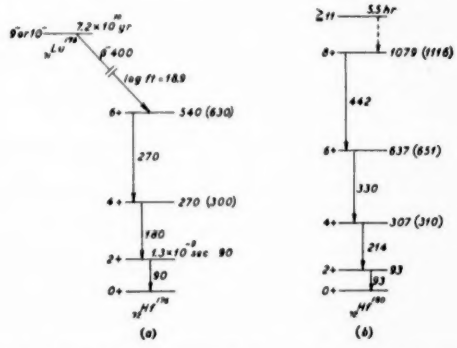

FIG. 2. Suggested decay schemes of $_{71}Lu^{176}$ and $_{72}Hf^{180}$. The gamma-ray energies as well as the β-decay data of Lu^{176} are taken from reference 2. The excitation energies listed in parentheses are obtained from Eq. (1) adjusted to give the energy of the first excited state. All energies are given in kev.

$_{72}Hf^{176}$: The β-decay of $_{71}Lu^{176}$ leads to a 540-kev state[2] of $_{72}Hf^{176}$ which decays in three steps to the ground state [see Fig. 2(a)]. The last transition (89 kev) is known to be of $E2$ type with a strongly enhanced transition probability.[1] The classification of the levels is consistent with the fact that the β-decay of Lu^{176} (measured spin ≥ 7) goes only to the highest (6+) member. The log (ft) value suggests a third-forbidden transition[2] which would lead to the assignment $I=9$ or 10, odd parity, for the Lu^{176} ground state.[8]

$_{72}Hf^{180}$: The decay of the 5.5-hr isomeric state of $_{72}Hf^{180}$ contains four gamma-rays which appear to be in cascade and the last of which (93 kev) has been identified as $E2$.[2] The classification in

Fig. 2(b) assigns an (8+) character to the 1079-kev member of the family and probably implies a spin of at least 11 for the 5.5-hr isomeric state.

* U. S. Atomic Energy Commission Fellow.

[1] A. Bohr and B. Mottelson, Phys. Rev. **89**, 316 (1953). For further details, see forthcoming paper in Kgl. Danske Videnskab. Selskab, Mat.-fys. Medd.

[2] M. Goldhaber and R. D. Hill, Revs. Modern Phys. **24**, 179 (1952).

[3] Hollander, Perlman, and Seaborg, *Table of Isotopes* (University of California Radiation Laboratory Report UCRL-1928, Berkeley, December, 1952).

[4] G. Scharff-Goldhaber, Phys. Rev. **90**, 587 (1953). We are indebted to the author for a private communication of results.

[5] The deviations from the strong coupling formula (1) have also been considered by K. Ford who has kindly communicated his results to us.

[6] Similar curves have been given by P. Preiswerk and P. Stahelin, Helv. Phys. Acta **24**, 623 (1951); S. Rosenblum and M. Valadares, Compt. rend. **235**, 711 (1952); F. Asaro and I. Perlman, Phys. Rev. **87**, 393 (1952); G. Scharff-Goldhaber, Physica **18**, 1105 (1952), and reference 4. Regularities like those in Fig. 1 are also observed for lighter elements, but the trends are somewhat more complicated due to the fact that neutrons and protons form closed shells for different A values.

[7] K. Ford (private communication) has pointed out a significant correlation between deformations deduced from quadrupole moments and those derived from excitation energies of the first excited states of even-even nuclei, interpreted as rotational levels.

[8] P. F. A. Klinkenberg [Physica **17**, 715 (1951)] has suggested the assignment (10−) for Lu^{178} from an analysis of its magnetic moment.

Recoil Effects in Meson-Nucleon Scattering

E. M. Henley* and M. A. Ruderman†
Columbia University, New York, New York
(Received March 25, 1953)

THE asymmetry about 90° of the pion-nucleon scattering cross section shows a considerable even state contribution in addition to a strong P state interaction. We have examined the even state scattering to be expected for pseudoscalar mesons coupled symmetrically to a nucleon with a coupling of the form

$$\sum_{j=1}^{3} g\tau_j \boldsymbol{\sigma}\cdot(\boldsymbol{\nabla}\phi_j - i\mathbf{V}\pi_j). \tag{1}$$

$\mathbf{V}$ is the average velocity of the nucleon before and after meson emission (absorption) so that (1) is Hermitean. The $\boldsymbol{\sigma}\cdot\mathbf{V}$ term[1] is necessary if the interaction is to be invariant under simple Galilean transformations.[2]

To terms in ω/M, the S and D wave phase shifts obtained from (1) are the same for perturbation theory and for the extended source model of Chew.[3] They do not contribute to the nonchargeexchange π^- scattering. The P wave phase shifts, on the other hand, depend critically on the model, but are only slightly affected by recoil effects.

Recoil corrections to the $\boldsymbol{\sigma}\cdot\boldsymbol{\nabla}\phi$ part of the interaction Hamiltonian give the S and D wave phase shifts shown in Table I.

TABLE I. S and D wave recoil phase shifts. Even wave phase shifts in degrees $\times 4\pi/g^2$ obtained from (1). $\eta=k/\mu$ and $\rho=k/\omega$. The superscript is twice the isotopic spin, and the subscript is the total angular momentum.

Phase shift	$S_{1/2}^{(3)}$	$S_{1/2}^{(1)}$	$D_{3/2}^{(3)}$	$D_{3/2}^{(1)}$	$D_{5/2}^{(3)}$	$D_{5/2}^{(1)}$
Recoil from $\boldsymbol{\sigma}\cdot\boldsymbol{\nabla}\phi$	$-5.8\eta^3\rho^2$	$2.9\eta^3\rho^2$	$1.2\eta^3\rho^2$	$-0.58\eta^3\rho^2$	$-4.6\eta^3\rho^2$	$2.3\eta^3\rho^2$
Galilean term	$35\eta^3$	$-17\eta^3$	0	0	0	0

The D wave phase shifts, although numerically smaller, give the main contribution (about twice that of the S wave) to the asymmetry of the cross section about 90°. In perturbation theory the calculated $d\sigma(180°)/d\sigma(0°)$ is independent of $g^2/4\pi$ and is in rough agreement with the asymmetry from the best $A+B\cos\theta+C\cos^2\theta$ fit to the experimental π^+ scattering on protons.[4] This is no longer true for Chew's model with $g^2/4\pi\approx 0.2$ to give best agreement with experiment. In this case $d\sigma(180°)/d\sigma(0°)\approx 1.3$ for 78–135 Mev incident π^+ mesons.

Inclusion of the Galilean term $\boldsymbol{\sigma}\cdot\mathbf{V}$ in (1) gives an S wave phase shift opposite in sign to that from the recoil effects of $\boldsymbol{\sigma}\cdot\boldsymbol{\nabla}\phi$, and dominates the even wave scattering as shown in Table I. The resultant asymmetry from both terms is opposite in sign to experiment, when combined with the P wave phase shifts from (1). With Chew's $g^2/4\pi$, the absolute magnitude of the S wave phase shift is about equal to that observed.

Combined with any short-range static repulsion, the fit of experiment and theory[5] for the S wave phase shifts is worse with the inclusion of the Galilean term in (1).

We wish to thank Professor R. Serber for helpful discussion.

* Frank B. Jewett Fellow.

† National Science Foundation Postdoctoral Fellow, on leave from the University of California, Berkeley, California.

[1] The usual $-\gamma_5\pi_j$ of the relativistic interaction becomes $-i\boldsymbol{\sigma}\cdot\mathbf{V}\pi_j$, when taken between positive energy states.

[2] R. P. Feynman, Proc. Annual Rochester Conference 1952 (to be published).

[3] G. F. Chew, Phys. Rev. **89**, 591 (1953).

[4] Anderson, Fermi, Nagle, and Yodh, Phys. Rev. **86**, 793 (1952). Experiment indicates a ratio ~2. Bodansky, Sachs, and Steinberger (to be published) find a best fit ratio ~4 at 59 Mev.

[5] R. E. Marshak, Phys. Rev. **88**, 1208 (1952).

The Transfer Rate of the Liquid Helium II Film near Zero Level Difference

Gerald S. Picus
Institute for the Study of Metals, University of Chicago, Chicago, Illinois
(Received March 30, 1953)

IT is well known that liquid He II will flow as a film over the walls of a beaker if there is a difference between the level inside the beaker and that of the surrounding bath. The rate of transfer per unit perimeter of the beaker (usually called the critical transfer rate) is practically independent of the level difference, but varies with the temperature.[1,2]

In order to investigate whether or not these transfer rates are due to a critical current density and perhaps to get some information concerning the mechanisms responsible for initiation and limitation of the flow rate, measurements have been made of the flow at very low level differences of the order of several hundredths to several tenths of a millimeter. These were accomplished by suspending an accurately turned Lucite plunger of diameter 7.62 mm inside of, and concentric with, a Pyrex beaker of i.d. 9.60 mm, leaving an annular space approximately 1 mm wide. The plunger could be moved up or down at any desired rate by an electric motor outside the cryostat appropriately geared to a shaft emerging from the top of the cryostat through a vacuum seal. The plunger was hung from a linen thread attached to the shaft.

The observations consisted of measuring the position of the level inside the beaker as a function of time for various rates of downward travel of the plunger. The most interesting results are obtained when the plunger motion is such that the rate at which it displaces liquid is less than the rate at which the beaker would be emptied by flow at the critical transfer rate. Figure 1 shows a

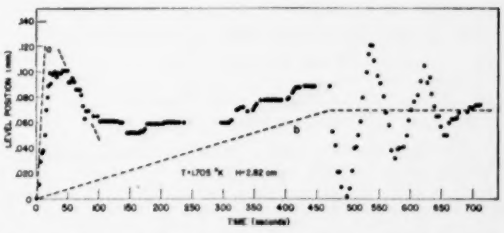

FIG. 1. Position of the level inside the beaker as a function of time.

typical run, made at a temperature of 1.705°K with the rim of the beaker at a height $H=2.82$ cm above the bath. At time $t=0$ sec, the levels inside and outside the beaker were equal, and the plunger was at that instant started down at a rate $x=55.12\times10^{-4}$ cm/sec. The dashed line a indicates the rate at which the level in

the beaker would rise if there were no film flow at all, and the line b indicates the rate at which the bath and beaker levels would rise together due to displacement of liquid by the plunger if at every instant the transfer rate was exactly that necessary to keep both levels equal.

The following features of the curve are regarded as the most significant:

(a) Initially, for $0<t<20$ sec the level rises very rapidly almost along the line a, indicating that during this time the flow rate is very close to zero. The duration of this initial rapid rise appears to increase as the height, H, of the beaker top above the bath is increased at a given temperature, and also as the temperature is increased at a given height H. Attempts are now being made to measure these dependences more precisely.

(b) At approximately $t=20$ sec a sharp break in the curve occurs, and from 50 sec to 100 sec the level moves downward in a stepwise fashion, indicating that the helium may be transferred in pulses rather than uniformly. If an average transfer rate is calculated from the slope of a straight line drawn through the points on this portion of the curve, the value obtained agrees with that measured at large level differences ($\sigma_0=8.81\times10^{-5}$ cc cm^{-1} sec^{-1}).

(c) From $t=100$ sec onwards, the curve levels off and then eventually rises gradually in a stepwise fashion, remaining on the average parallel to, but approximately 0.02 mm above, line b. The value of σ calculated for this portion of the curve is less than σ_0 and varies with the rate of plunger motion.

(d) When the plunger is stopped at $t=471$ sec, the level does not simply drop to zero, but executes what appears to be a damped oscillatory motion. The period of these oscillations is roughly linearly proportional to the film height H and is somewhat less than that calculated for our conditions from equations derived by Atkins.[3] From the fact that the eventual equilibrium position of the level in the beaker is lower than the level position when the plunger is stopped, and from the results in (c), we infer that a finite but small level difference is always necessary to sustain film flow, even at rates less than the critical value.

Investigations of these phenomena at different temperatures and film heights, H, are now being carried out in order to distinguish whether the initial sharp rise noted in (a) above is due to a critical level difference necessary to initiate film flow or to a critical time for transmission of the initial information of the changed conditions produced by the plunger motion. We also hope to determine the level differences necessary to maintain flow at less than the critical rate. A detailed paper will be published soon.

[1] J. G. Daunt and K. Mendelssohn, Proc. Roy. Soc. (London) **A170**, 424 (1939).
[2] K. Mendelssohn and G. K. White, Proc. Phys. Soc. (London) **A63**, 1328 (1950).
[3] K. R. Atkins, Proc. Roy. Soc. (London) **A203**, 240 (1950).

Scattering of 1.3[3] Mev Gamma-Rays by an Electric Field*

ROBERT R. WILSON
Cornell University, Ithaca, New York
(Received March 23, 1953)

A SEARCH has been made to detect the elastic scattering of gamma-rays by the electric field of the nucleus, an effect sometimes called Delbruck or potential scattering.[1] In the experimental arrangement shown in Fig. 1, 1.3-Mev gamma-rays from a 2.5-curie Co^{60} source are collimated by the conical opening in a lead block and are then incident on the scattering material. The scattered gamma-rays pass through a lead absorber of variable thickness and fall on an energy-sensitive detector comprised of a NaI(Tl) crystal (4 cm o.d. by 3 cm long) and an RCA 5819 electron multiplier tube, the energy resolution of the whole system being about ten percent. The large inelastic Compton scattering (about 10^4 times larger than that which might be reasonably expected for potential scattering) is discriminated against by biasing the detector above the energy of such scattered photons. Further energy discrimination is provided by the lead absorber.

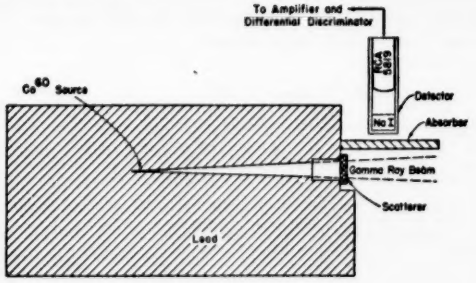

FIG. 1. Experimental arrangement.

The effect of Compton scattering from electrons was shown to be small by the use of a copper target containing the same number of electrons as the Pb target; the elastic scattering from copper should be negligible compared to that from heavy elements such as lead. When a sufficiently thick lead absorber was placed between target and detector, the scattering from copper was less than 20 percent of that from lead. The cross sections measured were not dependent on knowing the absolute calibration of the source nor on knowing the efficiency of the detector, over-all calibration being made by exposing the source directly to the detector placed at a large distance.

Gamma-rays can be scattered elastically by atoms in several ways: (a) by Thomson scattering through the motion of the whole nuclear charge; (b) by Rayleigh scattering from the tightly bound electrons; (c) by nuclear resonance scattering; and (d) by potential scattering through virtual pair production.

The Rayleigh scattering will be in phase with the Thomson scattering which is given by $R_0^2(1+\cos\theta)/2$, where $R_0=Z^2e^2/Mc^2$, Z and M being the charge and mass of the scattering nucleus. Using a Fermi-Thomas model, Franz[2] has made calculations of Rayleigh scattering which have been confirmed at 0.43 Mev by

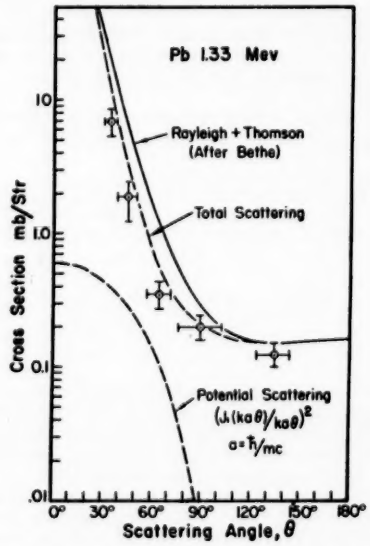

FIG. 2. The cross section in millibarns per steradian for the elastic scattering of 1.33-Mev gamma-rays by lead. The curve marked total scattering is a very rough estimate of Rayleigh, Thomson, and potential scattering combined.

Moon[3] and Storruste.[4] Bethe[5] has made similar calculations but using relativistic wave functions for the K electrons instead of the Thomas-Fermi distribution assumed by Franz. The compound effect of Rayleigh and Thomson scattering as calculated by Bethe is shown in Fig. 2.

Nuclear resonance scattering[6] should be very small except at resonance; the resonances should be less than 10^{-3} ev wide and spaced by at least several kev, hence one would be unlucky indeed to land near such a resonance. Measurements have also been made on Bi, Au, Pt which give very similar results to Pb. Thus nuclear resonance scattering is unlikely to contribute in any way to the measured results.

The experimental results for lead are plotted in Fig. 2, the horizontal bars indicating the angular resolution and the vertical bars, the standard statistical counting error. The measured cross sections agree with Bethe's calculation of Rayleigh-Thomson scattering at large angles, but are considerably lower at angles less than 90°.

Because the experimental difficulties all tend to make the measured cross sections come out too high, one is inclined to conclude (a) that the calculations of Rayleigh scattering at small angles are incorrect, or (b) that another scattering process is occurring which interferes destructively with the Rayleigh scattering to give the small cross sections actually observed. It does not seem likely that Bethe's calculation is wrong by a factor of five; hence the more probable conclusion is that potential scattering is responsible for the reduction of the cross section. Potential scattering would interfere destructively.

Now Rohrlich and Gluckstern[7] have calculated the potential scattering cross section in the forward direction and find it to be 0.6 millibarn per steradian at this energy. No calculation has been made as yet of the angular distribution. The curve plotted in Fig. 2 is on the assumption that the distribution is the same as that obtaining for a wave scattered by a black disk of radius $\hbar/mc$, i.e., diffraction scattering, and normalized to the theoretical result at zero degrees. The dashed curve marked "total scattering" is the result of compounding the amplitudes of the potential scattering and of the Rayleigh and Thomson scattering, assuming that they are exactly of opposite phase. That the measurements are in much better agreement with this curve can be taken as evidence for the occurrence of potential scattering, but this conclusion is subject to a refined calculation of the angular distribution of potential scattering and of the Rayleigh scattering at small angles.

I am grateful to H. A. Bethe, F. Rohrlich, and J. S. Levinger for many stimulating discussions.

* The measurements here reported were all made in 1951. Publication has been held up until now in the hope that the Rayleigh scattering could be calculated more accurately.

[1] R. R. Wilson, Phys. Rev. **82**, 295 (1951).
[2] W. Franz, Z. Physik **98**, 314 (1936).
[3] P. B. Moon, Proc. Phys. Soc. (London) **A63**, 1189 (1950
[4] A. Storruste, Proc. Phys. Soc. (London) **A63**, 1197 (1950).
[5] H. A. Bethe, private communication; see also J. S. Levinger, Phys. Rev. **87**, 656 (1952); G. Brown and J. Woodward, Proc. Phys. Soc. (London) **A65**, 972 (1952).
[6] J. S. Levinger, Phys. Rev. **84**, 523 (1951).
[7] F. Rohrlich and R. L. Gluckstern, Phys. Rev. **86**, 1 (1952).

Inner Bremsstrahlung and the Magnetic Moment of the Neutrino

E. J. Hellund
Argonne National Laboratory, Lemont, Illinois
(Received March 23, 1953)

RECENT measurements on the beta-spectrum of H^3 establish an upper limit of 250 ev for the neutrino rest mass.[1] It is of some interest to point out that the question of the magnitude of the neutrino rest mass is intimately related to the question of the magnitude of its magnetic moment.

During beta-decay, the neutrino is ejected from the neighborhood of the parent nucleus with a velocity very nearly equal to light velocity. Assuming the particle possesses a finite Pauli magnetic moment, one can calculate the intensity of inner bremsstrahlung.[2] The result shows that the total intensity is directly proportional to the square of the moment and inversely proportional to the square of the neutrino rest mass. Confirmation of this relation can be obtained also by a purely classical calculation in the manner outlined by Chang and Falkoff.[3]

A polar vector interaction in an allowed transition yields the following result for the intensity of neutrino inner bremsstrahlung (integrated over all directions):

$$I(k)dk \approx \frac{2\alpha}{\pi}\left(\frac{m}{\mu}\right)^2 g^2 k^2 (W_\nu - k)^2 dk, \quad \mu \to 0 \tag{1}$$

where α is the fine structure constant, m the electron rest mass, μ the neutrino rest mass, k the photon energy, W_ν the initial neutrino energy measured in units of mc^2, and g is the neutrino moment in Bohr magnetons.

The expression must be integrated over the neutrino spectrum corresponding to the probability for emission with energy W_ν. As superimposed on the normal β inner bremsstrahlung, the neutrino spectrum would appear as a spurious "line." Adopting the value 1/5000 Bohr magneton allowed by ionization measurements,[4] and Langer's upper bound for μ, the peak of this line would be about three times as great as the corresponding β inner bremsstrahlung for kinetic energies for both particles of 1 Mev. Identification of the entire inner bremsstrahlung by actual experimental observation as β-radiation[5] clearly necessitates the adoption of a smaller value for the upper limit of the neutrino moment, consistent with the limits of experimental error. Detection of the anomalous line would constitute direct observation of the neutrino.

[1] L. M. Langer and R. J. D. Moffat, Phys. Rev. **88**, 689 (1952). Later measurements indicate an upper limit of 100 ev.
[2] J. K. Knipp and G. E. Uhlenbeck, Physica **3**, 425 (1936); F. Bloch, Phys. Rev. **50**, 272 (1936).
[3] C. S. Wang Chang and D. L. Falkoff, Phys. Rev. **76**, 365 (1949). One only has to change the expression for the current density, i.e., $\mathbf{J} = C\nabla \times \mathbf{M}$ where $\mathbf{M}$ is the moment density, to make their derivation apply to the neutrino.
[4] M. E. Nahmias, Proc. Cambridge Phil. Soc. **31**, 99 (1935).
[5] T. B. Novey, Phys. Rev. **89**, 672 (1953); Bolgano, Madansky, and Rasetti, Phys. Rev. **89**, 679 (1953).

Possible Breakdown of Isotopic Spin and Charge Parity Selection Rules

D. H. Wilkinson
Cavendish Laboratory, Cambridge, England
(Received March 9, 1953)

IT is of interest to determine the purity of isotopic spin[1] and charge parity[2] states. In nuclei of moderate excitation it appears that the contamination of such states may amount to a few percent in *amplitude* from the two probable violations of the selection rules so far reported;[3] the many examples of the success of the rules are consistent with such a purity. A contamination of this order is expected even under perfect charge independence or charge symmetry of the specifically nuclear forces in view of the Coulomb perturbation.[4] It must be anticipated that at higher excitations these concepts of isotopic spin and charge parity will cease to have much significance, and effectively complete breakdown of the rules must be expected. This note indicates one probable and two possible breakdowns.

The reaction $N^{15}(p, \alpha)C^{12}$ (ground state) is strongly resonant, for a particular angle of observation, at a proton energy of 1020 kev; the total width of the resonance is about 160 kev.[5] The reaction $N^{15}(p, \gamma)O^{16}$ (ground state) is strongly resonant at a proton energy of 1050 kev with a total width of about 150 kev.[5] It seems reasonable to identify these resonances and to ascribe their small separation in energy to effects of neighboring levels. The first observation permits the spin of the compound state to be (0+)(1−)(2+), etc.; the second observation eliminates (0+). If we take (1−), we have $E1$ radiation with $(2J+1)\Gamma_\gamma = 450$ ev and $(2J+1)|M|^2 = 0.29$ in excellent accord with other $E1$ transitions

in light nuclei;[6] if we take $(2+)$, we have $E2$ radiation with $(2J+1)\Gamma_\gamma = 250$ or 1250 ev and $(2J+1)|M|^2 = 135$ or 675, which seems improbable. $(1-)$ is therefore the most plausible assignment; it is made almost certain by the angular distribution of the alpha-particles (A. V. Cohen and A. P. French, private communication). If we are correct in the identification and assignment, we have a breakdown of the isotopic spin and charge parity rules; the emission of alpha-particles demands here $T=0$, even charge parity, while the emission of $E1$ radiation demands here $T=1$, odd charge parity;[1,2,7] yet both widths are large ($\Gamma_\gamma = 150$ ev; $\Gamma_\alpha = 75$ kev) and neither may be supposed to have suffered a very large measure of discouragement. We may not rule out the possibility that there are two resonances and that what we are observing is the rules in action rather than their violation, though this seems unlikely in view of the agreement in position and width. The excitation in O^{16} is 13.1 Mev and the first $T=1$ level may be expected at about 12.5 Mev.[8]

The reaction $B^{11}(p,\alpha)Be^8$ (ground state) is resonant at somewhat over 1 Mev[9] in proton energy; $B^{11}(p,\gamma)C^{12}$ (ground state) is strongly resonant at 1.4 Mev[10] with a large radiative width. This may be a similar example but is not so clear-cut. The reactions $Be^9(p,\alpha)Li^6$ and $Be^9(p,d)Be^8$ are resonant at 0.94 Mev,[11] while $Be^9(p,\gamma)B^{10}$ has a strong, almost certain, $E1$ resonance of similar width at 0.998 kev;[12] but these may well involve two different states. In these last two examples we are in a region of excitation containing $T=1$ states.

[1] R. K. Adair, Phys. Rev. **87**, 1044 (1952).
[2] N. M. Kroll and L. L. Foldy, Phys. Rev. **88**, 1177 (1952).
[3] G. A. Jones and D. H. Wilkinson, following Letter [Phys. Rev. **90**, 722 (1953)].
[4] L. A. Radicati, Proc. Phys. Soc. (London) **A66**, 139 (1953).
[5] Schardt, Fowler, and Lauritsen, Phys. Rev. **86**, 527 (1952).
[6] D. H. Wilkinson, Phil. Mag. (to be published).
[7] L. E. H. Trainor, Phys. Rev. **85**, 962 (1952); L. A. Radicati, Phys. Rev. **87**, 521 (1952).
[8] T. Lauritsen, *Annual Review of Nuclear Science* (Annual Reviews, Inc., Stanford, 1952), p. 67.
[9] T. Huus, private communication.
[10] T. Huus and R. B. Day, Phys. Rev. **85**, 761 (1952).
[11] Thomas, Rubin, Fowler, and Lauritsen, Phys. Rev. **75**, 1612 (1949).
[12] W. A. Fowler and C. C. Lauritsen, Phys. Rev. **76**, 314 (1949).

The Purity of Isotopic Spin or Charge Parity States

G. A. Jones and D. H. Wilkinson
Cavendish Laboratory, Cambridge, England
(Received March 9, 1953)

WE have carried out two experiments to attempt to assess the purity of isotopic spin or charge parity states[1-3] of moderate excitation.

O^{16} possesses[4] a $(1-)$ state at 7.12 Mev, a $(2+)$ state at 6.91 Mev, a $(3-)$ state at 6.14 Mev and a $(0+)$ state at 6.05 Mev; the ground state is $(0+)$. All these states are expected[5] to have $T=0$; if we think in terms of charge symmetry alone, the charge parity is probably even. The $(1-)$ state decays to the ground state thereby violating the isotopic spin[6] or charge parity[7] rule. The $E2$ decay to the $(3-)$ state is uninhibited by the special rules; we have shown it to occur at least 120 times less probably than the forbidden $E1$ transition. We have also shown that the $(2+)$ state decays to the ground state at least 200 times more readily than to the $(3-)$ state, although, in the absence of the special rules this latter $E1$ transition would be preferred. The single-particle matrix elements[8] seem to be unexpectedly reliable[9] for the prediction of $E1$ radiative widths, and there is no evidence that they are grossly wrong for $E2$ transitions in light nuclei; if we apply them to this case, we obtain the result that the contamination of the $(1-)$ state is more than 0.2 percent in *amplitude* and that that of the $(2+)$ and $(3-)$ states is less than 3 percent in amplitude (assuming the ground state to be pure $T=0$). These estimates are probably reliable to a factor of five or better.

The first state with $T=1$ in B^{10} is at 1.74 Mev; the first excited state of Be^{10} is at 3.37 Mev and is $(2+)$. A doublet exists in B^{10} at 5.11 and 5.16 Mev; there is another state at 4.8 Mev. It seems that one member of the doublet should have $T=1$. We have measured the excitation function of the reaction $Li^6(\alpha,\gamma)B^{10}$. We locate the lowest state at 4.75 ± 0.02 Mev ($\omega\Gamma\sim0.15$ ev) and the upper element of the doublet at 5.162 ± 0.008 Mev ($\omega\Gamma\sim0.2$ ev), but we find no trace of the 5.11-Mev level ($\omega\Gamma<\sim0.004$ ev). The obvious explanation, that the 5.11-Mev state has $T=1$ and its formation is inhibited by the isotopic spin rule, is rendered unlikely by the implied "discouragement factor" of more than 2×10^4 (if we guess an "uninhibited" width of about 100 ev for the $l=2$ alpha-particles of 1.1 Mev), Radicati[10] having calculated that there is probably about 0.25 percent in *intensity* of $T=1$ in the ground state of Li^6.

It is then possible that the 5.16-Mev level has $T=1$ with an implied discouragement factor of order 500, which is consistent with Radicati's estimate. It is known[11] that one or other element of the doublet is $(1-)$ or $(2-)$; $(1-)$ we cannot admit, as the $E1$ transition to the lower $T=1$ level $(0+)$ would be allowed. We therefore suggest that this 5.11-Mev level may be $(2-)$ and would then see in its small width the operation of the isotopic spin selection rule on $E1$ transitions [the ground and first excited states of B^{10} are $(3+)$ and $(1+)$, respectively]; we would then be on fairly safe ground in inferring a contamination of less than 2 percent in *amplitude* (assuming the lower states to be pure $T=0$).

These observations of two possible violations and two possible successes of the pure isotopic spin or charge parity selection rules seem to accord with what might be expected from complete specifically nuclear charge independence or charge symmetry when the effect of the Coulomb perturbation is taken into account.

[1] R. K. Adair, Phys. Rev. **87**, 1044 (1952).
[2] N. M. Kroll and L. L. Foldy, Phys. Rev. **88**, 1177 (1952).
[3] D. H. Wilkinson, preceding Letter [Phys. Rev. **90**, 721 (1953)].
[4] For all energies and characteristics quoted here, we refer the reader to F. Ajzenberg and T. Lauritsen, Revs. Modern Phys. **24**, 321 (1952).
[5] T. Lauritsen, *Annual Review of Nuclear Science* (Annual Reviews, Inc., Stanford, 1952), Vol. 1, p. 67.
[6] L. A. Radicati, Phys. Rev. **87**, 521 (1952).
[7] L. E. H. Trainor, Phys. Rev. **85**, 962 (1952).
[8] V. F. Weisskopf, Phys. Rev. **83**, 1073 (1951).
[9] D. H. Wilkinson, Phil. Mag. (to be published).
[10] L. A. Radicati, Proc. Phys. Soc. (London) **A66**, 139 (1953).
[11] F. Ajzenberg, Phys. Rev. **88**, 298 (1952).

Angular Distribution of γ-Rays from Stripping Reactions

G. R. Satchler
Clarendon Laboratory, Oxford, England
(Received March 19, 1953)

THE angular distribution (about the recoil axis) of the γ-radiation following a deuteron-stripping reaction has been treated both in terms of the channel spin of the capture process[1,2] and in terms of the total angular momentum j of the captured particle.[3]

Stripping reactions enable nucleons to be captured into low-lying excited levels where the Mayer $j-j$ coupling scheme is

TABLE I. γ-ray angular distributions predicted by the shell model. J_i = spin of initial nucleus; j = total angular momentum (spin + orbital) of captured particle; J_e = spin of excited nucleus after capture; L = multipole order of γ-ray; J_f = nuclear spin after emission.

J_i	(j)	J_e	(L)	J_f	A_2	A_4
0	(3/2)	3/2	(1)	1/2	−0.500	···
			(1)	3/2	+0.400	···
			(1)	5/2	−0.100	···
			(2)	7/2	+0.143	···
0	(5/2)	5/2	(1)	3/2	−0.400	···
			(1)	5/2	+0.457	···
			(1)	7/2	−0.143	···
			(2)	1/2	+0.571	−0.571
3/2	(3/2)	2			Isotropy*	
5/2	(5/2)	2	(2)	0	−0.204	−0.367
5/2	(5/2)	4	(2)	2	+0.160	+0.139

* Isotropy in this case is a numerical coincidence.

expected to be valid. Hence the extent to which the angular distribution can be analyzed in terms of one j value forms a quantitative test of shell model assumptions.

A similar analysis in terms of unique L and S values for the initial and excited nuclear states would test the validity of the $L-S$ coupling scheme.

In this letter we give formulas relating the unique $j-j$ and unique $L-S$ cases to the channel-spin formalism. We give also some explicit γ-distributions of interest on the shell model hypothesis.[4]

The distribution function, Eq. (6) of reference 3, for a unique j may be expanded in terms of Legendre polynomials. Using the same notation for angular momenta as in reference 3 (see also caption of Table I),

$$W(\theta)=1+\Sigma_\nu \eta_\nu(jJ_iJ_e)F_\nu(LJ_fJ_e)P_\nu(\cos\theta),$$

where $\nu=2, 4, \cdots$, the F_ν are tabulated elsewhere,[5] and

$$\eta_\nu=(2J_e+1)^{\frac{1}{2}}(2j+1)(-)^{J_i-J_e-\frac{1}{2}}C_{0\frac{1}{2}-\frac{1}{2}}{}^{\nu jj}W(J_eJ_ejj;\nu J_i).$$

Comparing this expression with the general channel-spin formula [see Eq. (18), reference 6] we find that the corresponding proportional contribution of channel-spin $s(=J_i\pm\frac{1}{2})$ is given by $|A(s)|^2$, where

$$A(s)\sim(2j+1)(2s+1)^{\frac{1}{2}}W(J_ijsl;J_e\tfrac{1}{2}).$$

In the case of $L-S$ coupling one obtains[4]

$$A(s)\sim(2s+1)^{\frac{1}{2}}W(S_esLJ;L_iJ_e)W(L_iS_is\tfrac{1}{2};J_iS_e),$$

where $(J_iL_iS_i)$ and $(J_eL_eS_e)$, respectively, describe the initial nuclear state and the state after capture.

Thus angular distributions calculated with the channel-spin approach can be used to express the results of unique j and unique $L-S$ assumptions. Unique l is assumed since measurements are to be made in coincidence with outgoing nucleons of a definite l-peak.

Explicit angular distributions for unique j values depend on 5 parameters $(J_iJ_eLJ_f)$, but shell model predictions reduce the number of independent variables in some cases. Thus:

(a) initial nucleus even-even, final even-odd. $J_i=0$, $J_e=j$. If the ground and excited states form a doublet, $J_e=l-\frac{1}{2}$, $J_f=l+\frac{1}{2}$ and $L=1$.

(b) even-odd to even-even. $j=J_i$ if the captured nucleon enters the same orbit as the original "odd" one and forms an excited state by coupling with it. Then $J_e=2$ (or 4), $J_f=0$, (or 2) and $L=2$.

Writing

$$W(\theta)=1+\Sigma_\nu A_\nu P_\nu(\cos\theta),$$

we list in Table I the coefficients A_ν, for $j=3/2$ and $5/2$. ($j=\frac{1}{2}$ gives isotropic distributions always.)

The author is indebted to Dr. J. A. Spiers for advice on this problem.

[1] Biedenharn, Boyer, and Charpie, Phys. Rev. **88**, 517 (1952).
[2] L. J. Gallaher and W. B. Cheston, Phys. Rev. **88**, 684 (1952).
[3] G. R. Satchler and J. A. Spiers, Proc. Phys. Soc. (London) **A65**, 980 (1952).
[4] General formulas including admixtures, etc., will be published elsewhere with full tables of the relevant η_ν coefficients.
[5] L. C. Biedenharn and M. E. Rose, Revs. Modern Phys. (to be published).
[6] Biedenharn, Arfken, and Rose, Phys. Rev. **83**, 586 (1951).

The Ratio of Plateau to Minimum Grain Density for Electrons

R. P. MICHAELIS AND C. E. VIOLET
Radiation Laboratory, Department of Physics, University of California, Berkeley, California

(Received March 16, 1953)

RECENT experimental and theoretical work concerning the relativistic increase in ionization of a charged particle moving through matter is discussed elsewhere.[1] The purpose of the present study was to compare the grain density at saturation ionization (plateau) with that at minimum ionization for negative electrons in G5 emulsion.

A single 1 in.×3 in., 200-micron Ilford G5 emulsion was exposed to 300-Mev and 3-Mev electrons. The former were obtained by magnetic analysis of pairs produced from a tantalum converter in the bremsstrahlung beam of the Berkeley synchrotron. The latter were obtained by magnetic analysis of an electron linear accelerator beam. Primary electrons entering the emulsion at ~5 degrees to the emulsion air surface penetrated the emulsion in opposite directions and formed two adjacent bands of electron tracks. Grain counts were recorded in terms of a standard reticule unit, which, under the magnification used (~2500×) was 32 microns in length. For the purposes of comparing grain counts at the two energies, the following criteria were adopted:

(1) A grain was counted as one unit regardless of size.

(2) All grain counts were taken in a layer of developed emulsion between 40 and 10 microns from the emulsion air surface.

(3) Track sections were accepted for grain counting only if their dip angle was in the same sense as would be expected from the exposure set-up.

(4) Consistent with (3), only portions of track were grain counted where the angle of dip in the developed emulsion was between 0 and arc tan 0.059.

The grain density determined on the basis of criterion (1) is essentially proportional to that obtained when clumps are resolved into individual grains for the thin tracks used here. The fourth criterion allows one to neglect the error in track length because of the uncertainty in the shrinkage factor. By grain counting tracks of ~300-Mev electrons as they penetrated the emulsion, the gradient of development in the acceptable layer [criterion (2)] was found to be less than one percent. Because of the large multiple scattering of ~3-Mev electrons, and in light of criterion (4), it was not feasible to grain count successive intervals of these tracks. Instead, the following "field of view" method was adopted: Grain counts per standard unit were taken for all portions of ~3-Mev tracks in a field of view lying within ±22.5 degrees of the mean entrance angle. Tracks of ~300-Mev electrons were first grain counted by taking successive intervals of given tracks (7207 grains). Then the ~3-Mev tracks were grain counted by the "field of view" method. Finally, ~300-Mev tracks were grain counted by the latter method (7197 grains). The means and standard deviations of the two sets of ~300-Mev data agreed within the statistical errors. The error in track length due to multiple scattering over a standard unit is negligible. All counts were taken by one observer whose reproducibility was found to be better than one percent.

Our results are given in Table I. The two sets of ~300-Mev data are combined. The mean energies have been calculated taking into account the energy loss in the acceptable layer due to radiation[2] and ionization.[3] The ionization of 2.8-Mev electrons differs from minimum ionization by less than one percent.[3] From the standard deviations of Table I it is evident that the spreads of the distributions of counted grains are less than those given by Poisson distributions. This result is anticipated since the probability of success in rendering a grain developable is not vanishingly small. Thus, the conditions for a Poisson distribution are not met. The standard errors have been computed from the measured standard deviations in the usual way.[4] Assuming proportionality between grain density and ionization, the ratio in Table I is also that of saturation to minimum ionization.

TABLE I. Grain density measurements.

Mean energy (Mev)	No. of grains counted	Mean grain density with standard error of mean (grains/32μ)	Standard deviation (grains/32μ)	Ratio of mean grain densities with standard error
293	14 404	8.61 ±0.05	2.13	1.087 ±0.010
2.8	7 002	7.92 ±0.06	1.95	

We are indebted to Dr. W. H. Barkas for suggesting this problem to us and for his many helpful discussions. The assistance of Dr. R. S. White, Mr. J. W. McLeod, Mr. George C. McFarland, and the synchrotron crew is gratefully acknowledged.

[1] M. Huybrechts and M. Schonberg, Nuovo cimento **9**, 764 (1952).
[2] D. R. Corson, Phys. Rev. **80**, 303 (1950).
[3] R. M. Sternheimer, Phys. Rev. **88**, 851 (1952).
[4] P. G. Hoel, *Introduction to Mathematical Statistics* (John Wiley and Sons, Inc., New York, 1947), p. 66.

The Total Cross Sections of 37-Mev Pions in Hydrogen

C. E. ANGELL AND J. P. PERRY*
University of Rochester, Rochester, New York
(Received March 26, 1953)

THE total cross sections for the processes $\pi^+ + p$ and $\pi^- + p$ have been measured at a laboratory interaction energy for the pions of 37 ± 6 Mev, using the method previously described.[1]

The "slow pions" and proton contamination described in reference 1 have been eliminated from the pion beam by the use of a second focusing magnet, and the pulse-height resolution of the scintillation counter telescope has been improved. These facts enable the analysis of the data to be more nearly independent of the characteristics of the pulse-height circuitry than was previously possible. The second focusing magnet, in conjunction with higher cyclotron operating levels, has increased the incident pion beam intensity to 13 000 π^+/min and 5000 π^-/min through a 1 in.$\times$1in.$\times 5\frac{1}{4}$ in. telescope.

A summary of the results is shown in Table I. All numbers have been corrected for the muon and electron contamination of the beam. The errors indicated are the standard deviations owing to counting statistics or fluctuations from the mean, whichever is larger. Since the π^- cross section includes charge exchange scattering, the value of 5 ± 1.5 mb obtained by Roberts and Tinlot[2] at approximately this same energy has been used in calculating the total cross sections.

TABLE I. Measured and calculated cross sections of 37-Mev pions in hydrogen.

	Measured cross section (millibarns)	Calculated total cross sections (millibarns)		
		isotropic	$\sin^2\theta$	$\cos^2\theta$
π^+	16.0 ± 1.0	20.8 ± 1	18.8 ± 1	26.4 ± 2
π^-	17.3 ± 1.4	21.0 ± 2	19.4 ± 2	25.3 ± 3

The π^+ and π^- data are each based on 5.6×10^6 incoming pions. The measured cross section is that obtained from the attenuation of the pion beam by the CH_2 and carbon scatterers. It is then corrected for the solid angle subtended by the anticoincidence counter in order to obtain the total cross section. This is done for three assumed angular distributions in the center-of-mass system.

* Work performed under the auspices of the U. S. Atomic Energy Commission.
[1] Barnes, Clark, Perry, and Angell, Phys. Rev. **87**, 669 (1952).
[2] A. Roberts and J. Tinlot (to be published).

A Binding Energy Calculation on He^4 with Single-Particle Wave Functions

P. G. WAKELY
Department of Mathematics, University of Southampton, Southampton, England
(Received March 30, 1953)

A PHENOMENOLOGICAL two-body interaction potential of the form

$$V(r) = V_0 \frac{T_{12}}{3}\left\{\left[1 - \frac{g}{2} + \frac{g}{2}(\boldsymbol{\sigma}_1 \cdot \boldsymbol{\sigma}_2)\right]\frac{e^{-r/r_c}}{r/r_c} + \gamma S_{12}\frac{e^{-r/r_t}}{r/r_t}\right\},$$

where T_{12} determines the exchange character of the forces, has been shown, for suitable choice of the interaction parameters, to give a satisfactory description of low energy scattering processes and the deuteron properties,[1] and also to fit the triton binding energy.[2,3] It has further been shown by Irving[4] to give rise to a reasonable value for the binding energy of He^4. This Letter will show that results for He^4 comparable to those of Irving may be obtained on the basis of the nuclear shell model when interconfigurational mixing is taken into account.

TABLE I. Contributions of the single-particle states to the binding energy of He^4.

State	Percent	Contribution to binding energy[a]	Parameter value
Ψ_1	75.73	15.72 Mev	$\theta_1 = 0.665$
Ψ_2	21.88		$\theta_2 = 0.88$
Ψ_3	2.39	5.12 Mev	$\theta_3 = 0.58$
		20.84 Mev	

[a] The increase in the S state binding energy due to the admixture of Ψ_2 was 4.27 Mev.

We use a symmetric interaction $[T_{12} = (\boldsymbol{\tau}_1 \cdot \boldsymbol{\tau}_2)]$ rather than one of neutral or Serber type, since, although for the triton and alpha-particle the precise form of the exchange character is immaterial,[5] for the heavier light nuclei considerable excess binding results with the neutral and Serber interactions. [See work of Kronheimer[6] on Be^9, and of the writer on Ca^{40}.] A variation method is employed, with wave functions constructed by the methods of Jahn *et al.*,[7] and the energy matrix elements calculated using the techniques described by Elliott.[8] The interaction parameter set used is that calculated by Pease and Feshbach[2] to give 100 percent binding for the triton. Suitably adjusted for the symmetric case this is:

$$V_0 = 46.96 \text{ Mev}, \quad r_t = 1.70 \times 10^{-13} \text{ cm}, \quad g = 1.985,$$
$$r_t/r_c = 1.44, \quad \gamma = 0.5085.$$

Calculations were first made on the ^{11}S state arising from the lowest configuration $(1s)^4$, using two types of single-particle radial wave function, *viz.*, oscillator well: $u_{1s}(r) \sim \exp(-\frac{1}{2}r^2/r_c^2\theta^2)$: and "exponential": $u_{1s}(r) \sim \exp(-\frac{1}{2}\gamma r/r_c)$; θ, γ being the respective variation parameters. These calculations showed the oscillator functions to be slightly superior to the exponential functions, but in each case the $(1s)^4$ configuration gave an inadequate description of the He^4 ground state.

In taking inter-configurational mixing into account, the states $(9s)^2(2p)^2[4]^{11}S$ and $(1s)^2(2p)^2[22]^{15}D$ were considered, together with the $(1s)^4[4]^{11}S$ state. The symmetry characters here label the irreducible representations of the symmetric group S_4 to which the orbital parts of the wave functions belong. A further state which preliminary calculations indicated to be of importance comparable to that of the $(1s)^2(2p)^2[4]^{11}S$ state is the state $(1s)^2(2s)[4]^{11}S$. This state is not however considered here. Writing $1s \equiv s$, the wave functions for the remaining states were found to be:

$$\Psi_1 \equiv \Psi(s^4[4]^{11}S) = \sqrt{\tfrac{1}{2}}\Phi(s^2[2]^{13}S, s^2[2]^{13}S, {}^{11}S) - \sqrt{\tfrac{1}{2}}\Phi(s^2[2]^{31}S, s^2[2]^{31}S, {}^{11}S),$$

$$\begin{aligned}\Psi_2 \equiv \Psi(s^2p^2[4]^{11}S) = {} & \sqrt{\tfrac{1}{6}}[\sqrt{\tfrac{1}{2}}\Phi(s^2[2]^{13}S, p^2[2]^{13}S, {}^{11}S) - \sqrt{\tfrac{1}{2}}\Phi(s^2[2]^{31}S, p^2[2]^{31}S, {}^{11}S)] \\ & + \sqrt{\tfrac{1}{6}}[\sqrt{\tfrac{1}{2}}\Phi(p^2[2]^{13}S, s^2[2]^{13}S, {}^{11}S) - \sqrt{\tfrac{1}{2}}\Phi(p^2[2]^{31}S, s^2[2]^{31}S, {}^{11}S)] \\ & + \sqrt{\tfrac{2}{3}}[\sqrt{\tfrac{1}{2}}\Phi(sp[2]^{13}S, sp[2]^{13}S, {}^{11}S) - \sqrt{\tfrac{1}{2}}\Phi(sp[2]^{31}S, sp[2]^{31}S, {}^{11}S)],\end{aligned}$$

$$\begin{aligned}\Psi_3 \equiv \Psi(s^2p^2[22]^{15}D) = {} & \sqrt{\tfrac{1}{6}}\Phi(s^2[2]^{13}S, p^2[2]^{13}D, {}^{15}D) \\ & + \sqrt{\tfrac{1}{6}}\Phi(p^2[2]^{13}D, s^2[2]^{13}S, {}^{15}D) \\ & - \sqrt{\tfrac{1}{2}}\Phi(sp[2]^{13}P, sp[2]^{13}P, {}^{15}D) \\ & - \sqrt{\tfrac{1}{2}}\Phi(sp[11]^{33}P, sp[11]^{33}P, {}^{15}D).\end{aligned}$$

Here, $\Phi(s^2[2]^{13}S, p^2[2]^{13}S, {}^{11}S)$, for example, indicates a state formed by vector coupling the state $\Psi(s^2[2]^{13}S)$ of particles 1 and 2, with the state $\Psi(p^2[2]^{13}S)$ of particles 3 and 4, in spin, charge and orbit, to give the resultant ${}^{11}S$ state.

Oscillator-well single-particle radial wave functions were used, and different parameters $\theta_1, \theta_2, \theta_3$, assigned to the three states Ψ_1, Ψ_2, Ψ_3, respectively, so that the wave function Ψ_i is dependent only upon θ_i. The results, neglecting the Coulomb energy, are given in Table I. These results, in the absence of the $(1s)^2(2s)[4]^{11}S$ state, are poorer than those obtained by Irving.

The author is indebted to Professor H. A. Jahn for many stimulating discussions, and to the Ministry of Education for an award under the F.E.T. scheme.

[1] H. Feshbach and J. Schwinger, Phys. Rev. **84**, 194 (1951).
[2] R. L. Pease and H. Feshbach, Phys. Rev. **88**, 945 (1952).
[3] T. Hu and K. Hsu, Proc. Roy. Soc. (London) **A204**, 476 (1951).
[4] J. Irving, Phys. Rev. **87**, 519 (1952); Proc. Phys. Soc. (London) **A66**, 17 (1953).
[5] This is due to the predominantly totally symmetric nature of the orbital wave functions—as exhibited for He^4 in the wave functions given here.
[6] E. H. Kronheimer, (to be published).
[7] H. A. Jahn and H. Van Wieringen, Proc. Roy. Soc. (London) **A209**, 502 (1951); Elliott, Hope, and Jahn, (to be published).
[8] J. P. Elliott, thesis, London, 1952, unpublished.

THE AMERICAN INSTITUTE OF PHYSICS

INCORPORATED

57 East 55 Street New York 22, N.Y.

MEMBER SOCIETIES:

American Physical Society
KARL K. DARROW, *Secretary*, Columbia University, New York 27, New York.

Optical Society of America
ARTHUR C. HARDY, *Secretary*, Massachusetts Institute of Technology, Cambridge 39, Massachusetts.

Acoustical Society of America
WALLACE WATERFALL, *Secretary*, 57 East 55th Street, New York 22, New York.

Society of Rheology
G. J. DIENES, *Secretary*, Brookhaven National Laboratory, Upton, Long Island, New York.

American Association of Physics Teachers
R. F. PAULY, *Secretary*, University of Illinois, Urbana, Illinois.

AFFILIATED SOCIETIES:

American Crystallographic Association
American Society for Metals
Electron Microscope Society of America
Physical Society of Pittsburgh
Physics Club of Chicago
Physics Club of Philadelphia
Cleveland Physics Society
Physics Club of the Lehigh Valley
Sigma Pi Sigma

ASSOCIATES:

Over seventy-five leading industrial enterprises and other institutions which contribute to the support of the Institute.

JOURNALS:

The Physical Review
S. A. GOUDSMIT, *Editor*, Brookhaven National Laboratory, Upton, Long Island, New York.

Reviews of Modern Physics
J. W. BUCHTA, *Editor*, University of Minnesota, Minneapolis, Minnesota.

Journal of the Optical Society of America
WALLACE R. BRODE, *Editor*, National Bureau of Standards, Washington 25, D. C.

The Journal of the Acoustical Society of America
FLOYD A. FIRESTONE, *Editor*, 57 East 55th Street, New York 22, New York.

American Journal of Physics
THOMAS H. OSGOOD, *Editor*, Michigan State College, East Lansing, Michigan.

The Review of Scientific Instruments
GAYLORD P. HARNWELL, *Editor*, Randal Morgan Laboratory of Physics, University of Pennsylvania, Philadelphia, Pennsylvania.

The Journal of Chemical Physics
CLYDE A. HUTCHISON, JR., *Editor*, Institute for Nuclear Studies, University of Chicago, Chicago 37, Illinois.

Journal of Applied Physics
ELMER HUTCHISSON, *Editor*, Case Institute of Technology, Cleveland 6, Ohio.

Physics Today
GAYLORD P. HARNWELL, *Editorial Director*; ROBERT R. DAVIS, *Managing Editor*, American Institute of Physics, 57 East 55 Street, New York 22, New York.

OFFICERS
GEORGE R. HARRISON, *Chairman*
Massachusetts Institute of Technology
GEORGE B. PEGRAM, *Treasurer*
Columbia University

GOVERNING BOARD
J. W. BUCHTA
KARL K. DARROW
G. J. DIENES
S. A. GOUDSMIT
GEORGE R. HARRISON
FREDERICK V. HUNT
DUANE R. JUNE
HUGH S. KNOWLES
C. C. LAURITSEN
WILLIAM F. MEGGERS
PHILIP M. MORSE
BRIAN O'BRIEN
GAYLORD P. HARNWELL
I. I. RABI
DUANE ROLLER
FREDERICK SEITZ
WILLIAM SHOCKLEY
RICHARD M. SUTTON
J. H. VAN VLECK
MARK W. ZEMANSKY

Committee on Printing
MELVIN LOSS

ADMINISTRATIVE STAFF
HENRY A. BARTON, *Director*
WALLACE WATERFALL, *Executive Secretary*
THEODORA VOSBURGH, *Advertising Manager*
RUTH F. EVANS, *Publication Manager*
BETTY H. GOODWEILER, *Assistant Secretary*
EILEEN B. NEUMEISTER, *Circulation Manager*
KATHRYN SEITZ, *Assistant Treasurer*

THE American Institute of Physics was founded in 1931 as a federation of leading societies in the field of Physics. It combines into one operating agency those functions on behalf of physics which can best be done by the Societies jointly. Its purpose is the advancement and diffusion of physics and its applications to human welfare. To this end it publishes for itself or the Societies the nine journals listed on this page; promotes unity and effectiveness of effort among all who are interested in physics; renders numerous direct services to physicists and to the public; and cooperates with government agencies, national associations, educational institutions, technical industries, and others in such manner as to realize the opportunities and fulfill the responsibilities of physics as an important and constructive human activity.

CONTENTS

The Physical Review — Second Series, Volume 95, No. 4 — May 15, 1954

Energy Loss of Protons in Metallic Foils and Mica . . . David Katz 861

Penetration and Diffusion of Hard X-Rays: Polarization Effects . . . L. V. Spencer and Gameron Wilson 869

Corrected Values of Electron-Annihilation Radial Probability Functions $4f\sigma$ and $4d\sigma$ . . . H. S. Snyderman, H. Kronheim, and J. M. Hayward 887

Addendum . . . S. K. Mitra 896

Solubility of Silicon and Germanium in Sulfuric Acid Solutions . . . Peter H. Emmett and James Brunauer 891

Adiabatic Heat Effect in Ferromagnetics . . . V. A. Johnson and F. W. Sheard 898

Magnetic Susceptibility of Cobalt Ferrites (Cobalt from Fe^{++} to Co^{+++}) . . . C. W. Haas and C. Rangel 899

Energy Loss of Low Energy Protons in Some Gases . . . James A. Phillips 905

Ultraviolet Absorption Spectrum of $(CN)_2$ and C_2N_2 . . . S. L. Miller and C. H. Townes 909

Electronic Structure of O_2 . . . S. L. Miller, C. H. Townes, and M. Kotani 913

Accumulation of Electrons through Thin Metallic Foils . . . C. H. Cheek, C. L. Cleek, and H. Pomerantz 916

Capture and Loss of Electrons by Protons Emergent . . . Gilbert I. Bell 918

Radiation from Satellites? . . . Richard H. Jansen, L. Jacques Laslett, Dow S. Mortimer, Jr., Francis J. Murray, and Winston W. Peace 927

Measurement of the Transport Mean Free Path of Thermal Neutrons in D_2O by a Steady Poisoning Method . . . S. W. Kash and D. C. Wrenn 936

Spikes. IV . . . S. H. Higgins, A. S. Rood, and F. M. Porter 947

Photomesonic Fission of Bismuth . . . G. Bernardini, A. Rossi, and E. Saudi 953

B^{11} Level Structure from the $C^{13}(p,n)B^{13}$ Reaction . . . J. E. Rose, J. D. Kington, and H. B. Willard 958

Geometrical Characterization of Nuclear Fission and the Theory of Angular Correlations . . . W. Fano 971

Nuclear Levels Associated with Transitions of and Neutrons . . . J. M. Cassidy, J. M. Lindsay, D. W. Mingay, W. E. Stephens, and M. G. Strauch 979

Radiochemical Studies on the Photofission of Thorium . . . Dana M. Haines and Earl K. Hyde, Jr. 991

Quadrupole Moment of Li^7 . . . Richard G. Hagens and Hiroshi A. Shugart 1000

Excited States of Boron-Boron Nuclei . . . Cornelius Bargmann-Christensen 1007

Thermal Neutron Capture Cross Section of Hydrogen . . . E. Hammarsten, G. E. Hansen and S. Wexler 1008

Some Reconnaissance Associated with K^+ Capture in A^{37} . . . Carl A. Anderson, Gleason W. Wheeler, and W. W. Watson 1009

Quadrupole Moment Ratio of Ba^{135} and Ba^{137} from Pure Quadrupole Spectra . . . Ralph Livingston and Homer Reid 1009

Comparison of the Values of the Disintegration Constant of Re^{187} in Re Salts, and ReO . . . J. J. Engelkemeir, Clarence D. Wilson, and Raymond T. Birge 1009

Total Neutron Cross Sections of Gold, Chlorine, and Hydrogen . . . R. C. Stevenson and W. D. Whitehouse 1011

Total Cross Sections of Cadmium, Sodium, Titanium, and Rubidium for Slow Neutrons . . . H. H. Dupree and R. H. Little, Jr. 1012

Mean Lifetimes of Λ^0-Particles and Heavy Mesons . . . W. L. Alford and E. H. Lancaster 1013

Scattering of Protons by Protons . . . H. M. Hall and J. L. Thomas 1019

High Energy Charged Particles from Targets Bombarded by 300-Mev Protons . . . L. Eberhardt, W. E. Crandall, G. B. Harrison, D. A. Hicks, and A. V. Sielaff 1025

Time Distribution of Positrons Annihilated in Liquids and Solids . . . R. E. Bell and R. L. Graham 1035

Penetration and Leptonic Effect of Cosmic Rays at High Altitudes and Latitudes . . . E. V. Nesmo, V. S. Pradhan, and E. A. Sperry 1042

Nuclear Interactions of 730-Mev π^+-Mesons in Emulsion . . . A. E. Ignatenko 1076

Positron-Electron Scattering at 1.3 Mev . . . Sergio A. Rossi and K. E. Mortensen 1078

Radiation of a High Energy Electron in a Constant Magnetic Field . . . Harmon Nelson 1083

Feynman Theory of Scattering in a Given Time-Dependent Field . . . Abdus Salam and R. T. Matthews 1090

Spherically Symmetric Solutions in Nonquantized Field Theories. I. The Klein-Gordon Tensor . . . P. G. Yajnik 1094

Renormalization of Potentials in Quantum Field Theory . . . E. A. Kraut and E. M. Warner 1099

Letters to the Editor:

Temperature, Current, Magnetic Field Phase Diagram of Superconductivity . . . W. Shockley, F. Bozorth, and E. Kunzler 1101

Paramagnetic Effect in Ferromagnetism . . . Yuri B. Tsaliuk and H. H. Stephenson, Jr. 1102

Annealing of Bombardment Damage in Silicon . . . W. L. Brown, R. C. Fletcher, and J. Morgan 1103

Extra-Resistivity Owing to Vacancies in Copper . . . F. Seitz and J. S. Koehler 1104

Paramagnetic Resonance in Manganous Fluoride . . . D. J. E. Ingram 1111

Radiation Curve for Photoneutrons from Beryllium . . . David Lazarus 1112

Differential Cross Section for Elastic p-p Scattering at 450 Mev . . . W. E. Abbott, D. E. Dutton, J. G. Fox, and J. A. Kane 1113

Occurrence of Cosmic-Ray Mass Only One Third as Great . . . S. Lindsay Kelly and Herbert L. Valentine 1115

Angular Distributions of Electrons Produced in Mercury Vapor . . . M. Walt and W. E. Rothschild 1116

Elastic Scattering of Mesons in Emulsion . . . T. A. Romanowski 1118

High Energy Nuclear Interactions in Lead and Light Elements . . . M. F. Kaplon, D. M. Ritson, and W. D. Walker 1119

Resonance Trapping in Diffusion Experiments . . . John R. Beyster 1121

Rotational States in Boron-Boron Nuclei . . . Alex Zucker, John E. Hopkins, and E. Norman Hudson 1122

Recoil Effects in Mixed-Electron Emission . . . E. M. Hiesey and M. A. Zimmerman 1123

Transfer Rate of the Liquid Helium II Film Over Bare Level Surfaces . . . Gordon K. Teal 1125

Scattering of Λ^0 Mesons Near to an Atomic Nucleus . . . Samuel B. Treiman 1126

Possible Breakdown of Isotopic Spin and Charge Parity Selection Rules . . . D. E. Wilkinson 1131

Heavy Decomposition and the Energy and Momenta of the Products . . . E. J. Konopinski 1132

Parity of Isotopic Spin or Charge Parity Mixed . . . G. de Jonge and D. E. Wilkinson 1133

Angular Distribution of Gamma-Rays from Stripping Reactions . . . G. R. Satchler 1135

Ratio of Photons to Electrons Quota Quantity for Hydrogen . . . R. F. Mozley and C. E. Violet 1136

Total Cross Sections of Λ^0-MeV Pions in Hydrogen . . . C. E. Angelini and J. P. Perez 1141

Binding Energy Calculation on Rh and Single-Particle Wave Functions . . . F. C. Barker 1142

LANCASTER PRESS, INC., LANCASTER, PA.